United States
Environmental Protection
Agency

Office of Research and
Development
Washington DC 20460

EPA/600/R-01/070
September 2001

Development of Recommendations and Methods to Support Assessment of Soil Venting Performance and Closure

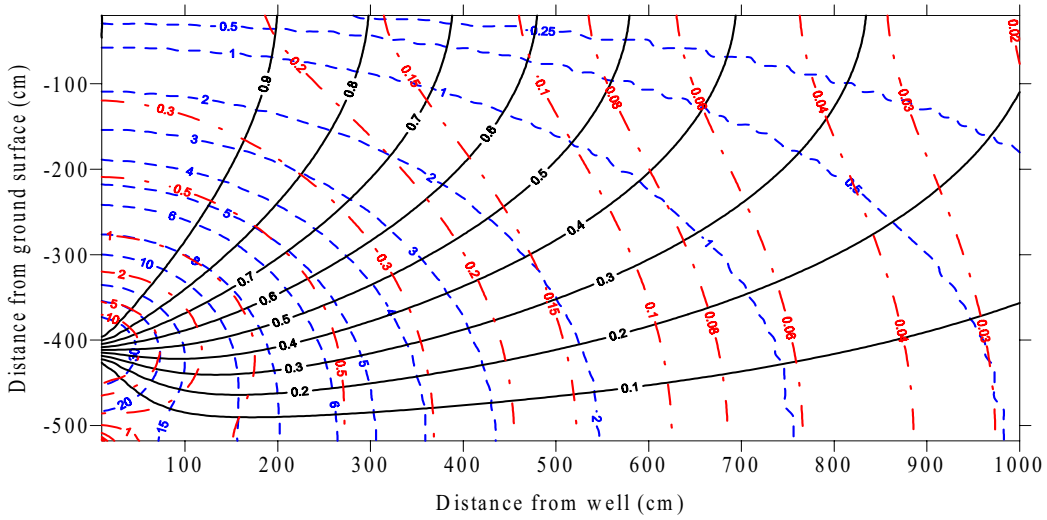

EPA/600/R-01/070
September 2001

DEVELOPMENT OF RECOMMENDATIONS AND METHODS TO SUPPORT ASSESSMENT OF SOIL VENTING PERFORMANCE AND CLOSURE

by

Dominic C. DiGiulio
Subsurface Protection and Remediation Division
National Risk Management Research Laboratory
Ada, Oklahoma 74820

and

Ravi Varadhan
(formerly with Dynamac Corporation)
Johns Hopkins University
School of Public Health
Baltimore, Maryland
Contract No. 68-C4-0031

Project Officer
Dominic C. DiGiulio
Subsurface Protection and Remediation Division
National Risk Management Research Laboratory
Ada, Oklahoma 74820

NATIONAL RISK MANAGEMENT RESEARCH LABORATORY
OFFICE OF RESEARCH AND DEVELOPMENT
U. S. ENVIRONMENTAL PROTECTION AGENCY
CINCINNATI, OHIO 45268

NOTICE

The U.S. Environmental Protection Agency through its Office of Research and Development funded and managed the research described here through in-house efforts and under Contract No. 68-C4-0031 to the Dynamac Corporation. It has been subjected to the Agency's peer and administrative review and has been approved for publication as an EPA document.

All data generated by EPA staff were subjected to the analytical Quality Assurance Plan for ManTech Environmental Research Services Corp. Results of field-based studies and recommendations provided in this document have been subjected to extensive external and internal peer and administrative review. This report provides technical recommendations, not policy guidance. It is not issued as an EPA Directive, and the recommendations of this report are not binding on enforcement actions carried out by the U.S. EPA or by the individual States of the United States of America. Neither the United States Government nor the authors accept any liability or responsibility resulting from the use of this document. Implementation of the recommendations of the document, and the interpretation of the results provided through that implementation, are the sole responsibility of the user.

Computer programs described within this report support analysis of gas flow and solute transport in porous media. Neither the United States Government nor the authors accept liability or responsibility resulting from the use of computer programs contained within this document. Use of these codes is the sole responsibility of the user. Mention of trade names or commercial products does not constitute endorsement or recommendation for use.

FOREWORD

The U.S. Environmental Protection Agency is charged by Congress with protecting the Nation's land, air, and water resources. Under a mandate of national environmental laws, the Agency strives to formulate and implement actions leading to a compatible balance between human activities and the ability of natural systems to support and nurture life. To meet these mandates, EPA's research program is providing data and technical support for solving environmental problems today and building a science knowledge base necessary to manage our ecological resources wisely, understand how pollutants affect our health, and prevent or reduce environmental risks in the future.

The National Risk Management Research Laboratory is the Agency's center for investigation of technological and management approaches for reducing risks from threats to human health and the environment. The focus of the Laboratory's research program is on methods for the prevention and control of pollution to air, land, water, and subsurface resources; protection of water quality in public water systems; remediation of contaminated sites and ground water; and prevention and control of indoor air pollution. The goal of this research effort is to catalyze development and implementation of innovative, cost-effective environmental technologies; develop scientific and engineering information needed by EPA to support regulatory and policy decisions; and provide technical support and information transfer to ensure effective implementation of environmental regulations and strategies.

The overall purpose of the report is to improve the "state of the art" and "state of the science" of soil venting application. Results of field-based research and comprehensive and detailed literature reviews on gas flow and vapor transport are provided to form the basis and defense of recommendations to improve site characterization, design, and monitoring practices in support of venting application.

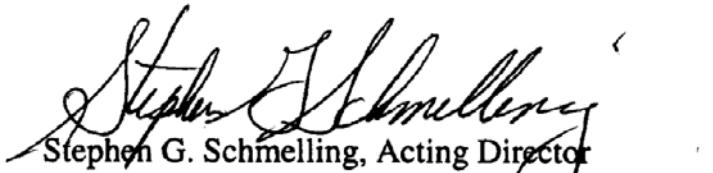

Stephen G. Schmelling, Acting Director
Subsurface Protection and Remediation Division
National Risk Management Research Laboratory

ABSTRACT

Soil venting, which includes gas extraction and/or gas injection, is the primary method used in the United States to remove volatile organic compounds (VOCs) from unsaturated subsurface porous media. The widespread use of venting is due to its above ground simplicity of operation and proven ability to remove contaminant mass inexpensively relative to competing technologies. However, there is little consistency in assessment of performance of the technology in U.S. EPA or State regulatory programs. Design, monitoring, and closure schemes are typically based on empirical methods with little consideration given to fundamental physical, chemical, and biological processes controlling mass removal during venting operation. This results in the technology not being utilized to its fullest potential, nor its limitations being well understood.

The purpose of this document was to improve the current "state of the art" and "state of the science" of soil venting application. This purpose was accomplished by attainment of three specific objectives. The first objective was to develop a regulatory approach to assess closure including measures to ensure consistency in ground-water and vadose zone remediation. The second objective was to provide comprehensive and detailed literature reviews on gas flow and vapor transport. These reviews formed the basis of recommendations and methods to improve venting design and monitoring. The third objective was to perform research to improve various aspects of venting application.

To fulfill the first objective, a strategy was proposed to base closure on regulatory evaluation of four components: (1) site characterization, (2) design, (3) monitoring, and (4) mass flux to and from ground water. Concurrent consideration of each component results in converging lines of reason or a "weight of evidence" approach thereby increasing the likelihood of correctly assessing the suitability for closure. Each component is interrelated requiring continuous evaluation during the life of the project. A vadose zone paradigm was developed to dynamically link the performance of ground-water remediation to vadose zone remediation. Substantial progress in remediating ground water translates to increasingly stringent soil venting closure requirements, while lack of progress in remediating ground water translates into less stringent closure requirements.

To fulfill the second objective, a detailed and comprehensive literature review describing laboratory and numerical experiments performed to elucidate and quantify rate-limited mass transport process during venting was provided. This literature review provided the basis for development of an innovative method of design based on attainment of a critical pore-gas velocity in contaminated media. A critical pore-gas velocity is defined as a pore-gas velocity which results in slight deviation from equilibrium conditions. Selection of a pore-gas velocity to support venting design requires consideration of rate-limited gas-NAPL, gas-water, and solids-water mass exchange on a pore-scale and rate-limited mobile-immobile gas exchange on a field-scale. Results of single- and multiple-well gas pressure and pore-gas velocity simulations demonstrated that a design based on attainment of a critical pore-gas velocity is superior to the

commonly used empirical method of radius of influence (ROI) testing. These simulations clearly showed that the ROI is an ill-defined entity and that ROI-based designs do not guarantee sufficient gas flow in porous media for timely remediation.

This literature review also revealed that observation of low asymptotic vapor concentrations in effluent gas is not a sufficient condition to demonstrate progress in mass removal from contaminated soils. Different mass retention and rate coefficients produce very similar effluent curves suggesting that effluent and vapor probe concentration data can not be used to estimate mass transport coefficients and remaining VOC mass. Thus, the ubiquitous empirical method of assessing venting performance based on observation of asymptotic vapor concentrations is questionable.

The third objective was fulfilled by conducting research in the following areas: (1) linearization of the gas flow equation, (2) one-dimensional steady-state gas flow with slippage, (3) two-dimensional steady-state gas flow and permeability estimation in a domain open to the atmosphere, (4) two-dimensional steady-state gas flow and permeability estimation in a semi-confined domain, (5) two-dimensional transient gas flow and permeability estimation, (6) radius of influence versus critical pore-gas velocity based venting design, (7) modification of a gas extraction well to minimize water-table upwelling, (8) rate-limited vapor transport with diffusion modeling, (9) respiration testing, and (10) one-dimensional, analytical, vadose zone transport modeling to assess mass flux to and from the capillary fringe. A number of public domain FORTRAN codes were developed to achieve these research objectives. Example input and output files and the source code for each program are contained within the appendices.

This page was intentionally left blank.

TABLE OF CONTENTS

TABLE OF CONTENTS

TABLE OF CONTENTS

TABLE OF CONTENTS

TABLE OF CONTENTS

LIST OF SYMBOLS

Latin

A	area [L^2]
A_{ia}	gas-water interfacial area [L^2L^{-3}]
C_{ia}	concentration at the gas-water interface [ML^{-3}]
C_g	concentration in gas phase [ML^{-3}]
C_g*	equilibrium vapor concentration [ML^{-3}]
C_g^{sat}	saturated vapor concentration [ML^{-3}]
C_n	NAPL phase concentration [ML^{-3}]
C_s	solids phase concentration [MM^{-1}]
C_{s1}	solids concentration in equilibrium domain [MM^{-1}]
C_{s2}	solids concentration in rate-limited domain [MM^{-1}]
C_T	total soil concentration [ML^{-3}]
C_w	concentration in bulk water or intra-aggregate space [ML^{-3}]
C_w^{sat}	saturated aqueous concentration [ML^{-3}]
D	dimensionless depth ($d_{U/}d$)
D_g	molecular gas diffusivity [L^2T^{-1}]
D_{ij}	dispersion coefficient [L^2T^{-1}]
D_m	mechanical dispersion coefficient [L^2T^{-1}]
D_w	molecular aqueous diffusion coefficient [L^2T^{-1}]
F	fraction of instantaneous sorption sites [-]
G_0	geometric shape factor of minipermeameter [-]
H	Henry's Law Constant [-]
ΔH_v	heat of vaporization [$ML^2T^{-2}mol^{-1}$]
ΔH_{vb}	heat of vaporization at boiling point [$ML^2T^{-2}mol^{-1}$]
I	inertial flow factor [L^{-1}]
J_0	zero-first-order Bessel functions of the first kind
J_1	first-order Bessel functions of the first kind
K_0	zero-order modified Bessel functions of the second kind
K_1	first-order modified Bessel functions of the second kind
K_d	equilibrium sorption coefficient [L^3M^{-1}]
K_F	Fishtine dipole moment factor [-]
K_{ia}	adsorption coefficient between gas and gas-water interface [L]
K_{ng}	NAPL - gas partition coefficient [-]
K_{nw}	NAPL - water partition coefficient [-]
K_{oc}	organic carbon - water partition coefficient [L^3M^{-1}]
K_{ow}	octanol-water partition coefficient [L^3M^{-1}]
L	dimensionless lengh (d_L/d)
L_c	characteristic contamination distance [L]

LIST OF SYMBOLS

M_g molecular weight of gas mixture [$Mmole^{-1}$]
M_i molecular weight of compound i [$Mmole^{-1}$]
M_n average molecular weight of NAPL [$Mmole^{-1}$]
P gas pressure [$ML^{-1}T^{-2}$]
$\overline{P}$ average pressure [$ML^{-1}T^{-2}$]
P_D prefix denominator [-]
Pe Peclet number [-]
P_v vapor pressure [$ML^{-1}T^{-2}$]
Q_m mass flow rate [MT^{-1}]
Q_v volumetric flow rate [L^3T^{-1}]
$\Re$ universal gas constant [ML^2/T^2molK]
R retardation factor [-]
R_D retardation factor used for prefix denominator [-]
Re Reynolds number [-]
R_s retardation factor used for bicontinuum sorption kinetics [-]
S_g gas saturation [-]
S_n NAPL saturation [-]
$S_{g,e}$ gas saturation at emergence point [-]
$S_{g,s}$ maximum gas saturation [-]
$\overline{S}_g$ effective gas saturation [-]
S_w water saturation [-]
$\overline{S}_w$ effective water saturation [-]
ΔS_{vb} entropy of vaporization at boiling point [$ML^2T^{-3}mol^{-1}$]
T temperature [K]
T_b boiling point [K]
T_c critical point [K]
U Kirckhoff transformed pressure
V_b borehole storage volume [L^3]
V_m molar gas volume [L^3mol^{-1}]
Y_0 zero-order Bessel function of the second kind
Y_1 first-order Bessel function of the second kind
Z gas compressibility factor [-]
a radius or aggregate radius [L]
b gas slippage or Klinkenberg parameter [$ML^{-1}T^{-2}$]
c geometric shape factor: spherical is 15, planar is 3
a_s total acceleration in Lagrangian framework [LT^{-2}]
d depth or thickness of a domain [L]
d’ thickness of semi-confining layer [L]
d_{50} mean grain diameter [L]

LIST OF SYMBOLS

d_L depth to lower portion of sand pack [L]
d_m molecular diameter [L]
d_p pore diameter [L]
d_U depth to upper portion of sand pack [L]
dS length of cylinder in potential formulation [L]
e $(k_r/k_z)^{½}$
e' $k'd/k_z d'$
f friction factor [-]
f_g mass fraction of contaminant in gas phase [MM^{-1}]
f_i mass fraction of contaminant accumulated at gas-water interface [MM^{-1}]
f_n mass fraction of contaminant in NAPL phase [MM^{-1}]
f_s mass fraction of contaminant on solid phase [MM^{-1}]
f_w mass fraction of contaminant in water phase [MM^{-1}]
f_{oc} fraction of organic carbon content [MM^{-1}]
g gravitational constant (980 cm s^{-2})
h capillary pressure [L]
h_d empirical Brooks-Corey fitting parameter [L]
$\underline{\underline{k}}$ gas permeability tensor [L^2]
$\underline{\underline{k_i}}$ intrinsic permeability tensor [L^2]
k' gas permeability of semi-confining layer [L^2]
k_r radial gas permeability [L^2]
k_{rg} relative permeability to gas [-]
$k_{i(r)}$ intrinsic radial permeability to gas [L^2]
k_x longitudinal gas permeability [L^2]
$k_{i(x)}$ intrinsic one-dimensional permeability to gas [L^2]
k_z vertical component of gas permeability [L^2]
$k_{i(z)}$ intrinsic vertical permeability to gas [L^2]
m_m molecular mass [M]
m numerical index in summation series, number of capillary tubes, or empirical van Genuchten water retention parameter []
n numerical index in summation series, number of molecules [-], or empirical van Genuchten water retention parameter
q volumetric specific discharge vector [LT^{-1}]
q_r radial component of specific discharge vector [LT^{-1}]
q_z vertical component of specific discharge vector [LT^{-1}]
q_m mass specific discharg vector [$ML^{-2}T^{-1}$]
r radial coordinate [L]
r_I radius of influence [L]
r_i inner radius of tip seal of minipermeameter [L]

LIST OF SYMBOLS

r_o outer radius of tip seal of minipermeameter [L]
r_w radius of well or filter pack [L]
t_c critical time necessary to remove 99% of contaminant mass [T]
v average linear pore-gas velocity [LT^{-1}]
$v_{c(ng)}$ critical pore-gas velocity for NAPL-gas exchange [LT^{-1}]
$v_{c(gw)}$ critical pore-gas velocity for gas-water exchange [LT^{-1}]
$v'_{c(a\text{-}gw)}$ critical pore-gas velocity for gas-water exchange using aggregate diffusion [LT^{-1}] from Gierke et al. (1992)
$v_{c(a\text{-}gw)}$ critical pore-gas velocity for gas-water exchange using aggregate diffusion [LT^{-1}] from Ng and Mei (1996)
$v_{c(D\text{-}gw)}$ critical pore-gas velocity for gas-water exchange using prefix denominator [LT^{-1}]
w average gas velocity in direction of flow in thin layer adjacent to pore wall [LT^{-1}]
y distance from a pore or capillary wall [L]
$\overline{y}$ average dist. from a pore wall in which the last molecular collision occurred [L]
z vertical coordinate [L]

Greek

Φ gas potential [L]
Φ_f gas potential loss due to friction [L]
Σ spreading coefficient
α empirical van Genuchten water retention fitting parameter []
δ_c characteristic diffusion path length or radius [L]
κ_c Boltzmann constant (1.38066×10^{-23} JK^{-1})
λ mean free path of gas molecules [L] or empirical Brooks-Corey water retention fitting value
λ_{gg} mobile gas-immobile gas first order rate [T^{-1}]
λ_{gw} gas-water first-order rate coefficient [T^{-1}]
λ'_{gw} gas-water first-order rate coefficient defined by Gierke et al. (1992) [T^{-1}]
λ_{ng} NAPL-gas first order rate coefficient [T^{-1}]
λ_{ws} water-solid first order rate coefficient [T^{-1}]
κ first-order degradation rate [T^{-1}]
μ_g dynamic gas viscosity [MTL^{-2}]
ω_{gw} gas-water Damkohler number [-]
ω_{sw} solids-water Damkohler number [-]
ρ_b bulk density of soil [ML^{-3}]
ρ_g gas density [ML^{-3}]
ρ_j density of compound j [ML^{-3}]
ρ_n NAPL density [ML^{-3}]
ρ_s particle density [ML^{-3}]

LIST OF SYMBOLS

σ_{gn} gas-NAPL interfacial tension
σ_{gw} gas-water interfacial tension
σ_{nw} NAPL-water interfacial tension
η porosity [L^3L^{-3}]
ϕ pressure squared [$M^2L^{-2}T^{-4}$]
ϕ_I pressure squared at radius of influence [$M^2L^{-2}T^{-4}$]
τ gas phase shearing stress [$ML^{-1}T^{-2}$]
τ_g gas phase tortuosity factor [-]
τ_w water phase tortuosity factor [-]
θ_g mobile volumetric gas content or inter-aggregate gas-filled porosity [L^3L^{-3}]
θ_n volumetric NAPL content [L^3L^{-3}]
θ_w volumetric water content or intra-aggregate porosity [L^3L^{-3}]
χ_i mole fraction of organic compound i in NAPL
γ_i activity coefficient of organic compound i in NAPL [-]
ψ streamfunction for gas flow
υ_g kinematic gas viscosity [L^2T^{-1}]

LIST OF FIGURES

LIST OF FIGURES

LIST OF FIGURES

LIST OF FIGURES

LIST OF FIGURES

LIST OF FIGURES

LIST OF FIGURES

LIST OF FIGURES

LIST OF TABLES

ACKNOWLEDGMENTS

The authors express their appreciation for helpful comments received from the following reviewers of this document:

Mr. Dave Becker
Hazardous, Toxic, and Radioactive Waste
Center of Expertise
U.S. Army Corps of Engineers
Omaha, Nebraska

Dr. Mark Brusseau
Soil, Water, and Environmental Science Department and
Hydrology and Water Resources Department
University of Arizona
Tucson, Arizona

Dr. Paul C. Johnson
Department of Civil and Environmental Engineering
College of Engineering and Applied Sciences
Arizona State University
Tempe, Arizona

Dr. Dave Kreamer
Water Resources Management Graduate Program
University of Nevada, Las Vegas
Las Vegas, Nevada

Ms. Michelle Simon
U.S. Environmental Protection Agency
National Risk Management Research Laboratory
Cincinnati, Ohio

The authors also wish to express appreciation to:

Ms. Anna Krasko
U.S. Environmental Protection Agency
New England Region
Boston, Massachusetts

for assistance in developing a number of portions of this document and for help in the field.

EXECUTIVE SUMMARY

Soil venting, soil vacuum extraction (SVE), and bioventing are terms commonly used to describe in-situ technologies in which gas flow is induced in subsurface unconsolidated or consolidated unsaturated media for the purpose of volatilizing or biodegrading organic chemicals. Gas (typically air) is injected and/or extracted from one or more wells causing a pressure differential and subsequent advective gas flow. Removal of volatile organic compounds (VOCs) is achieved by non-aqueous phase liquid (NAPL) evaporation, NAPL dissolution, desorption, air-water partitioning, biodegradation, and abiotic degradation. Removal of semi-volatile organic compounds is achieved partly through abiotic processes but primarily through biodegradation due to the effective delivery of oxygen.

Soil vacuum extraction (SVE), defined as including only gas extraction, is considered a presumptive remedy (a detailed technology screening process is not necessary for implementation) in the U.S. Environmental Protection Agency's (U.S. EPA) Superfund program. Bioventing, commonly defined as in-situ gas circulation designed to maximize contaminant mass removal through biodegradation while minimizing air flow rates and operating costs especially those associated with above-ground vapor treatment, is characterized by relatively "low" pore-gas velocities or pore-volume exchange rates. However, similar pore volume exchange rates or pore-gas velocities however may be optimal for operation under conditions of rate-limited mass transport. This observation and the fact that during venting, simultaneous volatilization and biodegradation occurs whether or not the latter process is intended suggests that the commonly used definition of bioventing is non-unique. In this document, an operational term, venting, is used to define gas injection and/or extraction without specific reference to biodegradation or any other subsurface processes. It is considered a general term encompassing SVE and bioventing.

Soil venting has become the primary method used in the United States to remove VOCs from unsaturated subsurface media. In 1997, SVE was applied or planned to be applied at 27% of Superfund sites. Since this statistic does not include gas injection or combined gas extraction and injection, venting application at Superfund sites likely exceeds 30%. The popularity and widespread use of venting is due to its simplicity of operation and proven ability to remove contaminant mass inexpensively compared to other technologies.

Despite the common use of venting in the Superfund program, there is little consistency in approach to assessment of performance and closure. Assessment of the technology's performance and eventual decisions on closure are based primarily on negotiations between responsible parties and regulators. In this process there is widespread use and reliance on empirical methods as opposed to an emphasis on understanding fundamental physical, chemical, and biological processes controlling mass removal during the venting operation. This results in the technology not being used to its fullest potential, nor its limitations being well understood.

The overall purpose of the work described in this document was to improve the "state of the art" and "state of the science" of soil venting application. This purpose was accomplished by

attainment of three specific objectives. The first objective was to develop an overall regulatory approach to assess venting performance and closure including measures to ensure consistency in ground-water and vadose zone remediation. The second objective was to provide comprehensive and detailed literature reviews on gas flow and vapor transport. These reviews formed the basis of recommendations and methods to improve venting design and monitoring. The third objective was to perform research to improve various aspects of venting application. This document should benefit regulators, practitioners, and research scientists needing detailed knowledge of soil venting application.

Research conducted to support soil venting application consisted of analysis of: (1) linearization of the gas flow equation, (2) one-dimensional steady-state gas flow with slippage, (3) two-dimensional steady-state gas flow and permeability estimation in a domain open to the atmosphere, (4) two-dimensional steady-state gas flow and permeability estimation in a semi-confined domain, (5) two-dimensional transient gas flow and permeability estimation, (6) radius of influence versus critical pore-gas velocity based venting design, (7) modification of a gas extraction well to minimize water-table upwelling, (8) rate-limited vapor transport with diffusion modeling, (9) respiration testing, and (10) one-dimensional, analytical, vadose zone transport modeling to assess mass flux to and from the capillary fringe. A number of FORTRAN codes were developed to achieve these research objectives. Example input and output files and the source code for each program are contained within the appendices.

Concise summaries of each section except section 1 (introduction) are presented below.

Section 2

It is clear that an environmentally protective, flexible, technically achievable, and consistently applied approach for assessment of performance and closure of venting systems is needed. Any approach used to assess performance of a venting system should encourage good site characterization, design, and monitoring practices since mass removal can be limited by poor execution of any of these components. Also, any approach used to assess closure of a venting system must link ground-water remediation to vadose zone remediation since the two are interrelated. A strategy is proposed in section 2 for assessment of venting performance and closure based on regulatory evaluation of (1) site characterization, (2) design, (3) performance monitoring, and (4) mass flux to and from ground water. These components form converging lines of evidence regarding performance and closure. Evaluation is on a pass/fail basis since this type of critique provides the greatest flexibility in decision making. Failure in evaluation of one or more component(s) results in overall venting closure failure. Such a “weight of evidence” approach increases the likelihood of correctly assessing the performance of a venting system and its suitability for closure. Each component is interrelated and requires continuous evaluation during the life of the project. Approval of individual components occurs concurrently at the perceived end of the project.

This closure approach encourages and will likely in some cases force good site

characterization, design, and monitoring practices. If evaluation of all these factors individually supports closure, then it is likely that closure is indeed appropriate. If one or more of the components does not support closure, then it is likely that either closure is inappropriate or that a conscious decision must be made to accept a limiting condition. For instance, in the presence of significant rate-limited vapor transport, closure would not proceed if there was potential for substantial continued mass flux to ground water. In this case, venting may need to be applied indefinitely at low pore-gas velocities or in a pulsed mode. Regulators however could decide to turn off the system if indefinite ground-water remediation or containment is anticipated or if the remaining mass moving into the ground water will not impact a potential receptor. Regardless of the situation, assessment of these components enables flexible, organized, and informed decision making.

The most common method of assessing whether to initiate, continue, or cease venting application or any other in-situ vadose zone remediation technology, involves periodic collection of soil samples for comparison with compound-specific, concentration-based standards which are often based on the results of vadose zone modeling. Remediation is considered complete when vadose zone modeling indicates that these standards will be attained in the future. Both soil-based and leachate-based standards are typically stringent because it is required that soils be remediated to the extent that mass flux to ground water not result in aqueous concentrations exceeding maximum contaminant levels (MCLs). However, at sites where it is unlikely that ground-water remediation will result in attainment of MCLs, the need for soil or soil-water based vadose zone remediation standards that assume attainment of MCLs becomes questionable. Stringent remediation standards and other factors such as mass transport limitations often make attainment of venting closure difficult at many sites.

Soil remediation goals must reflect the realities of ground-water remediation. This was accomplished by partitioning subsurface remediation areas into three distinct zones for performance evaluation purposes. The first zone is bounded on the upper end by the soil surface and on the lower end by the seasonally high water table. This zone consists of consistently unsaturated media (above the region of water table fluctuation) where mass flux to and from ground water occurs through infiltration and diffusion, and mass flux from ground water to the vadose zone occurs through diffusion.

The second zone consists of periodically de-saturated media due to water-table fluctuation or dewatering. Often, it will consist of a highly contaminated “smear” zone containing residual NAPL where venting is combined with dewatering to remove contaminant mass from a localized region. This zone is bounded on the upper end by the seasonally high water table and on the lower end by the maximum depth to ground water during dewatering.

The third zone is bounded on the upper end by a ground-water level with or without dewatering and on the lower end by the targeted depth of ground-water remediation. It represents media that remains saturated during venting. Ground-water concentrations in this zone vary temporally and determine compliance in the first two zones. The second zone is in compliance

when ground-water concentrations are less than or equal to ground-water concentrations in the third zone. This ensures that remediation of ground water within a smear zone will be attempted to levels consistent with maximum levels of deeper contamination. This ensures consistency in ground-water remediation efforts and avoids reduction of ground-water concentrations in the second zone to levels lower than what would occur through vertical recontamination from the third zone.

In the case of a light non-aqueous phase spill where ground-water concentrations within a "smear" zone are at much higher levels than beneath the “smear” zone, low concentrations in the third zone forces aggressive dewatering and venting application in the second zone. In the case of a dense non-aqueous phase spill where ground-water concentrations may be at high levels deep within an aquifer, remediation within the dewatered region or second zone proceeds only to the degree at which it is consistent with remediation in deeper regions or the third zone. The first zone is in compliance with the second zone when mass flux to ground water is close to zero or the direction of mass flux is primarily from ground water to the vadose zone (i.e. mass flux due to vapor diffusion from contaminated ground water exceeds mass flux due to vapor diffusion and infiltration from the vadose zone at the ground-water - vadose zone boundary). This ensures aggressive venting application in the vadose zone when ground water has very low levels of contamination, and less aggressive venting application when vapor diffusion will result in recontamination of cleansed soils. Thus, venting performance in the first and second zones is dynamically linked to the performance of ground-water remedial efforts in the third zone. Substantial progress in remediating ground water translates to increasingly stringent soil venting performance standards, while lack of progress in remediating ground water translates into less stringent soil remediation requirements.

Section 3

In section 3, two methods of linearization of the gas flow equation were evaluated. The governing equation for gas flow is by definition a non-linear partial differential equation because the dependent variable, ϕ or pressure squared, is expressed in a form other than unity. To solve this equation analytically, linearization of the $\sqrt{\phi}$ term is necessary. The most simplistic approach is to let $\sqrt{\phi}$ equal atmospheric pressure (P_{atm}) or some other constant pressure and to let $\phi = PP_{atm}$, thereby removing consideration of compressibility. A second approach is to let $\sqrt{\phi}$ equal P_{atm} but still solve for ϕ. A third approach is to replace $\sqrt{\phi}$ with a prescribed time-varying function which in some manner reflects the rate of change of initial pressure distribution. For analytical model development and derivations in this dissertation, only the first two approaches are practical.

Error incurred in pressure computation using the first and second approaches was evaluated using Kidder’s (1957) second-order perturbation solution to the one-dimensional transient gas flow equation. Maximum error occurred at low absolute pressures and were much less when solving directly for ϕ ($\approx$6 %) than when compressibility was neglected ($\approx$80%). It is often assumed that compressibility is of minor importance during vacuum extraction because near atmospheric pressure is commonly encountered in sandy soils. However, in recent years,

vacuum extraction has been increasingly applied in lower permeability soils such as silts and glacial till, where at least in the vicinity of gas extraction wells, low absolute pressure (less than 0.5 atmospheres) occurs.

This analysis demonstrated that solving directly for ϕ is adequate for solving gas flow problems while the $\phi = PP_{atm}$ approach incurs too much error and thus should not be used for venting application. In section 3, figures were generated illustrating error in pressure computation as a function of linearization method. These figures eliminate the need to solve Kidder's (1957) lengthy perturbation solution when assessing error due to linearization of the gas flow equation.

Section 4

In section 4, an analytical solution was derived for one-dimensional, steady-state gas flow incorporating the effect of gas slippage. This solution was then used to assess the impact of gas slippage on one-dimensional pressure and pore-gas velocity simulation as a function of flow rate and gas permeability. Simulations during gas extraction demonstrated that neglecting gas slippage results in underestimation of absolute pressure, whereas during air injection, neglecting gas slippage results in overestimation of absolute pressure. In both cases, pressure differential from atmospheric pressure was overestimated when neglecting gas slippage. For both gas extraction and injection, variation in pressure was greatest at the point of extraction or injection and at lower gas permeability values. However, the magnitude of error in pressure computation for gas injection was far lower than for gas extraction because of higher absolute pressures during gas injection. Even at the lowest gas permeability, maximum error for pressure computation during gas injection did not exceed 6%, whereas during gas extraction, error exceeded 80%. Thus, if gas slippage is neglected, gas injection should result in a better estimate of gas permeability than gas extraction.

Computed pore-gas velocities during gas injection were much lower than during gas extraction at the same flow rates because of increased gas density. Error in pore-gas velocity computation neglecting gas slippage during gas injection was much lower than during gas extraction (13% versus over 600%). Similar to gas extraction, error during gas injection increased with decreased permeability. However, unlike gas extraction, error increased with distance from the point of injection.

These findings have important implications for laboratory- and field-scale gas flow and vapor transport studies. For vapor transport column studies, it is apparent that lower and better controlled pore-gas velocity profiles can be attained by gas injection compared to gas extraction. At the field-scale, neglecting gas slippage may result in significant error in gas permeability estimation and severe error in pore-gas velocity computation during gas extraction. The impact of gas slippage on field-scale gas permeability estimation and venting design requires further investigation.

Section 5

In section 5, data collected from the U.S. Coast Guard Station in Traverse City, Michigan was used to demonstrate gas permeability estimation, pore-gas velocity calculation, and streamline generation in a domain open to the atmosphere. An analytical solution was derived for computation of streamlines to a finite-radius well. For gas permeability estimation, random guesses constrained with decreasing intervals of radial and vertical permeability and analysis of root mean square errors (RMSE) were used to ensure attainment of global versus local minimum values. Confidence in permeability estimation was demonstrated by providing plots of observed versus simulated pressure response. Plots of pore-gas velocity as a function of distance and flow rate were provided to provide a preliminary estimate of soil venting well spacing. Through discussion and example, a partial list of elements necessary for sound gas permeability estimation was provided. These include: (1) placement of narrowly screened pressure monitoring points close to a discretely screened gas extraction well to capture the vertical component of gas flow, (2) testing at several flow rates to establish reproducibility, (3) analysis of error using the RMSE of observed versus simulated pressure response, and (4) plots of observed versus simulated pressure response to provide confidence is permeability estimation.

Section 6

In section 6, data collected from a Superfund Site on the Atlantic Coastal Plain was used to demonstrate difficulties encountered when attempting to use radius of influence (ROI)-based pressure data and the pseudo-steady-state radial flow equation for gas permeability estimation. There are two primary concerns with use of radial flow equations and ROI pressure data for gas permeability estimation. First, one-dimensional transient and pseudo-steady-state radial flow equations may result in higher estimates of radial gas permeability compared to solutions allowing vertical leakage because for a given flow rate, confined flow or semi-confined flow with low leakance (vertical gas permeability of a semi-confining layer divided by its thickness) results in a higher pressure differential compared to unconfined flow. Strict confined conditions rarely if ever occur in the field. Even at sites where a concrete or asphalt cap exists, small cracks or flow through a gravel subbase can result in significant recharge from the atmosphere. Second, ROI test data may not be suitable for estimation of anisotropy, leakance, and subsequent computation of axisymmetric cylindrical (r,z) or Cartesian (x, y, z) components of pore-gas velocity because: (1) gas monitoring wells are often located so far away from gas extraction wells that resulting pressure differentials are too low to distinguish from atmospheric pressure, (2) sensitivity of both radial and vertical gas permeability estimation decreases considerably with increasing radial distance from a gas extraction well, and (3) vacuum extraction wells and monitoring points are screened over large portions of the vadose zone providing vertically integrated measurements of pressure differential as opposed to point values required for vertical permeability and leakance estimation using analytical axisymmetric cylindrical or three-dimensional numerical models.

Gas permeability testing at the Atlantic Coastal Plain site indicated that use of the

pseudo-steady-state radial flow equation provided a slight but consistent overestimation of radial permeability compared to solutions which allowed recharge at the upper boundary. However, little if any correlation between increased leakance and overestimation of radial permeability was observed. A comparison of radial gas permeability estimates for unconfined and semi-confined domains revealed that radial permeability estimation was relatively insensitive to leakance. Estimation of vertical gas permeability expressed in the ratio of k_r/k_z though was very sensitive to leakance and illustrated the difficulty in resolving the correlated effect of leakance and anisotropy with ROI pressure data. The assumption of high leakance or a domain open to the atmosphere resulted in higher k_r/k_z ratios compared to semi-confined conditions.

Section 7

In section 7, a sensitivity analysis and field application of an analytical solution for finite-radius, transient testing gas permeability estimation was presented. Line-source/sink analytical solutions are currently used exclusively for transient, axisymmetric, two-dimensional gas flow analysis and parameter estimation. The implicit assumption in use of these solutions is that borehole storage effects are insignificant except in the immediate vicinity of the wellbore. The radii away from a well and borehole storage volume over which borehole storage effects become important though have not been investigated for gas flow. Thus, use of pressure monitoring points very close to a gas extraction or injection well may introduce some unquantified error in gas permeability estimation. Borehole storage effects would be expected to be of greatest significance in single-interval, transient testing. Similar to slug testing in ground-water hydrology, single-interval testing provides permeability estimation over a relatively small volume of subsurface media thereby providing a mechanism for assessing physical heterogeneity or spatial variability in permeability on a scale much smaller than full scale field-scale tests.

Simulations comparing transient finite-radius and line source/sink solutions during gas injection revealed that the line-source/sink solution resulted in a more rapid rise in pressure at the wellbore at early time but then leveled off to a lower normalized pressure at late time compared to the finite-radius solution. The former effect was due to lack of a delayed response from borehole storage. The latter effect was likely due to the fact that for the line source/sink solution simulated pressure response into the formation at a distance equivalent to the wellbore radius. Lower pressure differential response at late time for the line-source/sink solution would likely lead to gas permeability overestimation for a given flow rate. At the wellbore, pressure was overestimated at early time for the line source/sink solution and underestimated over well shut-in by as much as 10% . Thus, for single-interval, transient testing, borehole storage effects can become a moderate source of error if not properly accounted for.

Under conditions of these simulations, error due to use of a line-source/sink solution disappeared at a relatively short distance from the wellbore. Thus, under typical testing conditions when a gas extraction or injection well is not used as the pressure monitoring point, transient gas permeability estimation using a line-source/sink solution would result in little error. A comparison of line-source/sink versus finite-radius simulations at the wellbore at different

vertical elevations revealed little error (less than 1.5%) associated with using a line-source/sink solution. Thus, for simulations conducted here, line-source/sink solutions appear appropriate for single well, multi-interval testing. However, conditions specified here are not reflective all potential testing conditions. Thus, when observation points are close to a gas extraction or injection well, it may be useful to utilize a transient, finite-radius solution to assess the importance of finite-radius and wellbore effects.

A sensitivity analysis of the finite-radius solution revealed that in single-interval testing, increased borehole storage volume results in an increased delayed response to steady-state conditions. Increased gas-filled porosity results in a somewhat similar transient response to increased borehole storage volume but the transient effects are much more prolonged. Single-interval simulations also demonstrated that higher k_r/k_z ratios prolong attainment of steady-state conditions and result in a higher normalized pressure response compared to lower k_r/k_z ratios. The effect of leakance on transient pressure response at the wellbore however appeared to be minor. Finally, single-interval simulations demonstrated that lower gas permeability significantly prolongs attainment of steady-state conditions and results in a much higher pressure differential.

The usefulness of transient, single-interval gas permeability testing was then demonstrated at the Picillo Farm Superfund Site in Rhode Island. Testing revealed that single-interval transient gas permeability testing is an improvement over single-interval steady-state gas permeability testing in that the former provides an estimate of gas-filled porosity and does not rely on attainment of steady-state conditions which is sometimes questionable for low permeability media (small pressure change in time after initial pressure or vacuum application). The method though provided little confidence in leakance and k_r/k_z estimation. Thus, resolution of anisotropy and leakance requires multiple interval testing.

Section 8

In section 8, a basic description of volatile organic compound (VOC) retention in porous media is provided to assist the reader in understanding subsequent sections in mass transport. An understanding of VOC retention in porous media is critical to designing, monitoring, and closing venting systems. Each phase in unsaturated porous media can contribute to the retention and mass transport of VOCs. Phases present are solid minerals, organic matter, bulk water, nonaqueous phase liquids (NAPL), and gas. Partitioning mechanisms related to these phases are solid mineral - water, solid mineral - gas, organic matter - water, water - gas, NAPL - water, and NAPL - gas.

Section 9

In section 9, a detailed and comprehensive literature review describing laboratory and numerical experiments conducted to elucidate and quantify rate-limited mass transport process during venting was provided. This review was used to support the development of a method of

venting design based on specification of a critical pore-gas velocity in subsurface porous media. A critical pore-gas velocity is defined as a pore-gas velocity which results in slight deviation from equilibrium conditions. Selection of a pore-gas velocity to support venting design requires consideration of rate-limited gas-NAPL, gas-water, and solids-water mass exchange on a pore-scale and rate-limited mobile-immobile gas exchange on a field-scale. During rate-limited mass transfer, as pore-gas velocity increases, vapor concentration decreases. However, an increased pore-gas velocity still results in an increased mass removal rate and hence shorter remediation time because of an increased concentration gradient between equilibrium and nonequilibrium vapor and soil-water concentrations. Thus, there is a trade-off between selection of a design pore-gas velocity and remediation time.

Five methods were described that could be used separately or concurrently to select a critical pore-gas velocity for venting application. The approach most suitable for use by practitioners appears to be use of algorithms and Damkohler numbers. However, a limitation of using Damkohler numbers and algorithms to estimate critical pore-gas velocities is that mass transport processes are considered independently when in reality complex interactions between these processes dictate overall mass removal. Also, there are additional complications to consider in selection of critical pore-gas velocities. Virtually all research on rate-limited vapor transport and development of algorithms for pore-gas velocity determination originated from controlled sand tank and laboratory column studies where field-scale heterogeneity was not a factor. Thus, optimal pore-gas velocities in the field are likely to be very site-specific and somewhat smaller than indicated by Damkohler numbers, algorithms, and published studies. Also, characteristic lengths of contamination used in Damkohler numbers and algorithms are not constant but decrease in time due to NAPL and sorbed mass removal thereby reducing calculated optimal pore velocities. Finally, the cost of well installation and venting operation (e.g., electricity, vapor treatment) should be considered since achievement of a minimum target pore-gas velocity at some sites may be prohibitively expensive. Thus, it is apparent that selection of a critical pore-velocity is not a straightforward process but involves some degree of judgement and iterative reasoning (gas flow modeling to see what pore-gas velocities can be achieved given certain well spacing and flow rates). However, while there are limitations to the use of algorithms and Damkohler numbers in selecting a design pore-gas velocity, these numbers provide a starting point after which more sophisticated analysis can proceed if desired.

Section 10

In section 10, data was utilized from a Superfund site (described in section 6) to describe limitations of ROI evaluation in more detail than had been done previously and to demonstrate an alternative method of design based on specification and attainment of a critical pore-gas velocity in contaminated subsurface media. Information was utilized from section 9 to provide the basis for selection of a critical or design pore-gas velocity (0.01 cm/s) for use at this site. ROI evaluation is by far the most common method used for venting design in the United States. In practice, ROIs are determined by plotting vacuum as a function of logarithmically transformed radial distance and applying linear regression to extrapolate to a distance at which a specified

vacuum would be observed. For SVE design, overlapping circles of ROIs for individual wells are then drawn on a site map to indicate an "effective" remediation area.

Results of single-well simulations demonstrated several important deficiencies in ROI evaluation. First, cross-sectional vacuum profiles were very curvilinear especially under conditions of high leakance values and k_r/k_z ratios clearly illustrating that the ROI is an ill-defined entity. Second, an ROI-based design resulted in subsurface pore-gas velocities lower than 0.01 cm/s especially at low leakance values and high k_r/k_z ratios. Third, attainment of a 0.01 cm/s pore-gas velocity could not be guaranteed by simply raising the magnitude of subsurface vacuum (e.g., from 0.05 to 0.1 inches of water). Observed vacuum was a function of boundary conditions (e.g., leakance), applied mass flow, anisotropy, permeability, and geometry of screened intervals requiring at a minimum, two-dimensional simulation.

Multi-well simulations illustrated additional deficiencies in ROI-based design practices. It was evident that as leakance decreased, a velocity profile for a given total flow rate became more uniform but vacuum required to maintain a pore-gas velocity of 0.01 cm/s increased significantly - a relationship that would not be apparent from ROI testing. In one simulation, a pore-gas velocity of 0.01 cm/s could not be achieved despite vacuum levels exceeding 3.5 inches of water whereas in other portions of the site a pore-gas velocity of 0.01 cm/s was achieved at less than 1.5 inches of vacuum. This reinforces previous observations with single-well simulations that the magnitude of a vacuum level in subsurface media is not an indication of effective gas flow contrary to assumptions made in ROI testing. It was apparent that the suitability of using a specified vacuum levels of 0.05 or 0.1 inches of water, typical of ROI testing, to ensure adequate gas circulation decreased with increasing k_r/k_z ratios and decreasing leakance values. ROI-based designs then are more likely to be appropriate as k_r/k_z ratios approach 1.0 or less and when significant leakance occurs.

Finally, it was demonstrated that when attempting to achieve a critical design pore-gas velocity, it is far more efficient from an energy and vapor treatment perspective to install additional wells rather than pump existing wells at a higher flow rate. In one simulation, the total flow rate from 6 wells would have had to exceeded 1000 scfm to meet a pore-gas velocity of 0.01 cm/s throughout contaminated soils. When the total number of wells was increased from 6 to 16 however, a pore velocity of 0.01 cm/s was achieved throughout the entire contaminated region at only 400 scfm. In addition, the use of additional vapor extraction wells resulted in a much more uniform pore-gas velocity throughout the contaminated area.

Section 11

In section 11, the concept of combining gas injection and extraction (CIE) in a single well to avoid water-table upwelling or to reduce ground-water recovery during vacuum extraction was described. Field testing was conducted at Vance Air Force Base located in northwestern Oklahoma. Typically, when vacuum is applied to a well screened in or near the water table, water-level rise occurs within the well which often reduces or completely obstructs gas flow.

Gas injection on the other hand results in soil-water movement away from a screened interval. Thus, it is logical that injection of pressurized gas or at least maintenance of atmospheric pressure at the base of a vacuum extraction well would reduce water recovery.

At Vance AFB, injection of air at the base of a gas extraction well reduced water recovery by greater than 90% compared to dual vapor extraction. Vacuum measurements in soil during combined air injection and extraction were similar to vacuum application alone for all but the deepest probes. Vacuum measurement in shallow probes indicated that combined air injection and extraction did not result in uncontrolled air flow and hence vapor migration toward the surface.

Section 12

In this section, a number of recommendations were provided for VOC monitoring of venting sites. Flow and total vapor concentration monitoring using a PID or FID or other suitable instrument should be performed at the vapor treatment or blower inlet because it provides an estimate of VOC mass removal rate and total VOC mass removed as a function of time for an entire venting system. Flow and vapor concentration monitoring using a PID or FID or other suitable instrument should be performed at individual gas extraction wellheads to determine the most heavily contaminated portions of a site requiring perhaps the most monitoring, and to enable potential optimization of the vapor treatment system (e..g., prioritization of venting operation at highly contaminated areas, vapor stream richness or leanness for catalytic oxidation unit overheating or supplemental fuel requirement). When utilizing an FID or PID for VOC screening, the user must be aware of fundamental differences in detector operation, ionization potential of target compounds, and gas matrix effects. The high ionization potential of many common VOCs will result in nondetection using a conventional 10.6 or even a 11.7 eV PID lamp. The high halogen content of many common VOCs will result in underestimation or nondetection of VOCs using an FID. Gas matrix effects such as humidity, carbon dioxide, and alkane (especially methane) dramatically decrease PID response. Gas matrix effects combine in a nonlinear manner resulting in a decreased PID response far greater than what would be expected from additive effects. PIDs are also much more prone to nonlinearly in response compared to FIDs. Gas matrix and linearity problems however can be overcome through the use of serial dilution techniques.

Observation of evaporation fronts in individual extraction well effluent gas and evaporation/condensation fronts in well-placed vapor probe clusters could potentially provide valuable information on the progress of venting remediation of NAPL contaminated soils. Under equilibrium conditions, individual components of a NAPL propagate through soil in a sequence of evaporation-condensation fronts at speeds proportional to their vapor pressure. Evaporation-condensation fronts have likely not been reported during field application because of nonuniform gas flow (bypass flow as opposed to through-flow conditions, fully three-dimensional flow as opposed to one-dimensional or radial flow, spatial variability of NAPL distribution, common monitoring practices (determination of total VOC with a PID or FID as opposed to identification

and quantification of individual compounds), and rate-limited transport. Under equilibrium conditions in the field, sharp evaporation-condensation fronts are not likely to be discernable but the vapor concentration of lighter components should decrease monotonically with time compared to heavier components which should increase for some time and then decrease. In contrast, under rate-limited transport conditions, extensive extensive effluent tailing should be observed with vapor concentrations profiles remaining fairly similar. Thus, use of GC/MS monitoring in gas extraction well and vapor probe clusters may reveal patterns of component removal from NAPL, NAPL removal itself, and rate-limited vapor transport.

There is no way to directly relate observation of an asymptote to an environmental benefit and little potential to ensure consistency in decision making. Vapor concentration of an asymptote at a highly contaminated site may be much higher than at a lesser contaminated site leading perhaps to less stringent remediation at the highly contaminated site. Observation of an effluent asymptote may be related to venting design (e.g., well screening and spacing) or gas flow patterns separate or in addition to rate-limited vapor transport. Since both design considerations and rate-limited vapor transport can cause extensive effluent tailing and ineffectual removal of accessible contaminant mass, it is critical to first rigorously assess venting design, implementation, and associated monitoring prior to concluding that rate-limited vapor transport significantly constrains mass removal. An asymptote can be observed in gas extraction wells while much of the contaminant mass remains in soils. Observation of low asymptotic vapor concentrations in effluent gas is not a sufficient condition to demonstrate progress in mass removal from contaminated soils. Different mass retention and rate coefficients can produce very similar effluent curves suggesting that effluent and vapor probe concentration data can not be used to estimate mass transport coefficients and VOC concentration in the aqueous and solids phase. Thus, effluent and vapor probe concentration data is insufficient to quantitatively assess the progress of soil venting remediation.

Some indicators of rate-limited transport in the field may be decreased vapor concentration with increased pore-gas velocity (flow variation) and extensive vapor concentration tailing accompanied by vapor rebound after cessation of operation (flow interruption). In both NAPL and non-NAPL contaminated soils, flow variation provides a simple yet powerful test of the validity of local equilibrium. For NAPL contaminated soils however, results of flow interruption results can be confusing if the propagation of evaporation-condensation fronts are not considered. One potential use of flow interruption or rebound data is to use vapor concentrations and partition coefficients to estimate total soil concentration. However, there is presently so much uncertainty and error inherent in estimation that calculations can at best only provide qualitative insight into soil concentration levels.

Section 13

In section 13, data collected from Norton AFB in California demonstrated that diffusion modeling can provide a simple yet powerful way of assessing rate-limited vapor transport in discrete lenses of low permeability. Vacuum extraction had been applied at the site for two

years. VOCs in gas extraction wells and vapor probes had approached low asymptotic levels. Lithologic examination of cores and sample analysis though revealed much higher levels of VOCs remaining in lenses of fine-grained material compared to surrounding coarser-grained material. This observation indicated that mass removal from fine-grained material was likely limited by diffusion.

The contaminant profile within a fine-grained lense was used to establish the initial condition for diffusion modeling. Effluent concentrations at the gas extraction well were used to establish first-type, time-dependent boundary conditions. At the moisture saturation at the time of sampling (95%), simulations indicated that in excess of 80 years would be required to reach a trichloroethylene (TCE) concentration of 10 ug/kg (remediation goal) because the high moisture content resulted in a low effective diffusion coefficient. Vadose zone transport simulations conducted by a remedial contractor however indicated that mass flux of remaining TCE in soils to ground water would be insignificant. These simulations and simulations conducted for diffusion modeling were used then to support venting closure at this site.

Section 14

In section 14, the results of respiration testing and core sampling during venting application at the U.S. Coast Guard Base in Elizabeth City, North Carolina were described. Since measurement of biodegradation rates at a field scale is difficult and expensive, indicators of aerobic microbial activity such as oxygen depletion and carbon dioxide production are commonly used to demonstrate microbial activity. During venting application, it has become common practice to use zero-order oxygen consumption rates to directly estimate hydrocarbon degradation rates. Problems associated with this practice are discussed at length in section 14.

Data from respiration tests were fitted to zero- and first-order kinetic relationships. The significance of distinguishing zero- and first-order kinetics for oxygen consumption is that oxygen depletion is constant for the former and a function of oxygen concentration for the latter. If the oxygen depletion rate is a function of oxygen concentration, then oxygen may become a limiting factor below some concentration level above zero. In this site study, discernment of zero- versus first-order oxygen depletion kinetics, was achieved at some but not all monitored locations due to too few data points at critical times. In areas of high contamination, oxygen depletion followed zero-order kinetics. Soil sampling at the test site after 18 months of venting revealed removal of BTEX compounds to very low concentrations but poor removal of higher molecular weight and lower volatility compounds.

Section 15

In section 15, a one-dimensional, analytical, unsaturated zone VOC transport model termed "VFLUX" was derived and described. One-dimensional analytical modeling may be appropriate under some conditions for regulatory decision making. However, even at this level of modeling, a sensitivity analysis of how model input and selected boundary conditions affect

model output and decision making is critical. VFLUX was used to assess the effect of water saturation, NAPL saturation, degradation-half-life, and selection of boundary conditions at the unsaturated zone - capillary fringe interface on model output and regulatory decision making in regard to vadose zone remediation, specifically venting initiation or closure.

Results of simulations revealed that selection of lower boundary conditions and highly sensitive input parameters such as water saturation, NAPL saturation, and degradation half-life significantly affected model output and decision making whether to initiate or cease venting application, especially when soil concentrations were low. The first-type boundary condition allowed mass transfer across the unsaturated zone - capillary fringe interface by infiltration and diffusion. The zero-gradient lower boundary condition only allowed mass transfer across the interface by infiltration with soil-water concentrations independent of boundary conditions. For highly contaminated soils, the first-type boundary conditions resulted in higher magnitude but shorter duration pulses of mass to the capillary fringe and a higher cumulative mass fraction to the capillary fringe compared to the zero-gradient lower boundary condition.

For highly contaminated soils, regardless of which boundary condition is chosen, model simulations clearly indicated a need to initiate or continue venting application. For soils at low contaminant levels however, use of the first-type boundary condition resulted in the primary direction of mass flux being from the capillary fringe to the unsaturated zone questioning the need to initiate or continue venting. The zero-gradient boundary condition on the other hand resulted in sustained but low magnitude mass flux to the capillary fringe perhaps prompting a decision to initiate or continue venting. Thus, the two boundary conditions resulted in contradictory decisions.

In reality, neither the first-type nor zero-gradient appeared to adequately represent mass transfer across the unsaturated zone - capillary fringe interface. Use of the first-type boundary condition appeared to overestimate mass flux to the capillary fringe when soils were highly contaminated while use of the zero-gradient boundary condition did not incorporate the effect of capillary fringe contamination on unsaturated zone VOC transport. Use of a third-type boundary condition does not remedy this situation since mass flux is a desired output of modeling and a diffusive boundary layer would eliminate the contribution of infiltration to mass flux. One solution to this problem would be to use numerical modeling and directly incorporate a capillary fringe and variable saturation with depth. In this way, a first-type, time-dependent boundary condition could still be utilized but the effect of vapor diffusion across the interface would be greatly dissipated and the linkage between vadose zone and ground-water remediation would remain intact. However, analytical screening models such as VFLUX should still be adequate for decision making when elevated levels of contamination indicate potential for prolonged mass flux to ground water using both types of boundary conditions.

1. INTRODUCTION

Soil venting, soil vacuum extraction (SVE), and bioventing are terms commonly used to describe in-situ technologies in which gas flow is induced in subsurface unconsolidated or consolidated unsaturated media for the purpose of volatilizing or biodegrading organic chemicals. Gas (typically air) is injected and/or extracted from one or more wells causing a pressure differential and subsequent advective gas flow. Removal of volatile organic compounds (VOCs) is achieved by non-aqueous phase liquid (NAPL) evaporation, NAPL dissolution, desorption, air-water partitioning, biodegradation, and abiotic degradation. Removal of semi-volatile organic compounds is achieved partly through abiotic processes but primarily through biodegradation due to the effective delivery of oxygen. At Superfund and RCRA sites, contaminated gas effluent from extraction wells is often treated above ground prior to discharge to the atmosphere.

Soil vacuum extraction (SVE), defined as including only gas extraction, is considered a presumptive remedy (a detailed technology screening process is not necessary for implementation) in the U.S. Environmental Protection Agency's (U.S. EPA) Superfund program. Bioventing, commonly defined as including gas extraction and/or injection, describes in-situ gas circulation designed to maximize contaminant mass removal through biodegradation as opposed to volatilization. Bioventing systems are characterized by relatively "low" pore-gas velocities or pore-volume exchange rates. However, relatively low pore-gas velocities may be optimal for operation under conditions of rate-limited mass transport. This observation and the fact that during venting, simultaneous volatilization and biodegradation occurs whether or not the latter process is intended suggests that the definition bioventing is non-unique. In this document, an operational term, venting, is used to define gas injection and/or extraction without specific reference to biodegradation or any other subsurface processes. It is considered a general term encompassing SVE and bioventing.

Soil venting has become the primary method used in the United States to remove VOCs from unsaturated subsurface media. In 1997, SVE was applied or planned to be applied at 27% of Superfund sites (Kovalick, 1999). Since this statistic does not include gas injection or combined gas extraction and injection, venting application at Superfund sites likely exceeds 30%. Recently, the technology has been used to control vapor migration to structures and hence reduce potential indoor air exposure. The popularity and widespread use of venting is due to its simplicity of operation and proven ability to remove contaminant mass inexpensively compared to other in-situ technologies. The technology can be implemented with minimal site disturbance and with standard readily available equipment (e.g., PVC pipe, blowers).

Despite the common use of venting in the Superfund program, there is little consistency in approach to assessment of performance and closure. This problem exists for most if not all subsurface remedial technologies. A recent Inspector General's audit submitted to Congress (USEPA, 1998a) pointed out that:

> "EPA is not consistently using a scientifically-based, systematic planning process to take actions at Superfund hazardous waste sites...[Because of a lack of preferred systematic planning processes] "the Agency completed Superfund actions without known quality data for decision making and without sufficiently documenting important decision criteria...Until a scientifically-based, systematic planning process is implemented consistently nationwide, [EPA] can not be sure that decision makers have the information needed to make the best decisions about response actions at Superfund sites."

Assessment of performance of venting systems varies widely among and within U.S. EPA's regional offices and their corresponding states. Eventual decisions on closure are commonly based on site-specific negotiations with responsible parties (e.g., industry, military agencies) and their supporting consultants and attorneys. Assessment of performance and closure becomes contingent upon the goals of those involved, their corresponding education and experience, and the availability of information necessary for informed data analysis and decision making. There is often a lack of understanding or even awareness of published research relevant to characterizing, designing, and monitoring venting sites by those tasked with conducting such studies. This is evidenced by the widespread use and reliance on empirical methods to design and evaluate venting performance as opposed to placing an emphasis on understanding fundamental physical, chemical, and biological processes controlling mass removal during the venting operation. This results in the technology not being utilized to its fullest potential, nor its limitations being well understood. Examples of empiricism are radius of influence (ROI) testing to support venting design and the use of effluent asymptotes to justify venting cessation. With regard to availability of information necessary for informed data analysis and decision making, a set of minimum site-specific data requirements is rarely outlined. However, even when state and federal agencies are clear on data objectives, data collection typically becomes a contentious process due to costs associated with site characterization and system monitoring. Thus, decisions are commonly made based on available data "at hand" fueling speculation and debate as to what the data actually means. These problems build throughout the life of a project, eventually climaxing when attempts are made to shut the system down.

Quite often closure negotiations consider the perceived effectiveness of a remediation system more so than the actual effectiveness of the system. In other words, a regulatory agency is likely to grant closure or allow the termination of SVE operation if they think the responsible party has done the best they could with the technology. Thus, if the parties involved do not understand the technology, then it might be misapplied or prematurely terminated. Thus, poorly designed and operated SVE systems may lead to quicker closures/system terminations than well-designed systems.

Assessment of soil venting performance and closure has become critically important in U.S. EPA regional offices because of lack of guidance in evaluating venting systems and the fact that many systems are operating without a definable or achievable endpoint. This issue is particularly important in California which has far more venting sites than any other state, many of which are closed military bases that are being converted to civilian use. The issue of

struggling with measures of “success” in subsurface remediation was recently highlighted in an editorial by Conant and Rao (2000). They point out that

> “In subsurface remediation, policy and technical concerns are inextricably linked in an iterative debate...Whether the desired goals can be achieved is not necessarily apparent at the outset...Restoration to very low or background levels cannot be achieved at a large percentage of sites, at least not in a time frame or at costs expected by any of the stakeholders. Gradual recognition of this fact has caused a return, whether in site-specific deliberations or the formulation of policy or guidance, to the broader discussion of appropriate, attainable remediation goals...[While] the public is understandably reluctant to abandon the ultimate cleanup objectives...parties responsible for site cleanup are equally reluctant to undertake open-ended actions when they can”t predict the likely results with any reasonable certainty, and when they have no assurance about what may be required of them in the future...[Our] experience has also taught us much about the complexity of the subsurface systems in which remediation technologies are applied, allowing for improvements in technology design and the monitoring strategies critical to measuring their success...It has also caused us to reconsider the ultimate uses and appropriateness of data collected.”

The purpose of this document is to address the problems described above by developing recommendations and methods to support assessment of soil venting performance and closure. This goal is to be accomplished by attainment of three objectives. The first objective is to develop an overall regulatory approach to assess performance and closure of venting systems including measures to ensure consistency in ground-water and vadose zone remediation. The second objective is to provide comprehensive and detailed literature reviews on gas flow and vapor transport. These reviews form the basis of recommendations and methods to improve venting design and monitoring. The third objective is to summarize research conducted to improve various aspects of venting application. Literature reviews and technical recommendations provided in this document are very detailed but not prescriptive. Thus, the user of the document retains considerable flexibility. A number of case studies were included the document to enhance understanding of important principles.

2. PROPOSED APPROACH FOR ASSESSMENT OF PERFORMANCE AND CLOSURE OF VENTING SYSTEMS

2.1 Limitations in the Use of Vapor Concentration Asymptotes

Cessation of venting application is often proposed based on attainment of an asymptote, a concentration level during asymptotic conditions, or some subjectively determined mass removal rate (e.g., pounds per day) from gas extraction wells. There are several concerns with this approach to assessment of performance and closure of venting systems.

First, there is no way to directly relate observation of an asymptote to environmental benefit and little potential to ensure consistency in decision making. Vapor concentration of an asymptote at a highly contaminated site may be much higher than at a lesser contaminated site leading perhaps to less stringent remediation at the highly contaminated site.

Second, observation of an effluent asymptote may be related to venting design (e.g., well spacing) or operating conditions (e.g. flow rate) separate or in addition to rate-limited vapor transport. Rathfelder et al. (1991) demonstrated that effluent tailing can be caused by gas flow dynamics. Hypothetical simulations in a homogeneous, two-dimensional axisymmetric flow domain with NAPL under equilibrium conditions resulted in decreasing effluent concentrations that could be construed as tailing. Direct recharge from the atmosphere and subsequent vertical flow resulted in clean retreating evaporation fronts both vertically above and radially distant from a gas extraction well. This caused the formation of a wedge-shaped contamination zone whereby some continually decreasing fraction of gas flow intersected contaminated soil leading to the appearance of an asymptote. Shan et al. (1992) demonstrated that in a domain open to the atmosphere, most gas flow to an extraction well originates from atmospheric recharge in the immediate vicinity of the well. Thus, after some period of vacuum operation, vapor concentrations from gas extraction wells become largely reflective of soil and contaminant conditions in the immediate vicinity of the wells while higher concentrations more distant from wells are largely diluted. Effluents in gas extraction wells then approach low concentrations and an asymptote while significant and accessible mass may remain in soils between gas extraction wells. This situation is exacerbated by placing venting wells too far apart - a condition typical of ROI-based designs. A similar situation occurs in stratified soils where gas flow occurs primarily in layers of greater gas permeability. Analogous to the first situation, mass removal occurs more rapidly in soils receiving greater gas flow. Vapor concentrations in gas extraction wells become largely reflective of soil and contaminant conditions in these layers while higher vapor concentrations from lenses of lower permeability are largely diluted. Rathfelder et al. (1991) simulated effluent tailing when a gas extraction well was placed across two stratigraphic layers having an order of magnitude difference in permeability. In this case as before, effluent tailing and apparent rate-limited mass removal was caused by variation in pore-gas velocity, not by rate-limited NAPL-gas exchange. Lowered local gas permeability in zones containing pure phase residual would cause the same effect. Other examples of design factors potentially causing the observation of an effluent asymptote include inadequate lowering of the water table, inadequate

dewatering of perched water table zones, and gas extraction wells not placed in or near source areas.

Third, changing mole fractions of individual components in NAPL may also cause the appearance of an asymptote in vapor effluent. Baehr et al. (1989) simulated mass removal of gasoline in medium-grained sieved sand. Experimental and simulated mass flux profiles matched well suggesting attainment of equilibrium conditions. The decrease in total mass flux with time though exhibited apparent tailing due to selective removal of more volatile hydrocarbons. This behavior is in contrast with column and sand tank studies using single component residually contaminated soils which show no reduction in mass flux until residual NAPL has evaporated. In a field setting, it would be easy to mistake tailing due for selective volatilization of a multi-component NAPL for rate-limited behavior.

Fourth, several groups of investigators (Fisher et al., 1996; Ng and Mei, 1996; and Armstrong et al., 1994) have clearly demonstrated in laboratory column, sand tank, and numerical experiments that observation of low asymptotic vapor concentrations in effluent gas is a necessary but not sufficient condition to demonstrate progress in mass removal from contaminated soils. An asymptote due to rate-limited mass exchange can be observed in gas extraction wells while much of the contaminant mass remains in soils. Ng and Mei (1996) simulated the time variation in effluent vapor and aqueous soil aggregate concentration. Effluent vapor concentration dropped rapidly with time to the point of having indistinguishable values, however the decay of the aqueous phase was significantly slower. Since sorptive equilibrium exchange was assumed within the aggregates, the aqueous phase was indicative of mass removal within aggregates. Thus, effluent vapor phase monitoring provided little insight on the rate of concentration reduction in soil. Armstrong et al. (1994) developed a numerical one-dimensional model which incorporated first-order gas-water and solids-water rate-limited mass exchange to simulate vapor effluent data obtained by McClellan and Gillham (1992). Virtually identical fits were obtained to effluent curves for both continuous and pulsed schemes using two parameter sets. Simulated remaining mass however differed sharply with the second parameter set resulting in far greater mass retention. Their sensitivity analysis and calibration of data showed that different mass retention and rate coefficients can produce very similar effluent curves suggesting that effluent and vapor probe concentration data can not be used to estimate mass transport coefficients and VOC concentration in the aqueous and solids phase. They concluded that effluent concentration data is insufficient to quantitatively assess the progress of soil venting remediation. Thus, it appears that effluent and vapor probe concentration data can only be used in a qualitative sense to assess performance.

2.2 Limitations of Rebound Testing

Another common method of assessing the performance and closure of venting systems is flow interruption or rebound testing. Presumably, minimal rebound or lack of rebound after some period of system cessation indicates remediation success and subsequent site closure. Alternatively, extensive effluent tailing and rebound after system cessation indicates rate-limited

mass exchange and little benefit for continued venting operation. Thus, rebound testing is invariably used to justify closure. However, as previously discussed, significant mass removal can occur over an extended period time even in the presence of substantial rate-limited mass exchange.

In NAPL contaminated soils, results of flow interruption testing can be confusing if propagation of evaporation-condensation fronts are not considered. Hayden et al. (1994) provide a good example of this. They introduced gasoline at a NAPL saturation value of 2% in two sandy soils and monitored column effluent concentrations of benzene, m-xylene, p-xylene, and naphthalene. Flow interruption testing during the initial period of venting application (1 hour) resulted in a decrease in benzene concentration and an increase in m-xylene, p-xylene and toluene effluent concentration. Flow interruption testing at 3 hours resulted in a decrease in benzene and toluene effluent concentration and an increase in m-xylene and p-xylene. Hayden et al. (1994) explain that reconciliation of this behavior is possible only if one considers evaporation-condensation fronts. During initial venting operation, high vapor pressure compounds such as benzene would be removed first from the intake portion of the column and increase in mole fraction and vapor concentration downstream as the evaporation front moves through the column. Cessation of venting then would cause a decrease at the effluent end of the soil column and an increase in the intake end of the column as vapor diffusion becomes the dominant transport mechanism. Upon re-start, effluent concentrations would actually drop. For compounds like m-xylene and p-xylene, mole fractions and vapor concentrations would initially increase at the inlet of the soil column. Thus, during flow interruption, vapor diffusion would cause an increase in vapor concentration downstream resulting in an increase in vapor concentration upon start-up. Thus, in Hayden et al.'s (1994) column experiments, increases in m-xylene and p-xylene upon start-up was not likely the result of rate-limited mass transport, but propagation of evaporation and condensation fronts. In a field setting, flow interruption testing would provide evidence of rate-limited transport for a particular compound only after its evaporation front exited the soil column. Otherwise, flow interruption testing could provide confounding results.

2.3 Estimation of Soil Concentration from Soil-Gas Concentration

Another common use of flow interruption data is to use vapor concentrations and partition coefficients to estimate total soil concentration. This would provide an indication of soil concentration reduction, or through extrapolation, mass reduction over time for specific compounds. Knowledge of soil concentration reduction is helpful if site closure is based on attainment of compound specific soil standards. Monitoring of VOC concentrations in vapor probes for this purpose would be preferable to vapor extraction wells because they draw soil gas from a much smaller volume of soil and thus are less likely to be affected by decreased vapor concentration due to large scale heterogeneity. Viewed superficially, the idea appears to have merit because soil sample collection is expensive, especially when drilling at extensive depths and in soils containing large rocks (e.g., glacial till). Drilling can cause disruption of venting operation and manufacturing processes at active operating facilities. Also, drilling often results

in the generation of a substantial amount of cuttings which must be disposed of as hazardous waste. It can also be argued that soil sample collection is by nature "hit" or "miss" because sample volume is small compared to the volume of soil affected by soil-gas collection. Thus, if contaminant mass remains in soil, there is a higher probability of detection with soil-gas sampling than soil-solids sampling. Finally, soil sample collection is obviously not appropriate for venting operation in fractured rock or other consolidated material.

Johnson and Kreamer (1994) showed that soil vapor concentrations were able to be correlated with soil concentrations in a sand tank study. However, other investigators (Stephens, 1995; Hahne and Thomsen, 1991; Kerfoot, 1991) have reported poor correlation between soil-gas and matrix concentration. Stephens (1995) reported poor correlation between trichloroethylene (TCE) concentrations in soil gas and soil matrix samples collected during drilling at approximately the same depth. He states that the more frequent detection of TCE in soil-gas compared to the soil matrix was due at least partially to much lower detection limits achieved for soil gas compared to the soil matrix. This statement is sensible when one considers that the vapor detection limit for TCE using EPA Method TO-14 is $\geq$ 0.1 ppbv which is equivalent to 4.28×10^{-04} ug/kg using equilibrium partition coefficients and the assumption of an organic carbon content of 0.1%, porosity of 0.4, and a volumetric water content of 0.2. This equivalent soil concentration is far below the EPA Superfund Contract Laboratory detection limit of 0.05 ug/kg. Stephens (1995) states that another factor likely causing poor correlation between trichloroethylene (TCE) concentrations in soil gas and soil matrix samples is the fact that the soil matrix is far more heterogeneous with respect to contaminant distribution compared to soil-gas. Another likely reason for poor correlation between soil gas and soil matrix samples is that significant VOC loss can occur during soil sample collection and storage resulting in reported VOC concentrations lower than expected (Siegrist and Jenssen, 1990).

Significant uncertainty in estimation of parameters making up a soil-gas partition coefficient and difficulty in measuring a steady-state vapor concentration in the field makes estimation of total soil concentration from vapor measurements challenging. Under equilibrium conditions, the relationship between a nonionic organic compound concentration in soil and soil gas is a function of a compound's chemical properties (Henry's Law Constant, organic-carbon-water partition coefficient, and NAPL-water or NAPL-air partition coefficient), fluid distribution (gas, water, and NAPL fluid saturations), and soil properties (soil organic carbon content, porosity, and particle density). If separate phase NAPL is available from a site, batch laboratory studies can used to directly determine NAPL-air or NAPL-water partition coefficients for compounds of concern. If free NAPL is not available, NAPL-water or NAPL-air partition coefficients can be estimated from a compound of interest's vapor pressure and molecular weight and mole fractions, densities, and molecular weights of individual compounds in the NAPL. At many sites though, there are so many compounds in NAPL contaminated soil that accurate mole fraction identification and quantification is impossible. An average NAPL density and molecular weight which can be used in place of individual NAPL constituent information if the mole fractions of dominant chemical classes in the NAPL can be quantified. However, equations used to estimate NAPL-water or NAPL-air partition coefficients reveal that these partition coefficients

will not be constant but change as a function of changing mole fractions of various compounds.

Since a compound's organic-carbon-water partition coefficient, Henry's Law Constant, vapor pressure, molecular weight can be found in the literature or estimated for many compounds, a soil-gas partition coefficient has 7 primary unknown parameters - gas, water, and NAPL saturation, particle density, porosity, average NAPL density, and average molecular weight. The parameters describing NAPL are of greatest interest because analysis of mass fractions reveals that the majority of contaminant mass is partitioned in the NAPL phase even at very low NAPL saturation (e.g., 0.5%). Error in estimation of NAPL saturation would dramatically affect estimates of soil concentration and contaminant mass. There is presently no standard method of estimating NAPL saturation in-situ in soil but gas-phase partitioning tracer testing shows promise. In-situ water saturation would need to be estimated with the use of a neutron probe or other downhole device. Gas saturation could be estimated from knowledge of porosity and volumetric water content. Each estimation procedure involves error, which from an analysis of variance, propagates non-linearly. Finally, there is no way to assess the accuracy of estimation of soil-concentration from soil-gas measurements because the volume of soil being affected by advective gas flow to a probe is likely far greater that the volume of soil typically sampled for laboratory analysis. Collection of soil samples for soil-gas estimation comparison also necessitates consideration of spatial variability which can be significant even on a small scale.

Estimation of soil concentration also requires measurement of steady-state soil-gas concentration. In a well designed venting system, mass removal will eventually limited by combined liquid and vapor diffusion from less permeable soil regions not receiving direct gas flow. In a poorly designed system, mass removal will be limited by these factors plus inadequate gas flow in regions still amenable to significant advective phase mass transport. In the former case, at the cessation of venting, vapors diffuse slowly from immobile regions into mobile domains where advective gas flow occurs. When a soil's moisture, organic carbon, or NAPL content is high, time for attainment of equilibrium conditions can be excessive. Thus, when collecting vapor samples for total soil concentration or mass estimation purposes, a correction factor is necessary for estimation of steady-state vapor concentration. Assuming that concentration is caused by vapor diffusion, estimation of steady-state vapor concentration will involve the use of some type of a diffusion-based model. The diffusion coefficient will incorporate the 7 unknown parameters of the soil-gas partition coefficient plus three additional unknown parameters - tortuosity in the gas and liquid phases and the diffusion path length. Tortuosity values could be estimated from fluid saturation and porosity. It is assumed that literature values can be found for molecular gas and water diffusion coefficients. Since there are likely to be numerous localized sources of vapors in contaminated soils, including contaminated ground water, the diffusion path length will represent some averaged distance. In practice, it would be necessary to fit a diffusion-based equation to vapor concentration versus time data during vapor rebound to estimate a lumped parameter incorporating the diffusion path length. This will of require the collection of several gas samples over time at each vapor sampling point followed by gas chromatography analysis. Another practical problem is devising an appropriate

methodology of vapor sampling. The collection of vapor samples may cause local dis-equilibrium, thus later vapor sampling results would be biased by earlier sampling efforts.

It is apparent that analysis of rebound testing and estimation of soil concentration from soil-gas measurement is a difficult process. It requires a substantial amount of work, expense (GC analysis of vapor), and thorough knowledge of subsurface conditions. Even under the best of conditions, appreciable estimation error can be expected. While drilling is expensive and disruptive, it still offers the best opportunity to evaluate vertical subsurface contamination profiles. While rebound or flow interruption testing could be a fruitful area of research, its use at present for quantitative assessment of venting performance and eventual closure does not appear defensible. Soil-gas monitoring during venting operation and periods of shut-down though might provide valuable qualitative insight into progress towards remediation and aid in timing of soil sample collection.

2.4 Vadose Zone Solute Transport Modeling

Probably the most common method of assessing whether to initiate, continue, or cease venting application or any other in-situ vadose zone remediation technology, involves periodic collection of soil samples for comparison with compound-specific, concentration-based standards which are often based on the results of vadose zone modeling. A variation of this approach, is attainment of "drinkable leachate" or soil-water concentrations adjusted for a "dilution-attenuation factor" at the vadose zone - ground-water interface. Remediation is considered complete when vadose zone solute transport modeling indicates that these standards will be attained in the future. Both soil-based and leachate-based standards are typically stringent because it is required that soils be remediated to the extent that mass flux to ground water not result in aqueous concentrations exceeding maximum contaminant levels (MCLs). The National Research Council (1994), however states that:

> "regulatory agencies should recognize that ground water restoration to health-based goals is impracticable with existing technologies at a large number of sites [and that] ...improvements are needed...to manage the large number of sites where technical limitations may present problems."

At sites where it is unlikely that ground-water remediation will result in attainment of MCLs, the need for soil or soil-water based vadose zone remediation standards that assume attainment of MCLs becomes questionable. Stringent remediation standards and other factors such as mass transport limitations often make attainment of venting closure difficult at many sites.

Mathematical models that simulate soil-water movement to ground water are often used to determine soil concentration-based remediation standards. These models vary in complexity from simple and conservative algebraic water-balance equations that neglect degradation and volatilization to more process descriptive finite-difference and finite-element numerical codes. Lack of data to support spatial discretization of soil properties (e.g., hydraulic conductivity,

porosity, bulk density, moisture content, total organic carbon content) and contaminant distribution, however, commonly limits the use of more complex models.

Considering that venting is often applied to remove contaminant mass from variably saturated media for ground-water protection, it would seem that only an analysis of mass flux to and from ground water is necessary for assessment of soil venting operation and closure. Unfortunately, vadose zone subsurface fate and transport processes are not understood well enough to permit the sole use of deterministic models for decision making. Though a basic understanding of the physics, chemistry, and biology of many fundamental subsurface processes exists, spatial and temporal distribution of contaminants in the subsurface are the end result of a vast number of processes whose complex interactions can not be effectively simulated. Thus, mass-flux modeling should only be one of several tools used to evaluate operation and closure of venting sites.

2.5 Proposed Approach for Assessment of Performance and Closure

It is clear that an environmentally protective, flexible, technically achievable, and consistently applied approach for assessment of performance and closure of venting systems is needed. Any approach used to assess performance of a venting system should encourage good site characterization, design, and monitoring practices since mass removal can be limited by poor execution of any of these components. Also, any approach used to assess closure of a venting system must link ground-water remediation to vadose zone remediation since the two are interrelated.

The following is a description of a general strategy proposed for assessment of performance and closure of soil venting systems. This discussion is followed by a proposed scheme for linking ground-water and vadose zone remediation. **There is no regulatory requirement that EPA or State regulators adhere to this strategy or recommendations given in this report.** The strategy is based on four components considered integral to successful venting application: (1) site characterization, (2) design, (3) performance monitoring, and (4) mass flux to and from ground water. These four components form converging lines of reasoning or a preponderance of evidence regarding performance and closure. Evaluation is on a pass/fail basis since this type of critique provides the greatest flexibility in decision making. Failure in evaluation of one or more component(s) results in overall venting closure failure. Such a "weight of evidence" approach greatly increases the likelihood of correctly assessing the performance of a venting system and its suitability for closure. The use of converging lines of evidence has become popular in evaluation of subsurface remedial technologies, especially bioremediation, as subsurface fate and transport processes are too complex to allow definitive assessment of progress. U.S. EPA's "Technical Protocol for Evaluating Natural Attenuation of Chlorinated Solvents in Ground Water" (USEPA, 1998b) most recently adopted this convergent lines of evidence approach.

Since each component is interrelated and requires continuous evaluation during the life of

the project, regulatory approval of individual components must occur concurrently and not until the perceived end of the project. Premature approval of a closure component would limit later corrective action. For example, performance monitoring may reveal deficiencies in design. Premature approval of a design then could limit implementation of measures needed for successful remediation. Notice of deficiencies in evaluation of individual components however could occur at any time since in many cases it will be apparent early on that deficiencies exist. For instance, during the site characterization phase, U.S. EPA and State regulators may be unconvinced that the vertical and lateral extent of contamination is sufficiently delineated for venting application. In this case, responsible parties would be notified up-front that venting closure will not be attained until this situation is rectified. Thus, this closure approach encourages and likely in some cases forces good site characterization, design, and monitoring practices.

If evaluation of all these factors individually supports closure, then it is likely that closure is indeed appropriate. If one or more of the components does not support closure, then it is likely that either closure is inappropriate or that a conscious decision must be made to accept a limiting condition. For instance, in the presence of significant rate-limited vapor transport, closure would not proceed if there was potential for substantial continued mass flux to ground water. In this case, venting may need to be applied indefinitely at low pore-gas velocities or in a pulsed mode. Regulators however could decide to turn off the system if indefinite ground-water remediation or containment is anticipated or if the remaining mass moving into the ground water will not impact a potential receptor. Regardless of the situation, assessment of these components enables flexible, organized, and informed decision making.

2.6 Mass Flux Assessment

Evaluation of mass flux to and from ground water is vital in integrating venting application with progress in ground-water remediation. Soil remediation goals must reflect the realities of ground-water remediation. As illustrated in Figure 2.1, subsurface remediation areas are partitioned into three distinct zones for performance evaluation purposes. Zone 1 is bounded on the upper end by the soil surface and on the lower end by the seasonally high water table. Zone 1 consists of consistently unsaturated media (above the region of water table fluctuation) where mass flux to ground water occurs through a combination of infiltration and diffusion or by diffusion alone. Mass flux from ground water to the vadose zone occurs through diffusion. Hughes et al. (1992) demonstrated that ground-water contamination can occur solely by vapor diffusion from residually contaminated soil by diffusion across the capillary fringe or by fluctuation in the water table which traps vapors in the zone of saturation.

Zone 2 consists of periodically de-saturated media due to water-table fluctuation or dewatering. Often, it will consist of a highly contaminated “smear” zone containing residual NAPL where venting is combined with dewatering to remove contaminant mass from a localized region. Zone 2 is bounded on the upper end by the seasonally high water table and on the lower end by the maximum depth to ground water during dewatering. The base of zone 2 will be

variable depending on targeted dewatering depths throughout a site area. The maximum depth of zone 2 will be dictated by the vertical profile of contamination and feasibility of dewatering to a depth of interest. If a smear zone exists in highly permeable media where dewatering is

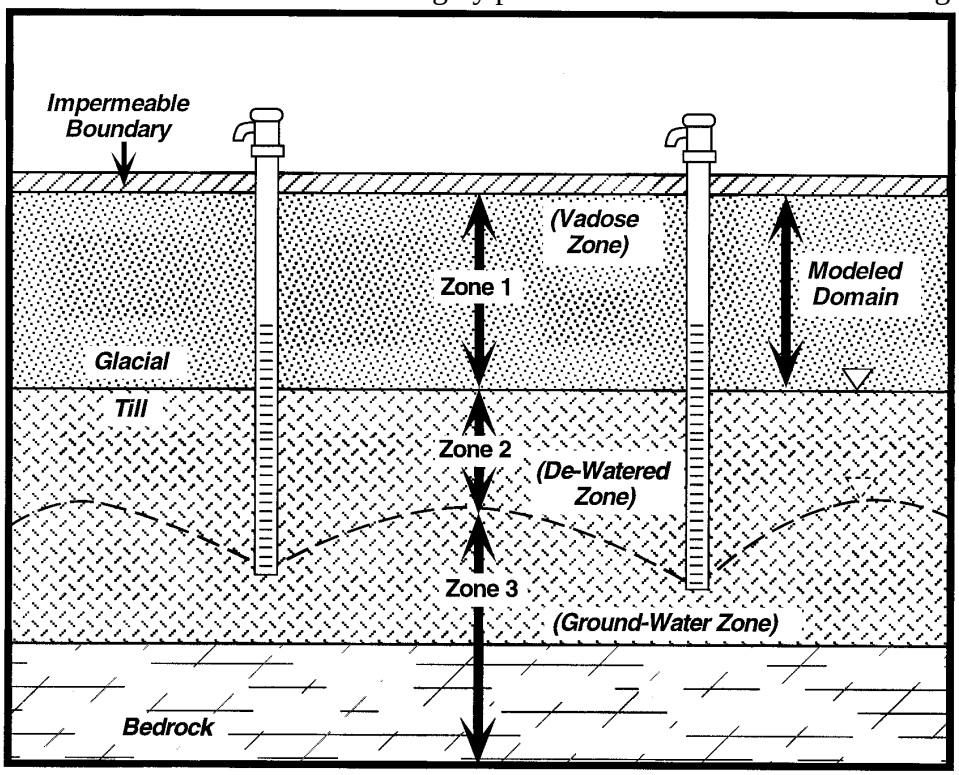

Figure 2.1 Schematic of remediation zones for mass flux assessment

technically infeasible or requires large pumping rates, zone 2 can be thought of as the region where another source control technology such as sparging is used. If dewatering is not to be used in conjunction with venting, then zone 1 is directly linked to zone 3.

Zone 3 is bounded on the upper end by a ground-water level with or without dewatering and on the lower end by the targeted depth of ground-water remediation. It represents media that remains saturated during venting. Ground-water concentrations in zone 3 vary temporally and determine compliance in zones 1 and 2. Zone 2 is in compliance when ground-water concentrations are less than or equal to ground-water concentrations in zone 3. This ensures that remediation of ground water within a smear zone will be attempted to levels consistent with maximum levels of deeper contamination. This ensures consistency in ground-water remediation efforts and avoids reduction of ground-water concentrations in zone 2 to levels lower than what would occur through vertical recontamination from zone 3. Implementation of this approach then requires adequate vertical profiling of ground-water concentrations in zone 2 and 3. This can be achieved by installation of short-screened multi-well clusters, multi-port monitoring wells, or diffusive samplers in fully screened wells.

In the case of a light non-aqueous phase spill where ground-water concentrations within a "smear" zone are at much higher levels than beneath the “smear” zone, low concentrations in zone 3 forces aggressive dewatering and venting application in zone 2. In the case of a dense non-aqueous phase spill where ground-water concentrations may be at high levels deep within an aquifer, remediation within the dewatered region or zone 2 proceeds only to the degree at which it is consistent with remediation in deeper regions or zone 3. Zone 1 is in compliance with zone 2 when mass flux to ground water is close to zero or the direction of mass flux is primarily from ground water to the vadose zone (i.e. mass flux due to vapor diffusion from contaminated ground water exceeds mass flux due to vapor diffusion and infiltration from the vadose zone at the ground-water - vadose zone boundary). This ensures aggressive venting application in the vadose zone when ground water has very low levels of contamination, and less aggressive venting application when vapor diffusion will result in recontamination of cleansed soils. Thus, venting performance for zones 1 and 2 is dynamically linked to the performance of ground-water remedial efforts in zone 3. Substantial progress in remediating ground water translates to increasingly stringent soil venting performance standards, while lack of progress in remediating ground water translates into less stringent soil remediation requirements. Regardless of the strategy chosen to close an venting site, there must be a link between ground-water and soils remediation. Remediation in the unsaturated zone should not proceed independently of ground-water conditions. Unfortunately, this aspect of closure is missing at most sites.

3. GAS FLOW IN POROUS MEDIA - FUNDAMENTAL PRINCIPLES

Systematic investigation of gas flow in porous and consolidated media originated in the petroleum industry to support characterization and development of natural gas reservoirs (Muskat and Botset, 1931). Gas exchange between soils and the atmosphere has been of interest to soil and agricultural scientists for decades. More recently, hydrologists, soil scientists, and environmental engineers have been interested in gas flow in porous media to support design of venting systems for remediation of contaminated soils containing VOCs or other compounds capable or aerobic biodegradation (Johnson et al., 1990a,b; Baehr and Hult, 1991; Shan et al., 1992; Baehr and Joss, 1995). Most recently, gas flow studies have been conducted to evaluate potential gaseous movement at proposed high-level radioactive waste sites (Ahlers et al., 1995, 1999; Shan et al. 1999) and barometric pressure propagation in soils (Shan, 1995, Rojstaczer and Tunks, 1995). Analysis of gas flow and permeability estimation in subsurface media requires a thorough knowledge of fundamental gas flow principles. The purpose of this section is to provide a review of background information necessary to formulate and apply analytical and numerical solutions to gas flow.

3.1 Compressibility

Compressibility is one of two primary factors differentiating gas flow from liquid flow. The second factor, gas slippage along pore walls, will be discussed later. Katz et al. (1959) were among the first investigators to derive analytical solutions for gas flow by utilizing the ideal gas law to express gas density. This approach however was found to be of limited use in the petroleum industry because of deviation from the ideal gas law at high pressures typical of gas reservoirs and large pressure variation near production wells.

At pressures typical of soil venting operation (less than atmospheric pressure up to perhaps 1.5 atm), deviation from the ideal gas law for gases of interest (primarily O_2 and N_2) will be insignificant and the ideal gas law can be used to estimate gas density, ρ_g [M L^{-3}] by

$$\rho_g = \frac{M_g P}{\Re T} \tag{3.1}$$

where M_g is the molecular weight of a gas mixture [M $mole^{-1}$] (atmospheric air = 28.8 g $mole^{-1}$), P is gas pressure [M L^{-1} T^{-2}] (1 atm = 1013250 g cm^{-1} s^{-2}), $\Re$ is the universal gas constant [M L^2 T^{-2} mol^{-1} K^{-1}] (8.3143 x 10^7 g cm^2 $mole^{-1}$ s^{-2} K^{-1}), and T is temperature [K]. Equation (3.1) is utilized to estimate gas density in virtually all analytical and numerical codes supporting venting application.

3.2 Viscosity

When a shearing stress is applied to a fluid, it deforms continuously. During laminar flow, adjacent layers (lamina) of fluid molecules move at different velocities with changes

gradually occurring from lamina to lamina. Velocity increases from zero (for non-slip conditions) at a planar stationary surface to a maximum value at the center of a tube or pore. Each layer experiences frictional force called viscous drag from adjacent slower-moving lamina. This effect is manifested as resistance to flow. According to Newton's Law for laminar flow, resistance to gas flow is expressed by

$$\frac{F}{A} = \tau = -\mu_g \frac{dv}{dy} \tag{3.2}$$

where F = a force applied along a lamina of flowing fluid [M L T^{-2}], A [L^2] = the area of contact along adjacent lamina, τ = gas phase shearing stress along adjacent lamina [M L^{-1} T^{-2}], μ_g = a constant of proportionality called dynamic gas viscosity [M T^{-1} L^{-1}] (μ_g for atmospheric gas at 20°C = 1.76 x 10^{-4} g cm^{-1} s^{-1}), v = gas velocity in lamina [L T^{-1}], and y = a distance from a fixed surface [L]. Viscosity sometimes appears in fluid flow problems in the form

$$\upsilon_g = \frac{\mu_g}{\rho_g} \tag{3.3}$$

where υ_g is called kinematic viscosity [L^2 T^{-1}]. Fluids for which shearing stress (τ) is linearly related to the rate of shearing strain (dv/dy) are designated as Newtonian fluids. All gases are Newtonian fluids.

Gas viscosity is largely independent of pressure up to 10 atmospheres (Bird, Stewart, and Lightfoot, 1960). For gases at low density, viscosity increases with increasing temperature whereas viscosity decreases with increasing temperature in liquids. If gas molecules are conceptualized as hard spheres without molecular interaction, gas viscosity can be estimated from momentum transfer principles by (Bird, Stewart, and Lightfoot, 1960)

$$\mu_g = \frac{2}{3\pi^{3/2}} \frac{\sqrt{m_m \kappa_c T}}{{d_m}^2} \tag{3.4}$$

where m_m = molecular mass [M], κ_c = Boltzmann constant (1.38066 x 10^{-23} J K^{-1}) , and d_m = molecular diameter [L]. From equation (3.4), gas viscosity theoretically increases with temperature to the ½ power. At low density typical of atmospheric conditions however, Bird, Stewart, and Lightfoot (1960) state that gas viscosity increases with temperature to the 0.6 to 1.0 power of temperature because of molecular interactions.

Gas viscosity is also a function of component mixture. Bird, Stewart, and Lightfoot (1960) provide an expression to estimate the viscosity of a multi-component gas mixture

$$\mu_g = \sum_{i=1}^{n} \frac{\chi_i \mu_i}{\sum_{j=1}^{n} \chi_j \Omega_{ij}} \tag{3.5}$$

where

$$\Omega_{ij} = \frac{1}{\sqrt{8}} \left(1 + \frac{M_i}{M_j} \right)^{-1/2} \left[1 + \left(\frac{\mu_i}{\mu_j} \right)^{1/2} \left(\frac{M_j}{M_i} \right)^{1/4} \right]^2 \tag{3.6}$$

and n = number of chemical species, and χ_i and χ_j, μ_i and μ_j, and M_i and M_j are gas phase mole fraction, viscosities, and molecular weights of species i and j, respectively. Bird, Stewart, and Lightfoot (1960) state that equation (3.5) has been able to reproduce measured values of viscosity of nonpolar gas mixtures within 2%. This equation however is not appropriate for polar (e.g., H_2O, NH_3) molecules because of angle dependent force fields existing between such molecules. Analytical codes require the assumption of constant gas viscosity for simulation of gas flow and estimation of gas permeability. However, during the course of venting, gas composition can change from a mixture of methane, carbon dioxide, nitrogen, and hydrocarbon vapors to a mixture more representative of atmospheric air. Numerical vapor transport codes such as MISER (Abriola et al., 1996) utilize equation (3.5) to account for variable gas composition.

3.3 Gas Potential Function

Using a force balance acting on an ideal (non-viscous) compressible fluid within a control volume, Bernoulli's Equation can be derived to express the components of potential (Φ) [L] for gas flow

$$\Phi = \frac{v^2 - v_{ref}^2}{2g} + \left(z - z_{ref} \right) + \frac{1}{g} \int_{P_{ref}}^{P} \frac{dP}{\rho_g(P)} = cons\tan t \tag{3.7}$$

where the first, second, and third terms represent inertial, gravitational, and pressure components in terms of energy per unit weight and P_{ref} v_{ref}, and z_{ref}, are reference pressure, velocity, elevation respectively. During gas permeability estimation and flow analysis both the velocity and elevation contributions to total potential are typically assumed to be negligible. The assumption of a negligible component of velocity potential may not be accurate in the immediate vicinity of an extraction or injection well. The assumption of negligible elevation potential may not be accurate for chlorinated contaminant laden gas present at many hazardous waste sites under low gradient conditions. Advective gas transport can be induced by density as well as pressure gradients. Density-driven flow may be of concern because of the relatively high vapor pressures and molecular weights of many common volatile contaminants. Density-driven flow will be most significant in soils that have high gas permeability in the vicinity of nonaqueous phase liquid present either as residual or mobile phase (Falta et al., 1989; Sleep and Sykes, 1989; and

Mendoza and Frind, 1990a,b). In addition, factors which reduce gas-phase concentration, such as partitioning to pore water and sorption, will reduce the significance of density-driven flow (Falta et al. 1989).

In real fluids, mechanical energy loss due to friction occurs during viscous fluid movement through soil pores, thus, potential does not remain constant. Fluid flow occurs from regions of higher to lower energy and is accompanied by an irreversible transformation of mechanical to thermal energy through the mechanism of fluid friction (Hubbert, 1940). Fluid potential loss (Φ_f) can be expressed as

$$\Phi_f \approx f(\tau)\frac{L}{d_p}\frac{v^2}{2g} \tag{3.8}$$

where d_p is pore diameter [L], L [L] is path length, and $f(\tau)$ is an expression a function of viscosity. Thus, frictional fluid potential loss increases linearly with increasing shear stress (viscosity) and distance of travel, increases linearly with decreasing pore diameter, and increases with the square of pore-gas velocity. Since gravitational and inertial components of gas potential are considered negligible in most gas flow models, the difference in gas potential between any two points in space is simply the integral term in equation (3.7).

3.4 Gas Slippage

The second factor differentiating gas flow from liquid flow is gas slippage along pore walls. In contrast to liquid flow, gas velocity at the pore wall can be significant. Klinkenberg (1941) derived an expression for specific discharge (q_x) [L T^{-1}] incorporating gas slippage

$$q_x = \frac{k_x}{u_g}\left(1+\frac{b}{\overline{P}}\right)\frac{dP}{dx} \tag{3.9}$$

where k_x = gas permeability at infinite gas pressure (high pressure where the effect of gas slippage is negligible) [L^2], $\overline{P}$ = mean pressure [M L^{-1} T^{-2}], and b = a gas slip factor [M L^{-1} T^{-2}] (expressed in terms of pressure). A general formulation of equation (3.9)

$$q_i = -\frac{1}{\mu_g}\left[\underline{\underline{k}}\left(1+\frac{b}{P}\right)\right]\frac{\partial P}{\partial x_i} \tag{3.10}$$

where q_i = Darcy specific discharge vector [L T^{-1}], and $\underline{\underline{k}}$ = gas permeability tensor [L^2] is commonly used in the literature to solve partial differential equations involving gas slippage (e.g., Kaluarachchi, 1995). Notice that in equation (3.10) mean pressure has been replaced by pressure at a point. In column studies though, the mean pressure (average of pressure at ends of column) formulation is retained. When the gas slippage factor is set to zero, equation (3.10)

reverts to the more commonly expressed equation for specific discharge

$$q_i = -\frac{\underline{\underline{k}}}{\mu_g}\frac{\partial P}{\partial x_i}\,. \tag{3.11}$$

Since values of b are always positive, equation (3.10) reveals that gas slippage results in specific discharge greater than would be predicted from equation (3.11) and that specific discharge increases with increasing values of the slip flow factor and decreasing pressure. As pressure goes to infinity, equation (3.10) reverts to equation (3.11). Another way of looking at equation (3.10) is that gas slippage flow results in an enhancement in apparent or observed gas permeability by a factor of (1 + b/P).

Klinkenberg (1941) derived the expression

$$\frac{4c\lambda}{d_p} = \frac{b}{\underline{\underline{P}}} \tag{3.12}$$

relating the slip flow factor, b, to the mean free path of gas molecules (λ) [L], pore diameter, and a proportionality constant (c). From equation (3.12), the gas slip factor and hence gas slippage should increase with decreased pore diameter. Thus, the slip factor should be larger for less gas permeable materials and smaller for more permeable material. Laboratory studies by Reda (1987) and Persoff and Hulen (1996) suggest that gas slippage can be important in fine-grained media. Baehr and Hult (1991) demonstrated through calculations that omission of gas slippage can result in pressure errors greater than 10% for soils having intrinsic permeabilities of less than 10^{-9} cm^2. Massmann (1989) related the relative importance of slip flow for low pressure systems. He calculated that materials with a pore radii greater that 0.001 mm would exhibit minimal effects of slip flow.

The constant b would be expected to decrease with increasing water saturation, especially in poorly sorted media, since only the largest pores would be available to conduct gas flow. Stonestrom and Rubin (1989b) reported that the slip correction factor ($b / \overline{P}$) decreased linearly with increasing water content in experiments with Oakley sand. However in studies with consolidated sandstones, Estes and Fulton (1956) reported fairly constant slip factors over a wide range of water contents as did Detty (1992) with Berino loamy fine sand. Thus, experimentally, the effect of water saturation on gas slippage is ambiguous.

From equation (3.12), gas slippage should also increase with increased mean free path. Mean free path is defined as the average distance traveled between consecutive collisions. Conceptually, the mean free path of molecules in a gas state at very high pressure should be equivalent to the mean free path of molecules in a liquid state. Bird, Stewart, and Lightfoot (1960) provide an equation for estimating mean free path incorporating relevant variables

$$\lambda = \frac{1}{\sqrt{2}\pi d_m^2 n} \tag{3.13}$$

where n equals number of molecules and d_m equals molecular diameter [L]. Equation (3.13) indicates that mean free path should decrease with the square of molecular diameter and number of gas molecules. Thus, gas slippage should increase with decreasing molecular diameter and gas density.

The traditional method used to determine the Klinkenberg or gas slippage factor in laboratory cores is to plot apparent gas permeability (dependent variable) versus the reciprocal of average pressure from steady-state tests. Using linear regression, the high pressure gas permeability (dependent variable intercept) and gas slip factor (slope divided by intrinsic permeability) can be calculated. Once the gas slip factor is known for a soil type, pressure and pore-gas velocity simulations can be conducted. Wu et al. (1998) however state that the traditional method of estimating the gas slip factor may not be appropriate because the pressure profile is not linear and therefore apparent permeability varies along the length of the column. This observation relates back to whether to express pressure in equation as an average or point pressure. The impact of gas slippage on one-dimensional analysis of gas flow will be assessed in detail in section 4 of this document.

3.5 Visco-Inertial Effects

Equation (3.10) or Darcy's Law is widely accepted as valid under conditions of viscous laminar flow. At high pore-gas velocities however, visco-inertial effects or non-laminar flow may become important. During non-laminar flow, higher pressure loss is observed for a given mass flux than expected. Departure from laminar flow is often indicated by the presence of high Reynolds numbers (Re) [dimensionless] defined by

$$\mathrm{Re} = \frac{d_p q_m}{\mu_g \theta_g} \tag{3.14}$$

where q_m equals specific mass flux [$ML^{-2}T^{-1}$] and θ_g = volumetric gas content [dimensionless]. Yu (1985) conducted column experiments to test the validity of Darcy's law for gas flow through various-sized sands and showed that Darcy's Law was valid for Re < 6.

One equation used to assess deviation from laminar flow originally presented by Forchheimer in 1901 is

$$-\frac{dP}{dx} = \frac{\mu_g q_x}{k} + \mathrm{I}\rho_g q_x^2 \tag{3.15}$$

where I is an inertial flow factor [L^{-1}]. This appears to be Darcy's law without gas slippage with

an additional term added on the right hand side of the equation to represent kinetic energy loss resulting from high velocity flow. In experiments with Berino loamy sand, Detty (1992) found that I increased two orders of magnitude as sample saturation increased. He states that the increased inertial flow corresponding to decreased gas permeability agrees with values reported by Keelan (1989). Detty (1992) also reported that data analysis using the Rawlins and Schellhardt (1936) equation indicated increased inertial flow at increased pressure gradients and gas flux as sample saturation increased. Detty (1992) concluded though that plots using Rawlins's and Schellhardt's (1936) and Forchheimer's equations provide a qualitative rather quantitative indication of visco-inertial flow. That is, the plots can be used to determine whether non-laminar flow is occurring or not but can not determine the actual degree of non-laminar flow.

The importance of visco-inertial flow in laboratory column and field-scale application of venting is unclear at present. However, it is apparent that if visco-inertial flow does occur, the effect would likely be underestimation of gas permeability since non-laminar flow increases energy loss relative to laminar flow.

3.6 Relative Permeability

Intuitively, it is apparent that the presence of water or a NAPL phase will interfere with the flow of gas. Quantitatively, this permeability reduction is expressed in terms of a relative permeability factor, k_{rg} [-], which varies from zero to one. The gas permeability tensor is related to relative permeability by

$$\underline{\underline{k}} = \underline{\underline{k}}_t k_{rg} \left(1 + \frac{b}{P} \right) \tag{3.16}$$

where $\underline{\underline{k}}_t$ is the intrinsic permeability tensor [L^2].

Gas flow in soils is generally described in terms of constitutive relationships between capillary pressure, gas-water saturation, and permeability for gas and water (Brooks and Corey, 1966; Stonestrom and Rubin, 1989a,b; Springer et al., 1995, Fischer et al., 1996; and Garbesi et al., 1996). However, in contrast to unsaturated water permeability, relatively few experimental studies have been conducted to evaluate the relationship between gas permeability, fluid saturation, and capillary pressure. In unsaturated media, gas is considered the nonwetting phase and water the wetting phase. In moist soil, water forms a continuous phase. A substantial portion of the gas phase though can be isolated in discontinuous, immobile domains entrapped by the aqueous phase (Bear, 1972; Stonestrom and Rubin, 1989a,b; Fisher et al., 1997). For modeling purposes, it is usually assumed that the gas phase is continuous up to the maximum water phase saturation (or residual gas phase saturation). During laboratory drainage experiments however, large discrepancies have been observed between residual gas-phase saturation and the "emergence point" of gas-phase permeability (Stonestrom and Rubin, 1989a,b;

Fisher et al., 1996, 1997; Dury et al., 1999). Stonestrom and Rubin (1989a,b) denote saturations at which gas permeability disappears and reappears during wetting and drainage experiments as extinction and emergence points respectively. These points delimit a range of saturation for wetting and drainage hysteresis branches over which both phases are continuous (i.e. conduct fluid flow). For the aqueous phase, the distinction between residual saturation and emergence point has been considered negligible (Brooks and Corey, 1964; Corey, 1986).

A plausible explanation of zero gas permeability at non-zero gas saturation is that gas permeability is directly related to the continuity of gas-filled pores connecting boundaries (Dury et al., 1999; White et al., 1972; Stonestrom and Rubin, 1989a) of which gas or water saturation are secondary indicators. Muskat (1949) proposed that relative permeability of a phase goes to zero when the phase's continuity is broken and that point might occur at saturations higher than residual saturation. Dury et al. (1999) state that extinction and emergence of gas flow above residual saturation is a phenomenon that arises through the transition from the microscopic to the macroscopic scale. On the microscopic scale, the three-dimensional structure of pore space can be explicitly accounted whereas on the macroscopic scale, spatial averaging and use of empirical terms such as the extinction and emergence point must be used to describe processes occurring on a microscopic scale.

Pore-scale network models can be used to explicitly account for the three-dimensional connectivity of pores. This is accomplished by representing the pore space as a lattice of pore bodies or sites which are connected to one another by pore throats or bonds. Probability distribution functions can then be used to generate distributions of bond and site radii. As explained by Fisher and Celia (1999) though, drainage and imbibition in bonds or sites are controlled not only by size but also by location and accessibility in a three-dimensional lattice. Fisher and Celia (1999) were able to predict extinction and emergence points for gas flow in a quartz sand mixture using a pore-scale network model. They state that as opposed to empirical retention and capillary bundle models, the discontinuity of the gas phase at high wetting saturation is inherent in network models and thus has significant conceptual advantages.

In principle, no additional manipulation of lattice topology should be required for the prediction of permeabilities after adjustment to retention data. However, in practice, generation of an appropriate network of pores to match retention data and predict permeabilities is difficult. Development of methods to more accurately describe liquid retention and permeability relationships is an active area of research. For instance Tuller et al. (1999) devised a new model considering both capillary and adsorptive contributions to liquid retention in angular pore space. Or and Tuller (1999) then developed a statistical framework for upscaling the pore size model to represent a sample size.

While pore-scale network models have long-term potential use, the empirical capillary pressure - water saturation relationships of Brooks and Corey (1964) and van Genuchten (1980) combined with the capillary bundle models of Burdine (1953) and Mualem (1976) are most often used to estimate gas and water permeability. With rescaling, these models can account for gas

entrapment or discontinuities. Lenhard and Parker (1987) partitioned nonwetting phases into continuous and discontinuous phases to develop a relationship for relative nonwetting phase permeability based on the capillary pressure - saturation relationship of van Genuchten (1980) and capillary bundle model of Mualem (1976). Luckner et al. (1989) adapted the van Genuchten (1980) and Mualem (1976) equations by rescaling nonwetting phase saturation to residual nonwetting phase saturation. Fisher et al. (1996) then extended Luckner et al.'s (1989) approach to scale effective nonwetting phase saturation to the emergence point of nonwetting phase conductance.

Using Fisher et al.'s (1996) approach, effective gas saturation ($\overline{S_g}$) [-] can be defined by

$$\overline{S_g} = \frac{S_g - S_{g,e}}{S_{g,\max} - S_{g,e}} \tag{3.17}$$

where S_g is gas saturation (volume of gas-filled pore space divided by total pore space) [-], $S_{g,e}$ is the gas phase emergence point saturation [-], and $S_{g,max}$ is a maximum gas-phase saturation [-]. Similarly, effective water saturation ($\overline{S_w}$) [-] can be defined by

$$\overline{S_w} = \frac{S_w - S_{w,e}}{S_{w,\max} - S_{w,e}} \tag{3.18}$$

where S_w is water saturation (volume of water-filled pore space divided by total pore space) [-], $S_{w,e}$ is the water-phase emergence point saturation [-], and $S_{w,max}$ is maximum water-phase saturation [-]. However, with respect to the wetting phase, the difference between residual saturation and emergence point has been considered to be negligible and irrelevant (Brooks and Corey, 1964).

In contrast to unscaled gas and water saturation values, effective or scaled gas and water saturations do not in general add up to one. Combining the retention models of Brooks and Corey (1964)

$$\overline{S_w} = \left(\frac{h_d}{h} \right)^{\lambda} \qquad h \geq h_d \tag{3.19}$$

$$\overline{S_w} = 1 \qquad h \leq h_d \tag{3.20}$$

and van Genuchten (1980)

$$\overline{S_w} = \left[1 + (\alpha h)^n\right]^{-m} \tag{3.21}$$

respectively where α, λ, h_d, m, and n are empirical parameters and h is capillary pressure given in units of length and the models of Burdine (1953)

$$k_{rg} = \left(1 - \overline{S_w}\right)^2 \left[\int_{\overline{S_w}}^{1} \frac{dx}{h^2(x)} \Big/ \int_{0}^{1} \frac{dx}{h^2(x)} \right] \tag{3.22}$$

and Mualem (1976)

$$k_{rg} = \left(1 - \overline{S_w}\right)^{1/2} \left[\int_{\overline{S_w}}^{1} \frac{dx}{h(x)} \Big/ \int_{0}^{1} \frac{dx}{h(x)} \right] \tag{3.23}$$

results in the formation of four gas-phase relative permeability models. Dury et al. (1999) observed that these four models have a similar mathematical form

$$k_{rg}\left(\overline{S}_w\right) = \left(1 - \overline{S}_w\right)^{\mu} \left(1 - \left(\overline{S}_W\right)^A\right)^B \tag{3.24}$$

or

$$k_{rg}\left(\overline{S}_g\right) = \overline{S}_g^{\mu} \left[1 - \left(1 - \overline{S}_g\right)^A\right]^B \tag{3.25}$$

which can be summarized by Table 3.1.

Table 3.1 Summary of capillary pressure - relative permeability models (from Dury et al., 1999)

Retention Model	Permeability Model	μ	A	B
Brooks and Corey (1964)	Burdine (1953)	2	$(2+\lambda)/\lambda$	1
Brooks and Corey (1964)	Mualem (1976)	0.5	$(1+\lambda)/\lambda$	2
van Genuchten (1980)	Burdine (1953)	2	1/m	m
van Genuchten (1980)	Mualem (1976)	0.5	1/m	2m

Dury et al. (1999) state that the term raised to the powers of A and B represent capillarity while the term raised to the power μ represents connectivity and tortuosity of the pores. They found that after scaling to an emergence point water saturation for drainage experiments, that selection of the permeability model was decisive for fitting experimental data. Prediction of gas permeability did not appear to be very sensitive to the choice of the retention model. Best fits to experimental data were found when μ was optimized. Dury et al. (1999) point out that the connectivity - tortuosity term μ is not based on theoretical considerations. The value of 0.5 used for the Mualem (1976) was based on empirical evidence from a variety of hydraulic conductivity data where μ ranged from -0.5 to 2.5 for different soils. No comparable studies have been conducted for gas permeability. The value of 2.0 used for the Burdine (1953) is also empirically based. Luckner et al. (1989) arbitrarily choose a value of 0.33 while Parker and Lenhard (1987) and Fisher et al. (1996) both used a value of $\mu = 0.5$ by analogy with hydraulic conductivity. Thus, there is no theoretical or practical reason to confine selection of μ to 0.5 or 2.0. Detty (1992) demonstrated that the relative permeability of gas is greater than water for the same saturation because water is the wetting fluid and occupies the smaller pores.

3.7 Components of Specific Discharge

Specific discharge is a macroscopic quantity defined as the volume of discharge of fluid over some representative area per time. It is a vector in three-dimensional space in Cartesian coordinates and in two-dimensional axisymmetric cylindrical coordinates. Darcy's law given in terms of its gas permeability tensor (expressed as a matrix) can be described by:

$$\begin{bmatrix} q_x \\ q_y \\ q_z \end{bmatrix} = -\frac{k_{rg}}{\mu_g}\left(1+\frac{b}{P}\right)\begin{bmatrix} k_{\iota(xx)} & k_{\iota(xy)} & k_{\iota(xz)} \\ k_{\iota(yx)} & k_{\iota(yy)} & k_{\iota(yz)} \\ k_{\iota(zx)} & k_{\iota(zy)} & k_{\iota(zz)} \end{bmatrix}\begin{bmatrix} \partial P/\partial x \\ \partial P/\partial y \\ \partial P/\partial z \end{bmatrix}. \tag{3.26}$$

or

$$\begin{bmatrix} q_r \\ q_z \end{bmatrix} = -\frac{k_{rg}}{\mu_g}\left(1+\frac{b}{P}\right)\begin{bmatrix} k_{\iota(rr)} & k_{\iota(rz)} \\ k_{\iota(zr)} & k_{\iota(zz)} \end{bmatrix}\begin{bmatrix} \partial P/\partial r \\ \partial P/\partial z \end{bmatrix} \tag{3.27}$$

In analytical gas permeability testing, it is commonly assumed that site-specific coordinates are aligned with the principal axes of gas permeability whereby equations (3.26) and (3.27) become

$$\begin{bmatrix} q_x \\ q_y \\ q_z \end{bmatrix} = -\frac{k_{rg}}{\mu_g}\left(1+\frac{b}{P}\right)\begin{bmatrix} k_{\iota(xx)} & 0 & 0 \\ 0 & k_{\iota(yy)} & 0 \\ 0 & 0 & k_{\iota(zz)} \end{bmatrix}\begin{bmatrix} \partial P/\partial x \\ \partial P/\partial y \\ \partial P/\partial z \end{bmatrix}. \tag{3.28}$$

or

$$\begin{bmatrix} q_r \\ q_z \end{bmatrix} = -\frac{k_{rg}}{\mu_g}\left(1+\frac{b}{P}\right)\begin{bmatrix} k_{i(rr)} & 0 \\ 0 & k_{i(zz)} \end{bmatrix}\begin{bmatrix} \partial P/\partial r \\ \partial P/\partial z \end{bmatrix} \tag{3.29}$$

However, this is done for mathematical convenience, specifically to allow development of analytical solutions. Actual principal directions of gas permeability may be quite different. This would become readily apparent if one injected a gas tracer and noted movement in a direction not parallel with the pressure gradient.

3.8 Continuity Equation for Gas Flow

The continuity equation for gas flow can be expressed by

$$\frac{\partial(\rho_g \theta_g)}{\partial t} + \frac{\partial}{\partial x_i}(\rho_g q_i) = 0\,. \tag{3.30}$$

The assumption of constant volumetric gas content, viscosity, temperature, and molecular weight yields

$$\mu_g \theta_g \frac{\partial P}{\partial t} = \frac{\partial}{\partial x_i}\left(k_{rg} \underline{\underline{k_i}} \left(1+\frac{b}{P}\right) P \frac{\partial P}{\partial x_j} \right) \tag{3.31}$$

If we let $\phi = P^2$ then

$$\frac{\mu_g \theta_g}{\sqrt{\phi}} \frac{\partial \phi}{\partial t} = \frac{\partial}{\partial x_i}\left(k_{rg} \underline{\underline{k_i}} \left(1+\frac{b}{\sqrt{\phi}}\right) \frac{\partial \phi}{\partial x_j} \right) \tag{3.32}$$

which is the governing partial differential equation commonly used for analytical and numerical gas flow analysis.

Baehr and Hult (1991) state that natural areal temperature variations can be neglected over the scale of a pneumatic test. Also, temperature variations due to energy transport associated with induced gas movement will be negligible as a result of the high thermal capacity of natural sediments and low-energy content of subsurface gas. The assumption of constant volumetric gas content however may impart error under aggressive operating conditions (e.g. high vacuum or pressure) in soils having a high moisture content. Redistribution of gas and water during pneumatic testing can change the original spatial distribution of gas permeability. Vacuum extraction will cause water to move towards the well while gas injection will cause water to move away from the well. Thus, gas extraction and gas injection pneumatic tests may provide different estimates of pneumatic permeability.

3.9 Linearization of Gas Flow Equation

Equation (3.32) is by definition a non-linear partial differential equation. To solve this equation analytically, linearization of the $\sqrt{\phi}$ term is necessary. The first and most simplistic approach is to let $\sqrt{\phi}$ equal atmospheric pressure (P_{atm}) or some other constant pressure and to let $P^2 = P*P_{atm}$, thereby solving for P not P^2 and removing consideration of compressibility. Johnson et al. (1988) used this linearization to solve the Theis equation for gas flow. A second approach is to let $\sqrt{\phi}$ equal to a constant pressure but still solve for ϕ or P^2. Baehr and Hult (1988) and Falta (1996) let $\sqrt{\phi} = P_{atm}$. Falta (1996) states that with this approximation, the gas is assumed to be compressible with a constant compressibility factor of $1/P_{atm}$. A third approach is to replace $\sqrt{\phi}$ with a prescribed time-varying function which in some manner reflects the rate of change of initial pressure distribution (Wu et al., 1998). Since the first and second approaches are easy to implement and commonly used for analytical and numerical solution of the gas flow equation, it is useful to evaluate error associated with these two linearization methods to determine whether use of the third approach is necessary.

Error incurred using the first and second approaches can be evaluated using Kidder's (1957) perturbation solution to the one-dimensional transient gas flow equation

$$\frac{\theta_g \mu_g}{k_x}\frac{\partial P}{\partial t} = \frac{\partial}{\partial x}\left(P\frac{\partial P}{\partial x}\right) \tag{3.33}$$

subject to

$$P(x,0) = P_0, \qquad 0 < x < \infty \tag{3.34}$$

$$P(0,t) = P_1, \qquad 0 \le t < \infty \tag{3.35}$$

$$\lim_{x\to\infty} P = P_0 . \tag{3.36}$$

Kidder's (1957) second-order perturbation solution is summarized as follows

$$\left(\frac{P}{P_0}\right)^2 = 1 - \alpha\varpi_0 - \alpha^2\varpi_1 - \alpha^3\varpi_2 \tag{3.37}$$

where

$$\alpha = \frac{P_0^2 - P_1^2}{P_0^2} \tag{3.38}$$

$$\varpi_0 = 1 - erf(\varsigma) \tag{3.39}$$

$$\varpi_1 = -\frac{1}{2\pi}\left\{\varpi_0\left[1+\pi^{1/2}\varsigma\exp(-\varsigma^2)\right]-\exp(-2\varsigma^2)\right\} \tag{3.40}$$

$$\varpi_2 = -\frac{\varpi_1}{\pi}+\frac{\varsigma\exp(-3\varsigma^2)}{8\pi^{3/2}}-\frac{\varpi_0}{2\pi}-\frac{\varsigma\left(5-2\varsigma^2\right)\exp(-\varsigma^2)}{16\pi^{1/2}}\varpi_0^2 + \frac{\left(2-\varsigma^2\right)\exp(-2\varsigma^2)}{4\pi}\varpi_0+\frac{3^{3/2}}{16\pi}\left[erf(3^{1/2}\varsigma)-erf(\varsigma)\right] \tag{3.41}$$

and

$$\varsigma = \left(\frac{\theta_g\mu_g}{k_x P_0}\right)^{1/2}\left(\frac{x}{2\sqrt{t}}\right). \tag{3.42}$$

Kidder (1957) provides an analysis to justify truncation at the second-order coefficient. Using Laplace transforms, it can be demonstrated that the zero-order solution

$$\frac{P^2}{P_0^2} = 1-\alpha\varpi_0 \tag{3.43}$$

is an exact solution to $\sqrt{\phi} = P_0$ linearized form of the one-dimensional transient gas flow equation for the boundary conditions described above. Linearization by letting $\phi = P^*P_0$ and $\sqrt{\phi} = P_0$ results in

$$\frac{P}{P_0} = 1-\alpha'\varpi_0 \tag{3.44}$$

where

$$\alpha' = \frac{P_0 - P_1}{P_0}. \tag{3.45}$$

Kidder's (1957) second-order perturbation solution and the dimensionless variable, ς, are used to compare the accuracy of the $\sqrt{\phi} = P_0$ combined with $P^2 = P^*P_0$ to the $\sqrt{\phi} = P_0$ approach to linearization. Results of simulations are summarized in Figures 3.1 and 3.2. Deviation from Kidder's second-order perturbation solution is defined here as

$$Deviation\ from\ \text{second order solution} = \frac{\left| \frac{P}{P_0} - \frac{P^{2nd-order}}{P_0} \right|}{\frac{P^{2nd-order}}{P_0}} \qquad (3.46)$$

As P_1/P_0 (ratio of pressure at x = 0 to pressure at infinite distance) approaches zero, the $\sqrt{\phi} = P_0$ approach to linearization provides a much more accurate approximation to P/P_0 (ratio of pressure at a prescribed distance and time to pressure at infinite distance) for various values of ς compared to the $P^2 = P*P_0$ approach to linearization. It is noteworthy that the maximum deviation from Kidder's (1957) second-order perturbation solution when solving directly for ϕ and linearizing $\sqrt{\phi}$ by $\sqrt{\phi} = P_0$ is less than 6 %. Error approaching 6% occurs as the ratio of P_1/P_0 approaches zero or as the pressure at x = 0 approaches a perfect vacuum. The $\sqrt{\phi} = P_0$ combined with $P^2 = P*P_0$ approach to linearization appears acceptable only when the ratio of P_1/P_0 is greater than 0.5. However, even under these conditions, solving directly for ϕ and linearizing $\sqrt{\phi}$ by $\sqrt{\phi} = P_0$ approach to linearization is clearly superior.

This analysis demonstrates that solving directly for ϕ and linearizing $\sqrt{\phi}$ by $\sqrt{\phi} = P_0$ approach to linearization is adequate for solving gas flow problems associated with venting application. This approach to linearization will be used for equation development throughout the remainder of this document.

3.10 Conclusions

1. At pressures typical of soil venting operation (less than atmospheric pressure up to perhaps 1.5 atm), deviation from ideality for gases of interest (primarily O_2 and N_2) will be insignificant and the ideal gas law can be used to estimate gas density.

2. Gas viscosity is largely independent of pressure up to 10 atmospheres. At low density, gas viscosity increases with temperature to the 0.6 to 1.0 power of temperature because of molecular interactions. Gas viscosity of a nonpolar multicomponent mixture can be estimated to within 2% from individual gas mole fractions, viscosities, and molecular weights.

3. Inertial and gravitational components of Bernoulli's equation are typically neglected in gas flow analysis. The assumption of a negligible component of inertial potential though may be inaccurate in the immediate vicinity of an extraction or injection well. The assumption of negligible gravitational potential may be inaccurate for chlorinated contaminant laden gas present near a NAPL source area under low gradient conditions.

4. Frictional fluid potential loss is proportional to shear stress and distance of travel, increases to the square of pore-gas velocity, and increases linearly with decreasing pore diameter. The last factor explains why gas potential dissipates over short distances in fine

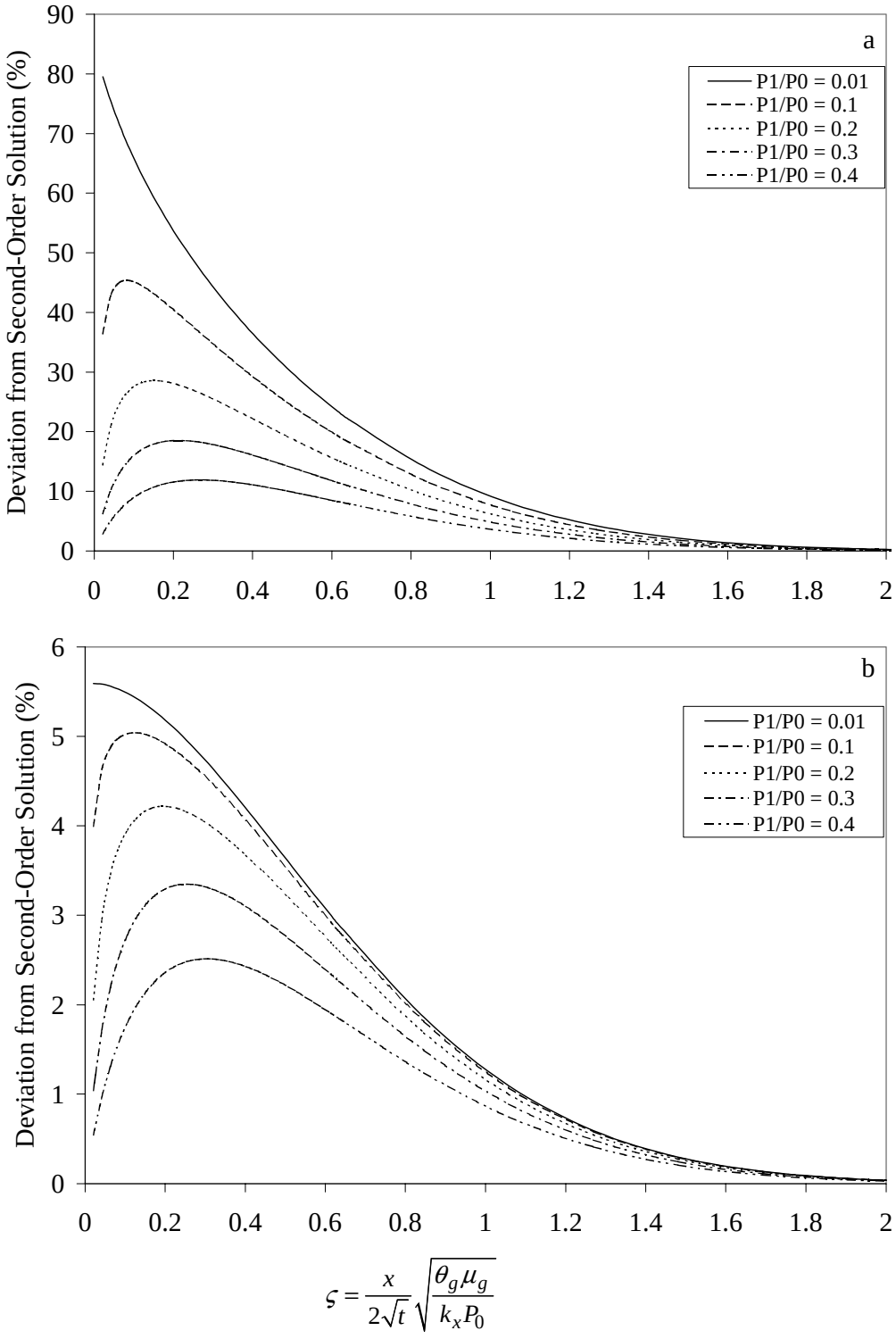

Figure 3.1 Percent deviation from Kidder's (1957) second-order perturbation solution for P_1/P_0 = 0.01 to 0.4 for (a) $\phi = PP_0$ in addition to $\sqrt{\phi} = P_0$ and (b) $\sqrt{\phi} = P_0$ alone

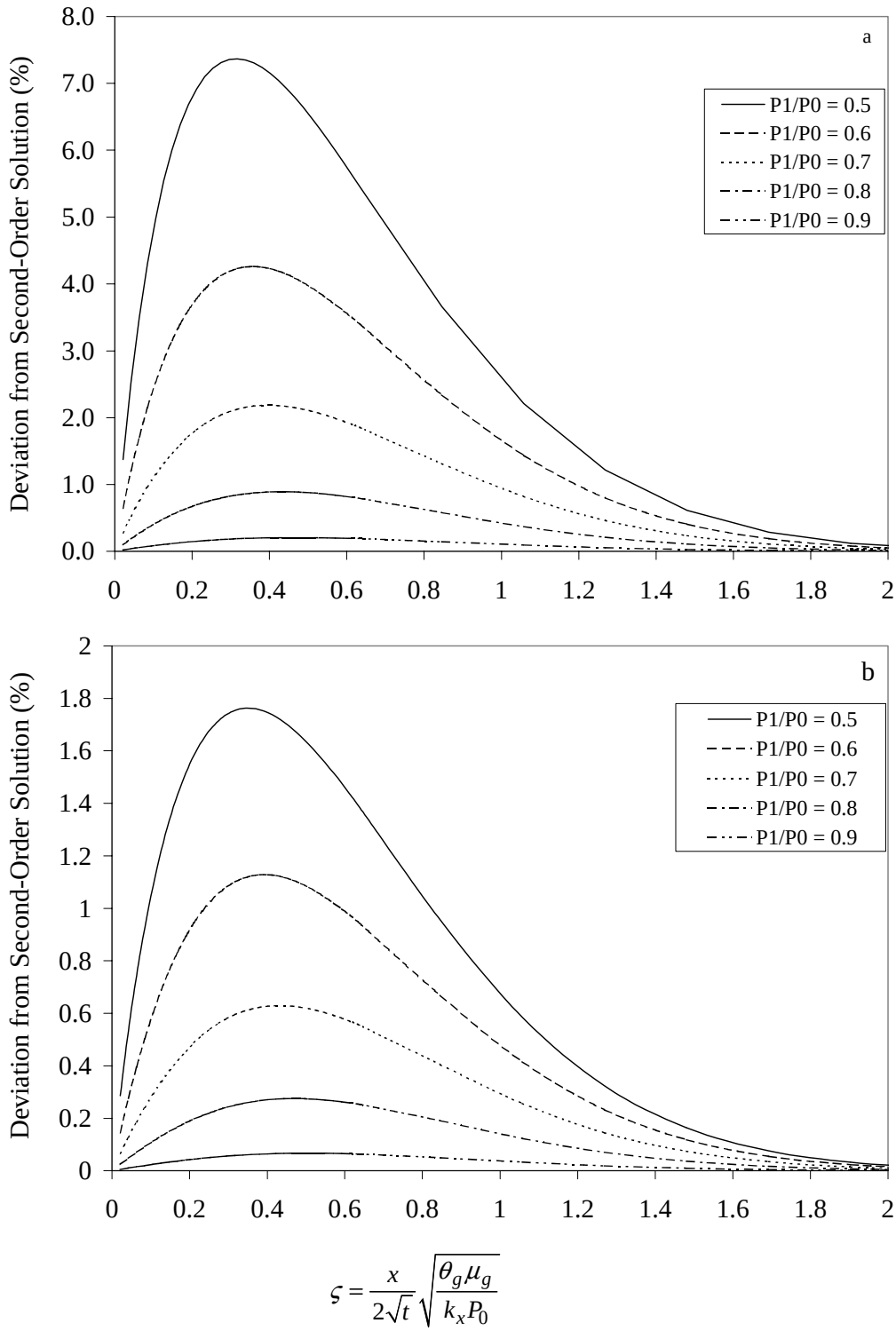

Figure 3.2 Percent deviation from Kidder's (1957) second-order perturbation solution for P_1/P_0 = 0.5 to 0.9 for (a) $\phi = PP_0$ in addition to $\sqrt{\phi} = P_0$ and (b) $\sqrt{\phi} = P_0$ alone

grained soils such as silts and clays.

5. A reduction in molecular diameter, pore diameter, and gas density should increase slip flow. Apparent gas permeability should be approximately a linear function of reciprocal pressure. Thus, in dry or water free media, apparent permeability extrapolated to the reciprocal of infinite pressure should give intrinsic (fluid independent) permeability. Since the gas slippage factor, b, is inversely proportional to the pore radii, it should be small for high gas permeable material and larger for low gas permeable materials. Also, the gas slippage factor would be expected to decrease with increasing water saturation since only the largest pores would conduct gas flow. However with the exception of one study, experimental evidence does not support this statement.

6. At high pore-gas velocities, visco-inertial effects or non-laminar (non-Darcy) flow may become important. For one-dimensional flow, Forchheimer's equations may provide a qualitative indication of visco-inertial flow.

7. Gas permeability is directly related to the continuity of gas-filled pores. A substantial portion of the gas phase is often isolated in discontinuous, immobile domains entrapped by the aqueous phase. Water saturation at which gas permeability disappears during wetting and reappears during drainage are referred to as extinction and emergence points respectively. These points delimit a range of saturation for wetting and drainage hysteresis branches over which both phases are continuous. With rescaling to incorporate gas entrapment, empirical capillary pressure - water saturation relationships of Brooks and Corey (1964) and van Genuchten (1980) combined with capillary bundle models of Burdine (1953) and Mualem (1976) can be used to estimate gas permeability from capillary pressure and water saturation information.

8. The gas flow equation is by definition a non-linear partial differential equation. To solve this equation analytically, linearization of the $\sqrt{\phi}$ term is necessary. The first and most simplistic approach is to let $\sqrt{\phi}$ equal atmospheric pressure (P_{atm}) or some other constant pressure and to let $P^2 = P*P_{atm}$, thus solving for P not P^2. A second approach is to let $\sqrt{\phi}$ equal to a constant pressure but still solve for ϕ or P^2. Comparison with Kidder's (1957) demonstrate that the latter approach is much more accurate at pressure differential exceeding 0.5 atmospheres.

4. ONE-DIMENSIONAL GAS FLOW AND PERMEABILITY ESTIMATION

While not representative of fully three-dimensional field-scale gas flow, one-dimensional flow analysis can provide valuable insight into fundamental gas flow processes such as the effect of compressibility and gas slippage on pressure and pore-gas velocity profiles. Analysis of one-dimensional gas flow is especially important in designing and interpreting laboratory column vapor mass transport studies where knowledge of pore-gas velocity profiles becomes critical. Because field-scale tests provide estimation of gas permeability over an integrated volume of porous media too large to discern small discrete layers of less permeable materials (e.g., lenses of silt and clay), gas permeability estimation in "minimally" disturbed samples could be useful in determining small-scale gas permeability variation in subsurface media. Testing with undisturbed or minimally disturbed soil cores though provides only an estimate of vertical permeability. However, variation in horizontal and vertical permeability of a soil core may be an order of magnitude or less than variation in permeability between distinct stratigraphic lenses. For example, variation in gas permeability between a sand and clay would be expected to be much greater than variation in horizontal and vertical permeability within the clay or sand core.

4.1 Permeameter Design

One-dimensional permeability estimation most often involves testing in laboratory-scale columns or permeameters. Basic features that permeameters should exhibit for accurate gas permeability estimation include: (1) a sample-holding device capable of forming a tight seal between the sample and container wall without significantly altering the geometry or physical properties of the sample; (2) end caps and filters which form a tight seal with the sample but do not restrict gas flow; and (3) a method to vary moisture content uniformly throughout the sample. Guidance for conducting gas permeability tests in permeameters such as the American Petroleum Institute's "Recommended Practice for Core-Analysis Procedure RP-40" (API, 1960) and American Society for Testing and Material's Method D4525-90 (ASTM, 1990) entitled "Standard Test Method for Permeability of Rocks by Flowing Air" is largely intended for rock cores. The preferred apparatus in ASTM Method D4525-90 is to have a rock specimen confined and compressed by an elastomer sleeve to avoid bypassing of air along the sample wall. In the Hassler (1944) permeameter, a rubber diaphragm inflated with high pressure liquid or air is used to seal the sample. In the Fancher (1933) permeameter, an elastomer bushing and compression yoke is used to confine and seal a rock specimen. In these methods, the rock specimen must be sufficiently hard and consolidated to resist cracking or other deformation since gas permeability estimation is extremely sensitive to bypass flow. Another approach, more appropriate for unconsolidated media, is to confine a sample with a rigid bushing or tube such as would occur during core collection with a shelby tube. This method however does not allow direct manipulation of moisture content as would be necessary for evaluation of gas permeability as a function of moisture content.

Corey (1986) developed an apparatus to determine gas permeability as a function of moisture content by placing a sample in an annulus between a water-wetted ceramic cylinder and

a rubber sleeve. The ceramic cylinder was used to ensure a constant and uniform moisture content in the sample during testing. Short circuiting of gas flow and poor contact with the ceramic cylinder along the sample wall boundaries was prevented by applying pneumatic pressure (50 to 100 kPa) across the rubber sleeve. Stonestrom (1987) modified Corey's (1986) design by adding concentrically grooved ceramic end plates to allow simultaneous water desaturation and air flow through the sample and peripheral features for co-determination of trapped gas, water-retention characteristics, and air and water permeability functions. Springer et al. (1998) describe an apparatus referred to as a "soil-air permeameter" in which soils are packed in a 1-bar rated ceramic cylinder to allow water extraction and uniform water content and capillary pressure throughout the column. This device has the capability to evaluate gas permeability as both a function of capillary pressure and water content.

When attempting to evaluate small-scale gas permeability variation in the field, use of permeameters such as those described by Corey (1986), Stonestrom (1987), and Springer et al. (1988) provide the opportunity of determining capillary pressure - gas permeability curves but require repacking of soil samples thereby compromising pneumatic sample integrity. Use of shelby tubes during core collection allows collection of minimally disturbed cores, but elimination of short-circuiting along the tube wall can not be guaranteed. Use of both permeameters and shelby tubes measure only the vertical component of the permeability tensor. Thus, it would appear that all laboratory-scale methods of measuring gas permeability have notable limitations. However, there is currently no other direct means to estimate gas permeability on the scale of centimeters in the field. Field-scale testing integrates gas permeability estimation on the scale of m^3 or larger.

4.2 Formulation of a One-Dimensional Steady-State Gas Flow Equation With Gas Slippage

Because of small sample size and hence very rapid transient response, estimation of gas permeability with permeameters or soil columns is typically accomplished using steady-state solutions. The governing equation for one-dimensional, steady-state gas flow incorporating gas slippage is

$$\frac{d}{dx}\left(k_{rg} k_{t(x)} \left(1 + \frac{b}{\sqrt{\phi}} \right) \frac{d\phi}{dx} \right) = 0 . \tag{4.1}$$

The boundary condition for equation (4.1) when gas is injected or extracted is represented by

$$k_{rg} k_{t(x)} \left(1 + \frac{b}{\sqrt{\phi}} \right) \frac{d\phi}{dx}\bigg|_{x=0} = -\frac{2 Q_m \Re T \mu_g}{M_g A} \tag{4.2}$$

where Q_m = mass flow rate [M T^{-1}]. The boundary condition where gas exits the column is represented by constant pressure

$$\phi(L) = \phi_L \,. \tag{4.3}$$

In the literature, flow rates are often expressed in terms of volume and sometimes in terms of mass. The mixing of units causes confusion. In this document, all flow units are expressed in terms of mass to maintain consistency and to emphasize the point that analytical solutions presented here demand a constant mass flux not volumetric gas flow into or out of the formation or column. The relationship between volumetric flow (Q_v) and mass flow (Q_m) is given by:

$$Q_v = \frac{Q_m \Re T}{P M_g} \,. \tag{4.4}$$

Negative values of Q_m denote gas extraction while positive values of Q_m denote gas injection.

The Kirchhoff transformation can be used to remove the non-linearity associated with gas slippage (Kaluarachchi, 1995) by letting

$$U = \int_{\phi_{ref}}^{\phi} \left(1 + \frac{b}{\sqrt{\tau}}\right) d\tau \,. \tag{4.5}$$

Integration of equation (4.5) results in

$$U = \phi + 2b\sqrt{\phi} - \phi_{ref} - 2b\sqrt{\phi_{ref}} \,. \tag{4.6}$$

Expressing ϕ in terms of P^2 and use of the quadratic equation on (4.6) results in

$$P = -b + \sqrt{b^2 + P_{ref}^2 + 2bP_{ref} + U} \,. \tag{4.7}$$

Differentiation of U in equation (4.6) results in

$$\frac{dU}{dx} = \left(1 + \frac{b}{\sqrt{\phi}}\right) \frac{d\phi}{dx} \,. \tag{4.8}$$

Equation (4.1) now becomes

$$\frac{d}{dx}\left(k_{rg} k_{t(x)} \frac{dU}{dx}\right) = 0 \tag{4.9}$$

with boundary conditions:

$$U(L) = 0 \tag{4.10}$$

and

$$k_{rg} k_{\iota(x)} \left. \frac{dU}{dx} \right|_{x=0} = -\frac{2Q_m \Re T \mu_g}{M_g A} . \tag{4.11}$$

Integration of equation (4.9) provides a solution

$$U(x) = \frac{2Q_m \Re T \mu_g}{M_g A k_{rg} k_{\iota(x)}} \left(L - x\right) \qquad 0 \le x \le L . \tag{4.12}$$

An exact solution to equation (4.1) in terms of pressure can now be expressed by

$$P(x) = -b + \sqrt{b^2 + P_L^2 + 2bP_L + \frac{2Q_m \Re T \mu_g}{M_g A k_{rg} k_{\iota(x)}} \left(L - x\right)} . \tag{4.13}$$

Specific discharge as function of distance within a soil column can then be calculated by

$$q(x) = -\frac{Q_m \Re T}{M_g A} \frac{1}{\sqrt{b^2 + P_L^2 + 2bP_L + \frac{2Q_m \Re T \mu_g}{M_g A k_{rg} k_{\iota(x)}} \left(L - x\right)}} . \tag{4.14}$$

When gas slippage is neglected during permeameter testing or b is assumed to equal zero, the commonly referenced equation

$$k_{rg} k_{\iota(x)} = \frac{2Q_m \Re T \mu_g L}{M_g A \left(P_0^2 - P_L^2\right)} = \frac{2Q_v P_0 \mu_g L}{A \left(P_0^2 - P_L^2\right)} \tag{4.15}$$

can be used to estimate gas permeability. The empirical equation

$$b = \left(3.98 \times 10^{-5}\right) \left(k_{rg} k_{\iota(x)}\right)^{-0.39} \tag{4.16}$$

based on data presented by Heid et al. (1950) can be used to estimate the Klinkenberg parameter where b is in atmospheres and k is in units of centimeters squared. Equation (4.17) is the American Petroleum Institute (API) standard correction for gas slippage and is based on air-dry consolidated media. Thus, there is some question to its applicability to porous media.

4.3 Analysis of Effect of Gas Slippage on One-Dimensional Pressure and Pore-Gas Velocity Simulation

Equations (4.13), (4.14), and (4.16) were used to evaluate the effect of flow rate on pressure and pore-gas velocity computation with and without gas slippage as a function of distance in a hypothetical 30 cm long soil column having diameter of 10 cm. Gas extraction occurs at x = 0. Simulations were conducted using gas permeabilities of 1.0×10^{-08} cm^2, 1.0×10^{-09} cm^2, and 1.0×10^{-10} cm^2. Mass flow rates were adjusted to maintain a constant $Q_m/k_{rg}k_{i(x)}$ ratio. From equation (4.14), when this ratio is held constant, non-slip-corrected pressure as a function of distance must be identical. This is not the case however for slip-corrected gas flow since b varies with gas permeability.

Figures 4.1 through 4.3 illustrate the effect of flow rate on pressure computation as a function of distance with and without gas slippage during gas extraction. For each figure, the disparity between slip-corrected and non-slip-corrected computed pressure increases with increasing flow rate and decreases with increased distance from the extraction point. At higher flow rates, neglecting gas slippage results in underestimation of absolute pressure and overestimation of pressure differential from atmospheric pressure. These effects become more severe as gas permeability and pressure is reduced.

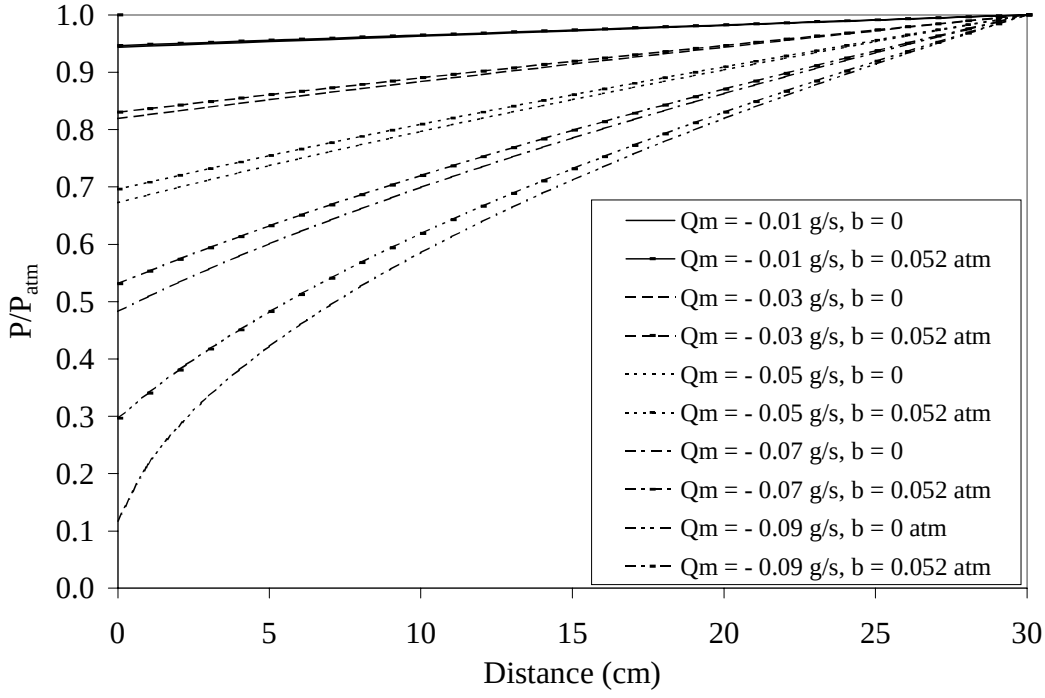

Figure 4.1 Normalized pressure computation as a function of mass flow rate, distance, and gas slippage factor ($k_{rg}k_{i(x)} = 1.0 \times 10^{-08}$ cm^2).

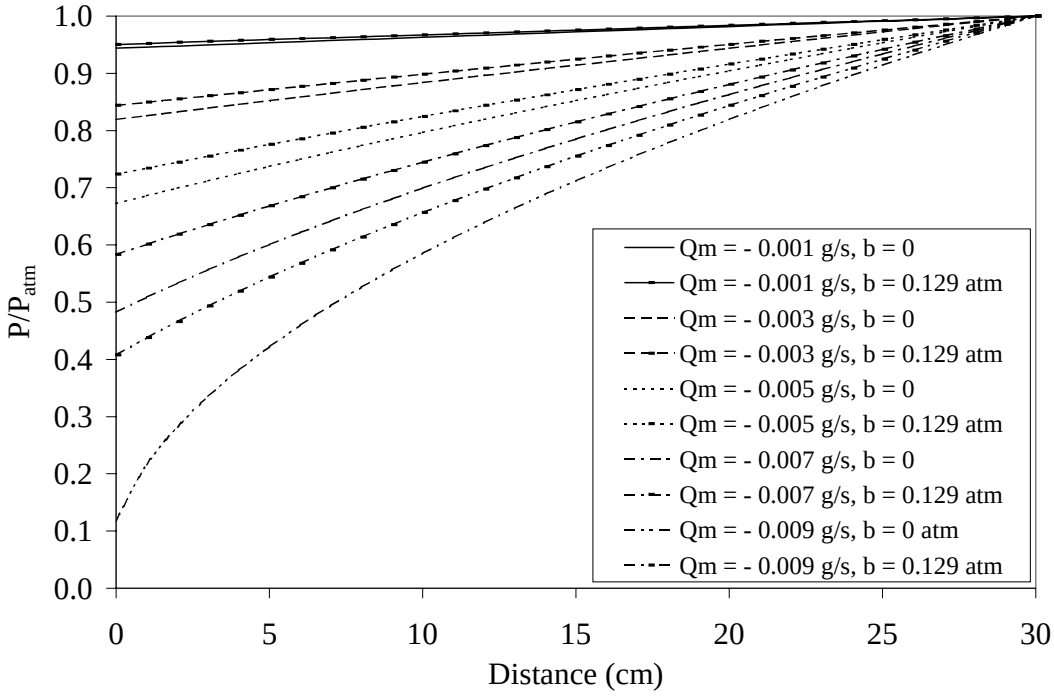

Figure 4.2 Normalized pressure computation as a function of mass flow rate, distance, and gas slippage ($k_{rg}k_{\iota(x)}$ = 1.0 x 10^{-09} cm^2).

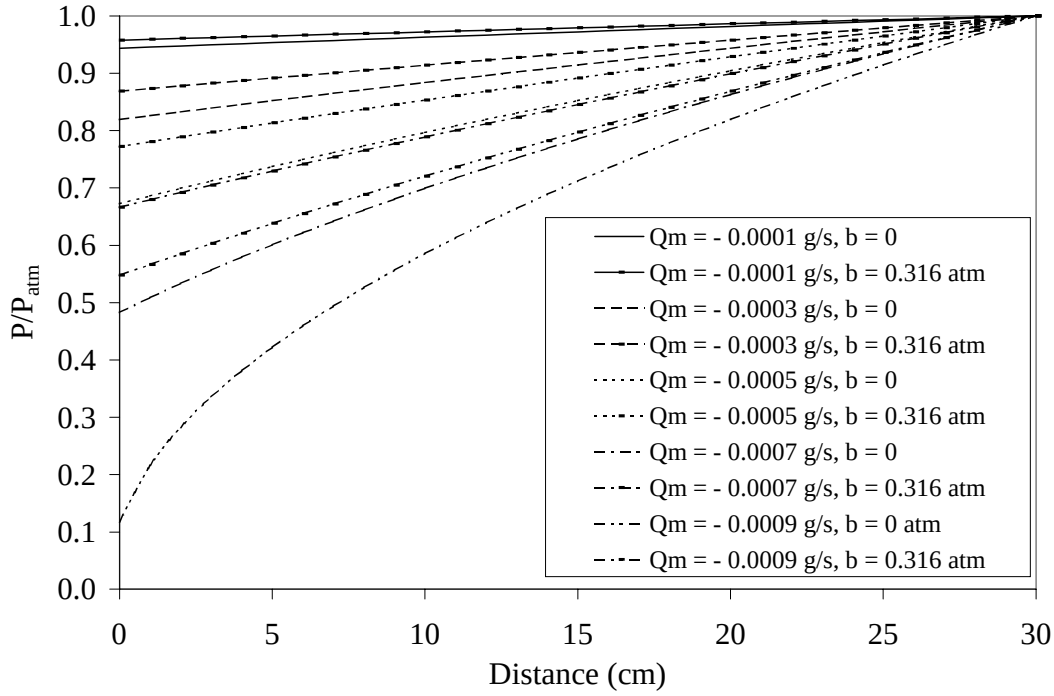

Figure 4.3 Normalized pressure computation as a function of mass flow rate, distance, and gas slippage ($k_{rg}k_{\iota(x)}$ = 1.0 x 10^{-10} cm^2).

Figures 4.4 through 4.6 illustrate error in pressure calculation due to gas slippage. Error is calculated by

$$Error\ in\ pressure\ calculation = \frac{P(b=0) - P(b \neq 0)}{P(b \neq 0)}. \qquad (4.17)$$

Error is negative since absolute pressure for slip-corrected flow is always greater than for non-slip-corrected flow under vacuum application. Error in pressure computation due to gas slippage increases with gas flow and decreased permeability. Note that error in pressure computation exceeded 60%, 70%, and 80% at gas permeability values of 1.0×10^{-08}, 1.0×1^{-09}, and 1.0×10^{-10} cm^2 respectively. The magnitude of these errors may necessitate consideration of gas slippage for laboratory and field-scale estimation of gas permeability in soils having when vacuum is applied. As will be discussed, consideration of gas slippage may not be necessary for estimation of gas permeability when gas is injected or pressure is applied.

Figures 4.7 through 4.9 illustrate the effect of flow rate on calculated pore-gas velocity as a function of distance assuming a volumetric gas content of 0.1 during air extraction. At the point of extraction, pore-gas velocity increases for both slip-corrected and non-slip-corrected gas flow because of lower gas density. However, at higher flow rates and low absolute pressures near the extraction point, calculated pore-gas velocities for non-slip corrected flow are much higher than for slip-corrected flow.

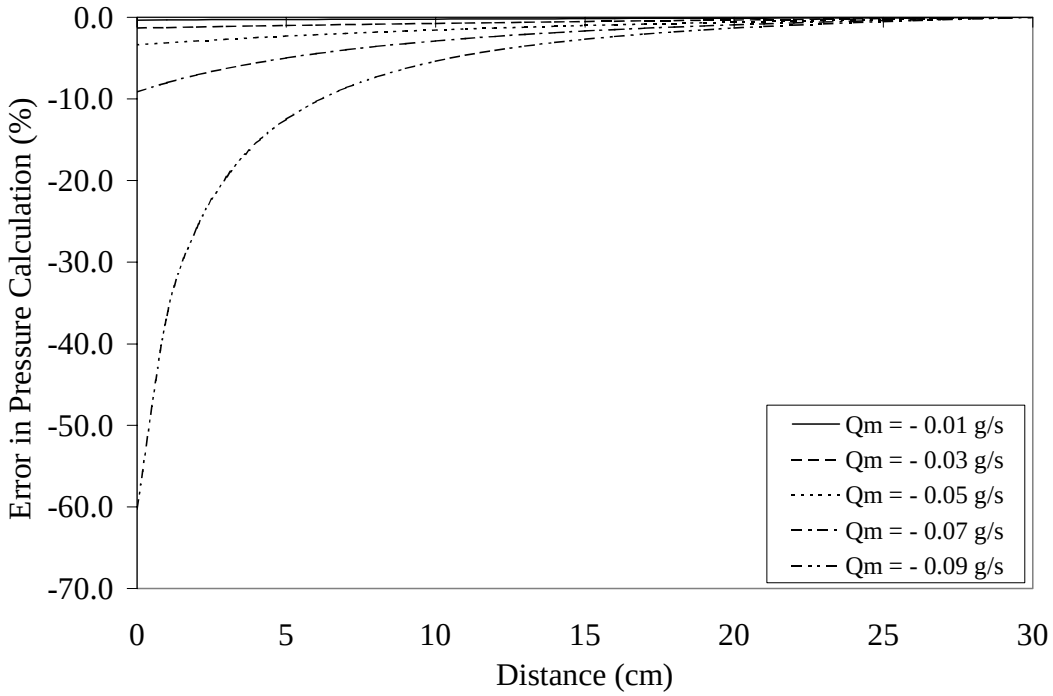

Figure 4.4 Error in pressure computation as a function of mass flow rate and distance when gas slippage is neglected ($k_{rg}k_{i(x)} = 1.0 \times 10^{-08}$cm^2).

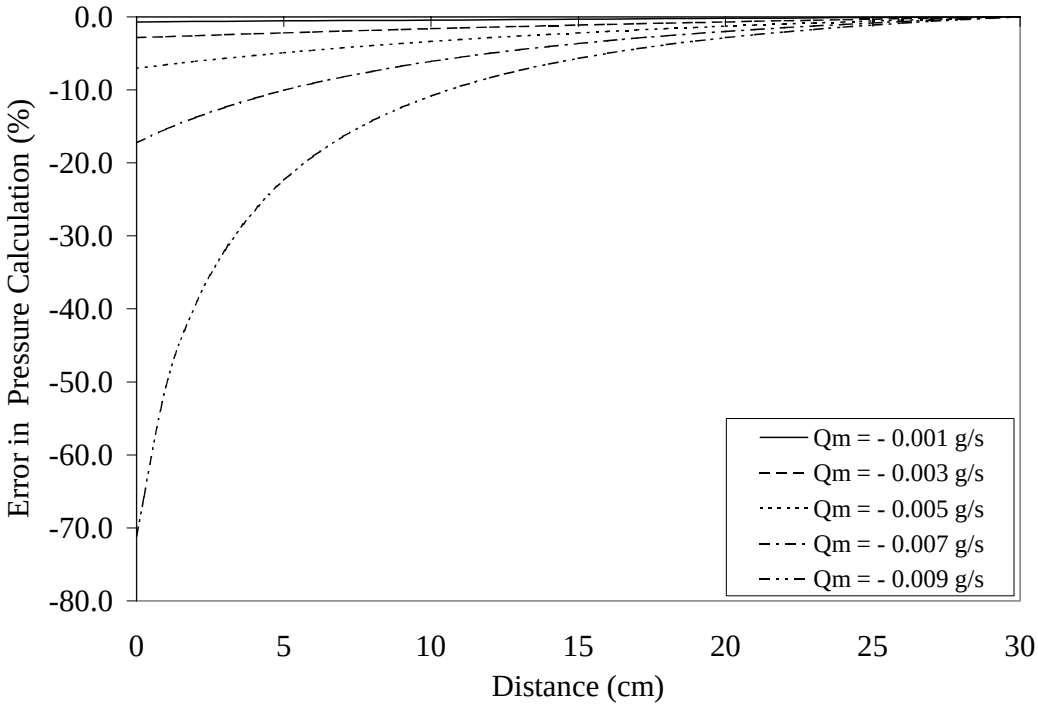

Figure 4.5 Error in pressure computation as a function of mass flow rate and distance when gas slippage is neglected ($k_{rg}k_{\iota(x)} = 1.0 \times 10^{-09} cm^2$).

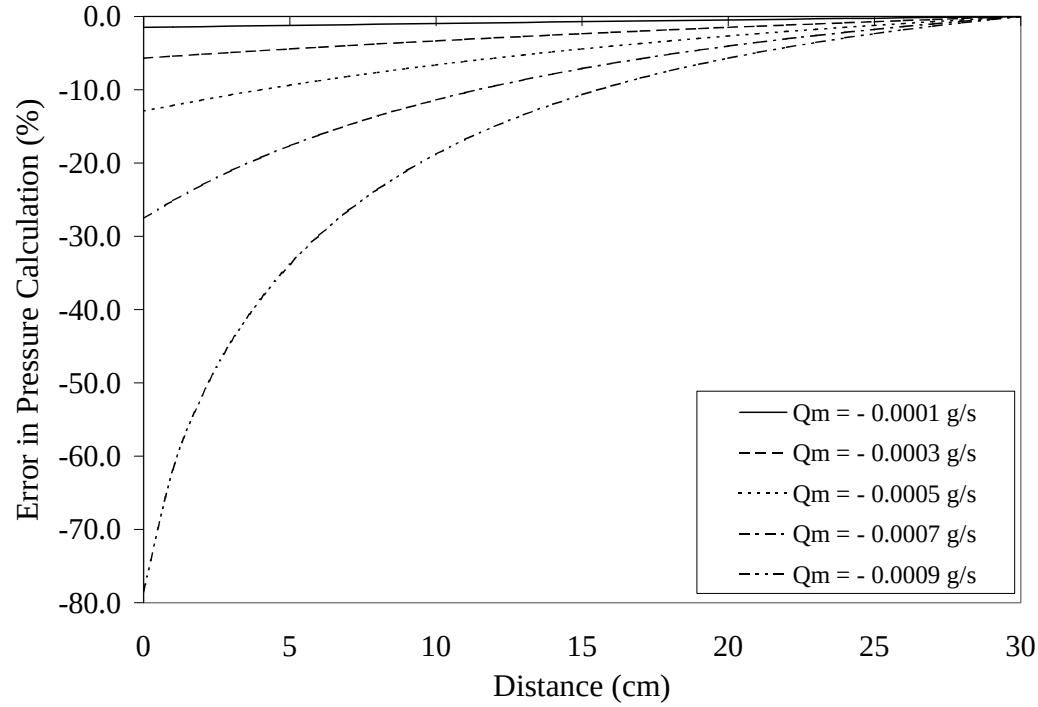

Figure 4.6 Error in pressure computation as a function of mass flow rate and distance when gas slippage is neglected ($k_{rg}k_{\iota(x)} = 1.0 \times 10^{-10} cm^2$).

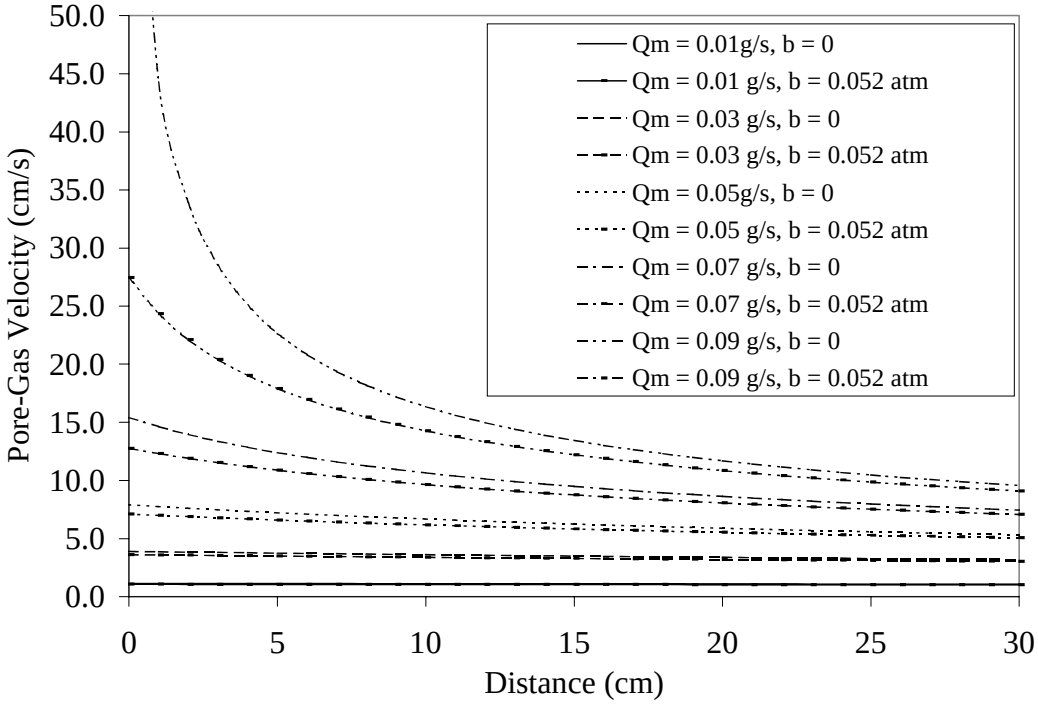

Figure 4.7 Pore-gas velocity computation as a function of mass flow rate, distance, and gas slippage ($\theta_g = 0.1$, $k_{rg}k_{i(x)} = 1.0 \times 10^{-08}$ cm^2).

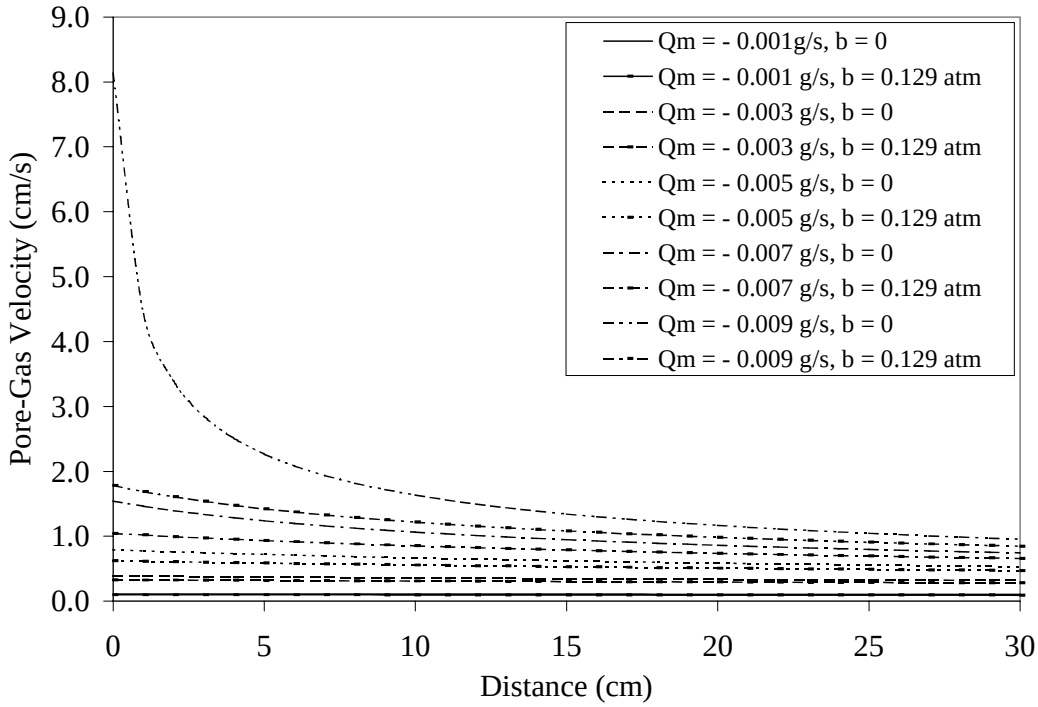

Figure 4.8 Pore-gas velocity computation as a function of mass flow rate, distance, and gas slippage ($\theta_g = 0.1$, $k_{rg}k_{i(x)} = 1.0 \times 10^{-09}$ cm^2).

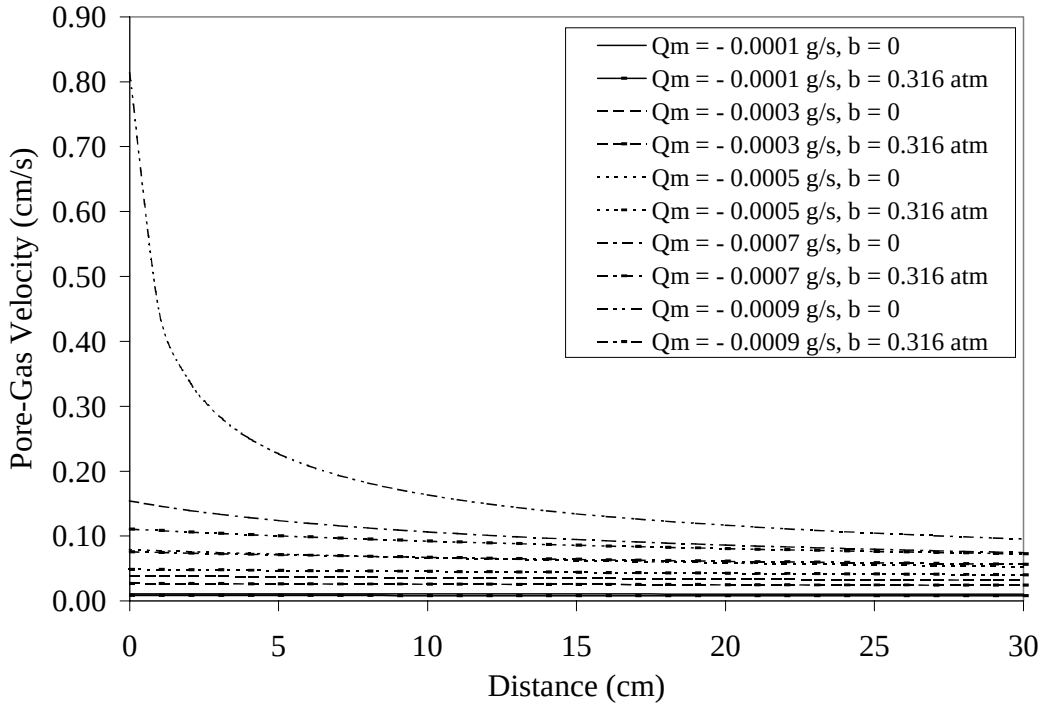

Figure 4.9 Pore-gas velocity computation as a function of mass flow rate, distance, and gas slippage ($\theta_g = 0.1$, $k_{rg}k_{i(x)} = 1.0 \times 10^{-10}$ cm^2).

Figures 4.10 through 4.12 illustrate error in pore-gas velocity calculation for slip-corrected and non-slip-corrected gas flow. Error is defined by

$$Error\ in\ pore-gas\ velocity\ calculation = \frac{v(b=0)-v(b\neq 0)}{v(b\neq 0)}. \qquad (4.18)$$

Positive values of error denote that pore-gas velocity is overestimated during vacuum application when slip flow is neglected. The magnitude of error increases with decreased absolute pressure and decreased gas permeability. As illustrated in Figure 4.12, at very low absolute pressure (near extraction point) and gas permeability, error exceeds 600%. This finding has important implications for laboratory column studies in silt or lower permeability media in which rate-limited vapor transport needs to be evaluated as a function of pore-gas velocity. The application of vacuum and neglecting gas slippage can result in a huge error in pore-gas velocity computation.

Now consider what happens during gas injection. As illustrated in Figures 4.13 through 4.15, simulated absolute pressure profiles incorporating gas slippage are lower than profiles neglecting gas slippage. During gas extraction, neglecting slippage results in underestimation of absolute pressure whereas during gas injection, neglecting gas slippage results in overestimation of absolute pressure. In both cases though, pressure differential from atmospheric pressure is

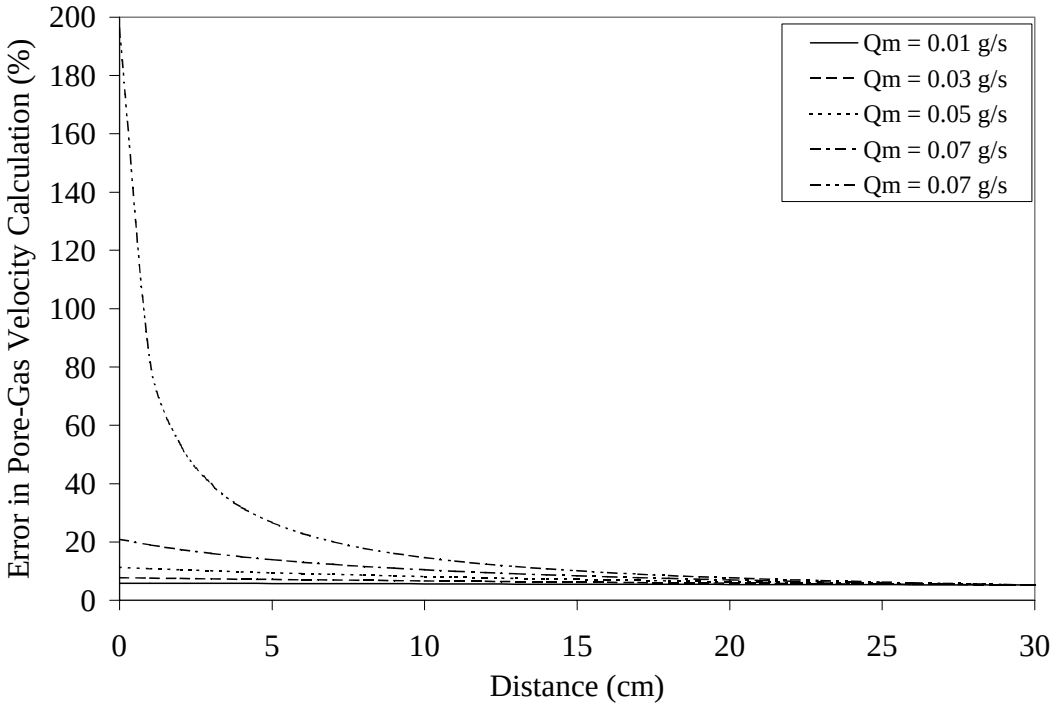

Figure 4.10 Error in pore-gas velocity computation as a function of mass flow rate and distance when gas slippage is neglected ($\theta_g = 0.1$, $k_{rg}k_{i(x)} = 1.0 \times 10^{-08}$ cm^2).

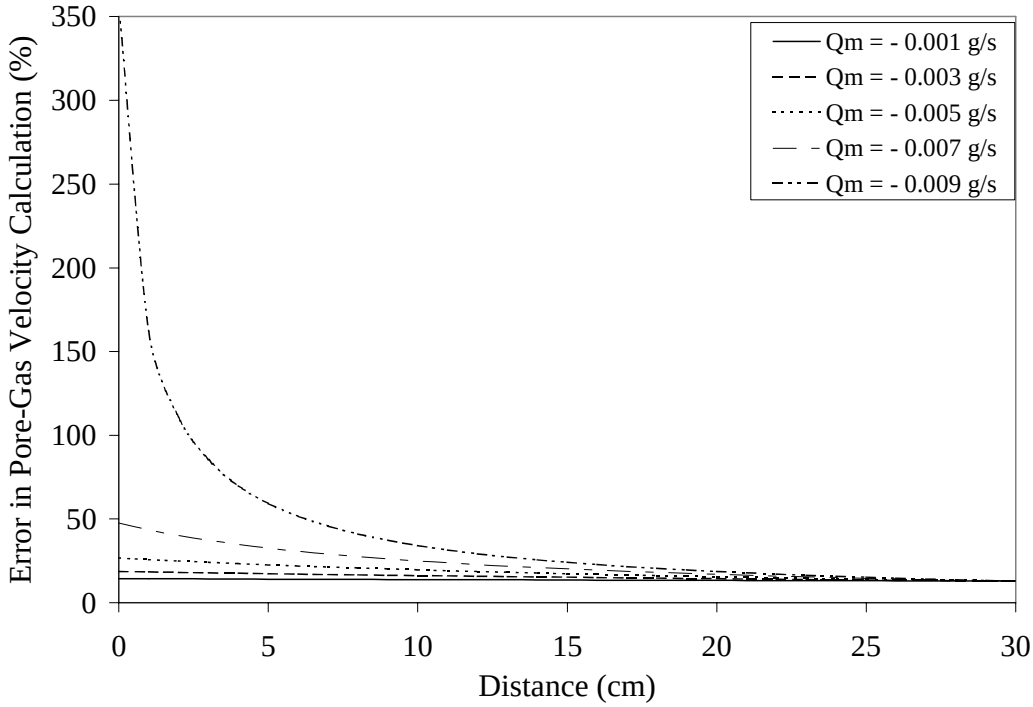

Figure 4.11 Error in pore-gas velocity computation as a function of mass flow rate and distance when gas slippage is neglected ($\theta_g = 0.1$, $k_{rg}k_{i(x)} = 1.0 \times 10^{-09}$ cm^2).

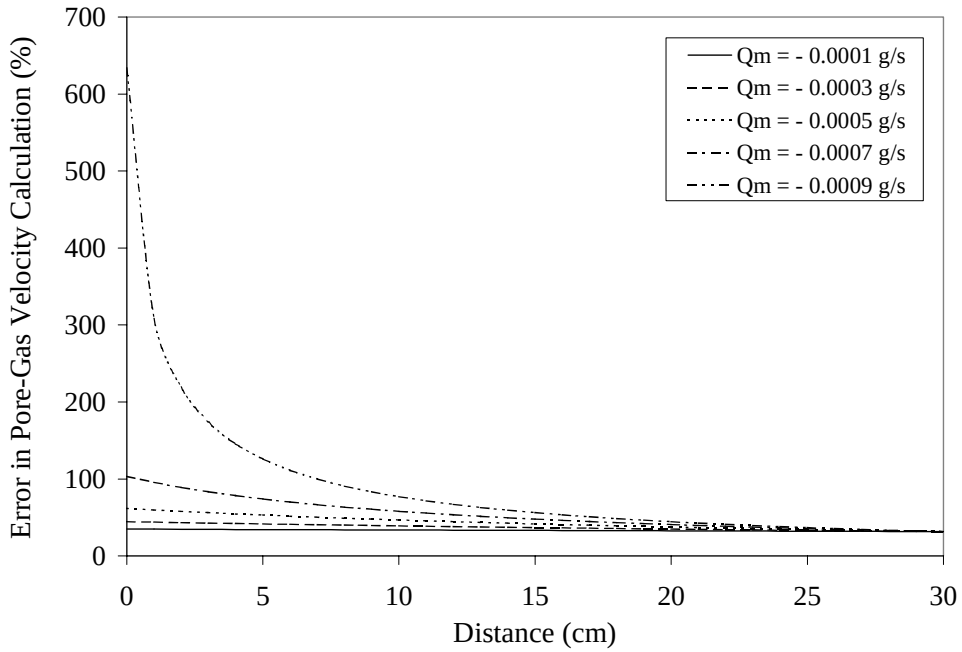

Figure 4.12 Error in pore-gas velocity computation as a function of mass flow rate and distance when gas slippage is neglected ($\theta_g = 0.1$, $k_{rg}k_{i(x)} = 1.0 \times 10^{-10}$ cm^2).

overestimated. For both gas extraction and injection, variation in pressure is greatest at the point of extraction or injection and lowest gas permeability values.

As indicated in Figures 4.16 through 4.18 however, the magnitude in error in pressure computation for gas injection is far lower than for gas extraction because of higher absolute pressures during gas injection. Even at the lowest gas permeability, maximum error does not exceed 6.0% whereas during gas extraction, error exceeded 80%. Thus, if gas slippage is neglected, gas injection should result in a better estimate of gas permeability than gas extraction. Fortunately, most permeameter testing is conducted by gas injection.

Figures 4.19 through 4.21 provide an analysis of pore-gas velocity as a function of flow rate and slip conditions during gas injection. Pore-gas velocities during gas injection are much lower than during gas extraction at the same flow rate because of increased gas density. Thus, it may be preferable to use gas injection during laboratory column studies as opposed to gas extraction to achieve lower and better controlled pore-gas velocities.

As illustrated in Figures 4.22 through 4.24, error in pore-gas velocity computation neglecting gas slippage during gas injection is much lower than during gas extraction. Similar to gas extraction though, error increases with decreased permeability. However, unlike gas extraction, error increases with distance from the point of injection. In any event, under worst case conditions, error during gas injection is less than 13% where it exceeded 600% during gas extraction simulations.

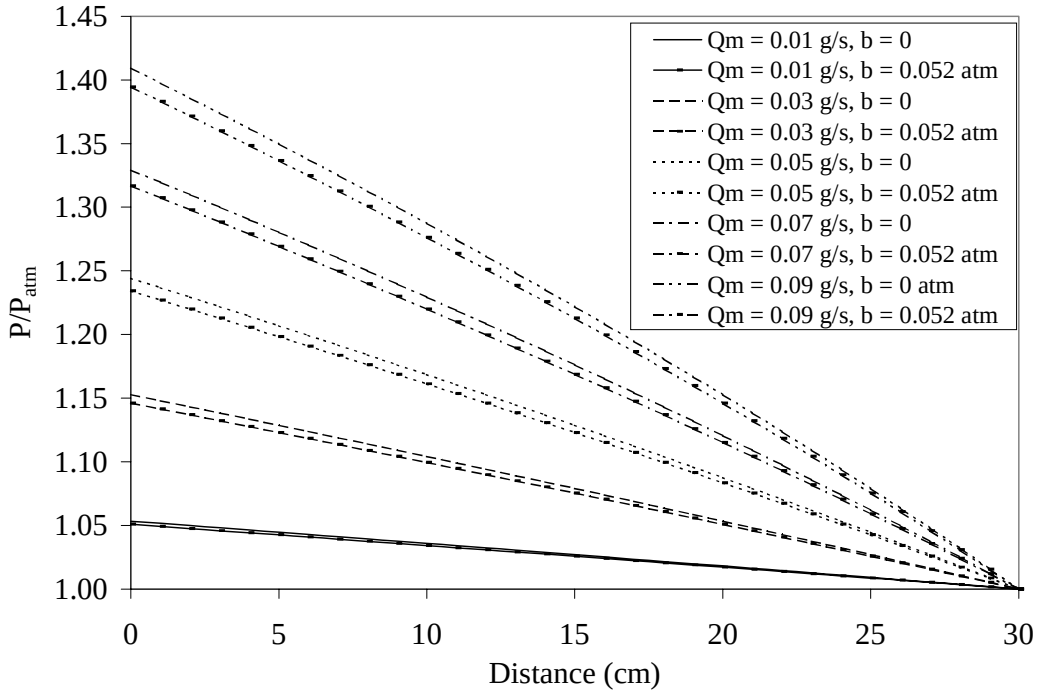

Figure 4.13 Pressure computation as a function of mass flow rate, distance, and gas slippage ($k_{rg}k_{\iota(x)}$ = 1.0 x 10^{-08} cm^2).

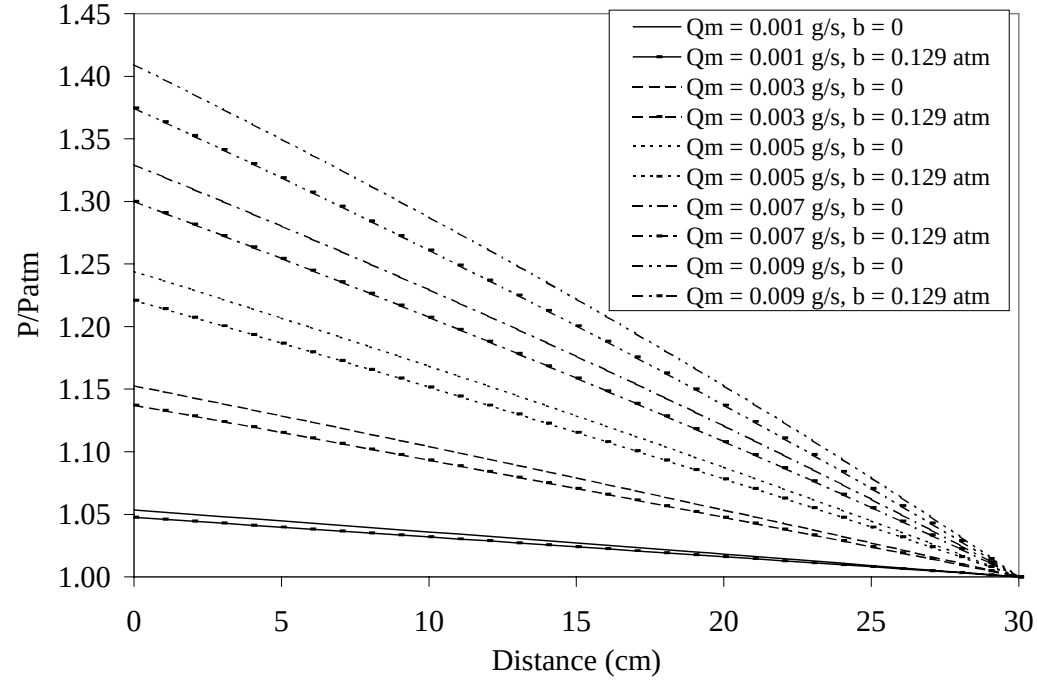

Figure 4.14 Pressure computation as a function of mass flow rate, distance, and gas slippage ($k_{rg}k_{\iota(x)}$ = 1.0 x 10^{-09} cm^2).

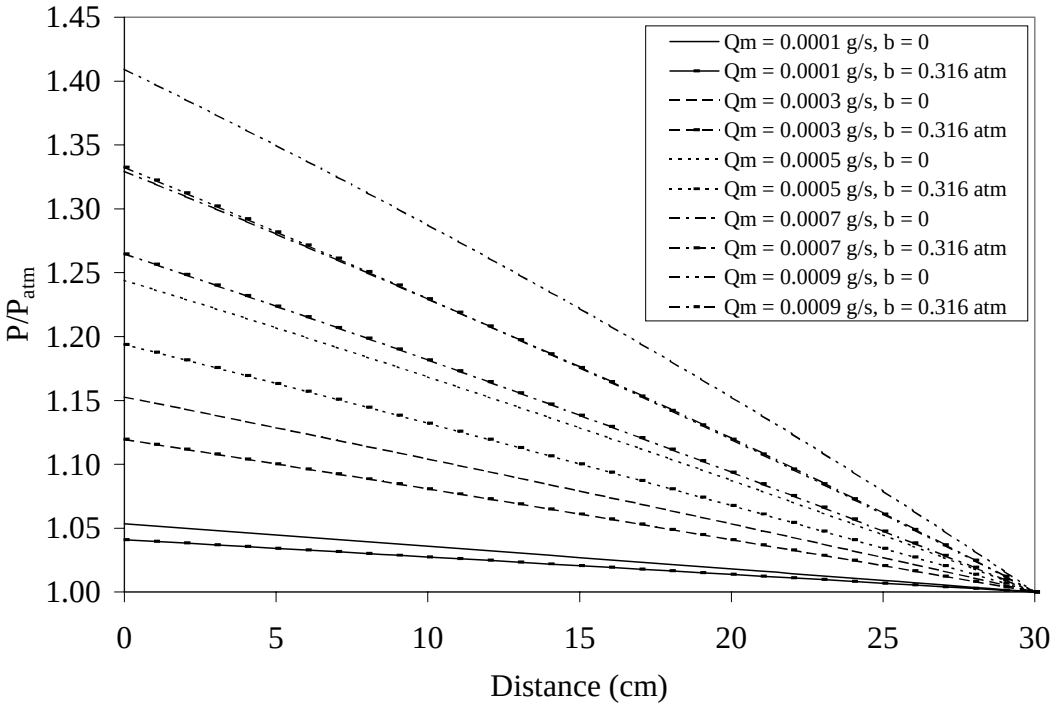

Figure 4.15 Pressure computation as a function of mass flow rate, distance, and gas slippage. ($k_{rg}k_{i(x)} = 1.0 \times 10^{-10}$ cm^2).

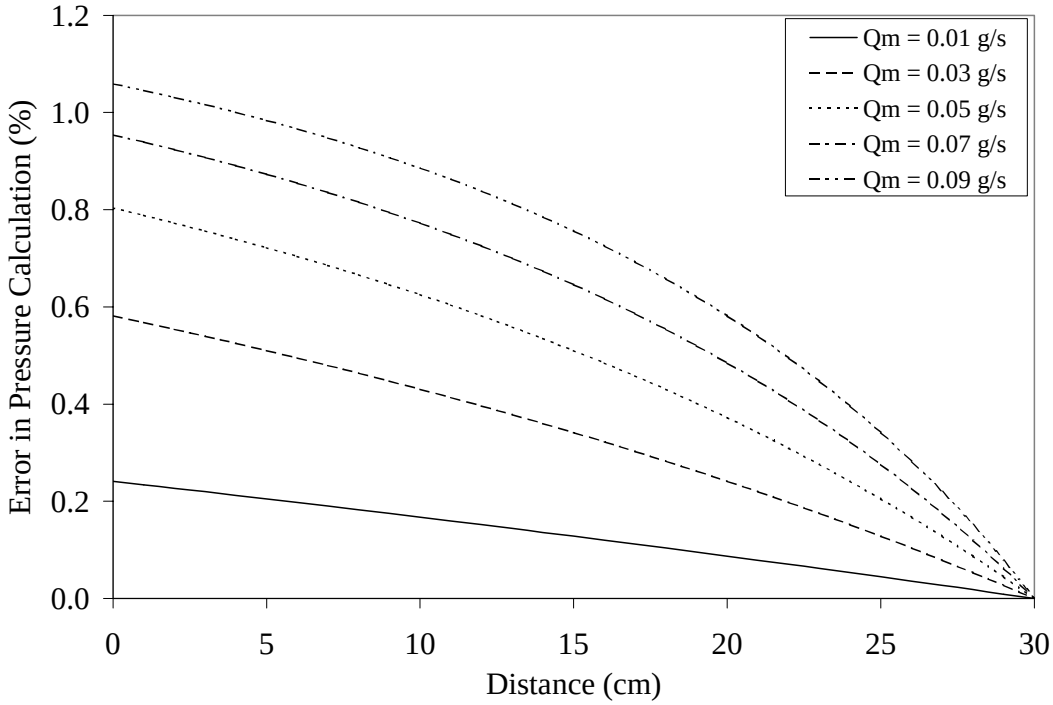

Figure 4.16 Error in pressure computation as a function of mass flow rate and distance when gas slippage is neglected ($k_{rg}k_{i(x)} = 1.0 \times 10^{-08}$cm^2).

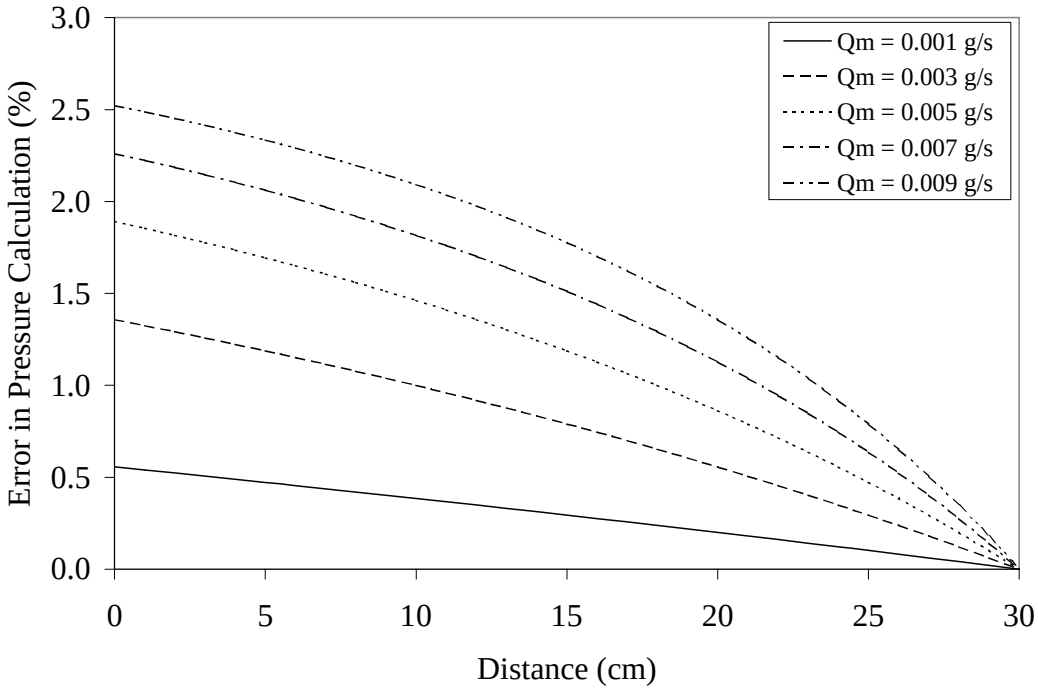

Figure 4.17 Error in pressure computation as a function of mass flow rate and distance when gas slippage is neglected ($k_{rg}k_{\iota(x)} = 1.0 \times 10^{-9} cm^2$).

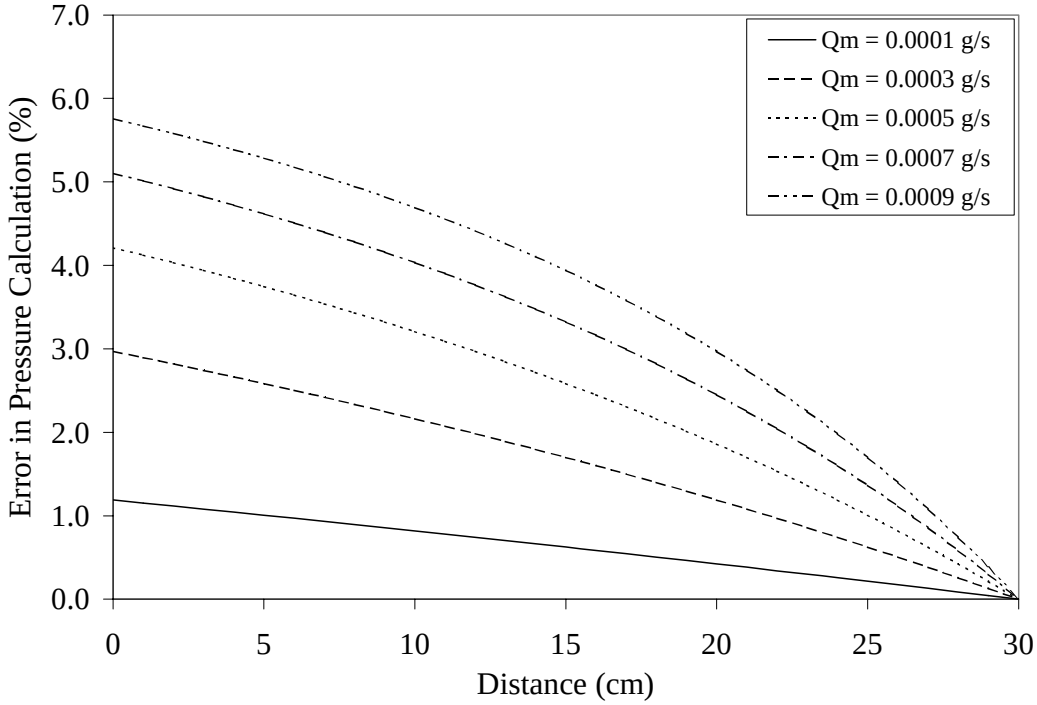

Figure 4.18 Error in pressure computation as a function of mass flow rate and distance when gas slippage is neglected ($k_{rg}k_{\iota(x)} = 1.0 \times 10^{-10}\ cm^2$).

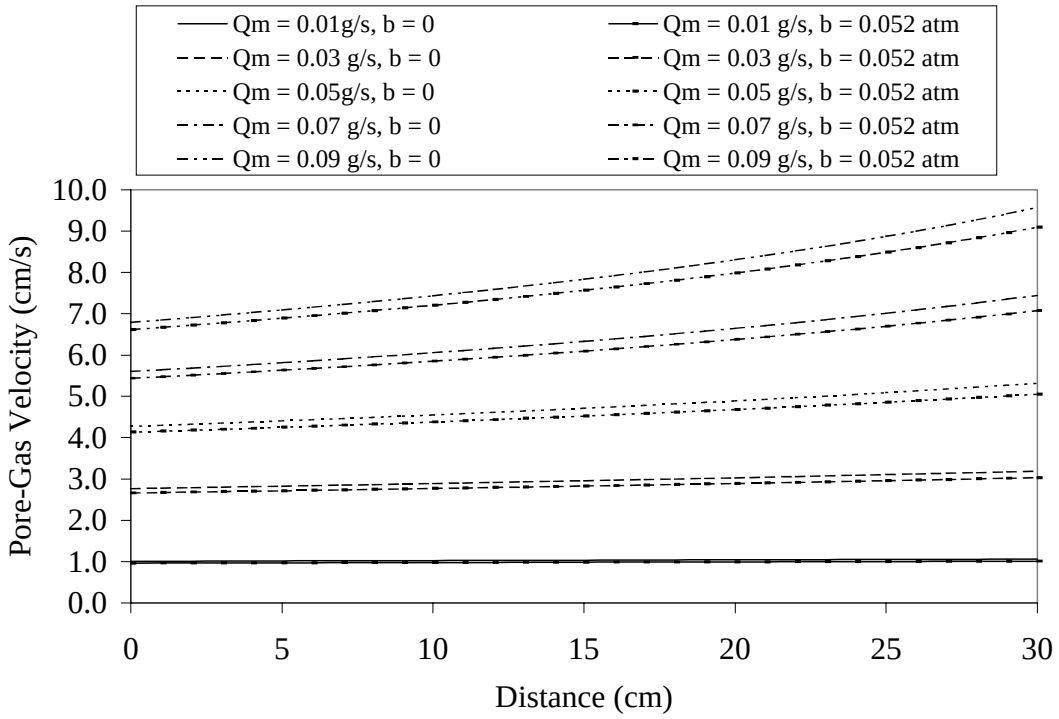

Figure 4.19 Pore-gas velocity computation as a function of mass flow rate, distance, and gas slippage ($\theta_g = 0.1$, $k_{rg}k_{i(x)} = 1.0 \times 10^{-08}$ cm^2).

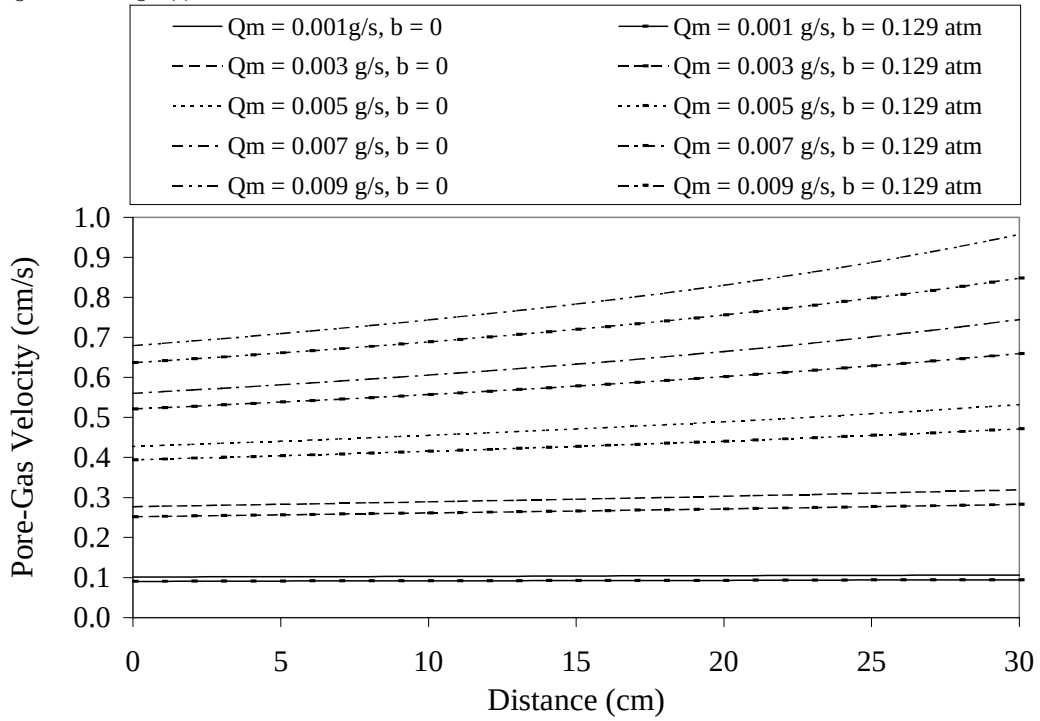

Figure 4.20 Pore-gas velocity computation as a function of mass flow rate, distance, and gas slippage ($\theta_g = 0.1$, $k_{rg}k_{i(x)} = 1.0 \times 10^{-09}$ cm^2).

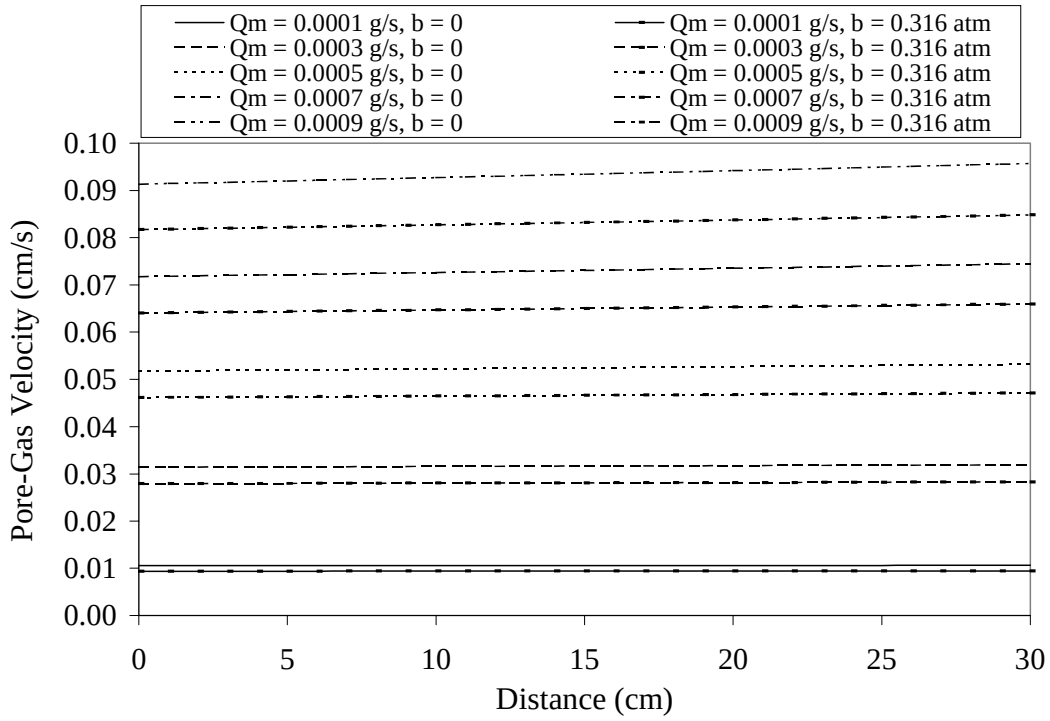

Figure 4.21 Pore-gas velocity computation as a function of mass flow rate, distance, and gas slippage ($\theta_g = 0.1$, $k_{rg}k_{i(x)} = 1.0 \times 10^{-10}$ cm^2).

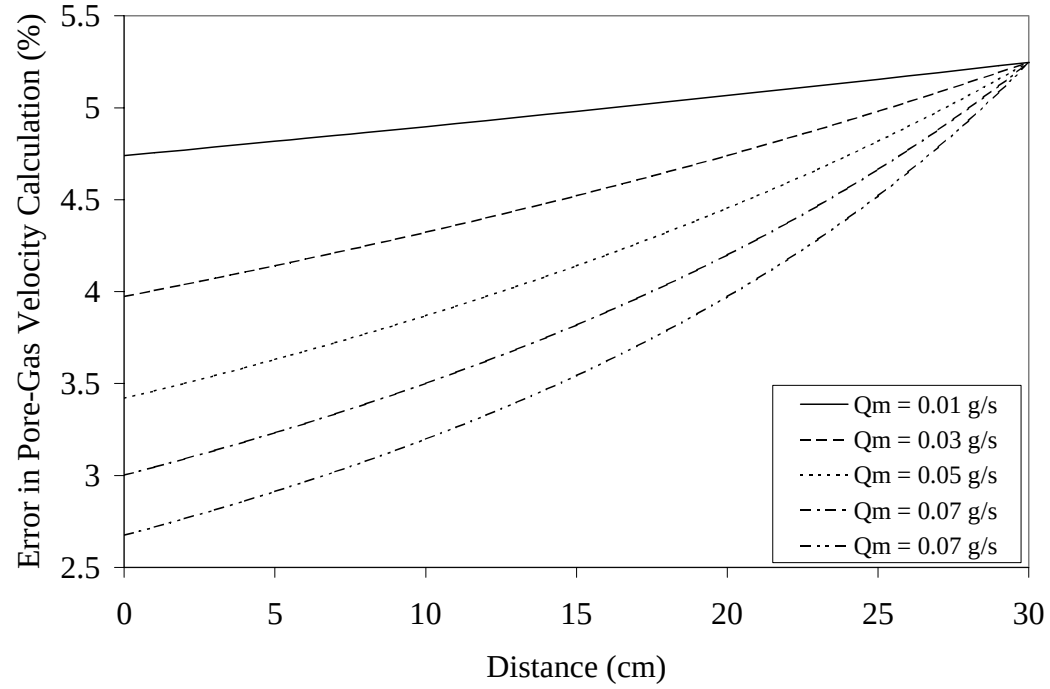

Figure 4.22 Error in pore-gas velocity computation as a function of mass flow rate and distance when gas slippage is neglected ($\theta_g = 0.1$, $k_{rg}k_{i(x)} = 1.0 \times 10^{-08}$ cm^2).

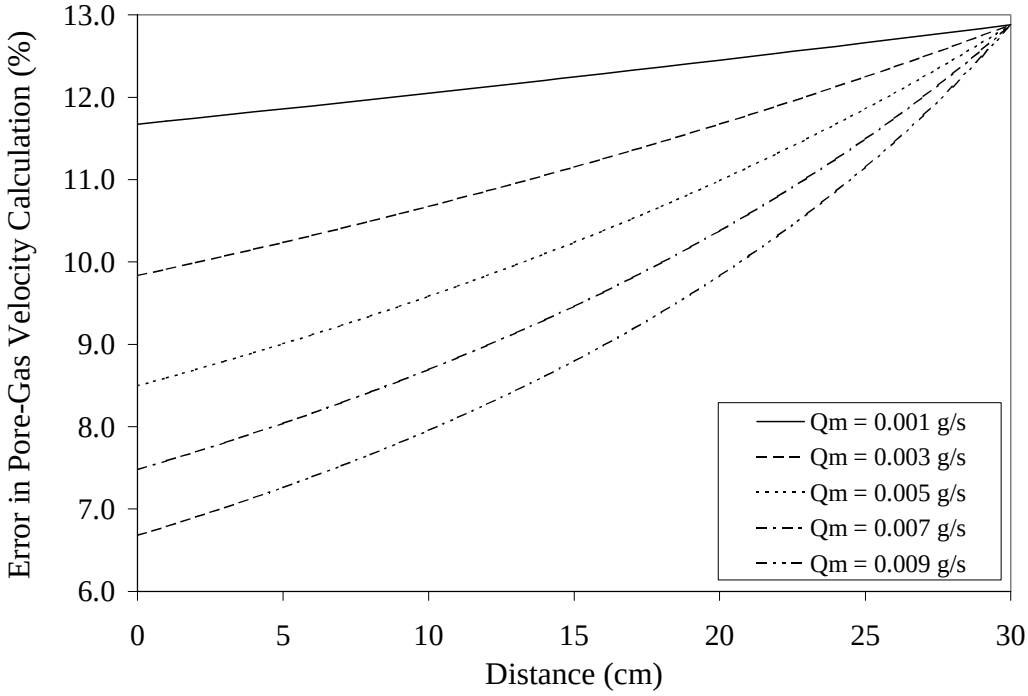

Figure 4.23 Error in pore-gas velocity computation as a function of mass flow rate and distance when gas slippage is neglected ($\theta_g = 0.1$, $k_{rg}k_{i(x)} = 1.0 \times 10^{-09}$ cm^2).

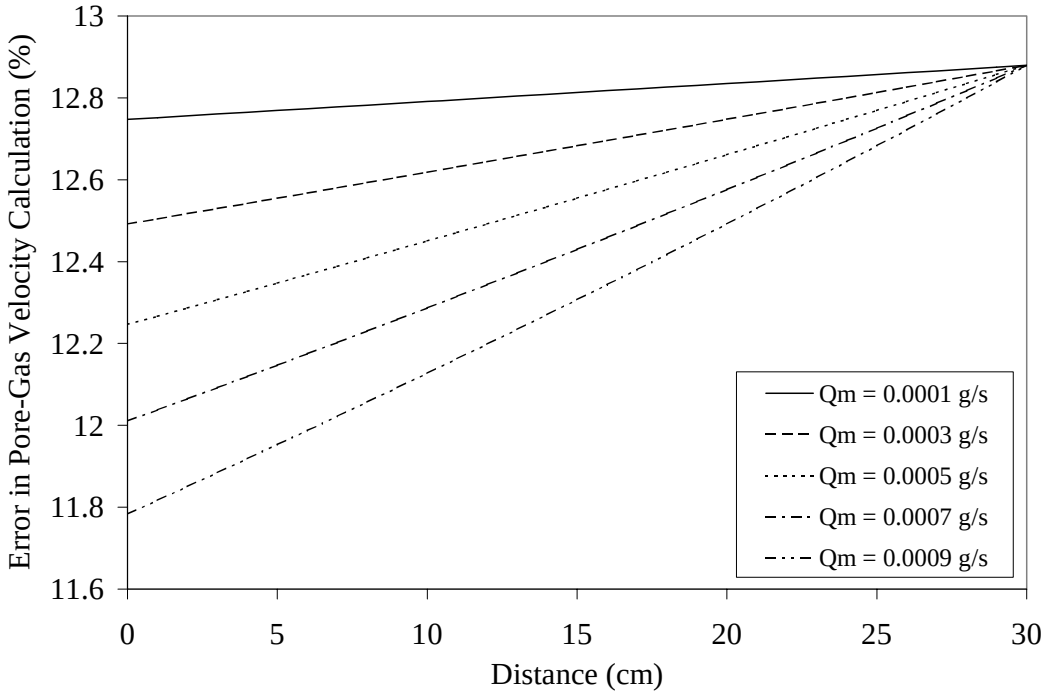

Figure 4.24 Error in pore-gas velocity computation as a function of mass flow rate and distance when gas slippage is neglected ($\theta_g = 0.1$, $k_{rg}k_{i(x)} = 1.0 \times 10^{-10}$ cm^2).

4.4 Minipermeamter Testing

Minipermeameter testing provides a rapid, nondestructive, inexpensive means of obtaining gas permeability estimates in exposed consolidated media or surface soils. One potential application for venting design is estimation of vertical gas permeability of a leaky confining layer (e.g., asphalt or concrete cap). Basic operation involves compression of a tip seal against rock or other test media through which gas is injected. Pressure differential and flow rate are then recorded to estimate gas permeability. Characteristics of the resulting flow field and sample support (volume of media affected) are dictated by the dimensions of the tip seal. To date, most minipermeameter studies have been performed using a single, small (about 0.31 cm inner radius) tip seal (Tidwell and Wilson, 1997). Originally developed in the petroleum industry (Eijpe and Weber,1971) for rapid field and laboratory acquisition of permeability data, the gas minipermeameter has found widespread use in characterizing the spatial distribution of permeability in outcrops as well as rock cores and slabs. Studies have been performed on a wide range of geologic media including eolian sandstones (Chandler et al., 1989; Goggin et al., 1988b), fluvial sandstones (Dreyer et al., 1990; Davis et al., 1993), carbonates (Kittridge et al., 1990) and volcanic tuffs (Fuller and Sharp, 1992). Three basic minipermeameter designs exist: a nonsteady, or pressure decay (Jones, 1992), high volume steady-state (e.g., Sharp et al., 1993), and low volume steady-state (Davis et al., 1994). Davis et al.'s (1994) method was designed to avoid particle movement in weakly lithified rocks and unconsolidated media typical of subsurface hydrology investigations. They used a glass syringe containing a piston falling under its own weight to inject air and demonstrated that the piston was capable of providing a small but constant pressure and flow rate over a period of several seconds. Using fabricated sandstone cores, Davis et al. (1994) found that their minipermeameter apparatus compared well with a minipermeameter using a constant supply of air. Their apparatus however underestimated gas permeability compared to one-dimensional core testing using the ASTM D4525 method. They state that this may be due to a scale effect. According to the analysis of Goggin et al. (1988a), the volume affected by gas flow is roughly a hemisphere with a radius four times the internal tip seal radius. For Davis et al.'s (1994) apparatus, this suggests that the volume affected is approximately 7.4 cm^3 whereas gas flowed through 100 cm^3 in one-dimensional column studies.

Tidwell and Wilson (1997) used a gas minipermeameter termed "multisupport permeameter" (MSP) to investigate permeability upscaling. They state that one of the major problems in aquifer/petroleum reservoir characterization stems from technological constraints that limit the measurement of material properties to sample support (volume of media sampled) much smaller than those that can be accommodated in current predictive models. This disparity in support requires measured data to be averaged or upscaled to yield effective properties at the computational grid block scale. Tidwell and Wilson (1997) state that quantitative investigation of permeability upscaling requires that measurement at different supports be consistent in four basic ways. First multisupport permeability data must be collected from the same physical sample, thus requiring the measurement technique to be nondestructive. Second, near exhaustive sampling is required at each support to avoid errors induced by sparse data effects. For this reason, large suites of data must be collected at each sample support, requiring measurements to

be rapid and inexpensive. Third, measurements must be sensitive to slight changes in permeability at all sample supports. Thus, measurement error must be small and consistent. Fourth, measurements must be consistent in terms of flow geometry, boundary conditions, and computational techniques as to provide a uniform basis for comparison. Also, as upscaling studies need to be performed on a wide variety of geologic media, the technique must have a large dynamic permeability range and ability to discern heterogeneities occurring at different length scales. They state that the gas minipermeameter meets these basic criteria.

Tidwell and Wilson (1997) and others use an equation developed by Goggin et al. (1988a) to estimate gas permeability

$$k_{rg}k_{i(r)} = \frac{2Q_v P_0 \mu_g}{r_i G_0\left(\frac{r_o}{r_i}\right)\left(P_0^2 - P_{atm}^2\right)} \tag{4.19}$$

where P_0 = pressure applied at the tip seal/rock interface, r_i = inner radius of tip seal [L], r_o = outer radius of tip seal [L], and $G_0(r_o/r_i)$ = geometric shape factor [-]. In this model, complexities associated with the flow field geometry are summarized by $G_0(r_o/r_i)$, a single, analytically derived, dimensionless function that varies according to the ratio of the outer tip seal radius to the inner tip seal radius. It is apparent that this equation is similar to the one-dimensional, steady-state gas flow equation when P_L is replaced by P_{atm} and (A/L) is replaced by $r_i G_0(r_o/r_i)$. For minipermeameter measurements subject to a homogenous, isotropic, semi-infinite half-space, the bounding surface of resultant gas flow field is approximated by a hemisphere (Goggin et al., 1988a). Tidwell and Wilson (1997) state that the effective radius of the bounding surface is governed primarily by the inner radius of the tip seal while the geometry of the diverging flow paths beneath the tip seal is controlled by the ratio r_o/r_i. They define the effective radius in terms of the radial distance at which the minipermeameter response is no longer sensitive to media heterogeneities. Numerical experiments conducted by Goggin et al. (1988a) indicate that the effective radius can vary from $2.5r_i$ to 4 r_i depending on whether a 10% or 5% change in minipermeameter response respectively is used as the defining criteria. Thus, variation in r_i may cause variation in permeability estimation and variation in r_o/r_i may lead variation in permeability estimation even when r_i is maintained constant. For this reason, Tidwell and Wilson (1997) used different inner radii (0.15, 0.31, 0.63, 1.27, and 2.54) in their investigations but maintained a constant r_o/r_i ratio of 2. Also, during their study, Tidwell and Wilson (1997) noted a consistent exponential decrease in permeability with increasing tip seal compression. They state that as compression stress is increased, the seal deforms into surface irregularities preventing gas flow from short-circuiting between the rock-seal interface. Thus, compression stress tests must be determined for each tip seal prior to permeability estimation. Acceptable compression then is the point where permeability estimation shows little decrease with increased compression.

4.5 Formulation of a One-Dimensional Transient Gas Flow Equation with Gas Slippage in a Semi-Infinite Domain

Derivation of an analytical solution for one-dimensional transient gas flow in a semi-infinite domain might be useful to evaluate pressure propagation as a function of time in semi-infinite media. The governing equation for one-dimensional transient gas flow is given by

$$\frac{\mu_g \theta_g}{\sqrt{\phi}} \frac{\partial \phi}{\partial t} = \frac{\partial}{\partial x}\left[k_{rg} k_{t(x)} \left(1 + \frac{b}{\sqrt{\phi}} \right) \frac{\partial \phi}{\partial x} \right] \tag{4.20}$$

A solution can be derived when equation (4.20) is subject to equation (4.2) and

$$\lim_{x \to \infty} \phi = \phi_{atm} \tag{4.21}$$

$$\phi(x, 0) = \phi_{atm} \, . \tag{4.22}$$

Use the Kirckhoff transformation modifies equation (4.21) to

$$\frac{\mu_g \theta_g}{\sqrt{\phi} + b} \frac{\partial U}{\partial t} = \frac{\partial}{\partial x}\left(k_{rg} k_{t(x)} \frac{\partial U}{\partial x} \right) \tag{4.23}$$

Allowing gas permeability to be constant, $\sqrt{\phi} = P_{atm}$ and

$$\alpha = \frac{k_{rg} k_{t(x)} \left(P_{atm} + b \right)}{\mu_g \theta_g} \tag{4.24}$$

results in

$$\frac{\partial U}{\partial t} = \alpha \frac{\partial^2 U}{\partial x^2} \tag{4.25}$$

with boundary and initial conditions:

$$\left. \frac{\partial U}{\partial x} \right|_{x=0} = -\beta \tag{4.26}$$

where

$$\beta = \frac{2Q_m \Re T \mu_g}{k_{rg} k_{t(x)} M_g A} \tag{4.27}$$

$$\lim_{x \to \infty} U = 0 \tag{4.28}$$

$$U(x,0) = 0\,. \tag{4.29}$$

Transforming the governing equation and boundary conditions to a Laplace Domain in time (s) and use of the inverse Laplace Transform from Abramowitz and Stegun (1970)

$$\frac{e^{-k\sqrt{s}}}{s^{3/2}} = 2\sqrt{\frac{t}{\pi}}\, e^{\frac{-k^2}{4t}} - k\, erfc\left(\frac{k}{2\sqrt{t}}\right) \tag{4.30}$$

where k is a constant results in

$$U(x,t) = \beta\sqrt{\alpha}\left[2\sqrt{\frac{t}{\pi}}\, \mathrm{e}^{-\frac{x^2}{4\alpha t}} - \frac{x}{\sqrt{\alpha}} erfc\left(\frac{x}{2\sqrt{\alpha t}}\right)\right] \tag{4.31}$$

where pressure is as defined in equation (4.7) and P_{atm} is substituted for P_{ref}. Equation (4.31) was checked by plugging it into (4.25) and observing no residual.

4.6 Formulation of a One-Dimensional Transient Gas Flow Equation With Gas Slippage in a Finite Domain

Now consider a finite domain where equation (4.20) is subject to equation (4.22), equation (4.2) at x = L, and

$$\phi(0,t) = \phi_{atm} \tag{4.32}$$

Again, use of the Kirckhoff transformation results in equation (4.25), with initial condition equation (4.29), a flux boundary at x = L similar to equation (4.26), and

$$U(0,t) = 0 \tag{4.33}$$

The solution is given by Carslaw and Jaeger (1959), p. 113 as:

$$U(x,t) = -\beta x + \frac{8\beta L}{\pi^2} \sum_{n=1}^{\infty} \frac{(-1)^n}{(2n+1)^2} e^{-\frac{\alpha(2n+1)^2 \pi^2 t}{4L^2}} \sin\left(\frac{(2n+1)\pi x}{2L}\right) \tag{4.34}$$

where equation (4.7) expresses the solution in terms of pressure. This solution could have potential in permeameter testing of low permeable media where pressure transducers are placed along the axis of flow.

4.7 Formulation of One-Dimensional Transient Gas Flow Equations Without Gas Slippage in a Finite Domain With Time-Dependent Boundary Conditions

Analytical solutions for one-dimensional, transient gas flow with time-dependent boundary conditions are useful when using variation in barometric pressure to estimate gas permeability in one or more layers. The method is based upon the observation that when atmospheric pressure changes at land surface, gas moves to or from the vadose zone to maintain a pressure balance between gas in the soil and the atmosphere. The rate of gas movement and the resultant rate of pressure change at depth are affected by both the gas permeability and gas-filled porosity of materials in the vadose zone (Weeks, 1978).

Movement of gas to and from the vadose zone due to variation in barometric pressure was first analyzed by Buckingham (1904). He presented an equation for the attenuation of the amplitude and phase lag of a periodic atmospheric pressure wave at any depth in a homogeneous layer bounded below by an impermeable boundary (e.g., water table). Later Stallman (1967) and Stallman and Weeks (1969) measured variation in barometric pressure and pressure variation at depth to determine in situ vertical gas permeability. Their method was based on the assumption that the unsaturated materials comprised a single homogeneous layer. Using the same assumptions, Roza et al. (1975) used an analytical solution and the principle of superposition to determine gas permeability of material comprising several nuclear chimneys (vertical sections of bedrock containing rubble caused by subsurface nuclear explosions) at the Nevada Test Site. The nuclear chimney rubble was assumed to consist of a homogeneous unit extending to infinity below land surface. Although the assumption that air movement can occur to infinite depth did not accurately represent actual boundary conditions, computed gas permeabilities compared well with those determined by numerical analysis of air injection data. Weeks (1978) used the methods of Stallman (1967) and Weeks and Stallman (1969) to estimate the gas permeability of discrete layers. He determined the gas permeability of each layer through trial and error. He ignored gas compressibility, assuming that it would result in insignificant error due to the relatively small magnitude of barometric pressure variations.

Consider the one-dimensional gas flow equation without gas slippage (since pressure differential is very low)

$$\frac{\mu_g \theta_g}{\sqrt{\phi}} \frac{\partial \phi}{\partial t} = k_{rg} k_{\iota(x)} \frac{\partial^2 \phi}{\partial x^2} \tag{4.35}$$

subject to an initial condition allowing pressure variation with distance

$$\phi(x,0) = f(x) \tag{4.36}$$

a no flux boundary at the water table (x = 0)

$$\left.\frac{\partial \phi}{\partial x}\right|_{x=0} = 0 \tag{4.37}$$

and time-dependent pressure variation at the surface (x = L)

$$\phi(L,t) = f(t) \tag{4.38}$$

The solution is given by Carslaw and Jaeger (1959), p. 104 as:

$$\phi(x,t) = \frac{2}{L} \sum_{n=0}^{\infty} e^{-\frac{\alpha(2n+1)^2 \pi^2 t}{4L^2}} \cos\left(\frac{(2n+1)\pi x}{2L}\right) \left\{ \frac{(2n+1)\pi\alpha(-1)^n}{2L} \int_0^t e^{\frac{\alpha(2n+1)^2 \pi^2 t'}{4L^2}} f(t')dt' + \int_0^L f(x') \cos\left(\frac{(2n+1)\pi x'}{2L}\right) dx' \right\} \tag{4.39}$$

where without gas slippage

$$\alpha = \frac{k_{rg} k_{\iota(x)} P_{atm}}{\mu_g \theta_g} . \tag{4.40}$$

If pressure variation is allowed at both boundaries then

$$\phi(0,t) = f_1(t) \tag{4.41}$$

$$\phi(L,t) = f_2(t) \tag{4.42}$$

The solution for this situation is given by Carslaw and Jaeger (1959), p. 104 as:

$$\phi(x,t) = \frac{2}{L}\sum_{n=1}^{\infty} e^{\frac{-\alpha n^2\pi^2 t}{L^2}} \sin\left(\frac{n\pi x}{L}\right)$$
$$\left\{\int_0^L f(x')\sin\left(\frac{n\pi x'}{L}\right)dx' + \frac{n\alpha\pi}{L}\int_0^t e^{\frac{\alpha n^2\pi^2 t'}{L^2}}\left[f_1(t') - (-1)^n f_2(t')\right]dt'\right\} \quad (4.43)$$

Shan (1995) used these two solutions to present two scenarios for testing: (1) a domain consisting of a region between the water table and the soil surface or at some depth in soil, and (2) a domain between any two points within the soil. The latter scenario provides a method to evaluate pneumatic permeability in discrete layers. Both methods require a minimum of three measurement points; one on each boundary and one between boundaries.

4.8 Formulation of the Pseudo-Steady-State Radial Gas Flow Equation

The pseudo-steady-state radial flow equation is the equation most commonly used by venting practitioners to estimate gas permeability in the field. The governing ordinary differential equation describing radial, pseudo-steady-state, confined gas flow is expressed as:

$$\frac{d^2\phi}{dr^2} + \frac{1}{r}\frac{d\phi}{dr} = 0 \quad (4.44)$$

with boundary conditions:

$$\phi(r_I) = \phi_I \quad (4.45)$$

$$r\frac{d\phi}{dr}\bigg|_{r=r_w} = -\frac{Q_m \Re T \mu_g}{M_g \pi d k_{rg} k_{t(r)}}. \quad (4.46)$$

The solution for the pseudo-steady-state flow equation is easily derived and given by:

$$\phi(r) = \phi_I + \frac{Q_m \Re T \mu_g}{M_g \pi d k_{rg} k_{t(r)}} \ln\left(\frac{r_I}{r}\right) \qquad r_I > r \quad (4.47)$$

where ϕ_I = pressure squared at r_I $[(ML^{-1}T^{-2})^2]$, r_I= arbitrary radial distance (radius of influence or ROI) at which a constant pressure is prescribed [L], r = radial distance from well center line [L], r_w = radius of well and filter pack [L], d = thickness of domain [L], and k_r = radial pneumatic permeability $[L^2]$.

Notice that in equation (4.47), when Q_m is negative (air extraction), ϕ goes to infinity as

the radius goes to infinity. When Q_m is positive (air injection), ϕ goes to negative infinity as the radius goes to infinity. Thus, the prefix "pseudo" reflects the fact that there is no true steady-state solution to the radial flow equation unless a constant pressure boundary (i.e., ROI) is specified since flow is assumed to occur under non-leaky or confined conditions. The limitations of using the pseudo-steady-state radial flow equation for gas permeability estimation will be discussed in detail in section 6 where a ROI data set from an actual site is used to estimate gas permeability.

4.9 Formulation of the Radial Transient Confined Gas Flow Equation

The transient, radial flow equation is expressed as:

$$\frac{\theta_g \mu_g}{\sqrt{\phi}} \frac{\partial \phi}{\partial t} = k_{rg} k_{t(r)} \left(\frac{\partial^2 \phi}{\partial r^2} + \frac{1}{r} \frac{\partial \phi}{\partial r} \right) \tag{4.48}$$

with boundary conditions:

$$r \lim_{r \to \infty} \phi = \phi_{atm} \tag{4.49}$$

$$r \lim_{r \to 0} \frac{\partial \phi}{\partial r} = -\frac{Q_m \Re T \mu_g}{\pi k_{rg} k_{t(r)} dM_g} \tag{4.50}$$

A solution to transient, radial flow equation using these boundary conditions, Laplace Transforms and the assumption that $\sqrt{\phi} = P_{atm}$ gives:

$$\phi(r,t) = \phi_{atm} + \frac{Q_m \Re T \mu_g}{2\pi d k_{rg} k_{t(r)} M_g} \int_u^\infty \frac{e^{-\tau}}{\tau} d\tau \tag{4.51}$$

where

$$u = \frac{\theta_g \mu_g r^2}{4 k_{rg} k_{t(r)} t P_{atm}} \tag{4.52}$$

The solution to equation (4.48) given by Johnson et al. (1988,1990a,b) is:

$$P' = \frac{Q_m \Re T \mu_g}{4\pi k_{rg} k_{t(r)} M_g dP_w} \int_u^\infty \frac{e^{-\tau}}{\tau} d\tau \tag{4.53}$$

where u is a previously defined and P' is a gauge pressure. The solution is obtained in P

instead of P^2 because Johnson et al. (1988, 1990a,b) linearized the radial, transient equation by letting $P^2 = P*P_{atm}$ instead of explicitly solving for P^2. As discussed in section 3.10, this linearization approach can lead to significant error when pressure differential exceeds 0.5 atmospheres. The integral on the right-hand-side of the equation is the well known exponential integral. When $u < 0.01$, it can be approximated by:

$$\int_u^{\infty} \frac{e^{-\tau}}{\tau} d\tau = -0.57721 - \ln u \qquad (4.54)$$

Regardless of the linearization procedure, derivations of both equations (4.51) and (4.53) require homogeneous conditions in addition to: (1) strict radial flow, (2) completely impermeable upper and lower boundaries (no leakage from the surface), (3) no wellbore storage (line sink). Beckett and Huntley (1994) modified the Hantush and Jacob (1955) equation for transient radial flow in a semi-confined domain by applying the linearization $P^2 = P*P_{atm.}$

4.10 Conclusions

1. While not representative of fully three-dimensional field-scale gas flow, one-dimensional testing and analysis can provide insight into fundamental processes such as the effect of compressibility and gas slippage on pressure and pore-gas velocity profiles. Analysis of one-dimensional gas flow is especially important in designing and interpreting laboratory column vapor mass transport studies where knowledge of pore-gas velocity profiles becomes critical. Because field-scale tests provide estimation of gas permeability over an integrated volume of porous media too large to discern small discrete layers of less permeable materials (e.g., lenses of silt and clay), gas permeability estimation in minimally disturbed or reconstructed samples could be useful in determining small-scale gas permeability variation in subsurface media.

2. When attempting to evaluate small-scale gas permeability variation in the field, use of permeameters such as those described by Corey (1986), Stonestrom (1987), and Springer et al. (1988) provide the opportunity of determining capillary pressure - gas permeability curves but require repacking of soil samples thereby compromising pneumatic sample integrity. Use of shelby tubes during core collection allows collection of "minimally" disturbed cores, but elimination of short-circuiting along the tube wall can not be guaranteed during testing. It would appear that while all laboratory-scale methods involve some degree of compromise in sample integrity, there is currently no other means to estimate gas permeability on the scale of centimeters in the field.

3. The governing equation for one-dimensional, steady-state gas flow incorporating gas slippage was derived and used to assess the impact of gas slippage on one-dimensional pressure and pore-gas velocity simulation. During gas extraction, neglecting gas slippage results in underestimation of absolute pressure whereas during air injection, neglecting gas slippage results in overestimation of absolute pressure. In both cases though, pressure

differential from atmospheric pressure is overestimated when neglecting gas slippage. For both gas extraction and injection, variation in pressure is greatest at the point of extraction or injection and at lower gas permeability values. However, the magnitude in error in pressure computation for gas injection was far lower than for gas extraction because of higher absolute pressures during gas injection. Even at the lowest gas permeability, maximum error for gas injection did not exceed 6.0% whereas during gas extraction, error exceeded 80%. Thus, if gas slippage is neglected, gas injection should result in a better estimate of gas permeability than gas extraction. Pore-gas velocities during gas injection were much lower than during gas extraction at the same flow rates because of increased gas density. Error in pore-gas computation neglecting gas slippage during gas injection was much lower than during gas extraction. Similar to gas extraction, error during gas injection increased with decreased permeability. However, unlike gas extraction, error increased with distance from the point of injection. Maximum pore-gas velocity computation error during simulations was less than 13% whereas it exceeded 600% during gas extraction simulations. Thus, for vapor transport column studies, it would seem that lower and better controlled pore-gas velocity profiles can be attained through gas injection.

5. TWO-DIMENSIONAL, AXISYMMETRIC, STEADY-STATE GAS PERMEABILITY ESTIMATION, PORE-GAS VELOCITY CALCULATION, AND STREAMLINE GENERATION IN A DOMAIN OPEN TO THE ATMOSPHERE

Field-scale estimation of gas permeability and subsequent computation of pore-gas velocity profiles are critical elements of sound soil venting design. Many venting practitioners however are unaware of equations and data interpretation methods appropriate for gas permeability estimation and pore-gas velocity computation. In this section, the governing equation for unconfined (open to the atmosphere), steady-state, axisymmetric cylindrical flow is presented along with an analytical solution derived by Baehr and Hult (1991). Data collected from a U.S. Coast Guard Station in Traverse City, Michigan is used to demonstrate gas permeability estimation, pore-gas velocity calculation, and streamline generation in a domain open to the atmosphere.

5.1 Model Formulation

The governing equation for unconfined (open to the atmosphere), steady-state, axisymmetric cylindrical flow is:

$$k_{rg} k_{t(r)} \left(\frac{\partial^2 \phi}{\partial r^2} + \frac{1}{r} \frac{\partial \phi}{\partial r} \right) + k_{rg} k_{t(z)} \frac{\partial^2 \phi}{\partial z^2} = 0 \, . \tag{5.1}$$

When subject to the following boundary conditions:

$$\phi(r, 0) = \phi_{atm} \tag{5.2}$$

$$\lim_{r \to \infty} \phi(r, z) = \phi_{atm} \tag{5.3}$$

$$\frac{\partial \phi}{\partial z}(r, d) = 0 \tag{5.4}$$

$$\frac{\partial \phi}{\partial r}(r_w, z) = 0, \qquad 0 < z < d_U \tag{5.5}$$

$$\frac{\partial \phi}{\partial r}(r_w, z) = \frac{-Q_m \Re T \mu_g}{\pi k_{rg} k_{t(r)} r_w (d_L - d_U)}, \qquad d_U < z < d_L \tag{5.6}$$

$$\frac{\partial \phi}{\partial r}(r_w, z) = 0, \qquad d_L < z < d \, . \tag{5.7}$$

Baehr and Hult (1991) provide a solution as follows

$$\phi = \phi_{atm} + \frac{2eQ_m\mu_g \Re T}{M_g \pi^2 r_w k_{rg} k_{\iota(r)} (d_L - d_U)} \left\{ \sum_{n=1}^{\infty} \frac{1}{m} \left[\frac{\cos\left(\frac{m\pi d_U}{d}\right) - \cos\left(\frac{m\pi d_L}{d}\right)}{\frac{m\pi}{d} K_1\left(\frac{m\pi}{d}\frac{r_w}{e}\right)} \right] K_0\left(\frac{m\pi}{d}\frac{r}{e}\right) \sin\left(\frac{m\pi z}{d}\right) \right\} \tag{5.8}$$

where

$$m = n - 1/2, \qquad e = \left(\frac{k_{rg} k_{\iota(r)}}{k_{rg} k_{\iota(z)}} \right)^{1/2} \tag{5.9}$$

and z = vertical distance below land surface [L], d_U = vertical distance to top of sand pack or well screen [L], d_L = vertical distance to bottom of sand pack or well screen [L], $k_{rg}k_{\iota(z)}$ = vertical gas permeability [L^2], K_0 = zero-order modified Bessel functions of the second kind, K_1 = first-order modified Bessel functions of the second kind, ϕ_{atm} = atmospheric pressure squared [$(ML^{-1}T^{-2})^2$]. Shan et al. (1992) solved equation (5.1) by approximating the well as a line sink of uniform strength. They argue that while this approximation leads to errors in simulating the pressure distribution in the immediate vicinity of a well screen, these errors are not expected to be large. Baehr and Hult's (1991) finite-radius solution though is generally preferred because it is more accurate near a wellbore, easy to program, and is utilized in the public domain gas permeability code AIR2D (Joss and Baehr, 1997). However, further work on steady-state analysis of gas flow which shows promise for field application continues (Warrick and Rojano, 1999)

Radial specific discharge, q_r [LT^{-1}], is calculated by

$$q_r = -\frac{1}{2} \frac{k_{rg} k_{\iota(r)}}{\mu_g} \frac{1}{\sqrt{\phi}} \frac{\partial \phi}{\partial r} \tag{5.10}$$

where

$$\frac{\partial \phi}{\partial r} = -\frac{2Q_m \mu_g \Re T}{M_g \pi^2 k_{rg} k_{\iota(r)} (d_L - d_U) r_w} \sum_{n=1}^{\infty} \frac{1}{m} \left[\frac{\cos\left(\frac{m\pi d_U}{d}\right) - \cos\left(\frac{m\pi d_L}{d}\right)}{K_1\left(\frac{m\pi}{d}\frac{r_w}{e}\right)} \right] K_1\left(\frac{m\pi}{d}\frac{r}{e}\right) \sin\left(\frac{m\pi z}{d}\right) \tag{5.11}$$

Vertical specific discharge, q_z [LT^{-1}], is calculated by

$$q_z = -\frac{1}{2} \frac{k_{rg} k_{\iota(z)}}{\mu_g} \frac{1}{\sqrt{\phi}} \frac{\partial \phi}{\partial z} \tag{5.12}$$

where

$$\frac{\partial \phi}{\partial z} = \frac{2eQ_m \mu_g \Re T}{M_g \pi^2 k_{rg} k_{t(r)} (d_L - d_U) r_w} \sum_{n=1}^{\infty} \frac{1}{m} \left[\frac{\cos\left(\frac{m\pi d_U}{d}\right) - \cos\left(\frac{m\pi d_L}{d}\right)}{K_1\left(\frac{m\pi}{d}\frac{r_w}{e}\right)} \right] K_0\left(\frac{m\pi}{d}\frac{r}{e}\right) \cos\left(\frac{m\pi z}{e}\right). \tag{5.13}$$

Pore-velocity is calculated by dividing specific discharge by the volumetric gas content conducting air flow. For venting design though, it is the norm, q [LT^{-1}], of the vector pair that is of interest which is calculated by

$$q = \sqrt{q_r^2 + q_z^2}\ . \tag{5.14}$$

In a domain open to the atmosphere, streamfunction computation is helpful to visualize the fraction of flow to a well as a function of radial distance. In homogeneous isotropic media, Cauchy-Riemann equations can be used to generate orthogonal families of equipotential and streamline curves. In anisotropic media, equipotential and streamline curves are not orthogonal but equations relating potential and streamfunction can be expressed by (Bear1972, p.235):

$$\frac{\partial \phi}{\partial r} = \frac{1}{r}\left(\frac{k_{rg} k_{t(z)}}{k_{rg} k_{t(r)}}\right)^{1/2} \frac{\partial \psi}{\partial z} \tag{5.15}$$

$$\frac{\partial \phi}{\partial z} = -\frac{1}{r}\left(\frac{k_{rg} k_{t(r)}}{k_{rg} k_{t(z)}}\right)^{1/2} \frac{\partial \psi}{\partial r}. \tag{5.16}$$

Solving for the streamfunction ψ results in

$$\psi(r,z) = \frac{2derQ_m \mu_g \Re T}{M_g \pi^3 k_{rg} k_{t(r)} (d_L - d_U) r_w} \sum_{n=1}^{\infty} \frac{1}{m^2} \left[\frac{\cos\left(\frac{m\pi d_U}{d}\right) - \cos\left(\frac{m\pi d_L}{d}\right)}{K_1\left(\frac{m\pi}{d}\frac{r_w}{e}\right)} \right] K_1\left(\frac{m\pi}{d}\frac{r}{e}\right) \cos\left(\frac{m\pi z}{d}\right)$$

$$+ const \tag{5.17}$$

Examination of this equation reveals that the streamfunction is undefined at r = 0 since

$$\lim_{r \to 0^+} K_1(r) = \infty\ . \tag{5.18}$$

Also, $\psi(r,b)$ equals a constant streamline along the lower impermeable boundary [$\cos(m\pi)=0$] or capillary fringe which will be set to zero. Normalized streamfunction values can now be calculated by dividing by the calculated streamfunction by the maximum streamfunction value. The difference in normalized streamfunction values then is equivalent to percent flow to the venting well. The analytical solution presented here for computation of the streamfunction is for a finite-radius well which differs from Shan's et al. (1992) solution for a line source/sink.

5.2 Computational Method

In the public domain program AIR2D (Joss and Baehr, 1997) a non-linear data fitting algorithm

$$\min imize \quad \sum_{i=1}^{N} \left(P(r_i, z_i) - \widehat{P}(r_i, z_i) \right)^2 \tag{5.19}$$

is used to estimated $k_{rg}k_{\iota(r)}$ and $k_{rg}k_{\iota(z)}$. The method serves to minimize the objective function, *f*, where $P(r_i, z_i)$ is the estimated pressure and $\widehat{P}(r_i, z_i)$ is the observed pressure at the observation point. Unlike linear fitting least squares fitting however, non-linear least squares fitting does not guarantee the minimum least squares solution. Non-linear fitting algorithms sometimes find a local minimum rather than a global minimum which represents the true least squares solution. Thus, good starting estimates are essential for non-linear algorithms. A different approach to estimation of $k_{rg}k_{\iota(r)}$ and $k_{rg}k_{\iota(z)}$ was pursued here to circumvent, to some degree, problems with finding a global minium. Random guesses (groups of 5000) constrained within decreasing intervals of $k_{rg}k_{\iota(r)}$ and $k_{rg}k_{\iota(z)}$ were used until the lowest root mean squared error (RMSE) defined

$$RMSE = \sqrt{\frac{\sum_{i=1}^{N} \left(p(r_i, z_i) - \widehat{p}(r_i, z_i) \right)^2}{n}} \tag{5.20}$$

was attained and the best 10 to 100 random guesses for $k_{rg}k_{\iota(r)}$ and $k_{rg}k_{\iota(z)}$ were constant. For instance, the first 5000 guesses were constrained for $k_{rg}k_{\iota(r)}$ values ranging from 1.0×10^{-10} to 1.0×10^{-06} cm^2 with $k_{rg}k_{\iota(r)}/k_{rg}k_{\iota(z)}$ ratios allowed to vary from 0.1 to 10.0. Examination of the RMSE for the top 100 guesses quickly revealed that by far the best guesses centered around a variation of k_r between 1.0×10^{-07} to 1.0×10^{-06} cm^2 with $k_{rg}k_{\iota(r)}/k_{rg}k_{\iota(z)}$ ratios between 1.0 and 5.0. The next 5000 guesses were then constrained within these limits to further narrow the estimation range. This procedure was continued 3 more times for a total of 25,000 guesses until estimates of $k_{rg}k_{\iota(r)}$ and $k_{rg}k_{\iota(r)}/k_{rg}k_{\iota(z)}$ ratios and RMSE for top 100 guesses were identical. Using this procedure, each guess can be individually examined to ensure that the set of lowest RMSE values do not give significantly different $k_{rg}k_{\iota(r)}$ and $k_{rg}k_{\iota(r)}/k_{rg}k_{\iota(z)}$ estimates. While somewhat tedious (taking 10 to 15 minutes for each flow rate in this application), this approach provided considerable insight

into the parameter estimation process and confidence in parameter estimates. Huang et al. (1999) used a trial-and-error approach for estimation of gas permeability and also argued that this type of approach offers the modeler insight into the parameter estimation process.

A FORTRAN program, MFROAINV, was written to facilitate parameter estimation computations. The source code and sample input and output files are included in Appendix A. Another FORTRAN program, SAIRFLOW was written to facilitate computation of pore-gas velocity and streamlines for one well in a domain open to the atmosphere. The source code and sample input and output files are included in Appendix B.

5.3 Site Description

A series of gas permeability tests were conducted at the U.S. Coast Guard Aviation Station in Traverse City, Michigan in April, 1990 to aid in design of a soil venting project. The Coast Guard reported that contamination of soil and ground water had been caused by an accidental release of an estimated 132,000 liters of aviation fuel in 1969. The spill created a ground-water plume about 80 meters wide and 300 meters long. Previous soil sampling efforts revealed that most of the mass from the spill was confined to a narrow band above and below the water table. Soils were characterized as well-sorted, coarse-grained sand with an mean grain size of 0.35 mm. At the time of testing, the water table was located 5.2 meters below land surface.

Wells and vapor probe clusters were installed into 15 cm diameter open boreholes drilled using hollow-stem augering. Two wells constructed of 12.5 cm diameter, schedule 40 PVC pipe were placed 6.1 meters apart. Factory slotted screens were set at 3.9 to 4.2 m below a topographically flat ground surface. As illustrated in Figure 5.1, vapor probes clusters were placed along a line between the two wells. Each vapor probe cluster consisted of three 5 cm long, 6.35 mm diameter stainless steel screens connected to the surface by 6.35 mm copper tubing and quick connectors. Probes in each cluster were placed at depths of 0.9, 2.7, and 4.2 m below ground surface. Wells and probe clusters were completed by backfilling native sand into open boreholes. Pressure gauges were installed on both wells to allow applied pressure or vacuum monitoring at the wellhead. Pressure differential in vapor probes were measured with magnehelic gauges. The lowest pressure differential that could be accurately measured with the magnehelic gauges was 0.13 cm or 0.05 inches of water or 0.00097 atm as wind appeared to affect readings below that level. Flow was measured with pitot tubes installed upgradient of wells.

5.4 Results and Discussion

Seven vacuum extraction tests were conducted to estimate radial and vertical gas permeability. Table 5.1 provides a summary of applied flow and pressure response while Table 5.2 provides a summary of radial and vertical gas permeability estimates for each test. Figure 5.2 illustrates observed versus simulated pressure response and a corresponding correlation coefficient (R^2) using linear regression for test 1. The other 6 tests showed similar responses and

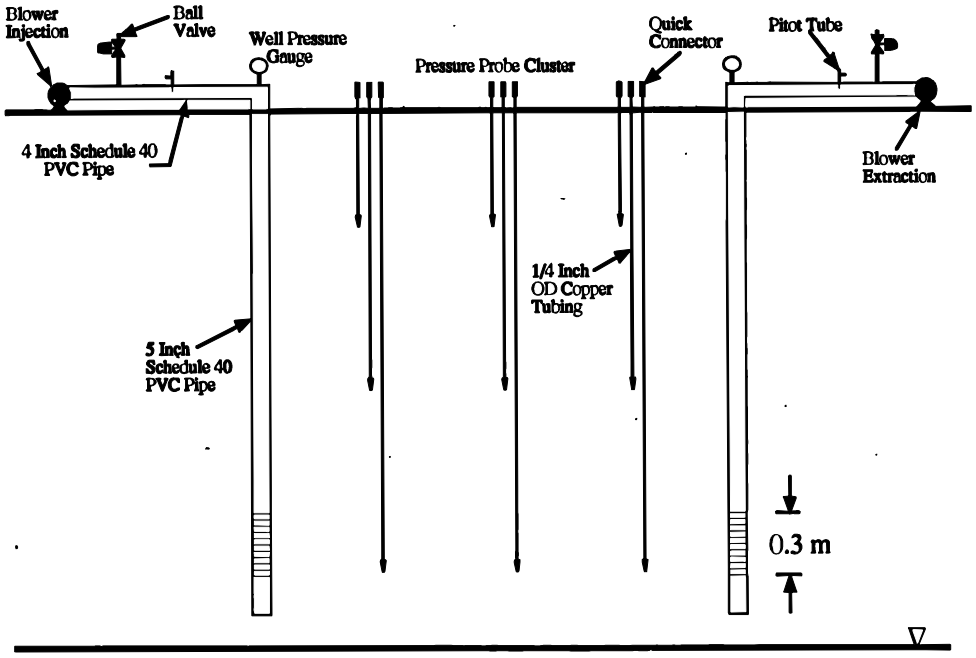

Figure 5.1 Gas permeability testing schematic at the USCG Station, Traverse City, MI

correlation coefficients. Plots of observed versus simulated pressure response did not visually indicate the presence of any systematic bias. Generally, as indicated by R^2 values in Table 5.2, observed versus simulated pressure response was good. Figure 5.3 illustrates a two-dimensional cross-sectional schematic of observed versus simulated pressure differential for test 1. Again, the other 6 tests showed a similar response. Observed versus simulated pressure differential showed close agreement providing additional confidence that gas permeability was correctly estimated and that relatively homogeneous conditions existed. The low standard deviation and 95% confidence interval (CI) for both $k_{rg}k_{\iota(r)}$ and $k_{rg}k_{\iota(r)}/k_{rg}k_{\iota(z)}$ ratio indicate reproducibility of results over a wide span of flow rates. There was no observable trend in permeability estimation as a function of applied flow and vacuum as would be expected from Klinkenberg (1941) effects (increased permeability with increased vacuum) or soil-water movement toward the well (decreased permeability with increased vacuum). Klinkenberg (1941) effects were not expected because of the high permeability of these sandy soils. Soil-water movement toward the well due to vacuum application was not expected to be significant because the sand appeared to be coarse-grained and well sorted meaning that fairly low capillary pressure would be needed to drain these soils to a low soil-water content. Examination of drill cuttings during well and probe installation appeared to indicate relatively homogeneous sand deposits. There was no indication of change in texture with depth. Thus $k_{rg}k_{\iota(r)}/k_{rg}k_{\iota(z)}$ ratios near 1.0 were expected and reasonable.

Figure 5.4 illustrates a two-dimensional, cross-sectional plot of pressure differential,

Table 5.1 Test results USCG Station, Traverse City, MI

r (cm)	**z** (cm)	**Test 1** (75.11 g/s) *P (atm)*	**Test 2** (66.57 g/s) *P (atm)*	**Test 3** (56.90 g/s) *P (atm)*	**Test 4** (47.23 g/s) *P (atm)*	**Test 5** (38.69 g/s) *P (atm)*	**Test 6** (32.43 g/s) *P (atm)*	**Test 7** (32.43 g/s) *P (atm)*
152.4	91.44	0.99803	0.99803	0.99852	0.99877	0.99926	0.99939	0.99963
152.4	274.32	0.99434	0.99434	0.99508	0.99607	0.99730	0.99779	0.99840
152.4	426.72	0.98574	0.98598	0.98820	0.99066	0.99361	0.99496	0.99607
304.8	91.44	0.99877	0.99877	0.99902	0.99926	0.99951	0.99963	0.99951
304.8	274.32	0.99680	0.99680	0.99730	0.99779	0.99877	0.99902	0.99902
304.8	426.72	0.99459	0.99434	0.99508	0.99607	0.99730	0.99791	0.99813
457.2	91.44	0.99926	0.99914	0.99939	0.99951	0.99951	0.99956	0.99970
457.2	274.32	0.99828	0.99828	0.99840	0.99877	0.99902	0.99921	0.99936
457.2	426.72	0.99730	0.99730	0.99791	0.99828	0.99862	0.99882	0.99904
609.6	91.44	0.99931	0.99924	0.99963	0.99948	0.99961	0.99970	0.99975
609.6	274.32	0.99877	0.99872	0.99926	0.99911	0.99936	0.99951	0.99961
609.6	426.72	0.99867	0.99865	0.99926	0.99907	0.99936	0.99951	0.99956
914.4	91.44	0.99961	0.99961	0.99970	0.99970	0.99975	0.99988	0.99988
914.4	274.32	0.99941	0.99948	0.99951	0.99956	0.99970	0.99988	0.99988
914.4	426.72	0.99921	0.99924	0.99934	0.99946	0.99966	0.99975	0.99975

Table 5.2 Gas permeability test summary for USCG Station, Traverse City, MI

Test	**Flow** *(g/s)*	**Pressure at well** *(atm)*	$\mathbf{k_{rg}k_{\iota(r)}}$ *(cm^2)*	$\mathbf{k_{rg}k_{\iota(z)}}$ *(cm^2)*	$\mathbf{k_{\iota(r)}/k_{\iota(z)}}$	**RMSE** *(atm)*	$\mathbf{R^2}$
1	75.11	0.877	6.10E-07	4.89E-07	1.25	6.50E-04	0.97
2	66.57	0.877	5.59E-07	4.24E-07	1.32	6.06E-04	0.96
3	56.90	0.897	5.27E-07	4.61E-07	1.14	5.24E-04	0.97
4	47.23	0.911	5.92E-07	4.41E-07	1.34	3.70E-04	0.97
5	38.69	0.941	7.50E-07	4.97E-07	1.51	2.75E-04	0.96
6	32.43	0.951	7.65E-07	5.47E-07	1.40	2.06E-04	0.97
7	32.43	0.961	1.12E-06	5.75E-07	1.95	1.45E-04	0.98
		Average	7.03E-07	4.91E-07	1.42	3.97E-04	
		Std Dev	2.05E-07	5.50E-08	0.26	2.00E-04	
		95% CI	1.52E-07	4.07E-08	0.19		

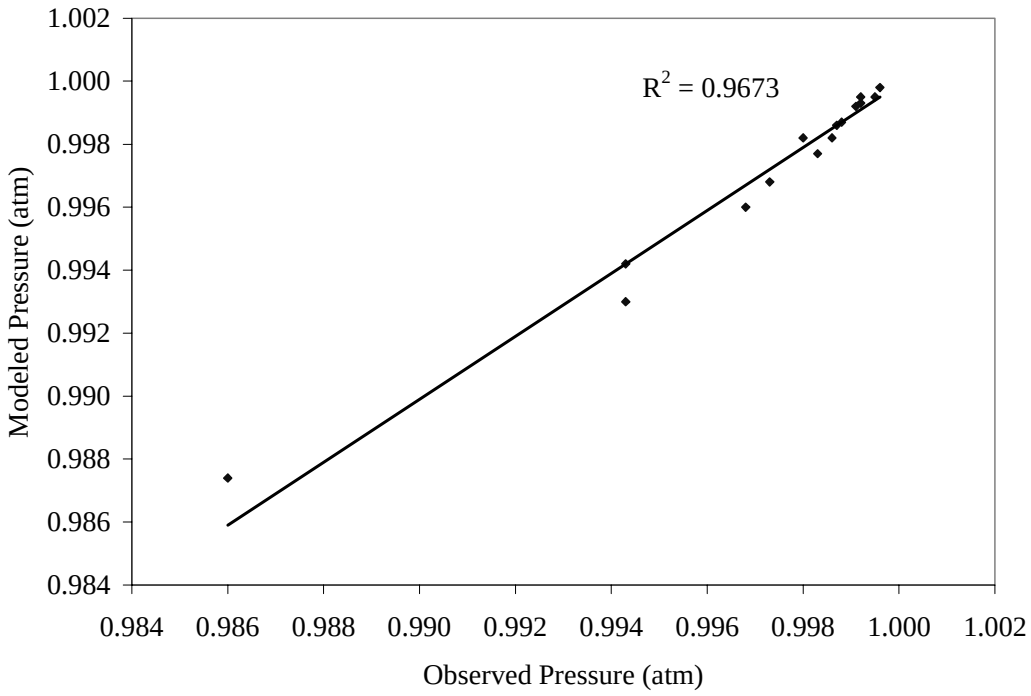

Figure 5.2 Observed versus predicted pressure for test . Applied flow and vacuum 75.11 g/s (131.8 scfm) and 0.877 atm respectively. Estimated $k_{rg}k_{\iota(r)}$ = 6.1x 10^{-07} cm^2, $k_{rg}k_{\iota(r)}/k_{rg}k_{\iota(z)}$ = 1.2, RMSE = 6.50 x 10^{-04} atm

pore-gas velocity (assuming a volumetric gas content of 0.2) , and streamlines for test 1. Each streamline originates at ground surface and terminates at the well screen. By convention, the top streamline, extending from r = 0, z = 0 to the well screen has a streamline value of one while the bottom streamline, extending from r = ∞, z = d, and up the well screen has a value of zero. This convention was used here and by Falta et al. (1993) but is the reverse of that used by Shan et al. (1992). In Figure 5.4, the area between pairs of streamlines represents 10% of flow going to the well. Iso-contours for pressure differential, velocity, and streamlines are all highly curvilinear due to the constant pressure boundary at the surface and partial penetration of the gas extraction well. Streamlines indicate that most gas recharge occurs in the immediate vicinity of the well (e.g., 70% of gas recharge occurs within 8 meters of the well). Pore-gas velocities are very high throughout the tested domain because of high gas permeability and applied flow rate (75.11 g/s or 131.8 scfm). These types of plots are useful for visualizing flow to a well. For instance, Wilson et al. (1988) and Shan et al. (1992) used plots of gas pressure and streamlines to argue that little gas flow occurs below a well screen suggesting that the screened intervals should always be placed below a zone of contamination.

Figure 5.5 illustrates pore-gas velocity along a vertical transect (depth at center point of well) as a function of radial distance and applied flow using average measured k_r and the $k_{rg}k_{\iota(r)}/k_{rg}k_{\iota(z)}$ values. Note that pore-gas velocity is on a logarithmic scale to encompass orders of magnitude decrease with increasing radial distance. An increase in mass flow at small applied

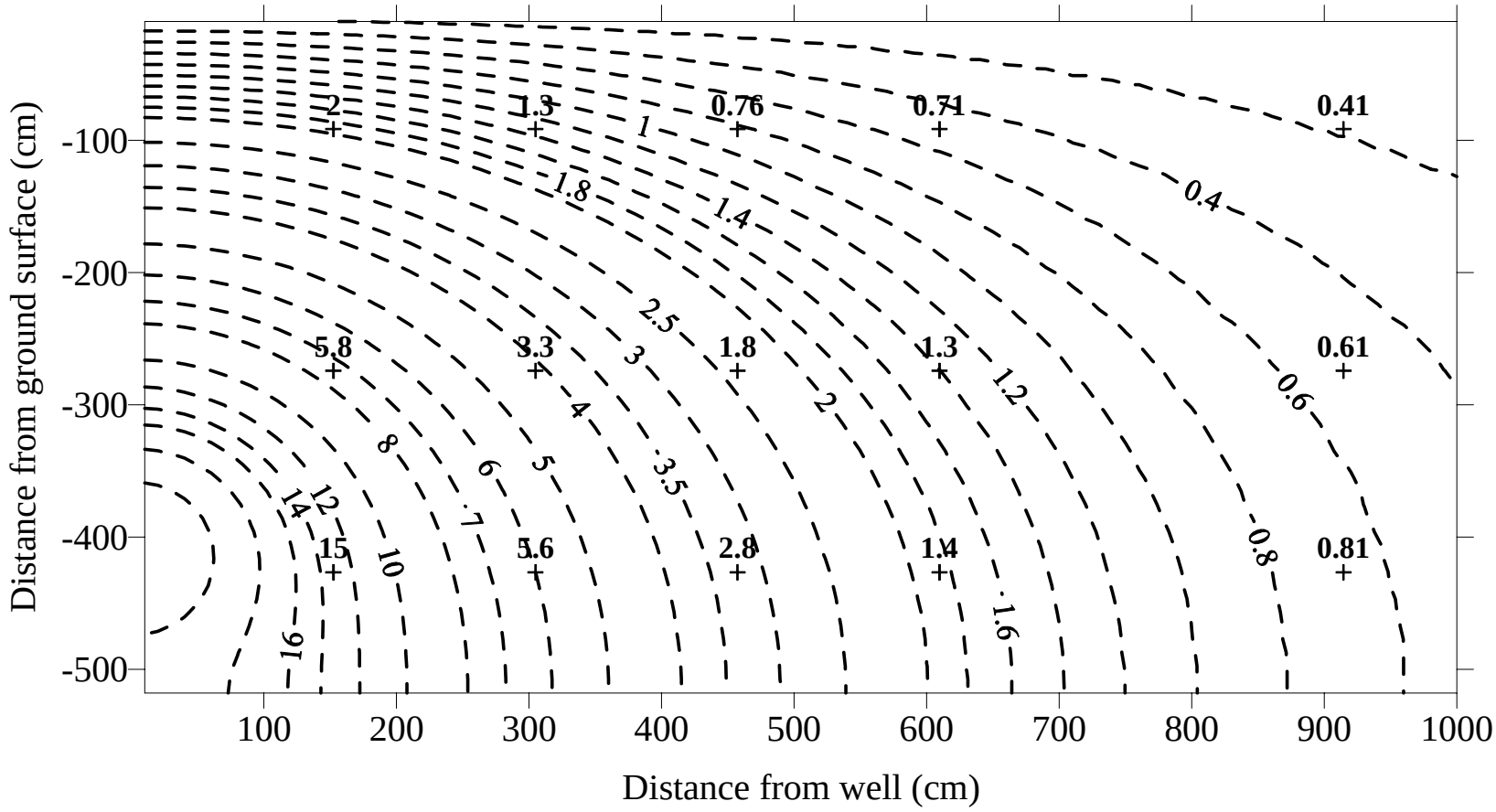

Figure 5.3 Observed (+) versus simulated (dashed lines) pressure differential (cm water) for test 1

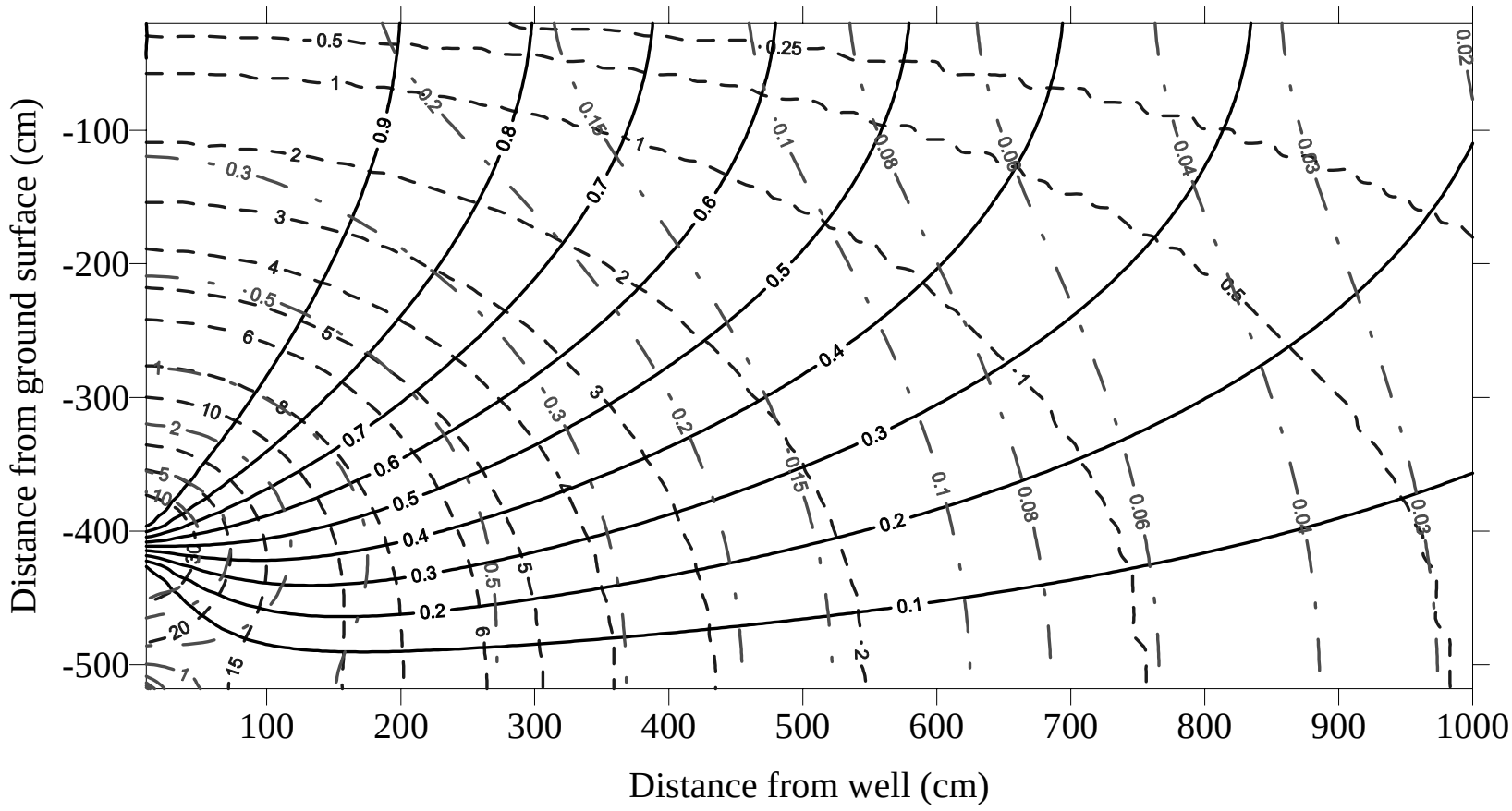

Figure 5.4. Calculated pressure differential (cm of water - dashed lines), pore-gas velocity (cm/s - dash-dot lines), and streamlines (solid lines) for test 1.

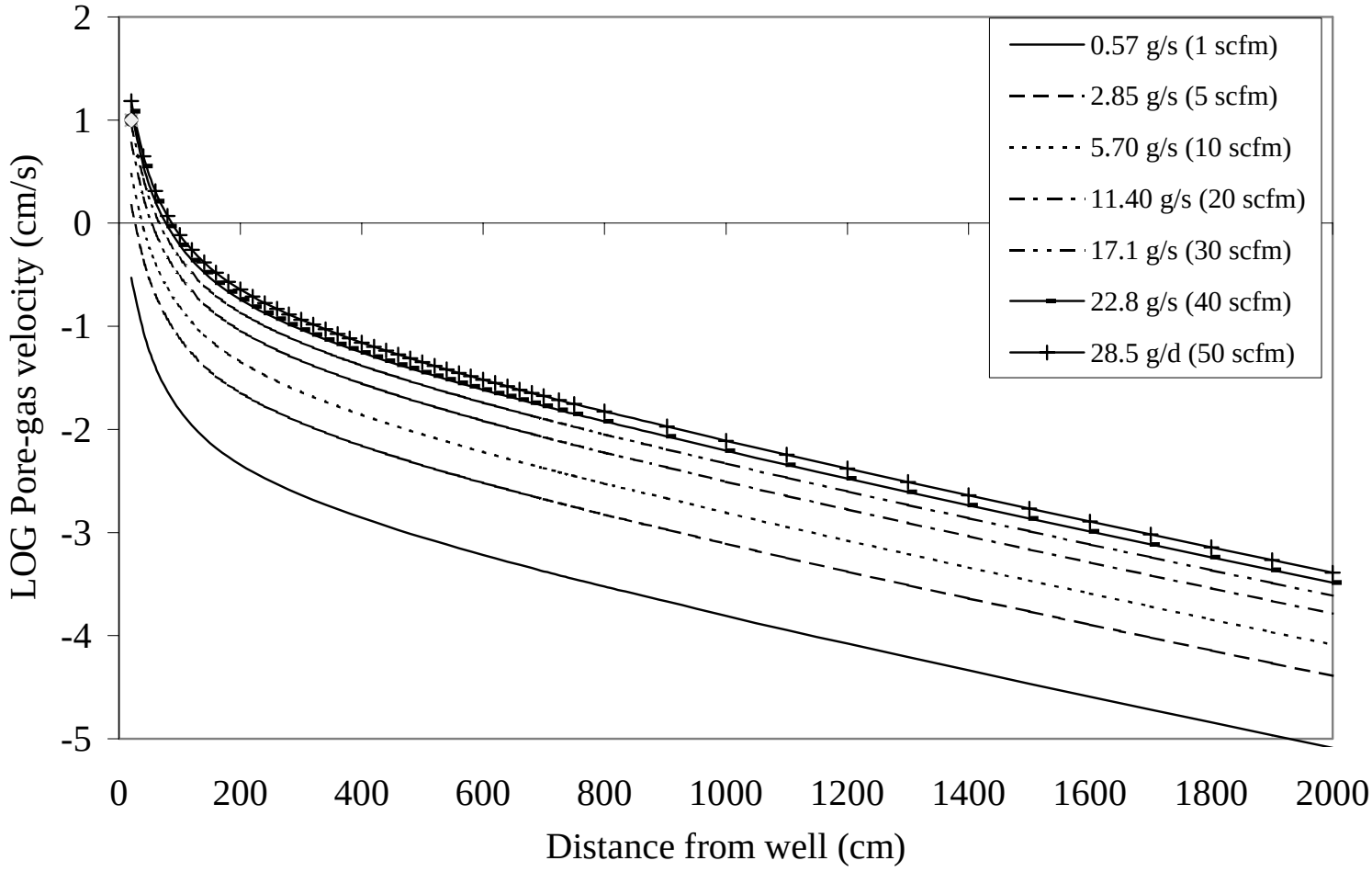

Figure 5.5 Pore-gas velocity along a transect (centerline of well) as a function of applied flow and radial distance using average k_r and $k_{rg}k_{\iota(r)}/k_{rg}k_{\iota(z)}$ ratio

flow rates (from 0.57 to 2.85 g/s) resulted in a significant increase in pore-gas velocity throughout the modeled domain. An increase in flow at high flow rates (22.8 to 28.5 g/s) however resulted in little additional increase in pore-gas velocity since most recharge, as indicated by Figure 5.4, is in the immediate vicinity of the well. Pore-gas velocity plots are useful to estimate initial well spacing based a desired flow rate and pore-velocity. For instance, at a flow rate of 2.85 g/s, attainment of a pore-gas velocity of 0.01 cm/s may require an approximate well spacing of about 200 cm (2 x 100 cm) whereas at a flow rate of 11.4 g/s, an approximate well spacing of 400 cm might be acceptable. However, because of pressure superposition effects, multiple well simulations would be necessary to more accurately space wells as a function of desired flow rate. It is obvious from Figure 5.5 though that there is a tradeoff between well spacing and flow rate as one would intuitively expect.

5.5 Conclusions

1. Data from a site was used to demonstrate radial and vertical gas permeability estimation in soils open to the atmosphere. Through discussion and example, a partial list of elements necessary for sound gas permeability estimation was provided: placement of narrowly screened pressure monitoring points close to a discretely screened gas extraction well to capture the vertical component of gas flow, testing at several flow rates to establish reproducibility, analysis of error using the RMSE of observed versus simulated pressure response, and plots of observed versus simulated pressure response to provide confidence is permeability estimation.

2. An illustration of how information on gas permeability can be used to generate plots of pore-gas velocity as a function of distance and flow rate, essential in venting design, was provided. Field-testing and data interpretation methods outlined here in addition to available software programs such as AIR2D (Joss and Baehr, 1997) and GASSOLVE (Falta, 1996) should be useful to practitioners tasked with estimating gas permeability.

6. TWO-DIMENSIONAL, AXISYMMETRIC, STEADY-STATE GAS FLOW, PORE-GAS VELOCITY CALCULATION, AND PERMEABILITY ESTIMATION IN A SEMI-CONFINED DOMAIN

In section 4, the governing equation for one-dimensional, pseudo-steady-state radial flow was presented. As previously discussed, the prefix "pseudo" reflects the fact that there is no true steady-state solution to the radial flow equation unless a constant pressure boundary (i.e., ROI) is specified since flow is assumed to occur under non-leaky or confined conditions. There are two primary concerns with use of the pseudo-steady-state radial flow equation and ROI data for gas permeability estimation. First, one-dimensional, transient and steady-state radial flow equations may result in higher estimates of radial gas permeability compared to solutions allowing vertical leakage. Strict confined conditions rarely if ever occur in the field. Even at sites where a concrete or asphalt cap exists, small cracks or flow through a gravel subbase can result in significant recharge from the atmosphere. Beckett and Huntley (1994) examined vertical leakage at five sites having asphalt and concrete caps and found that "vertical leakage was the rule, rather than the exception". Beckett and Huntley (1994) compared estimates of radial gas permeability using the Theis equation (1935) (fully confined flow) and the Hantush-Jacob equation (1955) (radial flow with vertical leakage). Both equations were modified for gas flow by invoking linearization of the dependent variable, $P^2 = P*P_{atm}$, thereby removing consideration of compressibility. Johnson et al. (1988, 1990a,b) describe this linearization for the Theis equation. Beckett and Huntley (1994) found that overestimation of radial gas permeability increased with increased leakage at the surface. At one site, use of the Theis equation (1935) compared to the Hantush-Jacob equation (1955) resulted in overestimation of radial gas permeability by a factor of 20. This is likely due to the fact that for a given flow rate, confined flow or semi-confined flow with low leakance results in a higher pressure differential compared to unconfined flow.

Second, and perhaps more importantly though, is that ROI test data may not be suitable for estimation of anisotropy, leakance, and subsequent computation of axisymmetric cylindrical (r,z) or Cartesian (x, y, z) components of pore-gas velocity. During ROI testing, gas monitoring wells are often located so far away from gas extraction wells that resulting pressure differentials are too low to distinguish from atmospheric pressure. Chen (1999) demonstrated that sensitivity of both radial and vertical gas permeability estimation decreases considerably with increasing radial distance from a gas extraction well. When pressure differential approaches zero, gas flow is no longer sensitive to radial and vertical gas permeability values. Also, during ROI testing, vacuum extraction wells and monitoring points are screened over large portions of the vadose zone providing vertically integrated measurements of pressure differential as opposed to point values required for vertical permeability and leakance estimation using analytical axisymmetric cylindrical or three-dimensional numerical models. Chen (1999) demonstrated that screening a gas extraction well deep within and over a relatively small portion of the modeled domain enhances vertical gas permeability estimation. Gas extraction wells used for ROI evaluation are typically screened over a large portion of the vadose zone. ROI monitoring practices all stem from a one-dimensional visualization of gas flow and attempting to "physically" locate a radius where pressure differential is near atmospheric pressure.

In this section, the governing equation for two-dimensional, axisymmetric, steady-state gas flow in a semi-confined domain will be presented along with an analytical solution derived by Baehr and Joss (1995). This solution will be applied to a site where radius of influence (ROI) testing and the pseudo-steady-state radial flow equation were used to estimate gas permeability.

6.1 Model Formulation

The governing partial differential equation for axisymmetric cylindrical gas flow is

$$k_{rg}k_{\iota(r)}\left(\frac{\partial^2\phi}{\partial r^2}+\frac{1}{r}\frac{\partial\phi}{\partial r}\right)+k_g k_{\iota(z)}\frac{\partial^2\phi}{\partial z^2}=0 \tag{6.1}$$

with boundary conditions:

$$k_{rg}k_{\iota(z)}\frac{\partial\phi}{\partial z}=\frac{k_{rg}k_{\iota(z')}}{d'}\left(\phi-\phi_{atm}\right) \qquad r>r_w,\ z=0 \tag{6.2}$$

$$\frac{\partial\phi}{\partial z}=0 \qquad r>r_w,\ z=d \tag{6.3}$$

$$\lim_{r\to\infty}\phi=\phi_{atm} \qquad 0<z<d \tag{6.4}$$

$$\frac{\partial\phi}{\partial r}=0 \qquad r=r_w,\ 0<z<d_U \tag{6.5}$$

$$\frac{\partial\phi}{\partial r}=-\frac{Q_m\mu_g\Re T}{\pi k_{rg}k_{\iota(r)}M_g\left(d_L-d_U\right)r_w} \qquad r=r_w,\ d_U<z<d_L \tag{6.6}$$

$$\frac{\partial\phi}{\partial r}=0 \qquad r=r_w,\ d_L<z<d \tag{6.7}$$

where: ϕ_{atm} = atmospheric pressure squared [$(ML^{-1}T^{-2})^2$], z = depth below semi-confining layer [L], d = depth below semi-confining layer to ground water [L], d_U = depth below semi-confining to top of sand pack [L], d_L = depth below semi-confining layer to base of sand pack [L], $k_{rg}k_{\iota(z)}$ = vertical gas permeability below semi-confining layer [L^2], $k_{rg}k_{\iota(z')}$ = vertical gas permeability in semi-confining layer [L^2], and d' = thickness of semi-confining layer [L]. Baehr and Joss (1995) incorporate the leakance term ($k_{rg}k_{\iota(z')}/d'$) in boundary condition (6.2) as opposed to adding a leakance term in the governing partial differential equation as previously done by Baehr and Hult (1991). Baehr and Joss (1995) state that boundary condition (6.2) is an approximation of the conservation of mass principle. It is obtained by using a finite-difference approximation of

specific discharge across the thickness of the layer of lower permeability and equating the resultant expression to the vertical component of mass flow defined in the domain as z approaches zero. Baehr and Joss (1995) state that this is a more rigorous approach than adding a leakance term to the governing partial differential equation. They did not however provide an analysis of error incurred by using the stated less rigorous approach. The solution provided by Baehr and Joss (1995) for axi-symmetric, cylindrical, steady-state, leaky confined flow is given by:

$$\phi = \phi_{atm} + \frac{2dee'Q_m\mu_g RT}{M_g \pi k_{rg} k_{\iota(r)} \left(d_L - d_U\right) r_w} \left\{ \sum_{n=1}^{\infty} \alpha_n \cos\left(\frac{q_n \left(d - z\right)}{d} \right) K_0 \left(\frac{q_n r}{de} \right) \right\} \tag{6.8}$$

where

$$e = \left(\frac{k_{rg} k_{\iota(r)}}{k_{rg} k_{\iota(z)}} \right)^{1/2} \qquad e' = \frac{k_{rg} k_{\iota(z')} d}{k_{rg} k_{\iota(z)} d'} \tag{6.9}$$

$$\alpha_n = \frac{\sin\left(\frac{q_n \left(d - d_U\right)}{d} \right) - \sin\left(\frac{q_n \left(d - d_L\right)}{d} \right)}{q_n^2 K_1 \left(\frac{q_n r_w}{de} \right) \left(e' + \sin^2 q_n \right)} \tag{6.10}$$

and q_n are positive solutions (n = 1,2,3...) to

$$\tan\left(q_n\right) = \frac{e'}{q_n} . \tag{6.11}$$

Radial and vertical volumetric specific discharge are as previously defined (5.10) and (5.12) respectively where

$$\frac{\partial \phi}{\partial r} = -\frac{2e'Q_m\mu_g RT}{\pi k_g k_{\iota(r)} M_g \left(d_L - d_U\right) r_w} \left\{ \sum_{n=1}^{\infty} q_n \alpha_n \cos\left(\frac{q_n \left(d - z\right)}{d} \right) K_1 \left(\frac{q_n r}{de} \right) \right\} \tag{6.12}$$

and

$$\frac{\partial \phi}{\partial z} = -\frac{2ee'Q_m\mu_g RT}{\pi k_{rg} k_{\iota(r)} M_g \left(d_L - d_U\right) r_w} \left\{ \sum_{n=1}^{\infty} q_n \alpha_n \sin\left(\frac{q_n \left(d - z\right)}{d} \right) K_0 \left(\frac{q_n r}{de} \right) \right\} \tag{6.13}$$

The norm or magnitude of the specific discharge vector is as previously defined in section 5. Pore-gas velocities are defined in terms of the norm of the specific discharge vector since it represents the overall magnitude of pore-gas velocity through soil and reduces complications incurred with analyzing two- and three-dimensional vector components of flow.

6.2 Computational Method

When attempting to estimate three parameters ($k_{rg}k_{\iota(r)}$, $k_{rg}k_{\iota(z)}$, and leakance) with few pressure measurements (some of which are of minimum usefulness because of near atmospheric pressure response), convergence to a local minimum and estimation non-uniqueness are major concerns. To circumvent these problems to some degree, the estimation approach described in section 5 was pursued here. A series of random guesses was applied (groups of 5000) constrained within decreasing intervals of $k_{rg}k_{\iota(r)}$, $k_{rg}k_{\iota(z)}$, and leakance until the lowest root mean squared error (RMSE) was attained for a set of $k_{rg}k_{\iota(r)}$, $k_{rg}k_{\iota(z)}$, and leakance estimates. In this way, variation in parameter estimations for the same or similar RMSE values were assessed. Little variation in parameter estimates would presumably be an indication of a satisfactory estimation. A FORTRAN program, MFRLKINV, was written in to facilitate computations. The source code and sample input and output files for this program are included in Appendix C. Huang et al. (1999) state that the inverse problem is usually ill posed and model structure error, which is difficult to estimate, often dominates other errors. As will be discussed, this observation proved valid at this site when attempting to compare parameter estimates from open and semi-confined domains.

6.3 Site Description

To demonstrate how ROI testing constrains gas permeability estimation, an attempt was made to estimate radial and vertical gas permeability and leakance through a semi-confined layer at a field site where ROI testing was used for venting design. The field site is located in an urban area in sandy soils along the Atlantic Coastal Plain. An asphalt layer (parking lot) is present on the site surface. Tables 6.1.a summarizes depths of screened intervals of gas extraction (W - series) and monitoring (v - series) wells. Table 6.1.b summarizes flow and vacuum response during ROI testing. Depth to ground water at gas extraction wells varied from about 12 to 15 feet below ground surface. Midpoint monitoring depths adjusted for water-table elevation were used as “point” values for gas permeability estimation. It was assumed that the thickness of the capillary fringe was insignificant compared to the thickness of the tested domain for sandy soils at the site. It is apparent from Table 6.1.b that monitoring points were placed at distant radii in an attempt to locate the radius at which vacuum approached 0.01 inches of water even though most vacuum dissipation and thus highest pressure gradients occurred within 15 feet of each well. Magnehelic gauges were used to measure vacuum. As evident in Table 6.1.b, many readings were at or below 0.05 inches of water. Cho and DiGiulio (1992) found when using magnehelic gauges they could not distinguish vacuum readings below 0.05 inches of water from ambient atmospheric pressure using due to wind velocity induced pressure variation in the vicinity of the gauges. Random variation in vacuum readings at or below 0.05 inches of water during testing at

Table 6.1.a Summary of well and vapor probe depths

well	*top of sandpack (ft)*	*bottom of sandpack (ft)*	*depth to water (ft)*	*Midpoint Monitoring. (ft)*
v-1	4.5	9.5		7.0
v-2	5.0	10.0		7.5
v-3	5.0	10.0		7.5
v-4	4.5	9.5		7.0
v-5	4.5	9.5		7.0
v-6	5.0	10.0		7.5
v-7	5.0	10.0		7.5
v-8	5.0	10.0		7.5
v-9	5.0	10.0		7.5
v-10	5.0	10.0		7.5
v-12	5.0	10.0		7.5
W-1	6.8	20.5	14.05	10.4
W-3	6.3	18.6	14.78	10.5
W-4	6.3	16.3	12.80	9.6
W-5	7.0	24.0	15.24	11.1
W-6	6.5	14.5	12.28	9.4
W-7	5.8	15.7	11.86	8.8

W-1 (31.3 ft - 66.5 ft), and W-6 (63.2 ft - 75.3 ft) support this observation.

6.4 Results and Discussion

Estimates of radial gas permeability using the pseudo-steady-state radial flow equation and linear regression were compared with radial gas permeability estimated using an analytical solution developed by Baehr and Joss (1995) for steady-state, two-dimensional, axisymmetric air flow in a semi-confined domain. The presence of an asphalt layer does not guarantee semi-confined conditions as a sand sub-base or fractures in the asphalt may result in significant gas recharge near an extraction well. Thus, gas permeability was estimated under conditions of high leakance (i.e., unconfined) and semi-confined domains as selection of the upper boundary condition can significantly affect vertical gas permeability estimation or anisotropy.

Table 6.2.a and 6.2.b provide a summary of gas permeability estimates for testing at each well assuming unconfined and semi-confined domains. Radial permeability estimated using the pseudo-steady-state radial flow equation is compared with radial permeability estimated using equation (6.8) under unconfined (high leakance) and semi-confined upper boundary conditions. In all cases but one (W-7 unconfined), use of the pseudo-steady-state radial flow equation appeared to provide a slight but consistent overestimation of radial permeability compared to solutions which allowed recharge at the upper boundary. However, little if any correlation between increased leakance and overestimation of radial permeability was observed. A comparison of radial gas permeability estimates for unconfined and semi-confined domains

Table 6.1.b Data for gas permeability estimation

W-1			**W-3**		
11 scfm (6.26 g/s)			20 scfm (11.38 g/s)		
Obs point	*distance (ft)*	*vacuum (in water)*	*Obs point*	*distance (ft)*	*vacuum (in water)*
v-10	15	0.24	v-5	15	1.2
v-9	31.3	0.04	v-12	36	0.31
v-8	49.5	0.01	v-6	40.6	0.33
v-4	56.8	0.05	v-4	48.5	0.27
v-5	59.9	0.02	W-7	51.9	0.16
W-3	66.5	0.01	v-7	52	0.1
			W-6	63.4	0.12

W-4			**W-5**		
9 scfm (5.12 g/s)			29 scfm (16.50 g/s)		
Obs point	*distance (ft)*	*vacuum (in water)*	*Obs point*	*distance (ft)*	*vacuum (in water)*
v-2	15	0.41	v-8	15	0.24
v-1	30.2	0.15	v-9	32.3	0.06
v-12	45.9	0.04	v-10	49.6	0.01
v-3	50.3	0.25	W-3	51.6	0.01
v-5	70.5	0.01			
v-6	85	0.02			

W-6			**W-7**		
11 scfm (6.26 g/s)			24 scfm (13.66 g/s)		
Obs point	*distance (ft)*	*vacuum (in water)*	*Obs point*	*distance (ft)*	*vacuum (in water)*
v-4	14.7	0.8	v-6	15	2.9
v-7	31.7	0.49	v-4	36	1.5
v-6	33.1	0.3	W-6	40.9	1.1
W-7	41	0.16	v-5	41.5	1.1
v-5	48.3	0.15	v-12	42.3	1.1
W-1	63.2	0.05	W-3	51.8	0.24
W-3	63.2	0.02	W-4	88.2	0.02
v-12	75.3	0.05			

revealed that radial permeability estimation was relatively insensitive to leakance.

As evident in Tables 6.2.a and 6.2.b however, estimation of vertical gas permeability expressed in the ratio of $k_{rg}k_{\iota(r)}/k_{rg}k_{\iota(z)}$ was very sensitive to selected boundary conditions and illustrates the difficulty in resolving the correlated effect of leakance and anisotropy with ROI test data. Use of (6.8) with high leakance or a domain open to the atmosphere resulted in higher $k_{rg}k_{\iota(r)}/k_{rg}k_{\iota(z)}$ ratios compared to semi-confined conditions. While higher leakance and $k_{rg}k_{\iota(r)}/k_{rg}k_{\iota(z)}$ ratios result in similar RMSE values compared to lower leakance and $k_{rg}k_{\iota(r)}/k_{rg}k_{\iota(z)}$

ratios, subsurface pressure and pore-gas velocity patterns for the two scenarios are quite different and can not be resolved without vertical profiling of vacuum or pressure data. Thus, accurate estimation of vertical permeability and leakance requires the use of small (relative to the thickness of the simulated domain) screened intervals for extraction wells and pressure observation points and placement of observation points relatively close to gas extraction wells. These criteria were not met at this site nor would be met at any site where ROI testing was performed to design a venting system. Given this situation, we are faced with the task of attempting to salvage ROI data for use in vertical permeability and leakance estimation. At this site, with the exception of well W-4, RMSE of estimates for gas permeability were slightly better for the semi-confined compared to the unconfined upper boundary condition. Estimation of leakance at well W-4 varied widely for the same RMSE of 1.83×10^{-4} (atm) which was probably due to field-scale heterogeneity (measurements of 0.04 and 0.25 inches of water at 45.9 and 50.3 feet respectively). Given this and the observation that $k_{rg}k_{\iota(r)}/k_{rg}k_{\iota(z)}$ values for the semi-confined domain are lower and perhaps more credible for sandy soils, use of the semi-confined upper boundary condition would appear reasonable. However as previously mentioned, because of the nature of ROI testing, two-dimensional cross-sectional diagrams for each test condition can not be plotted to compare simulated versus observed pressure response to demonstrate confidence in vertical permeability and leakance estimation.

6.5 Conclusions

1. This section provided an example of gas permeability and leakance estimation in a semi-confined domain and illustrated difficulties encountered when attempting to use ROI-based data for parameter estimation.

2. Use of the pseudo-steady-state radial flow equation appeared to provide a slight but consistent overestimation of radial permeability compared to solutions which allowed recharge at the upper boundary. However, little if any correlation between increased leakance and overestimation of radial permeability was observed. A comparison of radial gas permeability estimates for unconfined and semi-confined domains revealed that radial permeability estimation was relatively insensitive to leakance. Estimation of vertical gas permeability expressed in the ratio of $k_{rg}k_{\iota(r)}/k_{rg}k_{\iota(z)}$ though was very sensitive to leakance and illustrated the difficulty in resolving the correlated effect of leakance and anisotropy with ROI test data. The assumption of high leakance or a domain open to the atmosphere resulted in higher $k_{rg}k_{\iota(r)}/k_{rg}k_{\iota(z)}$ ratios compared to semi-confined conditions.

Table 6.2.a Summary of gas permeability estimation for domain open to atmosphere (high leakance)

well	$k_{rg}k_{i(r)}$* (cm^2)	*n*	$k_{rg}k_{i(r)}$** (cm^2)	$k_{rg}k_{i(r)}$*/$k_{rg}k_{i(r)}$**	$k_{rg}k_{i(r)}$**/$k_{rg}k_{i(z)}$**	*RMSE*** (atm)*
W-1	9.65×10^{-7}	19	3.20×10^{-7} (3.02×10^{-7} - 3.38×10^{-7})	2.85 - 3.20	2.76 (2.55 - 2.97)	4.87×10^{-5}
W-3	3.02×10^{-7}	113	1.86×10^{-7} (1.82×10^{-7} - 1.90×10^{-7})	1.59 - 1.66	6.92 (6.71 - 7.12)	1.23×10^{-4}
W-4	5.74×10^{-7}	235	4.98×10^{-7} (4.73×10^{-7} - 5.23×10^{-7})	1.10 - 1.21	21.93 (19.55 - 24.31)	1.83×10^{-4}
W-5	1.78×10^{-6}	1	7.28×10^{-7}	2.45	2.47	1.05×10^{-5}
W-6	3.16×10^{-7}	91	2.42×10^{-7} (2.38×10^{-7} - 2.45×10^{-7})	1.29 - 1.33	12.15 (11.94 - 12.63)	1.73×10^{-4}
W-7	1.99×10^{-7}	18	2.03×10^{-7} (1.99×10^{-7} - 2.06×10^{-7})	0.97 - 1.00	24.17 (23.55 - 24.79)	6.94×10^{-4}

Table 6.2.b Summary of gas permeability estimation for semi-confined domain

well	$k_{rg}k_{i(r)}$* (cm^2)	*n*	$k_{rg}k_{i(r)}^{+}$ (cm^2)	$k_{rg}k_{i(r)}$*/$k_{rg}k_{i(r)}$	$k_{rg}k_{i(r)}^{+}$/$k_{rg}k_{i(z)}^{+}$	*leakance (cm)*	*RMSE*$^{+}$(atm)*
W-1	9.65×10^{-7}	20	2.90×10^{-7} (2.80×10^{-7} - 3.00×10^{-7})	3.31 - 3.45	1.17 (0.85 - 1.49)	9.29×10^{-10} (7.07×10^{-10} - 1.15×10^{-9})	4.85×10^{-5}
W-3	3.02×10^{-7}	45	1.80×10^{-7} (1.75×10^{-7} - 1.85×10^{-7})	1.63 - 1.73	4.29 (3.07 - 5.50)	4.04×10^{-10} (2.18×10^{-10} - 5.89×10^{-10})	1.22×10^{-4}
W-4	5.74×10^{-7}	11	4.69×10^{-7} (4.28×10^{-7} - 5.09×10^{-7})	1.13 - 1.34	14.52 (5.80 - 23.23)	4.23×10^{-8} (1.28×10^{-10} - 8.45×10^{-8})	1.83×10^{-4}
W-5	1.78×10^{-6}	1	6.87×10^{-7}	2.6	1.01	2.24×10^{-9}	9.10×10^{-6}
W-6	3.16×10^{-7}	6	1.81×10^{-7} (1.73×10^{-7} - 1.88×10^{-7})	1.68 - 1.83	0.74 (0.52 - 0.96)	8.62×10^{-11} (8.24×10^{-11} - 9.00×10^{-11})	1.60×10^{-4}
W-7	1.99×10^{-7}	4	1.42×10^{-7} (1.41×10^{-7} - 1.43×10^{-7})	1.39 - 1.41	0.98 (0.91 - 1.05)	3.62×10^{-11} (3.61×10^{-11} - 3.63×10^{-11})	5.67×10^{-4}

* estimated using equation (4.54) and linear regression6

** mean estimated using equation (6.8) with high leakance (open to atmosphere) - values in parenthesis denote range at same RMSE

$^{+}$ mean estimated using equation (6.8) assuming semi-confined domain- values in parenthesis denote range at same RMSE

n number of guesses with equivalent RMSE

7. TWO-DIMENSIONAL, AXISYMMETRIC, TRANSIENT GAS FLOW AND PERMEABILITY ESTIMATION ANALYSIS

Transient gas permeability testing is not commonly performed during site characterization activities at sites in which soil venting is planned. The reason for may be because transient pressure response often occurs quicker than field technicians can make enough useful manual measurements. However, it may also have to do with the need for additional equipment (e.g., pressure transducers) and more sophisticated and time consuming data analysis. Transient testing though has some distinct advantages over steady-state testing. First, attainment of steady-state conditions can take hours or even days in low permeability media when the distance from extraction or injection well to a monitoring point is extensive. If gas extraction is used, a lengthy testing period may require use of vapor treatment equipment resulting in additional costs. If gas injection is used, prolonged uncontrolled release of VOCs from subsurface media to the atmosphere may create a health and safety issue. Short testing times, alleviates both of these problems. Second, after a relatively short period of initial pressure rise or drop, pressure change can be slow, especially in soils having very low gas permeability, making discernment of steady-state conditions difficult. Premature cessation of testing will likely result in overestimation of gas permeability since the utilized pressure differential is less than the true pressure differential for a given flow rate under steady-state conditions. Third, transient testing enables estimation of gas-filled porosity. Knowledge of gas-filled porosity is necessary for pore-velocity calculation to support venting design and monitoring activities. Fourth, the large number of data points collected during transient testing may enable more accurate parameter estimation. During steady-state testing, there are rarely more than 10 monitoring points for data analysis. Transient testing allows use of a hundred or more pressure measurements at each monitoring point. Finally, since periodic pressure measurement must be performed anyway to observe attainment of steady-state conditions it would appear wasteful not to increase pressure measurement frequency and utilize this data for quantitative analysis considering high personnel and drilling costs incurred to support gas permeability testing.

At present, only line-source/sink analytical solutions exist for transient, axisymmetric, two-dimensional gas flow analysis and parameter estimation. The implicit assumption in use of these solutions is that borehole storage effects are insignificant except in the immediate vicinity of the wellbore. The radii away from a well and borehole storage volume over which borehole storage effects become important though have not been investigated for gas flow. Thus, use of pressure monitoring points very close to a gas extraction or injection well may introduce some unquantified error in gas permeability estimation.

Borehole storage effects would be expected to be of greatest significance in single-interval, transient testing. Single-interval testing provides permeability estimation over a relatively small volume of subsurface media thereby providing a mechanism for assessing physical heterogeneity or spatial variability in permeability on a scale much smaller than full field-scale tests. The scale of single-interval tests however would still be larger than that obtained with collection of discrete soil core and subsequent laboratory testing. While there are

no published studies of single-interval, transient, gas permeability testing, single-interval, transient, hydraulic testing is common in ground-water hydrology (i.e., slug testing). Joss et al. (1992) conducted single-interval, steady-state, gas permeability testing. With single-interval, steady-state testing however parameter estimation is limited to one parameter, radial gas permeability, since only one pressure point can be used for each flow rate. Transient, single-interval testing would enable the use of many pressure measurements as a function of time thereby allowing estimation of radial permeability, vertical permeability, leakance, and gas-filled porosity.

The purpose of this section is to: (1) summarize available transient, axisymmetric, two-dimensional, source/sink analytical solutions, (2) introduce a solution for a finite-radius solution incorporating borehole storage, (3) conduct a sensitivity analysis for the finite-radius solution, and (4) evaluate the usefulness of transient, single-interval, finite-radius testing at a field site.

7.1 Model Formulation for Line-Source Open to the Atmosphere

The governing equation describing two-dimensional, axisymmetric gas flow in anisotropic, homogeneous media in a domain open to the atmosphere is (Baehr and Hult, 1991)

$$\frac{\mu_g \theta_g}{\sqrt{\phi}} \frac{\partial \phi}{\partial t} = k_{rg} k_{\iota(r)} \left(\frac{\partial^2 \phi}{\partial r^2} + \frac{1}{r} \frac{\partial \phi}{\partial r} \right) + k_{rg} k_{\iota(z)} \frac{\partial^2 \phi}{\partial z^2}; \quad r > r_w, \quad 0 < z < d \quad t > 0 . \tag{7.1}$$

When subject to the initial condition:

$$\phi = \phi_{atm}; \quad r > r_w, \quad 0 < z < d; \quad t = 0 \tag{7.2}$$

and boundary conditions:

$$\phi = \phi_{atm}; \quad r > r_w, \quad z = 0; \quad t > 0 \tag{7.3}$$

$$\frac{\partial \phi}{\partial z} = 0; \quad r > r_w, \quad z = d; \quad t > 0 \tag{7.4}$$

$$\lim_{r \to \infty} \phi = \phi_{atm} \qquad 0 < z < d; \quad t > 0 \tag{7.5}$$

$$\lim_{r \to 0} r \frac{\partial \phi}{\partial r} = - \frac{Q_m \Re T \mu_g}{M_g \pi k_{rg} k_{\iota(r)} \left(d_L - d_U \right)} \square z \qquad 0 < z < d; \quad t > 0 \tag{7.6}$$

where

$$\begin{aligned} \square(z) &= 1; \quad d_U \le z \le d_L \\ &= 0; \quad 0 < z < d_U, \quad d_L < z < d \end{aligned} \tag{7.7}$$

Falta (1993) provides a solution:

$$\phi(r,z,t) = \phi_{atm} - \frac{Q_m \Re T \mu_g}{\pi^2 M_g k_{rg} k_{\iota(r)} \left(d_L - d_U\right)} \sum_{n=1}^{\infty} \frac{1}{m} \left[\cos\left(\frac{m\pi d_U}{d}\right) - \cos\left(\frac{m\pi d_L}{d}\right) \right] \sin\left(\frac{m\pi z}{d}\right) W\left(u,\beta\right) \tag{7.8}$$

where

$$m = n - \frac{1}{2} \tag{7.9}$$

$$u = \frac{r^2 \theta_g \mu_g}{4 P_{atm} k_{rg} k_{\iota(r)} t} \tag{7.10}$$

$$\beta = r \left[\frac{k_{rg} k_{\iota(z)}}{k_{rg} k_{\iota(r)}} \left(\frac{m\pi}{d}\right)^2 \right]^{\frac{1}{2}} \tag{7.11}$$

and W(u,β) is the Hantush Leaky Well Function defined by

$$W\left(u,\beta\right) = \int_u^{\infty} \frac{1}{y} e^{\left(-y - \frac{\beta^2}{4y}\right)} dy \,. \tag{7.12}$$

This solution is coded in GASSOLVE (Falta, 1996); a program available from the author upon request.

7.2 Model Formulation for Line-Source with Leaky-Confined Flow

Baehr and Hult (1988) adapted Hantush's (1964) solution for two-dimensional, axisymmetric, ground-water flow to a partially penetrating well in a leaky-confined aquifer to evaluate gas flow in the unsaturated zone induced by a gas extraction well. Their solution to the gas flow equation requires the extraction or injection well to be modeled as an infinitesimal line source and the domain to be bounded above by layer of low permeability. They give the governing equation for leaky-confined, transient, cylindrical flow as:

$$\frac{\mu_g \theta_g}{\sqrt{\phi}} \frac{\partial \phi}{\partial t} = k_{rg} k_{\iota(r)} \left(\frac{\partial^2 \phi}{\partial r^2} + \frac{1}{r} \frac{\partial \phi}{\partial r} \right) + k_{rg} k_{\iota(z)} \frac{\partial^2 \phi}{\partial z^2} + \frac{k_{rg} k_{\iota(z')}}{d' d}; \quad r > r_w, \quad 0 < z < d \quad t > 0 . \quad (7.13)$$

When subject to the initial condition (7.2) and boundary conditions (7.4), (7.5), (7.6), and (7.7) in addition to boundary condition:

$$\frac{\partial \phi}{\partial z} = 0; \quad r > r_w, \quad z = 0; \quad t > 0 \quad (7.14)$$

Baehr and Hult's (1989) provide a solution as follows:

$$\begin{aligned} \phi = \phi_{atm} &- \frac{Q_m \Re T \mu_g}{2\pi M_g k_{rg} k_{\iota(r)} d} W(u, \beta_1) \\ &- \frac{Q_m \Re T \mu_g}{\pi^2 M_g k_{rg} k_{\iota(r)} (d_L - d_U)} \sum_{n=1}^{\infty} \frac{1}{n} \left[\sin\left(\frac{n\pi d_L}{d} \right) - \sin\left(\frac{n\pi d_U}{d} \right) \right] \cos\left(\frac{n\pi z}{d} \right) W(u, \beta_2) \end{aligned} \quad (7.15)$$

where u is as defined in (7.10) and

$$\beta_1 = r \left(\frac{k_{rg} k_{\iota(z')}}{k_{rg} k_{\iota(r)} d d'} \right)^{\frac{1}{2}} \quad (7.16)$$

$$\beta_2 = r \left(\frac{k_{rg} k_{\iota(z)}}{k_{rg} k_{\iota(r)}} \left(\frac{n\pi}{d} \right)^2 \frac{k_{rg} k_{\iota(z')}}{k_{rg} k_{\iota(r)} d d'} \right)^{\frac{1}{2}} \quad (7.17)$$

$$W(u, \beta_i) = \int_u^{\infty} \frac{1}{y} e^{\left(-y - \frac{\beta_i^2}{4y} \right)} dy . \quad (7.18)$$

This solution is also coded in GASSOLVE (Falta, 1996)

7.3 Model Formulation for a Finite-Radius Well with Leaky-Confined Flow

Varadhan and DiGiulio (2001) recently derived an analytical solution for two-dimensional, transient flow in a semi-confined domain with gas extraction or injection from a finite-radius well. Equation (7.1) is used as the governing partial differential equation describing two-dimensional, axisymmetric transient gas flow in anisotropic, homogeneous media. Initial

condition (7.2) and boundary conditions (7.4), and (7.5) are used in addition to

$$\frac{\partial \phi}{\partial z} = \frac{k_{rg} k_{t(z')}}{d'} \left(\phi - \phi_{atm} \right); \quad r > r_w, \quad z = 0, \quad t > 0 \tag{7.19}$$

which is the boundary condition used by Baehr and Joss (1995) for a semi-confined domain. The condition at the well ($r = r_w$) taking wellbore storage into consideration may be expressed as

$$-2\pi r_w (d_L - d_U) \frac{k_{rg} k_{t(r)}}{\mu_g} \left(\frac{M_g P}{\Re T} \right) \frac{\partial P}{\partial r} + V_b \left(\frac{M_g}{\Re T} \right) \frac{\partial P}{\partial t} = Q_m(t) \square(z); \quad 0 < z < d, \quad t > 0 \tag{7.20}$$

where $\square z$ is as defined in (7.7), $Q_m(t)$ is a time-dependent mass flow pump function [MT^{-1}] (negative when gas is extracted, positive when gas is injected), and V_b = wellbore storage volume [L^3]. The first term in equation (7.20) denotes the mass rate of gas entering the well from the soil domain. The second term denotes the rate of change of mass inside the wellbore. The wellbore storage term includes the volume of the pipe and associated tubing to the pump plus the air-filled porosity contained within the sandpack. For this reason, the wellbore storage term was expressed explicitly as a volume specified by the user instead of as a function of the dimensions of the well as is commonly done. It was assumed that the gas volume inside the wellbore remains constant and that the change in mass is due only to change in gas pressure.

Varadhan and DiGiulio (2001) express the governing partial differential equation and associated initial and boundary conditions in a non-dimensional form as follows:

$$\left(1 + \Phi\right)^{-\frac{1}{2}} \frac{\partial \Phi}{\partial T} = \frac{\partial^2 \Phi}{\partial R^2} + \frac{1}{R} \frac{\partial \Phi}{\partial R} + \zeta^2 \frac{\partial^2 \Phi}{\partial Z^2}; \quad R > 1, \quad 0 < Z < 1, \quad T > 0 \tag{7.21}$$

$$\Phi = 0; \quad R > 1, \quad 0 < Z < 1, \quad T = 0 \tag{7.22}$$

$$\frac{\partial \Phi}{\partial Z} = \mathrm{B}\Phi; \quad R > 1, \quad Z = 0, \quad T > 0 \tag{7.23}$$

$$\frac{\partial \Phi}{\partial Z} = 0; \quad R > 1, \quad Z = 1, \quad T > 0 \tag{7.24}$$

$$-\frac{\partial \Phi}{\partial R} + \Gamma \left(1 + \Phi\right)^{-\frac{1}{2}} \frac{\partial \Phi}{\partial T} = M \ g(T) \square(Z); \quad R = 1, \quad 0 < Z < 1, \quad T > 0 \tag{7.25}$$

$$\square(Z) = \frac{1}{L-D}; \quad D \le Z \le L \qquad = \quad 0; \qquad 0 < Z < D, \quad L < Z < 1 \qquad . \tag{7.26}$$

The dimensionless variables are defined by

$$\Phi = \frac{\phi}{\phi_{atm}} - 1 \tag{7.27}$$

$$T = \left(\frac{k_{rg} k_{\iota(r)} P_{atm}}{\mu_g \theta_g r_w^2} \right) t \tag{7.28}$$

$$R = \frac{r}{r_w}; \qquad Z = \frac{z}{d}; \qquad D = \frac{d_U}{d}; \qquad L = \frac{d_L}{d} \tag{7.29}$$

$$\zeta = \left(\frac{r_w}{d} \right) \left(\frac{k_{rg} k_{\iota(z)}}{k_{rg} k_{\iota(r)}} \right)^{\frac{1}{2}} \tag{7.30}$$

$$\mathrm{B} = \left(\frac{k_{rg} k_{\iota(z')} d}{k_{rg} k_{\iota(z)} d'} \right) \tag{7.31}$$

$$\Gamma = \frac{1}{2\theta_g \left(L - D \right)} \tag{7.32}$$

$$M = \frac{Q_0 \mu_g \Re T}{\pi M_g k_{rg} k_{\iota(r)} d P_{atm}^2} \tag{7.33}$$

where the pump function $Q_m(t) = Q_0 g(T)$; Q_0 (MT^{-1}) is the maximum of the absolute value of $Q_m(t)$, and $-1 \le g(T) \le 1$, for all $T > 0$.

Equation (7.21) and boundary condition (7.25) are nonlinear because of the radical term on the left hand side of the equation. To solve equation (7.21) analytically, linearization of the radial term is necessary. As discussed in section 3, the easiest method of linearization with little loss of accuracy is to let $(1+\Phi)^{½}$ or P/P_{atm} equal some constant. Baehr and Hult (1988) and Falta (1996) let P equal atmospheric pressure (P_{atm}) or $(1+\Phi)^{½} = 1$. Falta (1996) states that with this approximation, gas is assumed to be compressible with a constant compressibility factor of $1/P_{atm}$.

Varadhan and DiGiulio (2001) developed an exact analytical solution to equation (7.21) subject to (7.22) - (7.26)

$$\frac{\Phi(R,Z,T)}{2M} = \sum_{n=1}^{\infty} \mathbb{Z}(Z)\mathbb{R}(R,T) \tag{7.34}$$

where

$$\mathbb{Z}(Z) = \left[\sin\left(\lambda_n(1-D)\right) - \sin\left(\lambda_n(1-L)\right)\right] \frac{\mathrm{B}\cos\left(\lambda_n(1-Z)\right)}{\lambda_n(L-D)\left(\mathrm{B}+\sin^2\lambda_n\right)} \tag{7.35}$$

$$\begin{aligned}\mathbb{R}(R,T) = {} & \frac{2K_0(\xi_n R)}{K_0(\xi_n)}\left[2\Gamma - 1 + \frac{K_1^2(\xi_n)}{K_0^2(\xi_n)}\right]^{-1} \mathrm{H}\left(T,(\zeta^2\lambda_n^2 - \xi_n^2)\right) \\ & - \frac{2}{\pi}\int_0^{\infty} \mathrm{H}\left(T,(\zeta^2\lambda_n^2 + u^2)\right)\left[\frac{\mathrm{E}_1 J_0(uR) - \mathrm{E}_2 Y_0(uR)}{\mathrm{E}_1^2 + \mathrm{E}_2^2}\right] u\,du\end{aligned} \tag{7.36}$$

$$\mathrm{E}_1 = uY_1(u) - \Gamma\left(\zeta^2\lambda_n^2 + u^2\right)Y_0(u) \tag{7.37}$$

$$\mathrm{E}_2 = uJ_1(u) - \Gamma\left(\zeta^2\lambda_n^2 + u^2\right)J_0(u)\,. \tag{7.38}$$

The eigenvalues λ_n are obtained as the n-th positive roots of

$$\lambda\tan(\lambda) = \mathrm{B}\,. \tag{7.39}$$

The roots of ξ_n are determined by

$$\zeta^2\lambda_n^2 - \xi_n^2 = \frac{\xi_n K_1(\xi_n)}{\Gamma K_0(\xi_n)}; \quad \xi_n > 0\,. \tag{7.40}$$

J_0 and J_1 are zero- and first-order Bessel functions of the first kind, Y_0 and Y_1 are zero-and first-order Bessel function of the second kind respectively. The function H(T,A), where A is a dummy variable, depends on the pumping function g(T) as follows

$$\mathrm{H}(T,A) = e^{-AT}\int_0^T e^{A\tau} g(\tau)\,d\tau\,. \tag{7.41}$$

When the pumping rate is constant

$$\mathrm{H}(T,A)=\frac{1}{A}\left(1-e^{-AT}\right). \tag{7.42}$$

Computation of Φ(R,Z,T) is difficult because the integrand in (7.36) is slowly decaying and oscillatory. Furthermore, when the Fourier summation in (7.34) is slowly convergent, evaluation of (7.36) must be performed numerous times. Thus, while accurate, the solution is computationally inefficient. This led Varadhan and DiGiulio (2001) to pursue the use of a numerical inversion algorithm in place of (7.36). Specifically, transformation in time (T) using p as the Laplace transform variable yielded

$$\mathbb{R}(R,T)=invLaplace\left\{\frac{g(p)K_0\left(\omega_n R\right)}{\omega_n K_1\left(\omega_n\right)+p\Gamma K_0\left(\omega_n\right)}\right\} \tag{7.43}$$

where

$$\omega_n=\left(p+\zeta^2\left(n-1/2\right)^2\pi^2\right)^{1/2}. \tag{7.44}$$

Varadhan and DiGiulio (2001) used the Gaver-Stehfest algorithm (Stehfest, 1970) to invert (7.43). The Gaver-Stehfest algorithm has been widely used in well hydraulics and found to be efficient and acceptably accurate when a constant pumping function is used (Moench and Ogata, 1981; Dougherty and Babu, 1984; and Butler and Liu, 1993). Davies and Martin (1979) however found that the Gaver-Stehfest algorithm does not perform well for a sinusoidal pumping function. Varadhan and DiGiulio (2001) used a sinusoidal pumping function to check the performance of the Gaver-Stehfest algorithm for this application and found that the algorithm did indeed perform poorly and that performance deteriorated with time. Thus, while the Gaver-Stehfest algorithm is computationally more efficient than Varadhan and DiGiulio's (2001) exact analytical solution, it can not be used for sinusoidal or other oscillatory functions. In practice however, a constant or step function is usually specified. Under these conditions, the Gaver-Stehfest algorithm performs well and substantially speeds up computation compared to the exact solution.

7.4 Sensitivity Analysis of Finite-Radius, Transient Solution

Varadhan and DiGiulio (2001) did not perform a sensitivity analysis for their analytical solution nor provide an example application. A sensitivity analysis is provided here using input representative of conditions present at a field site where the solution will be tested. A FORTRAN program (TFRLK) was written to solve the forward solution of Varadhan and DiGiulio's (2001) solution. Example input and output files and the source code is provided in Appendix D. Figures 7.1 and 7.2 provide a comparison of normalized pressure (P/P_{atm}) and error

as a function of time and normalized radial distance (r/d) for finite-radius (FR) and line-source (LS) solutions in a semi-confined domain having a thickness of 600 cm, borehole storage volume of 15000 cm^3, volumetric gas content of 0.1, and leakance of 1.0×10^{-11} cm^2. Error is defined as

$$error = \left(\frac{\frac{P}{P_{atm}}(LS) - \frac{P}{P_{atm}}(FR)}{\frac{P}{P_{atm}}(FR)} \right). \tag{7.45}$$

As illustrated in Figure 7.1, during pumping at the wellbore (r/d = 0.017), the line-source/sink solution simulates a more rapid rise in pressure at early time but then levels off to a lower normalized pressure at late time compared to the finite-radius solution. The former effect is due to lack of a delayed response from borehole storage. The latter effect is likely due to the fact that the simulated distance r/d = 0.017 is the wellbore radius for the finite-radius solution and approximately 10 cm into the formation for the line source/sink solution. Lower pressure differential response at late time for the line-source/sink solution would likely lead to gas permeability overestimation for a given flow rate. As illustrated in Figure 7.2, at the wellbore, pressure is overestimated at early time for the line source/sink solution and underestimated over well shut-in by as much as 10% for the given mass flow rate. Thus, when conducting single-interval, transient testing, borehole storage effects become a significant source of error if not properly accounted for. Under conditions of these simulations, error due to use of a line-source/sink solution disappears at r/d = 0.150 or 90 cm (about 3 feet). Thus, under typical testing conditions when a gas extraction or injection well is not used as the pressure monitoring point and the closest observation point is greater than 150 cm away, transient gas permeability estimation using a line-source/sink solution would result in little error.

Figures 7.3 and 7.4 provide a comparison of line-source/sink and finite-radius simulations at the wellbore but at different vertical elevations to assess error associated with using the line-source solution for testing at different intervals in multi-level wells. It appears from Figure 7.4 that there is little error (less than 1.5%) associated with using a line-source/sink solution under conditions specified here. However, conditions specified here are not representative of all potential testing conditions. Thus, when observation points are close to a gas extraction or injection well, it may be useful assess the importance of finite-radius and wellbore effects.

Figure 7.5 illustrates the effect of borehole storage on the transient pressure response at the borehole during single-interval testing. Increased borehole storage volume results in an increased delayed response to steady-state conditions. Figure 7.6 illustrates the effect of volumetric gas content on transient pressure response at the borehole during single-interval testing. Increased gas-filled porosity results in a somewhat similar transient response to increased borehole storage volume but the transient effects are much more prolonged. If borehole storage volume if unknown or can only be roughly estimated because of uncertainties in the filter pack volume and volumetric gas content in the filter pack, similarity in response of borehole storage volume and volumetric gas content create the possibility of non-unique

parameter estimation due to correlated behavior. Figure 7.7 illustrates the effect of $k_{rg}k_{\iota(r)}/k_{rg}k_{\iota(z)}$ ratio or anisotropy on transient pressure response at the wellbore. Higher $k_{rg}k_{\iota(r)}/k_{rg}k_{\iota(z)}$ ratios prolong attainment of steady-state conditions and result in a higher normalized pressure response compared to lower $k_{rg}k_{\iota(r)}/k_{rg}k_{\iota(z)}$ ratios. Figure 7.8 illustrates the effect of leakance on transient pressure response at the wellbore. This effect, at least under the conditions specified in single-interval testing, was minor. As demonstrated in section 6 however, when conducting gas permeability testing on a larger scale, simulated pressure response becomes very sensitive to estimated leakance and the correlated effect of leakance and $k_{rg}k_{\iota(r)}/k_{rg}k_{\iota(z)}$ ratios becomes apparent. Finally, the effect of radial permeability estimation is illustrated in Figure 7.9. Lower gas permeability significantly prolonged attainment of steady-state conditions and resulted in a much higher pressure differential.

7.5 Description of Field-Site

The concept of transient single-interval gas permeability testing was tested at the Picillo Farm Superfund Site in Coventry, Rhode Island. Unsaturated and saturated subsurface media at the site are heavily contaminated with chlorinated and non-chlorinated cycloalkanes, alkanes, alkenes, phenolic, and aromatic hydrocarbons as a result drum and bulk liquid disposal in 1977. At least 10,000 drums and an undetermined volume of bulk liquid wastes containing industrial solvents, PCBs, paint sludges, plasticizers, explosives, resins, and still bottoms were disposed of in several trench areas throughout an eight-acre portion of the site. Between 1980 and 1982, U.S. EPA removed drums and remaining drum fragments offsite for disposal. In 1993, U.S. EPA

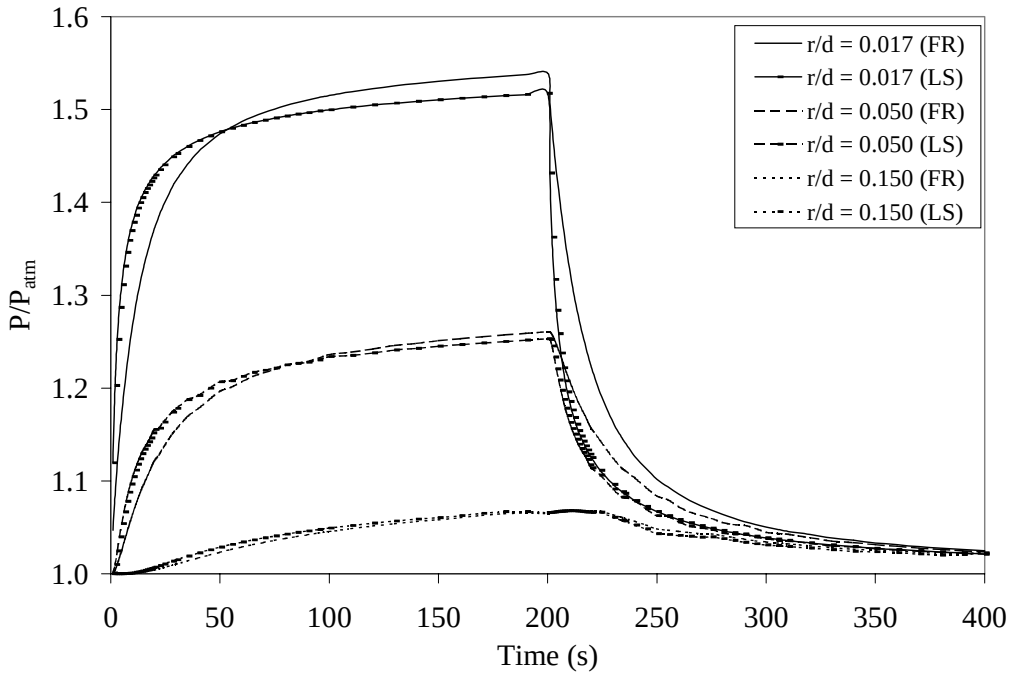

Figure 7.1. Pressure response as a function of time for finite-radius (FR) and line source solutions (LS) (d = 600 cm, $d_U/d = 0.683$, $d_L/d = 0.783$, $z/d = 0.733$, $r_w/d = 0.017$, $\theta_g = 0.1$, $k_{rg}k_{\iota(r)} = 1.0 \times 10^{-9}$ cm^2, $k_{rg}k_{\iota(r)}/k_{rg}k_{\iota(z)} = 1.0$, $Q_m = 1.0$ g/s, $V_b = 15000$ cm^3, $k_{rg}k_{\iota(z')}/d' = 1.0 \times 10^{-11}$ cm).

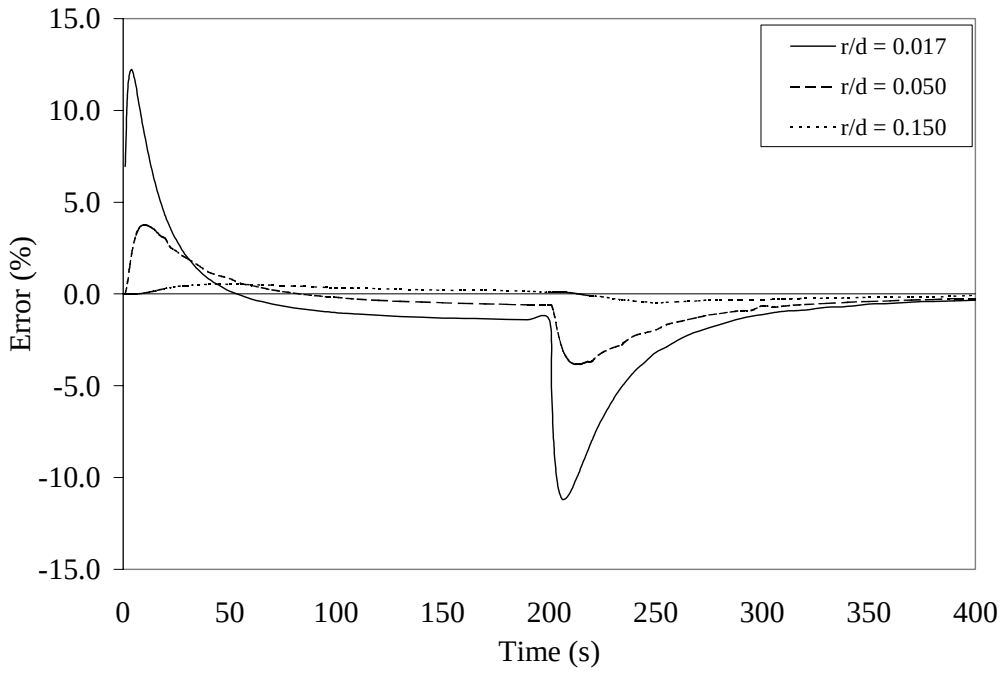

Figure 7.2. Error in pressure computation as a function of time for finite-radius (FR) and line source solutions (LS) (d = 600 cm, $d_U/d = 0.683$, $d_L/d = 0.783$, z/d = 0.733, $r_w/d = 0.017$, $\theta_g = 0.1$, $k_{rg}k_{\iota(r)} = 1.0 \times 10^{-9}$ cm^2, $k_{rg}k_{\iota(r)}/k_{rg}k_{\iota(z)} = 1.0$, $Q_m = 1.0$ g/s, $V_b = 15000$ cm^3, $k_{rg}k_{\iota(z')}/d' = 1.0 \times 10^{-11}$ cm).

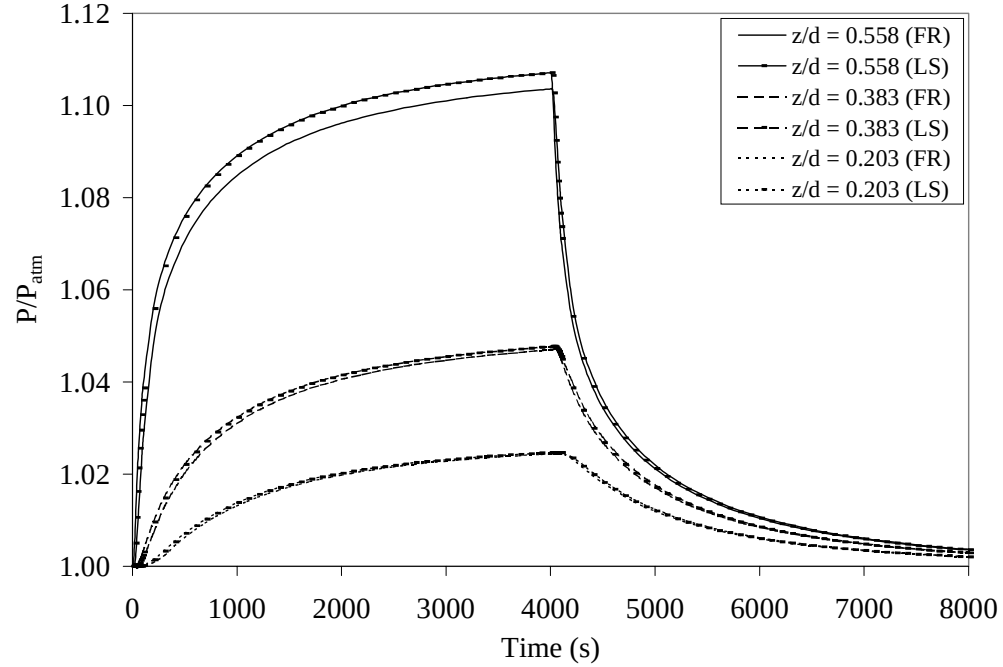

Figure 7.3 Pressure response as a function of time and vertical elevation for finite-radius (FR) and line source solutions (LS) (d = 600 cm, $d_U/d = 0.683$,$d_L/d = 0.783$, $r = r_w$, $\theta_g = 0.1$, $k_{rg}k_{\iota(r)} = 1.0 \times 10^{-9}$ cm^2, $k_{rg}k_{\iota(r)}/k_{rg}k_{\iota(z)} = 1.0$, $Q_m = 1.0$ g/s, $V_b = 15000$ cm^3, $k_{rg}k_{\iota(z')}/d' = 1.0 \times 10^{-11}$ cm).

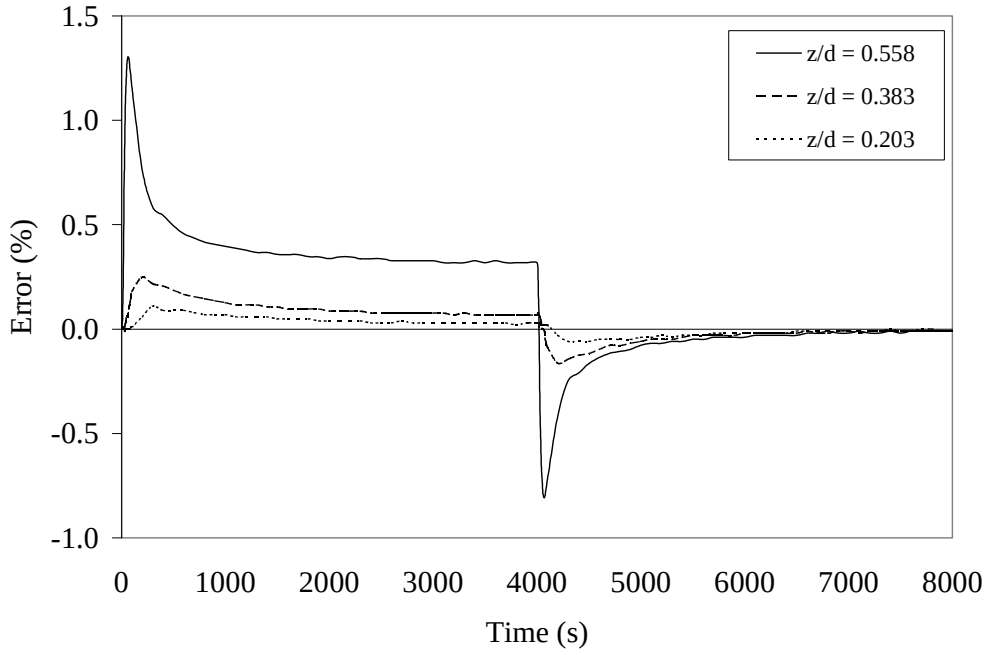

Figure 7.4 Error in pressure computation as a function of time and vertical elevation for finite-radius (FR) and line source solutions (LS) (d=600 cm, d_U/d = 0.683, d_L/d = 0.783, r = r_w, θ_g = 0.1, $k_{rg}k_{\iota(r)}$ =1.0 x 10^{-9} cm^2, $k_{rg}k_{\iota(r)}/k_{rg}k_{\iota(z)}$ =1.0, Q_m =1.0 g/s, V_b = 15000 cm^3, $k_{rg}k_{\iota(z')}/d'$= 1.0 x 10^{-11}cm

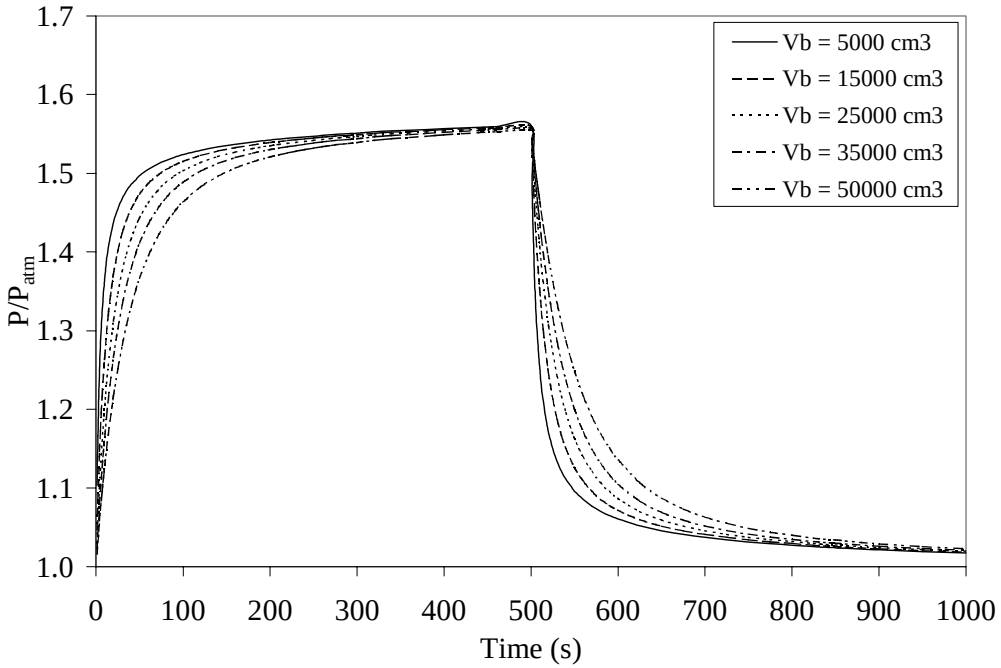

Figure 7.5 Pressure response as a function of time and borehole storage (d = 600 cm, d_U/d = 0.683, d_L/d = 0.783, z/d = 0.733, r = r_w, θ_g = 0.1, $k_{rg}k_{\iota(r)}$ = 1 x 10^{-9} cm^2, $k_{rg}k_{\iota(r)}/k_{rg}k_{\iota(z)}$ = 1.0, Q_m = 1.0 g/s, $k_{rg}k_{\iota(z')}/d'$ = 1.0 x 10^{-11} cm).

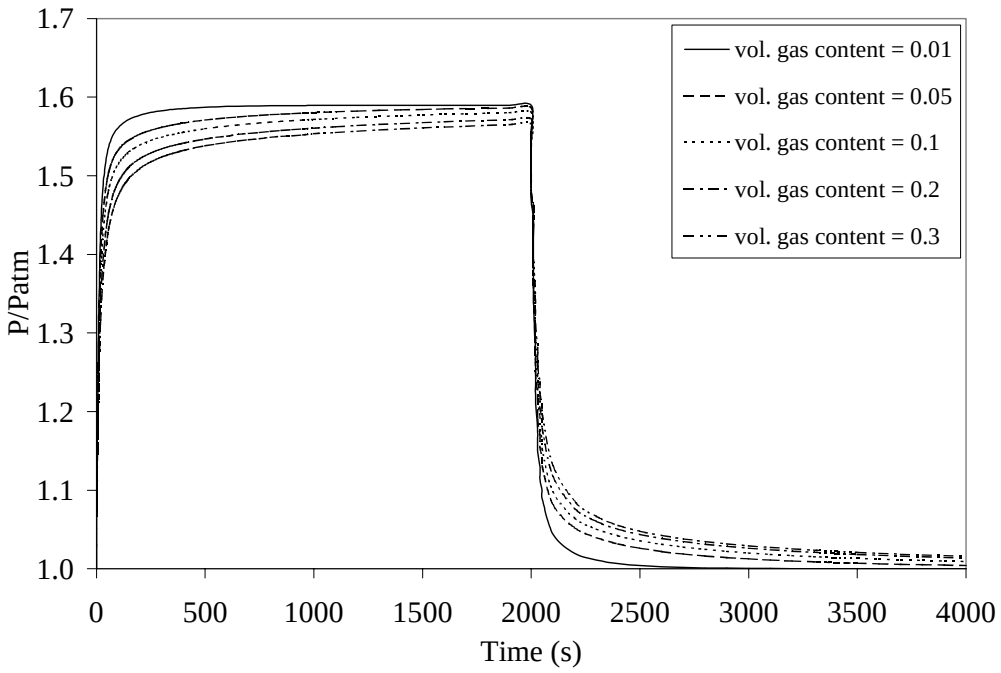

Figure 7.6 Pressure response as a function of time and volumetric gas content (θ_g) (d = 600 cm, d_U/d = 0.683, d_L/d = 0.783, z/d = 0.733, r = r_w, $k_{rg}k_{\iota(r)}$ = 1 x 10^{-9} cm^2, $k_{rg}k_{\iota(r)}/k_{rg}k_{\iota(z)}$ = 1.0, Q_m = 1.0 g/s, V_b = 15000 cm^3, $k_{rg}k_{\iota(z')}/d'$ = 1.0 x 10^{-11} cm)

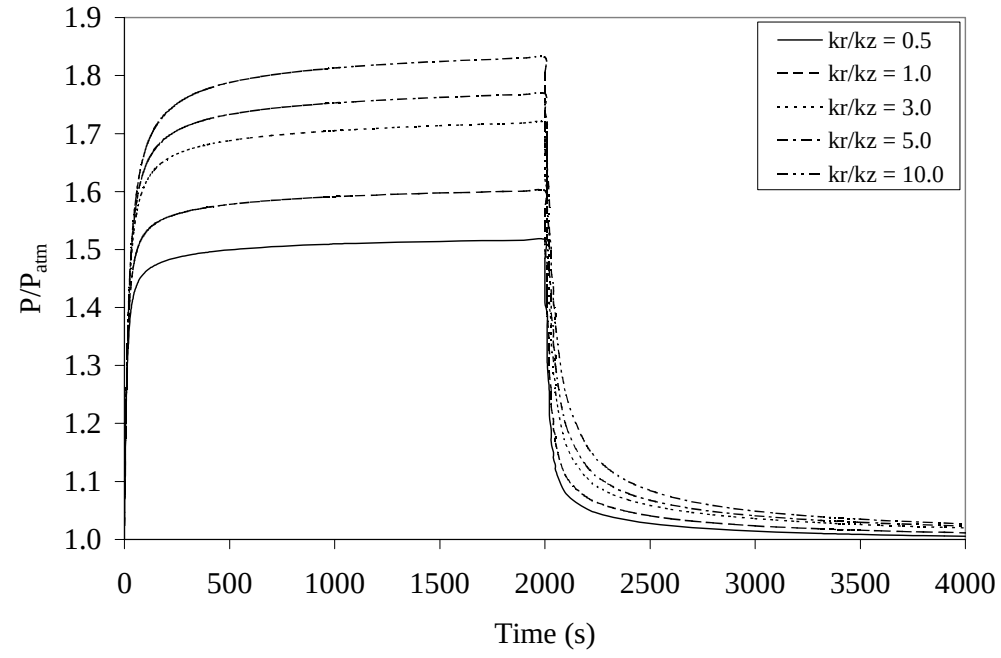

Figure 7.7 Pressure response as a function of time and $k_{rg}k_{\iota(r)}/k_{rg}k_{\iota(z)}$ (or k_r/k_z) ratio (d = 600 cm, d_U/d = 0.683, d_L/d = 0.783, z/d = 0.733, r = r_w, $k_{rg}k_{\iota(r)}$ =1.0 x 10^{-9} cm^2, θ_g =0.1, Q_m =1.0 g/s, V_b = 15000 cm^3, $k_{rg}k_{\iota(z')}/d'$ = 1.0 x 10^{-11} cm)

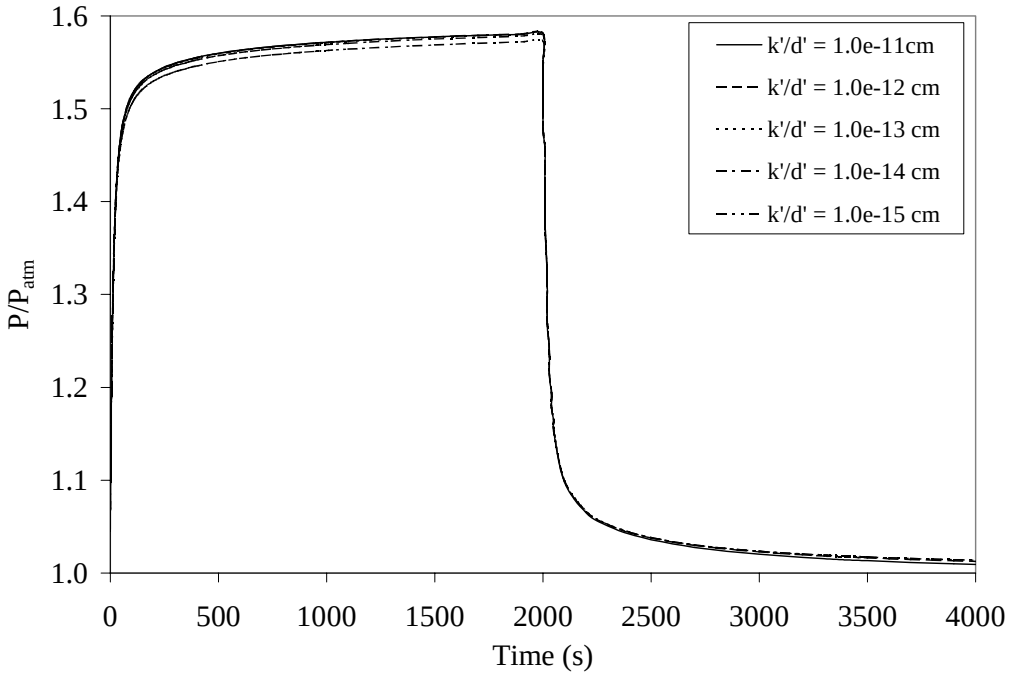

Figure 7.8 Pressure response as a function of time and $k_{rg}k_{\iota(z')}/d'$(or k'/d') (d = 600 cm, d_U/d = 0.683, d_L/d = 0.783, z/d = 0.733, r = r_w, $k_{rg}k_{\iota(r)}$ = 1.0 x 10^{-9} cm^2, $k_{rg}k_{\iota(r)}/k_{rg}k_{\iota(z)}$ = 1.0, θ_g = 0.1, Q_m = 1.0 g/s, V_b = 15000 cm^3)

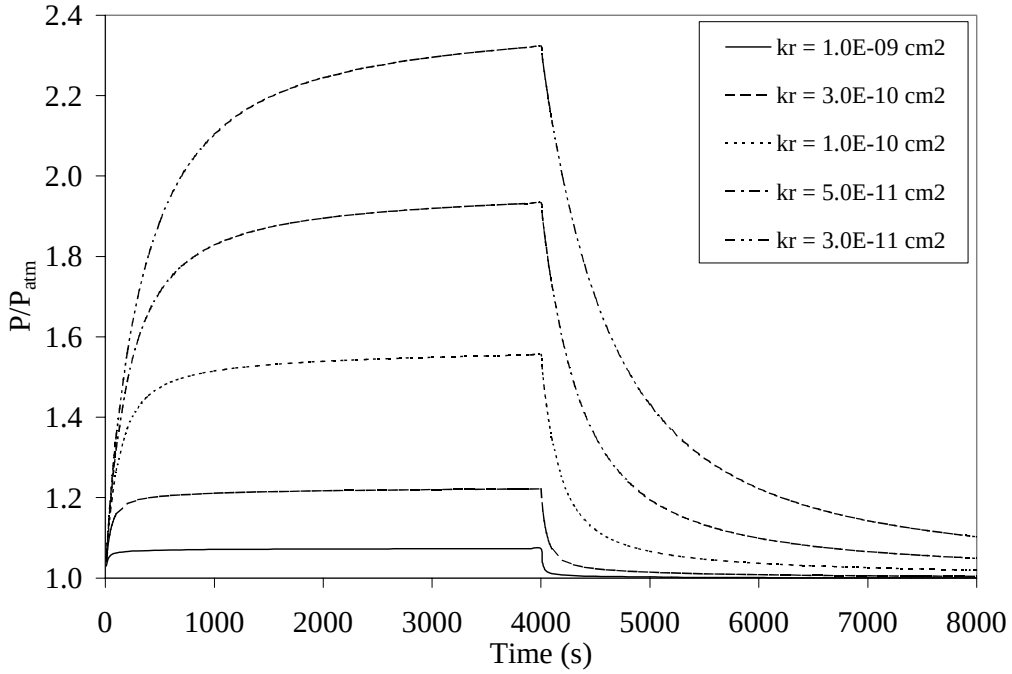

Figure 7.9 Pressure response as a function of time and $k_{rg}k_{\iota(r)}$ (or k_r) (d = 600 cm, d_U/d = 0.683, d_L/d = 0.783, z/d = 0.733, r = r_w, θ_g = 0.1, $k_{rg}k_{\iota(r)}/k_{rg}k_{\iota(z)}$ = 1.0, Q_m = 0.10 g/s, V_b = 15000 cm^3, $k_{rg}k_{\iota(z')}/d'$ = 1.0 x 10^{-11} cm).

issued a Record of Decision (ROD) to the responsible parties mandating the use of soil vacuum extraction and ground-water pump and treat to remove remaining contaminants in unsaturated and saturated subsurface media. The original well design for transient, single-interval testing at the Picillo Farm site was to install 5 cm (2-inch) boreholes with roto-sonic drilling followed by direct-push of 5 cm i.d., 7.6 cm o.d. (3 - inch) heavy gauge aluminum vertically slotted pipe. Roto-sonic drilling was selected as the preferred drilling method because of the presence of large cobbles and boulders encountered during previous drilling efforts. Aluminum was chosen for well construction because of its compatibility with neutron probe counts. Prior to gas permeability testing, the borehole was to be logged with a neutron probe to correlate moisture content with gas permeability estimates and potentially develop in-situ water-gas permeability curves. The use of aluminum as well casing however was abandoned in favor of vertically slotted 5 cm i.d. drill rod high strength carbon steel illustrated in Figure 7.10 because of concern with structural integrity and that casing would have to be pushed through boulders having a cored diameter slightly smaller that the outside diameter of the pipe. It was hoped that a tight fit between the carbon steel pipe and borehole wall, nearly continuous vertical slots, and straddle packers would enable gas permeability estimation over small intervals on the order of 10 cm.

Figure 7.10 Photograph of vertically slotted 5 cm i.d. high tensile carbon steel pipe initially installed for gas permeability testing at the Picillo Farm Superfund Site.

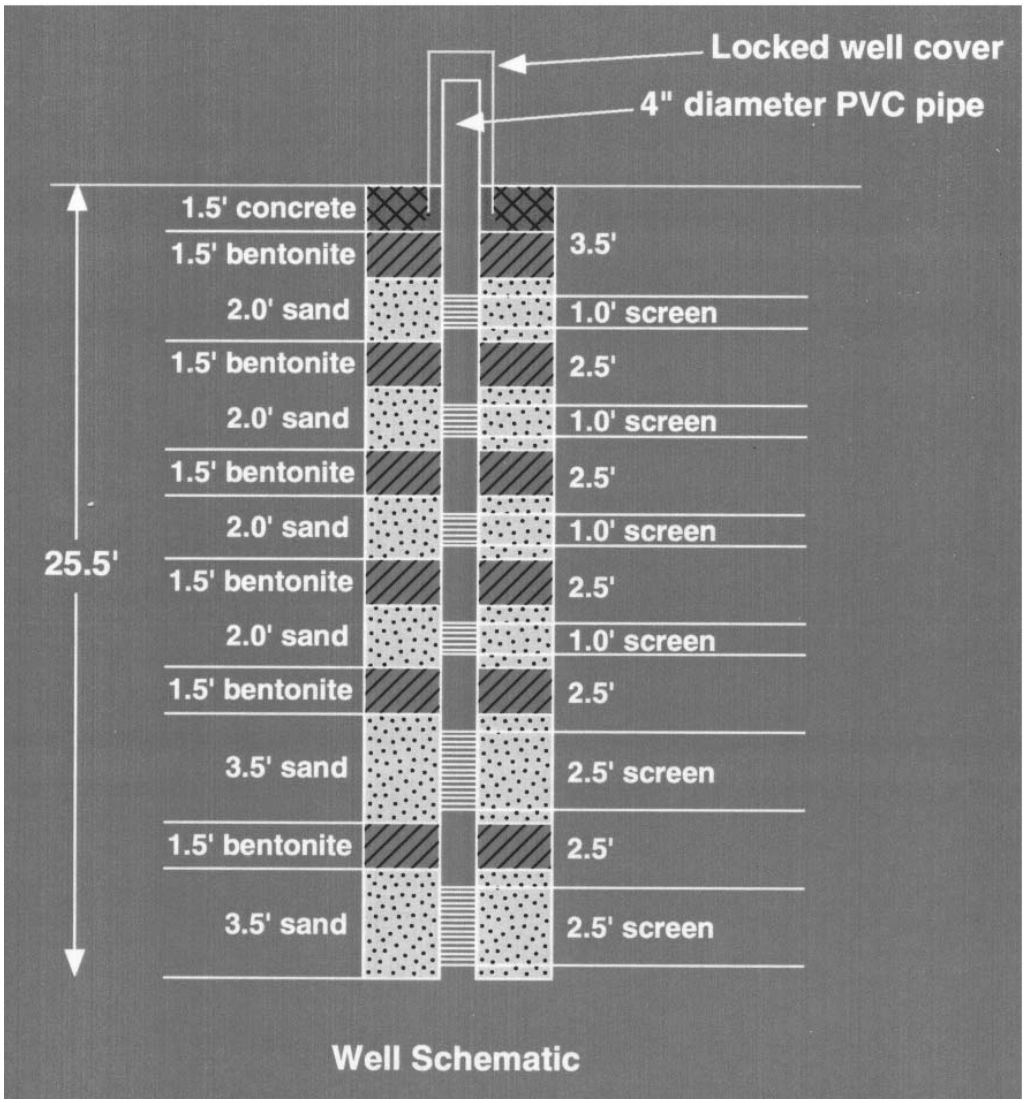

Figure 7.11 Typical well installation details for MWE wells installed at the Picillo Farm Superfund site.

However development of the well revealed severe problems with siltation and plugging of the vertical slots. During well development, a large quantity (20 liters) of a very fine sand was retrieved. Sounding with a water meter at the base of the well revealed that this material continued to flow into the well throughout the development process. Based on these observations, this well construction method was abandoned in favor of a more conventional but less desirable method illustrated in Figure 7.11. Actual completion intervals for sandpack and bentonite seals varied by about ± 8 cm (3 inches).

Dry granular bentonite was poured from the surface through the PVC well and borehole

annular space and hydrated in place through the addition of water. Coarse sand (grade #0) was deposited in a similar manner with the volume for each sandpack interval recorded to assist in borehole storage estimation. Wells and factor slotted screens (0.002 inch) were constructed of 4-inch internal diameter, schedule-40 PVC pipe. The installation of six discrete screened intervals allows measurement of gas permeability over more intervals than typically present (2 or 3) at hazardous waste sites but each screened interval and sandpack is fixed in place and covers a larger vertical interval (approximately 60 cm) than desired. Nevertheless, given the difficult drilling and subsurface conditions present at this site, this well installation method likely represents the limit of conventional well construction.

In 1998, U.S. EPA's Office of Research and Development, installed a test plot consisting of 13 multi-level wells within the west trench portion of the site. The wells were spaced approximately 150 cm (5 feet) apart. The purpose of the test plot is to gain a better understanding of gas flow and rate-limited mass transfer on a field-scale during soil venting application. Roto-sonic drilling was used to create 8-1/4 inch diameter boreholes for well installation. Soil cores were carefully logged with detailed observation of the vertical dimensions of lenses of silt and clay. Soil cores revealed a high heterogeneous subsurface environment consisting of trench backfill, sandy glacial till, and glaciofluvial sand, silt, and clay deposits. One soil core consisted entirely of sausage-shaped, polymer-like, white solid waste. Another soil core resulted in retrieval of a drum fragment containing a semi-solid dark brown to red viscous material. Chemical analysis of both waste materials revealed very high concentrations of chlorinated and non-chlorinated solvents.

During single-interval transient gas permeability testing, a 1.2 g/s capacity diaphragm pump was used to inject air into a riser pipe containing a 1.25-inch internal diameter, 6-inch, schedule-80 PVC screen separated by two 2-foot long inflatable packers. As illustrated in Figure 7.12, flow was measured and controlled at surface using a 150-mm flowmeter (± 2% accuracy) containing a high precision control valve. Air injection temperature was measured with a type-J thermocouple and a thermocouple thermometer (±0.5% of reading accuracy). Air injection pressure was measured with a digital manometer (± 1.0% of range accuracy) and magnehelic gauges. As illustrated in Figure 7.13, a quick-connect was used at the top of the packer riser pipe to prevent release of gas pressure during well shut-in. Pressure as a function of time at the gas injection interval and interval immediately above the injection interval was measured with wireless, self contained, 7/8-inch o.d. pressure transducers (Levelogger - Solinst Canada - accurate to 0.2% full scale). Compensation of pressure loss through subsurface piping and surface tubing was avoided by measurement of pressure in this manner. Pressure readings were taken every 0.5 seconds during testing. Rubber couplings were used between sections of PVC pipe to ensure minimal loss of pressure at the pipe threads. As illustrated in Figure 7.14, the wireless pressure transducer data was located between two pneumatic packers. After testing, data was downloaded into a laptop personal computer using an optical reader.

Single-interval, transient testing was demonstrated in well MWE-02 in a screened interval (MWE-02-03) having an annular sandpack extending from 298 to 354 cm below the base of an

asphalt cap. Depth to the water table was 521 cm below the base of the asphalt cap. Values of radial permeability, vertical permeability and leakance were allowed to vary freely, but borehole storage volume was constrained between 7500 and 12500 cm^3. Based on the volume of the annular sandpack, assumption of a volumetric gas content of 0.3 in the sandpack, and above and below ground piping and tubing, a borehole storage volume of 10,000 cm^3 was calculated. Borehole storage volume was allowed to vary 25% to incorporate uncertainty in volumetric gas content and annular sandpack volume estimation.

Figure 7.12 Flow, pressure, and temperature measurement at the surface during gas permeability estimation in well MWE-02

7.6 Results and Discussion

The approach to parameter estimation described in sections 5 and 6 was applied to parameter estimation here. A series of random guesses was applied (groups of 5000) constrained within decreasing intervals of $k_{rg}k_{\iota(r)}$, $k_{rg}k_{\iota(z)}$, leakance, borehole storage volume, and gas-filled porosity until the lowest root mean squared error (RMSE) was attained for a set of estimates. In this way, variation in parameter estimations for the same or similar RMSE values were assessed. A program was written in FORTRAN (FRLKINV) to facilitate computations. Example input and output files and the source code for this program is provided in Appendix E. Tables 7.1 through 7.4 provide a summary of the 10 best fit estimates (based on lowest RMSE) for each of

Figure 7.13 Close-up of quick-connect at top of 3.2 cm i.d., sch-80 PVC pipe to prevent gas pressure release at shut-in

Figure 7.14 Illustration of wireless pressure transducer clamped between pneumatic packers for use in single-interval and two-interval, transient gas permeability testing in MWE wells

four tests conducted at MWE-02-03. Figures 7.16 through 7.19 illustrate observed versus simulated pressure response for the fit in each test having the lowest RMSE. Values of radial permeability for the 10 best fits in all 4 tests provided very consistent results demonstrating reproducibility in testing at least for radial permeability estimation. Values of leakance though varied over an order of magnitude for the 10 best fits demonstrating uncertainty in this parameter. Ratios of $k_{rg}k_{\iota(r)}/k_{rg}k_{\iota(z)}$ also varied widely again demonstrating uncertainty in this parameter. Uncertainty in leakance and $k_{rg}k_{\iota(r)}/k_{rg}k_{\iota(z)}$ ratios occur because these parameters are correlated and single-interval testing provides no vertical resolution in pressure measurement. Estimates of gas-filled porosity however were very consistent despite modest variability in borehole storage volume demonstrating reproducibility in estimation of gas-filled porosity.

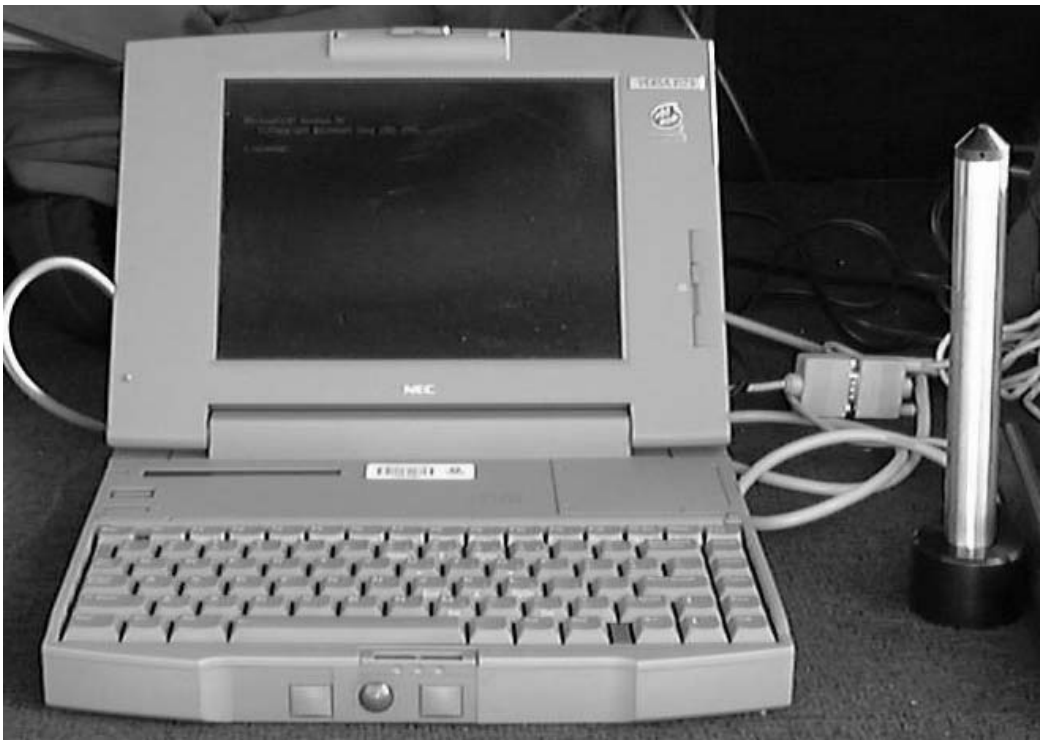

Figure 7.15 Photograph of downloading wireless pressure transducer data into a laptop computer using an optical reader.

7.7 Conclusions

1. During pumping at the wellbore, the line-source/sink solution simulated a more rapid rise in pressure at early time but then leveled off to a lower normalized pressure at late time compared to the finite-radius solution. The former effect was due to lack of a delayed response from borehole storage. The latter effect was likely due to the fact that for the line source/sink solution, simulation extended into the formation at a distance equivalent to the wellbore radius. Lower pressure differential response at late time for the line-source/sink solution would likely lead to gas permeability overestimation for a given flow

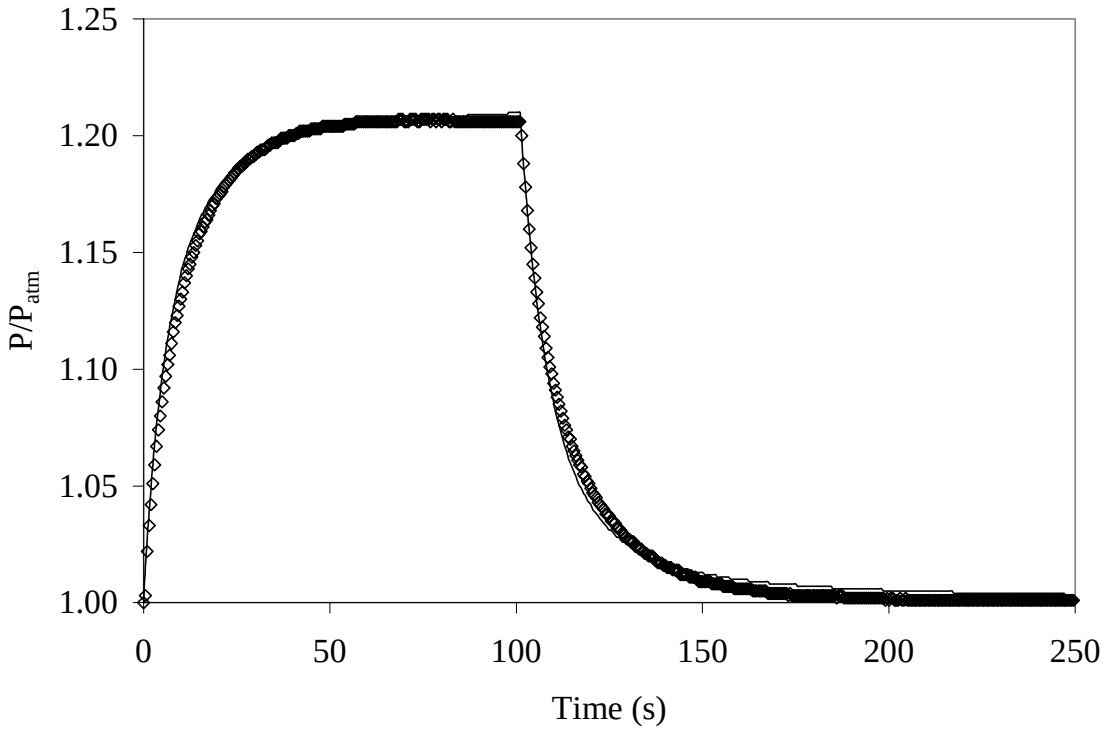

Figure 7.16 Observed versus fitted pressure response for Test 1 in MWE-02-03 ($k_{rg}k_{\iota(r)}$ = 1.54 x 10^{-9} cm^2, $k_{rg}k_{\iota(r)}/k_{rg}k_{\iota(z)}$ = 5.86, $k_{rg}k_{\iota(z')}/d'$ = 1.51 x 10^{-12} cm, θ_g = 0.011, V_b = 10,260 cm^3, RMSE = 3.121 x 10^{-3} atm)

Table 7.1 Ten best parameter estimation fits for test 1 in MWE-02-03

$k_{rg}k_{\iota(r)}$ (cm^2)	$k_{rg}k_{\iota(z)}$ (cm^2)	$k_{rg}k_{\iota(r)}/k_{rg}k_{\iota(z)}$	$k_{rg}k_{\iota(z')}/d'$ (cm)	θ_g	V_b (cm^3)	RMSE (atm)
1.54E-09	2.62E-10	5.86	1.51E-12	0.011	10260	3.121E-03
1.56E-09	3.51E-10	4.45	1.84E-11	0.014	12280	3.171E-03
1.78E-09	2.12E-10	8.40	3.25E-11	0.011	12330	3.230E-03
1.60E-09	3.28E-10	4.87	7.24E-11	0.014	12360	3.233E-03
1.46E-09	3.13E-10	4.68	1.85E-12	0.012	10360	3.243E-03
1.68E-09	2.89E-10	5.82	4.51E-12	0.011	12030	3.296E-03
1.77E-09	2.33E-10	7.59	4.97E-11	0.010	12190	3.322E-03
1.58E-09	3.29E-10	4.80	8.80E-11	0.012	11760	3.369E-03
1.38E-09	6.02E-10	2.29	2.25E-11	0.013	11630	3.403E-03
1.44E-09	3.51E-10	4.12	1.84E-12	0.011	9955	3.403E-03

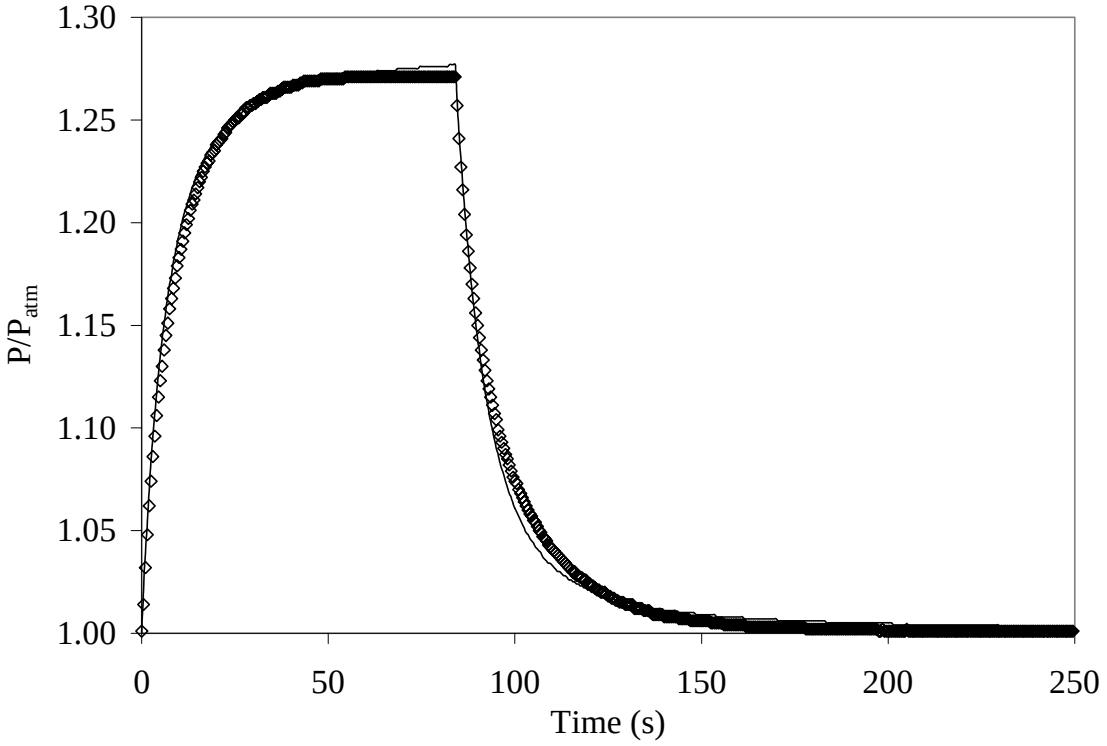

Figure 7.17 Observed versus fitted pressure response for Test 2 in MWE-02-03 ($k_{rg}k_{\iota(r)}$ = 1.81 x 10^{-9} cm^2, $k_{rg}k_{\iota(r)}/k_{rg}k_{\iota(z)}$ = 9.02, $k_{rg}k_{\iota(z')}/d'$ = 7.20 x 10^{-12} cm, θ_g = 0.008, V_b = 11,790 cm^3, RMSE = 3.23 x 10^{-3} atm)

Table 7.2 Ten best parameter estimation fits for test 2 in MWE-02-03

$k_{rg}k_{\iota(r)}$ (cm^2)	$k_{rg}k_{\iota(z)}$ (cm^2)	$k_{rg}k_{\iota(r)}/k_{rg}k_{\iota(z)}$	$k_{rg}k_{\iota(z')}/d'$ (cm)	θ_g	V_b (cm^3)	RMSE (atm)
1.81E-09	2.01E-10	9.02	7.20E-12	0.008	11790	3.23E-03
1.76E-09	2.31E-10	7.63	6.14E-12	0.008	11860	3.23E-03
1.76E-09	2.23E-10	7.91	6.46E-11	0.008	11860	3.27E-03
1.76E-09	2.35E-10	7.52	7.40E-12	0.008	11640	3.29E-03
1.80E-09	2.12E-10	8.46	6.80E-12	0.008	11510	3.30E-03
1.81E-09	2.00E-10	9.03	3.74E-11	0.009	11480	3.37E-03
1.74E-09	2.30E-10	7.58	5.05E-11	0.008	11670	3.37E-03
1.83E-09	1.86E-10	9.81	4.27E-12	0.008	11560	3.37E-03
1.71E-09	2.56E-10	6.70	5.80E-11	0.010	11710	3.39E-03
1.72E-09	2.47E-10	6.98	8.23E-12	0.009	11880	3.42E-03

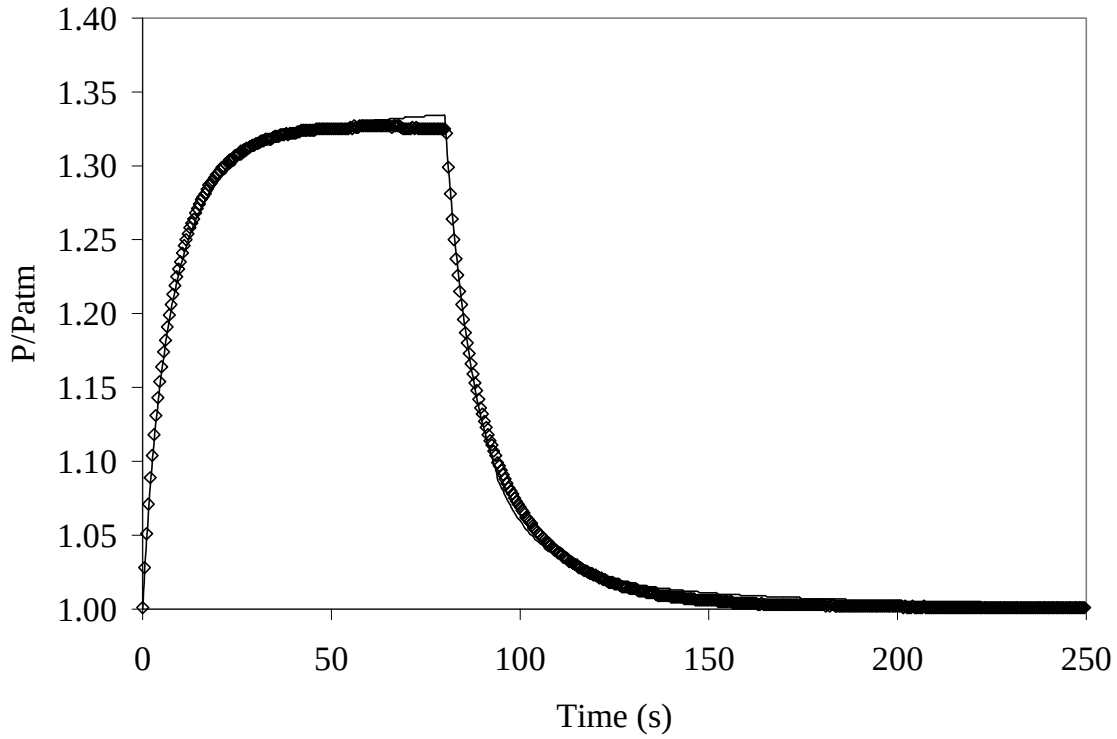

Figure 7.18 Observed versus fitted pressure response for Test 3 in MWE-02-03 ($k_{rg}k_{\iota(r)}$ = 1.60 x 10^{-9} cm^2, $k_{rg}k_{\iota(r)}/k_{rg}k_{\iota(z)}$ = 3.50, $k_{rg}k_{\iota(z')}/d'$ = 8.20 x 10^{-11} cm, θ_g = 0.010, V_b = 11,560 cm^3, RMSE = 4.655 x 10^{-3} atm)

Table 7.3 Ten best parameter estimation fits for test 3 in MWE-02-03

$k_{rg}k_{\iota(r)}$ (cm^2)	$k_{rg}k_{\iota(z)}$ (cm^2)	$k_{rg}k_{\iota(r)}/k_{rg}k_{\iota(z)}$	$k_{rg}k_{\iota(z')}/d'$ (cm)	θ_g	V_b (cm^3)	RMSE (atm)
1.60E-09	4.59E-10	3.50	8.20E-11	0.010	11560	4.655E-03
1.92E-09	1.94E-10	9.92	6.47E-12	0.012	10660	4.735E-03
1.47E-09	6.59E-10	2.24	1.60E-11	0.012	11520	4.756E-03
1.82E-09	2.57E-10	7.09	1.33E-11	0.010	10840	4.797E-03
1.73E-09	3.41E-10	5.07	8.28E-11	0.010	11870	4.831E-03
1.71E-09	3.35E-10	5.10	9.15E-12	0.012	10920	4.831E-03
1.40E-09	7.44E-10	1.88	1.78E-11	0.013	11240	4.897E-03
1.78E-09	2.85E-10	6.24	4.77E-11	0.013	10810	4.910E-03
1.92E-09	1.94E-10	9.88	7.67E-12	0.011	10330	4.997E-03
1.74E-09	3.52E-10	4.93	9.82E-12	0.011	11180	5.032E-03

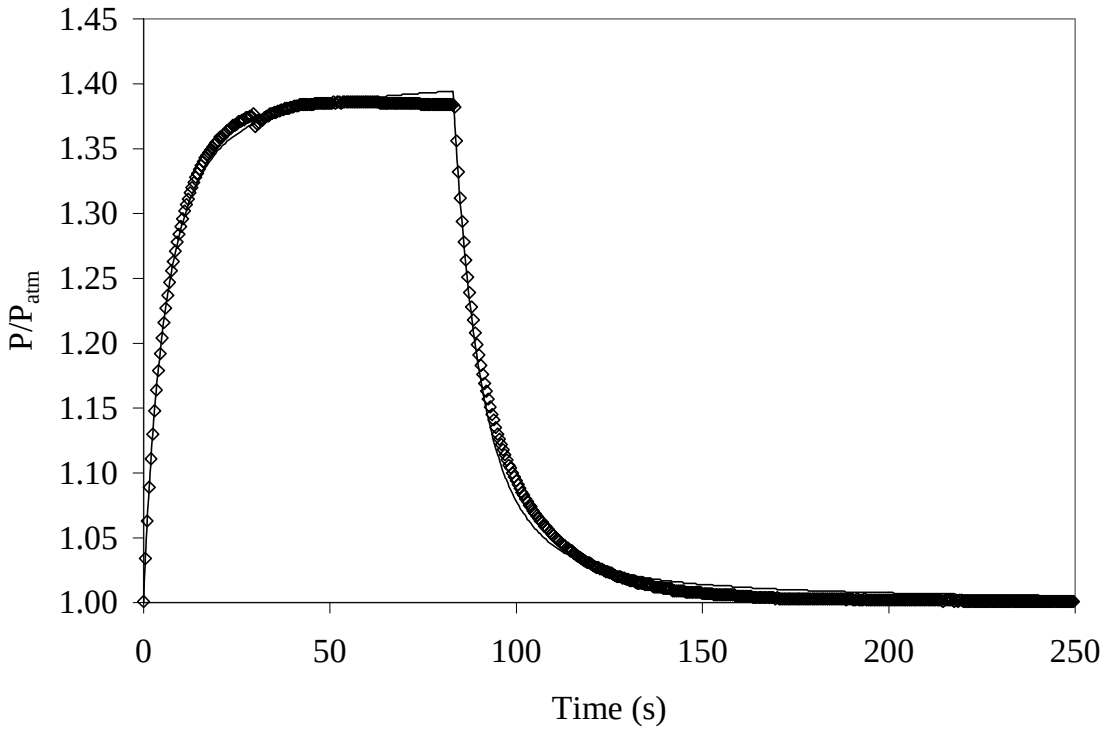

Figure 7.19 Observed versus fitted pressure response for Test 4 in MWE-02-03 (Q_m = 0.722 g/s, $k_{rg}k_{\iota(r)}$ = 1.60 x 10^{-9} cm^2, $k_{rg}k_{\iota(r)}/k_{rg}k_{\iota(z)}$ = 4.29, $k_{rg}k_{\iota(z')}/d'$ = 2.44 x 10^{-12} cm, θ_g = 0.011, V_b = 9,199 cm^3, RMSE = 6.35 x 10^{-3} atm)

Table 7.4 Ten best parameter estimation fits for test 4 in MWE-02-03

$k_{rg}k_{\iota(r)}$ (cm^2)	$k_{rg}k_{\iota(z)}$ (cm^2)	$k_{rg}k_{\iota(r)}/k_{rg}k_{\iota(z)}$	$k_{rg}k_{\iota(z')}/d'$ (cm)	θ_g	V_b (cm^3)	RMSE (atm)
1.60E-09	3.72E-10	4.29	2.44E-12	0.011	9199	6.35E-03
1.65E-09	4.28E-10	3.86	1.74E-11	0.016	10370	6.47E-03
1.46E-09	7.35E-10	1.98	3.02E-11	0.010	10870	6.53E-03
1.57E-09	3.78E-10	4.17	1.15E-12	0.013	9155	6.55E-03
1.64E-09	2.89E-10	5.68	1.03E-12	0.011	8925	6.55E-03
1.66E-09	4.41E-10	3.76	1.18E-11	0.018	10140	6.66E-03
1.63E-09	5.29E-10	3.08	9.05E-11	0.011	11310	6.69E-03
1.68E-09	2.68E-10	6.26	1.93E-11	0.010	8069	6.73E-03
1.68E-09	3.92E-10	4.28	1.98E-11	0.020	9777	6.78E-03
1.49E-09	7.42E-10	2.00	1.83E-11	0.013	10230	6.81E-03

rate. Thus, for single-interval, transient testing, borehole storage effects can become a significant source of error if not properly accounted for.

2. Under conditions of these simulations, error due to use of a line-source/sink solution disappeared at a relatively short distance from the wellbore. Thus, under typical testing conditions when a gas extraction or injection well is not used as the pressure monitoring point, transient gas permeability estimation using a line-source/sink solution would result in little error.

3. A comparison of line-source/sink versus finite-radius simulations at the wellbore at different vertical elevations revealed little error (less than 1.5%) associated with using a line-source/sink solution. Thus, for simulations conducted here, line-source/sink solutions appear appropriate for single well, multi-interval testing. However, conditions specified here are not reflective all potential testing conditions. Thus, when observation points are close to a gas extraction or injection well, it may be useful to utilize a transient, finite-radius solution to assess the importance of finite-radius and wellbore effects.

4. Single-interval simulations demonstrated that increased borehole storage volume results in an increased delayed response to steady-state conditions. Increased gas-filled porosity results in a somewhat similar transient response to increased borehole storage volume but the transient effects are much more prolonged.

5. Single-interval simulations demonstrated that higher $k_{rg}k_{\iota(r)}/k_{rg}k_{\iota(z)}$ ratios prolong attainment of steady-state conditions and result in a higher normalized pressure response compared to lower $k_{rg}k_{\iota(r)}/k_{rg}k_{\iota(z)}$ ratios. The effect of leakance on transient pressure response at the wellbore however appeared to be minor.

6. Single-interval simulations demonstrated that lower gas permeability significantly prolongs attainment of steady-state conditions and results in a much higher pressure differential.

7. Finally, testing at the Picillo Farms Superfund Site revealed that single-interval transient gas permeability testing is an improvement over single-interval steady-state gas permeability testing in that the former provides an estimate of gas-filled porosity and does not rely on attainment of steady-state conditions which is sometime questionable for low permeability media (small pressure change in time after initial pressure or vacuum application). The method though provided little confidence in leakance and k_r/k_z estimation necessitating testing in two or more vertically spaced intervals for which existing analytical solutions are available and appropriate.

8. VOC RETENTION IN POROUS MEDIA

An understanding of volatile organic compound (VOC) retention in porous media is critical to designing, monitoring, and closing venting systems. Each phase in unsaturated porous media can contribute to the retention and mass transport of VOCs. Phases present are solid minerals, organic matter, bulk water, nonaqueous phase liquids (NAPL), and gas. Partitioning mechanisms related to these phases are solid mineral - water, solid mineral - gas, organic matter - water, water - gas, NAPL - water, and NAPL - gas.

8.1 Vapor Concentration

Vapor concentration can be expressed in terms of volume of VOC per volume of gas (e.g., parts per million volume or ppmv), or mass per volume (e.g., ug/cm^3). Since from the Ideal Gas Law, volumetric concentration is equivalent to molar concentration (moles of VOC per moles of gas), conversion of from units of ppmv to ug/cm^3 can be accomplished by

$$C_g(ug/cm^3) = C_g(ppmv)\frac{M_i P}{1000\Re T} \tag{8.1}$$

where M_i (g/mole), P(atm), $\Re$ = 0.08205 (L atm/K mole), and T (°K). For instance, at 20°C (293.15°K) and atmospheric pressure, 100 ppmv benzene (M_i = 78.11 g/mole) is equivalent to 0.3247 ug/cm^3.

8.2 Vapor Pressure

Vapor pressure can be defined as the gas pressure exerted by the vapor of a compound in equilibrium with its pure condensed liquid or solid phase. At a given temperature, a number of molecules in the condensed phase will acquire sufficient energy to overcome molecule-molecule attractions in the condensed phase and escape to the vapor phase. Meanwhile in the vapor phase, continuous collisions of vapor molecules with the surface of the condensed phase will cause a return of some molecules to the condensed phase. The most commonly measured vapor pressure is the boiling point (T_b), which is the temperature at which vapor pressure is equal to 1 atmosphere.

Since molecules in the gas phase at or below a pressure of one atmosphere are separated by relatively large distances and thus have little molecular interaction, the extent to which compounds escape to the vapor phase is largely controlled by molecular interactions in the condensed phase. In the liquid phase, the summation of molecular interactions which cause molecule-molecule attraction is represented by the heat of vaporization (ΔH_v) [$ML^2T^{-2}mol^{-1}$]. Large heats of vaporization are associated with high boiling points. When attempting to estimate vapor pressures for compounds not having tabulated or referenced values, it is helpful to understand the nature of molecular interactions in the condensed phase. Schwarzenbach et al. (1993) provide a discussion on van der Waals, dipole-dipole and hydrogen bonding interactions

which cause increased attraction between like molecules. All compounds experience van der Waals forces. Even nonpolar molecules such as alkanes, which exhibit a time-average smooth distribution of electrons throughout their structure, experience instantaneous displacement of electrons such that momentary electron-rich and electron poor structural regions develop. This momentary redistribution of charges triggers a displacement of electrons in neighboring alkane molecules causing molecular attraction. Vapor pressure decreases and the heat of vaporization increases with increasing alkane size or carbon number because the summation of van der Waals forces or attraction is directly related to molecular size. Van der Waals forces are also responsible for decreasing vapor pressure with increasing size of alkyl groups on alkylbenzenes.

Schwarzenbach et al. (1993) explain that dipole interactions result from electron-attracting or electronegative properties of various types of atoms included in organic compounds (H, C, S, I<N, Br<Cl<O<F). Dipole interactions result from regions in molecules that are always deficient or enriched in electrons. In addition to van der Waals forces, dipoles align with other dipoles in a head to tail fashion. Further, if a dipole is positioned near an evenly charged structural region of an adjacent molecule, electrons in the neighboring molecule will be displaced resulting in an induced dipole attraction. The effect of dipole interaction can be seen in increased heats of vaporization and decreased vapor pressures for benzenes substituted with halogens such as dichlorobenzene. Other polar groups such as nitro ($-NO_2$) also cause marked increased heats of vaporization.

Finally, large differences in electronegativity of hydrogen, oxygen, and nitrogen, hydrogens bound to oxygens in alcohols, or to nitrogens in amines cause hydrogen bonding between like molecules. Thus, substituted benzenes with -COOH, -OH, $-CH_2OH$, and -NH2 show strongly increased heats of vaporization compared to unsubstituted benzenes.

Vapor pressure of an organic compound is strongly dependent on temperature. Equations that relate vapor pressure to temperature are derived from integration of the Clausius-Clapeyron equation

$$\frac{d \ln P_v}{dT} = \frac{\Delta H_v}{\Delta Z \Re T^2} \tag{8.2}$$

where T is temperature, P_v $[ML^{-1}T^{-2}]$is vapor pressure, $\Re$ is the ideal gas constant (8.3143×10^7 $gcm^2mol^{-1}s^{-2}K^{-1}$), and ΔZ [-] is a dimensionless gas compressibility factor (unity for an ideal gas). Grain (1990) states that most estimation and correlation methods are designed for greatest accuracy between T_b and the critical temperature T_c. This range is useful to industrial engineers who deal with high temperatures. Environmental studies however normally involve temperatures well below T_b where these estimation techniques are less accurate. Grain (1990) recommends the use of two methods for estimation of vapor pressure. The first method is the well known Antoine Equation while the second method is known as the Modified Watson Correlation. The former is suitable for estimation of vapor pressure of liquids and gases in the range of 10^{-3} to 760 mmHg while the latter is suitable for vapor pressure of liquids and solids in the range of 10^{-7} to

760 mmHg. The latter method is also less prone to error compared to the former method. Vapor pressure estimation techniques are valuable for compounds having low vapor pressures since experimental data is scare or may be unreliable.

The Antoine Equation has the general form

$$\ln P_v = A_2 - \frac{B_2}{T - C_2} \tag{8.3}$$

where

$$A_2 = \frac{B_2}{T_b - C_2} \tag{8.4}$$

$$B_2 = \frac{\Delta H_{vb}}{\Delta Z \Re T_b^2}\left[\left(T_b - C_2\right)^2\right] \tag{8.5}$$

and C_2 is estimated by Thomson's Rule or

$$C_2 = -18.0 + 0.19 T_b \tag{8.6}$$

ΔH_{vb} is the heat of vaporization at the boiling point [$ML^2T^{-2}mol^{-1}$]. Substituting equations (8.3) and 8.4) into equation (8.2) yields

$$\ln P_v \approx \frac{\Delta H_{vb}\left(T_b - C_2\right)^2}{\Delta Z_b \Re T_b^2}\left[\frac{1}{\left(T_b - C_2\right)} - \frac{1}{\left(T - C_2\right)}\right]. \tag{8.7}$$

In these equations P_v, T_b, and ΔH_{vb} are expressed in units of atmospheres, Kelvin, and cal/mole. The constant $\Re$ is given as 1.987 cal mol^{-1} K-1. The ratio $\Delta H_{vb}/T_b$ can be evaluated using a method introduced by Fishtine (1963):

$$\frac{\Delta H_{vb}}{T_b} = \Delta S_{vb} = K_F\left(8.75 + \Re \ln T_b\right) \tag{8.8}$$

where ΔS_{vb} is the entropy of vaporization at the boiling point and K_F is derived from a consideration of dipole moments of polar and nonpolar molecules. Grain (1990) provides a table of K_F for various compound classes. Equation (8.7) is a modification of the well known relationship of constant entropy of vaporization developed by Trouton in 1884.

From the Antoine Equation, plots of ln P_v (y-axis) versus the reciprocal of temperature (x-

axis) yield a straight line within a temperature range where phase change does not occur (liquid to solid). If the melting point of a compound lies within the temperature range considered, the vapor pressure curves shows a break at this transition temperature. Below the melting point, a compound vaporizes from the solid phase. This process is known as sublimation. The vapor pressure of a solid can be approximated by extrapolating the vapor pressure of an imaginary liquid (subcooled liquid) at the given temperature with modification using the entropy of melting, however, the second method of vapor pressure estimation which was developed for solids is more reliable (Crane, 1990).

The second method incorporates the temperature dependence of the heat of vaporization. Vapor pressure can be estimated by

$$\ln P_v \approx \frac{\Delta H_{vb}}{\Delta Z_b \Re T_b}\left[1-\frac{T_b}{T}\left(3-\frac{2T}{T_b}\right)^m - 2m\left(3-\frac{2T}{T_b}\right)^{m-1}\ln\left(\frac{T}{T_b}\right)\right]. \tag{8.9}$$

The value of m in equation (8.8) depends on the physical state of the compound at the temperature of interest. For solids, Grain (1990) recommends the following values

$$\frac{T}{T_b} > 0.6; \quad m = 0.36 \tag{8.10}$$

$$0.6 > \frac{T}{T_b} > 0.5; \quad m = 0.80 \tag{8.11}$$

$$\frac{T}{T_b} < 0.5; \quad m = 1.19 \tag{8.12}$$

When the boiling point is only available at a reduced pressure (P_1), Grain (1990) recommends estimation of vapor pressure by

$$\ln P_v \approx \ln P_1 + \frac{\Delta H_{v1}}{\Delta Z_b \Re T_1}\left[1-\frac{T_1}{T}\left(3-\frac{2T}{T_1}\right)^m - 2m\left(3-\frac{2T}{T_1}\right)^{m-1}\ln\left(\frac{T}{T_1}\right)\right] \tag{8.13}$$

The ratio $\Delta H_{v1}/T_1$ can then be evaluated by:

$$\frac{\Delta H_{v1}}{T_1} = K_F\left[8.75 + \Re\left(\ln T_1 - \ln P_1\right)\right]. \tag{8.14}$$

8.3 Henry's Law Constant

Partitioning from the gas phase to the aqueous phase can be expressed by

$$C_g = HC_w \tag{8.15}$$

where C_w = aqueous concentration [ML^{-3}] and H = is the "dimensionless" Henry's law constant. The "dimensionless" Henry's Law constant" is not really dimensionless but has units of [vol-liquid/vol-gas]. Henry's law constants are often given in units of atm-m^3/mole which can be converted to a dimensionless form by

$$H = \frac{H'}{\Re T} = \frac{H'}{8.205x10^{-5}\,T} \tag{8.16}$$

where H' is Henry's law constant expressed in atm-m^3/mole and T = temperature (°K). When a laboratory derived value can not be found, a Henry's Law Constant can be estimated by:

$$H = 16.04\frac{C_g^{sat} M_i}{C_w^{sat} T} \tag{8.17}$$

where C^{sat}_w, and C^{sat}_g are the saturation aqueous (solubility) and vapor phase (can be derived from vapor pressure) concentrations respectively [ML^{-3}]. For the equation above, C^{sat}_w, and C^{sat}_g are expressed in units of mg/l and mmHg respectively. M_i is the molecular weight [M/mole] of the compound of interest.

8.4 Gas-Water Interfacial Partitioning

In the absence of NAPL, retention of VOCs in porous media has generally been considered to include adsorption on mineral surfaces and partitioning in soil organic matter and water. However, Pennell et al. (1992), Hoff et al. (1993), Conklin et al. (1995), and Brusseau et al. (1997) found in laboratory experiments that retention was significantly greater than attributable to sorption and partitioning into bulk water. They attributed this additional retention to adsorption at the gas-water interface. For example, Hoff et al. (1993) estimated that 48-56% of the observed retention of straight-chain alkanes by sandy aquifer material was due to gas-water interfacial adsorption. Pennell et al. (1992) reported that accumulation at the gas-water interface accounted for about 50% of total p-xylene retention in unsaturated soils and clay minerals. Conklin et al. (1995) evaluated gas-water interfacial adsorption of benzene and p-xylene in desert sand having a low organic carbon content (0.097%) and sorption capacity (saturated soil-water partition coefficients for benzene and p-xylene 0.0380 and 0.240 cm^3g^{-1} respectively) at volumetric water contents of 0.10 and 0.18. Retardation coefficients estimated from column gas flow studies revealed that 34% and 61% of p-xylene was retained at the gas-water interface at volumetric water contents of 0.1 and 0.18 respectively while less than 10% of benzene was retained for either volumetric water content. Brusseau et al. (1997) evaluated gas-water

interfacial adsorption of methane, heptane, TCE, and benzene in glass beads (0.35 - 0.73 mm diameter), silica sand, and aquifer material (< 2mm fraction consisting of 89.5% sand, 4.1% silt, 6.4% clay, and 0.03% organic carbon) at volumetric water contents of 0.119, 0.094, and 0.16 respectively. Retardation coefficients estimated from column gas flow studies revealed that, 2.6%, 67.2%, and 83.5% of methane, TCE, and heptane respectively was retained at the gas-water interface in the silica sand system. In the glass bead system, 61.6% to 73.5% of TCE and 53.5% to 60.6% of benzene was retained at the gas-water interface. In the aquifer material system, 29.1% to 47.6% of TCE was retained at the gas-water interface. These experiments indicate that retention at the gas-water interface may be important in soils with low organic carbon or absent of NAPL.

The magnitude of interfacial partitioning is largely controlled by the specific interfacial area A_{ia} [L^{-1}]and the K_{ia} = the interfacial sorption coefficient [L]. Partitioning from the gas phase to the gas-water interface can be expressed by:

$$C_{ia} = K_{ia} C_g \tag{8.18}$$

where C_g = gas concentration [ML^{-3}], and C_{ia} = concentration at the gas-water interface [ML^{-2}]. Gvirtzman and Roberts (1991) state that maximum interfacial area should occur when water films are relatively thin and pendular rings form across adjacent mineral grains. As soil moisture content decreases further and approaches monolayer water coverage on mineral surfaces, A_{ia} will approach the specific surface area of the porous medium. Costanza and Brusseau (2000) state that physical soil characteristics such as soil texture, pore size distribution and wetting/drying cycles are factors that should affect the geometry of the soil water in porous media and thus are considerations in assessing A_{ia}. Gas-water interfacial area is important not only in determining retention at the interface but in gas-water mass exchange kinetics. It is expected that thin water films on mineral surfaces would have minimal mass-transfer rate limitations while aqueous diffusion limited mass transfer may be important for water-filled pores. Experimental evidence indicates that vapor adsorption at the gas-water interface may be considered instantaneous relative to other transport processes (Lorden et al. 1998) however there has been no systematic investigation to verify this assumption.

Karger et al. (1971), Pennell et al. (1992), and Hoff et al. (1993) established that increased hydrophobicity leads to greater retention at the gas-water interface. However, other physicochemical properties besides hydrophobicity determine retention at the gas-water interface. As Costanza and Brusseau (2000) explain, at a given vapor pressure, a low molecular weight compound such as methane will show much less interfacial adsorption than a higher molecular weight compound such as octane. This is attributed to the higher volatility of methane. As saturation vapor pressure is approached however, the trend is reversed where more volatile compounds like methane begin to exhibit greater total interfacial adsorption compared to compounds like octane. This is due to the much larger saturation vapor pressures of lower molecular weight compounds. Vapor pressure is proportional to the number of molecules in the vapor phase and subsequently, to the number of collisions with the gas-water interface. Larger

saturation vapor pressures of lower molecular weight compounds provide a greater probability of adsorption. Thus, less volatile compounds will dominate interfacial adsorption at lower vapor concentrations or partial pressures while more volatile compounds will dominate interfacial adsorption near saturation vapor pressure. Costanza and Brusseau (2000) state however that even in the presence of bulk NAPL, it would be rare for vapor concentrations to approach saturation levels.

The observation that greater hydrophobicity leads to greater retention at the gas-water interface appears to contradict the fact the interfacial partition coefficients are higher for more hydrophilic compounds. More polar compounds such as aromatics and chlorinated hydrocarbons tend to have higher interfacial partition coefficients compared to nonpolar compounds. More polar compounds though tend to partition strongly into the bulk water phase thereby reducing concentration at the gas-water interface. Thus water content becomes important in determining concentration at the interface. Costanza and Brusseau (2000) provide a summary of K_{ia} estimation methods and a table of literature values of K_{ia} for selected compounds.

8.5 Gas-Solids Partitioning

Partitioning coefficients have only been found to be relatively independent of the degree of saturation when gravimetric water contents exceed 2-5%. Direct sorption from the gas phase to the mineral surfaces may be neglected in most cases except under very arid conditions (Chiou and Shoup, 1985). In extremely dry soil-water systems, solid-vapor adsorption has been shown to be related to the mineral surface and moisture content of the soil (McCarty et al., 1981; Goss and Eisenreich, 1996). However, adsorption is no longer affected by moisture content upon coverage of the internal mineral surface by liquid water (Chiou and Shoup, 1985). Gas-solids partitioning will not likely be an important process for soil venting systems in a temperate environment. The importance of gas-solids partitioning during venting in an arid environment is unknown.

8.6 Solids-Water Partitioning

Partitioning from the aqueous phase to the solid phase can be expressed in the form of a linear Freundlich isotherm

$$C_s = K_d C_w \tag{8.19}$$

where C_s = solids concentration [MM^{-1}] and K_d = the sorption partition coefficient [L^3M^{-1}]. The mechanism underlying sorption of nonionic organic compounds from aqueous solution onto aquifer solids, sediments and soils is postulated to be hydrophobic partitioning into a stationary organic phase, such as soil organic matter (Karickhoff et al., 1979; Means et al., 1981; Chiou et al., 1979,1983; Gschwend and Wu, 1985). The soil-water partition coefficient (K_d) can be directly determined by laboratory testing or estimated by the empirical relationship

$$K_d \approx K_{oc}\, f_{oc} \tag{8.20}$$

where K_{oc} = organic-carbon-water partition coefficient (L^3M^{-1}) and f_{oc} = fraction of organic carbon [MM^{-1}]. This relationship is generally recognized as being valid when $f_{oc} > 0.001$ (McCarty et al., 1981; Schwarzenbach and Westall, 1981; Karickhoff, 1984). For soils with low organic carbon content ($f_{oc} < 0.1\%$), sorption to mineral grains may be dominant (Piwoni and Bannerjee, 1989) requiring direct measurement of soil-water partition coefficients. Organic carbon-water partition coefficients are often estimated from octanol-water partition coefficients or water solubility.

A compound's K_{oc} is typically estimated from a compound's water solubility or octanol-water partition coefficient. The applicability however of using octanol-water partition coefficient and aqueous solubility data to estimate K_{oc} has been questioned however because some organic compounds have similar aqueous solubility but very different octanol-water partition coefficients (Ellgehausen et al. 1981, Mingelgrin and Gerstl, 1983, Olsen and Davis, 1990). A more fundamental approach using molecular topology, specifically a parameter called the first-order connectivity index which describes the size and structure of an organic molecule, has been suggested to estimate K_{oc} (Koch, 1983; Sabljic, 1987, 1989; Sabljic and Protic, 1982). Fetter (1992) states that molecular topology has several advantages over the use of octanol-water partition coefficient and water solubility regression equations for estimation of an organic compound's K_{oc} value: (1) there is a theoretical basis to molecular topology for nonpolar organic compounds; (2) the literature contains a wide range of experimentally derived values for octanol-water partition coefficients and aqueous solubility values for nonpolar organic compounds where there is no way to know which values are correct; (3) some compounds with similar aqueous solubility values have quite different octanol-water partition coefficients; (4) there are a number of competing regression equations involving octanol-water and water solubility; (5) regression equations involving solubility and octanol-water coefficients to estimate K_{oc} were devised strictly for nonpolar organic compounds. Another advantage of using molecular topology is that the direct correspondence between molecular structure and molecular connectivity makes its possible to better understand the underlying mechanisms of sorption on a molecular level (Sablijc, 1989). Hu et al. (1995) estimated sorption mass transfer coefficients direct from molecular connectivity indexes.

8.7 NAPL-Gas/Water Partitioning

Equilibrium exchange between NAPL and the aqueous phase can be expressed by

$$C_w = \gamma_i \chi_i C_w^{sat} \tag{8.21}$$

where γ_i and χ_i are the activity coefficient [-] and mole fraction [-] of component i in the NAPL mixture respectively. Equilibrium exchange between NAPL and the gas phase can be expressed by

$$C_g = \gamma_i \chi_i C_g^{sat} \tag{8.22}$$

thus,

$$C_g = \gamma_i \chi_i C_g^{sat} = \gamma_i \chi_i H C_w^{sat} = H C_w . \tag{8.23}$$

A NAPL-gas partition coefficient, K_{ng} [-] can defined by

$$K_{ng} = \frac{C_n}{C_g} \tag{8.24}$$

where C_n = non-aqueous phase liquid concentration [ML^{-3}]. Since C_n can be expressed as

$$C_n = \frac{\chi_i M_i}{\sum_{j=1}^{N} \frac{\chi_j M_j}{\rho_j}} \tag{8.25}$$

and

$$C_g^{sat} = \frac{P_v M_i}{\Re T} \tag{8.26}$$

where P_v is the vapor pressure of an organic compound. K_{ng} can be expressed as a function of vapor pressure or water solubility

$$K_{ng} = \frac{\Re T}{\gamma_i P_v \sum_{j=1}^{N} \frac{\chi_j M_j}{\rho_j}} = \frac{M_i}{\gamma_i H C_w^{sat} \sum_{j=1}^{N} \frac{\chi_j M_j}{\rho_j}} \tag{8.27}$$

This equation can be simplified by

$$K_{ng} = \frac{\Re T \rho_n}{\gamma_i P_v M_n} = \frac{M_i \rho_n}{\gamma_i H C_w^{sat} M_n} \tag{8.28}$$

where M_n and ρ_n are the mean molecular weight [$Mmol^{-1}$] and density [ML^{-3}] of the NAPL mixture respectively. Alternatively, a NAPL-water partition coefficient (K_{nw}) can be expressed as

$$K_{nw} = \frac{M_i}{\gamma_i C_w^{sat} \sum_{j=1}^{N} \frac{\chi_j M_j}{\rho_j}} = \frac{M_i \rho_n}{\gamma_i C_w^{sat} M_n} \tag{8.29}$$

which is consistent with formulations of Lee et al.(1992) and Cline et al. (1992) for NAPL-water partitioning when the activity coefficient equals unity. The activity coefficient for a compound in a mixture of structurally similar compounds is close to unity. This has been shown for mixtures of aromatic compounds like benzene and toluene as well as saturated alkane constituents like hexane and octane (Leinonen et al 1973 and Sanemasa et al. 1987). Mixtures of alkanes and aromatic constituents, however show some deviation from ideality that can result in somewhat higher aqueous concentrations than predicted.

8.8 Advective-Dispersive Equation for Vapor Transport

Total retention of VOCs in porous media can be described by

$$C_T = C_g \theta_g + A_{ia} C_{ia} + C_w \theta_w + \rho_b C_s + C_n \theta_n \tag{8.30}$$

where C_T = total soil concentration [ML^{-3}], θ_g = volumetric gas content [L^3L^{-3}], θ_w = volumetric water content [L^3L^{-3}], θ_n = volumetric NAPL content [L^3L^{-3}], and ρ_b = bulk density [ML^{-3}]. Thus, under equilibrium conditions, the total soil concentration may be estimated from gas concentration by

$$C_T = C_g \left(\theta_g + A_{ia} K_{ia} + \frac{\theta_w}{H} + \frac{\rho_b K_d}{H} + \frac{\Re T \theta_n}{\gamma_i P_v \sum_{j=1}^{N} \frac{\chi_j M_j}{\rho_j}} \right). \tag{8.31}$$

The first generation of models designed to simulate gas-phase advective transport of volatile organic chemicals were based on the assumption of equilibrium or ideal transport (Johnson et al., 1988; Wilson et al., 1987, 1988; Baehr et al., 1989). That is rate-limited mobile-immobile gas (physical heterogeneity), gas-water, solids-water, and gas-NAPL exchange is insignificant or does not occur. The advective-dispersive equation including a storage term at the air-water interface is given by:

$$\theta_g \frac{\partial C_g}{\partial t} + A_{ia} \frac{\partial C_{ia}}{\partial t} + \theta_w \frac{\partial C_w}{\partial t} + \rho_b \frac{\partial C_s}{\partial t} + \theta_n \frac{\partial C_n}{\partial t} = \theta_g D_{ij} \frac{\partial}{\partial x_i} \left(\frac{\partial C_g}{\partial x_j} \right) - q_i \frac{\partial C_g}{\partial x_i} \tag{8.32}$$

where D_{ij} = dispersion coefficient tensor [L^2T^{-1}]. Invoking the assumption of local equilibrium

for the gas-water interface, gas-bulk water and solid-water phases results in the commonly expressed advective-dispersive equation

$$R\frac{\partial C_g}{\partial t} = D_{ij}\frac{\partial}{\partial x_i}\left(\frac{\partial C_g}{\partial x_j}\right) - v\frac{\partial C_g}{\partial x_i} \tag{8.33}$$

where the retardation coefficient R [-] equals

$$R = 1 + \frac{K_{ia}A_{ia}}{\theta_g} + \frac{\rho_b K_d}{\theta_g H} + \frac{\theta_w}{\theta_g H} + \frac{\Re T\theta_n}{\theta_g \gamma_i P_v \sum_{j=1}^{N}\frac{\chi_j M_j}{\rho_j}}. \tag{8.34}$$

Equation (8.34) is only valid when the volumetric NAPL content remains constant and mole fractions remain the same such as in the case of a recalcitrant waste oil. Using R, mass fractions in gas (f_s), gas-water interface (f_{ia}), water (f_w), solids (f_s), and NAPL (f_n) can be calculated as

$$f_g = \frac{1}{R} \tag{8.35}$$

$$f_{ia} = \frac{A_{ia}K_{ia}}{\theta_g R} \tag{8.36}$$

$$f_w = \frac{\theta_w}{H\theta_g R} \tag{8.37}$$

$$f_s = \frac{\rho_b K_d}{H\theta_g R} \tag{8.38}$$

$$f_n = \frac{\theta_n K_{ng}}{\theta_g R}. \tag{8.39}$$

8.9 Dispersion

When the advective-dispersion equation using the local equilibrium assumption is used to fit effluent breakthrough curves, rate-limited vapor transport results in breakthrough curves which give the "appearance" of increased dispersion. The dispersion coefficient however should not be used as a correction term to account for rate-limited mass transport. This has been attempted repeatedly with failure. To explicitly account for this rate-limited mass transport, the contribution of molecular diffusion and mechanical dispersion to dispersive flux must first be

quantified. The dispersion coefficient is defined as:

$$D = \frac{D_g}{\tau_g} + D_m v \tag{8.40}$$

where D_g = free-gas molecular diffusivity [L^2T^{-1}], τ_g = tortuosity factor of gas filled porosity [-], and D_m = mechanical dispersion coefficient [L], explicitly accounts for the combined effects of longitudinal molecular diffusion and mechanical dispersion. On the pore-scale (typical of a soil column study), mechanical dispersion is believed to be caused by: (1) fluid moving faster in the center of pores than along edges, (2) some fluid particles traveling along longer flow paths compared to other particles, and (3) larger pores conducting more fluid than smaller pores (Fetter, 1992). On a macroscopic or field scale, mechanical dispersion is much larger and appears to be caused primarily by spatial variation in hydraulic conductivity (Fetter 1992, and Domenico and Schwartz,1990). Since mechanical dispersion is combined with diffusion in the advective-dispersive equation, the contribution of mechanical dispersion to overall dispersion is often not clear. Pfannkuch (1962) conducted a series of column experiments to determine dispersion as a function of Peclet number (Pe) which he defined as

$$Pe = \frac{v d_{50}}{D_w} \tag{8.41}$$

where d_{50} is the mean grain size [L] and D_w is the aqueous molecular diffusion coefficient [L^2T^{-1}]. Pfannkuch (1962) plotted Peclet numbers versus dispersion coefficients normalized to free aqueous diffusion coefficients to determine the affect of pore velocity on mechanical dispersion. He observed that at high pore velocities or Peclet numbers when mechanical dispersion became dominant over aqueous diffusion, dispersion normalized for aqueous diffusion versus Peclet numbers plotted as a straight line with 45 degree angle indicating that pore velocity directly determined mechanical dispersion. Mechanical dispersivity then is considered a characteristic property in a medium and in a three dimension system, a tensor similar to hydraulic conductivity.

A number of ground-water field studies however have demonstrated that dispersion is scale dependent. In many of these studies physical heterogeneity and mechanical dispersion at the macroscopic scale appeared to have contributed significantly to overall dispersion. Values of dispersion are in general are two or more orders of magnitude greater in field studies compared to column experiments (Domenico and Schwartz, 1990). Stochastic theory (Gelhar, 1979) predicts that macroscale dispersivity should approach an constant or asymptotic value. These large values may however not be appropriate for simulation at the scale of interest. This makes selection of a mechanical dispersion coefficient difficult for model simulation. Domenico and Schwartz (1990) state that one way to explain spatially variable dispersivities is in relation to some representative elemental volume (REV). With the spreading of a solute, eventually a transition occurs from the microscale to the macroscale. The implicit assumption is that at each scale an REV exists where dispersivity is constant. In the zone of transition between scales, it may be difficult to define a

value for dispersivity however. As a consequence, small changes in volume could result in significant variability. Also, mass may not be normally distributed as classical theory would predict resulting in undefinable dispersivity values. Thus, in field-scale gas transport studies, mechanical dispersivity may be largely an undefinable input parameter requiring sensitivity analysis for each application to determine its importance in model output and decision making.

Diffusion in the gas phase is considerably more complex than in the aqueous phase. Gas-phase diffusion can occur not only by molecular diffusion but also by Knudsen diffusion and nonequimolar diffusion (Thorstenson and Pollock, 1989). Knudsen diffusion and nonequimolar diffusion are all molecular diffusion processes arising from random kinetic energy and motion of the molecules. They only differ in that specific conditions impose constraints and conditions on directions and rates of diffusion. Equations based on Fick's law are not adequate for representing diffusion in systems where contributions of Knudsen and nonequimolar diffusion are significant. In these systems, the "dusty gas" model is more appropriate (Thorstenson and Pollock, 1989). The contribution of Knudsen diffusion however will be negligible except for very fine grained materials (Thorstenson and Pollock, 1989). Equations based on Fick's law are also not appropriate for systems where the concentration in the gas phase is not dilute or where evaporative fluxes (mass transfer from organic liquid to the gas phase) occur (Baehr and Bruell, 1990). The assumption of dilute concentrations in the gas phase will be valid except when large sources of chemicals with large vapor pressures are present. During soil venting application, a detailed description of diffusion is probably unnecessary because the contribution of advective flux will overwhelm that of diffusive flux when pressure differences are on the order of 1% (Thorstenson and Pollock, 1989). Hence the use of equations based on Fick's law to describe diffusive flux is probably adequate in most cases. Molecular diffusion occurs from random molecular motion due to the thermal kinetic energy of individual molecules. This motion causes random spreading and mixing. The coefficient describing this motion is much larger in the gas phase compared to the liquid phase because molecules are much farther apart in the gas phase. D_g depends on the molecular weight of the chemical diffusing in soil gas and on soil temperature and pressure.

To directly assess the contribution of molecular diffusion and mechanical dispersion to dispersive flux during gas flow without the interfering effects of physical heterogeneity or rate-limited sorption, Popovičová and Brusseau (1997) conducted of a series of laboratory column experiments using carefully packed 0.59 mm dry glass beads to create a homogeneous media. Methane was used as a nonsorbing conservative tracer. Experiments were conducted at gas velocities ranging from 0.1 to 3.33 cm/s. Breakthrough curves for methane were symmetrical indicating no rate-limiting behavior. Peclet numbers, which arise during non-dimensionalization of the advective dispersion equation were defined as

$$Pe = \frac{vL}{D} \tag{8.42}$$

and determined through a non-linear, least squares optimization program. At high gas velocities

when mechanical dispersion is the primary cause of dispersion, Peclet numbers approach L/D_m because $D_g/\tau_g << D_m v$. Popovičová and Brusseau (1997) found that Peclet numbers were a function of gas velocity only at velocities less than 0.33 cm/s indicating that molecular diffusion was significant at velocities less than 0.33 cm/s. At gas velocities less than 0.33 cm/s, Popovičová and Brusseau (1997) assumed that molecular diffusion was the only process contributing to dispersion. Use of a literature value for the free air molecular diffusion for methane (0.28 cm^2/s) enabled calculation of a tortuosity for the homogeneous media. Fitted total dispersion values then allowed determination of the percent contribution of diffusion and mechanical dispersion to total dispersion as a function of gas velocity. They found that the contribution of molecular diffusion to total dispersion was less than 3% for gas velocities greater than 2.5 cm/s. Comparison of these results with those reported by Brusseau (1993) shows a difference of approximately three orders of magnitude between gas and water velocities at which the contribution of both longitudinal molecular diffusion and mechanical dispersion was 50%. This difference is expected since vapor-phase diffusion coefficients are approximately four orders of magnitude greater than aqueous diffusion coefficients. Thus, under typical field conditions where pore-gas velocities away from the immediate vicinity of a gas extraction well range from 0.001 to 0.1 cm/s, molecular diffusion will dominate the dispersion term.

During field-scale gas displacement experiments, low pore-gas velocities and high dispersion coefficients due to gaseous molecular diffusion will lead to low Peclet numbers. Brusseau et al. (1989) demonstrated that low Peclet numbers produce breakthrough curve asymmetry similar to nonideal transport. They used Brenner's solution to the advective-dispersive equation which is solved for a flux-type inlet boundary condition and finite zero-gradient outlet boundary condition, to assess the effect of Peclet numbers when R = 1 on generation of asymmetrical breakthrough curves. They noted that as the Peclet number increases in homogeneous material, breakthrough curves approach a symmetrical, sigmoidal shape. However, for Peclet numbers less than approximately 10, breakthrough curves are noticeably asymmetrical. While this analysis was conducted for solute transport, this finding is important for gas transport because under some column experimental conditions and likely under typical field conditions, the Peclet number will often be less than 10. Thus dispersion due to molecular diffusion could easily be mistaken for nonequilbrium behavior if not properly accounted for.

9. RATE-LIMITED VAPOR TRANSPORT: SELECTION OF CRITICAL PORE-GAS VELOCITIES TO SUPPORT VENTING DESIGN

The effectiveness of soil venting as a method to remove VOCs from unsaturated media basically relies on two factors: 1) the ability to move gas or air directly through contaminated media by advection and 2) rate-limited mass exchange. Anecdotal evidence from field studies and published studies (Krishnayya et al., 1988; Croisé et al., 1989; Ho and Udell, 1992; Kearl et al., 1991) indicate that physical heterogeneity on a large-scale such as lenses or layers of low permeability, perched water-table conditions, or regions of local saturation can severely limit the effectiveness of venting application. Reduced mass extraction due to physical heterogeneity can be overcome to some degree by improved venting design (e.g., increasing well spacing or improved placement of screened intervals). For instance, in the mid-western United States (e.g., Nebraska) it is common to have a thick layer of lower permeability loess overlaying a higher permeability layer of sand. When both media are contaminated, much better advective gas flow can be achieved in the loess by installing separate gas extraction wells in this material as opposed to screening wells across both stratigraphic layers whereby most gas flow would occur in the sand layer. It is impractical and in most cases infeasible though to selectively screen extraction wells in thin discontinuous lenses of silt or clay because of physical dimensions and inability to locate these lenses in the field. Because of the latter consideration, physical heterogeneity on this scale is not commonly explicitly described in numerical models but instead represented by first-order rate constants.

A growing number of published studies indicate that rate-limited gas-NAPL, gas-water, and water-solids mass exchange on a small, pore, or microscopic scale can also significantly limit the effectiveness of venting application. Laboratory column and sand tank studies such as those reported by McClellan and Gillham (1992) and Ng et al. (1999) have demonstrated that volatilization from NAPL in contact with the mobile gas phase ("free" NAPL) initially controls mass removal during venting operation. Following free NAPL removal, transfer of VOCs to the mobile gas phase is controlled by mobile- immobile gas (e.g., macropores such as that described by Popovičová and Brusseau, 1997, 1998), intraaggregate aqueous diffusion (Gierke et al., 1992; Ng and Mei, 1996), interparticle aqueous diffusion (Grathwohl and Reinhard, 1993; Conklin et al., 1995; Fisher et al., 1996), solids-water (Croisé et al., 1994; Lorden et al., 1998), or a combination of gas-water and solids-water (Brusseau, 1991) mass exchange.

The discussion that follows on selection of pore-gas velocities to support venting design then considers rate-limited gas-NAPL, gas-water, and solids-water mass exchange on a pore scale and rate-limited mobile-immobile gas exchange on field-scale where physical heterogeneity can not be explicitly represented or overcome by improved venting design.

9.1 Definition of Critical Pore-Gas Velocity

During rate-limited dominated mass transfer, as pore-gas velocity increases, vapor concentration decreases resulting in decreased "efficiency" in mass removal. Efficiency is

defined as mass removed per volume of extracted gas. However, an increased pore-gas velocity still results in an increased mass removal rate (mass removed per time) and hence shorter remediation time because of an increased concentration gradient between equilibrium and nonequilibrium vapor and soil-water concentrations. Thus, there is a trade-off between selection of a design pore-gas velocity and remediation time. The importance of maintaining a significant concentration gradient during rate-limited dominated vapor transport was demonstrated by Armstrong et al. (1994) during analysis of pulsed versus continuous venting operation. In pulsed pumping, the strategy is to extract gas only until the tailed portion of the effluent curve is reached. The gas extraction well is then shut-in to allow subsurface gas-phase concentrations to rebound. Pulsed pumping is intended to provide lower energy and vapor treatment costs compared too continuous operation. The length of on and off periods is dependent on kinetic mass transport coefficients and pore-gas velocity. In order to evaluate mass removal efficiency under a pulsed regime, Armstrong et al. (1994) investigated two pumping scenarios under gas-water and solids-water rate-limited mass exchange. The pumping schedules and corresponding pore-gas velocities were as follows: (1) 2 hours on at 0.14 cm/s, 8 hours off; and 2) 1 hour on at 0.14 cm/s, 4 hours off; each giving an average pore-gas velocity over the full cycle of 0.03 cm/s. These scenarios were compared to continuous pumping at 0.03 cm/s and 0.14 cm/s. As expected, continuous pumping at a rate at 0.14 cm/s resulted in the highest mass removal rate. Continuous pumping rate at 0.03 cm/s was more effective than the 1 - 4 hour pulsed pumping cycle at 0.14 cm/s. The slowest mass removal rate was the 2 - 8 hour cycle at 0.14 cm/s. Overall, the continuous but slow pumping rate or pore-gas velocity gave the best mass removal performance. Armstrong et al. (1994) state that this is because continuous pumping maximizes the concentration gradient for diffusive mass transfer for longer periods of time.

Armstrong et al. (1994) simulated the time hypothetically required to achieve 99% mass removal under continuous pumping as a function of pore-gas velocity. This relationship was highly nonlinear. The curve had two distinct parts, a slow part in which gas residence time was long allowing partitioning processes time to equilibrate and a fast part in which mass transport kinetics controlled mass removal. For the slow part, the limiting value corresponding to zero pore-gas velocity was the time required for 99% mass removal by diffusion. Applying even a low pore-gas velocity in this scenario resulted in a rapid decrease in remediation time compared to mass removal by vapor diffusion. Armstrong et al. (1994) selected a design or “critical” pore-gas velocity at the point or general location where the two portions of the curve met. A critical pore-gas velocity then is defined as a pore-gas velocity which results in slight deviation from equilibrium conditions.

9.2 Approaches to Estimating Critical Pore-Gas Velocities

There are conceivably at least five ways that could be used separately or concurrently to select a critical pore-gas velocity for venting application. The most rigorous approach would be to conduct site-specific field-scale tests to elucidate and quantify immobile gas - mobile gas (macropores, layers of different permeability), water-gas, solids-water, and NAPL-gas rate-limiting processes. However little research has been performed in this area, thus published field-

scale procedures are lacking. Development of field-scale procedures to identify and quantify rate-limited processes during venting constitutes a definitive research need.

A second method would be to conduct laboratory-scale tests with extrapolation of results to the field scale. A variety of procedures for conducting laboratory column tests can be found in the literature. However with the exception of just a few studies, methodologies have been designed to isolate or evaluate just one and at most two rate-limiting process in clean sieved sand, glass beads, or constructed media (e.g., fired clay aggregates) in which contaminants are artificially introduced into soil columns. These laboratory experiments have been valuable in understanding fundamental mass transport processes but are of limited use for direct application at hazardous waste sites.

A third approach would be to use fictitious but "representative" soils data and mass transport coefficients to conduct numerical modeling simulating rate-limited behavior. Rathfelder et al. (1995) state that of the three-phase (NAPL, water, gas) models which have been applied to venting application, only the models of Sleep and Sykes (1989), Rathfelder et al. (1991), and Lingineni and Dhir (1992) consider rate-limited NAPL-gas, gas-water, and water-solids mass exchange. Recently, Abriola et al. (1996) developed a two-dimensional, finite-element, two-phase flow, public domain model (MISER) which incorporates these rate-limited transport processes using first-order rate coefficients that would be suitable for estimation of a critical pore-gas velocity. The model is robust but complicated, requiring a considerable investment in time for proper use.

A fourth approach would be to review available literature in which rate-limited vapor transport has been observed for similar VOCs and soils (including moisture content) and select a pore-gas velocity lower than that which resulted in deviation from the local equilibrium assumption. Table 9.1 provides a summary of published studies on rate-limited NAPL-gas, gas-water, and solids-water mass exchange during gas advection. However, while a review of available literature provides valuable insight into rate-limited mass transport processes, it is unlikely to find a situation which matches site-specific conditions well. Also, pore-gas velocities used for laboratory column studies are often at least an order of magnitude higher (0.1 to 10 cm/s) than typical field application (0.01 cm/s or less). In addition, the characteristic transport length in which gas must pass through to observe rate-limited behavior is much smaller for a laboratory-scale study than would be expected in the field.

A fifth approach would be to utilize Damkohler numbers, which represent the ratio between reaction time and advection time and recently published algorithms for rate-limited gas-water, solids-water, and NAPL-gas mass transfer to calculate a critical pore-gas velocity. Bahr and Rubin (1987) concluded that the local equilibrium assumption is applicable if Damkohler numbers exceed 100. Jennings and Kirkner (1984) obtained good approximations to the local equilibrium assumption for Damkohler numbers as low as 10. Brusseau (1991) states that the dynamic range for Damkohler numbers is between 0.01 and 100 with values over 10 approaching the local equilibrium assumption. Thus, based on these analyses, it appears reasonable to

Table 9.1 Summary of column and sand tank studies where rate-limited vapor transport has been evaluated

pore-gas vel. (cm/s)	**media description**	**λ_{ng} (s^{-1})**	**λ_{gw} (s^{-1})**	**λ_{ws} (s^{-1})**	**author(s)**
0.178* - 0.703*	moist Borden sand, f_{oc} = 0.00017- 0.0008, S_o = 0.088, S_w = 0.25	not rate-limited	4.0×10^{-5} (after evaporation of NAPL)	5.0×10^{-5} (after evaporation of NAPL)	Armstrong et al. (1994) and McClellan and Gillham (1992)
2.07*, 4.47*, 10.92*	moist medium-grained sieved sand (avg. grain size = 0.90 mm), S_o = 0.075, S_w = 0.22,	not rate-limited	not evaluated	not evaluated	Baehr et al. (1989)
0.055	uniform sand with aggregated porous media (fired clay) (data from Gierke et al., 1991)	NAPL absent	3.06×10^{-4}	no sorption	Brusseau (1991)
0.636	desert soil (data from Roberts, 1990)	NAPL absent	2.78×10^{-2}	2.78×10^{-3}	Brusseau (1991)
0.016	Yolo loam (data from Brown and Rolston, 1980)	NAPL absent	1.28×10^{-3}	8.33×10^{-4}	Brusseau (1991)
0.144 - 0.545	moist sorted sand (median grain size 0.25 - 0.5 mm)	NAPL absent	3.0×10^{-4} - 5.5×10^{-4}	no sorption	Conklin et al. (1995)
0.009 - 0.018	moist clean quartz sand (grain sizes in the range of 0.08-1.2 mm)	NAPL absent	5.0×10^{-6} - 1.0×10^{-3}	no sorption	Fisher et al. (1996,1998)
0.01, 0.017, 0.020	moist coarse nonaggregated Ottawa sand (S_w = 0.26), dry aggregated porous media (fired clay)	NAPL absent	not rate-limited	no sorption	Gierke et al. (1992)
0.061	aggregated porous media (fired clay)	NAPL absent	aggregate diffusion	no sorption	Gierke et al. (1992)
0.1 - 0.2	silt loam, foc=0.025, water content 0.0, 0.16, 0.22 by weight	rate-limiting at 16% water content	not evaluated	not evaluated	Harper et al. (1998)
0.015* - 0.076*	two sandy soils having foc (0.001, 0.0165) and saturation (0.08, 0.43) values respectively. S_o = 0.02	rate-limited behavior unclear	not evaluated	not evaluated	Hayden et al. (1994)
7.83*	three mixtures of dry sand with average particle diameter of 1.2, 0.25, and 0.04 mm	not rate-limited	not applicable	not evaluated	Ho and Udell (1992)

pore-gas vel. (cm/s)	media description	λ_{ng} (s^{-1})	λ_{gw} (s^{-1})	λ_{ws} (s^{-1})	author(s)
1.5*	dry sand having average particle diameter of 0.25 mm	not rate-limited	not applicable	not evaluated	Ho et al. (1994)
0.002 - 0.161	coarse nonaggregated Ottawa sand (0.59 - 0.84 mm dia.) with initial uniform moisture content, countercurrent gas and water flow	NAPL absent	equilibrium	no sorption	Imhoff and Jaffe (1994)
9.35*,7.73*	dry and moist Monterey sand, mean grain size 0.25mm, S_o = 17% , S_w = 0 & 16%	not-rate limited	not evaluated	not evaluated	Liang and Udell (1999)
7.52*, 30.00*, 50.15*	dry glass beads (0.36-mm dia), S_o = 0.13	not rate-limited	not applicable	not evaluated	Lingineni and Dhir (1992)
0.29, 0.50	dry fine-grained sand	NAPL absent	not applicable	4.14×10^{-7} - 5.59×10^{-4}	Lorden et al. (1988)
0.0074	unspecified soil	rate-limited-aggregate diffusion modeling	aggregate diffusion modeling	aggregate diffusion modeling	Ng et al. (1999) and Ostendorf et al. (1997)
0.053*, 3.143*	unspecified soil from Superfund site	NAPL absent	not evaluated	1.15×10^{-6} , 2.27×10^{-6}	Nadim et al. (1997)
0.167 - 4.50	moistened glass beds (0.59 cm dia)	NAPL absent	3.15×10^{-3} - 6.96×10^{-2}	1.24×10^{-2} - 2.43×10^{-1}	Popovičová and Brusseau (1998)
0.27*	dry glass beads (0.50-1.0 mm dia) and dry Borden sand (0.25-0.50 mm dia)	not rate-limited	not applicable	tailing after evaporation of NAPL	Rathfelder et al. (1991) and Bloes et al. (1992)
0.35	moist fine to medium sand, foc=0.004, S_w=0.24	NAPL absent	rate-limited	rate-limited	Wehrle and Brauns (1994)

* calculated from information provided in publication

λ_{ng} NAPL - gas first-order rate constant

λ_{gw} gas - water first-order rate constant

λ_{ws} solids - water first-order rate constant

estimate critical pore-gas velocity based on Damkohler numbers of 10. A limitation using Damkohler numbers and algorithms to estimate critical pore-gas velocities is that mass transport processes are considered independently when in reality complex interactions between these processes dictate overall mass removal. It would appear that a combination of the fourth and fifth approaches is the easiest and most practical method of estimating critical pore-gas velocities for most venting practitioners until guidance for conducting laboratory and field-scale testing can be provided.

There are however additional complications to consider in selection of critical pore-gas velocities. Virtually all research on rate-limited vapor transport and development of algorithms for pore-gas velocity determination originated from controlled sand tank and laboratory column studies where field-scale heterogeneity was not a factor. Thus, optimal pore-gas velocities in the field are likely to be very site-specific and somewhat smaller than indicated by Damkohler numbers, algorithms, and published studies. Also, characteristic lengths of contamination used in Damkohler numbers and algorithms are not constant but decrease in time due to NAPL and sorbed mass removal thereby reducing calculated optimal pore velocities. Finally, the cost of well installation and venting operation (e.g., electricity, vapor treatment) should be considered since achievement of a minimum target pore-gas velocity at some sites may be prohibitively expensive. Thus, it is apparent that selection of a critical pore-velocity is not a straightforward process but involves some degree of judgement and iterative reasoning (gas flow modeling to see what pore-gas velocities can be achieved given certain well spacing and flow rates). Nevertheless, venting design based on attainment of critical pore-gas velocities is superior to the most commonly used soil venting design method, radius of influence (ROI) testing, which will be discussed in section10. A design based on attainment of critical pore-gas velocities in contaminated media involves consideration of fundamental subsurface gas flow and mass transport processes whereas a design based on ROI testing simply ensures attainment of vacuum in a contaminated region.

The fourth and fifth approaches to estimating a critical pore-gas velocity are considered here by providing a critical literature review of laboratory studies, Damkohler numbers, and algorithms published on rate-limited vapor transport. A large body of literature is developing on rate-limited vapor transport with contributions primarily from environmental engineering, soil and ground-water science. There exists no comprehensive detailed review that evaluates the impact of various nonequilibrium factors on vapor transport, their relative significance, and various modeling approaches used to describe rate-limited vapor transport. The following discussion provides such a review and provides additional insight into how an understanding of rate-limited vapor transport process can improve current practices in design. Operationally, rate-limited mass transfer exchange will be separated into four categories: (1) gas-water, (2) solids-water, (3) mobile-immobile gas and (4) gas-NAPL exchange.

9.3 Rate-Limited NAPL-Gas Exchange

An awareness of NAPL distribution in porous media under unsaturated conditions is

helpful in understanding rate-limited NAPL-gas exchange. In natural unsaturated porous media, NAPL is often distributed in two phases: "free" and "trapped" (Parker and Lenhard, 1987). Free NAPL is considered a thin film or lense in direct contact with mobile gas, while trapped NAPL is considered as discontinuous blobs or ganglia occluded within the bulk-water phase. NAPL entrapment in two-phase (NAPL-water) systems has been extensively studied. Typically, NAPL is the nonwetting phase while water is the wetting phase. The immiscible displacement of NAPL by water results in a fraction of the NAPL being snapped off and left behind as blobs or ganglia in an otherwise water-filled pore space (Chatzis et al., 1983; Wilson and Conrad, 1984). In a NAPL, water, gas system, fluid distribution is much more complex and may depend on the spreading coefficient of the NAPL. The spreading coefficient (Σ) is defined as:

$$\sum = \sigma_{gw} - \sigma_{nw} - \sigma_{gn} \tag{9.1}$$

where: σ_{gw} = gas-water interfacial tension, σ_{nw} = NAPL-water interfacial tension, and σ_{gn} = gas - NAPL interfacial tension. NAPLs exhibiting low interfacial tensions with water and gas have positive spreading coefficients and are theorized to spread as films on residual water. NAPLs exhibiting high interfacial tensions with water and gas have negative spreading coefficients and are theorized to exist as entrapped coalesced lenses or ganglia along air-water interfaces. Petroleum hydrocarbons generally have positive spreading coefficients while many halogenated solvents have negative spreading coefficients. NAPLs with positive spreading coefficients are expected to have a much higher NAPL-gas contact area and hence a high rate of mass transfer compared to nonspreading NAPLs. Soils contaminated with spreading NAPLs are expected to have lower residual saturations compared to nonspreading NAPLs. Blunt et al. (1995) however concluded that contrary to accepted theory, both spreading and nonspreading NAPLs may form thin films along water interfaces in three-phase water-wet porous media. They suggest that even nonspreading NAPLs may form films from thinning of previously thick NAPL layers during NAPL drainage. This is supported by Hayden and Voice (1993) who observed the existence of continuous NAPL films, as well as pendular rings and V-shaped wedges, for a nonspreading NAPL entrapped in a water-wet sandy aquifer material. In experiments with two spreading NAPLs, styrene and toluene, and one nonspreading NAPL PCE, Wilkins et al. (1995) noted that spreading coefficients had minimal influence on interphase NAPL-gas mass transfer indicating similarities in pore-scale NAPL distribution. Residual NAPL saturations were comparable for all three NAPLs ranging between 4 and 5%. These findings suggest that the influence of spreading coefficients in NAPL-gas mass exchange is ambiguous.

Wilkins et al. (1995) present a conceptual model for NAPL volatilization from unsaturated porous media. The wetting fluid, water, preferentially occupies the smallest pores, filling pore bodies and creating water films along soil particles. The invasion and drainage of NAPL produces intermediate wetting NAPL films along air-water interfaces, and in heterogeneous media, complex geometric patterns of residual NAPL. As a result, all residual NAPL may not be readily accessible to the mobile gas phase. Initially, mass transfer in NAPL contaminated soils is rapid due to the presence of NAPL films exposed directly to soil gas which provide a large surface area to volume ratio. Over extended periods of time however, NAPL

films are removed and the remaining NAPL mass exists as pendular rings, wedges surrounding aqueous pendular rings, filled pore throats, and NAPL isolated between aqueous wedges or within pore throats surrounded by water. Increases in fluid saturation and natural pore structure heterogeneity may further restrict the mobility of the gas phase, limiting access to entrapped NAPL. When NAPL is surrounded by water, mass removal becomes limited by aqueous diffusion in a manner similar to that for saturated zone processes. Thus, according to Wilkins et al.'s (1995) conceptualization, NAPL-gas mass transport should be constrained by increasing water content. This observation is important, since virtually all through-flow (gas flow directly through NAPL contaminated soils) laboratory column studies in which NAPL has been placed in dry porous media, have not shown rate-limited NAPL-gas mass transfer. Rate-limited NAPL-gas mass transfer has only been demonstrated in water wet soils, but this observation has not been consistent.

McClellan and Gillham (1992) conducted one-dimensional through-flow experiments in a steel box to evaluate mass transfer between uniformly mixed residual TCE and air. They mixed free phase TCE with moist Borden sand, resulting in residual NAPL and water saturation of 8.8% and 25% respectively. Effluent vapor concentrations during the first 72 hours of operation were relatively constant and at or near saturation (35,000 to 36,000 ppmv). During a 12 hour period, pore-gas velocity was increased from 0.18 to 0.63 cm/s (calculated from information provided by authors). Relatively constant concentrations were observed in the effluent indicating that local equilibrium had been maintained at the higher pore-gas velocity. Flow rate was directly proportional to mass flux rate. A sharp decline in vapor concentration (about 1.3 orders of magnitude) though was observed at approximately 100 hours. McClellan and Gillham (1992) believe that the sharp decline in concentration correspond to the time when the last liquid or residual TCE was removed and the kinetics of aqueous and sorbed phase mass removal became dominant. After this time, increased flow rate caused a reduction in vapor concentration. Further evidence of rate-limited transport was seen during flow interruption. The system was turned off for a period of one hour. Upon restarting the system, the effluent concentration increased significantly compared to effluent concentrations just prior to shut down but then quickly decreased to pre-test effluent concentrations. A second flow interruption test was then conducted with a shut down time of only 35 minutes resulting in a smaller rebound concentration upon restart. McClellan and Gillham (1992) attempted to assess the mass remaining in the steel box at the end of the study by using partition coefficients with an average soil gas concentration (16 ppmv) after a 19 hour shut down period. They concluded that in excess of 99% of contaminant mass had been removed prior to observation of rate-limited vapor transport.

Baehr et al. (1989) simulated mass removal of gasoline under through-flow conditions in pre-moistened medium-grained sieved sand having a NAPL saturation of 7.5% and water saturation of 22.4%. Experimental and simulated mass flux profiles matched well suggesting attainment of equilibrium conditions at a pore velocities of 2.07, 4.47, and 10.92 cm/s (calculated based on information provided by authors). They state that the ability of model simulations to describe experimental results conducted at three flow rates supports their hypothesis that local equilibrium conditions prevailed during mass removal. A plot of hydrocarbon mass removed as

a function of volume of air passed through their columns revealed no dependence on pore-gas velocity. Analysis of chromatograms indicated a loss of lower molecular weight compounds with time.

Rathfelder et al. (1991) and Bloes et al. (1992) simulated mass removal of a NAPL mixture of benzene, toluene, and TCE in dry glass beads and dry Borden sand under through-flow conditions. Distinguishable evaporation fronts of benzene, TCE, and toluene eluted in sequential order as expected from Raoult's law. Experimental and predicted effluent vapor concentrations matched well during evaporation of NAPL suggesting attainment of equilibrium conditions at a pore velocity of 0.27 cm/s (calculated based on information provided by authors). Some tailing in the glass beads and Borden sand was evident however at low vapor concentrations.

To simulate rate-limited gas-NAPL exchange, the NAPL storage term in the advective-dispersive equation (8.18) can be expressed by

$$\theta_n \frac{\partial C_n}{\partial t} = \theta_g \lambda_{ng} \left(C_g - \frac{C_n}{K_{ng}} \right). \qquad (9.2)$$

where λ_{ng} is a NAPL - gas first-order rate constant [T^{-1}]. Rathfelder et al. (1991) conducted hypothetical simulations of xylene removal in dry soils with a NAPL saturation of 1.0% using λ_{ng} values ranging from 2.23×10^{-6} to 2.23×10^{-5} s^{-1} in a radial flow system with an initial contaminated radius of 10 m. Simulations showed that λ_{ng} rates had little effect on time for complete mass removal as long as equilibrium vapor concentrations were established prior to reaching the gas extraction well. As λ_{ng} was reduced, the travel distance over which saturated vapor concentrations were established increased causing the evaporation front to become disperse.

Ho et al. (1994) conducted through-flow column studies in a dry sand with a multi-component NAPL mixture of benzene, toluene, and o-xylene. Using a local equilibrium model they successfully simulated evaporation fronts in the gas effluent. Similar to Rathfelder et al. (1991), they were able to predict the successive rise in effluent vapor concentration of heavier VOCs upon depletion of lighter VOCs.

Liang and Udell (1999) successfully simulated mass removal of a NAPL mixture of benzene, toluene, and o-xylene in dry and moist (water saturation = 15%) Monterey sand (mean particle diameter = 0.25 mm) in through-flow experiments using the assumption of local equilibrium. Pore-gas velocities for the moist and dry sand experiments were 9.35 and 7.73 cm/s respectively (calculated based on information provided by authors). Similar to Rathfelder et al. (1991) and Ho et al. (1994), they observed sharp evaporation fronts eluting in order of volatility or vapor pressure (benzene, toluene, o-xylene respectively). Breakthrough curves and the amount of time required to recover the compounds in both cases were nearly identical. Liang and

Udell (1999) concluded that at least in their experiments, the presence of residual water had virtually no effect on NAPL-gas mass transfer. Liang and Udell (1999) also conducted bypass experiments where gas flow in a glass column occurred only on the soil surface. In these experiments, extensive effluent tailing was observed.

Lingineni and Dhir (1992) introduced ethyl alcohol into dry 0.36-mm glass beads to achieve a residual NAPL saturation of 13% and observed temperature reduction along the axis of flow due to evaporation under through-flow conditions. They state that the latent heat of vaporization required to evaporate an organic liquid is partially provided by the incoming air, while the rest is absorbed from the porous media. After the fluid is completely evaporated, soil temperatures rise due to heat transfer from air to soils at higher temperature. Simulations of temperature and evaporation fronts at pore-gas velocities of 7.52, 30.00, and 50.15 cm/s (calculated based on information provided by authors) matched experimental data suggesting attainment of equilibrium conditions.

Hayden et al. (1994) introduced gasoline at NAPL saturation value of 2% in two sandy soils (less than 5% silt and clay) having organic carbon content of 0.1% and 1.65% and water saturation values of 8.0% and 43.0% respectively and monitored effluent concentrations of benzene, m,p-xylene, and naphthalene. They conducted flow variation and interruption testing to evaluate NAPL-gas rate-limited exchange. For the high organic content and water saturation soil, flow variation resulted in pore-gas velocities of 0.076 and 0.020 cm/s (calculated based on information provided by authors) while for the low organic carbon content and water saturation soil, flow variation resulted in calculated pore-gas velocities of 0.057 and 0.015 cm/s (calculated based on information provided by authors). Flow variation and interruption testing revealed that rate-limited behavior was not a function of moisture content and only occurred at very low component concentrations. Hayden et al. (1994) state that possible explanations of observed rate-limited behavior at low mole fractions or concentrations include: 1) heterogenous flow patterns and NAPL distribution, 2) rate-limited gas-water or solids-water exchange, 3) rate-limited gas-NAPL exchange, and 4) a combination of all or some of the factors above. They state that small-scale physical heterogeneity or permeability variation may result in unequal flow distribution causing some NAPL containing pore regions to experience much more gas movement than others. Mole fractions of components having high vapor pressure would then be higher in NAPL containing regions of low gas exchange compared to more weathered NAPL in regions of high gas exchange. This would cause tailing, and an increase in effluent vapor concentration upon reduction or stoppage of gas flow. It would also explain rate-limited behavior for compounds having high volatility while effluent monitoring of lower volatility compound show no rate-limited behavior. However, another viable explanation of rate-limited transport for compounds having high volatility would be almost complete mass removal from NAPL with remaining mass present in soil-water, humic material, and solids where rate-limited behavior is well documented in the literature. Thus, it is difficult to elucidate the cause of rate-limited behavior of compounds having high volatility at low concentrations in NAPL contaminated soil. It would appear then that Hayden et al.'s (1994) study can not be used to document rate-limited NAPL-gas exchange.

Harper et al. (1998) observed rate-limiting behavior in a silt loam using toluene and a mixture of toluene and m-xylene as a NAPL source at a gravimetric moisture content of 22% but not under air-dried conditions or at a gravimetric moisture content of 16%. At a gravimetric moisture content of 22% using a binary mixture of toluene and m-xylene, no distinct evaporation fronts were discernable. Effluent concentrations displayed rapid and extended tailing. In comparison to other published studies (e.g., Hayden et al., 1994), rate-limited behavior for NAPL components was present at high mole fractions or soil concentrations. Harper et al. (1998) state that the abrupt transition from equilibrium to nonequilibrium conditions with small changes in water content (16% to 22%) suggests a nonlinear dependence of mass transfer on soil water content. Harper et al. (1998) are among the first investigators to use non-sandy soils or glass beads to investigate NAPL-gas mass transfer and the first investigators to definitively demonstrate reduced NAPL-gas mass transfer with increased moisture content. As they point out, venting is often applied in silty soils, yet few investigators use silty or clayey soils for laboratory studies.

Of particular concern is that in contrast to typical published column studies where NAPL is placed in dried soils or in moist soils after pre-wetting, NAPL contaminated soils at a field site are subject to numerous wetting and drying cycles. This suggests that NAPL distribution on a pore-scale in natural soils may be more heterogeneous and NAPL-gas exchange may be more rate-limited than in artificially contaminated soils typically used in published studies. Ostendorf et al. (1997) provide one of the few published studies evaluating rate-limited NAPL-gas exchange in "naturally" contaminated media. Ng et al. (1999) developed an aggregate diffusion model similar to Ng and Mei (1996) and utilized Ostendorf et al's. (1997) laboratory column based data to simulate mass removal of individual compounds. In Ng et al.'s (1999) model, intraaggregate space is filled with trapped NAPL, water, and gas while interaggregate space is filled with mobile gas and a thin film of NAPL surrounding aggregate particles. NAPL constituents in intraaggregate space move to interaggregate space by NAPL dissolution and aqueous diffusion. Calibration of their model to vapor transport along the axis of the column of one of the most volatile constituents, 2-methylpentane, resulted in an estimated trapped NAPL fraction of 70% Simulated versus observed vapor concentrations of compounds having relatively high vapor pressures compared well. There were some discrepancies however for compounds having lower pressures which they attribute to not including enough lower volatility components in the simulated NAPL mixture. The important observation for venting design purposes however is observed deviation from equilibrium at a relatively low pore-gas velocity (0.0074 cm/s) reinforcing concern that NAPL-gas exchange in "naturally" contaminated soils may be of larger magnitude than in artificially contaminated soils.

Wilkins et al. (1995) conducted a series of soil column experiments to evaluate NAPL-gas rate-limited mass transfer. They packed air-dried sieved soils in columns to obtain four uniform sand size fractions and two graded sand mixtures. By achieving macroscopically homogeneous unsaturated porous media systems, they were able to study NAPL-gas mass transfer without the interfering affects of physical heterogeneity. Relatively uniform soil moisture and NAPL distribution was maintained in soils throughout the columns. Single

component NAPLs (styrene, toluene, and perchloroethylene) were used for experimentation.

Parameters considered for describing mass transfer process included (1) mean grain size (d_{50}), (2) grain size uniformity index, (3) NAPL residual saturation, (4) water saturation, (5) and effective air filled porosity. Multiple linear regression analyses were performed to determine the best fit model for experimental data. Wilkins et al. (1995) observed that mean grain size provided the most significant statistical correlation describing NAPL-air mass transfer. NAPL-vapor phase mass transfer decreased with decreased mean grain size. Correlation between the uniformity index and mass transfer was significantly weaker. A model based on the residual NAPL saturation resulted in a negative correlation, indicating an inverse relationship between mass transfer and the entrapped NAPL content. However, the statistical significance of this model was considerably less than the mean grain size model. Wilkins et al. (1995) explain that entrapped NAPL preferentially occupies medium-sized pores while forming films along gas-water interfaces. Water, the wetting fluid, preferentially occupies smaller pores inhibiting NAPL entry while gas, a nonwetting fluid occupies the largest pores. Thus the medium-sized pores, which correspond to the mean grain size, may control NAPL distribution and have the greatest effect on mass transfer. A decrease in mean grain size or an increase in residual fluid saturation would be expected to increase gas phase restriction to pore spaces and reduce interphase mass transfer.

Based on experimental observations, Wilkins et al. (1995) derived an empirical equation for estimation of the NAPL-gas mass transfer coefficient

$$\lambda_{ng} = 10^{-0.42} D_g^{0.38} v^{0.62} d_{50}^{0.44} . \tag{9.3}$$

Equation (9.3) can be used to estimate a critical pore-gas velocity for NAPL-gas exchange, $v_{c(ng)}$:

$$v_{c(ng)} = \left(\frac{10^{-0.42} D_g^{0.38} d_{50}^{0.44} L_c}{-\theta_g \ln\left(1 - \frac{C_g}{C_g^*}\right)} \right)^{2.63} \tag{9.4}$$

where L_c is a characteristic contamination length [L] and C_g^* is equilibrium vapor concentration [ML^{-3}]. For a slight deviation from equilibrium conditions (C_g/C_g^*) = 0.99, $v_{c(ng)}$, can be estimated by:

$$v_{c(ng)} = \left(\frac{D_g^{0.38} d_{50}^{0.44} L_c}{12.11 \theta_g} \right)^{2.63} . \tag{9.5}$$

9.4 Rate-Limited Gas-Water Exchange (First-Order Kinetics)

Armstrong et al. (1994) explain the use of a first-order rate coefficient to quantitatively describe rate-limited gas-water exchange. On a conceptual basis, it is assumed that diffusive mass transfer between the gas and water phase takes place through an aqueous boundary layer. The driving force for mass transport then is a gradient between the average aqueous phase concentration and an equilibrium aqueous concentration at the gas-water interface. To simulate rate-limited gas-water exchange, the water storage term in the advective-dispersive equation (8.18) can be expressed by

$$\theta_w \frac{\partial C_w}{\partial t} = \theta_g \lambda_{gw} \left(C_g - H C_w \right) \tag{9.6}$$

where λ_{gw} is a lumped first-order gas-water mass transfer coefficient [T^{-1}] which is the product specific interfacial area [L^{-1}] between gas and the aqueous phase and a gas-water mass transfer coefficient [LT^{-1}]. In the boundary layer model, λ_{gw} depends on the compound's aqueous diffusion coefficient and thickness of the boundary layer. The thickness however is not a measurable quantity since the process represents a variety of diffusion pathlengths in heterogeneous porous media. The gas-water mass transfer coefficient then has meaning only as a lumped parameter representing the integral of all physical nonequilibrium processes affecting movement of contaminants between the aqueous and gaseous phase including diffusion with the soil moisture and dead-end pore effects.

Conklin et al. (1995) evaluated rate-limited gas-water exchange of benzene and p-xylene in desert sand having a median grain size of 0.25 to 0.50 mm and organic carbon content of 0.097% at volumetric water contents of 10% and 18%. Conklin et al. (1995) observed significant interfacial gas-water adsorption for p-xylene but not for benzene. In experiments using pore-gas velocities varying from 0.139 to 0.545 cm/s, breakthrough curves for benzene indicated tailing only at a volumetric water content of 18% while breakthrough curves for p-xylene exhibited tailing at both volumetric water contents with tailing of p-xylene more pronounced than benzene at a volumetric water content of 18%. Conklin et al. (1995) state that since tailing was absent in breakthrough curves for benzene at a volumetric water content of 10%, it is unlikely that mass transport was limited by solids-water exchange. They noted that a first-order kinetics model could fit the initial but not the long tailing portion of the desorption curve of benzene at a volumetric water content of 18% suggesting that more than one rate-limiting process was occurring, possibly in series. The average mass transfer coefficients fitting the initial and long tailing portions of the desorption curve for benzene were $(5.8 \pm 2.4) \times 10^{-3}$ and $(5.5 \pm 2) \times 10^{-4}$ s^{-1} respectively. The mass transfer coefficients describing long tailing were consistent with calculations for sorption retarded aqueous diffusion assuming a diffusion path length equivalent to the particle radius. Thus, they concluded that lower mass transfer coefficients likely described aqueous intraparticle diffusion while higher mass transfer coefficients may have represented film diffusion. Similar results were found for p-xylene where the average mass transfer coefficients fitting the initial portion of the desorption curve ranged from $(3.7 \pm 0.8) \times 10^{-3}$ and (4.1 ± 2.0) x

10^{-2} s^{-1} at moisture contents of 18 and 10% respectively and (3.0 ± 2) x 10^{-4} s^{-1} for the long tailing portion of the desorption curve. Conklin et al's. (1995) experimental results indicate that soil-water content can significantly affect gas-water rate constants and hence the time scale of remediation. Higher moisture content results in more void space between and within particles filled with water thereby increasing the diffusion path length in the aqueous phase. Thus, design practices such as installation of a synthetic liner or asphalt cap to minimize infiltration or lower soil moisture content may increase gas-water mass exchange and thereby reduce remediation time.

Fisher et al. (1996) conducted tank studies with clean quartz sand (grain sizes in the range of 0.08-1.2 mm) to determine if mass removal during gas advection could be affected solely by rate-limited mass transfer in interparticle soil water (water between soil particles). They conducted soil-water partitioning batch studies and observed negligible sorption of tested volatile organic compounds. Fisher et al. (1996) also sought to evaluate whether departure from local equilibrium due to gas-water limited mass transfer could be described by a first-order kinetics approach and the effect of water saturation and physiochemical properties (especially H and K_d) on volatile organic compound mass removal. Volatile organic compounds 1,1,1-trichloroethane (1,1,1-TCA), 1,1,2-trichloroethane (1,1,2-TCA), perchloroethene (PCE), and trichloroethene (TCE) were tested. Differences in mass removal of 1,1,1-TCA and 1,1,2-TCA were of particular interest because the dimensionless Henry's law constant of the former and latter vary over an order of magnitude, 0.73 and 0.04 respectively. Four venting experiments were performed according to saturation profiles in the tank. Water content varied vertically throughout the tank providing nonuniform water contents. VOCs were introduced into the tank by gas diffusion or through saturation of sands containing dissolved constituents. Average linear velocities in the sand tank varied from 0 (no interconnected gas-filled porosity) up to 0.02 cm/s. Relative vapor concentrations were plotted against a dimensionless time (T) defined as

$$T = \frac{vt}{R_D L} \tag{9.7}$$

where L is a reference length [L] chosen as the distance between two monitoring points, and R_D is a retardation factor derived from the local equilibrium assumption and defined as

$$R_D = 1 + \frac{\theta_w}{\theta_g H} + \frac{\rho_b K_d}{\theta_g H}. \tag{9.8}$$

Relative vapor concentration was plotted on a logarithmic scale to effectively illustrate concentration reduction over two orders of magnitude. All tests were characterized by a steep initial decline in vapor concentration followed by a long tail. A sharp transition in relative vapor concentration reduction occurred at T = 2. For T < 2, relative vapor concentrations decreased linearly (indicative of equilibrium conditions), while for T > 2, tailing with eventual constant relative concentration occurred over time. Fisher et al. (1996) state that the similarity of all experimental curves suggests that vapor concentration reduction was controlled by the same

variables affecting T, namely, water saturation, linear velocity, and Henry's law constant and that different slopes of curves in the range of $T < 2$ and $T > 2$ indicate two different processes in mass removal. They hypothesize that the steep initial decrease in gas concentration likely corresponds to removal of VOCs from water films surrounding particle surfaces, which is not likely to be rate-limited, whereas tailing may have been caused by removal from wedges. While the extent and geometry of the films and wedges depend on water saturation, in general, the mean distance from the gas-water interface must be greater for wedges than for films. The tailing processes indicates that advective transport in the gas phase must have proceeded much faster than mass transfer into the gas phase. This finding means that even at remediation sites where the soil material is seemingly homogeneous, low in sorptive capacity, without secondary porosity, and at low water saturation, soil venting operation will likely be affected by local nonequilibrium. Significant departure from equilibrium for 1,1,1-TCA removal was noted at velocities as low as 0.00914 cm/s.

In their study, Fisher et al. (1996) found gas flow emergence and extinction points occurred at water saturations of 0.6 and 0.7 respectively. As discussed in section 3, the importance of minimizing soil-water content during venting is reinforced by the observation that advective gas flow does not occur until water saturation decreases to an "emergence point". In initially dry media, advective gas flow does not cease until water saturation increases to an "extinction point". Emergence and extinction points refer to water saturations in which interconnected gas voids are able to conduct advective flow. A number of investigators (Stonestrom and Rubin, 1989a,b; Fisher et al., 1997; and Dury et al. 1999) have documented the presence of trapped, nonconducting gas during capillary pressure - saturation and relative permeability measurement. Drainage requires a lower water saturation for gas flow to occur compared to wetting. The obvious implication for venting design and monitoring is that subsurface media must be significantly desaturated for advective gas transport to occur. Because water saturation emergence points are lower than extinction points due to hysteresis, this is particularly important during water table lowering or dewatering for venting application. Proper design and monitoring strategies then must involve determination of minimum gas saturations in specific media to induce advective gas flow and periodic in-situ monitoring to ensure that these gas saturations are maintained. When soils are dewatered to allow application of soil venting, water level monitoring in piezometers alone is not adequate to demonstrate sufficient desaturation to conduct gas flow. Piezometers do not provide useful information in estimating the thickness of the capillary fringe and the water saturation profile above the capillary fringe.

Relationships to estimate critical pore-gas velocities for gas-water exchange will now be explored. Brusseau (1991) states that if liquid-liquid mass transfer is the rate controlling step, then λ_{gw} can be related to the free-liquid diffusion coefficient by

$$\lambda_{gw} = \frac{cD_w\theta_w}{\tau_w\delta_c^2} \tag{9.9}$$

where D_w = free-aqueous molecular diffusivity [L^2T^{-1}], τ_w = tortuosity factor of water filled

porosity [-], c = a shape factor (15 for a sphere, 3 for a plane), and δ_c = a characteristic diffusion path length (e.g., radius of a sphere). A Damkohler number describing gas-water can be expressed by (Brusseau, 1991, Popovičová and Brusseau, 1998)

$$\omega_{gw} = \frac{\lambda_{gw} L}{v\theta_g} . \tag{9.10}$$

Using a value of 10 for the gas-water Damkohler number, a critical pore-gas velocity for gas-water exchange, $v_{c(gw),}$ can be estimated by

$$v_{c(gw)} = 1.5 \frac{D_w \theta_w L_c}{\theta_g \tau_w \delta_c^2} . \tag{9.11}$$

An alternative to using Damkohler numbers to estimate a critical pore-gas velocity for gas-water exchange, $v_{c(gw),}$ is to use the concept of a prefix denominator. Fisher et al. (1998) used a procedure termed "Separation of the Kinetically Influenced Term" (SKIT), developed by Bahr and Rubin (1997), to derive a dimensionless "prefix denominator"(P_D) defined by

$$P_D = \frac{\lambda_{gw} L H \theta_g}{v\theta_w} R_D \tag{9.12}$$

which provides a measure of the degree of departure from local equilibrium. The SKIT procedure consists of deriving equivalent dimensionless formulations of an equilibrium and kinetics model and identifying the additional term(s) in the kinetics model. Fisher et al. (1998) state that compared to a gas-water Damkohler number, use of the prefix denominator as an indicator of nonequilibrium has the advantage that it includes factors which represent gas and water saturation and physico-chemical properties such as a Henry's law constant and the solids-water partition coefficient. They found however that P_D values tend to decrease with time due to the fact that mass transfer coefficients describing gas-water exchange decrease with increasing time. Fisher et al. (1998) state that a critical velocity using the prefix denominator to optimize field application of venting can be expressed by:

$$v_{c(D-gw)} = \frac{\lambda_{gw} L_c R_D H \theta_g}{P_D \theta_w} . \tag{9.13}$$

Since gas-water mass transfer approaches equilibrium conditions as the P_D values approaches 10, Fisher et al. (1998) recommend using a P_D value of 10 to compute $v_{c(D\text{-}gw)}$. Assuming a P_D value of 10, a spherical shaped rate-limited domain, and equations (9.8), (9.9), and (9.13), a critical gas-water velocity using the prefix denominator can be estimated by:

$$\nu_{c(D-gw)} = 1.5\frac{D_w L_c}{\tau_w \delta_c^2}\left(H\theta_g + \theta_w + \rho_b K_d\right). \qquad (9.14)$$

9.5 Rate-Limited Gas-Water Exchange (Aggregate Diffusion Modeling)

Early development of the aggregate diffusion modeling took place in the chemical engineering field. Rao and co-workers (Nkedi-Kizza et al., 1982; Rao et al. 1980a,b) applied these models to describe sorption nonequilibrium during solute transport. Rate-limited sorption has been modeled by using diffusion equations based on Fick's law (Wu and Gschwend, 1986) and by using chemical reaction equations (Selim et al. 1976; Cameron and Klute, 1977). When using intraaggregate diffusion as the only causative factor for nonideality, accessibility to sorption sites becomes rate-limited but rate-limited solids-water exchange itself is not explicitly considered. Wu and Gschwend (1986) discuss a model involving retarded intraparticle liquid diffusion where sorption at the sorbent-solution interface is assumed to be instantaneous.

Rao et al. (1982) assessed whether solute diffusion from nonspherical aggregates could be approximated by diffusion from equivalent spheres. They showed that nonspherical aggregates could be represented by equivalent spherical aggregates whose radii are such that the sphere volume is equal to the volume of the nonspherical aggregate. Rasmuson (1985) extended a physical diffusion model developed for spherical aggregates to slabular and cylindrical shapes. A form factor was employed to adjust the intraaggregate diffusion equation to the selected shape. van Genuchten (1985) developed a method that extended the aggregate diffusion equation to more general conditions involving aggregates with nonspherical geometries. The method is based on the use of a geometry-dependent shape factor that can be used to transform an aggregate of a given shape and size into an equivalent sphere with similar diffusion characteristics.

Rao et al. (1982) described a method whereby a range of spherical aggregates can be reduced to a single, equivalent aggregate size. The method involves computing the equivalent radius from the volume-weighted radii of each aggregate-size class. Rao et al. (1982) demonstrated that the equivalent aggregate size could provide a good approximation of diffusion in actual mixed-sized medium. Nkedi-Kizza et al. (1982) observed that a distribution of aggregate sizes from 0.2 to 0.47 cm in diameter was well represented by an equivalent spherical aggregate size. Combining the shape transformations of van Genuchten (1985) with the aggregate size distribution transformation of Rao et al. (1982), porous medium consisting of different sizes and shapes of aggregates can be transformed in equivalent spherical aggregates of uniform size. In this manner, it may be possible to extend aggregate diffusion modeling to field-scale application.

Gierke et al. (1992) used 30 cm long, 5 cm i.d. glass columns packed with a uniform Ottawa sand and a manufactured aggregated porous soil material (APSM) to evaluate vapor transport in highly permeable nonaggregated and aggregated soils. Toluene vapor transport was observed in the sand and APSM under dry and wet conditions (27% and 67% water saturation). Sorption under wet conditions was assumed negligible because in previous studies (Gierke et al.,

1990) TCE sorbed neither to the sand in a water-saturated column nor to the APSM in an aqueous batch tests. For model development, Gierke et al. (1992) divided mass transport into two zones: (1) mobile gas and (2) aggregates composed of immobile water and solid soil particles. Gas was assumed to be a continuous phase. A Freundlich isotherm was included in model development to describe non-linear vapor-mineral surface sorption in dry experiments. One-dimensional gas flow was assumed to be steady and incompressible. Experiments with dry sand, moist sand, and dry APSM at pore-gas velocities of 0.017, 0.020, 0.01 cm/s showed no rate-limited behavior. Experiments with moist APSM however showed deviation of ideality at a pore-gas velocity of 0.061 cm/s indicating that intraaggregate diffusion controlled mass transport under these conditions.

Gierke et al. (1992) provide an equivalency relationship describing when dispersion, film transfer, and intraaggregate diffusion have similar impacts on the breakthrough curve of a linearly sorbed organic vapor

$$Pe = 15\left(1+\frac{1}{Dg}\right)^2 Ed = 3\left(1+\frac{1}{Dg}\right)^2 St \tag{9.15}$$

where

$$Ed = \frac{D_w \theta_w L}{\tau_w \theta_g H v \delta_c^2} \tag{9.16}$$

$$St = \frac{\lambda_{gw} L}{3v} \tag{9.17}$$

$$Dg = \frac{\theta_w + K_d \rho_b}{\theta_g H}. \tag{9.18}$$

They state that theoretically this equation is valid for linear isotherms, Pe > 40, and Ed > 13.33. In practice however, it can be used for values of Pe and Ed at least as low as 1. Parker and Valocchi (1986) used a moment analysis to derive an identical relationship. Gierke et al. (1992) state that this equation can be used to guide specification of an appropriate pore-gas velocity for venting application. They state that the chosen velocity should be low enough that Ed and St are large in comparison to Pe. Decreasing pore-gas velocity increases Ed and St and decreases Pe. However, the value of Pe though should be as high as possible to minimize the impact of gas diffusion on vapor transport. Gierke et al. (1992) provide an equation to estimate the gas-water mass transfer coefficient that would simulate the observed impact of intraaggregate diffusion

$$\lambda'_{gw} = 15\frac{D_w\theta_w}{\tau_w H\theta_g\delta_c^2}. \qquad (9.19)$$

Note that equation (9.19) differs from λ_{gw} defined in equation (9.9) by $H\theta_g$ in the denominator. Parker and Valocchi (1986) developed a relationship similar to equation (9.19) for equating first-order kinetics to spherical diffusion under saturated conditions. The motivation for development of these relationships is that numerically, intraaggregate diffusion requires more computational effort than first-order mass transfer. Gierke et al. (1992) state that for this reason, intraaggregate diffusion has not been included in field-scale models.

Ng and Mei (1996) simulated compressible gas flow and vapor transport within aggregated media in a radial coordinate system. They conceptualized soil as a periodic array of spherical aggregates and explicitly simulated mass transfer from water saturated aggregates to interaggregate pore gas. They neglected the presence of water and NAPL within interaggregate space and assumed: intraaggregate water to be immobile, negligible film resistance at aggregate-macropore interfaces, and equilibrium sorptive exchange between soil and aqueous phases inside aggregates. With this approach, solute concentration gradients within the aggregates or immobile regions is allowed. This is in contrast to the one-or two-site first-order rate models. Ng and Mei (1996) used high Peclet numbers (100-1000) for simulations assuming a radial extent of contamination near an SVE wells on the order of 10 meters, gas velocity from 0.001 to 0.01 cm/s and gas diffusion coefficients on the order of 0.01 cm^2/s. At high Peclet numbers, macroscale diffusion becomes insignificant compared to advection in the vapor phase.

Ng and Mei (1996) derived two dimensionless parameters, σ and ξ, to examine rate-limited vapor transport in the absence of NAPL.

$$\sigma = \frac{D_a L}{v\delta_c^2} \qquad (9.20)$$

and

$$\xi = \frac{\left[K_d\left(1-\theta_w\right)\rho_s + \theta_w\right]\left(1-\theta_g\right)}{H\theta_g} \qquad (9.21)$$

where

$$D_a = \frac{\theta_w D_w}{\tau_w\left[K_d\left(1-\theta_w\right)\rho_s + \theta_w\right]} \qquad (9.22)$$

where ρ_s = particle density $[ML^{-3}]$.

The parameter σ is the ratio of aggregate diffusion time which governs how fast compounds are removed from aggregates to global advection time. Local equilibrium exists when diffusion in aggregates is rapid or σ >>1. ξ is equal to the ratio of mass partitioned in aggregates to mass in the vapor phase per bulk volume of soil in the case of local equilibrium. A higher value of ξ means greater retardation of vapor transport. When σ >>1 and ξ << 1, vapor concentration is well predicted by local equilibrium theory. Ng and Mei (1996) examined the time necessary to reduce vapor and aqueous concentrations to 1% of their initial values in interaggregate and intraaggregate domains for values of σ ranging from 0.001 to 10 and three values of ξ (0.01, 1, 100). Since equilibrium sorptive exchange is assumed in aggregates, reduction to 1% of initial aqueous concentration is equivalent to 99% mass removal in aggregates. Based on the results of their simulations, Ng and Mei (1996) suggest that in the absence of NAPL and kinetically limited sorptive exchange, a critical pore-gas velocity occurs when mass removal is only slightly limited by diffusion in aggregates. They suggest that this occurs at:

$$(1+\xi)\sigma = 1 \tag{9.23}$$

or at a critical pore-gas or design velocity, $v_{c(a\text{-}gw)}$ [LT^{-1}], given by:

$$v_{c(a-gw)} = \frac{D_a L_c (1+\xi)}{\delta_c^2} . \tag{9.24}$$

When rate-limited vapor transport is due only to rate-limited gas-water exchange, aggregate diffusion models such as those developed by Gierke et al. (1992) and Ng and Mei (1996) may more accurately simulate long term mass reduction. For instance, both Fisher et al. (1996) and Conklin et al. (1995) noted that a single first-order gas-water mass transfer rate could not describe both early and late time data. Fisher et al.'s (1996) first-order rate coefficients used to fit early time data were consistently much higher (in one instance 10^{-4} versus 10^{-5} s^{-1}) than a second first-order rate used to fit late data. Fisher et al.'s (1996) work points out the danger in using first-order rate constants obtained from short term laboratory studies to estimate long term mass removal trends. Under these conditions, use of first-order rate constants obtained from short-term laboratory tests would result in overestimation of long term mass removal.

Rao et al. (1980a,b) demonstrated that first-order mass transfer coefficients cannot be expected to be constant because of the failure of the first-order models to account for the geometry and concentration gradient within intraaggregate space. Rao et al. (1980a,b) found that when a first-order kinetics model is used to simulate diffusion from spherical aggregates, the mass transfer coefficient decreases with time and approaches a constant value at large time.

9.6 Rate-Limited Solids-Water Exchange

Sorption data from batch experiments have been found to exhibit a two-stage approach to

equilibrium - a short initial phase of fast uptake, followed by an extended period of much slower uptake. Generally, about 50% of sorption occurs within the first few minutes to hours, with the remainder occurring over periods of days or months (Jaffe and Ferrara, 1983; Wu and Gschwend, 1986; Karickhoff, 1980; McCall and Agin, 1985; Oliver, 1985; Ball and Roberts, 1985; and Curtis et al., 1986). Diffusion within soil organic matter has been proposed as a plausible mechanism responsible for rate-limited sorption (Bouchard et al., 1988; Brusseau and Rao, 1989a; Brusseau et al., 1991; Karickhoff and Morris, 1985, Lee et al. 1988). Soil organic matter is essentially a three-dimensional network or randomly oriented polymer chains having a relatively open, flexible structure perforated with voids (Khan, 1978; Schnitzer, 1978). Brusseau (1994) summarizes experimental observations which support the hypothesis that sorbate diffusion into organic matter is a causative factor in rate-limited sorption.

The simplest approach in modeling sorption kinetics is to utilize a one-site, first-order model in which the sorption rate is taken as a function of the concentration difference between the sorbed and solution phases. To simulate rate-limited solids-water exchange, the solids storage term in the advective-dispersive equation can be expressed by:

$$\rho_b \frac{\partial C_s}{\partial t} = \theta_w \lambda_{ws} \left(C_w - \frac{C_s}{K_d} \right) \tag{9.25}$$

where λ_{ws} = water-solids first-order mass transfer coefficient [T^{-1}]. The one-site, first-order sorption rate model however has failed to fit experimental data well in both solute (Schwarzenbach and Westall, 1981; Rao and Jessup, 1983; and Wu and Gschwend, 1986) and vapor (Grathwohl and Reinhard, 1993; Wehrle and Brauns, 1994; and Croisé et al., 1994) transport experiments. Croisé et al. (1994) found that the solids-water mass transfer rate decreased exponentially with time during gas extraction. Kaleris and Croisé (1997) state that if a conservative estimate of remediation time is needed, a first-order kinetic approach can be considered provided a low mass transfer rate is assumed.

Selim et al. (1976) and Cameron and Klute (1977) were among the first investigators to use a first-order bicontinuum or two-site sorption model where sorption is assumed to be instantaneous for a fraction of the sorbent and rate-limited for the remainder. Two-site modeling has described sorption kinetics well in controlled laboratory batch and column studies. In bicontinuum or two-site modeling, solids-water mass exchange can be represented in the equilibrium domain by

$$\frac{\partial C_{s1}}{\partial t} = F K_d \frac{\partial C_w}{\partial t} \tag{9.26}$$

and in the rate-limited domain by

$$\frac{\partial C_{s2}}{\partial t} = \lambda_{ws} \left((1-F) K_d C_w - C_{s1} \right) \tag{9.27}$$

where F equals fraction of instantaneous sorption sites [-], C_{s1} equals solids concentration in equilibrium domain [MM^{-1}], and C_{s2} equals solids concentration in rate-limited domain [MM^{-1}]. The one-site model is a special case of the two-site model where F = 0 (all sites are rate-limited). In the two-site sorption model, equilibrium and rate-limited sites can be conceptualized as occurring in series or parallel. The former conceptualization is consistent with the viewpoint that soil organic matter is a polymeric like substance where sorption to the surface is rapid followed by liquid diffusion into the soil organic matter matrix. Mathematically however, both series and parallel sorption site conceptualizations are indistinguishable (Karickhoff, 1980; Karickhoff and Morris, 1985).

Popovičová and Brusseau (1998) derived a bicontinuum solids-water Damkohler number (ω_{sw}) for gas flow expressed by

$$\omega_{sw} = \frac{\lambda_{sw} L}{v} R_s \tag{9.28}$$

where

$$R_s = \frac{\rho_b}{\theta_g H}(1-F)K_d\ . \tag{9.29}$$

Assuming that rate-limited solids-water mass exchange approaches equilibrium conditions as ω_{sw} approaches 10, a solids-water critical pore-gas velocity, $v_{c(sw)}$ [LT^{-1}] can be estimated by

$$v_{c(sw)} = 0.1\frac{\lambda_{sw} L_c \rho_b K_d}{H\theta_g}(1-F) \tag{9.30}$$

Use of equation (9.30) to assess $v_{c(sw),}$ requires estimation of λ_{ws} and F. Brusseau and Rao (1989a) state that intra-sorbent mass transfer is a function of three factors: (1) aqueous diffusivity of the diffusing species, (2) resistance to diffusion associated with the sorbent matrix, and (3) diffusion path length. For nonionic, low polarity organic compounds, the soil-water partition coefficient (K_d) is predominately influenced by the compound's organic carbon-water partition coefficient (K_{oc}), and the fraction of organic carbon content (f_{oc}). The K_{oc} is a function of the size and molecular structure of the solute and therefore related to diffusivity while f_{oc} is related to the diffusion path length. For any given polymer (humic material) and solvent (water), the diffusion coefficient in a polymer decreases exponentially with increasing molecular weight or size of the diffusing molecule. This is especially true for polymer-sorbate systems where the size of the diffusing molecule is similar to the size of the polymer mesh (Brusseau et al., 1991) as is the case with humic material. Hence, if a diffusion mechanism is responsible for rate-limited sorption, an inverse relationship between λ_{sw} and K_d is expected. Brusseau and Rao (1989a,b) collected rate-limited sorption data from a number of investigators, plotted the logarithms of sorption rate constants and soil-water partition coefficients, and observed an inverse relationship

consistent with previous observations of Karickhoff (1980,1984), and Nkedi-Kizza et al. (1989). These and other correlations between λ_{sw} - K_d are summarized in Table 9.2. These correlation equations then can be used to estimate λ_{sw}.

Brusseau et al. (1991) investigated the effect of compound structure on sorption kinetics to assess when deviation from λ_{sw} - K_d correlations would be expected. Brusseau and Rao (1991) found that sorbates containing single or multiple substitutions of methyl or chlorine groups exhibited λ_{ws} - K_d relationships similar to unsubstituted aromatic hydrocarbons. Also, chlorinated alkenes/alkanes exhibited λ_{ws} - K_d relationships similar to unsubstituted and substituted aromatics. In addition, neutral species of ionogenic compounds exhibited λ_{ws} - K_d behavior similar to nonionic compounds. For these compounds, sorbate structure had a minor impact on the nature of rate-limited sorption as compared to K_d values. Brusseau and Rao (1991) state that the λ_{ws} - K_d correlation for simple molecules such as benzene and chlorobenzene represents a "standard-state" behavior, with deviations from the standard state being a function of the relative degree of additional sorbate-sorbent interactions. Sorbates with complex structures such as some pesticides may have additional constraints to diffusion and specific sorbate-sorbent interactions. For instance, Brusseau et al. (1991) evaluated the impact of single or multiple

Table 9.2 Correlation of solids-water mass transfer coefficients with soil-water partition coefficients

Equation (hr^{-1})	Compound Class	Reference
$\log \lambda_{ws} = 0.301 - 0.668 \log K_d$ ($r^2 = 0.95$)	wide variety of compounds with $\log K_d$ varying from -1.5 to 5.5	Brusseau and Rao (1989b)
$\log \lambda_{ws} = 0.960 - 0.836 \log K_d$ ($r^2 = 0.99$)	chlorobenzenes	Brusseau and Rao (1989b)
$\log \lambda_{ws} = 1.18 - 0.885 \log K_d$ ($r^2 = 0.99$)	chlorobenzenes	Brusseau et al. (1990)
$\log \lambda_{ws} = 0.944 - 0.830 \log K_d$ ($r^2 = 0.97$)	polynuclear aromatics	Brusseau and Rao (1989b)
$\log \lambda_{ws} = 0.56 - 0.47 \log K_d$ ($r^2 = 0.85$)	chloro-aliphatics, aromatics, chloro-aromatics, and chlorophenols	Brusseau and Rao (1991)
$\log \lambda_{ws} = 0.75 - 0.63 \log K_d$ ($r^2 = 0.99$)	aromatics and methyl-aromatics	Brusseau et al. (1991)
$\log \lambda_{ws} = 0445 - 0.86 \log K_d$ ($r^2 = 0.87$)	aromatics, chloroalkenes, polynuclear aromatics	Hu et al. (1994)

additions of methyl groups on the benzene molecule using toluene (methylbenzene), o-xylene (o-dimethylbenzene), p-xylene (p-dimethylbenzene), and trimethylbenzene. The addition of single methyl functional groups did not result in behavior deviating from the behavior exhibited by unsubstituted molecules. They also evaluated the impact of adding a single n-alkyl group on the benzene molecule by using ethylbenzene, n-propylbenzene, n-butylbenzene, and n-hexylbenzene. In this case, addition of an alkyl chain of three or more carbon units did alter the expected λ_{sw} - K_d correlation. Brusseau et al. (1991) argue that the presence of three- or four-carbon chain n-alkyl groups provides an increased opportunity for a diffusing molecule to become entangled with the polymer chain.

Estimation of the fraction of sorbent in instantaneous sorption occurs, F, does not appear as straightforward as estimation of $\lambda_{sw.}$ Values of F appear to vary with chemical and sorbent ranging from 0.12 to 0.52 for a combination of 24 chemicals and 11 sorbents (Karickhoff and Morris, 1985; Lee et al., 1988; and Brusseau et al., 1991). Lee et al. (1988) reported a median value of 0.17 for F in the transport of trichloroethene and p-xylene in columns packed with Borden and Lula sandy low-organic aquifer material. Brusseau et al (1991) observed a linear increase in F with increasing log K_{ow} (octanol-water partition coefficient) for a number of compounds. Brusseau et al. (1991) state that since K_{ow} is directly related to the molecular size of a solute, this behavior is consistent with the intra-organic matter diffusion model. They state that the polymeric mesh may act as a molecular sieve, whereby larger sorbate molecules are excluded from some portion of the internal volume because of size constraints. Thus the size of the rate-limited domain may vary with sorbate size. Molecular hindrance would cause F to increase assuming that the instantaneous fraction of sorption sites remains constant. Lee et al. (1991) found an increase in F with increasing log K_d for ionized chlorophenols. For pentachlorophenol (PCP). They observed that F values decreased linearly with increasing methanol addition. Lee et al. (1992) argue that since organic cosolvents are known to cause swelling of the organic matter matrix, this increase may be primarily in interior of the organic matter matrix or within the rate-limited domain. They also noted that F increases with increasing ionic strength of the solute containing solution. They explain that this is most likely a result of a tightening of the organic matter matrix with increasing divalent cation concentration.

Recently, there have been efforts to generalize the sorbent surface into parallel classes of reaction sites with each site having its own unique rate constant. For instance, Lorden et al. (1998) describe a γ-distribution model that generalizes two-site sorption heterogeneity into a continuum of sorption sites that are grouped into different classes according to a γ probability density function for both equilibrium and rate parameters. They conducted gas flow column studies to evaluate the performance of the γ-distribution model against the more commonly used two-site, first-order and spherical diffusion models. Laboratory columns consisted of packed air dried fine-grained sand (93% sand, 6.3% silt) having an organic carbon content of 0.91%. Gravimetric measurements indicated a gas-filled porosity of 52%, and moisture content of 1.6% by weight. Lorden et al. (1998) state that at this moisture content, soil particles were covered by approximately 18 molecular layers of water (based on measured BET surface area of 3.3 m^2/g and a surface area of 10.8 x 10^{-20} m^2 for a molecule of water). Soils were maintained at 90%

relative humidity (RH) for all transport experiments. TCE was injected into the columns at 90% (472.5 mg/l) and 10% (52.5 mg/l) of vapor saturation to simulated flow close to a NAPL source. Flow rates were chosen so that resulting pore-gas velocities ranged between 0.1 to 0.8 cm/s. Equilibrium sorption experiments were conducted at 90% RH over a wide range of vapor concentrations revealing a non-linear isotherm. Lorden et al. (1998) however state that concentration dependency on the partition coefficient probably did not have a significant affect on the ability of the γ-distribution model to fit BTC data because of the strong departure from equilibrium. The only cause of asymmetric effluent breakthrough curves during experimentation was postulated to be from sorption kinetics since symmetric breakthrough curves were observed using a conservative tracer (4% by volume methane in nitrogen). Particular emphasis was placed on the relative ability of each model to fit the slow tailing or low concentration portion of the breakthrough curves. C/C_o was plotted on a log scale to facilitate visual observation of fit at low vapor concentrations.

BTCs revealed that when the equilibrium sorption partition coefficient remained fixed at a laboratory measured value, both the two-site model and spherical diffusion model were unable to fit effluent C/Co concentrations below 0.1 and 0.01 respectively while the γ-distribution model was able to successfully fit data through C/Co concentrations of 0.001. When the partition coefficient was included as a fitting parameter, the quality of fit improved significantly for the spherical diffusion model but remained poor for the two-site first-order model. The two-site first-order model tended to provide sharp and straight concentration declines as opposed to a smooth transition in concentration with pore volume exchanges. Also, mass transport coefficients increased with velocity for the spherical diffusion and two-site model when the partition coefficient was included as a fitting parameter. There is no way to directly use Lorden et al.'s work to estimate a critical pore-gas velocity for solids-water exchange, but it is important to realize that there may be limitations to two-site and spherical diffusion modeling in assessing mass transfer.

9.7 Combined Rate-Limited Gas-Water and Solids-Water Exchange

Wehrle and Brauns (1994) describe column experiments conducted in moist fine to medium sand with f_{oc} = 0.4% and water saturation = 24%. Vapor effluent curves and flow interruption tests displayed significant rate-limited mass transport behavior at a pore-gas velocity of 0.35 cm/s. Vapor concentration increased over two orders of magnitude during flow interruption testing. A comparison of tests with and without organic carbon removed revealed less but still significant rate-limited behavior with organic carbon removed. Thus, vapor transport was likely limited by both gas-water and solids-water exchange. At the end of the experiments, 97% of contaminant mass had been removed after approximately 50,000 pore volumes.

McClellan and Gillham (1992) reported effluent tailing and significant concentration rebound after flow interruption tests. Vapor concentrations in the effluent persisted even after 22,650 pore volumes of air had passed through soils. Armstrong et al. (1994) developed a

numerical one-dimensional model incorporating first-order gas-water and solids-water rate-limited mass exchange to simulate vapor effluent data obtained by McClellan and Gilham (1992). Virtually identical fits were obtained to effluent curves for both continuous and pulsed schemes using two parameter sets: 1) K_d and λ_{gw} values of 2.1 cm^3/g and 2 x 10^{-5} s^{-1} respectively (equilibrium sorption) and 2) K_d, λ_{gw}, and λ_{ws} values of 10.1 cm^3/g, 4 x 10^{-5} s^{-1}, and 5 x 10^{-5} s^{-1} respectively. Simulated remaining mass however differed sharply with the second parameter set resulting in far greater mass retention. Their sensitivity analysis and calibration of data showed that different rate constants and mass retention characteristics can produce very similar effluent curves suggesting that effluent and vapor probe concentration data can not be used to estimate mass transport coefficients and VOC concentration in the aqueous and solids phase.

Brusseau (1991) developed a model which included a mobile and immobile domain with rate-limited solids-water exchange in both domains and simulated experimental results of Roberts (1990) and Brown and Rolston (1980) using independent derived data (i.e.simulation without curve fitting). Deviation from local equilibrium was evident in all three studies where pore-gas velocities ranged from 0.016 to 0.635 cm/s. Goltz and Oxley (1994) modified Brusseau's (1991) one-dimensional formulation to enable simulation of radial flow using a numerical Laplace transform inverse routine. Huang and Goltz (1999) provided: (1) an exact solution to Brusseau's (1991) formulation in radial coordinates for Peclet numbers less than 12; (2) an exact solution to Brusseau's (1991) formulation in radial coordinates for infinite Peclet numbers (no dispersion); and (3) an approximate solution to Brusseau's (1991) formulation in radial coordinates over a wide range of Peclet numbers.

To assess combined gas-water and solids-water rate-limited exchange during gas flow without the interfering effects of physical heterogeneity, Popovičová and Brusseau (1998) packed 0.59 mm moistened glass beads to create a homogeneous media with a volumetric water content of 11.9%. Methane was used as a nonsorbing conservative tracer while trichloroethene, benzene, and toluene were used as sorbing tracers. Experiments were conducted at gas velocities ranging from 0.1 to 3.33 cm/s. Breakthrough curves for methane were symmetrical for all tested pore-gas velocities indicating absence of rate-limited mobile - immobile gas exchange. Breakthrough curves for trichloroethene and benzene however were noticeably asymmetric. In addition, the degree of tailing increased with increasing velocity. Peclet numbers obtained by applying the ideal advective-dispersive model to trichlorethene and benzene transport were lower than those obtained for methane under the same experimental conditions indicating increased dispersion from rate-limited behavior. Values of gas-water and solids-water Damkohler numbers less than 10 indicated a significant degree of nonequilibrium caused by diffusion in water and rate-limited sorption.

9.8 Rate-Limited Mobile-Immobile Gas Exchange

The mobile-immobile domain concept has been used for solute transport analysis for many years with a large number of associated publications. Coats and Smith (1964) were among the first investigators to perform mobile-immobile domain modeling for nonsorbing solutes.

Later, van Genuchten and Wierenga (1976) extended the model for sorbing solutes. In mobile-immobile domain formulations, rate-limited mass exchange is represented by a two-site model where a concentration gradient between the mobile and immobile domain and a first-order rate constant controls mass exchange. When using the two-site, first-order rate modeling approach, an average immobile-region concentration is assumed in contrast to the aggregate diffusion model where a concentration gradient within the immobile domain is allowed.

For soil venting application, gas-filled regions where advective flow occurs is defined as the mobile domain while gas- and water-filled regions where advective flow does not occur is defined as the immobile domain. Mass exchange from water-filled regions has been previously discussed in the context of gas-water mass transfer using first-order rate constants or spherical diffusion modeling. Immobile domains have been conceptualized as lenses or layers of low permeability media surrounded by higher permeability media, intra-aggregate porosity, dead-end pores, bulk water, surface films, and matrix porosity of fractured media. In stratified media, gas will flow primarily through layers of higher gas permeability. Vapors in highly permeable strata will be extracted first by advection. As the contaminant from these strata becomes depleted, diffusion from the lower permeable strata will control mass removal.

Krishnayya et al. (1988), Croisé et al. (1989), Ho and Udell (1991), and Kearl et al. (1991) demonstrated the effect of layered porous media on gas transport. Rathfelder et al. (1991) demonstrated that effluent tailing can occur because of gas flow being channeled in stratigraphic layers of lesser contamination but greater permeability.

Kearl et al. (1991) conducted gas transport experiments in a column packed with layers of sand and silty clay with moisture contents of 2 and 10% respectively. They concluded that diffusion between layers of different permeability controlled transport and removal of contaminants at gas velocities ranging from 2 to 45 cm/s. These pore-gas velocities though are very high compared to typical pore-gas velocities expected in the field (0.001 to 0.1 cm/s).

Kaleris and Croisé (1999) used a well-mixed reservoir (WMR) model to evaluate the effect of variation in permeability and retardation factor in a two-layer system. They compared simulation results of their WMR model with a finite-element numerical model to assess conditions under which the WMR model was valid. Ho and Udell (1992) considered cases in which gas flow occurred only through a layer of high permeability media with contaminant removal from a layer of low permeability media occurring only through diffusion from a NAPL source.

To assess the effect of physical heterogeneity due only to mobile and immobile gas mass transfer without the interfering effects rate-limited gas-water and rate-limited solids-water exchange during soil venting, Popovičová and Brusseau (1997) conducted of a series of laboratory column experiments using dry 0.59 mm glass beads and a centered 5 mm o.d. stainless steel screen to represent a macropore. Methane was used as a nonsorbing conservative tracer while trichloroethene, benzene, and toluene were used as sorbing tracers. Experiments were

conducted at gas velocities ranging from 0.1 to 3.33 cm/s. In the heterogeneous media, increased tailing or BTC asymmetry for methane was evident with increasing velocity. At low pore-gas velocities (e.g., 0.1 cm/s) BTCs were symmetrical. Popovičová and Brusseau (1997) explain that as the residence time of the vapor decreases with increasing velocity, the departure from equilibrium increases due to insufficient time available for mass exchange between macropore and micropore domains. To compare contributions of molecular diffusion, mechanical dispersion, and micropore-macropore exchange to overall dispersion, a mechanical dispersivity value was estimated from experiments previously conducted without the macropore at pore-gas velocities in excess of 1.67 cm/s. At a pore-gas velocities greater than 2.0 cm/s, micropore-macropore exchange contributed greater than 50% of total dispersion. At a pore gas velocity of 3.33 cm/s, micropore-macropore exchange contributed greater than 80% of total dispersion. BTC asymmetry appeared to increase for sorbing tracers in the heterogeneous system. However, when the micropore-macropore first-order exchange coefficients were adjusted to incorporate differences in the free-gas molecular diffusion coefficients, this increased asymmetry was effectively accounted for and thus was not due to sorption kinetics.

In this experimental system, it is likely that advective transport occurred in the micropore as well as the macropore domain. Thus, breakthrough asymmetry could have been influenced by pore-gas velocity variation as well as from diffusive micropore-macropore exchange. If significant advective flow occurred in the micropore region, then fairly high pore-gas velocities would be required to induce breakthrough curve asymmetry. This is not analogous to a field situation where micropore-macropore or stratigraphic layer exchange may be completely constrained by diffusion. Thus, much lower pore-gas velocities could induce breakthrough asymmetry due to physical heterogeneity.

A Damkoher number for mobile gas - immobile gas transfer can be expressed by

$$\omega_{gg} = \frac{\lambda_{gg} L}{v\theta_g} \tag{9.31}$$

where λ_{gg} is an immobile gas - mobile gas first-order mass transfer coefficient [T^{-1}]. By analogy to Brusseau's (1991) estimation of λ_{gw}, λ_{gg} could be estimated by

$$\lambda_{gg} = \frac{cD_g\theta_g}{\tau_g\delta^2} \tag{9.32}$$

Thus, assuming that immobile gas - mobile gas exchange approaches equilibrium conditions as ω_{gg} approaches 10 and a spherical shaped immobile domain, a critical pore-gas velocity for immobile gas - mobile gas exchange can be estimated by

$$v_{c(gg)} = 1.5\frac{D_g L_c}{\tau_g \delta_c^2} \tag{9.33}$$

9.9 Combined Rate Limited Mobile-Immobile Gas and Gas-Water Exchange

Popovičová and Brusseau (1998) conducted of a series of laboratory column experiments similar to Popovičová and Brusseau (1997) except that 0.59 mm glass beads were saturated and allowed to drain to achieve a volumetric gas porosity of 9.9% prior to conducting experiments. As before, a centered 5 mm o.d. stainless steel screen was added to their column to represent a macropore and methane was used as a nonsorbing conservative tracer while trichloroethene, benzene, and toluene were used as sorbing tracers. Experiments were conducted at gas velocities ranging from 0.1 to 3.33 cm/s. Their model formulation allowed for retention at the gas-water interface, assumed instantaneous sorption, and allowed consideration of rate-limited: (1) mobile-immobile gas exchange, (2) mobile gas-mobile water exchange, and (3) immobile gas-immobile water exchange.

Transport of methane through the heterogeneous system exhibited asymmetric breakthrough which increased with pore velocity. Analysis of data indicated that advective flux was not confined to the macropore. Gas advection also in occurred in the glass bead domain. The magnitude of their mobile - immobile gas Damkohler numbers (0.88-2.83) indicated significant rate-limited mobile-immobile gas exchange. Popovičová and Brusseau (1998) state that generally, diffusive mass transfer in the gas phase is considered relatively rapid, especially compared to aqueous-phase diffusion. However, the results of their experiments illustrate that gas-phase mass transfer can be rate limited at the pore-gas velocities used for their column studies. The transport of TCE exhibited greater breakthrough asymmetry and decreasing Peclet numbers compared to methane at similar pore gas-velocities indicating the presence of additional rate-limiting processes which they attributed to diffusion within immobile water and rate-limited sorption.

9.10 Conclusions

1. Selection of pore-gas velocities to support venting design requires consideration of rate-limited gas-NAPL, gas-water, and solids-water mass exchange on a pore-scale and rate-limited mobile-immobile gas exchange on a field-scale. During rate-limited dominated mass transfer, as pore-gas velocity increases, vapor concentration decreases. However, an increased pore-gas velocity still results in an increased mass removal rate and hence shorter remediation time because of an increased concentration gradient between equilibrium and nonequilibrium vapor and soil-water concentrations. Thus, there is a trade-off between selection of a design pore-gas velocity and remediation time.

2. Five ways that could be used separately or concurrently to select a critical pore-gas velocity for venting application were described. The approach most suitable for use by practitioners appears to be use of algorithms and Damkohler numbers. As mentioned

though, a limitation using Damkohler numbers and algorithms to estimate critical pore-gas velocities is that mass transport processes are considered independently when in reality complex interactions between these processes dictate overall mass removal. Also, there are additional complications to consider in selection of critical pore-gas velocities. Virtually all research on rate-limited vapor transport and development of algorithms for pore-gas velocity determination originated from controlled sand tank and laboratory column studies where field-scale heterogeneity was not a factor. Thus, optimal pore-gas velocities in the field are likely to be very site-specific and somewhat smaller than indicated by Damkohler numbers, algorithms, and published studies. Also, characteristic lengths of contamination used in Damkohler numbers and algorithms are not constant but decrease in time due to NAPL and sorbed mass removal thereby reducing calculated optimal pore velocities. Finally, the cost of well installation and venting operation (e.g., electricity, vapor treatment) should be considered since achievement of a minimum target pore-gas velocity at some sites may be prohibitively expensive. Thus, it is apparent that selection of a critical pore-velocity is not a straightforward process but involves some degree of judgement and iterative reasoning (gas flow modeling to see what pore-gas velocities can be achieved given certain well spacing and flow rates). However, while there are limitations to the use of algorithms and Damkohler numbers in selecting a design pore-gas velocity, these numbers provide a starting point after which more sophisticated analysis can proceed if desired.

10. LIMITATIONS OF ROI EVALUATION FOR SOIL VENTING DESIGN: SIMULATIONS TO SUPPORT VENTING DESIGN BASED ON ATTAINMENT OF CRITICAL PORE-GAS VELOCITIES IN CONTAMINATED MEDIA

By far, the most common method used for venting design in the United States is radius of influence (ROI) evaluation. In a review of over 100 Superfund and Resource Conservation and Recovery Act (RCRA) sites at U.S. EPA's Office of Research and Development, National Risk Management and Research Laboratory in Ada, Oklahoma, only one documented case could be found where a non-ROI method had been used for venting design. ROI testing involves evaluating the maximum radial extent of induced subsurface vacuum to some arbitrarily specified level (typically 0.01 to 0.1 inches of water) in single well tests. As illustrated in Figure 10.1, in practice, ROIs are determined by plotting vacuum as a function of logarithmically transformed radial distance and applying linear regression to extrapolate to the distance at which a specified vacuum would be observed. Vacuum monitoring points are often located significant distances from gas extraction wells in an attempt to "physically" locate ROIs for given flow rates. For SVE design, overlapping circles of ROIs for individual wells are then drawn on a site map to indicate an "effective" remediation area.

Johnson et al. (1990a,b) first discussed ROI assessment as a method for spacing SVE

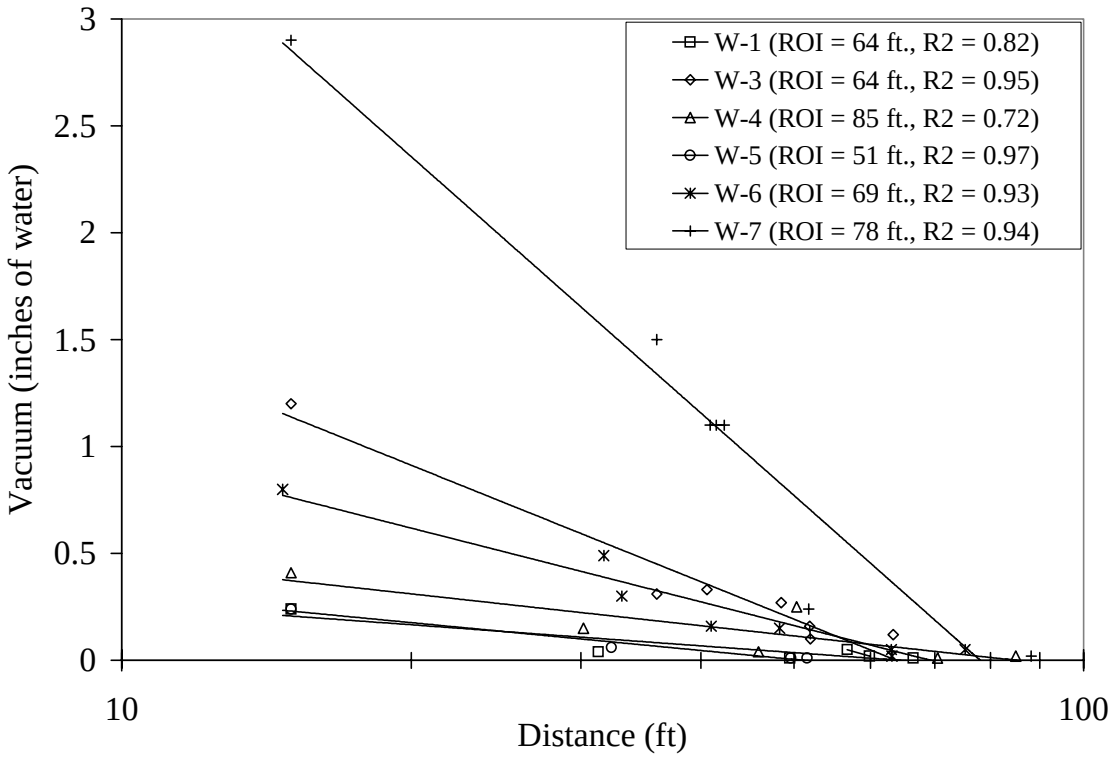

Figure 10.1 Observed vacuum as a function of logarithmically transformed radial distance at tested wells for ROI determination. Line represent result of linear regression with correlation coefficients R2 as provided.

wells. The U.S. EPA (1991) later incorporated ROI measurement into guidance for SVE design. The implicit assumption in ROI-based designs is that observation of subsurface vacuum ensures sufficient gas flow in contaminated soils for timely remediation. However, measurement of vacuum at best only ensures containment of contaminant vapors (Johnson and Ettinger, 1994). This is even in question when the magnitude of applied vacuum in soil is comparable to pressure differential caused by variation in barometric pressure and/or fluctuation of the water table. Diurnal barometric pressure changes in soil can be on the order of a few mbar (Massmann and Farrier, 1992) where 0.1 inch water vacuum is equivalent to 0.25 mbar. Cho and DiGiulio (1992) illustrated how specific discharge decreases dramatically with radial distance from gas extraction and injection wells and recommended that venting design be based on subsurface gas flow analysis instead of ROI testing. Johnson (1988) described how the addition of 13 extraction wells within the ROI of other extraction wells increased blower VOC concentration by 4000 ppmv and 40 kg/day. Johnson (1988) concluded that the ROI was not an effective design parameter for locating extraction wells and that operation costs could be reduced by increasing the number of extraction wells as opposed to pumping at higher rates with fewer wells.

In this section, data was utilized from a Superfund site (described in section 6) where ROI testing was conducted by a remedial contractor to describe limitations of ROI evaluation in detail and to demonstrate an alternative method of design based on specification and attainment of critical pore-gas velocities in contaminated subsurface media. Other than ROI assessment, little has been published on alternative quantitative design criteria for venting systems (Sawyer and Kamakoti,1998). Information was utilized from section 9 to provide the basis for selection of a minimum or critical pore-gas velocity for use at this site. Using single-well gas flow simulations, an assessment was made whether a selected critical pore-gas velocity could be achieved at measured ROI's. A series of multiple-well gas flow simulations were then conducted to assess how variation in anisotropy and leakance affect three-dimensional vacuum and pore-gas velocity profiles and determination of an ROI. Finally, an assessment was made when attempting to achieve a critical design pore-gas velocity, whether it is more efficient to install additional wells or pump existing wells at a higher flow rate.

10.1 Critical Pore-Gas Velocity Estimation for Test Site

At the test site described in section 6, preliminary single- and multiple-well gas flow modeling indicated that a critical pore-gas velocity of 0.01 cm/s was easily achievable. Many of the soils related input parameters required by Damkohler numbers and algorithms were not available and thus had to be estimated from literature values summarized in Table 10.1. A critical pore-gas velocity for gas-water exchange using a gas-water Damkohler number of 10 was calculated to be 2.70 cm/s. A critical pore-gas velocity for gas-water exchange using a prefix denominator value of 10 was calculated to be 5.23 cm/s. Using relationship developed by Ng and Mei (1996) for aggregate diffusion, a critical gas-water pore-gas velocity of 5.80 cm/s was calculated. Use of a solids-water Damkohler number of 10 and assumption that F = 0 resulted in computation of a critical pore-gas velocity for solids-water exchange at 2.22 cm/s. Information was not available to calculate a critical pore-gas velocity for mobile-immobile gas exchange but

Table 10.1 Input parameters for estimation of pore-gas velocity

	Description	Value	Units	Ref.
S_w	water saturation	0.26	[-]	1
η	porosity	0.33	[-]	1
ρ_s	particle density	2.65	g/cm^3	1
τ_g	gas phase tortuosity	2.9	[-]	1
τ_w	water phase tortuosity	1.4	[-]	1
δ_c	aggregate radius	0.035	cm	1
d_{50}	mean grain size	0.08	cm	2
L_c	radius of contaminated region	800	cm	3
K_d	soil-water partition coefficient	0.300	cm^3/g	4
H	Henry's Law Constant	0.26	[-]	1
D_g	gas diffusion coefficient	0.082	cm^2/s	1
D_w	water diffusion coefficient	1.1×10^{-05}	cm^2/s	1

11. Value used by Gierke et al. (1992) for sand
12. Value used for Wilkins et al. (1995) for graded sand mixture
13. Based on 53 foot (average distance between closest wells) well spacing
14. Assumed based on K_{oc} of 300 cm3/g for toluene and $f_{oc} = 0.001$

at pore-gas velocity of 0.01 cm/s, an immobile gas region having a radius greater that 61 cm would be necessary to limit mass removal. The relationship developed by Wilkins et al. (1995) using a C/C_o vapor concentration of 0.99 yielded an extremely high and unrealistic pore-velocity for deviation from equilibrium conditions. At a pore-gas velocity of 0.01 cm/s, a characteristic contamination of length of less that 1 cm would be necessary to achieve near equilibrium conditions in NAPL contaminated soils. Thus, use of the information provided in Table 10.1 without consideration of field-scale heterogeneity indicates that a fairly high pore-gas velocity could be utilized at this site. However, given the potential for overestimation of critical pore-gas velocities due to field-scale heterogeneity, overestimation of the characteristic length of contamination, and observation during gas flow modeling that pore-gas velocities on the magnitude of 1 cm/s would require very close well spacing, a critical pore-gas velocity of 0.01 cm/s was chosen for use at this site. Using similar reasoning, a design pore-gas velocity of 0.01 cm/s was also selected for use at the Picillo Farms Superfund site containing glacialfluvial outwash and glacial till (Woodward-Clyde and Envirogen, 1998) based on three-dimensional

numerical gas flow modeling with the public domain model AIR3D (Joss and Baehr, 1995).

10.2 Single-Well Simulations

Results from ROI testing are summarized in Table 10.2 for vacuum levels of 0.1, 0.05, and 0.0 inches of water and graphically displayed in Figure 10.1 with associated linear regression correlation coefficients. It is apparent that monitoring points were placed at distant radii in an attempt to "physically" locate the radius at which vacuum approached 0.01 inches of water even though most vacuum dissipation and thus highest pressure gradients occurred within 15 feet of each well. Using a ROI-based design, wells would be spaced 60 - 146, 80 - 150, and 128 - 170 feet apart for ROI vacuum of 0.1, 0.05, and 0.0 inches of water respectively. Yet as shown in Table 10.3 and Figures 10.3 through 10.8, adjacent wells were typically placed 43 to 65 feet apart. Thus, well spacing at this site is conservative for an ROI-based design.

With the exception of well W-4, Figure 10.2 illustrates two-dimensional profiles of calculated vacuum and vector norm pore-gas velocities using the arithmetic mean of gas

Table 10.2 Radii of Influence (ft) as a function of observed vacuum

well	0.1 in. water	0.05 in. water	atm. press.
W-1	32	45	64
W-3	57	60	64
W-4	55	65	85
W-5	30	40	51
W-6	58	64	69
W-7	73	75	78

Table 10.3 Well spacing (ft)

	W-1	W-3	W-4	W-5	W-6	W-7
W-1	0	67	123	65	66	94
W-3	67	0	59	53	64	53
W-4	123	59	0	79	118	89
W-5	65	53	79	0	104	106
W-6	66	64	118	104	0	43
W-7	94	53	89	106	43	0

permeability and leakance values in Table 6.2b. Calculations for well W-4 were not conducted because the range of leakance and anisotropy values were too wide to allow selection of representative values. Vacuum profiles are curvilinear especially near wells due to partial penetration of gas extraction wells, aniostropy, and leakance of air from the surface. The definition of a ROI however implies a constant pressure differential at a given radius. As k_r/k_z ratios increase, vacuum contours become increasing curvilinear until eventually as illustrated for well W-3, there is too much vertical variation to assign a vacuum level to any specific radial distance. If a vacuum level of 0.05 inches of water had been used to designate a ROI for W-3, the ROI would have varied from 54 to 78 feet. Thus, the ROI is an ill-defined and nondescript term for anisotropic soils or where there is significant leakance or partially penetrating gas extraction wells. This reality however is missed during ROI testing because gas monitoring wells are typically screened over an extensive portion of the vadose zone thereby integrating pressure or vacuum measurements and giving the impression that pressure differential is only a function of radial distance.

Recognizing, that ROI measurement does not incorporate vertical variation in pressure differential, Chen and Gosselin (1998) proposed using an area of influence or zone of influence (ZOI) to describe the effectiveness of a gas extraction well. This area or zone then would be a two-dimensional surface over which "effective" gas flow would occur. While an improvement over the ROI concept, the ZOI concept still requires arbitrary specification of a pressure differential which again does not guarantee attainment of a design critical pore-gas velocity. For instance, vacuum readings of 0.05 inches of water at wells W-1, W-3, W-5, W-6, and W-7, resulted in approximate computed pore-gas velocities of 0.002 - 0.003, 0.0007 - 0.001, 0.005 - 0.007, 0.0007, and less that 0.001 cm/s respectively. Vacuum readings of 0.1 inches of water (typically the highest vacuum that practitioners use to establish a ROI) at wells W-1, W-3, W-5, W-6, and W-7 resulted in approximate computed pore-gas velocities of 0.005 - 0.007, 0.0015 - 0.003, 0.01 - 0.02, 0.0015, and less than 0.001 cm/s respectively. In only one case did a vacuum of 0.1 inches of water result in attainment of 0.01 cm/s or higher (W-5). For wells W-1, W-3, W-5, W-6, and W-7, vacuum measurements of approximately 0.25, 0.5, 0.1, 0.5, and 1.0 inches of vacuum respectively would be necessary to ensure attainment of a pore-gas velocity of 0.01 cm/s.

The results of single-well simulations demonstrate several important deficiencies in ROI evaluation. First, as previously discussed, cross-sectional two-dimensional simulations clearly illustrate that the ROI is an ill-defined entity. Vacuum profiles are very curvilinear especially under conditions of high leakance values and k_r/k_z ratios. Second, an ROI-based design, may result in subsurface pore-gas velocities too low for optimal gas circulation especially at low leakance values and high k_r/k_z ratios. Third, attainment of critical pore-gas velocities can not be guaranteed by simply raising the magnitude of vacuum during venting application from say 0.05 inches of water to some other arbitrarily specified level (e.g., 0.1 inches of water). Observed vacuum is a function of boundary conditions (e.g., leakance), applied mass flow, anisotropy, permeability, and geometry of screened intervals. In some cases, relatively high vacuum (e.g., greater than 1 inch of water) must be maintained between wells to ensure sufficient subsurface gas flow.

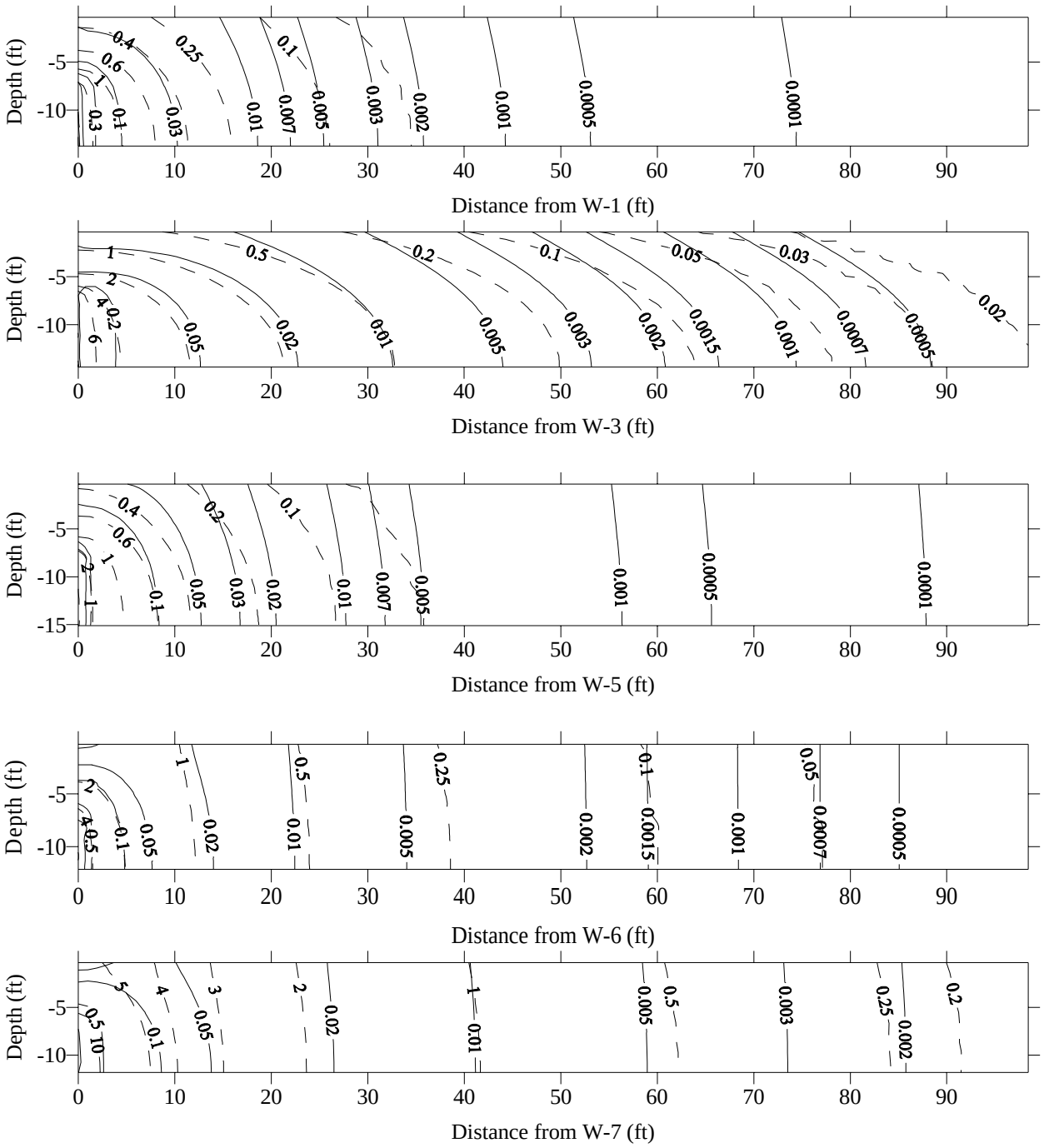

Figure 10.2 Vacuum (inches of water) (dashed lines) and pore-gas velocity (cm/s) (solid lines) plots for tested wells.

10.3 Multi-Well Simulations

To assess expected performance of a fully operational system, mean gas permeability and leakance values estimated at wells W-1, 3, 5, 6, and 7 were utilized to conduct a series of three-dimensional multi-well simulations. Steady-state vacuum and pore-gas velocities (vector norm) were simulated in three-dimensional space by applying superposition theory to (6.8) and converting radial coordinates to Cartesian coordinates. A FORTRAN program was written, MAIRFLOW, to compute a three-dimensional gas pressure and pore-gas velocity field from multiple gas injection or extraction wells. The code also allows particle tracking using the Simple Runge-Kutta (second-order) method. Sample input and output files in addition to the source code are located in Appendix F.

A depth of 15 feet was chosen for all multiple-well simulations because most contaminants in the vadose zone are located near the water table. An analytical modeling approach was appropriate at this site since distinct stratigraphic layers were not encountered necessitating numerical analysis of vacuum and pore-gas velocity profiles. As illustrated in Figure 10.3, isotropic conditions (k_r/k_z = 1.01) and high leakance (2.24 x 10^{-09} cm) resulted in significant recharge from the surface causing poor areal coverage of the 0.01 cm/s pore velocity contour and low vacuum (0.1 - 0.15 inches of water) between extraction wells. A similar k_r/k_z ratio (1.17) and slightly lower leakance (9.29 x 10^{-10} cm) depicted in Figure 10.4, resulted in minimal improved areal coverage of the 0.01 cm/s pore velocity contour but somewhat higher vacuum (0.2 - 0.5 inches of water) between extraction wells. Again nearly isotropic conditions (k_r/k_z ratio = 0.98) but significantly lower leakance (3.62 x 10^{-11} cm) shown in Figure 10.5 resulted in dramatic improvement in the areal coverage of the 0.01 cm/s pore velocity contour and much higher vacuum (3.0 - 4.0 inches of water) between extraction wells. It is evident that as leakance decreases, a velocity profile for a given total flow rate becomes more uniform but vacuum required to maintain a critical design pore-gas velocity increases significantly - a relationship not apparent from ROI testing. Notice the large area in the left center portion of Figure 10.5 where a pore-velocity of 0.01 cm/s was not achieved despite vacuum levels exceeding 3.5 inches of water whereas in other portions of the site a pore-velocity of 0.01 cm/s was achieved at less than 1.5 inches of vacuum. This reinforces previous observations with single-well simulations that the magnitude of a vacuum level in subsurface media is not an indication of effective gas flow contrary to assumptions made in ROI testing. When the k_r/k_z ratio is reduced to 0.74 and leakance increased to 8.62 x 10^{-10} cm as illustrated in Figure 10.6, the areal coverage of the 0.01 cm/s contour decreased as expected because of increased vertical flow and recharge from the surface. A comparison of anisotropy and leakance values estimated from testing at wells W-1 (k_r/k_z = 1.17, k'/b' = 9.29 x 10^{-10} cm) and W-3 (k_r/k_z = 4.29, k'/b'= 4.04 x 10^{-10} cm) illustrated in Figure 10.4 and 10.7 respectively reveals that for similar leakance values, higher k_r/k_z ratios significantly increase the areal coverage of a critical design pore-gas velocity and increase vacuum between wells. A comparison of anisotropy and leakance values estimated from testing at wells W-6 (k_r/k_z = 0.74, k'/b' = 8.62 x 10^{-11} cm) and W-3 (k_r/k_z = 4.29, k'/b' = 4.04 x 10^{-10} cm) illustrated in Figure 10.6 and 10.7 respectively reveals fairly similar pore-gas velocity and vacuum profiles. This indicates that at least at the targeted depth of 15 feet,

decreased leakance largely made up for a decreased k_r/k_z ratio. However, inspection of Figure 10.2 for W-3 reveals that increased k_r/k_z ratios result in much more curvilinear flow and the similarity in pore-gas velocity and vacuum profiles is limited to this depth. Regardless of specific k_r/k_z ratios and leakance values used for simulation however, it is apparent that the suitability of using vacuum levels of 0.05 or 0.1 inches of water, typical of ROI testing and ROI-based designs, to ensure adequate gas circulation decreases with increasing k_r/k_z ratios and decreasing leakance values. As illustrated in Figures 10.2 and 10.3 for well W-5, ROI-based designs are more likely to be appropriate as k_r/k_z ratios approach 1.0 or less and when significant leakance occurs. The latter two situations though are in direct conflict with assumptions made in derivation of pseudo-steady-state equation, the equation in which ROI-testing is based.

The effect of well screen placement on vacuum and pore-gas velocity profiles while not evaluated here was demonstrated by DiGiulio (1998c) and Shan et al. (1992). Specifically, DiGiulio (1988c) showed in simulations assuming a domain open to the atmosphere, isotropic conditions, $k_r = 1.5 \times 10^{-7}$ cm^2 and flow = 10 scfm that a pore-gas velocity of 0.01 cm/s could not be achieved directly below a well screened 0.1 to 0.3 times the length of domain below land surface even though a pressure differential between 0.3 to 0.5 inches of water vacuum was present.

Finally, when attempting to achieve a critical design pore-gas velocity, it is more efficient from a vapor treatment perspective to install additional wells rather than pump existing wells at a higher flow rate. As illustrated in Figure 10.8, using permeability and leakance information from well W-5, total flow from existing wells would have to exceed 1000 scfm to meet a pore-gas velocity of 0.01 cm/s at a depth of 15 feet throughout most of the contaminated region. Note however though that there was a small region between wells W-1 and W-3 were this design velocity could not be achieved. As illustrated in Figure 10.9, when the total number of wells was increased from 6 to 16, nearly a nearly continuous pore velocity of 0.01 cm/s was achieved throughout the entire contaminated region at only 400 scfm. Depending on the depth and media through which drilling occurs, capital costs associated with well construction may be more than offset by savings in vapor treatment costs. Another benefit of installing additional vapor extraction wells is that pore-gas velocity is much more uniform throughout a contaminated area. When only 6 wells were used to simulate venting operation at 1000 scfm, there were large regions in which pore-gas velocities exceeded 0.05 and 0.1 cm/s. When the number of wells was increased to 16, pore-gas velocity was maintained below 0.05 cm/s throughout the vast majority of the contaminated region. At lower pore-gas velocities, vapor transport would be less affected by mass transport limitations. Thus, an increased number of wells would result in more concentrated vapor stream, which is advantageous from a vapor treatment perspective.

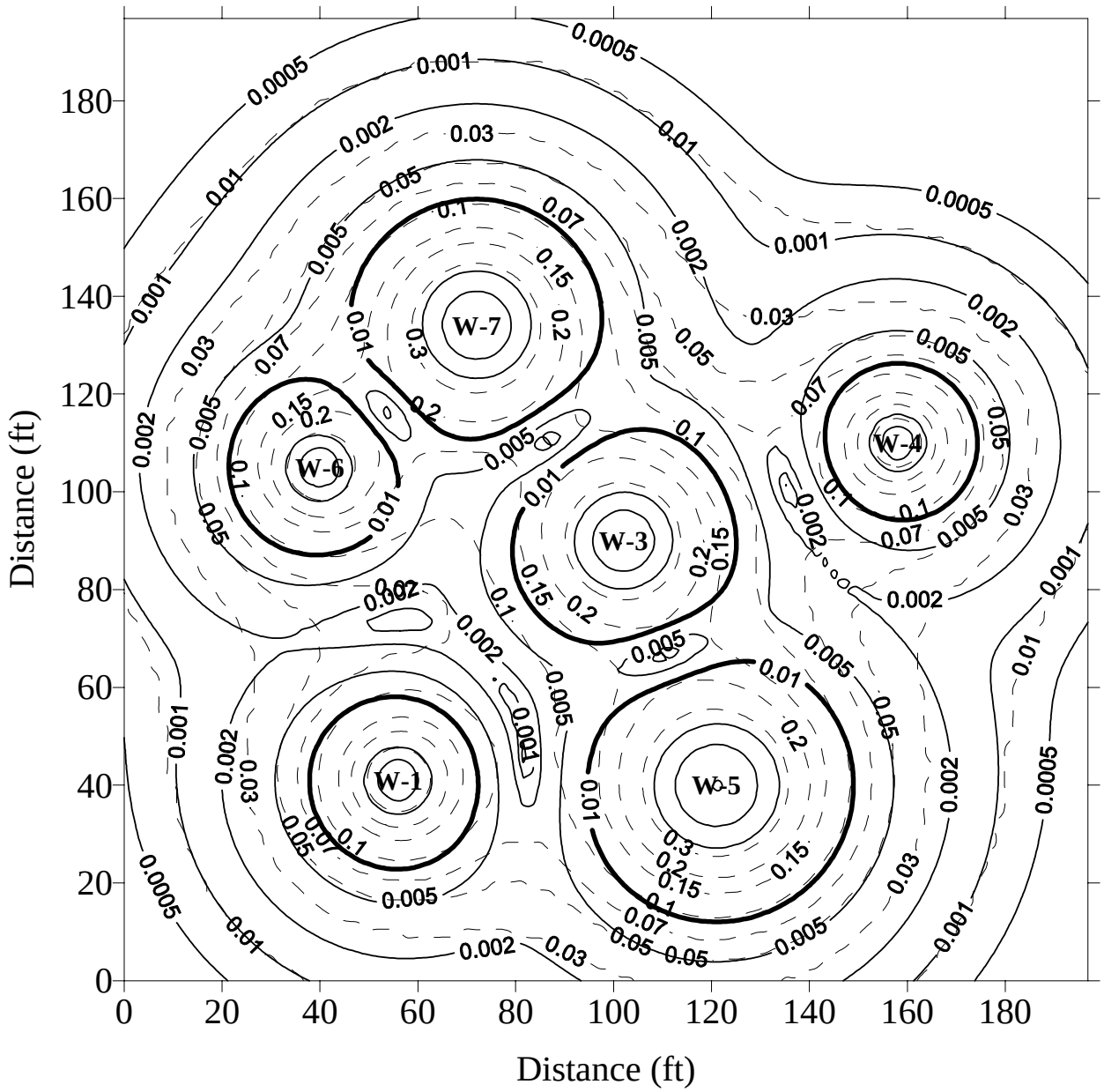

Figure 10.3 Multi-well simulation using permeability and leakance data from well W-5 (k_r = 6.87 x 10^{-7} cm^2, k_r/k_z = 1.01, leakance = 2.24 x 10^{-09} cm). Depth = 15 feet. Dashed lines denotes vacuum (inches of water), solid lines denote pore-gas velocity (cm/s).

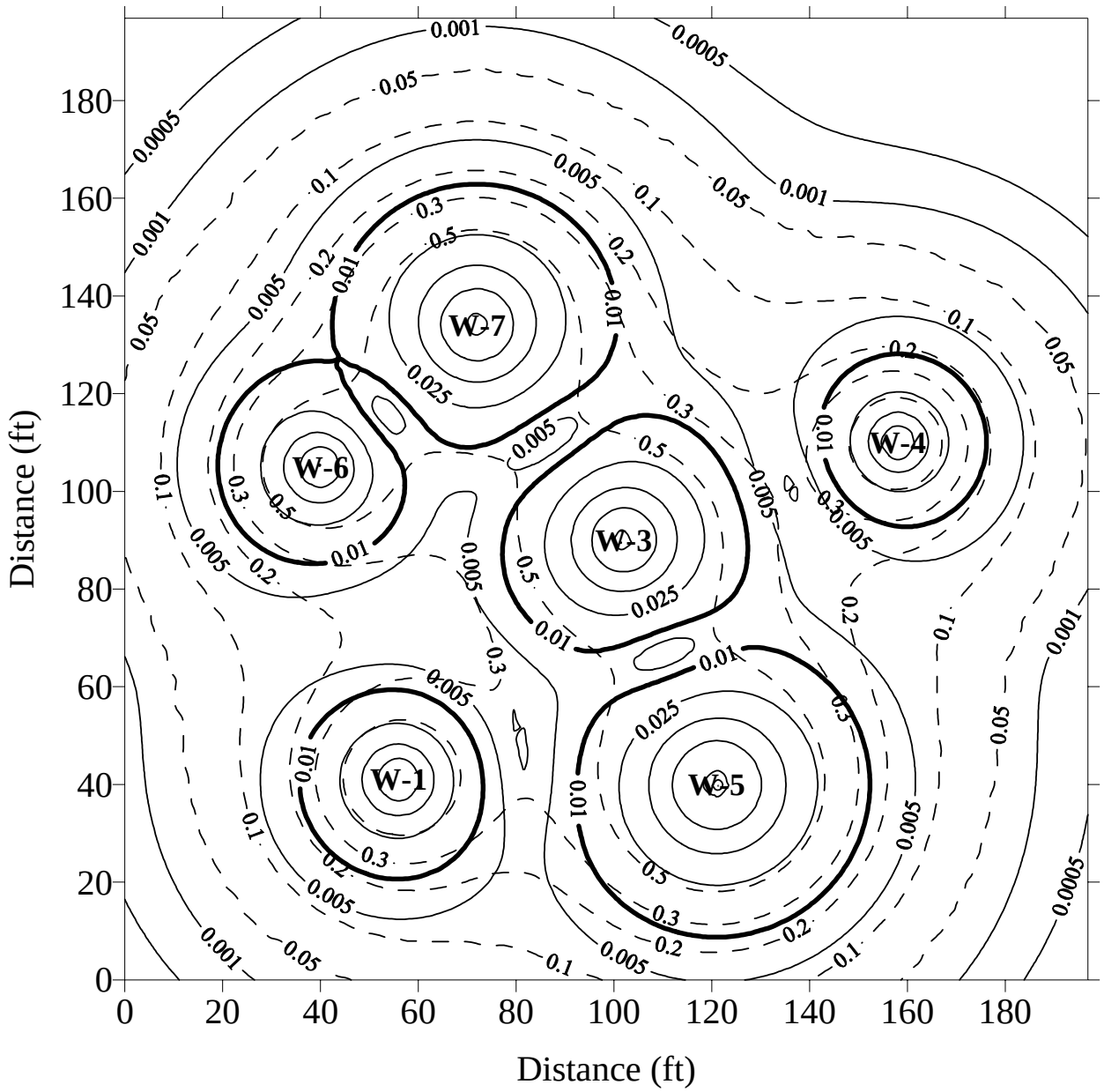

Figure 10.4 Multi-well simulation using permeability and leakance data from well W-1 (k_r = 2.90 x 10^{-7} cm^2, k_r/k_z = 1.17, leakance = 9.29 x 10^{-10} cm). Depth = 15 feet. Dashed lines denotes vacuum (inches of water), solid lines denote pore-gas velocity (cm/s)

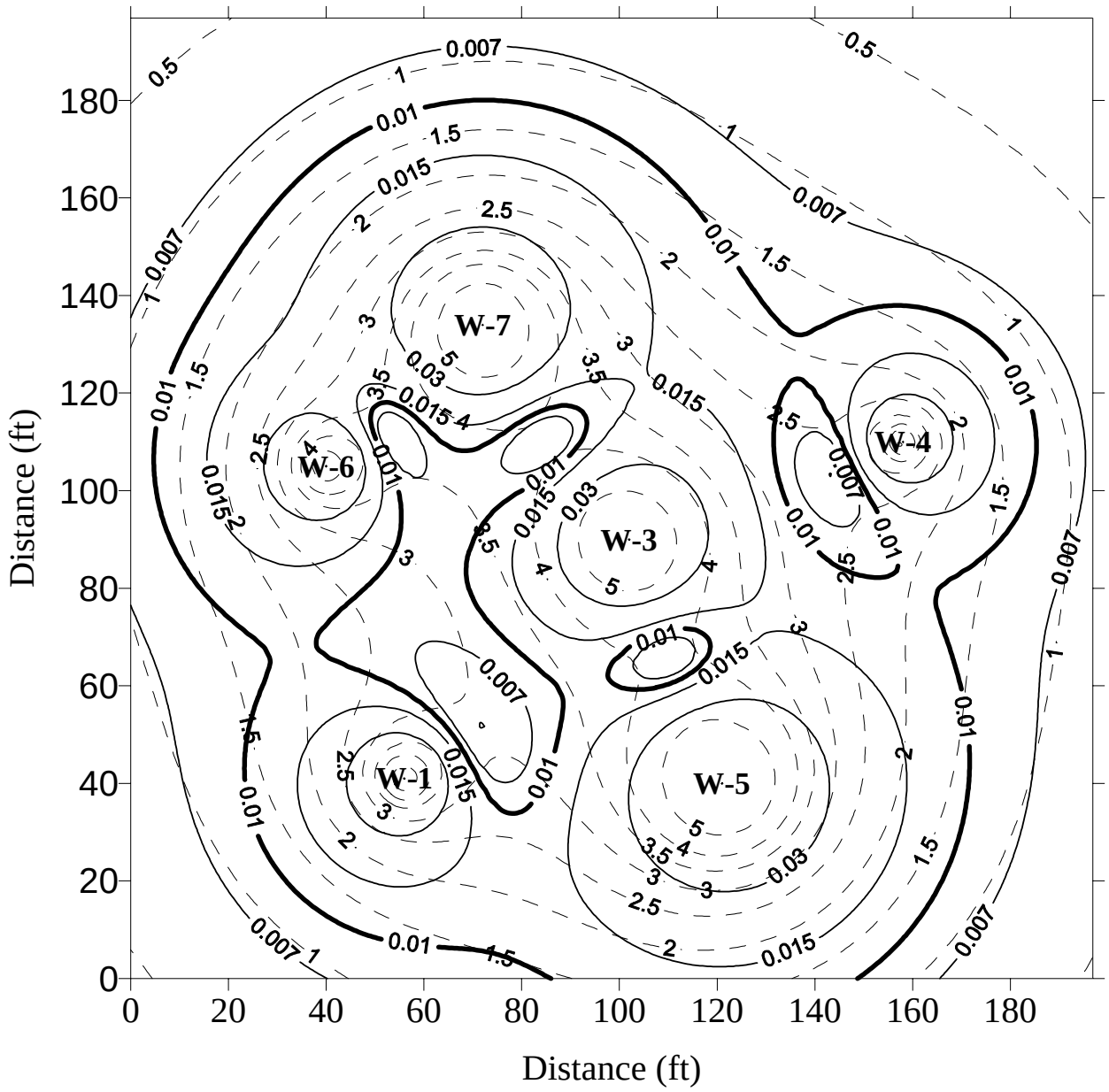

Figure 10.5 Multi-well simulation using permeability and leakance data from well W-7 (k_r = 1.42 x 10^{-7} cm^2, k_r/k_z = 0.98, leakance = 3.62 x 10^{-11} cm). Depth = 15 feet. Dashed lines denotes vacuum (inches of water), solid lines denote pore-gas velocity (cm/s).

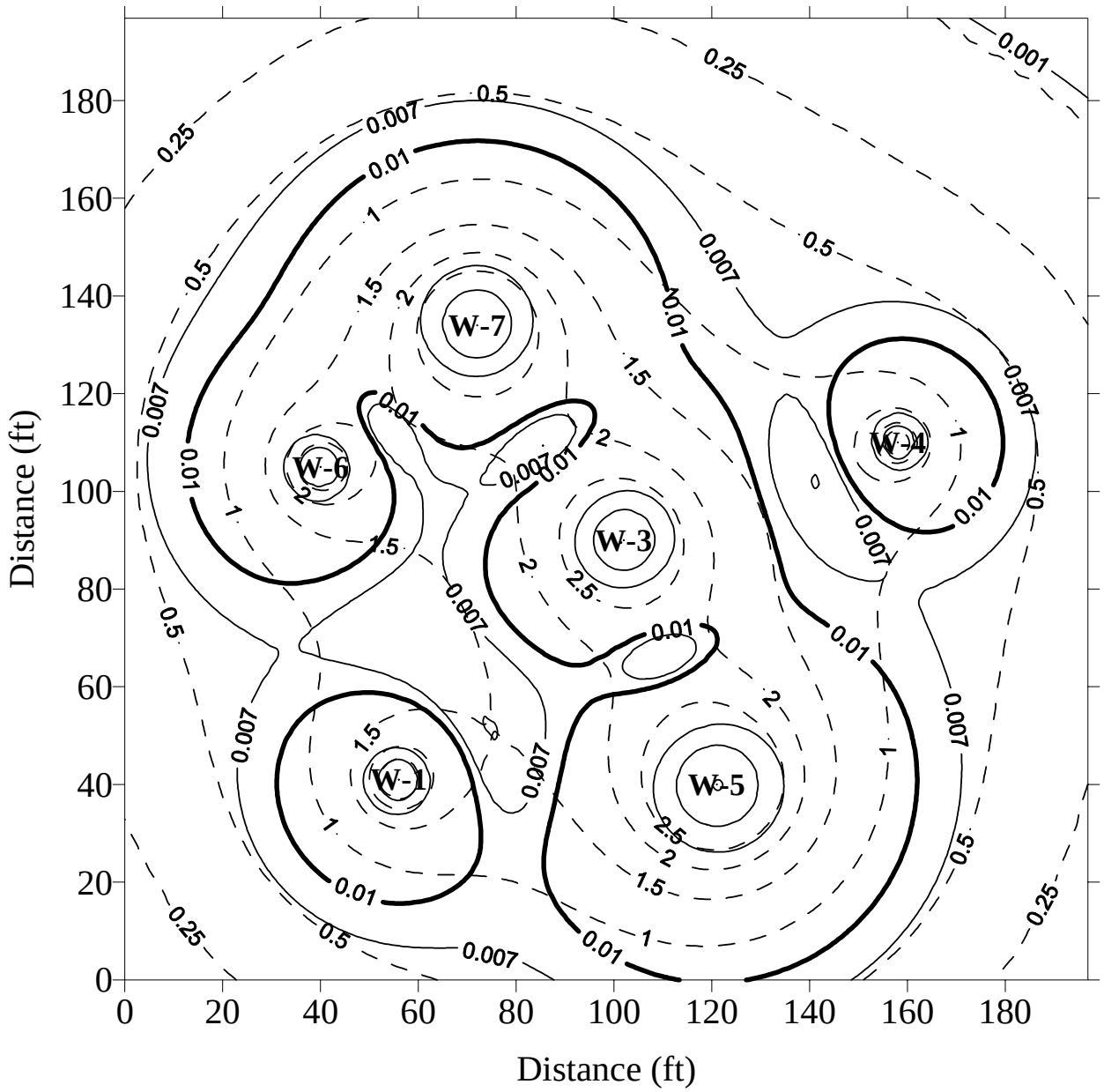

Figure 10.6 Multi-well simulation using permeability and leakance data from well W-6 (k_r = 1.81 x 10^{-7} cm^2, k_r/k_z = 0.74, leakance = 8.62 x 10^{-11} cm). Depth = 15 feet. Dashed lines denotes vacuum (inches of water), solid lines denote pore-gas velocity (cm/s).

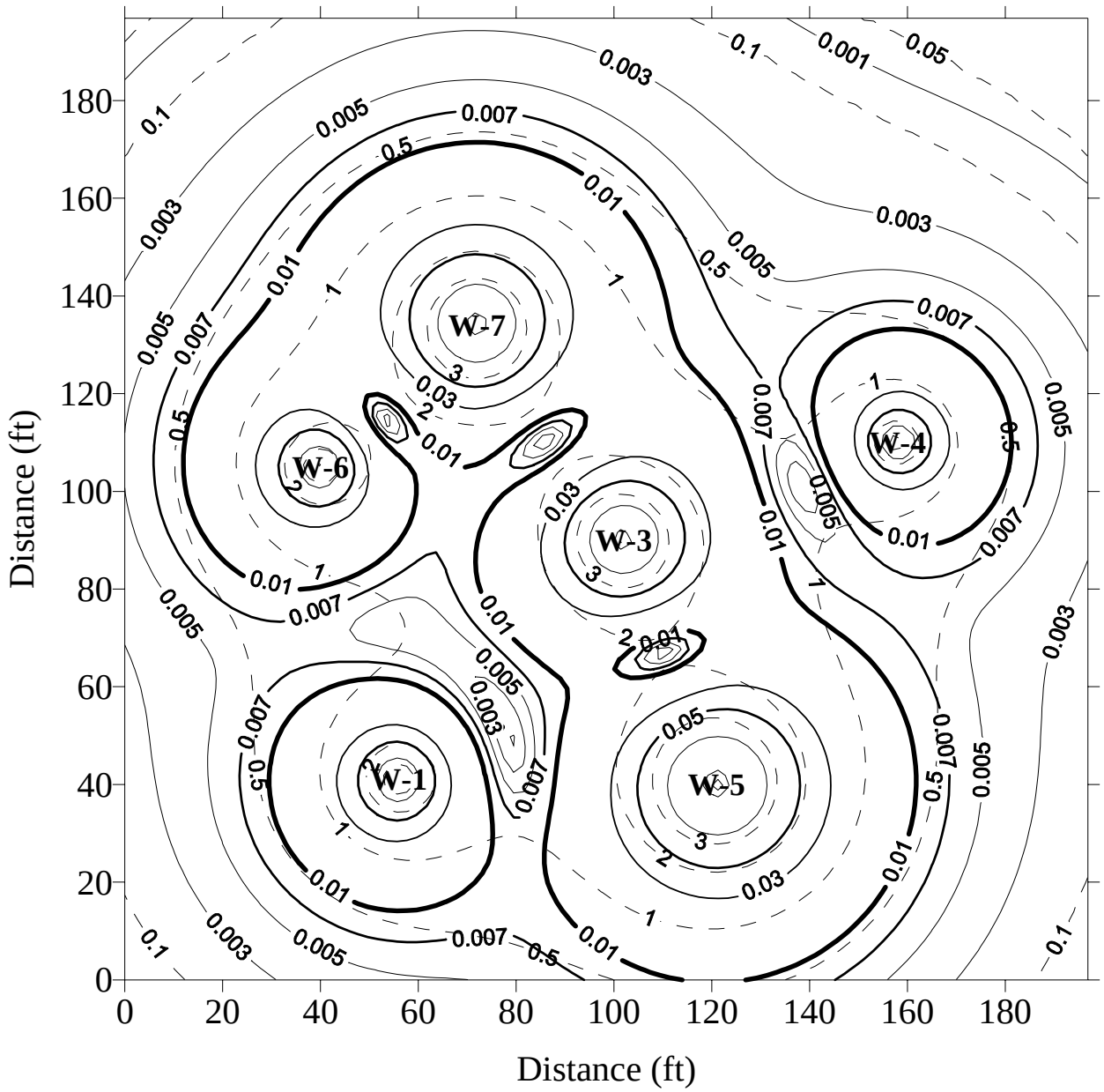

Figure 10.7 Multi-well simulation using permeability and leakance data from well W-3 (k_r = 1.80 x 10^{-7} cm^2, k_r/k_z = 4.29, leakance = 4.04 x 10^{-10} cm). Depth = 15 feet. Dashed lines denotes vacuum (inches of water), solid lines denote pore-gas velocity (cm/s)

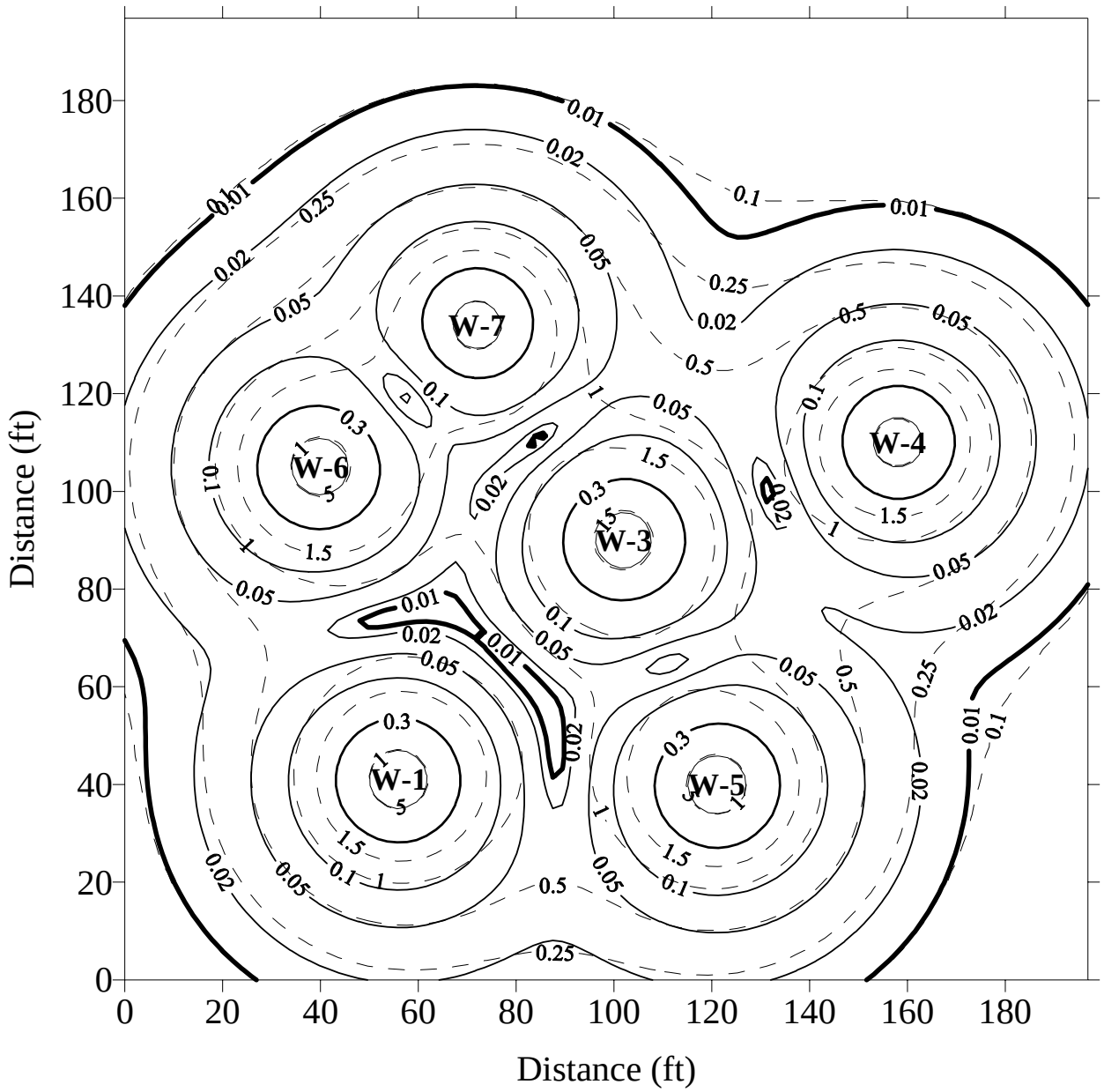

Figure 10.8 Vacuum and pore-gas velocity at the ground water interface using permeability and leakance data from well W-5 (k_r = 6.87 x 10^{-7} cm^2, k_r/k_z = 1.01, leakance = 2.24 x 10^{-09} cm). Depth = 15 feet. Total flow = 1000 scfm, wells W-1, 3, 5, 6 = 175 scfm, wells W-4, 7 = 150 scfm

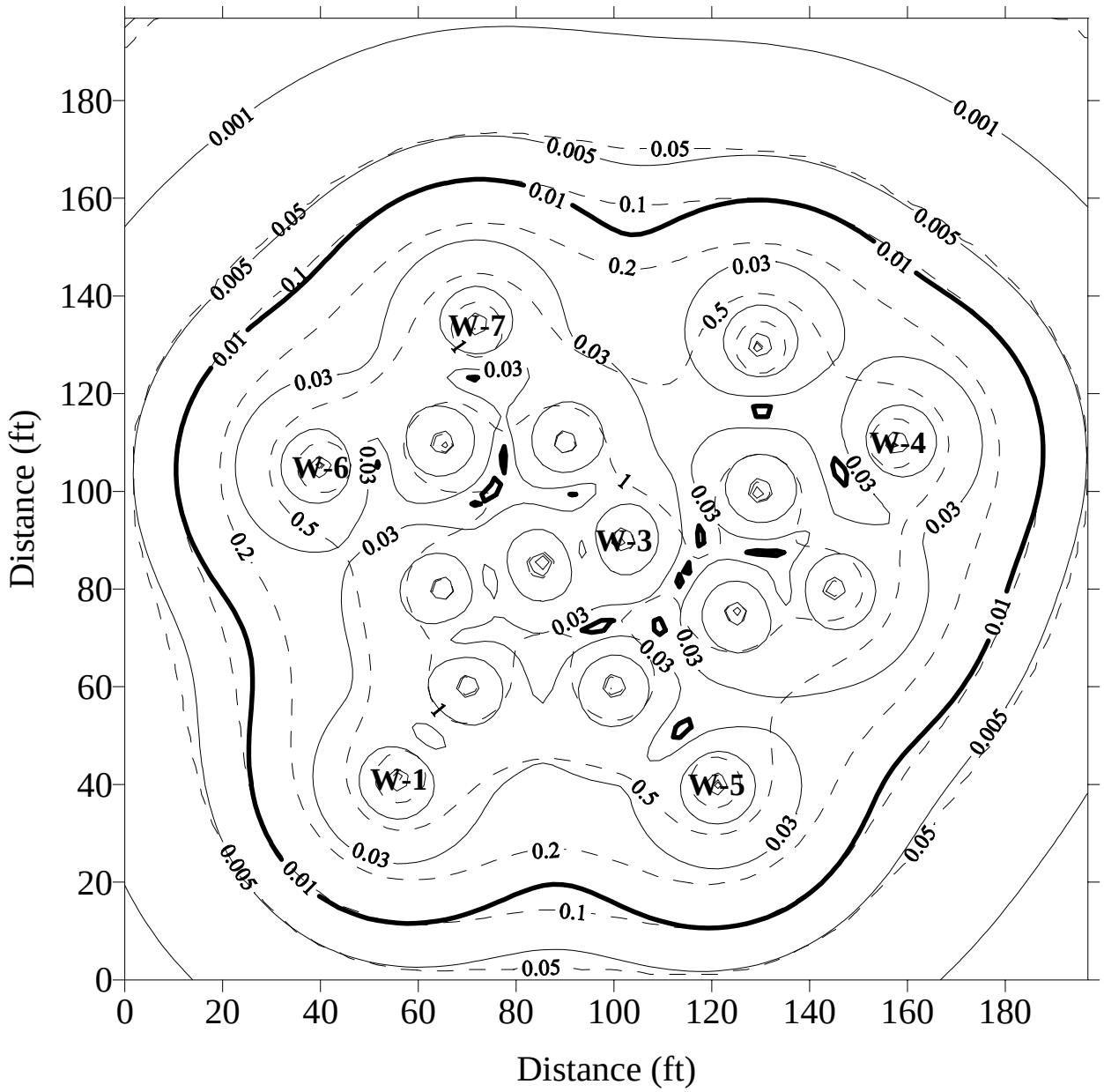

Figure 10.9 Vacuum and pore-gas velocity at the ground water interface using permeability and leakance data from well W-5 (k_r = 6.87 x 10^{-7} cm^2, k_r/k_z = 1.01, leakance = 2.24 x 10^{-09} cm). Depth = 15 feet. Total flow = 400 scfm, 16 wells with 25 scfm at each well.

10.4 Design Strategy

Using attainment of a critical pore-gas velocity as a design criteria, optimal well spacing, screened interval placement, and flow rate selection could be determined using three-dimensional analytical or numerical models. Numerical analysis can be very useful when distinct stratigraphic layers or complex boundary conditions are present at a site. Simulations could be conducted iteratively (trial and error) or perhaps more efficiency through the use of optimization routines such as those described by Sawyer and Kamakoti (1998), and Sun et al. (1996). The trial and error approach while tedious and time consuming allows greater insight into site-specific conditions determining design while the latter approach is more computationally efficient and allows easier evaluation of economic factors important to design. Ideally, information on spatial variability of radial and vertical gas permeability would be available to support three-dimensional numerical gas flow modeling. Since gas permeability is a function of moisture content, spatial variability of gas permeability for any given geologic environment will be far greater than for saturated hydraulic conductivity determined for ground-water investigations. Unfortunately, this level of detail necessary to support numerical modeling is invariably absent at field sites.

10.5 Conclusions

1. By far, the most common method used for venting design in the United States is radius of influence (ROI) evaluation. In practice, ROIs are determined by plotting vacuum as a function of logarithmically transformed radial distance and applying linear regression to extrapolate to the distance at which a specified vacuum would be observed. For SVE design, overlapping circles of ROIs for individual wells are then drawn on a site map to indicate an "effective" remediation area. In this section, data was utilized from a Superfund site (described in section 6) where ROI testing was conducted by a remedial contractor to describe limitations of ROI evaluation in more detail than has been done previously and to demonstrate an alternative method of design based on specification and attainment of critical pore-gas velocities in contaminated subsurface media. Information was utilized from section 9 to provide the basis for selection of a minimum or critical pore-gas velocity for use at this site.

2. The results of single-well simulations demonstrated several important deficiencies in ROI evaluation. First, cross-sectional two-dimensional simulations clearly illustrate that the ROI is an ill-defined entity. Vacuum profiles were very curvilinear especially under conditions of high leakance values and k_r/k_z ratios. Second, an ROI-based design, resulted in subsurface pore-gas velocities too low for optimal gas circulation especially at low leakance values and high k_r/k_z ratios. Third, attainment of critical pore-gas velocities could not be guaranteed by simply raising the magnitude of vacuum during venting application from say 0.05 inches of water to some other arbitrarily specified level (e.g., 0.1 inches of water). Observed vacuum was a function of boundary conditions (e.g., leakance), applied mass flow, anisotropy, permeability, and geometry of screened

intervals.

3. Multi-well simulations illustrated additional deficiencies in ROI-based design practices. It was evident that as leakance decreased, a velocity profile for a given total flow rate became more uniform but vacuum required to maintain a critical design pore-gas velocity increased significantly - a relationship that would not be apparent from ROI testing. In one simulation, a design pore-velocity of 0.01 cm/s could not be achieved despite vacuum levels exceeding 3.5 inches of water whereas in other portions of the site a pore-velocity of 0.01 cm/s was achieved at less than 1.5 inches of vacuum. This reinforces previous observations with single-well simulations that the magnitude of a vacuum level in subsurface media is not an indication of effective gas flow contrary to assumptions made in ROI testing. It was apparent that the suitability of using vacuum levels of 0.05 or 0.1 inches of water, typical of ROI testing and ROI-based designs, to ensure adequate gas circulation decrease with increasing k_r/k_z ratios and decreasing leakance values. ROI-based designs are more likely to be appropriate as k_r/k_z ratios approach 1.0 or less and when significant leakance occurs.

4. Finally, it was demonstrated that when attempting to achieve a critical design pore-gas velocity, it is more efficient from a vapor treatment perspective to install additional wells rather than pump existing wells at a higher flow rate. In one simulation, it was demonstrated that the total flow rate from 6 wells would have to exceed 1000 scfm to meet a pore-gas velocity of 0.01 cm/s. When the total number of wells was increased from 6 to 16 however a pore velocity of 0.01 cm/s was achieved throughout the entire contaminated region at only 400 scfm. The use of additional vapor extraction wells resulted in a much more uniform pore-gas velocity throughout the contaminated area.

11. USE OF A COMBINED AIR INJECTION/EXTRACTION (CIE) WELL TO MINIMIZE VACUUM ENHANCED WATER RECOVERY

The application of vacuum decreases energy potential in soils and hence induces water movement toward the screened interval of a gas extraction well. Increased moisture content results in reduced gas permeability in the vicinity of the gas extraction. Also, when vacuum is applied to a gas extraction well screened in or near the water table, water-level rise occurs within the well (upwelling) reducing or completely obstructing gas flow. Gas injection on the hand, results in soil-water movement away from and hence increased gas permeability in the vicinity of screened interval.

Since, the application of vacuum causes water-table upwelling, soil-water flow, and decreased gas permeability in the immediate vicinity of a gas extraction well, it is logical that injection of pressurized gas or at least maintenance of atmospheric pressure at the base of a vacuum extraction well would reduce water recovery. Gas injection however poses its own problems. Since gas injection is inherently more effective than gas extraction there is a possibility of uncontrolled advective vapor transport away from the base of a combined air injection and extraction well. Also, subsurface vacuum would be reduced perhaps leading to less effective capture of vapors. The concept of combined air injection and extraction (CIE) was evaluated during a pilot study at Vance Air Force Base located in northwestern Oklahoma. The information presented in this section is also discussed in DiGiulio (1995).

11.1 Field Methods and Materials

Testing was conducted in July and August of 1994 at Site-8 on Vance Air Force Base (AFB) located in northwestern Oklahoma. Soils and ground-water are contaminated with petroleum hydrocarbons, trichloroethene (TCE) and vinyl chloride. Five leaking underground storage tanks were removed in January, 1989. Four of the tanks stored lubricating oil, diesel fuel, and kerosene. The remaining tank stored waste oils and solvents. Contaminated soils in the immediate vicinity of the tanks were excavated and replaced with fill consisting primarily of silt. After compaction of the fill, the site was completely paved with a 25 cm concrete slab.

Figure 11.1 illustrates the location of wells and probe clusters installed by the U.S. Army Corps of Engineers. MW-8-4 was installed during a previous investigation. All boreholes were drilled to a diameter of 20.3 cm using hollow-stem augering techniques. As illustrated in Figure 11.2, numerous isolated saturated or near saturated regions, often associated with a sandstone-gravel/silt mixture, were identified by visual and manual examination of continuous split-spoon cores during drilling. As outlined in Table 11.1, the results of particle size tests indicate that in the study area, residuum above weathered shale and sandstone consists of silt loam soils. Soil textural analysis was conducted by the U.S. Army Corps of Engineers' Southwestern Division Laboratory located in Dallas, Texas.

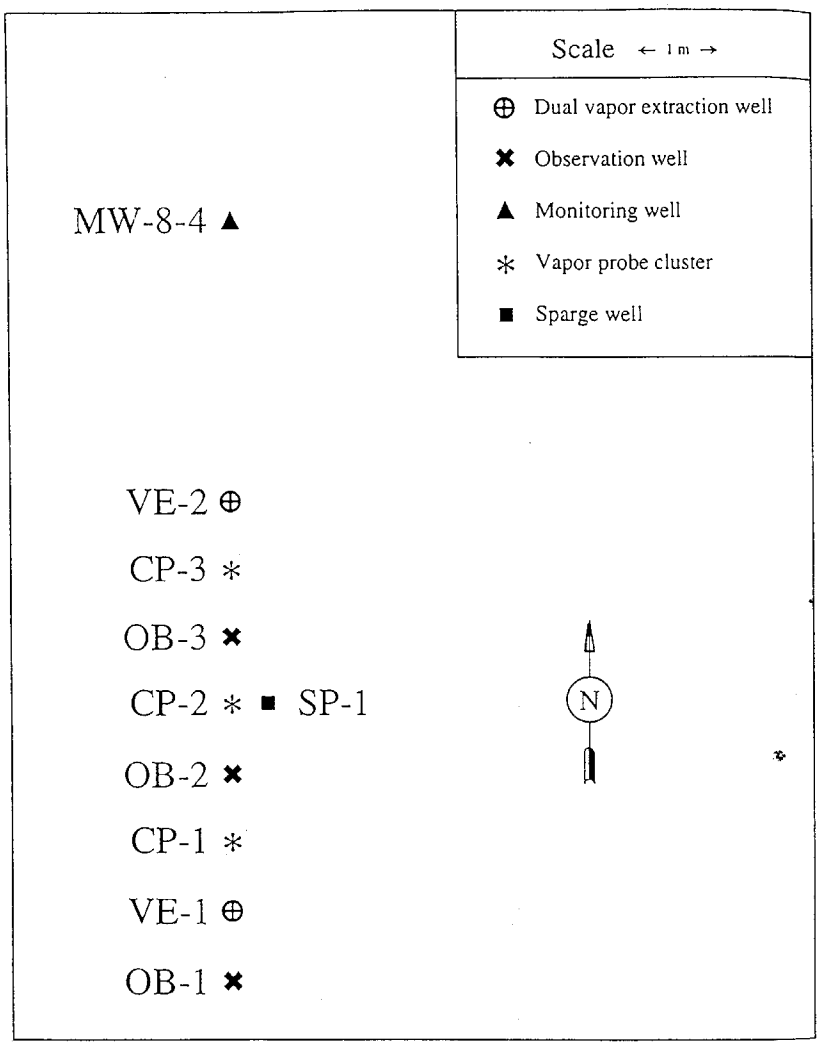

Figure 11.1 Locations of dual vapor extraction wells (VE-series), observation wells (OB-series), sparging well (SP-1) and vapor probe clusters (CP-series) used in study at Site 8, Vance AFB

Table 11.1 Soil Textural Analysis from OB-2

Depth (m)	Sand (%)	Silt (%)	Clay (%)	USDA Soil Textural Class	Moisture Content (% by mass)
0.0 - 0.61	6	65	29	silt loam	28.9
1.52 - 3.05	2	77	21	silt loam	16.0
4.57 - 6.10	4	76	20	silt loam	20.8
4.57 - 6.10	4	73	23	silt loam	21.1

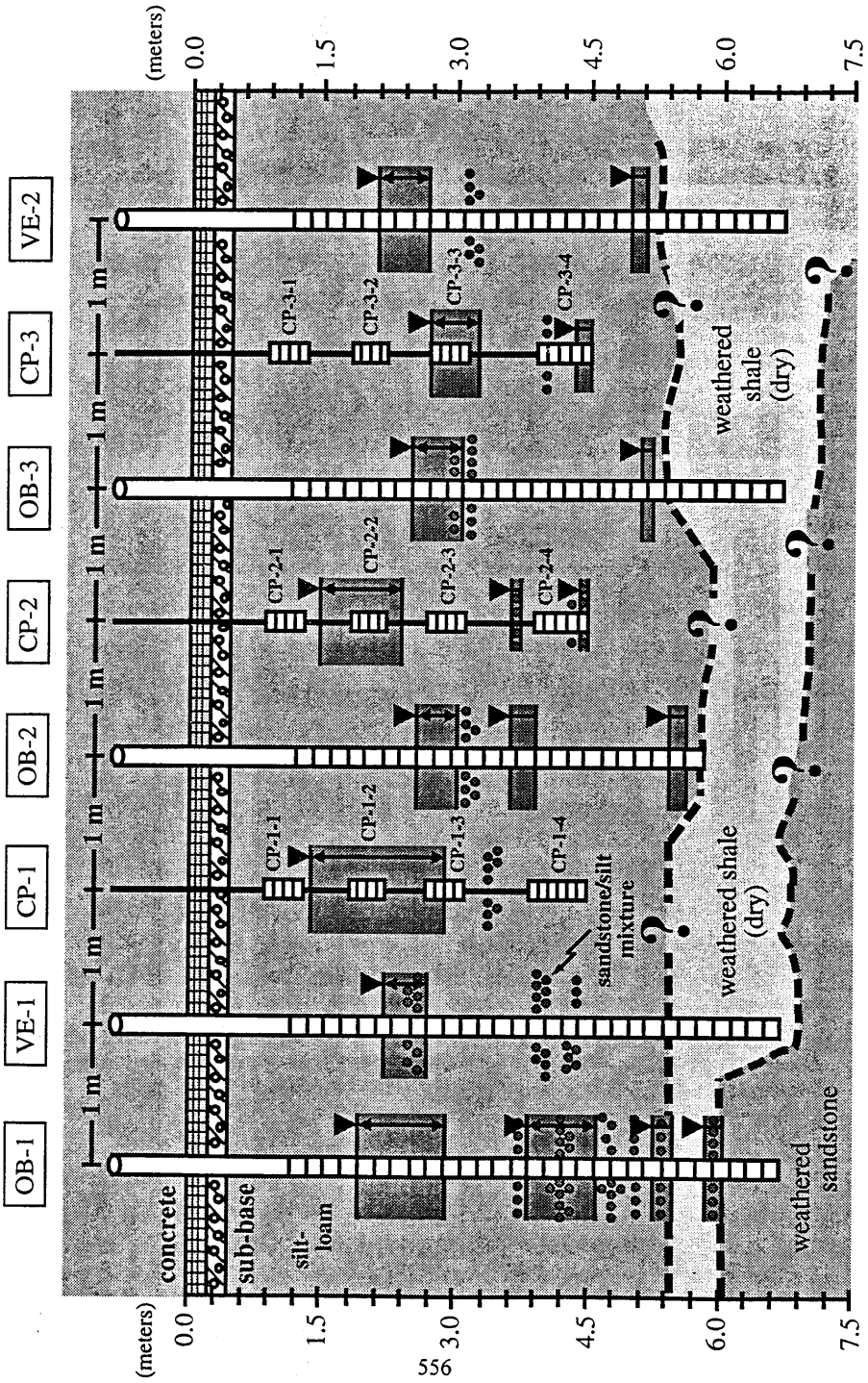

Figure 11.2 Cross-sectional schematic of DVE wells, observation wells, vapor probe clusters and soil conditions encountered during drilling.

Figure 11.3 illustrates equipment used during testing. Water was extracted from dual vapor extraction (DVE) wells (tubes sticking up), passed through an air-water separation tank (smaller cylindrical tank), and pumped into a 190,000 liter rectangular storage container. Contaminated vapors were treated with granular activated carbon (GAC) (larger cylindrical tank) prior to discharge to the atmosphere. Figure 11.4 illustrates construction details of DVE wells used to extract air and water during vapor extraction. Combined extraction of air and water was maintained by insertion of a 2.54 cm outside diameter tube at the base of a 10.16 cm outside diameter well from which vacuum from a common source was applied to both the tube and well annulus. Air and water extraction was facilitated by the use of "bleed" air at the top of the well. Operationally, when water-table upwelling occurs during vacuum extraction, the inner tube is supposed to remove water to prevent screen obstruction. DVE is often applied below the water-table to produce a cone of depression and enable simultaneous air and ground-water extraction. The mass flow rate of extracted air was measured using 2.54 cm annubars and manometers to determine pressure differential. Gas flow measurement though was complicated by constant surging of water flow and erratic variation of manometers. "Bleed" air flow rate was measured using a Dwyer flowmeter. Extracted gas temperature was measured using Cole-Parmer 6.35 mm NPT pipe thermocouples and a Cole-Parmer digital thermometer.

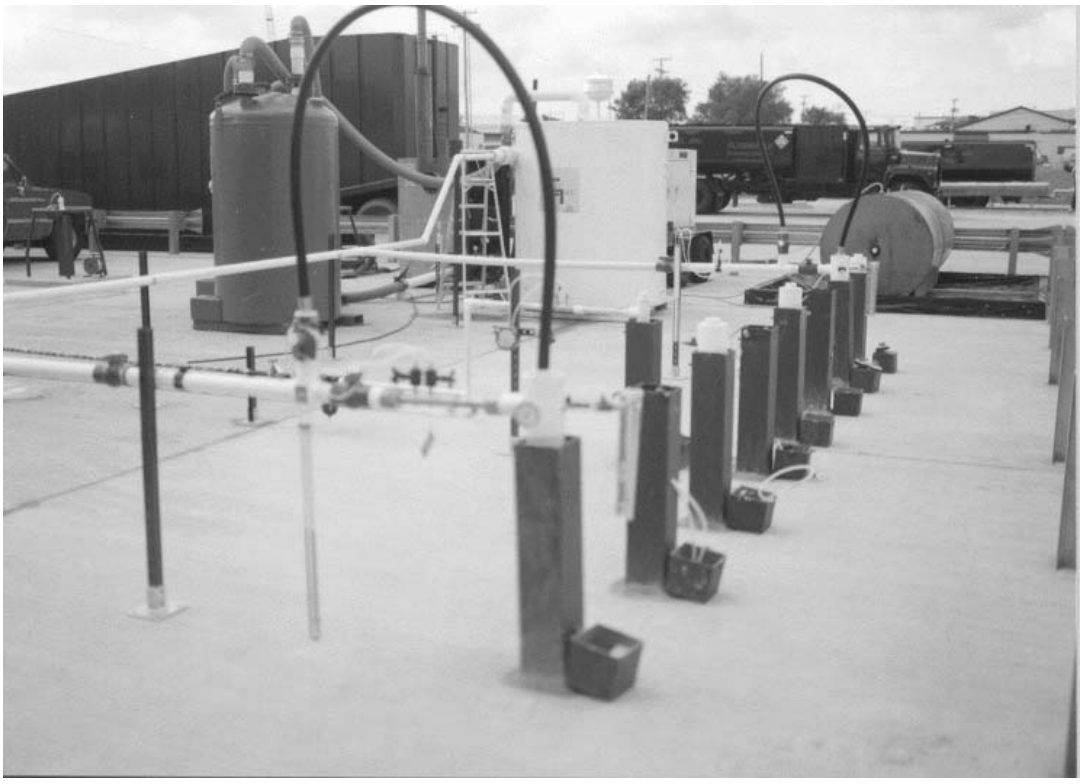

Figure 11.3. Photograph of DVE wells (wells with tubes sticking up - DVE-1 in foreground), observation wells, vapor probe clusters, air water separation tank (cylindrical tank with label), GAC units, and frac tank for contaminated water storage (rectangular shaped structure)

Figure 11.5 illustrates construction details of sparging well SP-1. Mass air flow was measured using a Dieterich standard annubar DNT-10 in a 2.54 cm steel diameter pipe with a Dwyer Capsehelic gauge to determine pressure differential. Static injection pressure was determined using a Dwyer Magnehelic gauges while temperature was measured using Cole-Parmer pipe thermocouples and a Cole-Parmer digital thermometer. Mass flow was calculated using software provided by MD Controls, a distributor of Dieterich annubars. Sparging during DVE operation was conducted to determine whether injection of air and subsequent decrease in vacuum near the water-table around SP-1 would decrease water recovery at the DVE wells.

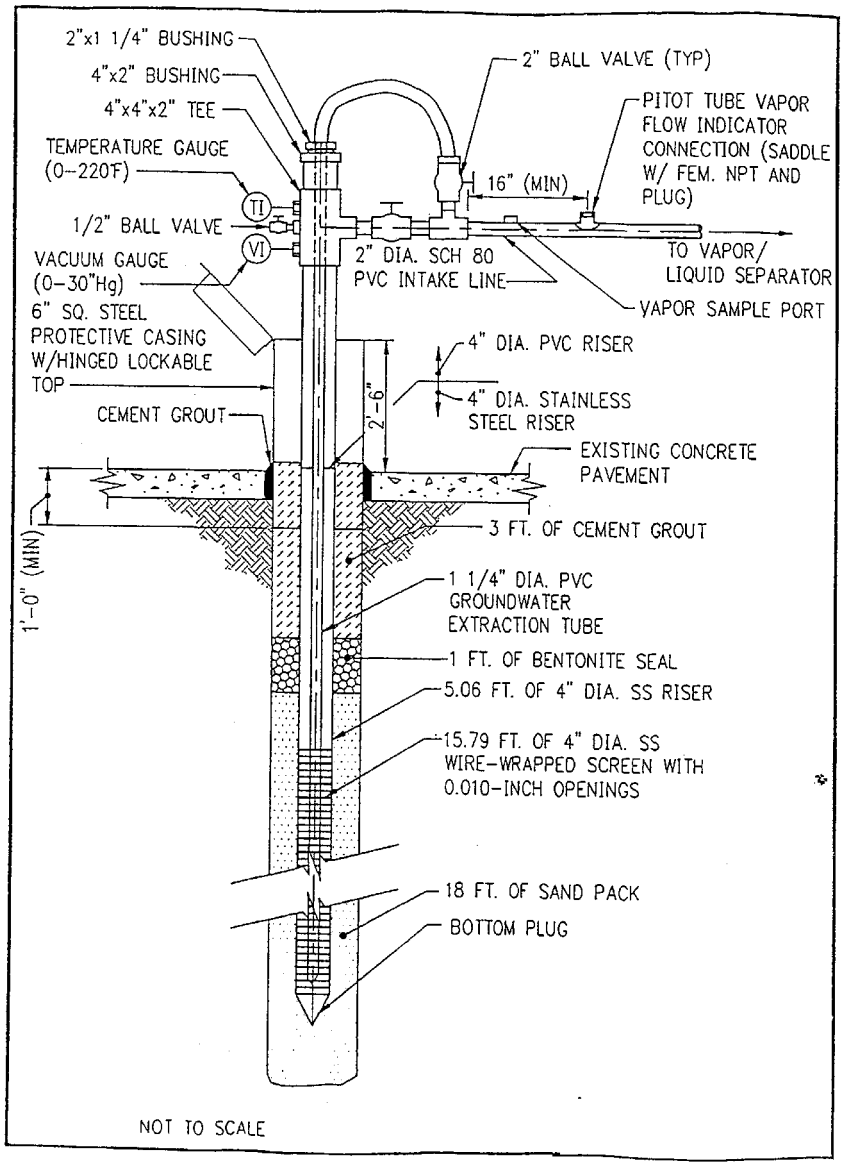

Figure 11.4 Schematic of a dual vacuum extraction (DVE) well used at Site 8,Vance, AFB

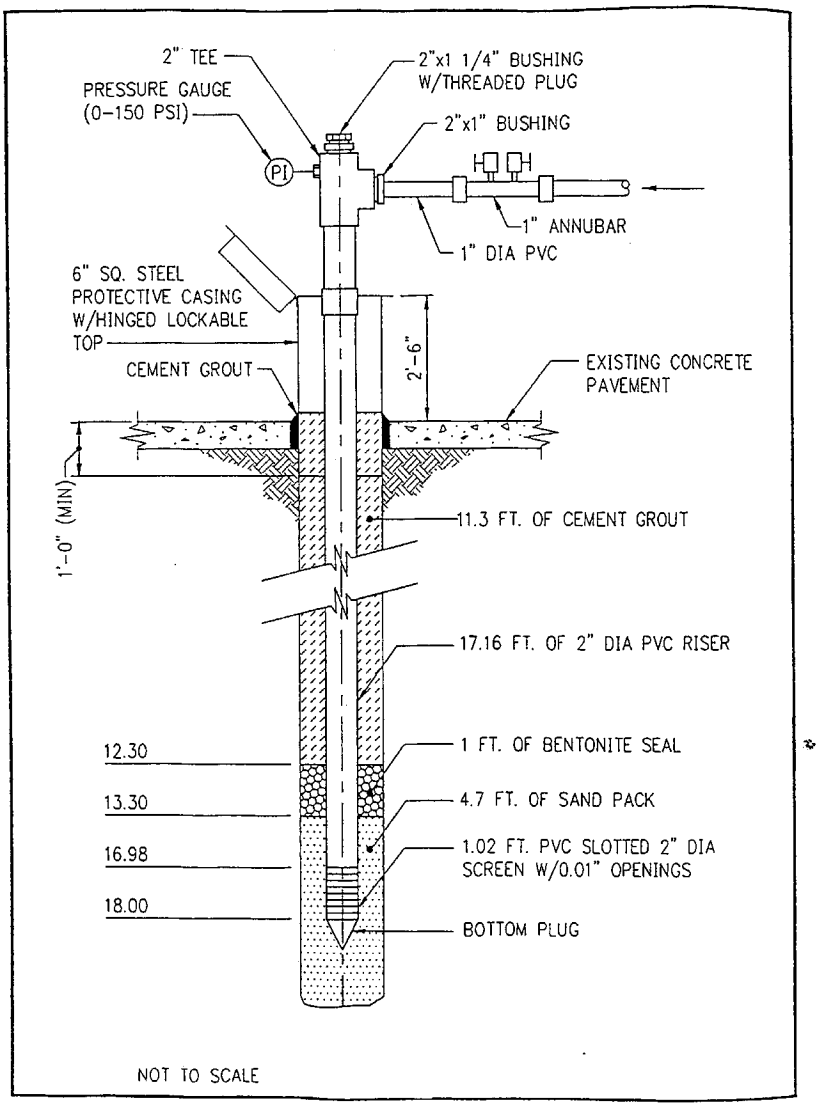

Figure 11.5 Schematic of sparging well used at Site 8,Vance, AFB

Figure 11.6 illustrates typical construction of observation wells. The primary purpose of these wells was to monitor water levels during DVE and sparging application. Figure 11.7 illustrates construction details of vapor probe clusters used to monitor subsurface pressure and vacuum. Stainless-steel, 6.35 mm diameter, 27 mm long wire screen probes obtained from the Geoprobe Corporation were used to monitor pressure and vapor concentrations. Probes were connected to 6.35 mm outside diameter copper tubing and Swagelok quick connects using compression fittings. The shallowest probe in each cluster was connected to probes by 3.18 mm outside diameter stainless-steel tubing. Cole Parmer thermocouples were placed adjacent to probes at each depth to measure soil temperature.

Figure 11.8 illustrates construction details of observation well OB-3 modified for

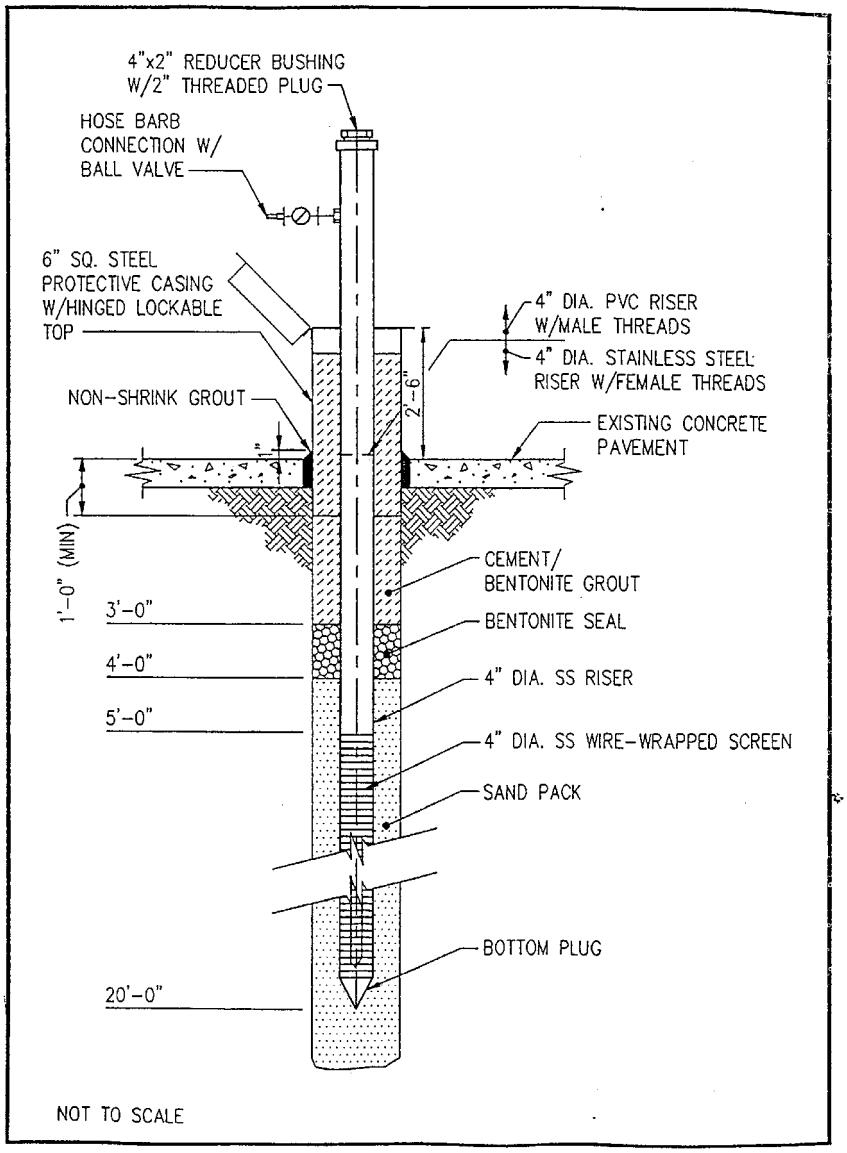

Figure 11.6 Schematic of an observation well used at Site 8,Vance, AFB

combined air injection and extraction (CIE). This observation well was modified in the field when it became apparent that DVE wells were producing water at rate (6 liters per minute) much higher than that encountered during well development. It appeared that vacuum from DVE wells was causing water-table upwelling while water extraction during well development consisted of perched water. Depth to the true water table however was never identified, thus this observation is speculative. The purpose of the modification was to figure out a way to extract gas at the targeted depth while minimizing ground-water extraction. Modification consisted of insertion of a 2.54 cm schedule 40 PVC pipe into the 10.16 cmoutside diameter observation well OB-3. Numerous small-diameter holes were manually drilled over a length of 60 cm at the base of the

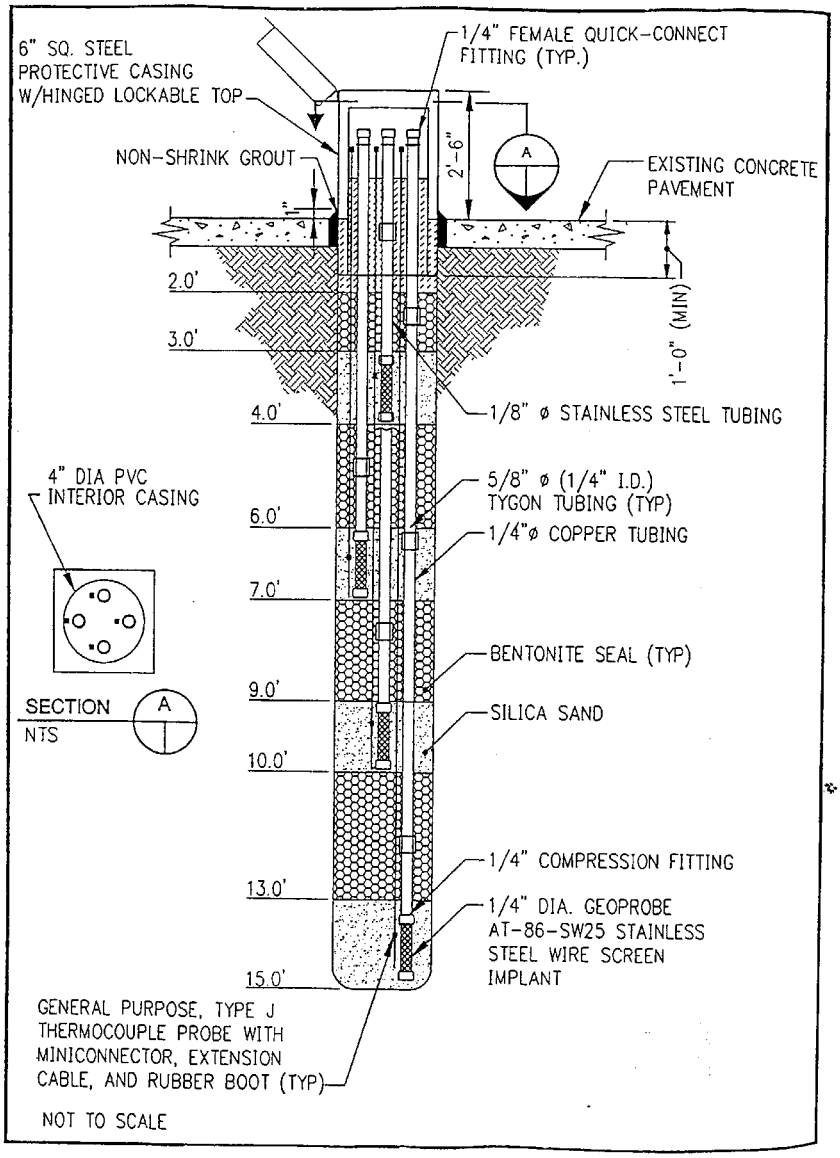

Figure 11.7 Schematic of a vapor probe cluster used at Site 8,Vance, AFB

2.54 cm pipe. The annulus between the region of air injection and extraction was separated by 30 cm of bentonite and 60 cm of cement. Cement was added to prevent potential fluidization of the bentonite seal due to positive pressure addition. Pressurized air was directed through a 2.54 cm schedule 40 PVC manifold used for sparging application. Mass flow of injected air was measured by the same methodology used for sparging. Mass flow of extracted air was measured off a manifold from the DVE wells. Measurement methodology was similar to that used during DVE operation. Figure 11.9 provides an above ground photograph of the CIE well.

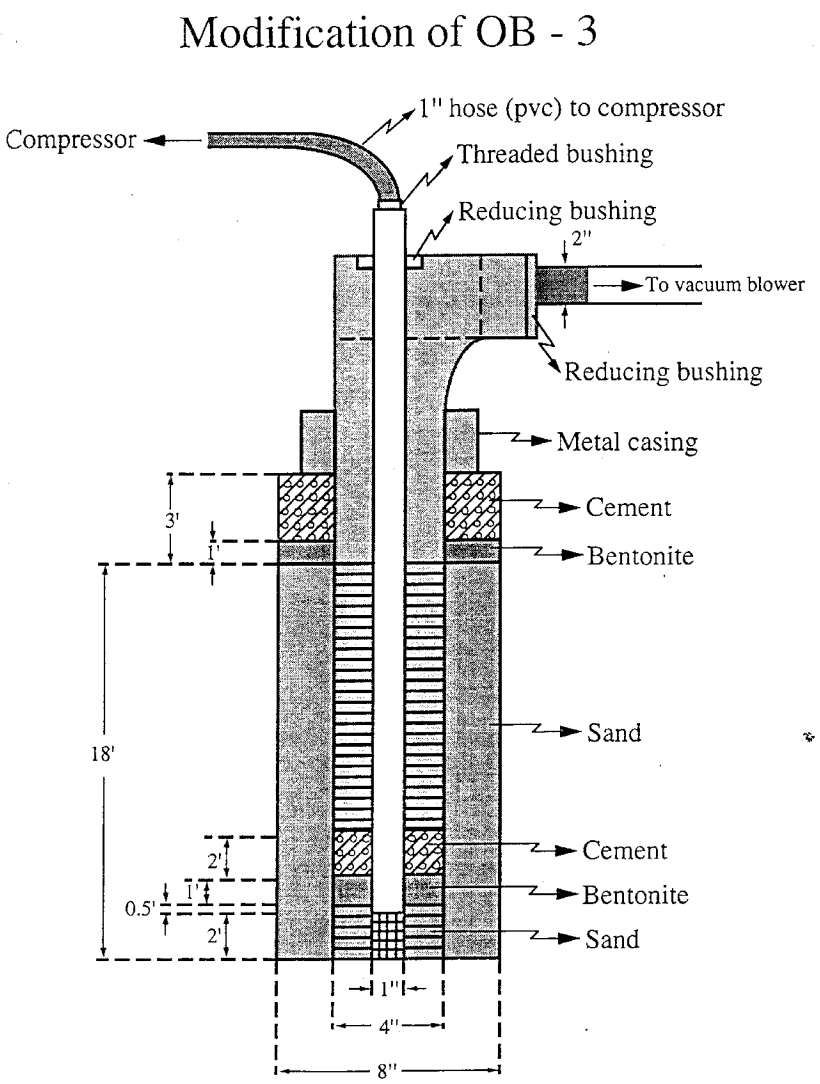

Figure 11.8 Schematic of modified observation well 3 to enable combined air injection and extraction at Site 8, Vance, AFB

11.2 Results and Discussion

Water recovery rates were estimated by periodic purging (twice per day) of an air/water separator. During the four week test period, over 128,700 liters of contaminated water were produced by the two DVE wells. Bleed air was needed continuously in both wells to maintain air extraction. Figure 11.10 illustrates water recovery rates from operation of dual vacuum extraction alone, dual vacuum extraction in conjunction with sparging, and operation of combined air injection and extraction (CIE) in OB-3. Sparging in conjunction with DVE resulted in a measurable reduction in water recovery compared to the operation of DVE alone. Combined air injection and extraction resulted in a further reduction in water recovery. Compared to DVE operation alone, water recovery was reduced over 90% with the CIE well.

Figure 11.9. Photograph of modified observation well, OB-3

The reduction in water recovery from the CIE well could be caused by two mechanisms: (1) elimination of water table upwelling, and (2) reduction in vacuum enhanced recovery of perched water. While the location of the true water-table was never discerned, previous drilling activities suggest its presence in the underlying weathered shale and sandstone. The application of positive pressure at the base of the CIE well would eliminate a water potential gradient for water-table upwelling. In fact, water recovery during combined air injection and extraction was similar (0.4 liters per minute) to water recovery in observation wells during well development prior to DVE operation (i.e., no applied vacuum). The design of the CIE well however would also result in less vacuum within the lower annulus of the well and thus reduce water recovery from perched water or soil-water movement. Similar water recovery rates prior to DVE operation and CIE operation appear to indicate that water-table upwelling was either the major or a contributing causative factor in high water recovery.

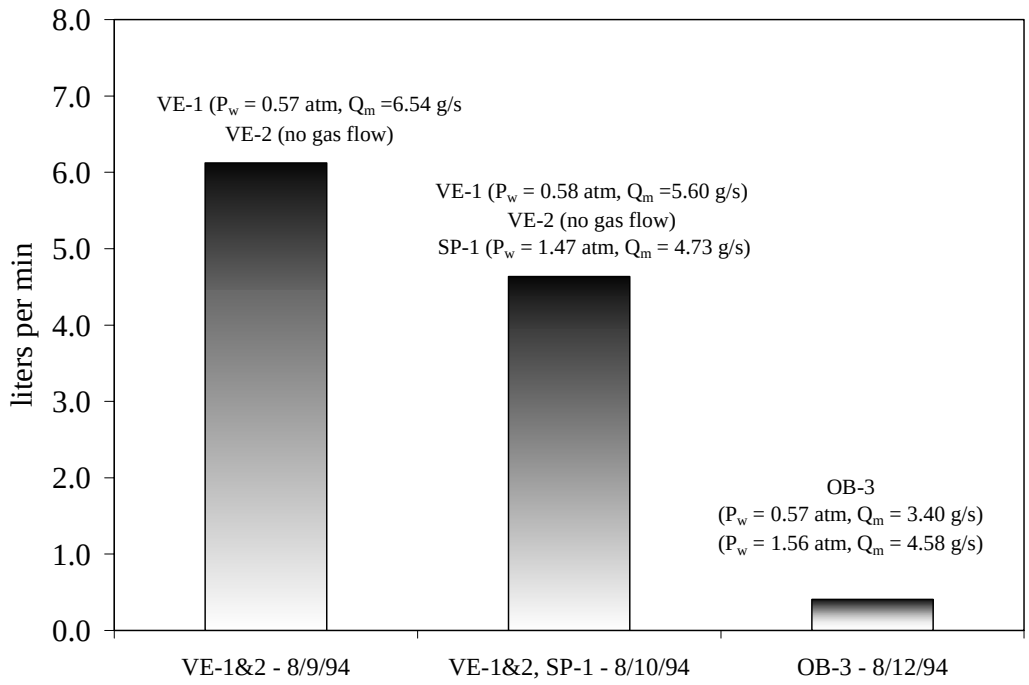

Figure 11.10 Water recovery during vacuum extraction, vacuum extraction and sparging, and combined air extraction/injection at OB-3

Water recovery may have been reduced somewhat during sparging by reducing vacuum near the water table and thus reducing water-table upwelling. Reduced vacuum in the deepest probes was noted during sparging. Examination of Figure 11.11 shows that positive pressure was detected in probe cp-1-4 during DVE operation as a result of previous sparging activities. Apparently an isolated, unsaturated region under positive air pressure had formed in a perched-water zone during sparging. Positive pressure in CP-1-4 increased during combined air extraction and injection in OB-3.

Figure 11.11 illustrates vacuum/pressure measurements in soils under three operating conditions: VE-2 alone, VE-1&VE-2, and CIE alone. Vacuum measurements in soil from combined air extraction and injection are similar for all but the deepest probes as would be expected for deeper air injection. DVE application resulted in greater vacuum with depth. The performance of the CIE well was surprising good considering that no seal was present in the well annulus between the injection and extraction intervals. Vacuum measurement in shallow probes indicates that combined air injection and extraction did not result in uncontrolled air flow toward the surface.

11.3 Conclusions

1. When vacuum is applied to a well screened near the water table, water-level rise occurs

within and near a gas extraction well which often reduces or completely obstructs gas flow. Gas injection on the hand, results in soil-water movement away from and hence increased gas permeability in the vicinity of screened interval. Since, the application of vacuum causes water-table upwelling, soil-water flow, and decreased gas permeability in the immediate vicinity of a gas extraction well, it is logical that injection of pressurized gas or at least maintenance of atmospheric pressure at the base of a vacuum extraction well would reduce water recovery.

2. The concept of combined air injection and extraction (CIE) was evaluated during a pilot study at Vance Air Force Base located in northwestern Oklahoma. Injection of air at the base of a gas extraction well reduced water recovery by 90% compared to dual vapor extraction. Vacuum measurements in soil from combined air extraction and injection were similar for all but the deepest probes. Vacuum measurement in shallow probes indicated that combined air injection and extraction did not result in uncontrolled air flow toward the surface.

3. Additional research is necessary to improve the design of the CIE well and assess it applicability at other sites.

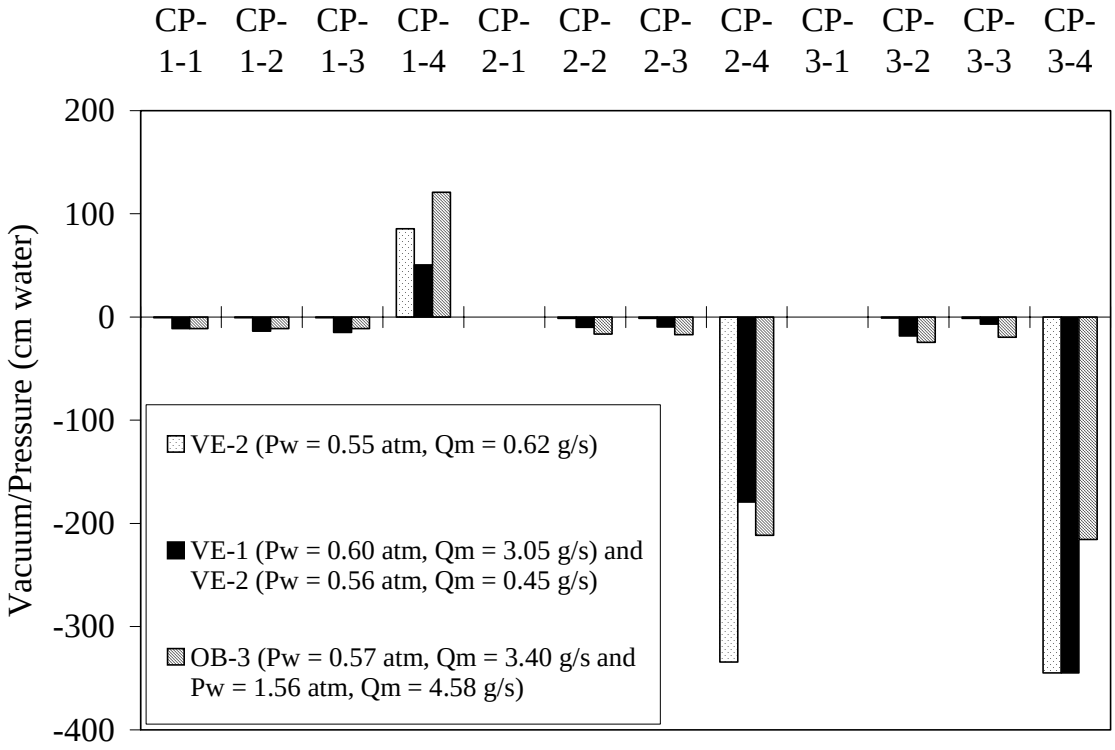

Figure11.11 Pressure differential measurements in vapor probes from DVE well and the combined air injection/extraction well at OB-3.

12. MONITORING STRATEGIES TO ASSESS CONCENTRATION AND MASS REDUCTION

During venting operation, VOC monitoring using a portable photoionization detector (PID) or flame ionization detector (FID) at the vapor treatment or blower inlet, gas extraction wells, and vapor probes invariably becomes the primary method of assessing venting performance. Vapor analysis using gas chromatography (GC) or gas chromatography/mass spectroscopy (GC/MS) is commonly viewed as being too expensive. Other methods of performance assessment such as collection and analysis of soil samples are often viewed as too disruptive and expensive. As will be discussed, monitoring the vapor treatment inlet, gas extraction wells, and vapor probes with a portable PID or FID provides useful information to assess the performance of a venting system. However, monitoring of evaporation-condensation fronts of individual components can provide valuable information in assessing venting performance in NAPL contaminated soils. This type of analysis requires GC or GC/MS analysis of vapor at individual gas extraction wells and vapor probe clusters between wells. Because of rate limited vapor transport effects, there is considerable uncertainty as to what decreasing vapor concentrations in extraction wells and vapor probes actually represent. Vapor concentration asymptotes in gas extraction wells may or may not be indicative of rate-limited vapor transport. Flow variation testing may reveal the presence of rate-limited vapor transport in NAPL and non-NAPL contaminated soils. Flow interruption (rebound) testing to evaluate rate-limited vapor transport however may only be applicable in non-NAPL contaminated soils. Thus, vapor concentration monitoring to assess venting performance is not straightforward. There are many complications, seldom appreciated, which lead to a false sense of accomplishment in venting remediation. Ultimately, assessment of concentration and mass reduction may necessitate soil sample collection and analysis.

12.1 VOC Monitoring at the Vapor Treatment Inlet and Individual Wellheads Using a Portable PID or FID

Flow and vapor concentration monitoring at the vapor treatment or blower inlet provides a direct estimate of the VOC mass removal rate and total VOC mass removed as a function of time for the entire venting system. Monitoring of carbon dioxide concentration has sometimes been used to estimate the mass removal rate and total mass removed as a function of time by biodegradation. Flow, CO_2, and vapor monitoring at individual wellheads has been used to estimate mass removal by volatilization and biodegradation at specific locations throughout a site in the same way as that used at the vapor treatment or blower inlet. Flow and vapor concentration monitoring at individual wellheads can be used to determine the most heavily contaminated portions of a site requiring perhaps the most intensive monitoring and to optimize vapor treatment. For instance, if a vapor treatment system has insufficient capacity to treat gas flow from all operating wells, flow and concentration information form each well can be used to initially operate wells yielding the greatest mass flux. VOC monitoring at the wellhead enables prioritization of venting operation at high contaminated areas. If catalytic oxidation is used to treat gas effluent, a vapor stream too rich in VOCs may cause overheating of the catalyst while a

vapor stream too lean in VOCs may require addition of supplemental fuel. Selectively operating gas extraction wells may enable minimization of vapor treatment costs. Flow and vapor monitoring at individual wellheads then allows assessment of mass flux from various regions of a site and enhances flexibility in vapor treatment operation.

VOC monitoring at the vapor treatment inlet and gas extraction wellhead is typically performed using a PID or FID. PIDs utilize photons from ultraviolet (UV) light to remove the outermost electron from many organic and some inorganic compounds. Ions formed are collected on a charged plate producing a current proportional to compound concentration. The ion current is then amplified and displayed on the meter as parts per million volume (ppmv). Electrons subsequently return to positively charged ions reforming the original vapor allowing non-destructive VOC detection. The energy required for ionization is measured in electron volts (eV). Ionization occurs when the energy supplied by a UV lamp exceeds a compound's ionization potential (IP). UV lamps are commercially available in 8.3, 9.5, 10.6 and 11.7 eV, with the 10.6 eV lamp being the most common. The 11.7 eV lamp extends the range of compounds detected with a PID but is seldom used because it is relatively expensive, requires constant maintenance and frequent replacement. The 11.7 eV lamp has a window made of lithium fluoride which is degraded by UV light, is very hygroscopic, and readily absorbs water from air even when not in use. This causes the window to swell and decreases the amount of light transmitted through the window. PIDs are very sensitive to aromatic hydrocarbons (e.g., benzene, toluene, ethylbenzene, xylene isomers) and chlorinated compounds with carbon-carbon double bonds (e.g., trichloroethylene, perchoroethylene).

FIDs use ionization as the method of detection much the same as PIDs except that ionization is accomplished by the use of a hydrogen flame. A pump draws sample gas from a hand-held probe and passes it to a mixing chamber which is fed with pure hydrogen gas from a small cylinder through a regulator. The mixture is ignited, producing organic ions and electrons which generate a current through the gas. FIDs respond to organic compounds that burn or ionize in the presence of a hydrogen and air flame (i.e., compounds containing large numbers of carbon-hydrogen bonds). The magnitude of ionization is proportional to the number of carbon atoms within the sample. FID like PID response though varies among various compounds requiring the use of correction factors to estimate a specific vapor concentration from a calibration gas concentration. FID response is a function of carbon content, arrangement of carbon atoms in a molecule, and the presence and arrangement of non-carbon functional groups. FIDs are very sensitive to petroleum hydrocarbons (especially methane), less sensitive to compounds having carbonyl, alcohol, halogen, and amine functional groups, and relatively insensitive to heavily halogenated compounds such as carbon tetrachloride.

Table 12.1 contains the maximum concentration (determined with GC/MS analysis) and associated IPs of VOCs detected during pilot scale testing at the Picillo Farm Superfund Site. It is apparent that use of a 10.6 eV lamp would result in detection of only 2 of the 6 target VOCs occurring in the highest concentration. However, FID response to the other 4 compounds would also be expected to be poor given the heavily halogenated nature of these compounds. Thus,

Table 12.1. Maximum concentration and associated IPs of VOCs detected during pilot scale testing at the Picillo Farm Site.

Compound	Highest vapor phase conc. (ppmv)	IP* (eV)
toluene	3500	8.82
1,1,1-trichloroethane	2500	11.00
chloroform	1100	11.37
methylene chloride	911	11.32
hexane	810	10.13
trichlorofluoromethane (Freon 11)	800	11.77
trichloroethene	730	9.47
total xylenes	720	8.44 - 8.56
methylpentanes	340	10.06 - 10.08
benzene	320	9.25
ethylbenzene	317	8.77
methylcyclopentanes	280	9.85
methylhexanes	180	?
tetrachloroethene	173	9.32
methylcyclohexanes	170	9.64
cyclohexane	160	9.86
heptane	150	9.92
methylheptanes	145	9.84
1,2,2-trichloro-1,2,2-trifluoroethane (Freon 113)	140	11.99
1,2-dichloroethane	89	11.04
1,1-dichloroethane	80	11.06
dimethylcyclohexanes	75	9.41-9.98
pentane	75	10.35
1,2-dichloroethene (total)	74	9.66
dichlorofluoromethane (Freon 21)	57	12.39
styrene	53	8.43
dimethylcyclopentanes	30	9.92-9.95
2-butanone (MEK)	17	9.51
trimethylbenzenes (total)	13	8.27 - 8.48
acetone	13	9.71
chlorobenzene	12	9.06
1,1-dichloroethene	12	9.79
1,3-dichloropropene (total)	10	?
4-ethyltoluene	8	?
chloroethane	6	10.97
bromomethane	6	10.54
vinyl chloride	6	9.99
carbon tetrachloride	5	11.47
bromodichloromethane	5	10.6
1,1,2-trichloroethane	5	11.00
chloromethane	5	8.90
dibromochloromethane	5	10.59
1,2-dichloropropane	5	10.87
1,1,2,2-tetrachloroethane	4	11.10
bromoform	4	10.48
1,2-dichlorobenzene	3	9.06

* CRC Handbook of Chemistry and Physics, 73rd Edition, D.R. Lide (Ed.), CRC Press (1993).

screening with a portable PID or FID may result in underestimation of total VOC concentration and mass removal at this site.

There are other considerations in PID and FID use. Robbins et al. (1990a) found decreased response with decreased flow rate for both a tested FID and PID, although the PID was particularly sensitive to decreased flow rate. PID response was found to be sensitive even to the presence of a slight vacuum in sampling tedlar bags. This problem was overcome by placing a weight on the bag during measurement. The weight induced a slight positive pressure in the bag and resulted in increased consistency in PID readings. Robbins et al. (1990a) state that response as a function of flow rate would introduce non-linearity in the correlation between measured and actual concentration. PID manufacturers state that response is essentially independent of gas flow rate as long as it is sufficient to satisfy the pump demand. If a gas bag or sample jar is used having sufficient volume, the instrument will draw gas at its normal flow rate.

The range of linear response is generally greater for FIDs compared to PIDs. For instance through the use of a serial dilution technique, Robbins et al. (1990a) demonstrated a linear response to benzene, methane, isobutylene, and vapors from unleaded gasoline at concentrations up to 1000 ppmv using an FID. Comparison of FID and PID response to benzene at concentrations up to 1000 ppmv revealed nonlinearity (underestimation of concentration) of the PID response above 125 ppmv. Comparison of FID and PID response to gasoline vapors also revealed nonlinearity of the PID response above 125 ppmv. These observations indicate that PIDs may underestimate vapor concentration when elevated levels of contamination are present.

In comparison to FID response, PID response can be significantly quenched by high moisture, methane or alkane, and CO_2 content. Robbins et al. (1990a) evaluated the effect of relative humidity (0 to 90%) on FID and PID response to benzene. The FID showed no discernable effect while the PID response markedly decreased at relative humidity as low as 10%. Since soil gas exits a gas extraction well at or near100% relative humidity, PIDs likely systematically underestimate vapor concentration. Methane and alkanes also have a quenching effect on PID response. Robbins et al. (1990a) observed a decreased PID response to isobutylene in the presence of elevated levels of methane (2000 - 12000 ppmv) and butane (500 - 3000 ppmv). Methane has an IP of 12.51 eV and thus can not be detected with a PID. FIDs though respond strongly to methane. Methane if present in significant concentrations in effluent gas, would cause a higher FID compared to PID response. Robbins et al. (1990a) also evaluated FID and PID response to benzene in the presence of carbon dioxide concentrations varying from 0 to 30%. PID response decreased with increasing carbon dioxide concentration while FID response increased slightly as carbon dioxide concentrations rose. Neither FIDs or PIDs ionize carbon dioxide, thus both responses are due to matrix or gas composition effects.

Robbins et al. (1990a) demonstrated that when a variety of gas compositional conditions cause a decreased PID or FID response, the overall effect is not additive but instead equal to the product of each response factor. Since PIDs are much more sensitive to gas compositional effects compared to FIDs, high humidity, methane, alkane, and carbon dioxide concentrations

could cause PID response to be a small fraction of expected response based on calibration of a dry, clean calibration gas. Also, since response factors due to gas compositional effects are generally non-linear and gas composition varies from sample to sample, estimation of actual total vapor concentration (to a calibrated hydrocarbon) from measured values becomes intractable unless serial dilution as explained by Robbins et al. (1990a,b) is performed. Serial dilution allows evaluation of gas composition on instrument response, calculation of response factors, and extrapolation to initial gas sample concentrations. Robbins et al. (1990a) demonstrated that without serial dilution, PID readings are unreliable and generally underestimate total vapor concentration.

12.2 Observation of Evaporation/Condensation Fronts

Observation of evaporation fronts in individual extraction well effluent gas and evaporation/condensation fronts in well-placed vapor probe clusters could potentially provide valuable information on the progress of venting remediation of NAPL contaminated soils. Removal of NAPL under equilibrium conditions in single component laboratory-scale through-flow (a term commonly used to denote absence of bypass-flow or where gas is forced directly through contaminated soils) experiments is characterized by a sharp evaporation front or very rapid decline in effluent concentration. For instance, during sand tank studies in a moist Borden sand, McClellan and Gillham (1992) observed a sharp decline in TCE vapor concentration (about 1.3 orders of magnitude) after an extensive period of essentially constant concentration. They state that this abrupt decrease in vapor concentration corresponded to the time when the last liquid or residual TCE was removed and the kinetics of aqueous and sorbed phase mass removal became dominant.

Abrupt decreases in effluent vapor concentration has also been observed in multi-component NAPL contaminated soils but is complicated by changing mole-fractions of individual components throughout the soil column during gas through-flow. Rathfelder et al. (1991) conducted through-flow column studies in dry glass beads and dry Borden sand with a multi-component NAPL mixture of benzene, toluene, and TCE. Using a local equilibrium model, they successfully simulated sharp evaporation fronts eluting in sequential order of decreased vapor pressure (benzene, TCE, toluene respectively) as expected from Raoult's law. Ho et al. (1994) conducted through-flow column studies in a dry sand with a multi-component NAPL mixture of benzene, toluene, and o-xylene. Similar to Rathfelder et al. (1991), they successfully simulated successive evaporation fronts in the gas effluent using a local equilibrium model. Ho et al. (1994) found that individual components of a NAPL propagate with separate evaporation fronts at speeds proportional to their vapor pressure. This is consistent with mathematical analysis of Zaidel and Zazovsky (1999) who found that the velocity and sequence of evaporation-condensation fronts can be predicted by a component's vapor pressure even at low NAPL saturations. Hayden et al. (1994) found mass removal was controlled by the presence of NAPL and component vapor pressures even at high organic carbon contents (1.65%) At very low NAPL saturations however, gas-water and solids-water partitioning must be taken into account in addition to NAPL-gas partitioning.

Ho et al. (1994) observed and successfully simulated evaporation-condensation fronts along the length of a soil column. Condensation of less volatile components, as measured by total concentration analysis, occurred downstream of evaporation fronts. For instance, total concentrations of toluene and o-xylene increased significantly at the location of the benzene evaporation front. After evaporation of benzene, concentrations of o-xylene concentrations increased significantly at the toluene evaporation front. As clean gas sweeps through the upstream portion of NAPL contaminated soil, more volatile components are preferentially volatilized thereby reducing the mole fractions of more volatile compounds and increasing the mole fractions of less volatile compounds. This increases vapor concentrations of less volatile compounds which are transported downstream to areas where their mole fractions are lower, causing condensation and increased concentrations above initial levels. Upstream evaporation and downstream condensation occur through a soil column until all but the last component is removed. They observed that a sharp decrease in effluent concentration occurs when a compound's evaporation front has reached the exit and near complete removal from the soil column has occurred. Ho et al. (1994) also observed that effluent vapor concentrations remain fairly constant prior to the first evaporation front reaching the exit. Based on this observation, they state that mole fractions of individual compounds in a NAPL mixture can be calculated from knowledge of a compound's vapor pressure and initial concentration.

Ostendorf et al. (1997) carried out a venting experiment on an intact core taken from a site having soils contaminated with weathered fuel. Along the axis of flow, the vapor concentration of lighter components decreased monotonically with time compared to heavier components which increased for some time and then decreased. Ng et al. (1999) successfully simulated Ostendorf et al's. (1997) data using a vapor transport model coupling macroscale advective-dispersive vapor transport with microscale aggregate diffusion. In their model, the macroscale region consisted of mobile gas and free NAPL while aggregates consisted of water, gas, and trapped NAPL. All transport to and from microscale and macroscale regions was assumed to be controlled by aqueous diffusion.

Ng et al. (1999) then conducted hypothetical simulations of propagation of evaporation fronts and downstream condensation in aggregated and nonaggregated soils contaminated by a NAPL mixture of benzene, toluene, and o-xylene in a radial flow system. For aggregated soils, the o-xylene vapor concentration exhibited a downstream increase with time approaching its saturated vapor concentration similar to nonaggregated soils. However, in contrast to nonaggreated soils, a sharp evaporation front was not observed. Vapor concentrations of o-xylene decayed slowly and exhibited extensive tailing due to slow release from aggregates. Ng et al. (1999) observed that in aggregated media, mass removal of compounds having lower volatility is prolonged a disproportionate period of time compared to compounds having higher volatility. In simulations with benzene, toluene, and o-xylene, Ng et al. (1999) observed that during condensation, the feeding of o-xylene into aggregates lasted substantially longer than benzene and toluene. While benzene and toluene were being removed, o-xylene continued to be stored in aggregates. This trend only stopped when the macropore o-xylene vapor concentration began to drop or when free NAPL saturation vanished at a macroscale position. The o-xylene

aqueous concentration inside aggregates then exhibited a discontinuous gradient. In the outer regions of aggregates, o-xylene diffused outward while in the inner region the o-xylene aqueous concentration continued to rise in response to lower o-xylene concentrations in the interior. Thus, in multi-component NAPL contaminated soils in a field setting, time for mass removal of compounds having lower volatility or vapor pressure will be extensive. Ng et al.'s (1999) radial flow simulations also show that even under nonequilibrium conditions, the time at which the vapor concentration of the compound with the lowest vapor pressure drops abruptly is the time in which the free NAPL is completely volatilized. Under nonequilibrium conditions, this abrupt decrease in vapor concentration is accompanied by extensive tailing.

The pattern of a sharp decline in effluent concentration at removal or evaporation of a NAPL component observed in through-flow experiments though has not been reported during field application in NAPL contaminated soils. This is most likely because of nonuniform gas flow (bypass flow as opposed to through-flow conditions), fully three-dimensional flow as opposed to radial flow as simulated by Ng et al., 1999), spatial variability of NAPL distribution, common monitoring practices (determination of total VOC with a PID or FID as opposed to identification and quantification of individual compounds), and rate-limited vapor transport. Given the first two factors, even under equilibrium conditions, NAPL removal during field operation is more likely to be characterized by a gradual rather than sharp reduction in total and individual component concentration. Ho and Udell (1992) conducted a series of sand tank experiments which demonstrate this point well. They used three sorted dry sands to assess deviation from equilibrium conditions in homogeneous and two-layer soil systems containing one and two-component NAPL formulations. During the first experiment, a single component NAPL (toluene) was injected into a 0.25 mm mean diameter sand to achieve a residual saturation of 12%. Effluent concentration remained relatively constant for the first 20 minutes but at only 60% of its saturated value. Based on the cross-sectional area of NAPL contaminated soils coming in contact with gas flow, approximately 70% of the saturated concentration should have been achieved. The presence of NAPL though likely reduced gas permeability in contaminated soils causing some bypass flow. Effluent concentrations then rapidly declined over the next 40 minutes with residual NAPL visually disappearing (dyed red). A sharp evaporation front though was not observed. Ho and Udell (1992) state that the gradual decrease in effluent concentration could have been caused by reduced gas-NAPL contact area, decreased critical length for equilibration, or reduced mass transfer coefficients as the toluene evaporated. They argue however that since the length of contaminated media required for equilibration was likely short, by the time the NAPL contaminated area had shrunk to a size with violated equilibrium conditions, much of the contaminant had already been removed. Thus, equilibrium conditions within NAPL contaminated soils likely prevailed with decreasing concentrations due solely to decreasing gas flow contact area. This experiment was repeated using a mixture of toluene and o-xylene at similar mole fractions at a residual saturation of 17%. Toluene effluent concentration decreased in a manner similar to the single component experiment but as its vapor concentration decreased, the vapor concentration of o-xylene increased as predicted by Raoult's law. At exhaustion of toluene the o-xylene concentration remained constant for a short time before decreasing in a manner similar to toluene. Discernable but not sharp evaporation fronts were

observed.

Ho and Udell (1992) then injected free-phase toluene into a lower permeability layer overlain by a higher permeability layer (14:1 ratio). Pore-gas velocities (calculated using formation provided by the authors) in the higher and lower permeability regions were 10.96 and 0.86 cm/s respectively. Slow recession of toluene residual occurred at the upgradient gas flow end similar to the unlayered soil system indicating significant gas flow through the layer of lower permeability. Thus, mass removal in the lower permeability lense was still controlled by advection. In contrast to unlayered tests though, effluent concentrations showed a prolonged, steady and somewhat linear decrease in effluent concentration over time. Repeating this experiment with a toluene - o-xylene mixture indicated a continued decrease in o-xylene concentration throughout the experiment as opposed to an increase in o-xylene concentration as toluene evaporated. The o-xylene effluent concentration however did not decrease as rapidly as the toluene concentration and eventually a cross-over point occurred where o-xylene concentration became higher than toluene concentration. While evaporation fronts were not discernable in this experiment, it was still apparent that preferential volatilization of toluene was occurring.

Finally, free-phase toluene and a toluene and o-xylene mixture was injected into a lower permeability layer overlain by a higher permeability layer with a 160:1 ratio. Pore-gas velocities (calculated using information provided by the authors) in the higher and lower permeability regions were 5.1 and 0.03 cm/s respectively. Comparison of dyed NAPL residual removal with an experiment where the low permeability layer was overlain by air, indicated that mass removal was controlled by diffusion. In contrast to all previous experiments, extensive effluent tailing was observed. While a cross-over point between toluene and o-xylene effluent concentration occurred, the concentration profiles were very similar.

Liang and Udell (1999) conducted a series of bypass-flow experiments with toluene and o-xylene where gas flow in a glass column was allowed to occur above but not through NAPL contaminated soils. This would occur in the field for instance when air flow occurs around a silt or sand lense. They demonstrated that an evaporation front slowly penetrates into the bypassed media and that a zone of variable liquid mole fractions grows in length ahead of the front because of continual evaporation and diffusion to the region of advective flow. The mole fractions of higher volatility compounds are lower than lower volatility compounds at the evaporation front but the liquid mole fractions farther away from the evaporation front remain at initial values. As a result, the measured mass ratio of compounds in effluent gas during bypass flow stays close to the initial mass ratio of compounds in the effluent gas. This effluent pattern is very different from increasing ratios of lower volatility compounds seen during advectively dominated flow.

Studies by Rathfelder et al. (1991), Ho and Udell (1992), Ho et al. (1994), Liang and Udell (1999), and Ng et al. (1999) make a strong case for monitoring individual NAPL components as opposed to just monitoring total hydrocarbons in gas extraction well effluent and vapor probes to assess the progress of remediation. At the start of venting, component ratios are

indicative of initial mole fraction ratios of residual NAPL providing valuable insight into the composition of residual NAPL in contaminated soils. During the period in which mass removal is dominated by advection, there could be a series of muted evaporation fronts in gas extraction wells where compounds with high vapor pressures show steady decline and compounds with lower vapor pressures show a temporary increase in vapor concentration prior to dropping in concentration. Patterns of increasing and subsequent decreasing vapor concentrations of lower volatility compound could be indicative of removal of these compounds from NAPL. A decrease in compounds having the lowest vapor pressure could be indicative of evaporation of accessible NAPL. Monitoring of vapor concentrations in well placed vapor probe clusters could provide evidence of the movement of evaporation-condensation fronts radially toward gas extraction wells and again provide evidence of successful removal of NAPL during venting application. In a complex multi-component NAPL, a mixture of high, medium, and low vapor pressure compounds could be targeted for monitoring in individual well gas effluent and in vapor probe clusters. As NAPL-gas exchange becomes dominated by diffusion or bypass flow, component concentrations in the effluent gas and vapor probes should return to ratios close to what was initially observed again reinforcing the need to estimate initial NAPL mole fractions.

12.3 Vapor Effluent Asymptotes

Often, cessation of venting application is proposed based on attainment of an asymptote, a concentration level during asymptotic conditions, or some subjectively determined mass removal rate (e.g., pounds per day) from gas extraction wells. However, there is no way to directly relate observation of an asymptote to environmental benefit and little potential to ensure consistency in decision making. Vapor concentration of an asymptote at a highly contaminated site may be much higher than at a lesser contaminated site leading perhaps to less stringent remediation at the highly contaminated site. Observation of an effluent asymptote may be related to venting design (e.g., well spacing) or operating conditions (e.g. flow rate) separate or in addition to rate-limited vapor transport. Rathfelder et al. (1991) demonstrated that effluent tailing in NAPL contaminated soil can be caused by flow dynamics. Hypothetical simulations in a homogeneous, one-dimensional, confined radial flow system with a NAPL and water saturation of 1% and 15% respectively showed that under equilibrium conditions, the bulk of contaminant volatilization occurred along a clean retreating radial evaporation front as air flow is forced directly through contaminated soil. During two-dimensional axisymmetric flow however, direct recharge from the atmosphere and subsequent vertical flow results in clean retreating evaporation fronts both vertically above and radially distant from a gas extraction well. This caused the formation of a wedge-shaped contamination zone whereby some continually decreasing fraction of gas flow intersected contaminated soil leading to decreasing effluent concentrations that could be construed as tailing. Shan et al. (1992) demonstrated that in a domain open to the atmosphere, most gas flow to an extraction well originates from atmospheric recharge in the immediate vicinity of the well. Thus, after some period of vacuum operation, vapor concentrations from gas extraction wells become largely reflective of soil and contaminant conditions in the immediate vicinity of the wells while higher concentrations more distant from wells are largely diluted. Effluents in gas extraction wells then approach low concentrations and an asymptote while

significant and accessible mass may remain in soils between gas extraction wells. This situation is exacerbated by placing venting wells too far apart - a condition typical of radius of influence based designs discussed in section10.

A similar situation occurs in stratified soils where gas flow occurs primarily in layers of greater gas permeability. Analogous to the first situation, mass removal occurs more rapidly in soils receiving greater gas flow and vapor concentrations in gas extraction wells become largely reflective of soil and contaminant conditions in these layers while higher vapor concentrations from lenses of lower permeability are largely diluted. Rathfelder et al. (1991) simulated effluent tailing when a gas extraction well was placed across two stratigraphic layers having an order of magnitude difference in permeability. In this case as before, effluent tailing and apparent rate-limited mass removal was caused by variation in pore-gas velocity, not by rate-limited NAPL-gas exchange. Lowered local gas permeability in zones containing pure phase residual would cause the same effect. Other examples of design factors potentially causing the observation of an effluent asymptote include inadequate lowering of the water table, inadequate dewatering of perched water table zones, and gas extraction wells not placed in or near source areas.

Changing mole fractions of individual components in NAPL may also cause the appearance of an asymptote in vapor effluent. Baehr et al. (1989) simulated mass removal of gasoline in medium-grained sieved sand. Experimental and simulated mass flux profiles matched well suggesting attainment of equilibrium conditions. The decrease in total mass flux with time and exhibited apparent tailing due to selective removal of more volatile hydrocarbons. This behavior is in contrast with column and sand tank studies using single component residually contaminated soils which show no reduction in mass flux until residual NAPL has evaporated. In a field setting, it would be easy to mistake tailing due to selective volatilization of a multi-component NAPL for rate-limited behavior.

Since both design considerations and rate-limited vapor transport can cause extensive effluent tailing and ineffectual removal of accessible contaminant mass, it is critical to first rigorously assess venting design, implementation, and associated monitoring prior to concluding that rate-limited vapor transport significantly constrains mass removal. If gas flow and design considerations can be eliminated as a causative factors in the observation of asymptotes, then the possibility of rate-limited mass exchange must be considered. Controlled laboratory experiments (Armstrong et al., 1994; Conklin et al., 1995; Fisher et al., 1996, Gierke et al., 1992; Grathwohl et al., 1990; McClellan and Gillham, 1990) have shown that very long effluent tailing can occur as a result of rate-limited mass exchange indicating that soils venting may be inefficient in achieving complete removal of VOCs. Several groups of investigators (Fisher et al., 1996; Ng and Mei, 1996; and Armstrong et al., 1994) have clearly demonstrated in laboratory columns, sand tank studies, and mathematical analysis that an asymptote can be observed in gas extraction wells while much of the contaminant mass remains in soils and that observation of low asymptotic vapor concentrations in effluent gas is not a sufficient condition to demonstrate progress in mass removal from contaminated soils.

Ng and Mei (1996) demonstrated the inadequacy of assessing the effectiveness of a SVE system using only effluent vapor monitoring. They simulated the time variation in effluent vapor and aqueous aggregate concentration. Effluent vapor concentration dropped rapidly with time to the point of having indistinguishable values however the decay of the aqueous phase was significantly slower. Since sorptive equilibrium exchange was assumed within the aggregates, the aqueous phase was indicative of mass removal within aggregates. Thus, effluent vapor phase monitoring provided little insight on the rate of concentration reduction in soil.

Armstrong et al. (1994) developed a numerical one-dimensional model which incorporated first-order gas-water and solids-water rate-limited mass exchange to simulate vapor effluent data obtained by McClellan and Gillham (1992). Virtually identical fits were obtained to effluent curves for both continuous and pulsed schemes using two parameter sets: 1) K_d and λ_{gw} values of 2.1 cm^3/g and 2 x 10^{-5} s^{-1} respectively (equilibrium sorption) and 2) K_d, λ_{gw}, and λ_{ws} values of 10.1 cm^3/g, 4 x 10^{-5} s^{-1}, and 5 x 10^{-5} s^{-1} respectively. Simulated remaining mass however differed sharply with the second parameter set resulting in far greater mass retention. Their sensitivity analysis and calibration of data showed that different mass retention and rate coefficients can produce very similar effluent curves suggesting that effluent and vapor probe concentration data can not be used to estimate mass transport coefficients and VOC concentration in the aqueous and solids phase. Thus, effluent and vapor probe concentration data is insufficient to quantitatively assess the progress of soil venting remediation. When coupled with uncertainty in initial mass distribution, it appears that effluent and vapor probe concentration data can only be used in a qualitative sense to assess performance.

12.4 Flow Variation and Interruption Testing

Results of controlled column and sand tank studies reveal that some indicators of rate-limited transport may be decreased vapor concentration with increased pore-gas velocity (flow variation) and extensive vapor concentration tailing accompanied by vapor rebound after cessation of operation (flow interruption). In laboratory-scale gas flow or miscible displacement studies, flow variation and interruption is commonly used to determine the validity of the local equilibrium assumption. If no change vapor or solute effluent concentration occurs during an increase, decrease, or start-up upon periodic stoppage of flow, then it is assumed that the local equilibrium assumption holds. In both NAPL and non-NAPL contaminated soils, flow variation could provide a simple yet powerful test of the validity of local equilibrium. For NAPL contaminated soils however, results of flow interruption testing could be confusing if the propagation of evaporation-condensation fronts are not considered. Hayden et al. (1994) provide a good example of this. They introduced gasoline at NAPL saturation value of 2% in two sandy soils (less than 5% silt and clay) having organic carbon content of 0.1% and 1.65% and water saturation values of 8% and 43% respectively and monitored effluent concentrations of benzene, m,p-xylene, and naphthalene. For the high organic content and water saturation soil, flow variation resulted in pore-gas velocities (calculated from information provided) being varied between 0.076 and 0.020 cm/s while for the low organic carbon content and water saturation soil, flow variation resulted in calculated pore-gas velocities (calculated from information provided)

being varied between 0.057 and 0.015 cm/s. Flow variation had no effect benzene, m,p-xylene, and naphthalene effluent concentrations during initial period of venting indicating the validity of the local equilibrium assumption. However after a prolonged period of venting, benzene effluent concentration decreased abruptly (indicating elution of the benzene evaporation front) and variation in flow rate caused a decrease in benzene concentration with an increase in flow rate and an increase in benzene with a decrease in flow rate. During this time period m,p-xylene, toluene, and naphthalene effluent concentration remained unaffected by flow variation. Thus, at low soil or NAPL benzene concentrations, mass removal appeared to become rate-limited and the method of flow variation worked well in discriminating between rate-limited and non-rate-limited transport. The results of flow interruption testing though were more difficult to discern. Flow interruption testing during the initial period of venting application (1 hour) resulted in a decrease in benzene concentration and an increase in m,p-xylene and toluene effluent concentration. Flow interruption testing at 3 hours resulted in a decrease in benzene and toluene effluent concentration and an increase in m,p-xylene. Reconciliation of this behavior is possible only if one considers evaporation-condensation fronts. During initial venting operation, high vapor pressure compounds such as benzene would be removed first from the intake portion of the column and increase in mole fraction and vapor concentration downstream as the evaporation front moves through the column. Cessation of venting then would cause a decrease at the effluent end of the soil column and an increase in the intake end of the column as vapor diffusion becomes the dominant transport mechanism. Upon re-start, effluent concentrations would drop. For compounds like m, p-xylene, the mole fraction and vapor concentration would initially increase at the inlet of the soil column. Thus during flow interruption, vapor diffusion would cause an increase in vapor concentration downstream resulting in an increase in vapor concentration upon start-up. Thus, the increase in m, p-xylene upon start-up was likely not the result of rate-limited mass transport, but propagation of evaporation and condensation fronts. In a field setting, flow interruption testing would provide evidence of rate-limited transport for a particular compound only after its evaporation front exited the soil column. This might be accomplished by sampling an array of vapor probes situated between a relative clean-gas boundary and a extraction well. Otherwise, flow interruption testing could provide confounding results.

12.5 Use of Flow Interruption Testing to Estimate Soil Concentration

One potential use of flow interruption or rebound data is to use vapor concentrations and partition coefficients to estimate total soil concentration. Monitoring of VOC concentrations in vapor probes for this purpose is preferable to vapor extraction wells because probes draw soil gas from a much smaller volume of soil and thus are less likely to be affected by vapor concentration variation due to large scale heterogeneity. Viewed superficially, the idea appears to have merit because soil sample collection can be expensive, especially when drilling at extensive depths and in soils containing large rocks (e.g., glacial till). Drilling can cause disruption of venting operation and manufacturing processes at active operating facilities. Also, drilling often results in the generation of a substantial amount of cuttings which must be disposed of as hazardous waste. Other benefits of vapor measurement to estimate total soil concentration are that volatile

organic compound (VOC) loss occurs during sample collection, storage, and analysis. VOC loss during sample collection can be significant for highly volatile compounds in soils with low organic carbon and moisture content. Vinyl chloride is often not detected in soils samples even when high concentrations are detected in soil gas. It can be argued that soil sample collection is by nature "hit" or "miss" because sample volume is small compared to the volume of soil affected by soil-gas collection. Thus, if contaminant mass remains in soil, there is a higher probability of detection with soil-gas sampling than soil-solids sampling. Finally, soil sample collection is obviously not appropriate for venting operation in fractured rock or other consolidated material.

Several investigators have attempted to correlate soil-gas concentrations with total soil concentrations. Stephens (1995) reported poor correlation between trichloroethylene (TCE) concentrations in soil gas and soil matrix samples collected during drilling at approximately the same depth. TCE was detected in 36 of 39 soil-gas samples but only 10 of 83 soil matrix samples with a detection limit of 50 ug/kg. Stephens (1995) states that the more frequent detection of TCE in soil-gas compared to the soil matrix is probably partially due to the much lower detection limits achieved for soil gas compared to the soil matrix and the fact that the soil matrix is far more heterogeneous with respect to contaminant distribution compared to soil-gas. Soil matrix samples with detectable TCE, the concentrations reported by the analytical laboratory were far below those that would be predicted based on equilibrium with measured TCE concentrations in adjacent soil-gas making reasonable assumptions regarding soil moisture, bulk density, and organic carbon content. Stephens (1995) states that if vapor phase equilibrium between soil-gas and soil matrix is assumed, then the discrepancy most likely reflects the shortcomings of soil matrix analytical procedures which often result in reported VOC concentrations lower than expected as reported by Siegrist and Jenssen (1990). Hahne and Thomsen (1991) and Kerfoot (1991) also report poor correlation between soil-gas and matrix concentration.

Significant uncertainty in estimation of parameters making up a soil-gas partition coefficient and difficulty in measuring a steady-state vapor concentration in the field makes estimation of total soil concentration from vapor measurements challenging. Under equilibrium conditions, the relationship between a nonionic organic compound concentration in soil and soil gas is a function of: (1) a gas-water partition coefficient (Henry's Law Constants), an organic-carbon-water partition coefficient, and NAPL-water or NAPL-gas partition coefficients, (2) gas, water, and NAPL fluid saturations, and (3) soil organic carbon content, porosity, and particle density. If separate phase NAPL is available from a site, batch laboratory studies can used to directly determine NAPL-gas or NAPL- water partition coefficients for compounds of concern. If free NAPL is not available, NAPL-water or NAPL-gas partition coefficients can be estimated from a compound of interest's vapor pressure and molecular weight and mole fractions, densities, and molecular weights of individual compounds in the NAPL. At many sites though, there are so many compounds in NAPL contaminated soil that accurate mole fraction identification and quantification is impossible. An average NAPL density and molecular weight can be used in place of individual NAPL constituent information if the mole fractions of dominant chemical

classes in the NAPL can be quantified. However, equations used to estimate NAPL-water or NAPL-air partition coefficients reveal that these partition coefficients will not be constant but change as a function of changing mole fractions of various compounds. Since a compound's organic-carbon-water partition coefficient, Henry's Law Constant, vapor pressure, molecular weight can be found in the literature or estimated for many compounds, a soil-gas partition coefficient has 7 primary unknown parameters - gas, water, and NAPL saturation, particle density, porosity, average NAPL density, and average NAPL molecular weight. The parameters describing NAPL are of greatest interest because analysis of mass fractions reveals that the majority of contaminant mass is partitioned in the NAPL phase even at very low NAPL saturation (e.g., 0.5%). Error in estimation of NAPL saturation would dramatically affect estimates of soil concentration and contaminant mass. There is presently no standard method of estimating NAPL saturation in-situ in soil but partitioning tracer testing shows promise. In-situ water saturation would need to be estimated with the use of a neutron probe or other downhole device. Gas saturation could be estimated from knowledge of porosity and volumetric water content. Each estimation procedure involves error, which from an analysis of variance, propagates non-linearly. Finally, there is no way to assess the accuracy of estimation of soil-concentration from soil-gas measurements because the volume of soil being affected by advective gas flow to a probe is likely greater that the volume of soil typically sampled for laboratory analysis. Collection of soil samples for soil-gas estimation comparison also necessitates consideration of spatial variability which can be significant even on a small scale.

Estimation of soil concentration also requires measurement of steady-state soil-gas concentration. In a well designed venting system, mass removal will eventually limited by combined liquid and vapor diffusion from less permeable soil regions not receiving direct airflow. In a poorly designed system, mass removal will be limited by these factors plus inadequate air flow in regions still amenable to significant advective phase mass transport. In the former case, at the cessation of venting, vapors diffuse slowly from immobile regions into mobile domains where advective gas flow occurs. When a soil's moisture, organic carbon, or NAPL content is high, time for attainment of equilibrium conditions can be excessive. Thus, when collecting vapor samples for total soil concentration or mass estimation purposes, a correction factor is necessary for estimation of steady-state vapor concentration. Assuming that concentration is caused by vapor diffusion, estimation of steady-state vapor concentration will involve the use of some type of a diffusion-based model. The diffusion coefficient will incorporate the 7 unknown parameters of the soil-gas partition coefficient plus three additional unknown parameters - tortuosity in the gas and liquid phases and the diffusion path length. Tortuosity values could be estimated from fluid saturation and porosity. Literature values can be found for molecular gas and water diffusion coefficients. Since there are likely to be numerous localized sources of vapors in contaminated soils, including contaminated ground water, the diffusion path length will represent some averaged distance. In practice, it will be necessary to fit a diffusion-based equation to vapor concentration versus time data during vapor rebound to estimate a lumped parameter incorporating the diffusion path length. This will require the collection of several gas samples over time at each vapor sampling point followed by gas chromatography analysis. Another practical problem is devising an appropriate methodology of

vapor sampling. The collection of vapor samples may cause local dis-equilibrium, thus later vapor sampling results would be biased by earlier sampling efforts.

It is apparent that defensible estimation of soil concentration from soil-gas measurement is a difficult process. It requires a substantial amount of work, expense (GC analysis of vapor), and thorough knowledge of subsurface conditions. Even under the best of conditions, substantial estimation error can be expected. While drilling and subsequent soil sampling is expensive and disruptive, it may still offer the best opportunity to evaluate vertical subsurface contamination profiles. Soil-gas monitoring during venting operation and periods of shut-down however might provide insight on the timing of soil sample collection.

12.6 Use of Gas Phase Partitioning Tracer Testing to Assess Residual NAPL Removal During Venting Application

Partitioning tracer tests have been widely used since the 1970's in the petroleum industry to estimate residual oil saturation and assess the effectiveness of enhanced oil recovery (Allison et al., 1991; Cooke, 1971; Deans, 1978, Ferreira et al., 1992; Lichtenberger, 1991; Sheely, 1978; Sheely and Baldwin, 1982; Tang, 1992; Tang and Harker, 1991a,b; and Tomich et al., 1973). Jin et al. (1995) state that single-well partitioning tracer tests have been conducted at over 300 oil field reservoirs throughout the world in a wide variety of geologic settings. More recently, aqueous-phase partitioning tracers have been used in ground-water (Annable et al., 1998; Brusseau et al., 1999; Cain et al., 2000, Jin et al., 1997; Nelson and Brusseau, 1996; Young et al., 1999; Wilson and Mackay, 1995) and vadose zone (Deeds et al., 1999; Mariner et al., 1999; Whitley et al., 1999) systems. In the environmental field, partitioning tracer studies have been used to: (1) locate subsurface NAPL pools, lenses, and residual, (2) estimate NAPL saturation, and (3) provide a means of assessing the performance of NAPL removal during remediation. Most recently, Nelson et al. (1999) used gas-phase partitioning tracers in the field to estimate in-situ water content. Brusseau et al. (1997) had previously examined the potential of using gas-phase tracers for measuring soil-water content and gas-water interfacial area in column studies.

The theoretical bases for the retention of dissolved or gaseous compounds by immobile, immiscible liquid phases has been described by Jin et al. (1995) and Brusseau et al. (1997). Basically, when tracers having different NAPL-fluid partition coefficients are injected into the subsurface, nonpartitioning tracers remain in and travel with the velocity of the transporting fluid phase while partitioning tracers move back and forth (in response to concentration gradients) between stationary NAPL and the transporting fluid. During gas-phase partitioning tracer tests in the vadose zone, it is commonly assumed that water and NAPL are immobile during the short duration of the test. The net result is that transport of partitioning tracers lags behind or is retarded compared to nonpartitoning tracers. The magnitude of retardation is primarily dependent upon NAPL-fluid partition coefficients and saturation of NAPL in subsurface systems. For a given partitioning tracer, the greater the chromatographic separation in breakthrough curves, the greater the NAPL saturation.

The ratio of residence times or average travel times of partitioning and nonpartitioning tracers can be expressed by

$$R = \frac{\overline{t_p}}{\overline{t_n}} \tag{12.1}$$

where R [-] is a retardation factor and $\overline{t_p}$ [T] and $\overline{t_n}$ [T] are travel times for partitioning and nonpartitioning tracers respectively. The retardation described in terms of fluid saturation can be expressed by

$$R = 1 + \frac{K_{ia} A_{ia}}{\eta S_g} + \frac{\rho_b K_d}{\eta S_g H} + \frac{S_w}{S_g H} + \frac{K_{ng} S_n}{S_g} . \tag{12.2}$$

Use of Raoult's and Henry's Laws allows the NAPL-gas partition coefficient (K_{ng}) [-] to be approximated in a number of ways

$$K_{ng} = \frac{\Re T}{\gamma_i P_v \sum_{j=1}^{N} \frac{\chi_j M_j}{\rho_j}} = \frac{\Re T \rho_n}{\gamma_i P_v M_n} = \frac{P \overline{V_g}}{\gamma_i P_v \overline{V_n}} = \frac{M_i \rho_n}{\gamma_i H C_w^{sat} M_n} . \tag{12.3}$$

Tracer travel times can be estimated by comparing specific points of respective breakthrough curves (Cooke, 1971; Deans 1971; Tang 1992, 1995) or by fitting data to various forms of the advective-dispersive equation. The most widely used and preferred method however is computation of first temporal moments because this method is less sensitive to rate-limited mass transfer and is not dependent on a suite of assumptions necessary in modeling analysis. Temporal moments are defined by Jin et al., 1995)

$$\overline{t_p} = \frac{\int_0^f t C_p(t) dt}{\int_0^f C_p(t) dt} - \frac{t_s}{2} \tag{12.4}$$

and

$$\overline{t_c} = \frac{\int_0^f t C_c(t) dt}{\int_0^f C_c(t) dt} - \frac{t_s}{2} \tag{12.5}$$

where t_s [T] is the tracer injection duration, t_f [T] is the duration of the test, and $C_p(t)$ and $C_c(t)$

represent partitioning and conservative tracer concentrations respectively [ML^{-3}] as a function of time. The moment method is susceptible to error when breakthrough curves are incomplete due to premature termination of field test or when concentrations fall below detection limits. These conditions occur when mass transfer constraints become extreme (substantial fraction of recovered tracer mass in tail of response curve). Application of high flow rates exacerbate effluent tailing and thus should be avoided. The response curve tail though can be extrapolated to zero concentration by fitting a straight line to late time data on a semilog plot (Skopp, 1984 and Pope et al., 1994) to improve the accuracy of moment estimation. Deeds et al. (1999) reported that in all but a few of 72 gas-phase tracer studies conducted at a site, extrapolation had only a minor effect on NAPL saturation estimation. In most cases, greater error originated from estimation of partition coefficients.

Average NAPL saturation (S_n) can be calculated by (Deeds et al., 1999)

$$S_n = \frac{\left(\overline{t_p} - \overline{t_c}\right)\left(1 - S_w\right)}{\overline{t_c}\left(K_{ng} - 1\right) + \overline{t_p}}. \tag{12.6}$$

This equation differs from computation of S_n in saturated systems by inclusion of the factor (1-S_w). If water saturation is estimated using a gas-water partition coefficient, equation (12.16) must be solved simultaneously with (Deeds et al., 1999)

$$S_w = \frac{\left(\overline{t_w} - \overline{t_c}\right)\left(1 - S_n\right)}{\overline{t_c}\left(H - 1\right) + \overline{t_w}}. \tag{12.7}$$

The pore volume, V_p [L^3] ($\theta_g + \theta_w + \theta_n$), swept by the tracers is given by (Deeds et al., 1999)

$$V_p = \frac{Q_v \overline{t_c}}{1 - S_w - S_n} \tag{12.8}$$

where Q_v is the flow rate of subsurface gas through NAPL. Q_v is not necessarily the volumetric flow rate of an extraction/injection well pair because of gas recharge and discharge from and to the atmosphere. The total volume of NAPL detected, V_n is given by (Deeds et al., 1999)

$$V_n = S_n V_p = \frac{\left(\overline{t_p} - \overline{t_c}\right) Q_v}{K_{ng}} \tag{12.9}$$

Nonpartitioning and partitioning tracers should ideally: (1) be initially absent from or at a very low concentration in subsurface media, (2) be readily available and relatively inexpensive, (3) be non-toxic at concentrations employed, (4) be resistant to mass loss (e.g., degradation), and

(5) have a low analytical detection limit. A low detection limit enables tracer detection over a scale of three to four magnitudes and injection at relatively low concentrations. Addition of tracers at low concentrations ensures that the transport of tracers will not be affected by changes in fluid density. Perfluorcarbons generally meet all of these criteria and thus have been widely used for gas-phase partitioning tracer studies. Perfluorcarbons however have been identified as powerful reactants in global warming leading to restricted use. The mass injected for field-scale testing however is insignificant compared to industrial use and it can be argued that testing yields a net environmental benefit. Thus, concern over global warming should not be a limiting factor for testing. Table (12.2) summarizes specific tracers used for gas-phase tracer studies.

Partitioning tracers used for laboratory and field tests should have NAPL-gas partition coefficients large enough so that NAPL-gas partitioning dominates tracer retention. This minimizes consideration of competing retention processes such as interfacial gas-water partitioning, gas-bulk water partitioning, and sorption. NAPL-gas partition coefficients should also be large enough to ensure that breakthrough curves of partitioning tracers are clearly distinguishable from nonpartitioning tracers but small enough such that the length of the test remains practical. For field-scale studies, Whitley et al. (1999) suggest that retardation factors should be greater than 1.2 and less than 4. If an approximate range of NAPL saturations to be encountered is known, partitioning tracers can be selected to provide retardation factors within a desired range. Since a range of NAPL saturations is frequently unknown (indeed the purpose of testing is often to determine NAPL saturation), it is useful to use multiple partitioning tracers with different partition coefficients providing a range of potential retardation. The potential presence of a very low NAPL saturation may necessitate the use of a gas tracer having a fairly high NAPL-gas partition coefficient. When multiple partitioning tracers are used, travel-time analysis can be conducted using various pairs of partitioning tracers as well as partitioning - nonpartitioning tracers. This approach can increase the robustness of the results. Vapor transport simulations can be very useful in design of a partitioning tracer test (Deeds et al., 1999; Nelson et al., 1999). The tracer breakthrough concentrations must be in a detectable range throughout the course of the test. Simulations provide an estimate of the injected tracer mass necessary to yield these concentrations and an estimate of the duration of the test. However, despite pretest analytical or numerical simulation of breakthrough curves, proper selection of gas-phase tracers may require actual testing and retesting.

NAPL-gas partition coefficients can be directly determined by batch equilibrium partitioning tests. However, NAPL composition changes significantly during venting application resulting in spatial and temporal variation in NAPL-gas partition coefficients. VOCs will be removed from NAPL in order of their vapor pressures eventually leaving higher molecular weight lower volatility compounds as NAPL residual. Using phase equilibria theory, Deeds et al. (1999) calculated a decrease in perfluorocarbon partition coefficients ranging from 15.9 to 22.0% resulting from NAPL weathering. They state that variation in tracer gas partition coefficients can result in substantial error in NAPL saturation estimation. Thus, variation in gas-phase tracer partition coefficients as a function of NAPL weathering or composition should be assessed during batch gas-phase partitioning tracer studies.

Partitioning tracer tests typically consist of simultaneous injection of several tracers with different NAPL-fluid partition coefficients at one or more injection wells and subsequent measurement of tracer concentrations at one or more extraction or monitor wells. A number of well configurations could be used for testing. One well configuration involves the use of a single extraction well and a non-pumping or passive injection well where the passive well is used to introduce the gaseous tracer solution into the flow field created by the extraction well which is used for sampling. A second configuration involves use of a single pumping injection well and one or more monitoring wells surrounding an injection well. A third configuration involves use of a combination of pumping injection and extraction wells. If multi-level sampling devices are used during testing, a three-dimensional distribution of NAPL saturation can be developed. When partitioning tracer tests are used to assess the performance of remedial actions at NAPL-contaminated sites, initial tracer tests are conducted to establish baseline conditions followed by periodic testing throughout the time of active remediation. By virtue of sampling a much larger volume of the subsurface in comparison to soil cores, the partitioning tracer method has a much greater chance of detecting NAPL saturation. The sensitivity of the partitioning tracer method for NAPL detection is a function of the area of influence of the tracer test (swept volume), amount of NAPL in the swept volume, the NAPL-gas partition coefficient of the tracer, and constraining factors such as rate-limited mass transfer and physical heterogeneity.

During testing, mass exchange between partitioning tracers and NAPL is assumed to be instantaneous. However, this assumption is valid only when the time required for tracer diffusion within NAPL regions is short comparted to advective transport time. When a partitioning tracer initially comes in contact with NAPL, a concentration gradient exists between exterior and interior regions of the NAPL region. This causes the partitioning tracer to diffuse into interior regions of the NAPL zone. When the tracer pulse is followed by tracer-free gas, the concentration gradient reverses causing partitioning tracer movement back toward exterior regions of the NAPL zone. If the time of the tracer pulse is insufficient to allow the tracer to fully penetrate the NAPL zone prior to injection of clean gas, an inward concentration gradient will still exist in the interior of the NAPL zone. This could significantly delay recovery of a partitioning tracer to a gas extraction well and give the impression of mass loss. Recovery of a partitioning tracer gas could also be caused by failure to capture all injection well flow lines (e.g., escape of tracer gas to the atmosphere). However, analysis of mass recovery of conservative tracers correct for this possibility.

Measured residual saturation values may underestimate true saturation values because of bypass flow (gas flow around a NAPL zone due to reduced relative permeability), rate-limited mass transfer, and mass loss. Thus, residual NAPL saturation values obtained with partitioning tracer tests are, at least initially, considered underestimates of actual values. When interpreting results of partitioning tracer tests, it is important to realize that residual saturation values represent “global” or average values within a tested domain. A small localized mass of NAPL could have a small impact on retardation as measured at an extraction well and thus the signal from this mass could be lost in normal noise associated with field data. This effect though can be

Table 12.2. Summary of tracers used for vadose zone partitioning tracer studies

Tracer	Use	Investigators
methane (CH_4)	conservative	Deeds et al. (1999), Mariner et al. (1999), Nelson et al. (1999)
argon	conservative	Whitley et al. (1999)
sulfur hexafluoride (SF_6)	conservative	Mariner et al. (1999)
trifluoromethane (CF_3)	NAPL-gas	Whitley et al. (1999)
carbon tetrafluoride (CF_4)	NAPL-gas	Whitley et al. (1999)
difluoromethane (CF_2H_2)	gas-water/ NAPL-gas	Mariner et al. (1999)
bromochlorodifluoromethane ($CBrClF_2$)	gas-water	Nelson et al. (1999)
dibromodifluoromethane (CBr_2F_2)	gas-water	Nelson et al. (1999)
hexafluoroethane (C_2F_6)	NAPL-gas	Whitley et al. (1999)
octafluoropropane (C_3F_8)	NAPL-gas	Whitley et al. (1999)
octafluorocyclobutane (C_4F_8)	NAPL-gas	Mariner et al. (1999), Whitley et al. (1999)
dodecafluorodimethylcyclobutane (C_6F_{12})	NAPL-gas	Mariner et al. (1999), Whitley et al. (1999)
perfluoromethylcyclohexane (C_7F_{14})	NAPL-gas	Deeds et al. (1999)
perfluoro-1,3-dimethylcyclohexane (C_8F_{16})	NAPL-gas	Deeds et al. (1999), Mariner et al. (1999), Whitley et al. (1999)
perfluoro-1,3,5-trimethylcyclohexane (C_9F_{18})	NAPL-gas	Deeds et al. (1999), Mariner et al. (1999), Whitley et al. (1999)
perfluorodecalin ($C_{10}F_{18}$)	NAPL-gas	Deeds et al. (1999)

minimized by using closely spaced wells where the swept volume is small. Another complicating effect in tracer test evaluation is variable flow conditions. For instance Cain et al. (2000) noted that variation in ground-water elevation and flow caused considerable variation in tracer test results since different NAPL regions were accessed for different hydrodynamic situations.

12.7 Soil Sample Collection, Storage, and Analysis

Effective June 13, 1997, EPA limited use of SW-846, Method 5030 to water samples and methanol extracts of solids (e.g., soils, sediments, and solid waster) samples. EPA established Method 5035 to provide an alternative to Method 5030 for low level (< 200 ug/kg) soil analysis and to incorporate chemical preservation and sample storage techniques to limit volatilization and biodegradation of organic compounds during sample storage and handling of both low and high concentration ($\geq$200 ug/kg) samples. Method 5035 can be used in conjunction with any appropriate gas chromatography (GC) procedure, including, but not limited to Methods 8015 (GC/FID), 8021 (GC/PID), and 8260.

For low concentration samples, 1 gram of sodium bisulfate and 5 ml of organic-free reagent water are added to glass sample 40-ml vials prior to sample collection to form an acid solution (pH $\leq$ 2) thereby reducing or preventing biodegradation during sample storage. Sodium bisulfate should not be used however if a sample contains high levels of carbonates which may result in sample effervescence and subsequent loss of VOCs. A clean magnetic stirring bar is also added to each vial as a means of stirring the sample unless sonication or another mechanical means is to be used. A sample (approximately 5 g) is then placed in a vial, sealed with a septum lined screw-cap, and stored at 4°C until analysis. Several techniques can be used to transfer a sample to the relatively narrow opening of the low concentration sample vial. These include devices such as the EnCore™ sampler, the Purge-and-Trap Soil Sampler™, or a cut plastic syringe. At the laboratory, the entire vial is placed unopened into a closed-system purge-and-trap system. Immediately before analysis, organic-free reagent water, surrogates, and internal standards are added without opening the sample vial. The vial containing the sample is then heated to 40°C and the VOCs are purged using an inert gas into a trap. When purging is complete, the trap is heated and backflushed with helium to desorbed the trapped sample components into a GC for analysis using the appropriate method. for analysis. Since the sample is never exposed to the atmosphere after sampling, losses of VOCs during sample transport, handling, and analysis is considered negligible. Since samples can be contaminated by diffusion of VOCs (particularly methylene chloride and fluorocarbons) through the septum seal of a sample vial during shipment and storage, a trip blank containing organic-free reagent water should be carried through sampling, handling, and storage protocols to serve as a check on contamination.

In Method 5035, there is an option to preserve high concentration samples in the field with an organic solvent. In the procedure, 10-ml of the organic solvent is added to 40-ml vials prior to sample collection. If the sample is oil-free, a water-miscible solvent such as methanol or polyethylene glycol or (PEG) can be used. If the sample contains oil, a water immiscible solvent such as hexadecane can be used if the oil is insoluble in a water miscible solvent (e.g., methanol, PEG). In the laboratory, an aliquot from the vial is introduced into the GC system. If the vial contains oily waste or soil, Method 5030 is used if the oil is soluble in a water-miscible solvent and Method 3585 is used if the oil is soluble in a water-immiscible solvent. If the solubility of the oil in water miscible or immiscible solvents is unknown, the sample should be stored without

the use of any solvents. If the oil is insoluble in methanol, PEG, and hexadecane, the use of other solvents should be investigated. In any event, the sample should be stored at 4°C prior to analysis.

There are two problems however associated with use of methanol as a preservative though. First, the use of methanol introduces a significant dilution factor that raise the method quantitation limit. The exact dilution factor depends on the masses of solvent and sample, but generally exceeds 1000. Thus, when low sample concentrations are suspected, duplicate samples should be collected for use of the low concentration preservation technique in addition to methanol preservation. The second problem is that addition of methanol is likely to cause the sample to fail the ignitability characteristic test.

Studies conducted by Liikala et al. (1996) and Siegrist and Jennsen (1990) have demonstrated conclusively that volatilization during soil sample collection, handling, and storage imparts a significant negative bias on VOC analytical results and that this bias can be minimized by sample preservation in methanol. Liikala et al. (1996) demonstrated that some VOC loss can occur even in soil samples preserved with methanol. Liikala et al. (1996) spiked 10 ml of methanol contained in 40-ml amber vials with bromochloromethane, chloroform, carbon tetrachloride, m-dichlorobenzene, trichloroethylene, 1,2-dibromomethane, 1,1,2,2-tetrachloroethane, and 1,2-dibromo-3-chloropropane. A number of vials were kept refrigerated at 4°C in the laboratory for 82 days while other vials were transported on ice to a field site where 2.5 to 9.0 g of soil was added to vials. These vials were then stored at 4°C for 82 days prior to analysis. Mean recoveries from vials containing methanol stored in the laboratory ranged from 80.7% for choroform to 88.0% for bromochloromethane. Mean recoveries from vials containing methanol transported to the field ranged from 74.0% for trichloroethylene to 80.3% for bromochloromethane.

Liikala et al. (1996) assessed the commonly used bulk storage method (minimal headspace) with methanol preservation for 50 soil sample pairs at a site contaminated by chlorinated and petroleum solvents. For bulk storage, subsamples were collected using stainless steel trowels and tightly packed into 4-oz wide mouth jars with Teflon-lined screw-top lids. For methanol preservation, 3.67 to 11.4 grams of soil were placed in 40-ml amber vials containing 10 ml of purge-and-trap grade methanol. All samples were stored on ice. For the bulk method analysis, 15g aliquot of soil sample was placed into a purge vessel. Five ml of laboratory grade organic free water was then transferred to the vessel, heated to 40°C, and purged with ultra-high-purity helium. Tenax traps were then desorbed at 225°C for 4 minutes with the sample transferred to a gas chromatograph. In the methanol method of analysis, a 2.5-ml aliquot was removed from the 40-ml vial, placed into a 50-ml flask, and diluted to 50-ml with boiled Milli-Q water. A second VOA vial was then filled to zero headspace and used for direct injection into a purge-and-trap system similar to the bulk storage method. Analysis revealed that benzene concentrations using methanol storage were 1-2 orders of magnitude greater than the bulk storage method for 26 of 34 sample pairs. Toluene concentrations using methanol storage were 1-3 orders of magnitude greater than bulk storage for 29 of 43 sample pairs. Ethylbenzene

concentrations using methanol storage were 1 order of magnitude greater than bulk storage for only 7 of 40 sample pairs. Concentrations of m+p-xylene using methanol storage were 1-2 orders of magnitude greater than bulk storage for 18 of 41 samples. Finally, concentrations of o-xylene using the methanol method were 1-2 orders of magnitude greater than bulk storage for only 8 of 41 samples. Liikala et al. (1996) state that considering that vapor pressures at 20C for benzene, toluene, ethylbenzene, and m,o,p-xylene are 76, 22,7, and 5 mmHg respectively, it is likely that losses occurred from volatilization during sample transport, storage, and handling .

Siegrist and Jenssen (1990) compared VOC retention from five soil sample collection and storage methods:

(1) undisturbed samples in glass bottles with high headspace (1.5 cm i.d., 10 cm long core extruded directly into a Teflon-sealed, 128 ml glass bottle with headspace volume about 85% of container volume),

(2) undisturbed samples in glass bottles with low headspace (3.0 cm i.d., 10 cm long core extruded into a Teflon-sealed, 128 ml glass bottle with headspace volume about 40% of container volume),

(3) undisturbed samples immersed in methanol in glass bottles (3.0 cm i.d., 10 cm long cores extruded into a Teflon-sealed, 300 ml glass bottle with 100 ml reagent grade methanol and headspace volume about 40% of container volume),

(4) disturbed samples in glass bottles with low headspace (3.0 cm i.d., 10 cm long cores emptied in 7 - 10 aliquots with a stainless steel spoon and deposited in a Teflon-sealed 128 ml glass bottle with a headspace volume about 40% of container volume),

(5) disturbed samples in empty plastic bags with low headspace (40 ml soil sample emptied in 7 - 10 aliquots with a stainless steel spoon and deposited into a 500 ml laboratory-grade plastic bag with zip closure and a headspace volume about 40% of container volume).

With the exception of methanol containing samples, VOC analyses of soil samples involved extracting a 10 g of sample with 10 ml of 2-propanol and 4 ml pentane and then extracting it again with 5 ml of 2-propanol and 4 ml pentane prior to GC injection. VOC analyses of soil samples containing methanol involved removing a 4 ml aliquot of methanol from the sample vial followed by addition of 2 ml water and 2 ml pentane. The pentane extract was removed and the procedure repeated. The two pentane extracts were then combined prior to GC injection.

The undisturbed soil samples preserved with methanol consistency yielded the highest VOC concentrations. Negative bias was greatest for lack of methanol immersion (up to 81%), followed by headspace volume (up to 17%), soil disturbance (up to 15%). Negative bias for sample storage in plastic bags was greatest (up to 100%). In general, sampling bias declined with

increasing sorption affinity and lower Henry's Law constant. Siegrist and Jenssen (1990) state that the principal mechanism underlying negative bias for compounds evaluated (methylene chloride, 1,2-dichloroethane, 1,1,1-trichloroethane, trichloroethylene, toluene, and chlorobenzene) was likely volatilization. They state further that analyses of VOCs in soils having relatively low sorption affinity, particularly where concentrations are anticipated in the range of cleanup action levels, may require collection of undisturbed samples with infield immersion in methanol.

12.8 Conclusions

Research on development of field-scale methods to elucidate and quantify rate-limited vapor transport is needed to allow stakeholders at particular sites to make informed decisions on modification of design, operation, and eventual closure. At present, it is difficult to even ascertain whether vapor transport is occurring in the field let alone attempt to elucidate and quantify the process. Under rate-limited conditions, mass removal is dictated by kinetic rate constants which are for the most part unknown at venting sites. However, if design and implementation factors can be eliminated as major contributing causes of reduced mass flux and extensive vapor concentration tailing, it is possible that mass removal is constrained by rate-limited vapor transport.

Given discussion in this section, the following recommendations can be provided for VOC monitoring of venting sites.

1. Flow and total vapor concentration monitoring using a PID or FID or other suitable instrument should be performed at the vapor treatment or blower inlet because it provides an estimate of VOC mass removal rate and total VOC mass removed as a function of time for an entire venting system.

2. Flow and vapor concentration monitoring using a PID or FID or other suitable instrument should be performed at individual gas extraction wellheads to determine the most heavily contaminated portions of a site requiring perhaps the most monitoring, and to enable potential optimization of the vapor treatment system (e..g., prioritization of venting operation at highly contaminated areas, vapor stream richness or leanness for catalytic oxidation unit overheating or supplemental fuel requirement).

3. When utilizing an FID or PID for VOC screening, the user must be aware of fundamental differences in detector operation, ionization potential of target compounds, and gas matrix effects. The high ionization potential of many common VOCs will result in nondetection using a conventional 10.6 or even a 11.7 eV PID lamp. The high halogen content of many common VOCs will result in underestimation or nondetection of VOCs using an FID. Gas matrix effects such as humidity, carbon dioxide, and alkane (especially methane) dramatically decrease PID response. Gas matrix effects combine in a nonlinear manner resulting in a decreased PID response far greater than what would be

expected from additive effects. PIDs are also much more prone to nonlinearly in response compared to FIDs. Gas matrix and linearity problems however can be overcome through the use of serial dilution techniques.

4. Observation of evaporation fronts in individual extraction well effluent gas and evaporation/condensation fronts in well-placed vapor probe clusters could potentially provide valuable information on the progress of venting remediation of NAPL contaminated soils. Under equilibrium conditions, individual components of a NAPL propagate through soil in a sequence of evaporation-condensation fronts at speeds proportional to their vapor pressure. Evaporation-condensation fronts have likely not been reported during field application because of nonuniform gas flow (bypass flow as opposed to through-flow conditions, fully three-dimensional flow as opposed to one-dimensional or radial flow, spatial variability of NAPL distribution, common monitoring practices (determination of total VOC with a PID or FID as opposed to identification and quantification of individual compounds), and rate-limited transport. Under equilibrium conditions in the field, sharp evaporation-condensation fronts are not likely to be discernable but the vapor concentration of lighter components should decrease monotonically with time compared to heavier components which should increase for some time and then decrease. In contrast, under rate-limited transport conditions, extensive extensive effluent tailing should be observed with vapor concentrations profiles remaining fairly similar. Thus, use of GC/MS monitoring in gas extraction well and vapor probe clusters may reveal patterns of component removal from NAPL, NAPL removal itself, and rate-limited vapor transport.

5. There is no way to directly relate observation of an asymptote to an environmental benefit and little potential to ensure consistency in decision making. Vapor concentration of an asymptote at a highly contaminated site may be much higher than at a lesser contaminated site leading perhaps to less stringent remediation at the highly contaminated site.

6. Observation of an effluent asymptote may be related to venting design (e.g., well screening and spacing) or gas flow patterns separate or in addition to rate-limited vapor transport. Since both design considerations and rate-limited vapor transport can cause extensive effluent tailing and ineffectual removal of accessible contaminant mass, it is critical to first rigorously assess venting design, implementation, and associated monitoring prior to concluding that rate-limited vapor transport significantly constrains mass removal.

7. An asymptote can be observed in gas extraction wells while much of the contaminant mass remains in soils. Observation of low asymptotic vapor concentrations in effluent gas is not a sufficient condition to demonstrate progress in mass removal from contaminated soils.

8. Different mass retention and rate coefficients can produce very similar effluent curves

suggesting that effluent and vapor probe concentration data can not be used to estimate mass transport coefficients and VOC concentration in the aqueous and solids phase. Thus, effluent and vapor probe concentration data is insufficient to quantitatively assess the progress of soil venting remediation.

9. Some indicators of rate-limited transport in the field may be decreased vapor concentration with increased pore-gas velocity (flow variation) and extensive vapor concentration tailing accompanied by vapor rebound after cessation of operation (flow interruption). In both NAPL and non-NAPL contaminated soils, flow variation provides a simple yet powerful test of the validity of local equilibrium. For NAPL contaminated soils however, results of flow interruption results can be confusing if the propagation of evaporation-condensation fronts are not considered.

10. One potential use of flow interruption or rebound data is to use vapor concentrations and partition coefficients to estimate total soil concentration. However, there is presently so much uncertainty and error inherent in estimation that calculations can at best only provide qualitative insight into soil concentration levels.

13. ASSESSMENT OF RATE-LIMITED VAPOR TRANSPORT WITH DIFFUSION MODELING

After venting has been applied at a site for some time and VOCs in gas extraction wells and vapor probes approach low levels, soil samples are often collected to evaluate actual concentration reduction in soils. Lithologic examination of cores and sample analysis often reveals much higher levels of VOCs remaining in lenses of fine-grained material compared to surrounding coarser-grained material. This observation likely indicates that mass removal from fine-grained material is diffusion limited. It stands to reason then that the material properties of these lenses (e.g., diffusion path length, moisture content, organic carbon content) will eventually dictate venting performance. Thus, information collected during soil core collection should be used in some quantitative manner.

From previous discussions, it appears that well conceived field-scale tests and fairly sophisticated data analysis will be necessary to elucidate and quantify rate-limited mass exchange processes during venting. These tests however require an investment in research and time for development. One obvious method of data analysis of soil cores is to conduct diffusion modeling to assess time for mass removal under current operating conditions. While soil core collection will likely not reveal the lateral extent or geometry of the fine-grained lense, other properties required for modeling such as the thickness, moisture content, and organic carbon content of the lense are readily available from field observation and sample analysis. The purpose then of this section is demonstrate this concept at an actual site.

13.1 Model Formulation

Since lenses of fine-grained material often exhibit a plate-like structure, it would appear inappropriate to conduct diffusion modeling in spherical coordinates. Since the lateral extent and actual geometric shape of a lense is typically unknown, an assumption will be made that the lense extends infinitely thereby enabling the use of one-dimensional modeling. The governing equation describing one-dimensional diffusion is given as:

$$\frac{\partial C_T}{\partial t} = k \frac{\partial^2 C_T}{\partial x^2} \tag{13.1}$$

where C_T = total soil concentration [ML^{-3}] and k = effective diffusion coefficient [L^2T^{-1}]. The initial condition describing soil concentration as a function of depth in the lense is given by

$$C_T(x,0) = f(x) \tag{13.2}$$

where f(x) is the initial total soil concentration distribution [ML^{-3}]. Upper and lower boundary conditions must now be specified. Since only vapor concentration will be known outside the modeled domain, it would appear that first-type, time-dependent boundary conditions are

appropriate for the upper and lower domains. The assumption is made here that these concentrations are equivalent. Upper and lower boundary conditions then are expressed by

$$C_T\left(0,t\right)=g\left(t\right) \tag{13.3}$$

$$C_T\left(L,t\right)=g\left(t\right) \tag{13.4}$$

where: L = diffusive path length [L], and g(t) = soil concentration at boundaries as a function of time [ML^{-3}]. The effective diffusion coefficient k can be defined by:

$$k=\frac{\tau_g D_g+\tau_w D_w}{H\theta_g+\theta_w+K_d\rho_b} \tag{13.5}$$

From equation (13.5), is assumed that NAPL is absent.

A solution to equation (13.1) with initial and boundary conditions (13.2) through (13.4) is found in Carslaw and Jaeger (1959), p. 104

$$C_T\left(x,t\right)=\frac{2}{L}\sum_{n=1}^{\infty}e^{-kn^2\pi^2t/L^2}\sin\left(\frac{n\pi x}{L}\right)\left[\int_0^L f\left(x'\right)\sin\left(\frac{n\pi x'}{L}\right)dx'+n\left(1-\left(-1\right)^n\right)\frac{\pi k}{L}\int_0^t e^{kn^2\pi^2t'/L^2}g\left(t'\right)dt'\right] \tag{13.6}$$

The expression for f(x') can be integrated in j partitions where:

$$\int_0^L f\left(x'\right)\sin\left(\frac{n\pi x'}{L}\right)dx'=\frac{L}{n\pi}\left[f_1+\sum_{i=1}^{j-1}\left(f_{i+1}-f_i\right)\cos\left(\frac{x_i n\pi}{L}\right)+\left(-1\right)^{n+1}f_j\right] \tag{13.7}$$

An average matrix concentration is useful for comparison as a function of time. Integration of (13.6) with respect to x from 0 to L, followed by dividing by L leads to:

$$C_{T(avg)}\left(t\right)=\frac{2}{\pi L}\sum_{n=1}^{\infty}\left(\frac{1-\left(-1\right)^n}{n}\right)\left[e^{-kn^2\pi^2t/L^2}\int_0^L f\left(x'\right)\sin\left(\frac{n\pi x'}{L}\right)dx'+\left(1-\left(-1\right)^n\right)\frac{n\pi k}{L}\int_0^t e^{-kn^2\pi^2/L^2\left(t-t'\right)}g\left(t'\right)dt'\right] \tag{13.8}$$

A FORTRAN program written to implement equation (13.8) is given in Appendix G.

13.2 Site Description

Soil cores collected and analyzed by a remedial contractor (Earth Tech, 1997) near Building 763 of Norton AFB in California were used for diffusion modeling. Building 763 was used for aircraft maintenance for over 50 years. Information for diffusion modeling was extracted from borehole CB-1 where a silty clay unit was found between 38.0 and 40.5 feet bgs. Gravelly, silty sandy soils above and clayey, sandy, silty soils below this unit contained trichloroethylene (TCE) concentrations near the detection limit (2 ug/kg) while as illustrated in Figure 13.1, the silty clay unit contained concentrations ranging from 1300 to 6100 ug/kg TCE. Figure 13.1 provides the initial condition for modeling purposes. This suggested that vapor transport was limited by diffusion from the silty clay lense to surrounding soils of higher permeability. The current cleanup standard for TCE contaminated soil prescribed in the Record of Decision (ROD) was 5 ug/l TCE concentration in leachate as determined using the Toxic Characteristics Leaching Procedure (TCLP) by EPA Method 1311/8240. Using soil property information collected during soil collection (95% water saturation, porosity = 38%, organic carbon content = 0.68%) and literature values for chemical properties (dimensionless Henry's law constant = 0.38, organic carbon - water partition coefficient = 126 cm^3/g), this is equivalent to approximately 10 ug/kg which was the goal set for modeling.

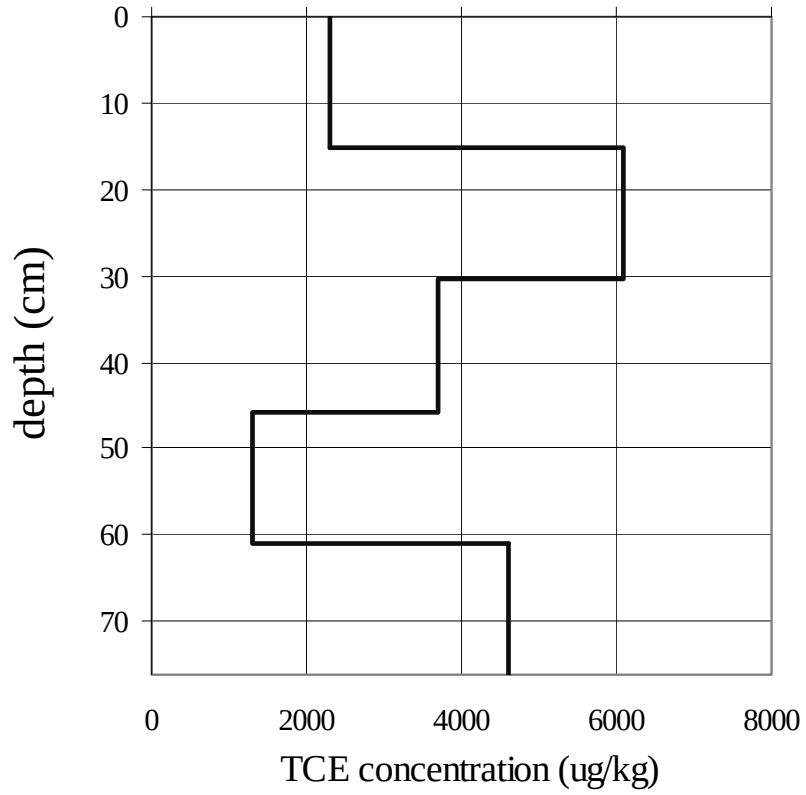

Figure 13.1 Concentration (dry wt.) profile in clay lense.

The boundary conditions require knowledge of vapor concentration at the top and bottom of the clay lense as a function of time. As illustrated in Figure 13.2, the decrease in vapor concentration at the extraction well during the period of operation can be adequately described by a simple analytical expression. This expression can then be used to estimate future effluent vapor concentrations at the well if venting were to continue indefinitely. Vapor concentrations at the well were then used to estimate vapor concentrations at the top and bottom of the clay lense although it was preferable to have actual vapor concentration data as a function of time near the soils being simulated. Unfortunately, this information was not available. Table 13.1 summarizes site-specific input data used for simulation. For soil-air and soil-water tortuosity estimates, we use a theoretically based model derived by Millington and Quirk (1961).

13.3 Results and Discussion

Figure 13.3 illustrates the average concentration of TCE in the clay lense as a function of time and four moisture saturations. At the moisture saturation at the time of sampling (95%), in excess of 80 years would be required to reach a concentration of 10 ug/kg because the high moisture content results in a very low effective diffusion coefficient. This level is reached in just 15 years when saturation is reduced to 86% because of the nonlinear effect of the diffusion coefficient on soil concentration. However, a water saturation of 95% is expected to remain constant in the clay lense. Water saturation was varied in the model simulations to illustrate the sensitivity of moisture content.

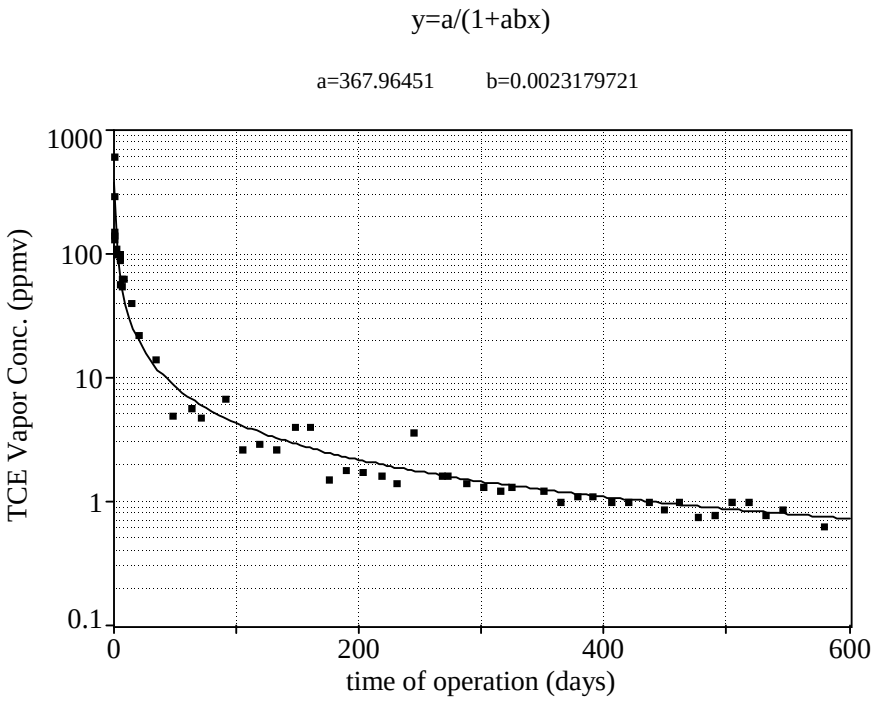

Figure 13.2 Best fit line of TCE vapor concentration profile as a function of time at the gas extraction well.

Table 13.1 Input for diffusion modeling

	Description	Value	Units
θ_g	volumetric air content	varies	cm^3_{air}/cm^3_{soil}
θ_w	volumetric water content	varies	cm^3_{water}/cm^3_{soil}
ϕ	porosity	0.38	cm^3_{pore}/cm^3_{soil}
ρ_b	bulk density	1.68	g_{solids}/cm^3_{soil}
H	Henry's Law Constant for TCE	0.38	$(ug/cm^3_{air})/(ug/cm^3_{water})$
K_d	soil-water partition coeff.	0.857*	$(ug/g_{solids})/(ug/cm^3_{water})$
D_g	free air diffusion coeff. for TCE	6366.8	cm^2/d
D_w	free water diffusion coeff. for TCE	0.804	cm^2/d

*Estimated by $K_d = K_{oc} * f_{oc}$ where $f_{oc} = 0.0068$, $K_{oc} = 126$ cm3/g

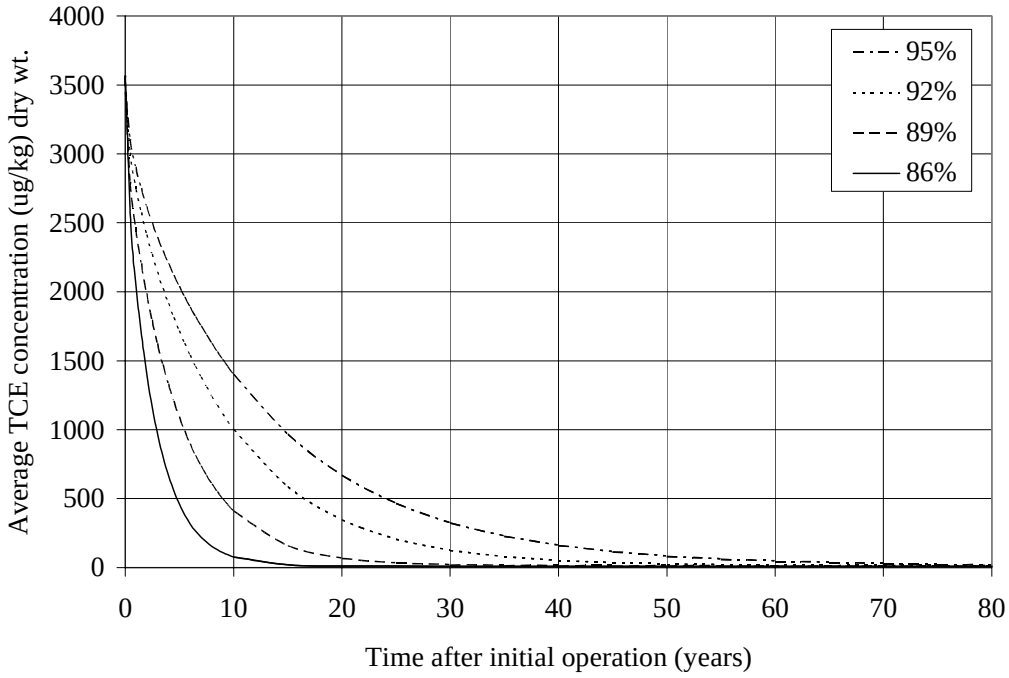

Figure 13.3. Simulated average TCE concentration in clay lense as a function of time and moisture content.

Vadose zone VOC transport simulations conducted by the remedial contractor indicated that mass flux of remaining TCE in soils to ground water would be insignificant. For a well characterized, designed, and monitored SVE system where contaminant mass flux to ground-water will be insignificant, it may be difficult to justify prolonged venting operation to meet a 10 ug/kg TCE concentration level. Thus, simulations conducted here support venting closure at this site.

13.4 Conclusions

Diffusion modeling provides a simple yet powerful way of assessing rate-limited vapor transport from discrete lenses of low permeability. Diffusion modeling could be extended to two- or three-dimensions for more sophisticated analysis if assumptions on the geometric shape of lenses are made.

14. USE OF RESPIRATION TESTING TO MONITOR SUBSURFACE AEROBIC ACTIVITY

During its initial use, venting was applied primarily to enhance volatilization of organic compounds from unsaturated consolidated and unconsolidated geologic media. However, large-scale tank experiments conducted by Texas Research Institute (TRI) (1980, 1984) demonstrated that biodegradation could be a major mass removal mechanism for compounds which biodegrade under aerobic conditions. In their studies, TRI (1980, 1984) indicated that biodegradation may have accounted for as much as 38% of the mass removal of gasoline from vented soils. Field-scale studies suggest that subsurface air circulation can indeed enhance aerobic biodegradation of fuel oils and other aerobically biodegradable compound mixtures in oxygen deficient soils. Subsurface advection of air allows rapid exchange of oxygen from the atmosphere as opposed to gaseous diffusion which dominates in non-vented soils.

The use of subsurface air circulation to enhance aerobic biodegradation is commonly referred to as "bioventing". Operationally, bioventing is supposed to be distinguished from "conventional" venting in that lower pore-gas velocities or pore-volume exchange rates are used for the former to minimize volatilization. For instance, Hinchee et al. (1991) state that approximately one pore volume exchange of air per day is sufficient to support biodegradation. The *U.S. Army Corps of Engineers (USACE)(1995)* state that recent field experience with full-scale systems suggests that 0.25 to 0.5 pore volumes exchanges per day may be optimal to maximize biodegradation while minimizing volatilization. However as previously discussed, rate-limited vapor transport may also require low pore-gas velocities to optimize mass removal efficiency through volatilization. Thus, bioventing is an ill-defined term when one considers that enhanced aerobic biodegradation occurs during venting whether intended or not. Bioventing should possess a definition which clearly distinguishes the technology from conventional venting. For example, the addition of methane to an air injection well to enable or enhance cometabolism of trichloroethylene represents a significant departure from conventional venting application and would logically fall within the realm of bioventing.

For removal of VOCs there is a trade-off between maximizing the rate of total hydrocarbon removal (volatilization plus biodegradation) and hydrocarbon removal primarily through biodegradation. Because volatilization is a more rapid removal mechanism than biodegradation, the application of high pore-gas velocities results in more rapid remediation. However, energy and vapor treatment costs are higher resulting in a trade-off between cost and remediation time. To properly assess this trade-off, quantification of factors affecting volatilization and biodegradation are necessary. Increased understanding of these factors may eventually lead to successful prediction of remediation time under a variety of operating conditions.

14.1 Discussion of Favorable Conditions for In-Situ Biodegradation

Enhanced aerobic biodegradation through venting application has potential in soils having: (1) organic compounds readily biodegradable under aerobic conditions; (2)

environmental conditions (e.g., nutrients, moisture, temperatuare, pH, Eh, salinity, toxicity) suitable for microbial growth; and (3) sufficient gas permeability to allow adequate air (oxygen) circulation. The rate of microbial growth or metabolism will be limited by the factor present at its minimum level.

Determination of limiting factors and practical alteration in the soil environment can enhance biodegradation during venting application. Information on the "intrinsic" aerobic biodegradability of many organic compounds and physiological tolerance limits for isolated microbial populations is available from the literature. However, since microbial interactions in a contaminated soil environment are complex, laboratory based treatability studies are sometimes conducted to evaluate the effect of various environmental variables. When treatability studies are conducted, singular or multivariable evaluations of temperature, nutrients, and moisture are common. For instance, Hinchee and Arthur (1991) evaluated the influence of moisture and nutrient addition on JP-4 contaminated soils from Hill AFB.

Laboratory microcosms possess distinct advantages over field testing. Since microcosms are replicable and their external environment is controllable, much greater statistical rigor can be achieved than is possible in the field. Ease of manipulation allows relatively straightforward evaluation relative to field studies of physical and geochemical factors affecting respiration rates and correlation to actual biodegradation. The question remains however whether these results can be extrapolated to the field. Physical and geochemical conditions in the field will differ from the laboratory environment. Also, determination of microbial activity in disturbed, displaced environmental samples incubated in the laboratory may be quantitatively and even qualitatively different from the same determination in situ.

Most field studies conducted to evaluate enhanced biodegradation during venting application have been conducted in jet fuel and gasoline contaminated soils. Most petroleum related hydrocarbons are natural substrates for microorganisms which have evolved mechanisms for their degradation. They are anthropogenic or xenobiotic only in the sense that they occur at waste sites at higher than accepted levels. For enhanced biodegradation to be feasible, an organic chemical must be inherently biodegradable under aerobic conditions. n-Alkanes constitute a significant proportion jet fuels (e.g., JP-4, JP-5, diesel fuel and gasoline. There are many references on microbial attack and the diversity of microorganisms involved in alkane metabolism. A wide range of n-alkanes are susceptible to biodegradation, however some microorganisms preferentially utilize only short chain molecules while others metabolize only longer chain structures. The initial oxidation of n-alkanes involves the incorporation of molecular oxygen, a common occurrence with all petroleum hydrocarbons. It is somewhat more difficult for microorganisms to utilize cycloalkanes as a sole source of carbon and energy, however, it is clear that individual or mixtures of microorganisms can metabolize cycloalkanes. As with n-alkanes, molecular oxygen is incorporated, but in this case in two separate steps. Branched alkanes and cycloalkanes in the C10 to C22 range are less biodegradable than n-alkanes of equivalent size. Cycloalkane biodegradation requires the presence of two or more species for complete metabolism (Dragun, 1988). Branched aliphatic hydrocarbons are generally more resistant to biodegradation than unsubstituted hydrocarbons. In general, as the number of

substitutions increase, the greater the resistance to biodegradation. Oxygen plays a critical role in the metabolism of aromatic hydrocarbons. All of the major pathways require oxygen as a coreactant. In addition, organisms catalyzing these reactions use oxygen as a terminal electron acceptor. Therefore, hydrocarbon metabolism puts a large demand on oxygen resources. Aromatic hydrocarbons can generally be used as primary substrates under aerobic conditions. In the absence of oxygen, degradation rates are slow. There is a large body of information describing the biodegradation of polyaromatic hydrocarbons (PAHs) under aerobic conditions. Most studies on PAH biodegradation indicate that low solubility of PAHs is the primary factor limiting biodegradation.

In general, biodegradability increases with water solubility. VOCs with functional groups containing nitrogen, sulfate, or oxygen typically are fairly water soluble and therefore are rapidly degraded. Low molecular weight aliphatic alcohols and ketones such as ethanol and methyl ethyl ketone (MEK) can biodegrade very rapidly in the presence of sufficient oxygen. Aromatic compounds such as toluene, ethylbenzene, and xylene biodegrade under aerobic conditions at moderate rates. Benzene, however, has been found to biodegrade at relatively slow rates.

Prior to venting, oxygen is typically depleted in soils containing high concentrations of organic compounds which biodegrade under aerobic conditions. Loss of oxygen as a metabolic electron acceptor induces a change in the activity and composition of the soil microbial population. Soil venting provides air to the vadose zone and thus carries oxygen that can be used as the terminal electron acceptor by soil microorganisms to biodegrade chemicals aerobically. Air has a much greater potential than water for delivering oxygen to soil on a weight-to-weight basis and volume-to-volume basis.

The feasibility of enhanced biodegradation at a site may largely be dependent on the ability to adequately circulate air through contaminated soils. Clayey soils pose a challenge in that gas permeability can be very low due to low intrinsic permeability and high moisture content. In these types of soils, diffusion may control VOC and oxygen transport. However, high oxygen concentrations in more permeable soils provide a large driving force for diffusion.

Soil water serves as the transport medium through which many nutrients and organic chemicals diffuse to the microbial cell, and through which metabolic waste products are removed (Sorensen and Sims, 1992). Atlas and Bartha (1993) state that optimal conditions for activity of aerobic microorganisms occur between 50% to 70% of “water holding capacity”, a term which is not rigorously defined. Soil moisture should be maintained in the range of 40 to 70% of field capacity. If soils are dried excessively, microbial activity can be seriously inhibited or stopped. Because individual species are seldom eliminated in extremely wet or dry soil, the rewetting of a dry soil should reestablish microorganism activity. However, between extreme conditions (dry vs. saturated), soil moisture content should have an undramatic effect on the microbiological degradation of organic chemicals (Brown and Donnelly, 1983).

Microbial metabolism and growth is dependent upon adequate supplies of essential macro- and micronutrients. At a minimum, the following nutrients must be available in the

proper form and amount for microbial proliferation: nitrogen, phosphorus, potassium, sodium, sulfur, calcium, magnesium, iron, manganese, zinc, copper, cobalt, and molybenum (Alexander, 1977). When an organic chemical enters the soil environment, the soil's supply of essential elements is frequently inadequate to support desirable biodegradation rates (Dragun, 1988). If soils are high in carbonaceous materials and low in nitrogen and phosphorus, the soils may become depleted of available nitrogen and phosphorus (Sorensen and Sims, 1992). Microbial cells contain 5 to 15 parts of carbon to 1 part nitrogen but 10:1 is a reasonable average for aerobic microorganisms (Alexander, 1977). A carbon, nitrogen, phosphorus (C:N:P) ratio of 250:10:3 is considered optimum for biodegradation in soil but 100:10:2 has been used in some applications (Staps, 1989). In general, one unit of nitrogen assimilated into cell material is accompanied by 10 units of carbon volatilized as CO_2 (Alexander, 1977). The 100:10:2 ratio assumes that all carbon is assimilated into cell mass while the 250:10:3 ratio considers CO_2 volatilization but does not consider recycling of organic nitrogen or phosphorus. If the ratio of C:N:P is wider than approximately 300:15:1 (weight basis), supplemental nitrogen or phosphorus should be added (Alexander, 1977). Mineral nutrients are typically supplied as soluble salts. Minor nutrients are usually present in soils in sufficient amounts. The availability of nutrients to microorganisms is strongly influenced by pH. The easiest method to determine if adequate nutrients are present in soils at proper pH levels is to collect soil samples for analysis.

One method of determining the effect of nutrient addition in the field on biodegradation is monitoring increased oxygen depletion or carbon dioxide production. Hinchee and Arthur (1991) conducted bench scale studies using soils from Hill AFB and found that both moisture and nutrients became limiting after aerobic conditions were achieved. This led to the addition of moisture and nutrients in the field. Moisture addition increased oxygen deficit in extraction well offgas but nutrient addition did not. Hinchee and Ong (1992) postulate that the failure to observe increased oxygen demand after nutrient addition could be explained by a number of factors including: (1) the failure of nutrients to move vertically through the soil column (pore-water and soils were not sampled to determine if nutrients had percolated in soils to depths of interest); (2) remediation of the site was entering its final phase, and nutrient addition may have been too late to result in an observed change; and (3) nutrients simply may not have been limiting. At Tyndall AFB, Miller (1990) observed no changes in oxygen depletion or carbon dioxide production as a result of moisture and nutrient addition. However pore-water and soils were not sampled to determine if nutrients had percolated in soils to depths of interest.

While most microorganisms will tolerate a pH range of about 4 to 9, the pH range within which bioremediation processes are considered to operate most efficiently is 6 to 8. Degradation of hydrocarbons generates carbon dioxide, which may lower pH. Degradation of chlorine, sulfur, and nitrogen containing compounds generates strong acids which require buffering capacity to maintain favorable pH conditions. Soils should be analyzed for pH prior to and at the completion of venting ensure that adverse pH levels are not present.

Microbiological reactions often increase as temperature increases. The upper temperature limit is thought to be about 50°C (122°F) because essential microbial enzymes are denatured above this temperature. Soils typically exhibit diurnal and seasonal temperature variation.

Diurnal variation is less pronounced in wet soils because of the high specific heat of water. Variation decreases with distance below the surface. During field testing at Tyndall AFB, Miller (1990) observed that O_2 depletion rates were approximately twice as high at 25°C than at 18°C. He used the van Hoff-Arrhenius equation to model of temperature effects.

In many cases, oxygen consumption and degradation rates will be lower upon start-up than following a period of acclimation. After the introduction of oxygen, microorganisms will adapt to the composition and concentrations of biodegradable compounds. Acclimation times can vary from a few days to a few months. Cessation of operation for more than a few days may result in detrimental changes to microbial populations and necessitate another period of acclimation before optimum performance is achieved.

14.2 Respiration Testing

Proof of in-situ biodegradation requires demonstration that contaminant mass or concentration reduction has decreased as a direct result of microbial activity. Proof however is elusive because of difficulties in: (1) identification and enumeration of microorganisms proliferating as a result of contaminants present in soils, (2) extreme spatial variability in contaminant concentration, and (3) differentiation of concentration reduction due to abiotic and biotic processes. Since measurement of biodegradation rates on a field scale is difficult and expensive, indicators of aerobic microbial activity such as oxygen depletion and carbon dioxide production have been used to demonstrate microbial activity. At operating sites, oxygen depletion or carbon dioxide production rates are determined in vapor probes during well shut-in periods. Zero or first-order kinetic constants are subsequently determined for each probe and adjusted for a background oxygen depletion or carbon dioxide production rate from probes lying in an uncontaminated area. Hinchee and Ong (1992) and van Eyk and Vreeken (1989a,b) have observed that O_2 consumption is often a more sensitive measure of aerobic metabolism than CO_2 production because of CO_2 sinks in soil (e.g., carbonate precipitation). One exception was at Tyndall AFB where soils had low alkalinity and pH (Miller, 1990). At Fallon NAS and Eielson AFB where soils had higher alkalinity and pH, little carbon dioxide production was measured (Hinchee and Ong, 1992).

It has become common practice to use zero-order oxygen consumption rates to directly estimate hydrocarbon degradation rates. A reference compound such as benzene or hexane is typically chosen for estimation purposes. The stoichiometry for mineralization of benzene is

$$C_6H_6 + 7.5\ O_2 \rightarrow 6\ CO_2 + 3\ H_2O \quad (14.1)$$
(3.1 g O_2/g C_6H_6)

while for hexane it is

$$C_6H_{14} + 9.5\ O_2 \rightarrow 6\ CO_2 + 7\ H_2O \quad (14.2)$$
(3.5 g O_2/g C_6H_{14}).

Stoichiometric relationships allow derivation of an equivalency equation to estimated a referenced hydrocarbon degradation rate to an oxygen consumption rate

$$K_{\deg} = 10^4 \frac{\theta_g \rho_{O_2}}{\rho_b R_{O_2/C_xH_y}} K_{O_2} \qquad (14.3)$$

where K_{deg} is the reference hydrocarbon degradation rate (mg $Kg^{-1}day^{-1}$), ρ_{O2} = pure oxygen density (gcm^{-3}), R_{O2}/C_xH_y = oxygen/hydrocarbon mass ratio (g g^{-1}), and K_{O2} = oxygen consumption rate (% O_2 day^{-1}).

One obvious limitation of this method is that the reference hydrocarbon used for the stochiometric mass ratio between hydrocarbon degradation and oxygen consumption may not be representative of many compounds present at a spill or hazardous waste site. Another limitation is that field data may show first-order degradation rates while equation (14.3) requires a zero-order rate. Also, respiration tests provide estimates of total hydrocarbon degradation rates but regulatory programs, specifically Superfund and RCRA, mandate specific contaminant concentration reduction of which these tests provide little information. The greatest concern however is the error involved in using oxygen depletion rates to directly calculate hydrocarbon degradation rates. Equations (14.1) and (14.2) represent the minimum oxygen requirement to completely mineralize benzene and hexane respectively. They are based on the assumption that either there is no cell synthesis or endogenous respiration, or that cell synthesis and endogenous respiration are occurring at the same rate with no net accumulation of biomass.

Oxygen serves as a terminal electron acceptor not only in the degradation of organic matter but also in the oxidation of reduced inorganic compounds by microorganisms which obtain energy through chemical oxidation. For example, different microbial populations carry out the two steps of nitrification. In the first reaction, molecular oxygen is incorporated into the nitrite molecule. In the second step, oxygen is derived from water and molecular oxygen serves as an electron acceptor. In the presence of molecular oxygen, reduced sulfur compounds can support microbial metabolism. For instance H_2S can be converted to elemental sulfur which can subsequently be converted to H_2SO_4 or sulfate. Under neutral and alkaline conditions, ferrous iron is rapidly oxidized to ferric iron. The greenish-grey color of contaminated soils is often associated with reduced iron. Reduced Mn^{+2} is stable under aerobic conditions at pH values below 5.5 and at higher pH values under anaerobic conditions. Various soil microorganisms which catalyze manganese oxidation have been identified.

Thus, use of oxygen consumption tests to estimate biodegradation rates may result in overestimation of mass loss through biodegradation. Perhaps the best use of respiration testing is as an indicator of soil amendment (moisture, temperature, nutrients, etc.) effectiveness and of microbial activity in general. Respiration testing could be used to indicate inhibition of degradation. For instance, if oxygen and carbon dioxide monitoring reveal low oxygen consumption and carbon dioxide generation in soils containing high concentrations of readily biodegradable compounds, further studies could be conducted to determine if biodegradation is

being limited by insufficient moisture content, toxicity (e.g. metals), or nutrients. Persistent, low oxygen levels may indicate an insufficient supply of oxygenated air at a location suggesting the need for air injection, higher extraction well vacuum, additional extraction wells, or additional soils characterization which may indicate high moisture content or the presence of immiscible fluids impeding the flow of air. Thus, respiration testing can be very useful in monitoring venting operation. Taken alone however, they do not provide proof of biodegradation and quantitative estimation of biodegradation rates. When used with other indicators of increased microbial activity or biodegradation however, respiration tests can provide one of several convergent lines of independent evidence to document biodegradation.

14.3 Site Description

Respiration testing was conducted at a field site, U.S. Coast Guard Base, Elizabeth City, North Carolina, to evaluate the use of respiration testing as a general indicator of bioremediation. In February, 1988, the U.S. Coast Guard detected a JP-4 fuel leak in a 10 cm (4 inch) diameter pipeline at its support center in Elizabeth City, North Carolina. Soils and ground water were subsequently contaminated by JP-4 constituents over an area of approximately 1200 square meters.

Surficial soils at the site consisted of 1.5 m of a dark brown silty clay underlain by a medium-grained sand. Ground water, which fluctuated ± 60 cm seasonally, was located about 2 m below the soil surface in the sand. During the spring, sandy soils were completely saturated while during summer and fall, ground-water levels dropped to the point that 1.0 to 1.5 m of sandy soils were available for venting. Ground-water temperature varied seasonally from 12 to 14°C. Air injection tests were conducted to assess gas permeability and leakance. The program AIR2D (Joss and Baehr, 1997) was used for parameter estimation. Average gas permeability values were 8.22×10^{-8} cm^2 assuming isotropic conditions and leakance was estimated at 2.06×10^{-10} cm^2.

A soil venting system consisting of 42 air injection/extraction wells and 34 piezometer/vapor probe clusters was installed at the site in December, 1992. Figure 14.1 provides a plan view of 18 piezometer/vapor probe clusters (70A through 70X) used for VOC and respiration monitoring and combined benzene, toluene, ethylbenzene, and xylene (BTEX) ground-water concentrations prior to commencement of venting in January, 1993. Vapor probes were constructed from 1.3 cm diameter, 316 stainless steel pipe having a length of 7.6 cm. The pipe was manually slotted with a bandsaw and wrapped in a fine stainless steel mesh to exclude particles. Brass compression fittings were used to connect the probes to 0.64 cm o.d. flexible copper tubing which was connected at the surface to brass quick-connects. The probes were installed in coarse sand 0.33 meters below the base of the clay layer (1.3 meters below surface). The annular space above the probes was sealed with granular bentonite to 0.3 meters below surface and cement to the surface. Differential pressure was measured with magnehelic gauges. Vapor concentration was measured using a GasTech Trace-Techtor hydrocarbon analyzer calibrated to hexane. The Trace-Techor utilizes a catalytic combustion sensor to oxidize hydrocarbons and a change in electrical resistance to quantify vapor concentration. The vapor

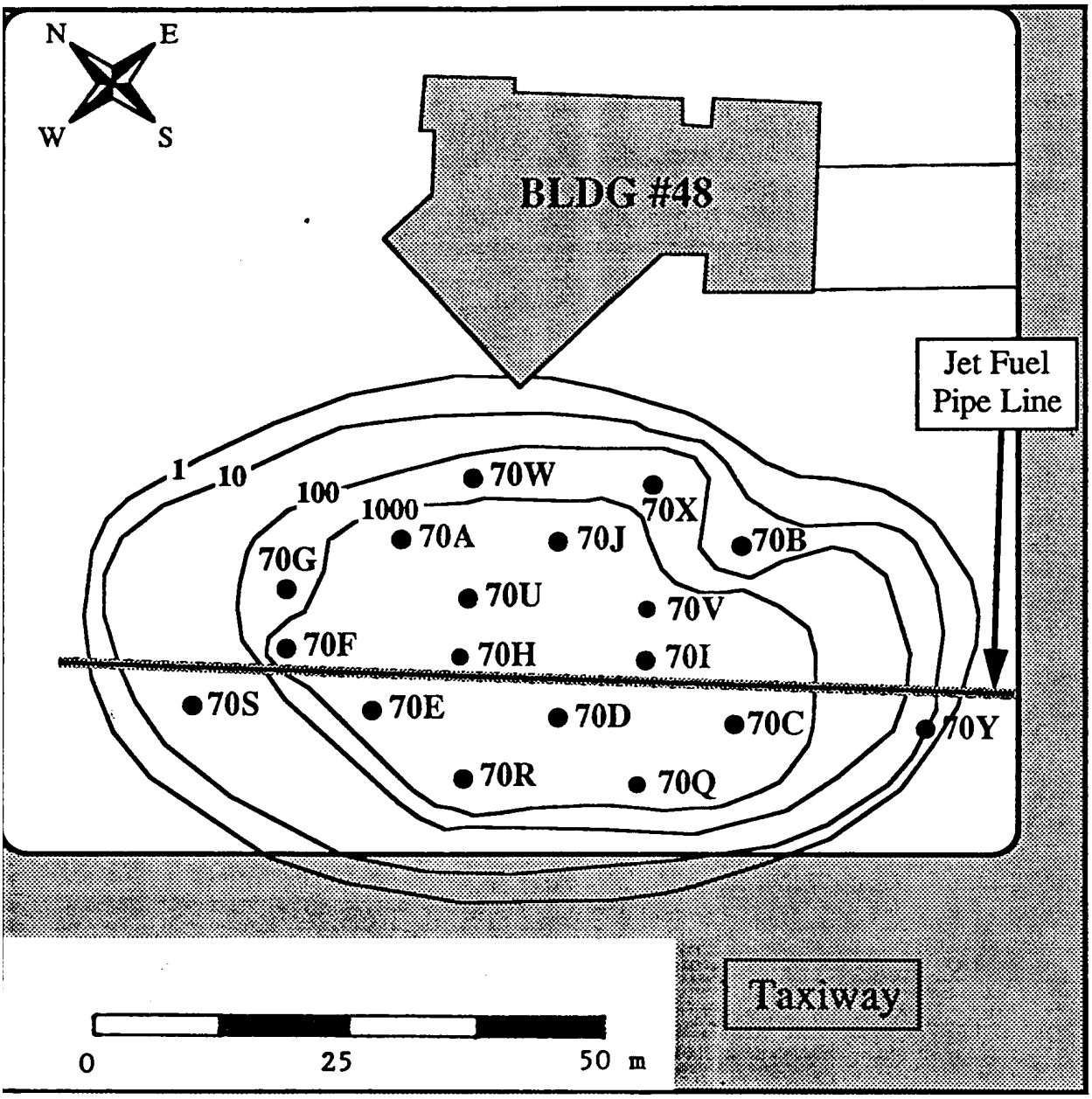

Figure 14.1 Dissolved combined benzene, toluene, ethylbenzene, and xylene (BTEX) concentrations before venting at Elizabeth City USCG Base, January, 1993.

analyzer has three settings: 0 to 100 ppmv, 0 to 1,000 ppmv, and 0 to 10,000 ppmv.

Soil sampling during installation of piezometer/vapor probe clusters was conducted to delineate the vertical extent of initial contamination. In August, 1992, 320 samples were obtained from 16 locations. Samples were collected during hollow stem augering in stainless-steel core barrels having an outside diameter and length of 5 and 120 cm respectively. Samples were preserved in 40 ml vials containing 5 ml methylene chloride and 5 ml distilled water and

analyzed for benzene, toluene, ethylbenzene, and xylene (BTEX), and total petroleum hydrocarbons (TPH). In September, 1994, after 18 months of venting operation, soils were sampled close (within 30 cm) of original sampling locations using a direct-push (Geoprobe) technique. A thin wall core barrel with a detachable piston was used to collect cores into plastic liners which were cut into 15 cm section for sampling and preservation as before. A total of 71

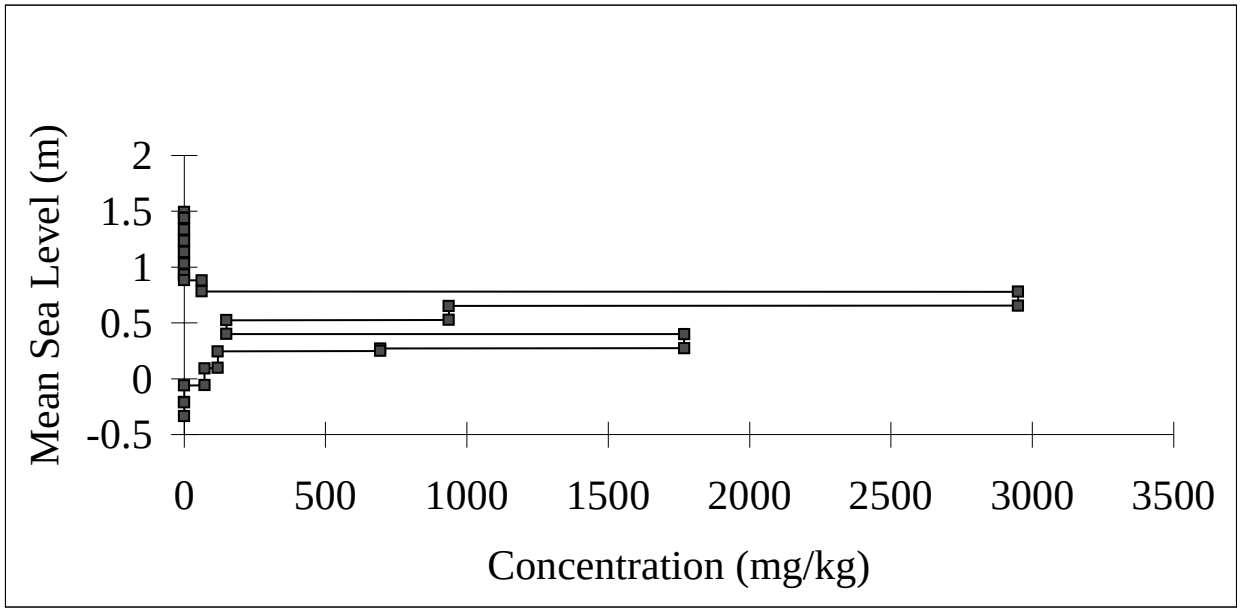

Figure 14.2 Total (wet) Petroleum Hydrocarbon (TPH) profile in 70E

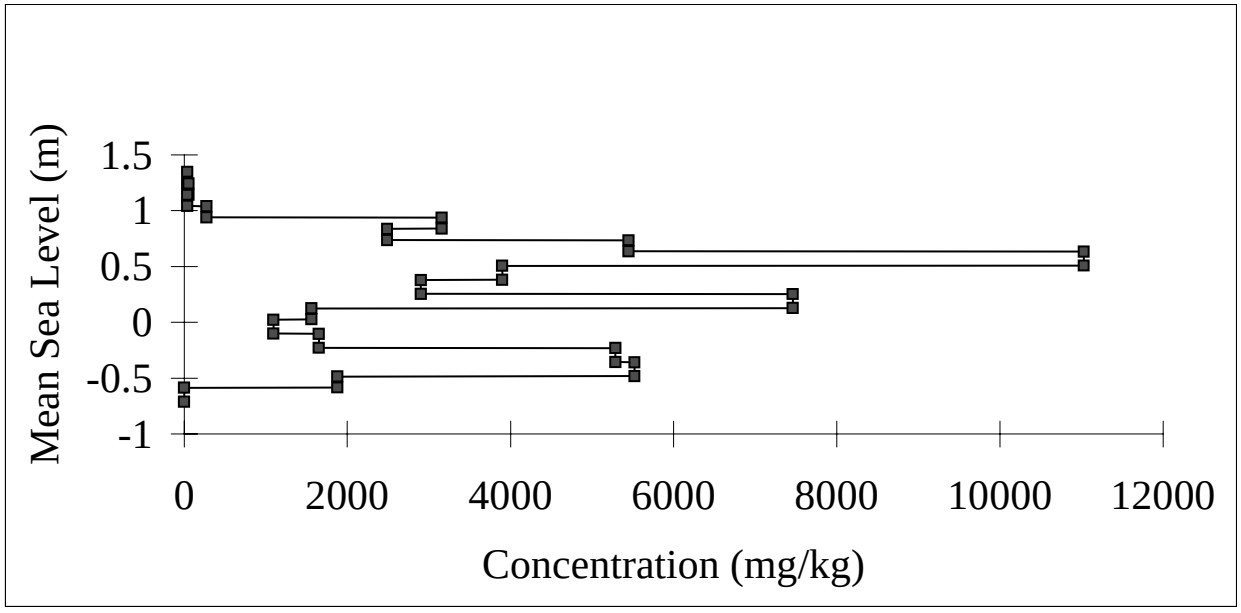

Figure 14.3 Total (wet) Petroleum Hydrocarbon (TPH) profile in 70D

samples from 8 locations were collected. Figures 14.2 and 14.3 illustrate initial vertical distribution of TPH in boreholes 70D and 70E. One meter MSL corresponds to the interface between the sand and clay. Thus, contaminated soils were generally restricted vertically between the interface of the sand and clay loam and approximately 2 m below this interface. After 7 months of operation, the first in-situ respiration or oxygen consumption test was conducted. Percent oxygen concentration was measured with a Gastech model 3252OX meter which utilizes an electrochemical cell for detection. A purge time of 5 minutes was calculated based the flow rate of the meters and volume of the probe and surrounding annulus. However, purge time was reduced to one minute since O_2 levels consistently stabilized within this time frame. Data from each oxygen depletion test was fitted to zero- and first-order kinetic relationships. For zero-order oxygen consumption kinetics:

$$\frac{dO_2}{dt} = -K_{O_2} \tag{14.4}$$

which after integration and assumption that $O_2 = O_{2o}$ at time zero equals

$$O_2 = -K_{O_2} t + O_{2_o} \tag{14.5}$$

where $O_{2o} = O_2$ concentration at time zero. For first-order kinetics:

$$\frac{dO_2}{dt} = -K^1_{O_2} O_2 \tag{14.6}$$

which after integration equals

$$\ln O_2 = -K^1_{O_2} t + C \tag{14.7}$$

or

$$O_2 = O_{2_o} e^{-K^1_{O_2} t} \tag{14.8}$$

where K^1_{O2} = a first-order oxygen consumption rate [T^{-1}]. Oxygen depletion rates were determined by linear regression to (14.5) and (14.7) and reported with associated correlation coefficients. The significance of distinguishing zero- and first-order kinetics is reflected in the formulation of (14.4) and (14.6) where oxygen depletion as a function to time is constant for the former and a function of oxygen concentration for the latter. If the oxygen depletion rate is a function of oxygen concentration, then oxygen may become a limiting factor below some concentration level above zero. Thus, observation of first-order kinetics has direct design implications. That is, oxygen levels would have to be maintained above some level to maximize aerobic microbial activity or indirectly biodegradation.

14.4 Results and Discussion

Figures (14.4) through (14.24) present the results of respiration tests while Table 14.1 provides a summary of zero- and first-order rates at each location. Rates of oxygen depletion observed at the Elizabeth City facility were very rapid compared to rates observed at Hill and Tyndall Air Force Bases which were also contaminated by JP-4 fuel oil. For comparison,

Table 14.1 Summary of zero- and first-order oxygen depletion rates at Elizabeth City USCG Base

Vapor Probe	zero-order rate ($\%O_2$/hr)	first-order rate (hr^{-1})
70A	- 0.1239	- 0.0072
70B	- 0.0434	- 0.0023
70C	- 2.0257	- 0.1780
70D	- 5.9280	----------
70E	-1.6179	- 0.1080
70F	- 0.8259	- 0.0522
70G	- 0.3432	- 0.0291
70H	- 1.7500	- 0.8570
70I	- 3.0650	- 0.6990
70J	- 1.5621	- 0.1716
70K	- 1.8664	- 0.1176
70M	- 3.6147	- 0.6456
70N	- 4.1243	----------
70P	- 2.6200	- 0.2151
70Q	- 3.3093	- 0.6216
70R	- 1.7044	- 0.1389
70S	- 0.2977	- 0.0343
70T	- 0.0128	----------
70U	- 0.6036	- 0.0547
70V	- 0.9202	- 0.0578
70X	- 0.5767	- 0.1307

consider first-order rates for oxygen consumption observed at a JP-4 spill location at Hill Air Force Base in Utah ranging from -0.000366 to -0.06 hr^{-1} where at Elizabeth City first-order rates varied from -0.00230 to -0.8570 hr^{-1}, an increase of at least one order of magnitude. At Tyndall Air Force Base, an average zero-order oxygen consumption rate of -0.24 $\%O_2$/hr was observed whereas at Elizabeth City zero-order rates varied from -0.013 to -5.93 $\%O_2$/hr.

A number of observations can be drawn from these tests. At 70A, 70B, 70G, 70S, and 70T, zero-order- and first-order oxygen depletion kinetics provide nearly identical fits to data over the tested period making it impossible to identify the governing relationship. Longer-term testing on the order of 50 to 100 hours at several of these locations would be necessary to discern trends. At locations 70C, 70I, 70J, 70M, 70P, and 70Q, oxygen depletion kinetics could follow either zero- or first-order kinetics depending on the time at which time zero concentration was first achieved. The zero concentration data point was not used for linear regression in these plots because zero concentration may have been maintained for some time prior to measurement. Thus, again the governing relationship was indeterminate. At locations 70E, 70F, 70H, 70K, 70R, 70U, and 70V it appears likely that oxygen depletion kinetics did not follow first-order kinetics. Since the time to zero concentration may have occurred near the x-axis intercept, it appears possible that oxygen depletion kinetics followed zero-order kinetics. At locations 70D and 70N, it appears that oxygen depletion did follow zero-order kinetics. Lack of data at intermediate times precluded determination of oxygen depletion kinetics at 70X.

Given the previous discussion, it is evident that one of the goals of this investigation, discernment of zero- and first-order oxygen depletion kinetics, was not achieved due to too few data points at critical times. Unfortunately, this situation could not be addressed during subsequent site visits as site accessibility became limited. Oxygen depletion tests did however demonstrate fairly intense aerobic activity in highly contaminated areas compared to areas with lesser contamination. For instance, at locations such as 70D and 70I, zero-order oxygen depletion rates of -5.93 and -3.07 $\%O_2$/hr were observed respectively while at 70B and 70T, zero-order oxygen depletion rates of only -0.04 and -0.01 $\%O_2$/hr were observed respectively. In the portion of the site encompassed by high oxygen depletion rates (70D, 70N, 70M, 70P, 70R, and 70Q), free LNAPL was observed in piezometers. Thus, as demonstrated here, respiration tests can provide an inexpensive and rapid means of assessing in-situ aerobic metabolic activity. From a soil venting monitoring perspective, respiration testing should be conducted periodically to assess change in oxygen depletion rates. As remediation progresses, oxygen depletion rates would be expected to decrease over time, eventually in some cases approaching background conditions.

Finally, figures 14.25 and 14.26 illustrate the vertical distribution of benzene and TPH respectively collected during installation of 70D and within 30 cm of 70D after 18 months of venting. Sample comparison reveals that volatile BTEX compounds had been removed to very low concentrations but higher molecular weight and lower volatility compounds remained at fairly high concentrations. This situation is common at venting sites, where lower volatility and more biologically recalcitrant compounds remain or only slowly dissipate in concentration. The fundamental question here is whether the remaining compounds pose an environmental risk.

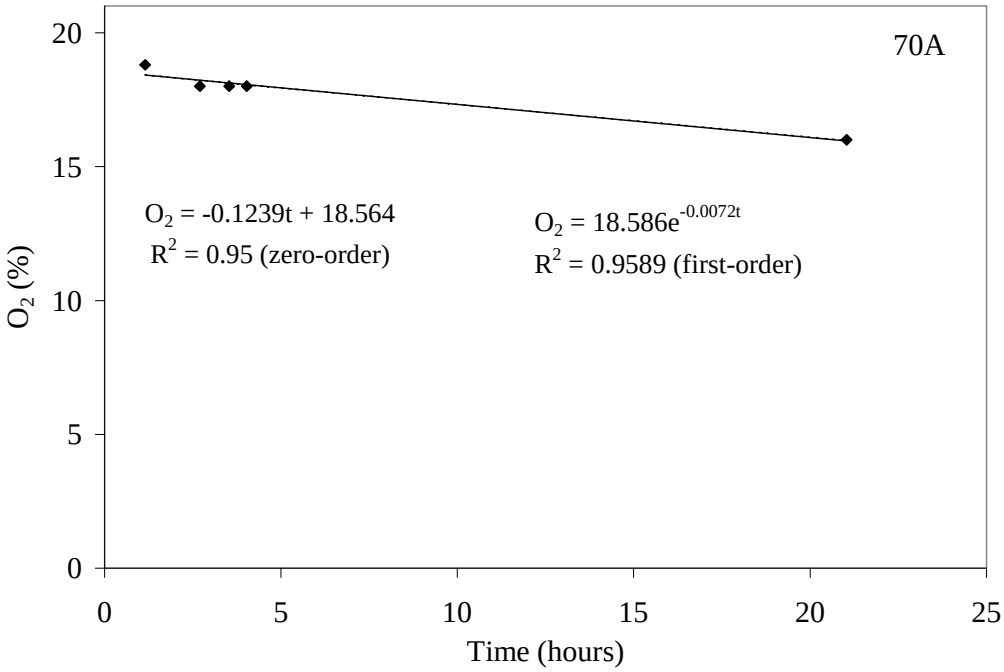

Figure 14.4 Oxygen depletion test at vapor probe 70A. Solid and dashed lines denote linear regression for zero- and first-order kinetics respectively.

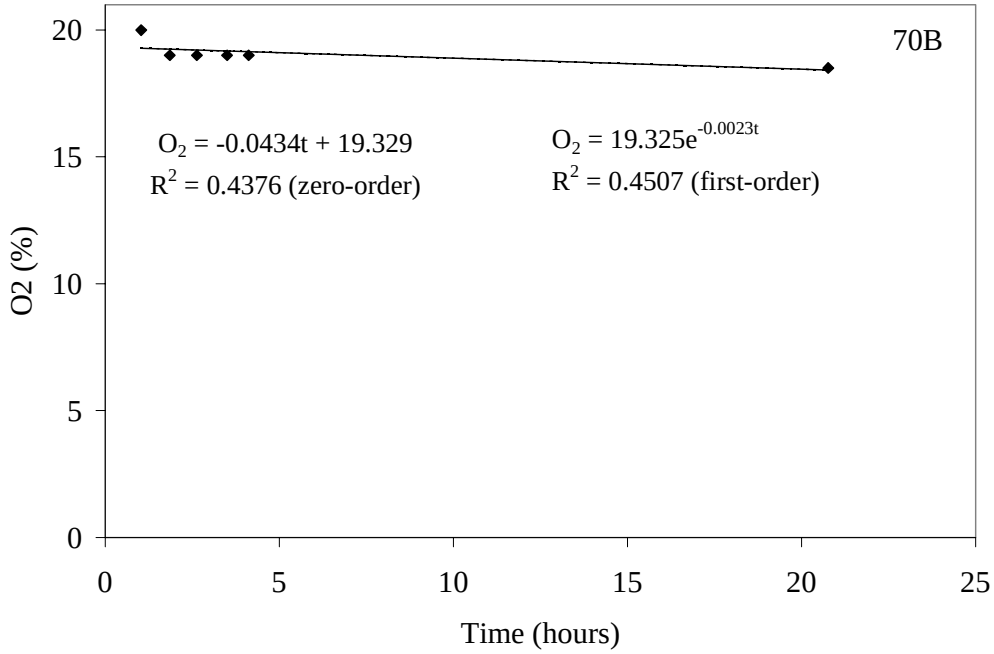

Figure 14.5 Oxygen depletion test at vapor probe 70B. Solid and dashed lines denote linear regression for zero- and first-order kinetics respectively.

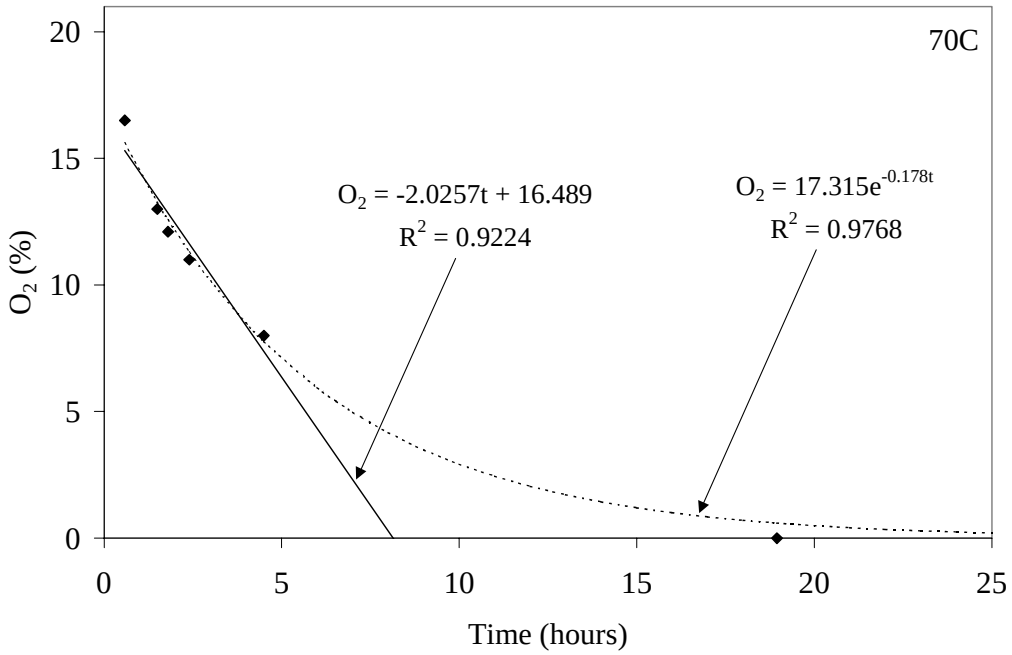

Figure 14.6 Oxygen depletion test at vapor probe 70C. Solid and dashed lines denote linear regression for zero- and first-order kinetics respectively not using zero concentration data point.

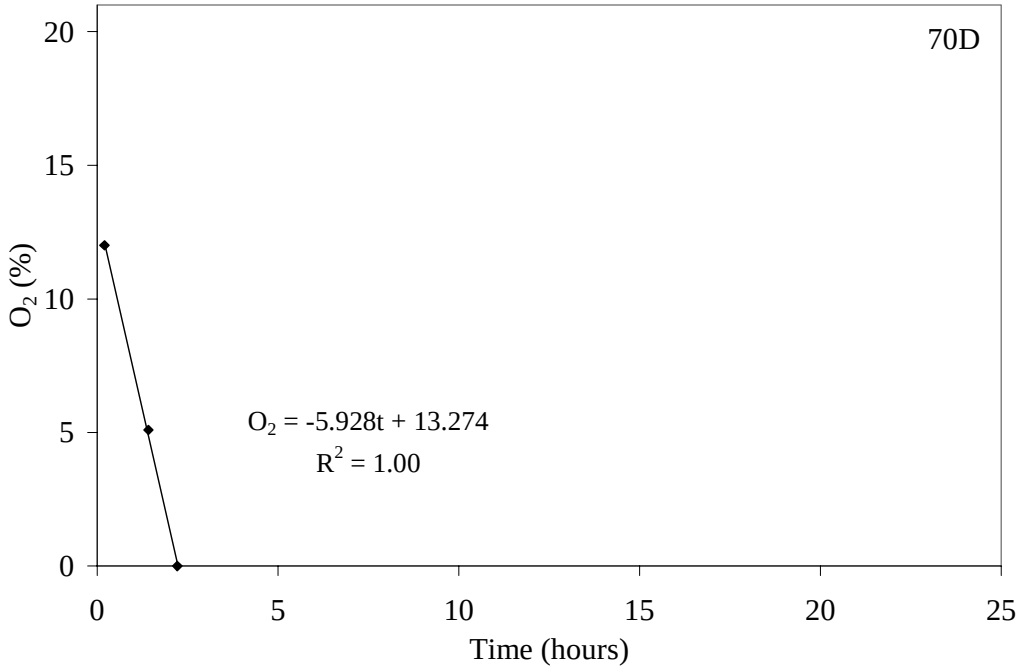

Figure 14.7 Oxygen depletion test at vapor probe 70D. Solid line denotes linear regression for zero-order kinetics not using last data point at zero concentration.

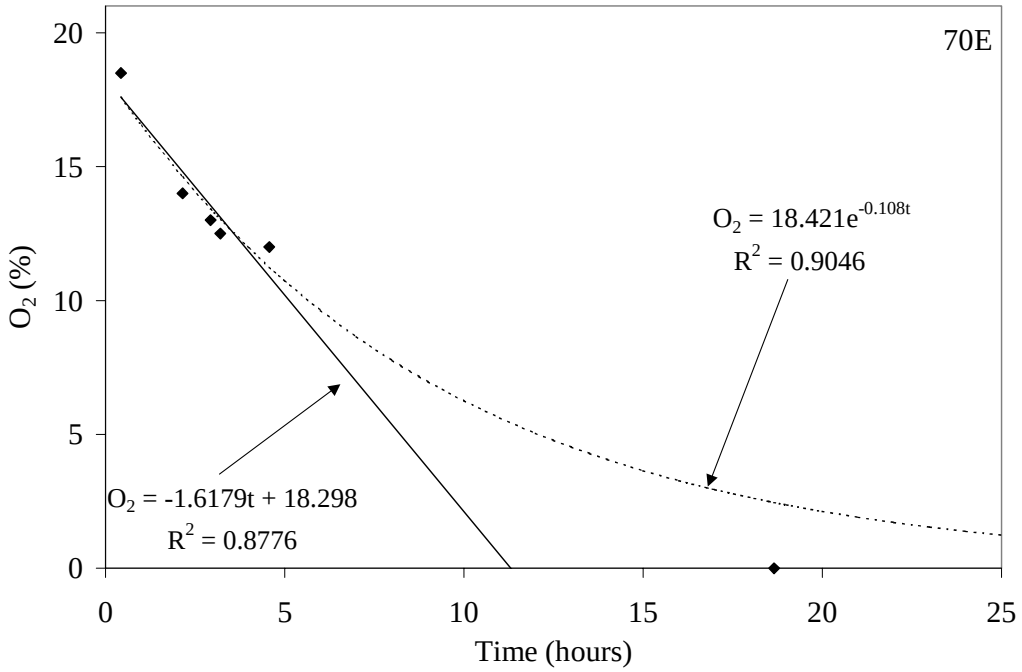

Figure 14.8 Oxygen depletion test at vapor probe 70E. Solid and dashed lines denote linear regression for zero- and first-order kinetics respectively excluding last data point at zero concentration.

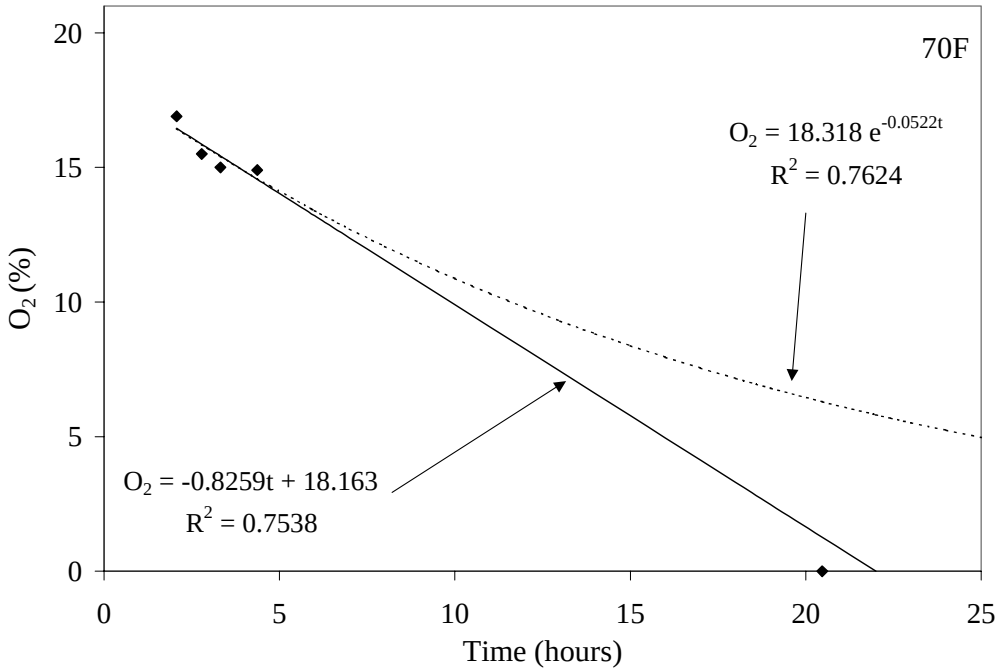

Figure 14.9 Oxygen depletion test at vapor probe 70F. Solid and dashed lines denote linear regression for zero- and first-order kinetics respectively excluding last data point at zero concentration.

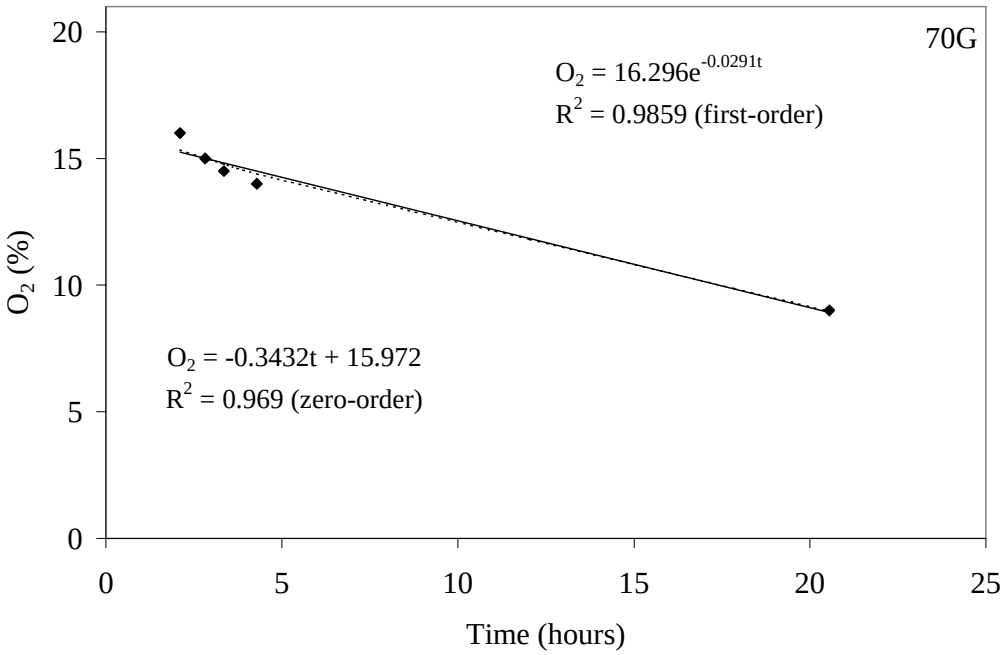

Figure 14.10 Oxygen depletion test at vapor probe 70G. Solid and dashed lines denote linear regression for zero- and first-order kinetics respectively.

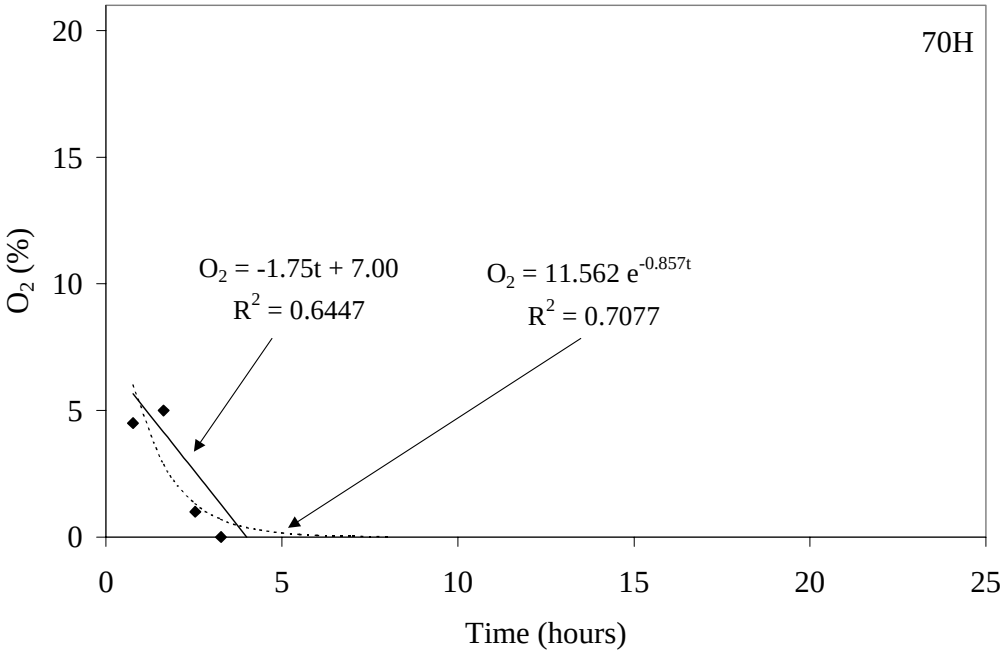

Figure 14.11 Oxygen depletion test at vapor probe 70H. Solid and dashed lines denote linear regression for zero- and first-order kinetics respectively excluding last data point at zero concentration.

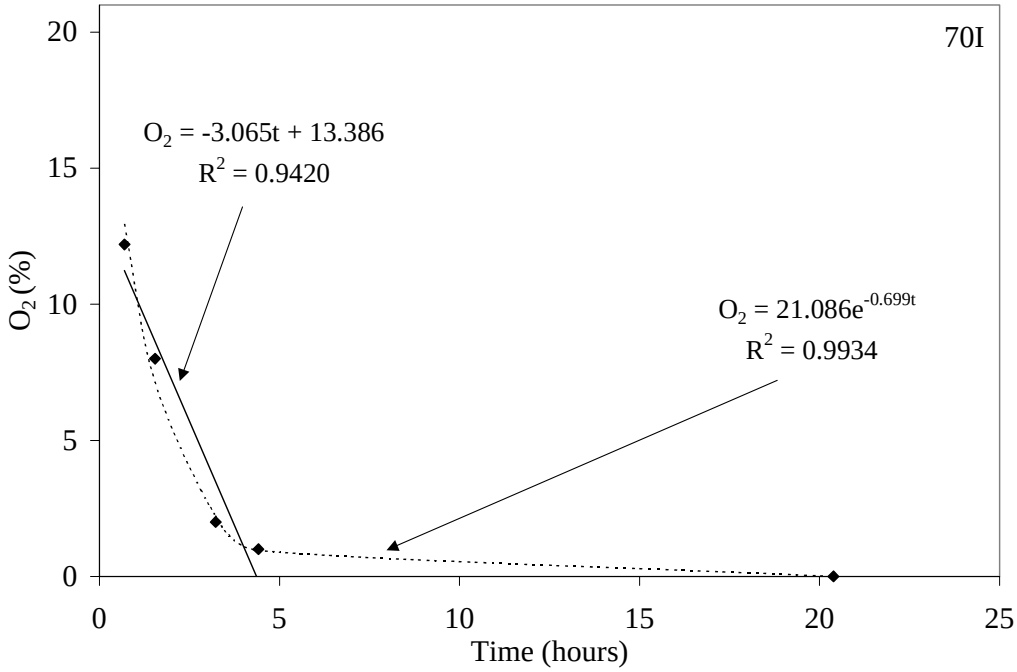

Figure 14.12 Oxygen depletion test at vapor probe 70I. Solid and dashed lines denote linear regression for zero- and first-order kinetics respectively excluding last data point at zero concentration.

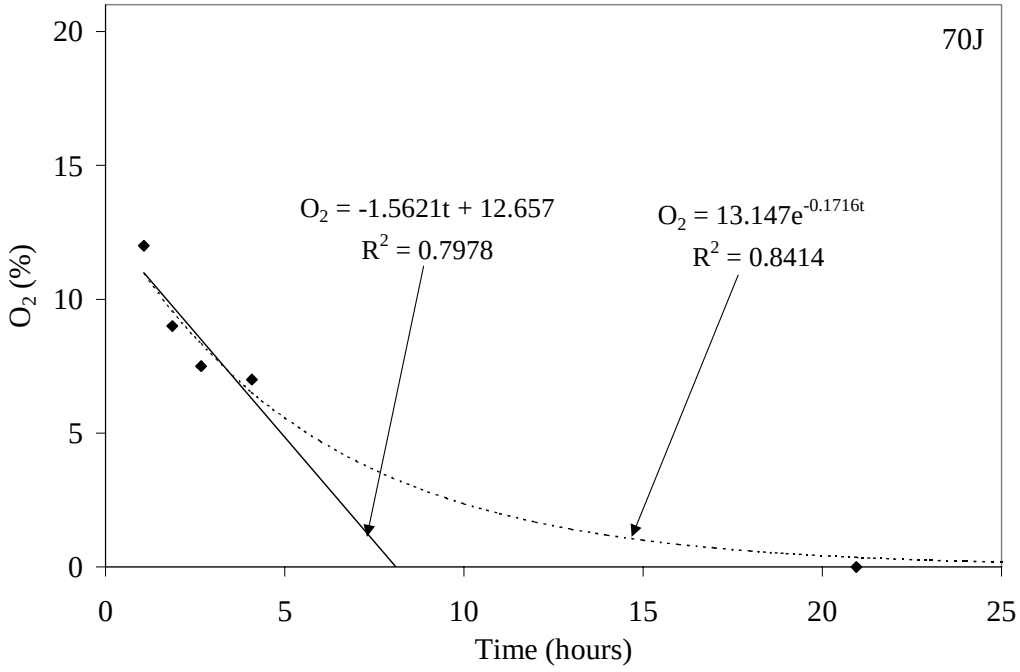

Figure 14.13 Oxygen depletion test at vapor probe 70J. Solid and dashed lines denote linear regression for zero- and first-order kinetics respectively excluding last data point at zero concentration.

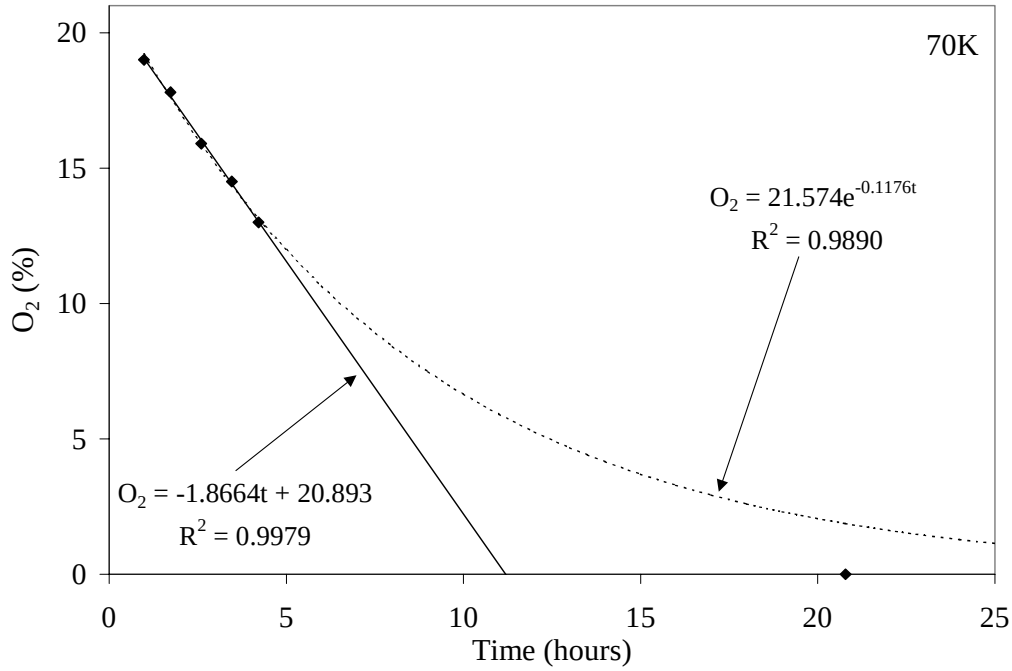

Figure 14.14 Oxygen depletion test at vapor probe 70K. Solid and dashed lines denote linear regression for zero- and first-order kinetics respectively excluding last data point at zero concentration.

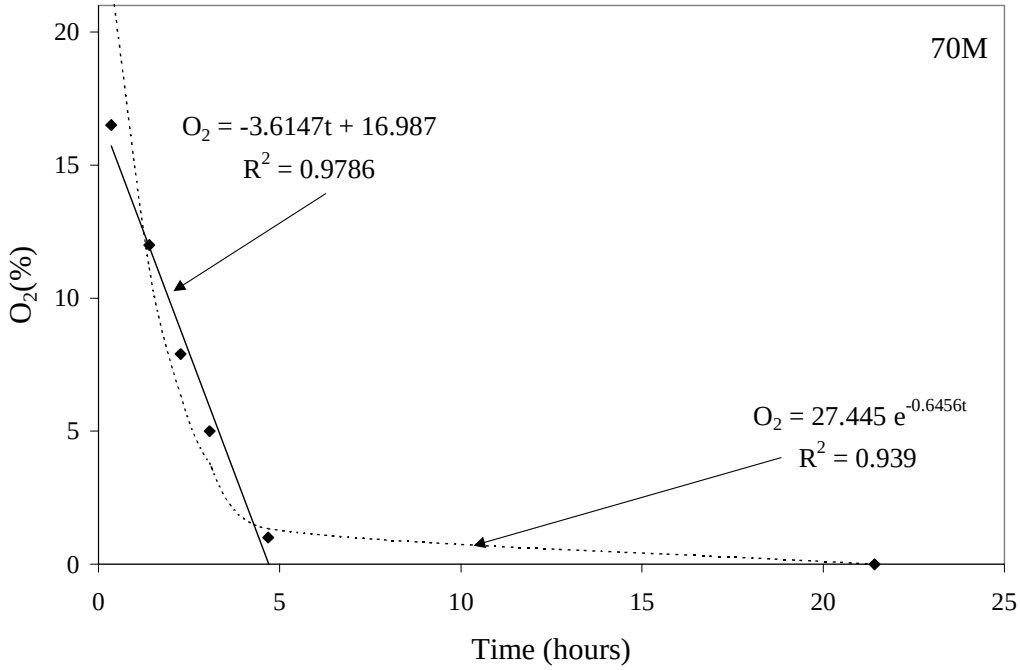

Figure 14.15 Oxygen depletion test at vapor probe 70M. Solid and dashed lines denote linear regression for zero- and first-order kinetics respectively excluding last data point at zero concentration.

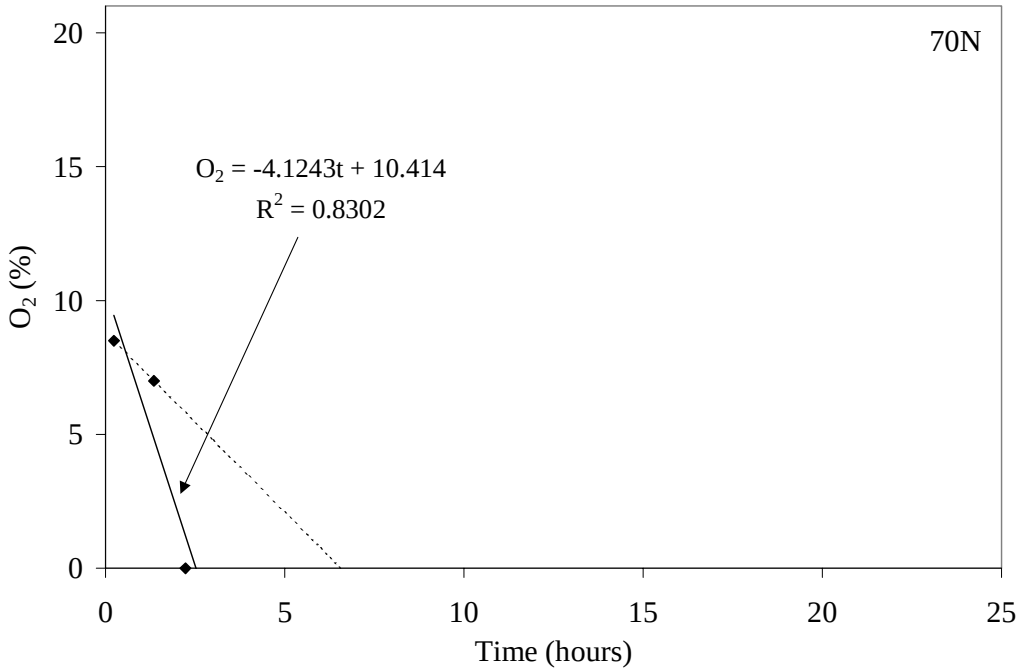

Figure 14.16. Oxygen depletion test at vapor probe 70N. Solid and dashed lines denote linear regression using and not using last data point at zero concentration respectively.

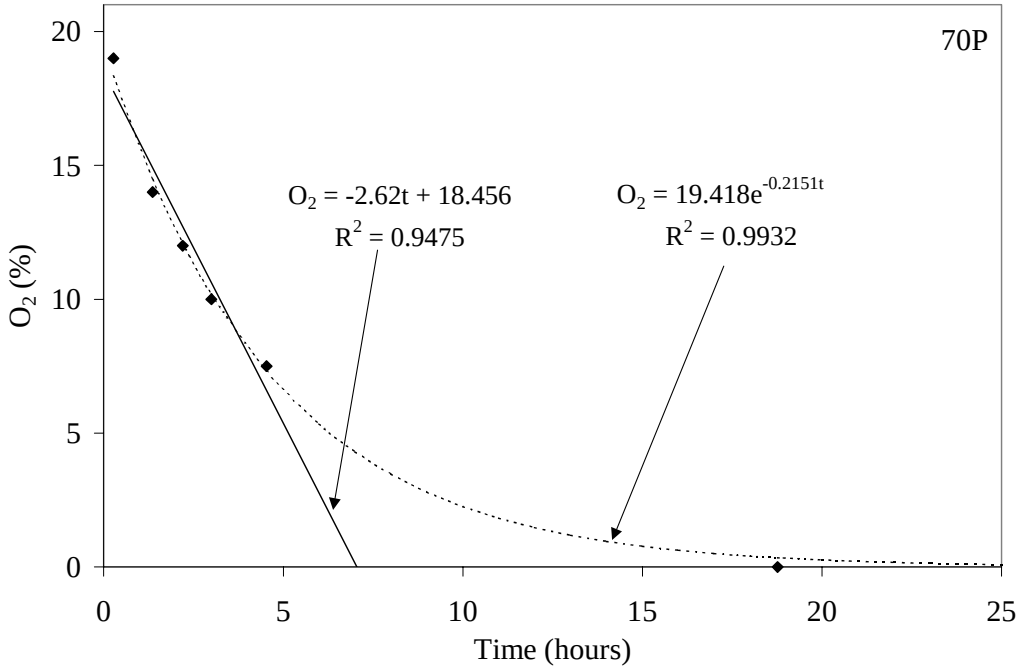

Figure 14.17. Oxygen depletion test at vapor probe 70P. Solid and dashed lines denote linear regression for zero- and first-order kinetics respectively excluding last data point at zero concentration.

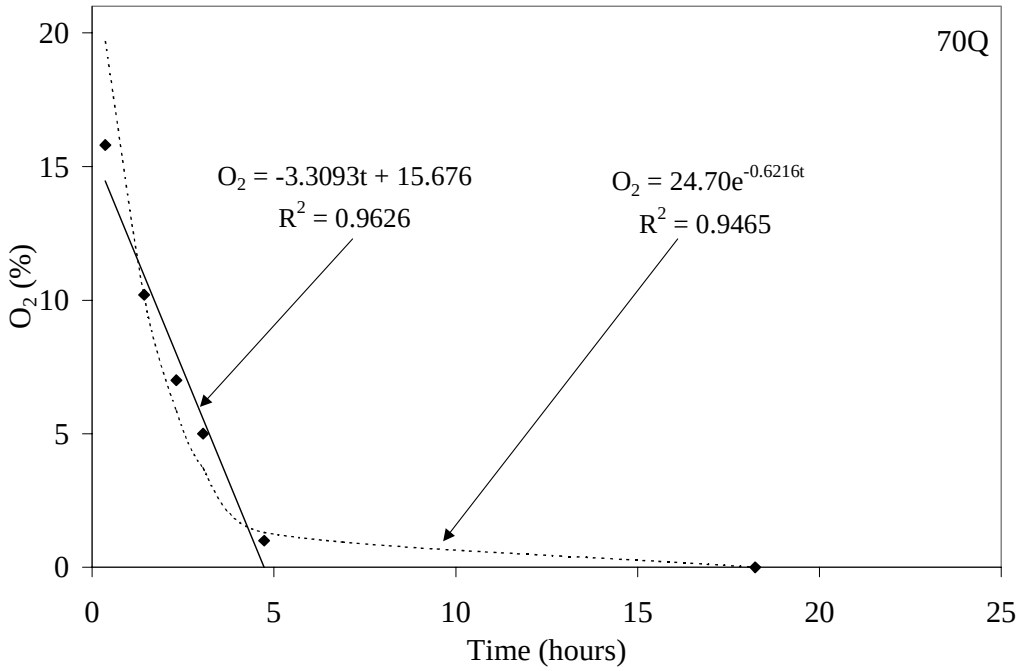

Figure 14.18. Oxygen depletion test at vapor probe 70Q. Solid and dashed lines denote linear regression for zero- and first-order kinetics respectively excluding last data point at zero concentration.

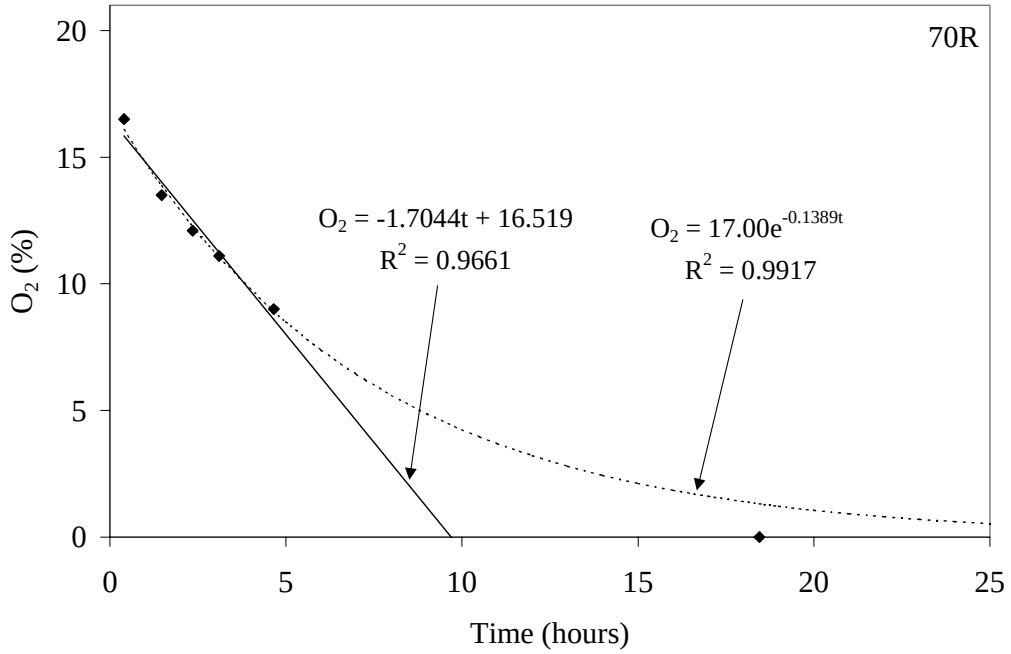

Figure 14.19. Oxygen depletion test at vapor probe 70R. Solid and dashed lines denote linear regression for zero- and first-order kinetics respectively excluding last data point at zero concentration.

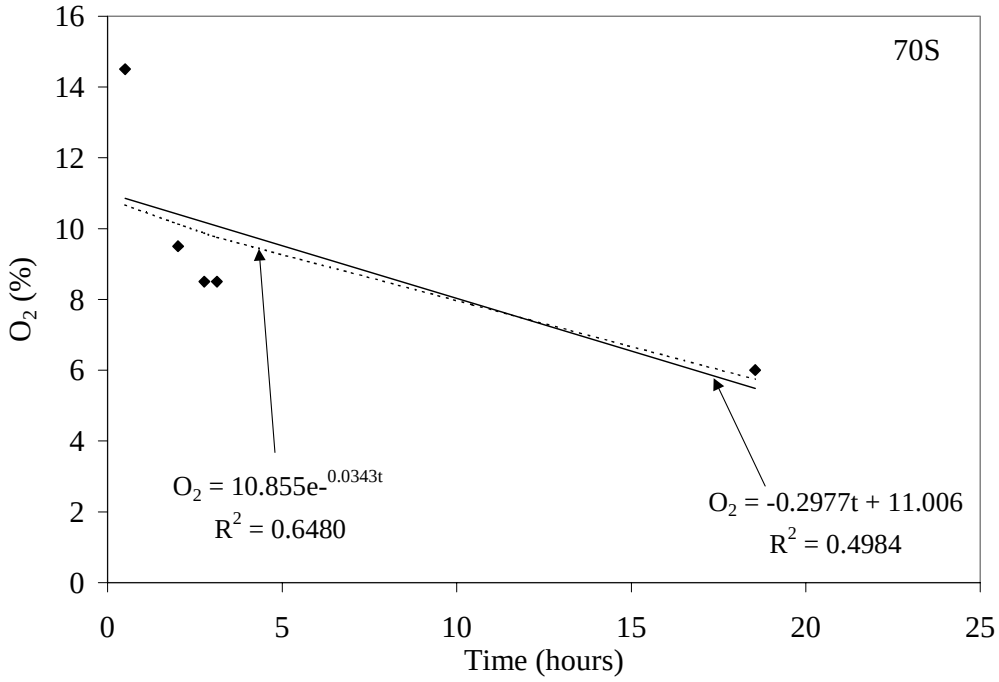

Figure 14.20. Oxygen depletion test at vapor probe 70S. Solid and dashed lines denote linear regression for zero- and first-order kinetics respectively.

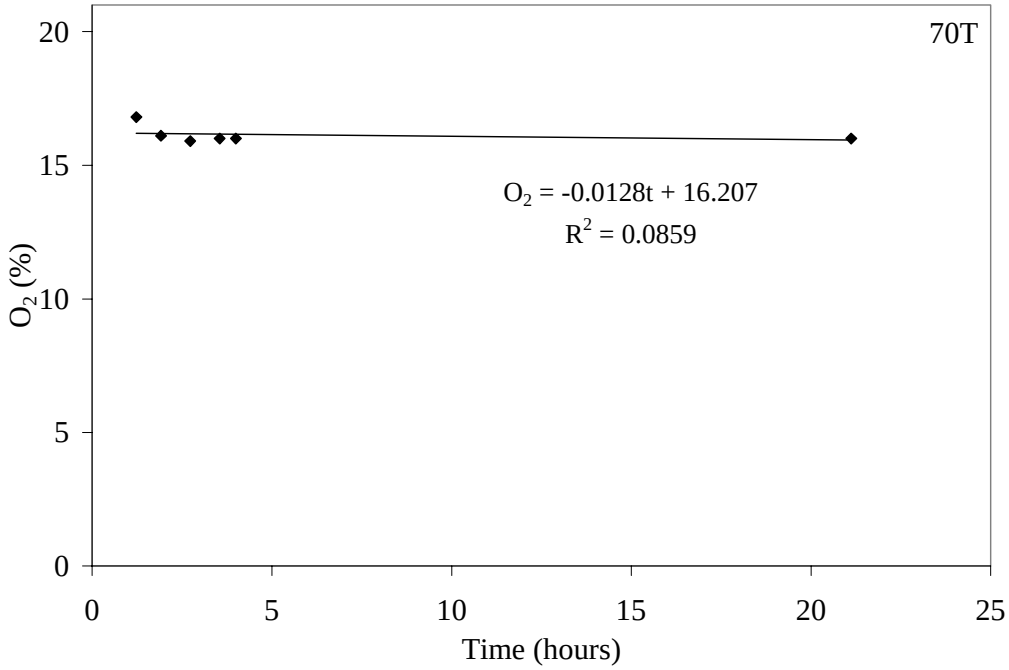

Figure 14.21. Oxygen depletion test at vapor probe 70T. Solid line denotes linear regression for zero-order kinetics.

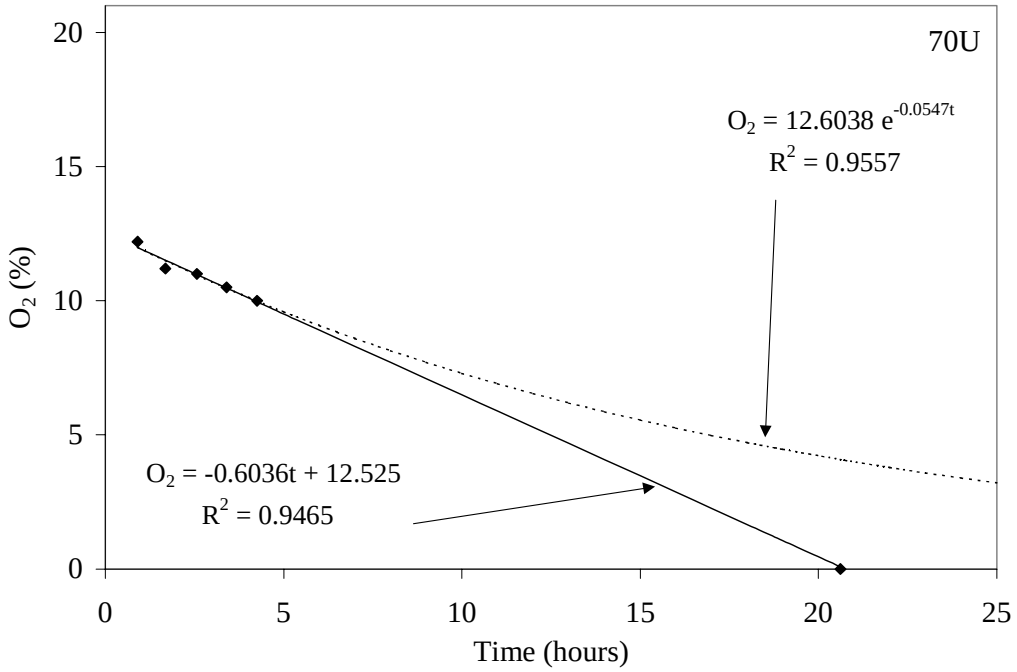

Figure 14.22. Oxygen depletion test at vapor probe 70U. Solid and dashed lines denote linear regression for zero- and first-order kinetics respectively excluding last data point at zero concentration.

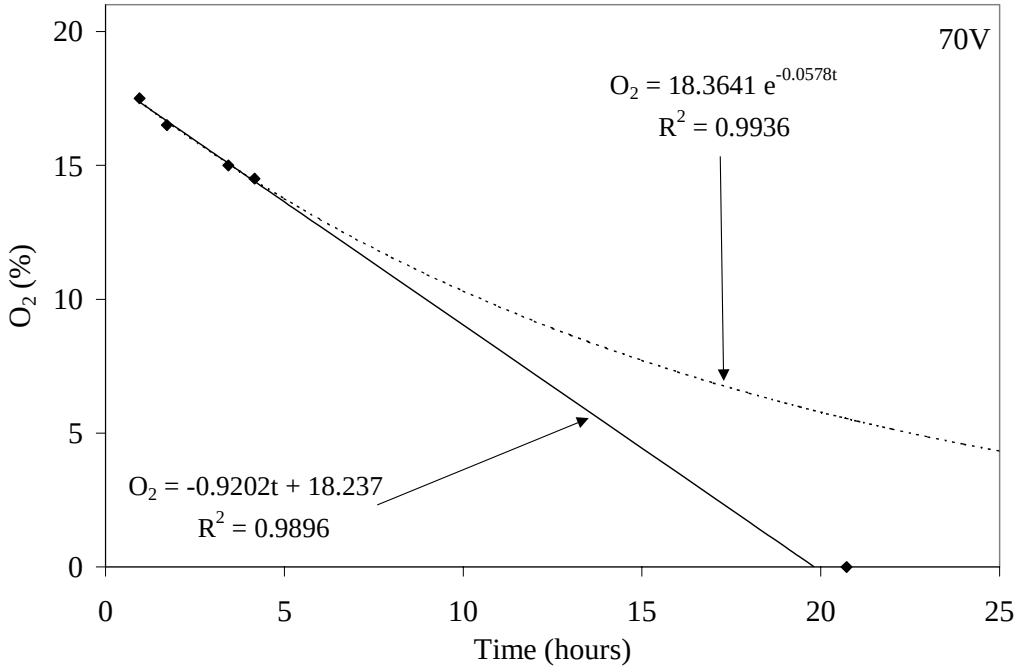

Figure 14.23. Oxygen depletion test at vapor probe 70V. Solid and dashed lines denote linear regression for zero- and first-order kinetics respectively excluding last data point at zero concentration.

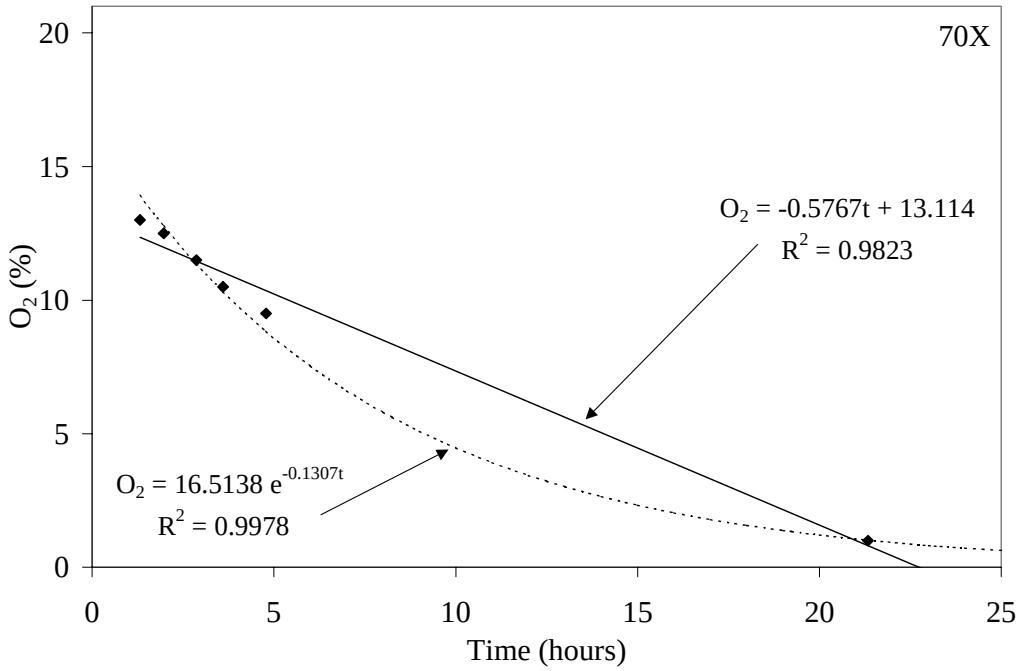

Figure 14.24. Oxygen depletion test at vapor probe 70X. Solid and dashed lines denote linear regression for zero- and first-order kinetics respectively excluding last data point at zero concentration.

14.5 Conclusions

1. Respiration tests provide an inexpensive and rapid means of assessing in-situ aerobic metabolic activity. From a soil venting monitoring perspective, respiration testing should be conducted periodically to assess change in oxygen depletion rates. As remediation progresses, oxygen depletion rates would be expected to decrease over time, eventually in some cases approaching background conditions.

2. It has become common practice to use zero-order oxygen consumption rates to directly estimate hydrocarbon degradation rates. Limitations of this method include: (1) reference hydrocarbons used for the stochiometric mass ratio between hydrocarbon degradation and oxygen consumption may not be representative of compounds present at a spill or hazardous waste site; (2) field data may show first-order degradation rates; (3) regulatory programs, specifically Superfund and RCRA, mandate specific contaminant concentration reduction; (4) the hydrocarbon-oxygen equivalency equation represents the minimum oxygen requirement to completely mineralize a reference compound based on the assumption that either there is no cell synthesis or endogenous respiration, and that oxygen does not serves a terminal electron acceptor in the oxidation of reduced inorganic compounds. Thus, it is possible that the hydrocarbon-oxygen equivalency equation will overestimate actual hydrocarbon degradation rates.

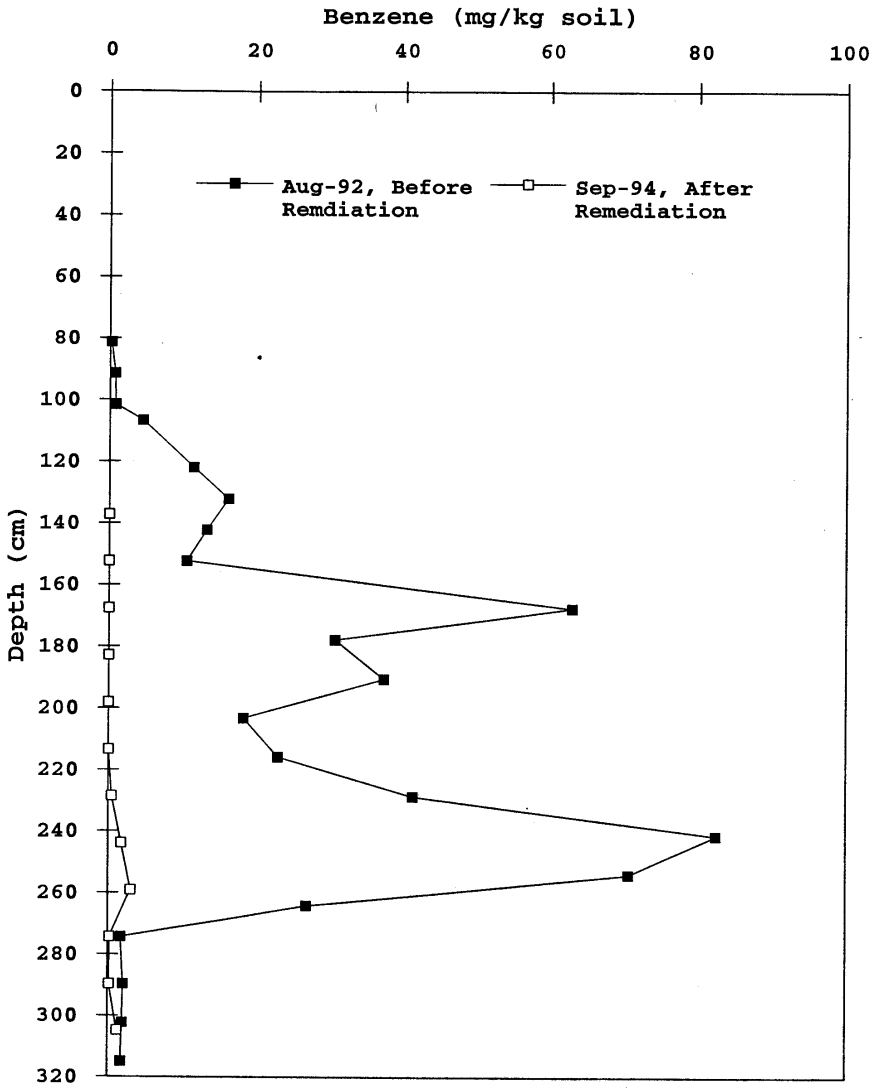

Figure 14.25. Vertical distribution of benzene at 70D before and after venting

3. The best use of respiration testing appears to be as a general indicator of soil amendment (moisture, temperature, nutrients, etc.) effectiveness and microbial activity. Respiration testing could be used to indicate inhibition of degradation. For instance, if respiration testing reveals low oxygen consumption and carbon dioxide generation in soils containing high concentrations of readily biodegradable compounds, further studies could be conducted to determine if biodegradation is being limited by insufficient moisture content, toxicity, or nutrients. Persistent, low oxygen levels may indicate an insufficient supply of oxygenated air at a location suggesting the need for air injection, higher extraction well vacuum, additional extraction wells, or additional soils characterization which may indicate the presence of immiscible fluids impeding the flow of air.

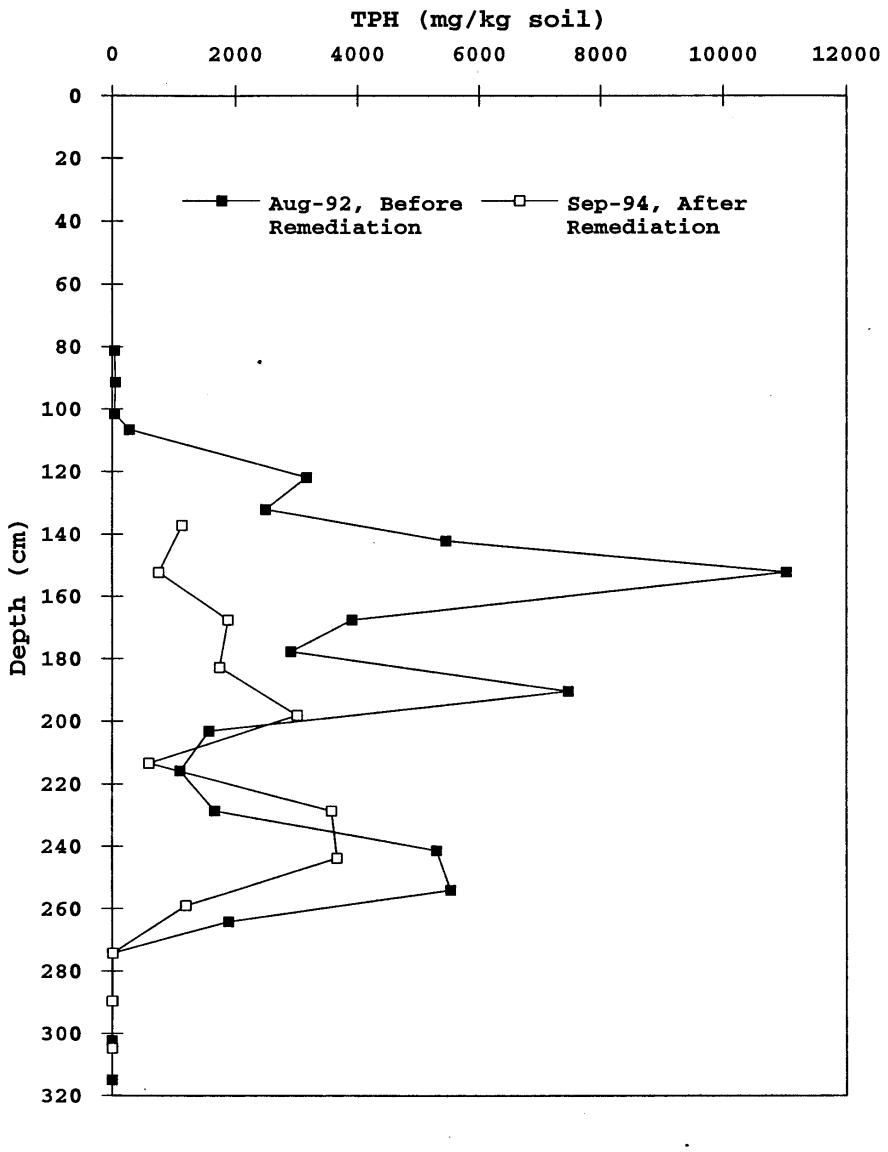

Figure 14.26 Vertical distribution of total petroleum hydrocarbons (TPH) at 70D before and after venting

4. The significance of distinguishing zero- and first-order kinetics for oxygen consumption is that oxygen depletion is constant for the former and a function of oxygen concentration for the latter. If the oxygen depletion rate is a function of oxygen concentration, then oxygen may become a limiting factor below some concentration level above zero. In the site study, discernment of zero- versus first-order oxygen depletion kinetics, was achieved at some but not all monitored locations due to too few data points at critical times. In areas of high contamination, oxygen depletion followed zero-order kinetics.

5. Soil sampling at the test site after 18 months of venting revealed removal of BTEX

compounds to very low concentrations but poor removal of higher molecular weight and lower volatility compounds.

15. EVALUATION OF MASS EXCHANGE TO THE ATMOSPHERE AND GROUND WATER

The inability to meet soil and soil-water concentration-based standards has led to the development of alternative methods to assess venting performance and closure. In section 2, a strategy for assessment of venting performance and closure was proposed based on regulatory evaluation of four components: (1) site characterization, (2) design, (3) monitoring, and (4) mass flux to and from ground water. These four components form "converging lines of reasoning" or a "preponderance of evidence"; an approach common in complex scientific analysis and decision making. Such an approach increases the likelihood of correctly assessing the performance of a venting system and its suitability for closure. Considering that venting is often applied to remove contaminant mass from variably saturated media for ground-water protection, it would seem that only an analysis of mass flux to and from ground water is necessary for assessment of soil venting operation and closure. There is, however, so much uncertainty in vadose zone solute transport modeling and difficulty in field validation that sole use of vadose zone mathematical modeling for decision making appears unwise. Nevertheless, mass flux evaluation is still a crucial component of the performance assessment and closure strategy.

15.1 Modeling Approach

Mathematical models which simulate soil-water movement to ground water vary in complexity from simple and conservative algebraic water-balance equations that neglect degradation and volatilization to more process descriptive finite-difference and finite-element numerical codes incorporating Richards' equation for soil-water flow and mass transport kinetics. Unsaturated zone modeling should ideally: (1) be rigorous enough to incorporate major fate and transport processes, (2) have input parameters that can be readily collected, and (3) be sufficiently user-friendly to enable use by consultants and regulators. Unfortunately, simultaneous attainment of all of these goals is unrealistic. Lack of data to support spatial discretization of soil properties (e.g., capillary pressure parameters, hydraulic conductivity, porosity, bulk density, moisture content, total organic carbon content) and contaminant distribution, commonly limits the use of sophisticated mathematical models. One approach to this problem is to use fictitious but "reasonable" input for numerical two- or three-dimensional modeling. This approach is applicable when attempting to simulate contaminant transport in a layered or high heterogeneous soil environment, when complex boundary conditions exist, or when consideration of mass transport kinetics is desirable. Another approach, is to start with commonly collected data and use fairly simplistic, one-dimensional, analytical screening models to gain insight into the potential magnitude of solute transport to and from ground water. This approach is similar to screening models developed by Jury et al. (1984a-c). More sophisticated numerical modeling can then be utilized if additional supporting data becomes available or a more detailed analysis of the problem is desired. Regardless of sophistication, all modeling is a simplification of reality containing considerable uncertainty in simulated results.

When choosing and interpreting output from a mathematical model, it is important to

keep in mind the intended objective of modeling. During regulatory decision making in regard to unsaturated zone remediation, the purpose of mathematical modeling is often simply to determine whether or not (yes or no) a long term potential risk to ground water exists. If there is a perceived immediate or long-term risk, then unsaturated zone remediation is initiated or continued. If not, then model output is combined with other factors such as the adequacy of site characterization, to forgo remediation or commence closure. In sharp contrast to fluid flow (ground-water and gas) modeling efforts, vadose zone soil-water movement and contaminant transport simulations are rarely calibrated or validated because of the time scale of modeling (years), extensive site characterization needs, and related cost. Thus, for regulatory decision making, one-dimensional analytical or numerical modeling may be appropriate under some conditions. However, even at this level of modeling, a sensitivity analysis of how model input and selected boundary conditions affect model output and decision making is critical. The objective here then is to conduct one-dimensional VOC transport simulations to assess the effect of water saturation, NAPL saturation, degradation-half-life, and selection of boundary conditions at the vadose zone - ground-water interface on model output and regulatory decision making in regard to vadose zone remediation, specifically venting initiation or closure. A one-dimensional analytical, public domain code, termed VFLUX (Vertical Flux) , was developed to support these simulations. Table 15.1 provides a summary of the model's characteristics and capabilities

VFLUX was written to replace VLEACH (Ravi and Johnson, 1997), a one-dimensional, finite-difference code, which is by far the most commonly used model to assess initiation or closure of vadose zone remediation. VFLUX has all the capabilities of VLEACH in addition to allowing a time-dependent, first-type lower boundary condition, and consideration of the effect of degradation and NAPL saturation on VOC removal and partitioning. The time-dependent boundary condition is the centerpiece of the mass flux assessment because it dynamically links performance of ground-water remediation to venting closure. VFLUX is a significant improvement over VLEACH because of these increased capabilities and exact method of solution. The governing equation with associated initial and boundary conditions of VLEACH were solved numerically, even though it could have easily been solved analytically. The determination of mass flux requires calculation of a spatial derivative at the water table interface, which is prone to large error when spatial discretization is coarse and a sharp concentration gradient exists between grid blocks. The analytical solutions of VFLUX provides exact values of mass flux at any location. Also, in order to calculate concentration profiles at a specified time, the transport equation has to be solved numerically at each time step starting from the initial distribution. Analytical methods allow direct solution at the time of interest. In addition, analytical solutions are not subject to convergence and stability problems arising from the use of coarse spatial grids and large time steps. Thus, there is less chance that an inexperienced user will generate inaccurate output due to poor specification of numerical simulation criteria (e.g., grid size).

Table 15.1 Summary of VFLUX Model Capabilities

Capability	Description
availability	public domain (to be available without cost on EPA internet site)
dimensionality	one-D
method of solution	analytical
upper boundary condition	first-type (zero concentration)
lower boundary condition	choice of first-type, time-dependent or finite, zero-gradient
initial condition	variable (input soil concentration as a function of depth)
mass transport kinetics	none - local equilibrium assumption
degradation	first-order (input as degradation half-life)
water saturation	constant in time and space
NAPL saturation	constant in time and space (NAPL assumed nonvolatile and nondegradable)
infiltration rate	constant
computation soil-gas and soil-water tortuosity coefficients for diffusion	Millington-Quirk relationship
hydrodynamic dispersion	function of infiltration rate
model output	- parameter file summarizing input - flux file showing average concentration and flux to ground water at the atmosphere as a function of time - mass balance file showing remaining mass in soil profile and mass lost to ground water, atmosphere, and decay

15.2 Model Formulation

Analysis of VOC transport in unsaturated media starts with a mass balance or continuity equation for each organic compound in soil. The continuity equation states that change in storage equals the divergence of flux. This can be represented mathematically by

$$\frac{\partial}{\partial t}\left(\theta_g C_g + \theta_w C_w + \rho_b C_s + \theta_n C_n\right) - r = -\frac{\partial J_T}{\partial z} \qquad (15.1)$$

where J_T = mass flux across a vertical plane [$ML^{-2}T^{-1}$] and r = a reaction term [$ML^{-3}T^{-1}$]. This equation can be represented more compactly as

$$\frac{\partial C_T}{\partial t} - r = -\frac{\partial J_T}{\partial z} \tag{15.2}$$

where

$$C_T = RC_w = \frac{R}{H} C_g \tag{15.3}$$

and

$$R = H\theta_g + \theta_w + K_{oc} f_{oc} \rho_b + \frac{M_i \theta_n}{\gamma_i C_w^{sat} \sum_{j=1}^{N} \chi_j M_j / \rho_j}. \tag{15.4}$$

If it is assumed that NAPL composition does not change with time, R may be approximated by

$$R = \left(H\theta_g + \theta_w + K_{oc} f_{oc} \rho_b + \frac{M_i \rho_o \theta_o}{\gamma_i C_w^{sat} M_o} \right). \tag{15.5}$$

Volatile organic compound transport in the vadose zone is caused by soil-water advection, mechanical dispersion, and diffusion (aqueous and gaseous). In derivation of the advective-dispersive equation, mechanical dispersion and diffusion are combined to form an overall dispersion coefficient. Transport by other mechanisms such as gaseous advection due to barometric pressure variation, gas density variation, and infiltration fronts is normally considered negligible. Advective soil-water flux, J_w is expressed as

$$J_w = q_w C_w \tag{15.6}$$

where q_w = infiltration flux of water [LT^{-1}]. Flux due to molecular diffusion in the liquid and gaseous phases ($J_{d,w}$ and $J_{d,g}$ respectively) is described by Fick's First Law

$$J_{d,w} = -D_w \frac{\partial C_w}{\partial z} \tag{15.7}$$

and

$$J_{d,g} = -D_g \frac{\partial C_g}{\partial z}. \tag{15.8}$$

The negative sign enables values of flux to be positive since movement is from areas of greater concentration to areas of lesser concentration resulting in a negative slope or gradient. Fick's First Law is a subset of a more general group of equations called "gradient flux laws" where flux is a function of a some property (in this case diffusion coefficients) and a gradient. Other examples are Darcy's Law (fluid flow), Fourier's Law (heat conduction), and Ohm's Law (electrical conductivity). Diffusion will occur as long as a concentration gradient exists.

In porous media, diffusion can not proceed as fast as it can in free water or gas because solute molecules collide with solids and must travel tortuous paths around mineral grains. Thus, diffusion coefficients for water and gas must be modified to account for the distance of the flowpath followed by solute molecules. Modification is accomplished by use a tortuosity factor. Flowpaths in a well-sorted soil would be expected to be shorter than those in a poorly sorted soil in which smaller grains fill in the pore spaces of larger grains (Fetter, 1992). To incorporate the effect of tortuosity, Ficks First Law can be modified by

$$J_{d,w} = -\tau_w D_w \frac{\partial C_w}{\partial z} \tag{15.9}$$

and

$$J_{d,g} = -\tau_g D_g \frac{\partial C_g}{\partial z}. \tag{15.10}$$

A number of expressions have been developed to estimate tortuosity factors for gas and aqueous diffusion. It stands to reason that the presence of soil-water will interfere with gas diffusion and increase the flowpath for vapor molecules. The theoretically based model derived by Millington and Quirk (1961) relationship

$$\tau_g = \frac{\theta_g^{10/3}}{\eta^2} \tag{15.11}$$

can be used to estimate τ_g. The equation illustrates the importance of volumetric gas content in estimation of a gas tortuosity. This model has been shown to be in good agreement with data over a wide range of water saturations (Sallam et al., 1984). Soil-gas will interfere with aqueous diffusion by forcing aqueous diffusion across pendular rings instead of directly across a pore. Because liquid tortuosity modifies liquid diffusion in the same way that gas tortuosity modifies gas diffusion, the Millington-Quirk (1961) tortuosity relation may also be used to estimate τ_w by (Jury et al. 1991)

$$\tau_w = \frac{\theta_w^{10/3}}{\eta^2} . \tag{15.12}$$

Total mass flux across any plane in the vadose zone can now be represented by

$$J_T = q_w C_w - \left(D_m \nu_w + D_w \tau_w\right) \frac{\partial C_w}{\partial z} - D_g \tau_g \frac{\partial C_g}{\partial z} \tag{15.13}$$

where D_m is a mechanical dispersion coefficient [L]. Equation (15.13) is equivalent to:

$$J_T = \frac{q_w}{R} C_T - \frac{D}{R} \frac{\partial C_T}{\partial z} \tag{15.14}$$

where

$$D = D_m \nu_w + D_g \tau_g H + D_w \tau_w . \tag{15.15}$$

It is important to note from equation (15.15) that mechanical dispersion coefficient has been combined with the aqueous diffusion coefficient to represent flux as a function of a concentration gradient. This in essence describes mechanical dispersion as a Fickian process or flux that is a function of a concentration gradient. In reality, it is known that mechanical dispersion is not a Fickian process but the end result is the same, namely contaminant spreading. Considering mechanical dispersion as a Fickian process simplifies solution of the advective-dispersive equation and has become the accepted method of handling overall dispersion which is considered a combination of diffusion and mechanical dispersion.

Because of the presence of a capillary fringe and variation in moisture content with depth, the dispersion coefficient will not be constant in a homogeneous media. One method of accounting for this variation is by specifying an effective dispersion coefficient (D_{eff}) defined as

$$D_{eff} = D_m \nu_w + L \left[\int_0^L \frac{dz}{H D_g \tau_g(z) + D_w \tau_w(z)} \right]^{-1} . \tag{15.16}$$

The integral expression in equation (15.16) can be approximated by

$$L \left[\int_0^L \frac{dz}{H D_g \tau_g(z) + D_w \tau_w(z)} \right]^{-1} \approx L \left[\sum_{i=1}^{N} \frac{L_i / \eta^{4/3}}{\left[H D_g \left(1 - S_{w,i}\right)^{10/3} + D_w S_{w,i}^{10/3} \right]} \right]^{-1} \tag{15.17}$$

where water saturation in each discrete layer ($S_{w,i}$) of length L_i is represented. In this way, the reduction in dispersion due to the presence of a capillary fringe and other layers of media having high water saturation can be explicitly accounted for. Equation (15.17) can then be used to determine an effective water saturation for model input such that

$$\eta^{4/3}\left[HD_g\left(1-S_w\right)^{10/3}+D_wS_w^{10/3}\right]=L\left[\sum_{i=1}^{N}\frac{L_i/\eta^{4/3}}{\left[HD_g\left(1-S_{w,i}\right)^{10/3}+D_wS_{w,i}^{10/3}\right]}\right]^{-1} \tag{15.18}$$

Johnson and Ettinger (1991) used a similar approach to calculate and effective diffusion coefficient in unsaturated media to assess the impact of upward VOC migration into buildings.

The only remaining factor in deriving the advective-dispersive equation is how to handle the sink or degradation term. Since degradation rates published in the literature are not referenced to specific phase (e.g., aqueous), the reaction term, r, is expressed as a function of total soil concentration and a first-order degradation constant (κ) [T^{-1}]

$$r=-\kappa C_T\ . \tag{15.19}$$

Degradation half-life ($t_{1/2}$) [T] equals:

$$t_{1/2}=\frac{0.693}{\kappa}\ . \tag{15.20}$$

Finally, the governing equation for one-dimensional transport of a volatile organic compound can be expressed as:

$$R\frac{\partial C_T}{\partial t}=-q_w\frac{\partial C_T}{\partial z}+D\frac{\partial^2 C_T}{\partial z^2}-\kappa RC_T\ . \tag{15.21}$$

15.3 Representation of the Initial Condition

Use of the advective-dispersive equation consists of choosing a set of initial and boundary conditions which may be accepted as adequate to the real situation then finding an analytical or numerical solution. Often selection of boundary conditions to the advective-dispersive equation is neither straightforward nor intuitive. In simulations to follow, initial conditions describe total (solids, NAPL, water, and air) soil concentrations as a function of depth at time zero. In application, total soil concentrations would presumably be determined directly from soil core analysis (solvent extraction). The initial condition can be represented by analytical expression or by a piecewise continuous function. The latter approach was utilized in VFLUX because any initial total soil concentration profile can be specified at any desired resolution without

modification of the code. Mathematically, the initial condition is represented by:

$$C_T(z,0) = f(z) \tag{15.22}$$

where f(z) [ML^{-3}] is a piecewise continuous function.

15.4 Selection of the Upper Boundary Condition

At the upper end of the modeled domain (z = 0), a first-, second-, or third-type boundary condition could conceivably be specified for solute transport modeling. Use of a first-type boundary condition simply states that concentration is varied as a function of time or held constant by some means at a boundary. For instance, if it is assumed that clean air and water is present at the surface, a first-type, constant (zero) concentration boundary condition could be specified by

$$C_T(0,t) = 0\ . \tag{15.23}$$

A boundary condition of the second-type represents a fixed gradient at a boundary surface expressed as a time-dependent function, a constant value, or zero. For instance, the finite zero-

gradient condition represented by

$$\left.\frac{\partial C_T}{\partial z}\right|_{z=0} = 0 \tag{15.24}$$

could be used to simulate no dispersive flux at soil-atmosphere boundary. However, since diffusive transfer from soil to the atmosphere is a desired output of modeling, this boundary condition is inappropriate. A boundary condition of the third-type represents mass flux into the modeled domain proportional to the difference in concentration at the boundary and surrounding medium. The inlet third-type boundary condition for this application can be expressed by

$$\left.\left(-\frac{D}{R}\frac{\partial C_T}{\partial z} + \frac{q_w}{R}C_T\right)\right|_{z=0^+} = \frac{q_w}{R}C_T^{surf}(t) \tag{15.25}$$

where C^{surf}_T (t) is a "flux" concentration at the soil surface as a function of time. This boundary condition though fixes flux into the domain when diffusive flux out of the domain is a desired model output. Jury et al. (1984 a,b) and Yates et al. (2000) formulated a third-type boundary condition at the surface by assuming that VOCs had to pass through a boundary layer by vapor diffusion before entering a well-mixed region of the atmosphere. This boundary layer could be a surface crust, compacted zone, or a resistive material such as polyethylene. For this application, an upper boundary expressed by

$$-\frac{D}{R}\frac{\partial C_T}{\partial z}\bigg|_{z=0} = h\left(C_T^{surf}(t) - C_T(0,t)\right) \tag{15.26}$$

could be utilized where h is a mass transfer coefficient [LT^{-1}] which could be approximated by $h = D_g/b$ where b is the thickness of air boundary [L].

Selection of an appropriate boundary condition at the surface is complicated by mass balance and concentration continuity considerations. In a flowing fluid, the concentration of a solute can be defined in two ways - "resident" and "flux" detection. Kreft and Zuber (1978) define resident detection as the mass of solute per unit volume of fluid contained in an elementary volume at a given instant. They define flux detection as the mass of solute per unit volume of fluid passing through a given cross section at an elementary time interval or the ratio of solute flux to volumetric fluid flux. Both concentrations though are in fact volume averaged (Kreft and Zuber, 1986). Kreft and Zuber (1978) state that in practice, flux detection is realized by measuring the mean concentration in an outflowing fluid. Referring to miscible displacement studies, Parker and van Genuchten (1986) state that in the case of a laboratory column where flow from the entire cross-section is collected, a definite measure of flux concentration is obtained. Measurement of flux detection inside a column though is usually impossible without disturbing flow lines. Parker and van Genuchten (1986) state that the question arises over the magnitude of local perturbation in the flow field caused by fluid withdrawal and the installation of sampling devices. Uncertainty is compounded by problems with time averaging. Measurement of resident concentration requires that the time to obtain the sample is small in comparison to the time in which fluxes occur (Parker and van Genuchten, 1986).

Kreft and Zuber (1978) also discuss differences between flux and resident injection. For resident injection, a first-type boundary condition is utilized and concentration continuity across the interface is maintained. For flux injection, concentration continuity is lost across the interface to allow flux across the interface as is apparent from equation (22). Kreft and Zuber (1978) state that flux injection is achieved in practice by introducing fluid with a solute through the whole entrance cross-section with no back mixing. van Genuchten and Parker (1984) state that for miscible displacement experiments, a third-type boundary condition or flux injection results in conservation of mass whereas resident injection does not maintain solute flux continuity across the inlet position. In one-dimensional miscible displacement studies, it is now generally agreed that the flux injection boundary condition is the correct inlet boundary condition (van Genuchten and Parker, 1984; Parker and van Genuchten, 1984, Barry and Sposito, 1988; and Novakowski, 1992 a,b). However, this is not necessarily true for gas displacement or diffusive vapor transport. Gimmi and Flühler, (1996) demonstrated that the selection of a resident or flux injection boundary condition for gas transport is directly dependent on the ratio of the cross-sectional areas of the tubing leading to a column and the column itself. Low gas velocity and a large tubing to column ratio (in field-scale unsaturated solute transport, this ratio is essentially unity) favor specification of a resident injection or type-one boundary condition. They state that for flux injection, the influence of diffusion must be negligible compared to the influence of mechanical dispersion. This typically occurs for miscible displacement experiments

but occurs for gas flow experiments only under conditions of high velocity and low tubing to column cross-sectional area ratios. Gimmi and Flühler (1996) state that for gaseous advective-dispersive transport, the exchange of solutes at a boundary will resemble a resident injection unless diffusive flux is restricted at the boundary. They state that in most cases it should be possible to model vapor exchange directly at the soil surface using a first-type boundary condition unless mixing with the atmosphere is strongly restricted by an upper boundary.

15.5 Selection of Lower Boundary Condition

Use of a third-type boundary condition similar to equation (15.25) would appear unreasonable at the domain outlet because it again fixes flux out of the domain when in fact the one objective of modeling is to calculate flux into and out of ground water. Flux from an outlet can not be known a priori but must be measured or simulated. Intuitively, a diffusive flux boundary however could conceivably be used similar to equation (15.26). This boundary condition though negates advection from the vadose zone to ground water. A first-type time-dependent boundary condition represented by

$$C_T(L,t) = g(t) \tag{15.27}$$

where g(t) = time-dependent soil concentration [ML^{-3}], though could be used to link ground-water and unsaturated zone aqueous concentrations at the base of the modeled domain. The time-dependent term could be described by an analytical expression as is common for exponential decay of a source term or by pulse loading of constant concentrations for fixed periods of time. The latter approach takes advantage of the principle of superposition and allows development of a general analytical solution for any pulse loading function whereas use of former requires either separate development of analytical solutions for each analytical loading expression or modification of computer code and subsequent numerical integration for time dependent function. A first-type lower boundary condition though is not appropriate if one wishes to use soil-water concentration at the outlet with a ground-water dilution attenuation factor to assess regulatory compliance since outlet concentrations are set by the boundary condition itself.

At the base of modeled domain, a finite or semi-infinite (z goes to infinity) zero-gradient boundary condition could also be utilized. Operationally, the primary difference between a finite and semi-infinite domain zero-gradient lower boundary condition is that the former allows only advective mass transfer to ground water while the latter allows diffusive and advective mass transfer to ground water since the interface is not distinguishable from any other plane over which mass transfer occurs. Use of a semi-infinite zero-gradient boundary condition requires the assumption that the exit boundary does not influence the system. In miscible displacement laboratory column studies, this condition is ensured by the use of small diameter tubing at the column effluent to prevent backward diffusion (Gimmi and Flühler, 1996). This laboratory configuration though is irrelevant to the field.

Neither a finite or semi-infinite zero-gradient boundary condition allows diffusive mass transfer from ground water to the unsaturated zone. Also, the use of a zero-gradient boundary condition is questionable when ground water containing elevated levels of VOCs underlies soils containing low levels of VOCs. In this situation, the primary direction of mass flux could be from ground water to the vadose zone as a result of diffusive exchange. As Kreft and Zuber (1986) state, it is difficult to imagine a boundary permeable to convective flow but impermeable to dispersive flow. Kreft and Zuber (1986) and Parker and van Genuchten (1986) point out that considerable ambiguity remains regarding the physical conditions under which various outlet boundary conditions are valid. In VFLUX, the user was given the option of selecting a first-type, time-dependent or a finite, zero-gradient lower boundary condition.

15.6 Derivation of Analytical Solutions for First-Type, Time-Dependent Lower Boundary Condition

Equation (15.21) can be expressed in dimensionless units:

$$\frac{\partial C_T}{\partial T} = -2\mathrm{A}\frac{\partial C_T}{\partial Z} + \frac{\partial^2 C_T}{\partial Z^2} - \mathrm{K}C_T \tag{15.28}$$

where:

$$T = \frac{Dt}{RL^2} \tag{15.29}$$

$$Z = \frac{z}{L} \tag{15.30}$$

$$\mathrm{A} = \frac{q_w L}{2D} \tag{15.31}$$

$$\mathrm{K} = \frac{\kappa RL^2}{D} \tag{15.32}$$

with initial and boundary conditions:

$$C_T(0,T) = 0 \tag{15.33}$$

$$C_T(1,T) = g(T) \tag{15.34}$$

$$C_T(Z,0) = f(Z) \tag{15.35}$$

The dimensionless parameter, A, is equivalent to a Peclet number if it is divided by the volumetric moisture content and multiplied by two. In this model, A has been termed the half-Peclet number.

Equation (15.28) subject to equations (15.33) through (15.35), is linear and hence can be solved by the principle of superposition. The solution can be written as:

$$C_T(Z,T) = C_T^I(Z,T) + C_T^{II}(Z,T) \tag{15.36}$$

where C^I_T (Z,T) and C^{II}_T (Z,T) are subject to different initial and boundary conditions. The first solution, C^I_T (Z,T) is due to a nonuniform initial condition, and the second solution, C^{II}_T (Z,T) is due to a nonhomogeneous lower boundary condition. The conditions are as follows:

$$C_T^I(Z,0) = f(Z) \tag{15.37}$$

$$C_T^I(0,T) = 0 \tag{15.38}$$

$$C_T^I(1,T) = 0 \tag{15.39}$$

and

$$C_T^{II}(Z,0) = 0 \tag{15.40}$$

$$C_T^{II}(0,T) = 0 \tag{15.41}$$

$$C_T^{II}(1,T) = g(T) \tag{15.42}$$

A solution to C^I_T (Z,T) can be obtained by the separation of variables technique

$$C_T^I(Z,T) = \sum_{n=1}^{\infty} A_n \exp(\mathrm{A}Z - \omega_n^2 T)\sin(n\pi Z) \tag{15.43}$$

where

$$\omega_n^2 = \mathrm{K} + \mathrm{A}^2 + n^2\pi^2 \tag{15.44}$$

and

$$A_n = 2\int_0^1 \exp(-\mathrm{A}Z')\sin(n\pi Z')\, f(Z')dZ' \tag{15.45}$$

To avoid numerical integration of complex analytical functions, f(Z) can be given by as a piecewise-constant function

$$f(Z) = C_{T(k)} \qquad Z_k \le Z < Z_{k+1} \qquad k = 0,1,2,...,M-1 \tag{15.46}$$

where $Z_0 = 0$, $Z_M = 1$, and M = number of sample intervals. Then

$$A_n = \frac{2}{\mathrm{A}^2 + n^2\pi^2} \sum_{k=0}^{M-1} \left[h\left(Z_k\right) - h\left(Z_{k+1}\right) \right] C_{T(k)} \tag{15.47}$$

where

$$h(z) = e^{-\mathrm{A}Z} \left[\mathrm{A}\sin(n\pi Z) + n\pi\cos(n\pi Z) \right] \tag{15.48}$$

C^{II}_T (Z,T) can be obtained by using Laplace transform techniques by first assuming that g(T)=1, and then obtaining the solution for any arbitrary function of time using superposition. The solution C^{II}_T (Z,T) for g(T)=1 can be called F(Z,T). Taking the Laplace transform with respect to the variable T subject to g(T)=1, and solving the resulting ordinary differential equation in Z yields:

$$\overline{F}(Z,p) = \exp\left(\mathrm{A}(Z-1)\right) \frac{\sinh(\delta Z)}{p\sinh(\delta)} \tag{15.49}$$

where

$$\delta = \left(\mathrm{A}^2 + \mathrm{K} + p\right)^{1/2} \tag{15.50}$$

and p is the transformed time variable. Equation (15.49) must now be inverted using Laplace inversion techniques in order to obtain C^{II}_T (Z,T). This is accomplished using the residue theory. The poles of (15.49) are located at p = 0 and $p = -(A^2+n^2\pi^2+K)$ for n = (1,2,...). The residue at p = 0 is

$$\exp\left(\mathrm{A}(Z-1)\right) \frac{\sinh(\delta Z)}{\sinh(\delta)} \tag{15.51}$$

where δ is now defined as

$$\delta = \left(\mathrm{A}^2 + \mathrm{K}\right)^{1/2}. \tag{15.52}$$

The residues at p = - $(A^2+n^2\pi^2+K) = -\omega_n^2$ (for n=1,2,...) are

$$\exp\left(\mathrm{A}(Z-1)\right)(-1)^n \frac{2n\pi}{\omega_n^2}\exp\left(-\omega_n^2 T\right)\sin(n\pi Z)\,. \tag{15.53}$$

Therefore,

$$F(Z,T) = \exp\left(\mathrm{A}(Z-1)\right)\left[\frac{\sinh(\delta Z)}{\sinh(\delta)} + 2\pi\sum_{n=1}^{\infty}(-1)^n \frac{n}{\omega_n^2}\exp\left(-\omega_n^2 T\right)\sin(n\pi Z)\right]. \tag{15.54}$$

Now, the solution for any arbitrary function g(T) can be approximated as closely as desired by a sum of j discrete step functions (superposition with time) as follows:

$$g(T) = C^*_{T(1)}U(T-T_o) + \sum_{j=1}^{N}\left(C^*_{T(j+1)} - C^*_{T(j)}\right)U(T-T_j) \tag{15.55}$$

where the asterisk denotes soil concentration at the vadose zone - ground-water interface and $U(T-T_j)$ is the Heaviside unit-step function defined such that it is equal to one when $T>T_j$, and equal to zero when $T\leq T_j$. The accuracy of the approximation to a smooth analytical function is improved by increasing N. In practice, any realization of temporal variation in ground-water concentration can be approximated by a series of discrete time steps. The solution for $C^{II}_T(Z,T)$ now can be expressed as

$$C^{II}_T(Z,T) = C^*_{T(1)}F(Z,T-T_o)U(T-T_o) + \sum_{j=1}^{N}\left(C^*_{T(j+1)} - C^*_{T(j)}\right)F(Z,T-T_j)U(T-T_j) \tag{15.56}$$

The solution for $C_T(Z,T)$ can be obtained as the sum of $C^{I}_T(Z,T)$ and $C^{II}_T(Z,T)$

$$C_T(Z,T) = \sum_{n=1}^{\infty} A_n e^{\left(\mathrm{A}Z-\omega_n^2 T\right)}\sin\left(n\pi Z\right) + C^*_{T(1)}e^{\mathrm{A}(Z-1)}\left[\frac{\sinh(\delta Z)}{\sinh(\delta)} + 2\pi\sum_{n=1}^{\infty}\frac{n(-1)^n}{\omega_n^2}e^{-\omega_n^2 T}\sin(n\pi Z)\right]$$
$$+\sum_{j=1}^{N}\left(C^*_{T(j+1)} - C^*_{T(j)}\right)e^{\mathrm{A}(Z-1)}\left[\frac{\sinh(\delta Z)}{\sinh(\delta)} + 2\pi\sum_{n=1}^{\infty}\frac{n(-1)^n}{\omega_n^2}e^{-\omega_n^2(T-T_j)}\sin(n\pi Z)\right]U(T-T_j) \tag{15.57}$$

Average total soil concentration of a compound as a function of dimensionless time, T, can be calculated by:

$$C_T(T)_{avg} = \int_0^1 C_T(Z,T)dZ \tag{15.58}$$

or

$$C_T(T)_{avg} = \sum_{n=1}^{\infty} A_n e^{-\omega_n^2 T} \frac{n\pi\left(1+(-1)^{n+1}e^{\mathrm{A}}\right)}{\mathrm{A}^2+n^2\pi^2} + C^*_{T(1)}e^{-\mathrm{A}}\left[\frac{(\mathrm{A}-\delta)e^{\mathrm{A}+\delta}-(\mathrm{A}+\delta)e^{\mathrm{A}-\delta}+2\delta}{2\sinh(\delta)\left(\mathrm{A}^2-\delta^2\right)}\right]$$

$$+2\pi^2 C^*_{T(1)}e^{-\mathrm{A}}\sum_{n=1}^{\infty}\frac{n^2(-1)^n e^{-\omega_n^2 T}}{\omega_n^2\left(\mathrm{A}^2+n^2\pi^2\right)}\left(1+(-1)^{n+1}e^{\mathrm{A}}\right)$$

$$+\sum_{j=1}^{N}\left(C^*_{T(j+1)}-C^*_{T(j)}\right)e^{-\mathrm{A}}\left[\frac{(\mathrm{A}-\delta)e^{\mathrm{A}+\delta}-(\mathrm{A}+\delta)e^{\mathrm{A}-\delta}+2\delta}{2\sinh(\delta)\left(\mathrm{A}^2-\delta^2\right)}\right]U\left(T-T_j\right)$$

$$+2\pi^2\sum_{j=1}^{N}\left(C^*_{T(j+1)}-C^*_{T(j)}\right)e^{-\mathrm{A}}\left[\sum_{n=1}^{\infty}\frac{n^2(-1)^n e^{-\omega_n^2(T-T_j)}}{\omega_n^2\left(\mathrm{A}^2+n^2\pi^2\right)}\left(1+(-1)^{n+1}e^{\mathrm{A}}\right)\right]U\left(T-T_j\right) \tag{15.59}$$

Total mass per unit area of a compound at any given dimensionless time, T, can be calculated by

$$M_T(T) = LC_{T(avg)} = L\int_0^1 C_T(Z,T)dZ\ . \tag{15.60}$$

Total (advective and diffusive) mass flux of a compound at the ground-water - unsaturated zone interface (Z=1) at any given dimensionless time, T, can be expressed by

$$J_T\left(1,T\right) = \frac{q_w}{R}C_T\left(1,T\right) - \frac{D}{R}\frac{\partial C_T}{\partial Z}\bigg|_{Z=1} \tag{15.61}$$

or

$$J_T\left(1,T\right)=C^*_{T(1)}\left[\frac{q_w}{R}-\frac{D}{RL}\left(\mathrm{A}+\delta\coth\left(\delta\right)+2\pi^2\sum_{n=1}^{\infty}\frac{n^2e^{-\omega_n^2T}}{\omega_n^2}\right)\right]$$

$$+\sum_{j=1}^{N}\left(C^*_{T(j+1)}-C^*_{T(j)}\right)\left[\frac{q_w}{R}-\frac{D}{RL}\left(\mathrm{A}+\delta\coth\left(\delta\right)+2\pi^2\sum_{n=1}^{\infty}\frac{n^2e^{-\omega_n^2\left(T-T_j\right)}}{\omega_n^2}\right)\right]U\left(T-T_j\right) \qquad (15.62)$$

$$-\pi\frac{D}{RL}\sum_{n=1}^{\infty}A_n n(-1)^n e^{\left(\mathrm{A}-\omega_n^2T\right)}$$

Since the orientation of the z-axis is positive downwards, positive values of mass flux denote migration to ground water while negative values of mass flux denote migration from ground water to the vadose zone. Cumulative total (advective/diffusive) mass transfer to and from ground water at any selected dimensionless time, T, can be expressed by

$$M_T\left(1,T\right)=\frac{RL^2}{D}\int_0^T J_T\left(1,T\right)dT \qquad (15.63)$$

or

$$M_T\left(1,T\right)=LC^*_{T(1)}\left[\frac{q_wLT}{D}-\left(\left(\mathrm{A}+\delta\coth\left(\delta\right)\right)T+2\pi^2\sum_{n=1}^{\infty}\frac{n^2\left(1-e^{-\omega_n^2T}\right)}{\left(\omega_n^2\right)^2}\right)\right]+L\sum_{j=1}^{N}\left(C^*_{T(j+1)}-C^*_{T(j)}\right)$$

$$\left[\frac{q_wL}{D}\left(T-T_j\right)-\left(\left(\mathrm{A}+\delta\coth\left(\delta\right)\right)\left(T-T_j\right)+2\pi^2\sum_{n=1}^{\infty}\frac{n^2\left(1-e^{-\omega_n^2\left(T-T_j\right)}\right)}{\left(\omega_n^2\right)^2}\right)\right]U\left(T-T_j\right)$$

$$-\pi L\sum_{n=1}^{\infty}\frac{A_n n(-1)^n}{\omega_n^2}\left(e^{\mathrm{A}}-e^{\left(\mathrm{A}-\omega_n^2T\right)}\right) \qquad (15.64)$$

Total mass flux (in this case only diffusive transfer) of a compound, at any dimensionless time, T, to the atmosphere (Z=0) can be calculated by

$$J_T\left(0,T\right)=-\frac{D}{R}\frac{\partial C_T}{\partial Z}\bigg|_{Z=0} \qquad (15.65)$$

or

$$J_T\left(0,T\right)=-\frac{D}{RL}\left[\pi\sum_{n=1}^{\infty}nA_n e^{-\omega_n^2 T}+2\pi^2 C^*_{T(1)}e^{-\mathrm{A}}\sum_{n=1}^{\infty}\frac{n^2\left(-1\right)^n}{\omega_n^2}e^{-\omega_n^2 T}\right]$$
$$-\frac{D}{RL}\left[\sum_{j=1}^{N}\left(C^*_{T(j+1)}-C^*_{T(j)}\right)e^{-\mathrm{A}}\left(\frac{\delta}{\sinh\left(\delta\right)}+2\pi^2\sum_{n=1}^{\infty}\frac{n^2\left(-1\right)^n}{\omega_n^2}e^{-\omega_n^2\left(T-T_j\right)}\right)\right]U\left(T-T_i\right) \quad (15.66)$$

Since the orientation of the z-axis is positive downwards and a first-type boundary condition of zero constant concentration at the surface has been set, mass flux to land surface will always contain negative values. Cumulative diffusive mass transfer to the atmosphere at any selected dimensionless time, T, can be calculated by

$$M_T\left(0,T\right)=\frac{RL^2}{D}\int_0^T J_T\left(0,T\right)dT \quad (15.67)$$

or

$$M_T\left(0,T\right)=-L\left[\pi\sum_{n=1}^{\infty}\frac{nA_n\left(1-e^{-\omega_n^2 T}\right)}{\omega_n^2}+2\pi^2 C^*_{T(1)}e^{-\mathrm{A}}\sum_{n=1}^{\infty}\frac{n^2\left(-1\right)^n\left(1-e^{-\omega_n^2 T}\right)}{\left(\omega_n^2\right)^2}\right]$$
$$-L\left[\sum_{j=1}^{N}\left(C^*_{T(j+1)}-C^*_{T(j)}\right)e^{-\mathrm{A}}\left(\frac{\delta}{\sinh\left(\delta\right)}\left(T-T_j\right)+2\pi^2\sum_{i=1}^{\infty}\frac{n^2\left(-1\right)^n\left(1-e^{-\omega_n^2\left(T-T_j\right)}\right)}{\left(\omega_n^2\right)^2}\right)\right]U(T-T_j) \quad (15.68)$$

When mass flux at the unsaturated zone - capillary fringe is unidirectional to the capillary fringe, mass lost to decay can now be calculated by

$$M_{T,\deg}(T)=M_T(T)-M_T(1,T)-M_T(0,T)\,. \quad (15.69)$$

15.7 Derivation of Analytical Solutions for Zero-Gradient Lower Boundary Condition

Consider equation (15.28) subject to

$$\left.\frac{\partial C_T}{\partial Z}\right|_{Z=1}=0 \quad (15.70)$$

instead of equation (15.34). Separation of variables where

$$C_T(Z,T) = F(Z)G(T) \tag{15.71}$$

can be used to reduce the governing partial differential equation into two ordinary differential equations

$$\frac{d^2F}{dZ^2} - 2\mathrm{A}\frac{dF}{dZ} + (\omega^2 - \mathrm{K})F = 0 \tag{15.72}$$

$$\frac{dG}{dT} = G\omega^2 . \tag{15.73}$$

If

$$-\lambda^2 = \mathrm{A}^2 + \mathrm{K} - \omega^2 \tag{15.74}$$

then, complex roots result in

$$F(Z) = e^{\mathrm{A}Z}\left(A_1 \cos \lambda Z) + A_2 \sin \lambda Z\right) \tag{15.75}$$

while

$$G(T) = A_3 e^{-\omega^2 T} \tag{15.76}$$

results in

$$C_T(Z,T) = e^{\left(\mathrm{A}Z - \omega^2 T\right)}\left(A_1 \cos \lambda Z + A_2 \sin \lambda Z\right) . \tag{15.77}$$

The specified boundary conditions results in $\mathrm{A}_1 = 0$ and determination of the eigenvalue

$$\lambda = -\mathrm{A} \tan \lambda . \tag{15.78}$$

Since there are an infinite number of roots for this relationship

$$C_T(Z,T) = \sum_{n=1}^{\infty} A_n e^{\left(\mathrm{A}Z - \omega^2 T\right)} \sin\left(\lambda_n Z\right) . \tag{15.79}$$

The initial condition and use of a generalized Fourier series results in

$$A_n = \frac{\int_0^1 e^{-\mathrm{AZ}} f(Z)\sin(\lambda_n Z)dZ}{\int_0^1 \sin^2(\lambda_n Z)dZ}. \tag{15.80}$$

Use of the eigenvalue relationship and several trigonometric identities results in simplification of this expression

$$A_n = \frac{2\left(\mathrm{A}^2 + \lambda_n^2\right)}{\mathrm{A} + \mathrm{A}^2 + \lambda_n^2} \int_0^1 e^{-\mathrm{AZ}} f(Z)\sin(\lambda_n Z)dZ \ . \tag{15.81}$$

Similar to the derivation for the time-dependent boundary condition, f(Z) can be given by a piecewise-constant function

$$f(Z) = C_{T(k)} \qquad Z_k \le Z < Z_{k+1} \qquad k = 0,1,2,...,M-1 \tag{15.82}$$

where $Z_0 = 0$ and $Z_M = 1$. Then

$$A_n = \frac{2}{\mathrm{A} + \mathrm{A}^2 + \lambda_n^2} \sum_{k=0}^{M-1} \left[h\left(Z_k\right) - h\left(Z_{k+1}\right) \right] C_{T(k)} \tag{15.83}$$

where

$$h(Z) = e^{-\mathrm{AZ}} \left[\mathrm{A}\sin(\lambda_n Z) + \lambda_n \cos(\lambda_n Z) \right]. \tag{15.84}$$

Average soil concentration as a function of time can be represented by:

$$C_T(T)_{avg} = \int_0^1 C_T(Z,T)dZ \tag{15.85}$$

or

$$C_T(T)_{avg} = \sum_{n=1}^{\infty} A_n e^{-\omega_n^2 T} \frac{e^{\mathrm{A}} \left(\mathrm{A}\sin(\lambda_n) - \lambda_n \cos(\lambda_n)\right) + \lambda_n}{\mathrm{A}^2 + \lambda_n^2}. \tag{15.86}$$

As before, total mass per unit area of a compound, i, at any given dimensionless time, T, can be calculated by $LC_{T(avg)}$. Flux at the ground-water interface equals

$$J_T(1,T) = \frac{q_w}{R} C_T(1,T) = \frac{q_w}{R} \sum_{n=1}^{\infty} A_n e^{(\mathrm{A} - \omega_n^2 T)} \sin(\lambda_n) . \tag{15.87}$$

Cumulative advective mass transfer to ground water at any selected dimensionless time, T, can be expressed by

$$M_T(1,T) = \frac{RL^2}{D} \int_0^T J_T(1,T) dT \tag{15.88}$$

or

$$M_T(1,T) = \frac{L^2 q_w}{D} \sum_{n=1}^{\infty} A_n e^{\mathrm{A}} \frac{\left(1 - e^{-\omega_n^2 T}\right)}{\omega_n^2} \sin(\lambda_n) . \tag{15.89}$$

Flux at the surface is

$$J_T(0,T) = -\frac{D}{RL} \left. \frac{\partial C_T}{\partial Z} \right|_{Z=0} = -\frac{D}{RL} \sum_{n=1}^{\infty} A_n \lambda_n e^{-\omega_n^2 T} . \tag{15.90}$$

Cumulative diffusive mass transfer to the atmosphere at any selected dimensionless time, T, can be calculated by

$$M_T(0,T) = \frac{RL^2}{D} \int_0^T J_T(0,T) dT \tag{15.91}$$

or

$$M_T(0,T) = -L \sum_{n=1}^{\infty} A_n \lambda_n \frac{\left(1 - e^{-\omega_n^2 T}\right)}{\omega_n^2} . \tag{15.92}$$

As before, mass lost to decay is calculated as before.

Appendix H provides sample input and output files and the source code for VFLUX. Model input is in a free FORTRAN format. This format provides easy and rapid model. Text output files can easily be open as a spreadsheet file and manipulated for graphing.

15.8 Example Simulations

Table 15.2 summarizes input used for VFLUX simulations. Degradation half-life, water saturation, and NAPL saturation were left as variable as these input parameters likely represent

the greatest sources of uncertainty and sensitivity to model output. Use of equation (15.18) assuming a vadose zone thickness (unsaturated media + capillary fringe) of 520 cm, a capillary fringe thickness of 10 cm, and saturation values above the capillary fringe varying from 0.1 to 0.9 resulted in effective water saturations varying from 0.703 to 0.902. Thus, effective water saturations of 0.7, 0.8, and 0.9 were used for model simulation to bracket and provide for a wide range of model output possibilities. With the exception of simulations conducted to assess the impact of infiltration rate on mass flux to ground water, illustrated in Figure 15.4, a relatively low infiltration rate (0.035 cm/d or 5.04 inches/year) was selected for remaining simulations to represent venting application in arid regions of the United States and in more humid regions where an asphalt cap or synthetic liner is placed on the soil surface to minimize infiltration. Trichloroethene (TCE) was chosen for simulation because of its frequent detection at Superfund sites.

Table 15.2 Input for modeling

	Description	Value	Units
S_w	water saturation	variable	$cm^3_{water}/cm^3_{pore\ space}$
S_n	NAPL saturation	variable	$cm^3_{NAPL}/cm^3_{pore\ space}$
η	porosity	0.35	$cm^3_{pore\ space}/cm^3_{soil}$
ρ_b	bulk density	2.15	g_{solids}/cm^3_{soil}
ρ_n	density of NAPL	1.462	g_{NAPL}/cm^3_{NAPL}
C^{sat}_w	water solubility for TCE	1.1E-03	g/cm^3
H	Henry's Law Constant for TCE	0.38	$(ug/cm^3_{air})/(ug/cm^3_{water})$
K_d	soil-water partition coefficient	0.126	$(ug/g_{solids})/(ug/cm^3_{water})$
M_o	average molecular weight of NAPL	131.5	g/mole
M_i	molecular weight of TCE	131.5	g/mole
D_g	free air diffusion coefficient for TCE	6366.8	cm^2/d
D_w	free water diffusion coefficient for TCE	0.804	cm^2/d
q_w	infiltration flux of water	0.035	cm/d
D_m	longitudinal mechanical dispersivity	30.0	cm
κ	first-order degradation rate	variable	1/d

A hypothetical Gaussian-shaped soil concentration profile, illustrated in Figure 15.1, was used to represent the initial condition. Soil concentrations were input in 10 cm increments for model simulation. A hypothetical ground-water concentration versus time profile, typical of many systems undergoing pump and treat aquifer remediation and illustrated in Figure 15.2, was used to represent the lower first-type, time-dependent boundary condition. Ground-water concentrations were input at one year increments for model simulation. Mass flux to ground water as a function of three infiltration rates (0.000, 0.035, and 0.050 cm/d) and two water saturations (0.7 and 0.9) is illustrated in Figure 15.3. As would be expected, mass flux to ground water increased significantly with increased infiltration rate (advective transport) and decreased water saturation (diffusive transport). Of particular interest however, is the duration and potentially environmentally significant magnitude of diffusive mass flux to ground water at high water saturation and zero infiltration rate illustrated in the embedded image of Figure 15.3. This figure reveals why isolating highly contaminated soil (even low permeability soil having a high moisture content) in a capped landfill decreases but does not eliminate mass flux to ground water. Isolation of highly contaminated soil or waste may not be environmentally protective in many circumstances and thus may simply delay but not preclude the use of a source control technology such as venting.

Mass flux to ground water as a function of time and water saturation for first-type, time-dependent and zero-gradient lower boundary conditions are illustrated in Figure 15.4. Since the orientation of the z-axis is positive downwards, positive mass flux for the first-type lower

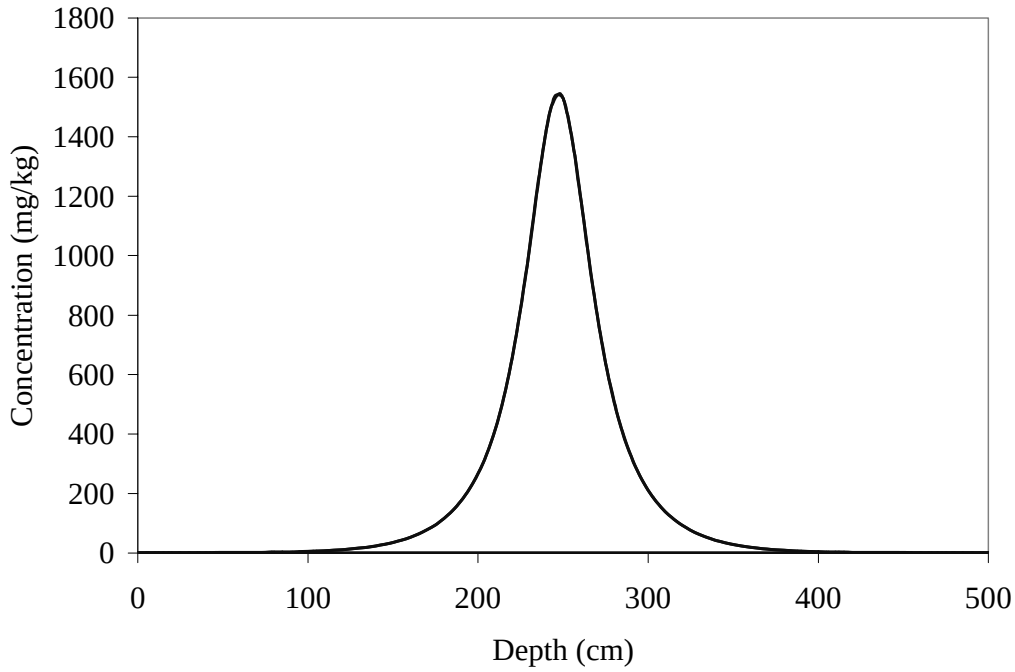

Figure 15.1 Hypothetical initial soil concentration profile.

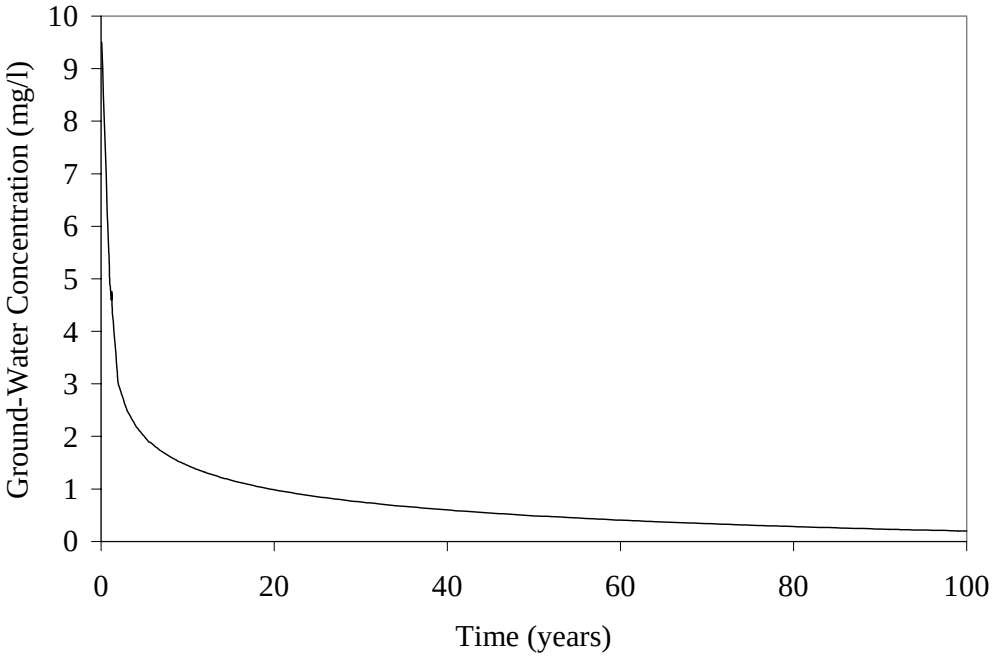

Figure 15.2 Hypothetical ground-water concentration profile

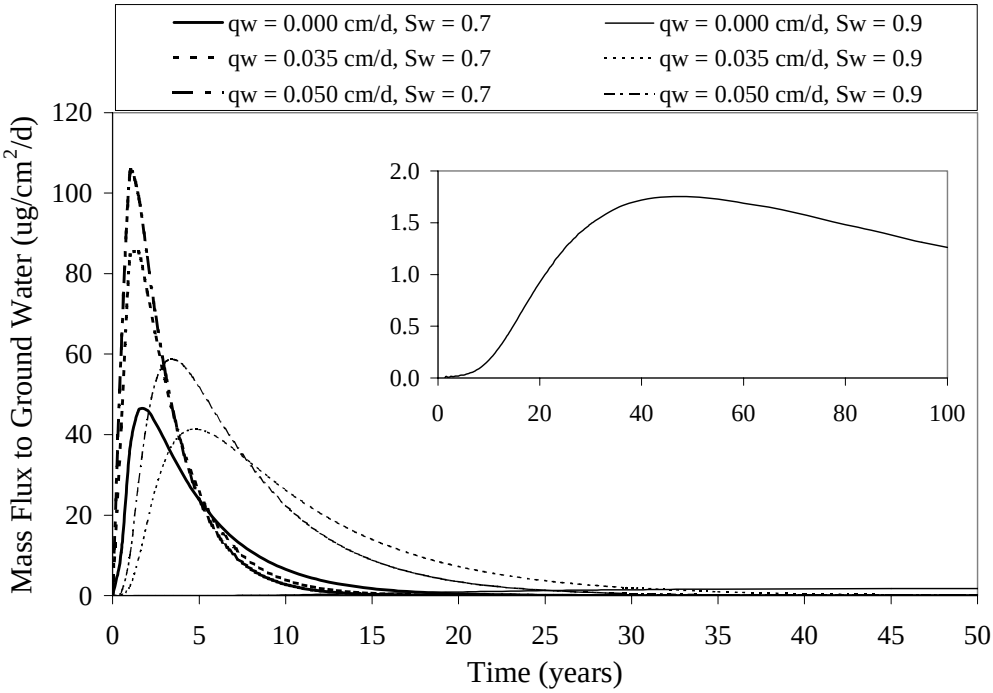

Figure 15.3 Mass flux to ground water as a function of time, infiltration rate, and water saturation for a first-type, time-dependent (TD) lower boundary condition. NAPL absent, no degradation.

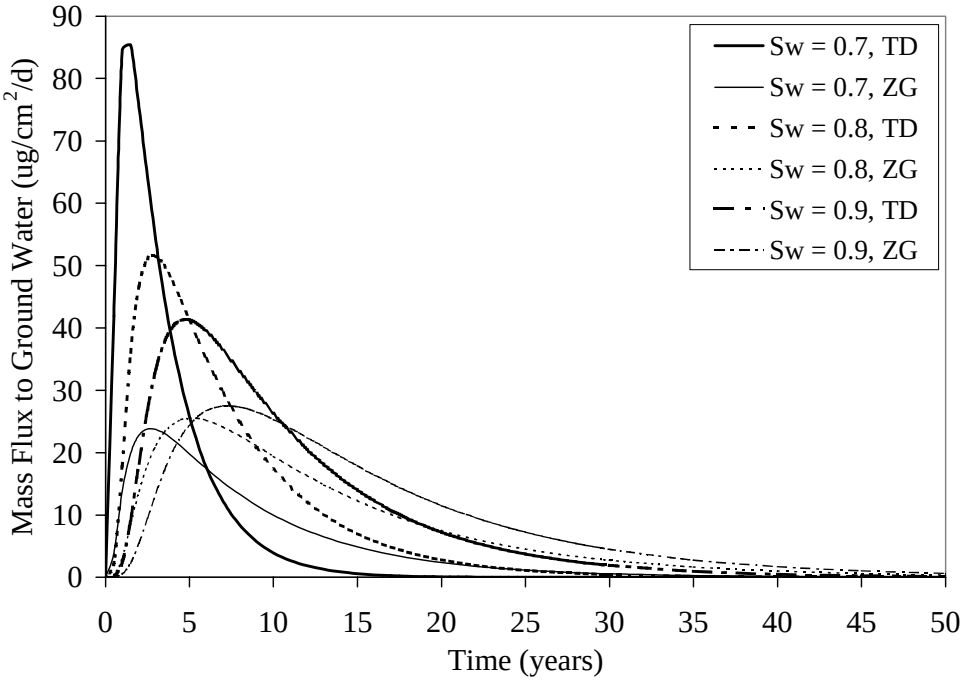

Figure 15.4 Mass flux to ground water as a function of time and water saturation for first-type, time-dependent (TD) and zero-gradient (ZG) lower boundary conditions. NAPL absent, no degradation, q_w = 0.035 cm/d.

boundary condition denotes flux from the vadose zone to ground water while negative mass flux numbers denotes mass flux by diffusion from ground water to the vadose zone. As previously mentioned, for the finite, zero-gradient lower boundary condition, mass transfer from ground water to the vadose zone can not be simulated by virtue of the specified boundary condition. Thus, mass flux values for the finite, zero-gradient lower boundary condition are always positive. For soil concentration vertical profile illustrated in Figure 15.1, mass flux to ground water is always positive for the first-type boundary condition indicating a need to initiate or continue venting application. For the first-type, time-dependent lower boundary condition, increasing water saturation results in a smaller magnitude but longer duration pulse of TCE to ground water with time to reach the maximum mass flux rate shifted to increasing time. For the finite, zero-gradient lower boundary condition, there is also a shift in increasing time to reach the maximum mass flux rate to ground water but the magnitude of the peak mass flux rate remains about the same. Since the infiltration rate was held constant at 0.035 cm/d, the shift in peak mass flux rate to increasing time is due to an increase in the retardation factor from increased water saturation.

As illustrated in Figure 15.5, increased water saturation results in decreased diffusive loss to the atmosphere (1- mass fraction to ground water since degradation loss = 0) and hence a greater mass fraction of initial mass going to the ground water for both types of boundary conditions. However, the mass fraction of initial mass lost to ground water is greater for the first-type, time-dependent lower boundary condition compared to the finite, zero-gradient

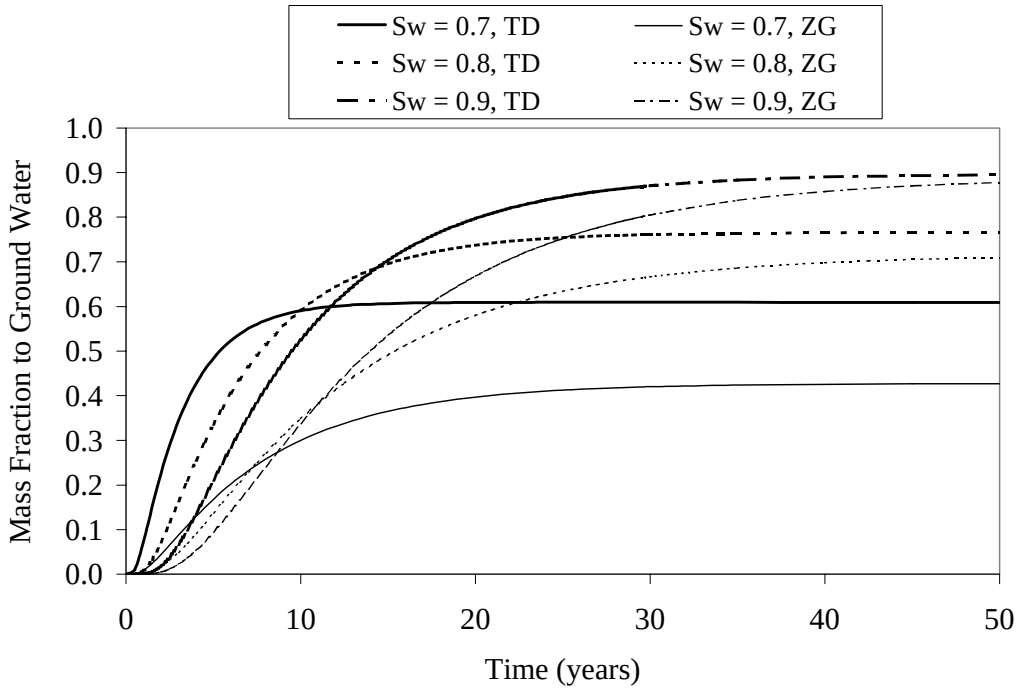

Figure 15.5 Mass fraction of initial mass to lost to ground water as a function of time and water saturation for first-type, time-dependent (TD) and zero-gradient lower boundary conditions. NAPL absent, no degradation, q_w = 0.035 cm/d.

boundary condition for any given water saturation. This is likely due to the fact that the first-type, time-dependent lower boundary condition allows advective and diffusive transfer across the lower boundary while the finite, zero-gradient lower boundary conditions allows only advective transfer.

Figure 15.6 illustrates average soil concentration as a function of time and water saturation for the two lower boundary conditions. Average soil concentration computation supplements mass balance calculations in gaining easy and rapid insight into patterns of mass removal with time. Figure 15.6 shows that average soil concentration was reduced below 1 mg/kg after approximately 50 years for both lower boundary conditions. However, concentration reduction was always more rapid with the use of the first-type, time-dependent boundary condition, especially at lower water saturations because of diffusive movement across the vadose zone - ground-water interface. Figures 15.3 through 15.6 clearly demonstrate that water saturation and selection of a lower boundary condition has a profound affect on the rate of concentration reduction and mass flux from the modeled domain and thus should be carefully considered when simulating VOC transport in the unsaturated zone.

Figures 15.7 and 15.8 illustrate differences in soil concentration as a function of time and depth for the two lower boundary conditions at a water saturation value of 0.9. Soil concentration at the vadose zone - ground-water interface is directly determined by the specified

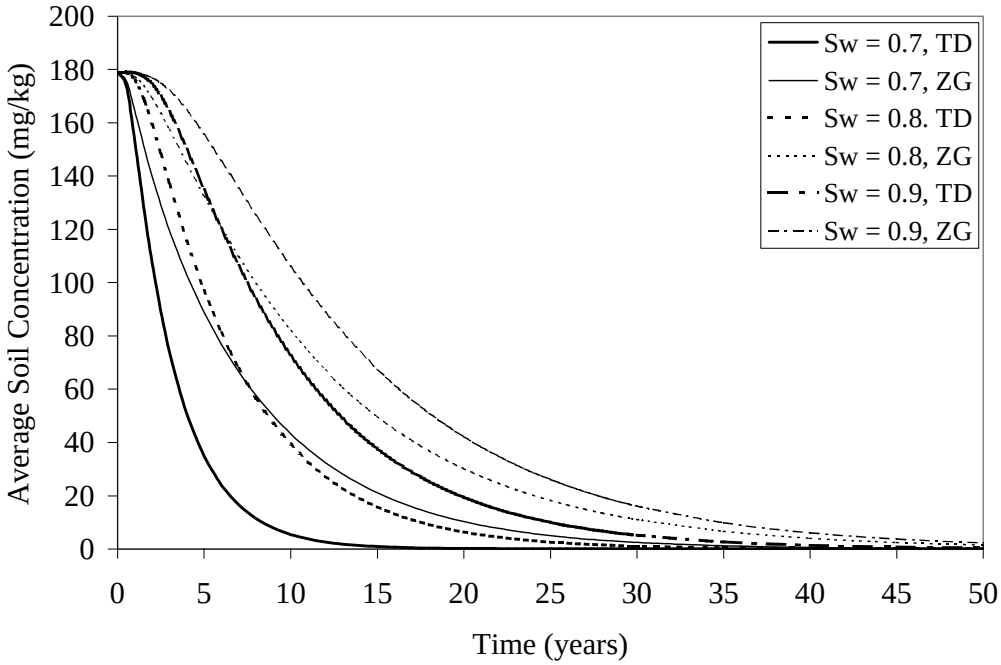

Figure 15.6 Average total soil concentration as a function of time and water saturation for first-type, time-dependent (TD) and zero-gradient (ZG) lower boundary conditions. NAPL absent, no degradation, q_w = 0.035 cm/d.

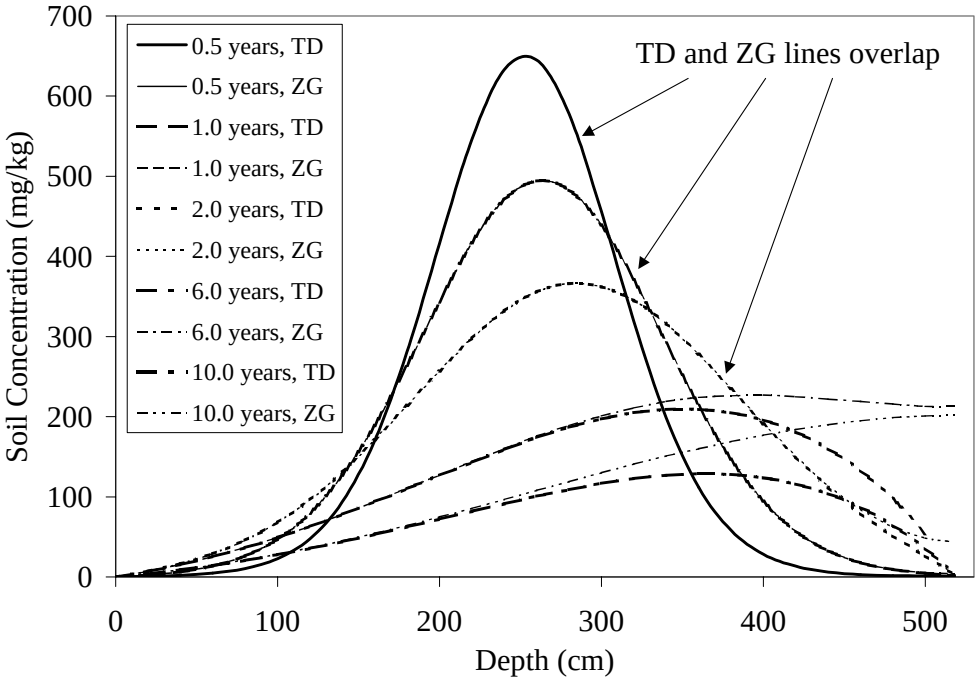

Figure 15.7 Total soil concentration as a function of time (0.5 - 10.0 years) and depth for first-type, time-dependent (TD) and zero-gradient (ZG) lower boundary conditions. Water saturation = 0.9, NAPL absent, no degradation, q_w = 0.035 cm/d.

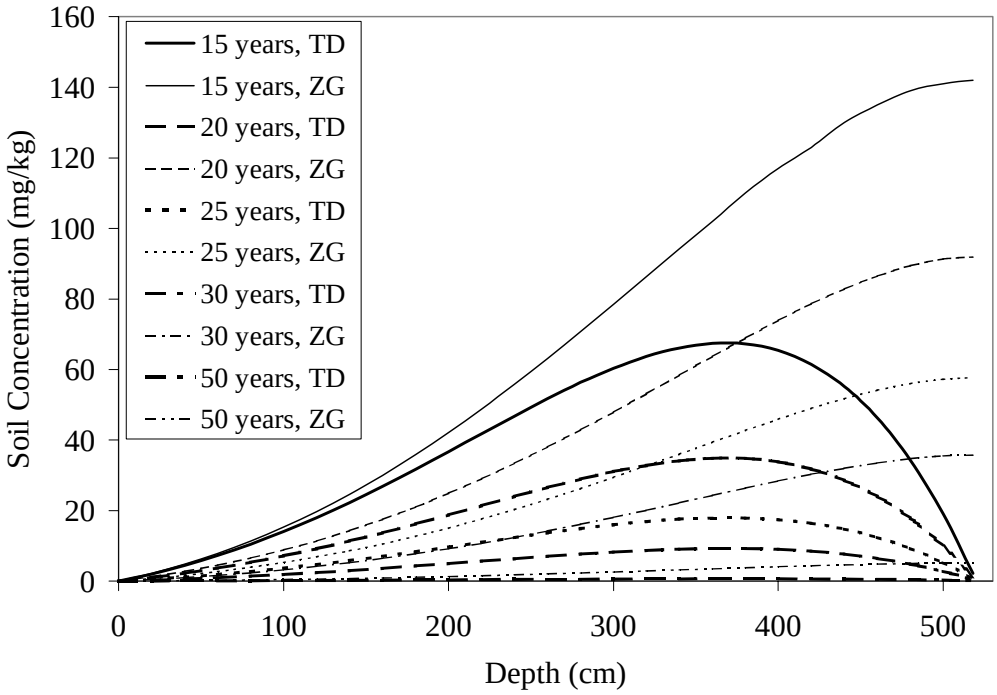

Figure 15.8 Total soil concentration as a function of time (15 - 50 years) and depth for first-type, time-dependent (TD) and zero-gradient (ZG) lower boundary conditions. Water saturation = 0.9, NAPL absent, no degradation, q_w = 0.035 cm/d.

first-type, time-dependent, lower boundary condition whereas soil concentration for the finite, zero-gradient lower boundary condition is allowed to vary independently of temporally varying ground-water concentrations. The effect of the lower boundary condition propagates up the soil column (toward z = 0) with time. For early time (0.5, 1.0, and 2.0 years), soil concentrations are nearly identical throughout the entire profile for the two boundary conditions. At 6 and 10 years simulation time though, soil concentration profiles for the two boundary conditions are identical only at depths less than 300 and 200 cm respectively and show clear deviation with approach to the water table. By 20 years simulation time, the effect of lower boundary condition selection has propagated up the entire soil column. Differences in soil concentration at the vadose zone - ground-water interface for the two boundary conditions increase with time up until approximately 10 years after which they begin to decrease as the contaminant pulse moves through the soil.

Figures 15.9, and 15.10 illustrate the effect that selection of degradation half-life has on mass flux to ground water, cumulative mass lost to degradation, and average soil concentration as a function of time. As would be expected, selection of a high degradation rate or low half-life significantly decreases the magnitude and duration of mass flux to ground water, increases the cumulative mass fraction lost to degradation, and decreases average soil concentration with time for both boundary conditions. Model output results are very sensitive to selection of a degradation half-life, an input parameter in which little is known at the time of modeling. Small

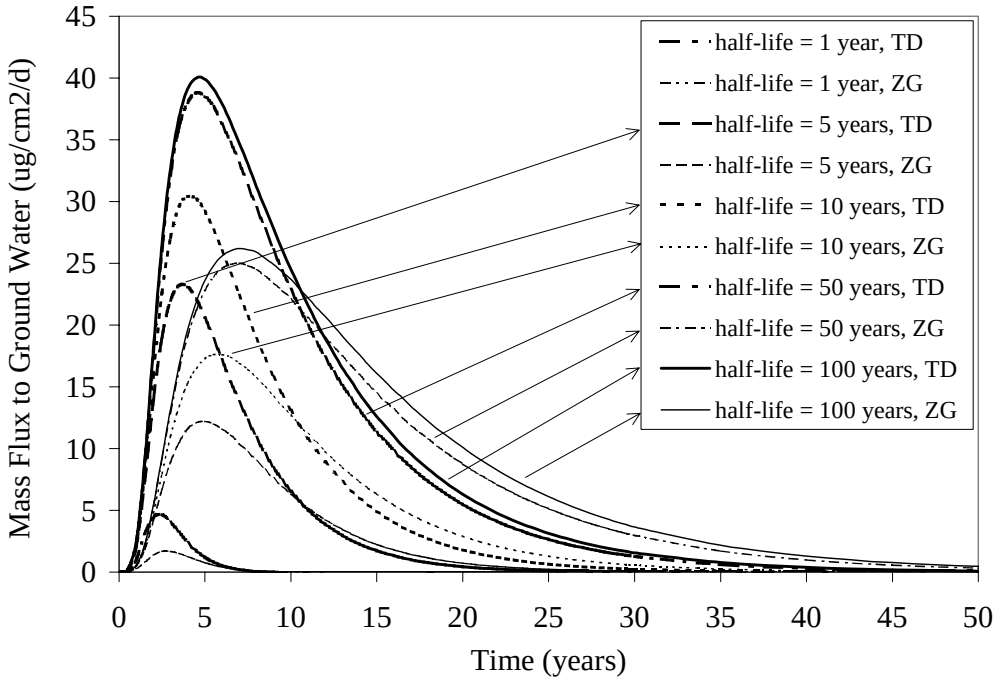

Figure 15.9 Mass flux to the capillary fringe as a function of time and degradation half-life for first-type, time-dependent (TD) and zero-gradient (ZG) lower boundary conditions. Water saturation = 0.9, NAPL absent, q_w = 0.035 cm/d.

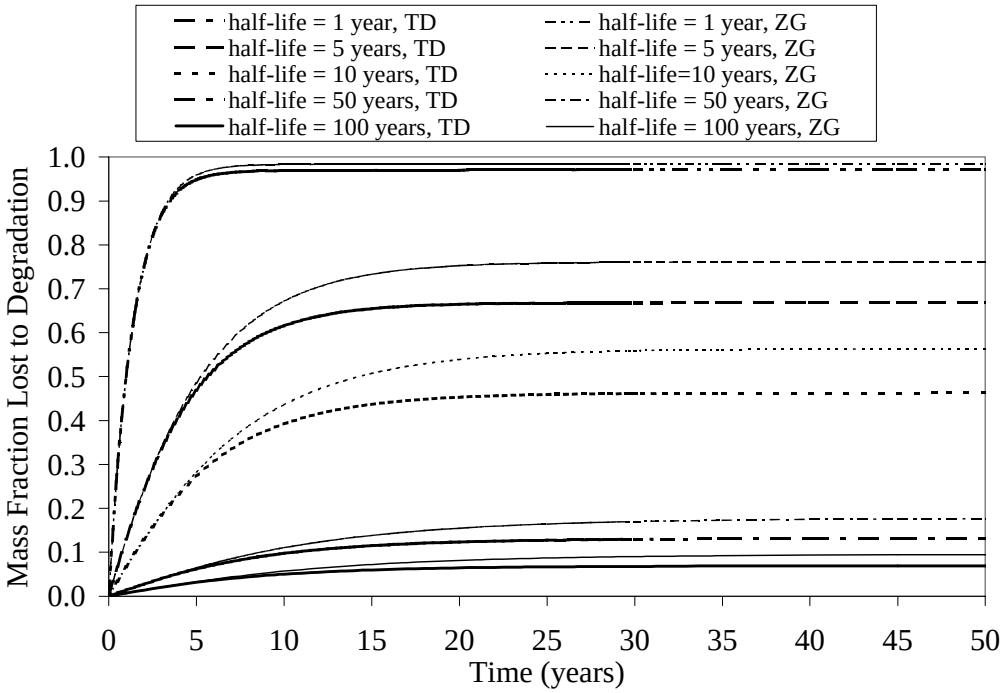

Figure 15.10 Mass fraction of initial mass lost to degradation as a function of time and degradation half-life for first-type, time-dependent (TD) and zero-gradient (ZG) lower boundary conditions. Water saturation = 0.9, NAPL absent, q_w = 0.035 cm/d.

changes in low half-lives (e.g., 1, 5 years) substantially affect model output whereas large changes in large half-lives (e.g., 50 to 100 years) have minimal effect. Notice however from Figure 15.10 that use of a finite, zero-gradient lower boundary condition consistently results in more cumulative mass loss due to degradation compared to a first-type, time-dependent lower boundary condition especially at degradation half-lives of 5 and 10 years. This is likely due to the to the observation that the zero-gradient boundary condition results in higher prolonged concentrations in the soil column compared to the first-type boundary condition. In advection-dispersion problems, delayed transport provides a greater opportunity for degradation.

Figures 15.11, 15.12 and 15.13 illustrate the effect that of NAPL residual saturation on mass flux to ground water, cumulative mass fraction lost to ground water, and average soil concentration. Formulation of equation (15.5) required constant volumetric NAPL content and that NAPL composition not change with time. Thus, NAPL is represented in VFLUX as a nonvolatile, nondegradable oil matrix. A volatile, degradable NAPL would decrease in volumetric content and change in composition (increasing mole fractions of compounds with lower vapor pressure) with time. Because of significantly increased retardation, NAPL saturation decreases the magnitude but dramatically increases the duration of mass flux to ground water for both boundary conditions. For instance, for the first-type boundary condition with no NAPL saturation, mass flux to ground water ceases after 15 years but continues for over 50 years at a NAPL saturation of 0.01. At higher NAPL saturations (0.05), as illustrated in the embedded figure in Figure 15.11, smaller but still potentially environmentally significant mass flux occurs to ground water in excess of the simulation period due to exceeding high retardation factors. As illustrated in figures 15.12 and 15.13, at a NAPL saturation of 0.05, little mass removal or concentration reduction occurs over a 100 year period. The argument of allowing VOCs in the vadose zone to migrate freely to ground water for subsequent removal during pump- and treat is less tractable when NAPL is present in soils because of exceeding long duration of mass flux to ground water. From Figures 15.11, 15.12. and 15.13, it is apparent that model output is very sensitive to specification of NAPL saturation and thus care must be exercised when inputting NAPL saturation values into VOC transport codes.

An important observation for all of the previous simulations is that at high initial soil concentrations, both lower boundary conditions indicated significant mass flux to ground water suggesting the need to initiate or continue venting operation. It is useful now to consider the case of much lower contaminant concentrations in the unsaturated zone, typical of prolonged venting application, to see if both lower boundary conditions result in consistent decision making on whether to initiate or continue venting application. Initial soil concentration levels were reduced by three orders of magnitude. Figure 15.14 illustrates mass flux to ground water as a function of water saturation and boundary condition. Mass flux profiles for the finite, zero-gradient boundary condition are as illustrated in Figure 15.4 but at a 1000 fold reduction. Use of a first-type, time-dependent lower boundary condition though having the same ground-water concentration profile as before though results in entirely different mass flux profile compared to Figure 15.4. At a water saturation of 0.7, the direction of mass flux is initially from the vadose zone to ground water but then switches to mass flux from ground water to the vadose zone after

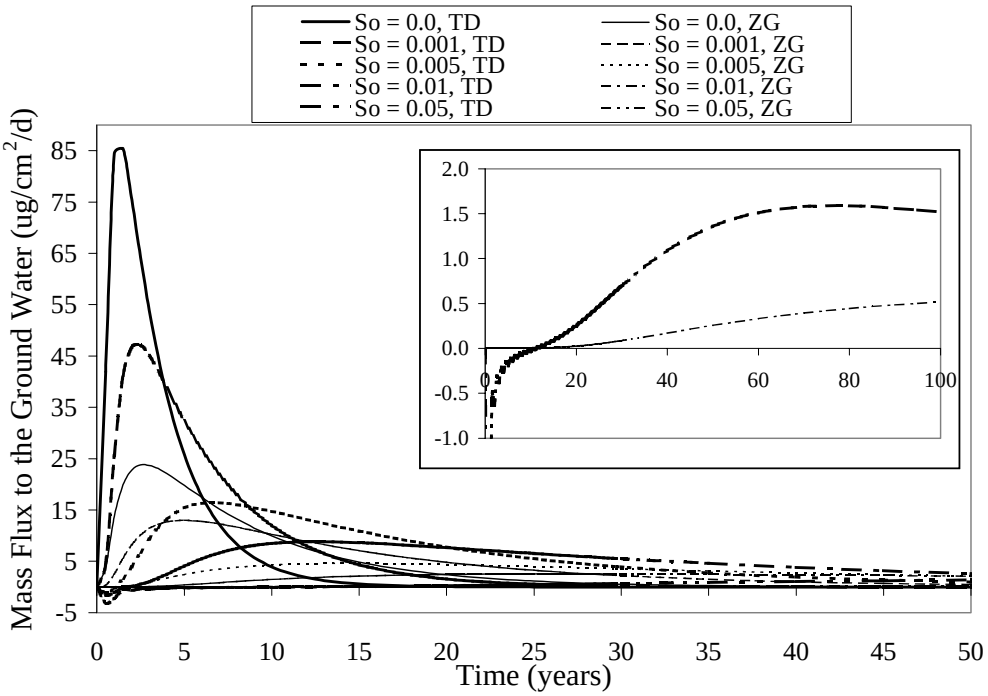

Figure 15.11 Mass flux to ground water as a function of time and NAPL saturation for first-type, time-dependent (TD) and zero-gradient (ZG) lower boundary conditions. Water saturation = 0.7, no degradation, q_w = 0.035 cm/d.

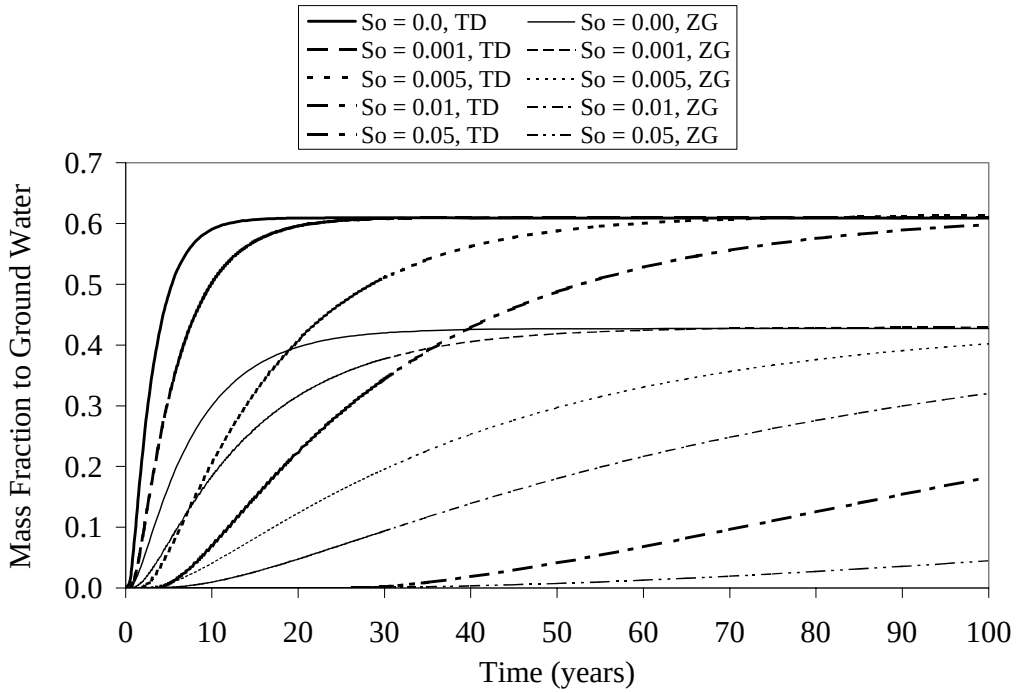

Figure 15.12 Mass fraction of initial mass lost to ground water as a function of time and NAPL saturation for first-type, time-dependent (TD) and zero-gradient (ZG) lower boundary conditions. Water saturation = 0.7, no degradation, q_w = 0.035 cm/d.

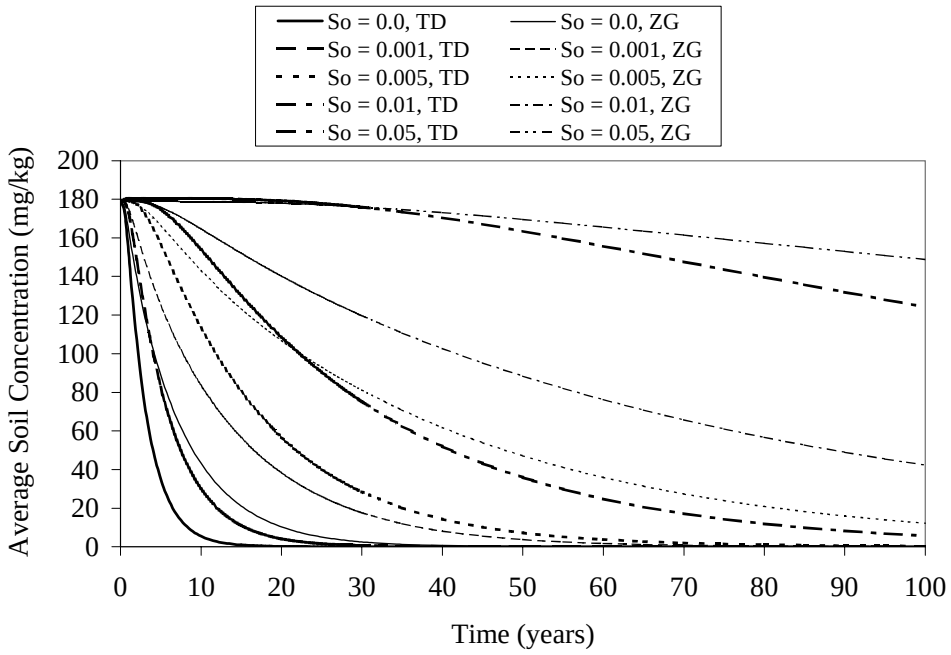

Figure 15.13 Average total soil concentration as a function of time and NAPL saturation for first-type, time-dependent (TD) and zero-gradient (ZG) lower boundary conditions. Water saturation = 0.7, no degradation, q_w = 0.035 cm/d.

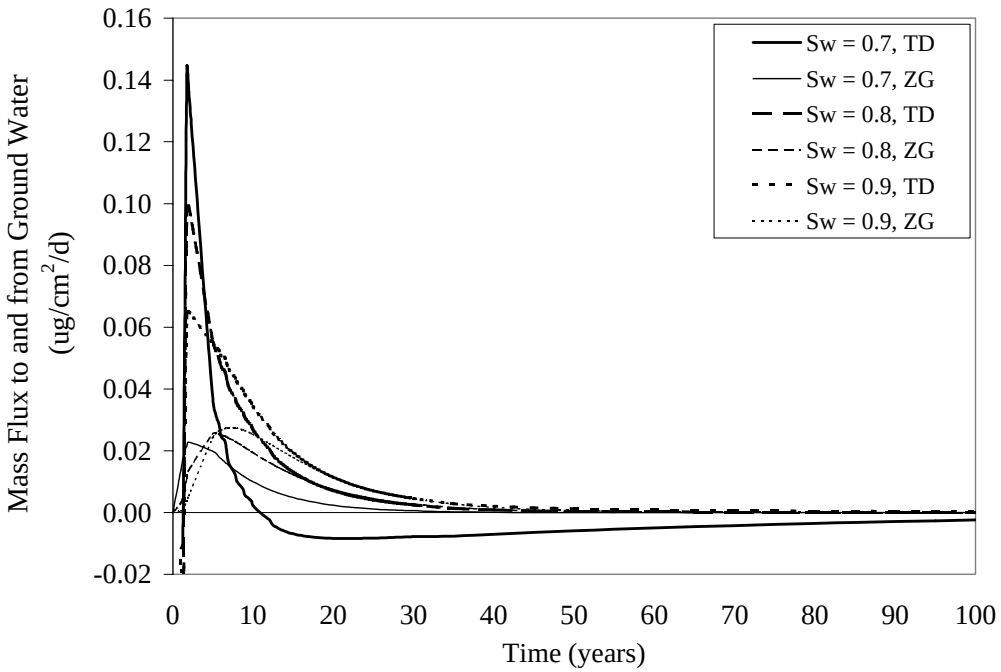

Figure 15.14 Mass flux to ground water as a function of time and water saturation (0.7 - 0.9) for first-type, time-dependent (TD) and zero-gradient (ZG) lower boundary conditions. NAPL absent, no degradation, q_w = 0.035 cm/d.

about 10 years. For higher water saturations (0.8 and 0.9) the direction of mass flux is consistently from the vadose zone to ground water as vapor diffusion to the atmosphere is repressed. Figure 15.15 illustrates average soil concentration as a function of time. The average soil profile illustrates the "inhibitive" effect that the first-type, time-dependent lower boundary condition can have on mass removal from the vadose zone especially at low water saturations. At low initial soil concentration levels, the first-type, time-dependent lower boundary condition consistently results in longer average soil concentration or mass reduction compared to the finite, zero-gradient lower boundary condition. This is opposite of what previously observed in Figure 15.4 at higher initial soil concentration levels. For the first-type, time-dependent lower boundary condition, Figure 15.15 indicates that residual mass remains in soil for over 100 years compared to complete removal after 40 or 50 years for the finite, zero-gradient lower boundary condition. Also, notice that for the first-type, time-dependent lower boundary condition, lower water saturation prolongs the amount of time for average concentration or mass reduction in soil - again opposite of what was previously observed at high soil concentration levels.

Figures 15.16 and 15.17 provide further insight as to how selection of the lower boundary condition affects simulation results when water saturation is held constant at 0.9. As illustrated in Figures 15.16 and 15.17, for the finite, zero-gradient lower boundary condition, soil concentration at the vadose zone - ground-water interface slowly increase with

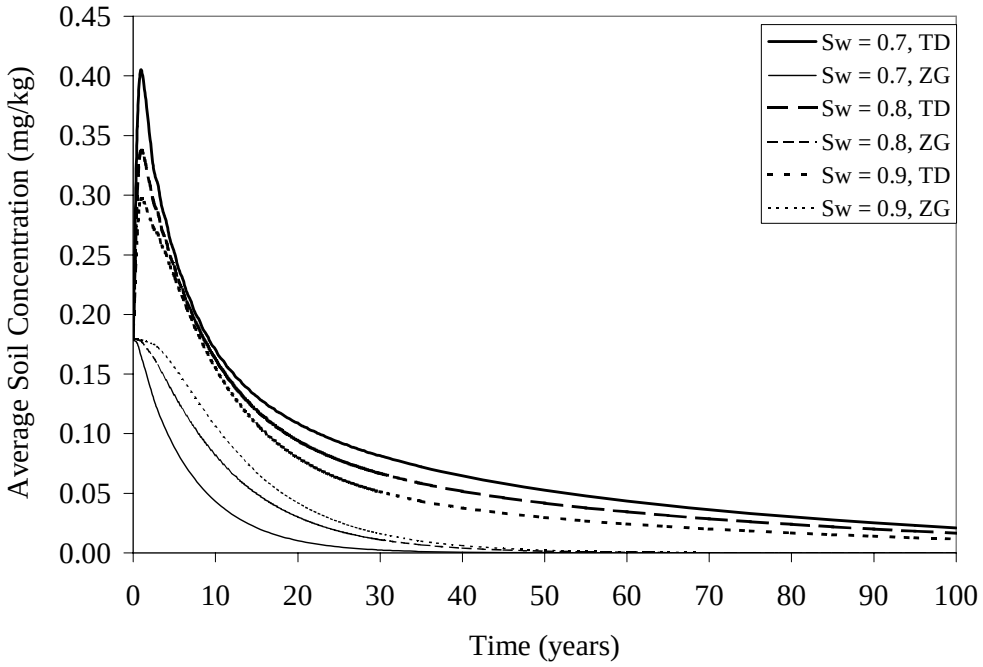

Figure 15.15 Average total soil concentration as a function of time for the low initial soil concentration profile for first-type, time-dependent (TD) and zero-gradient (ZG) lower boundary conditions. NAPL absent, no degradation, q_w = 0.035 cm/d.

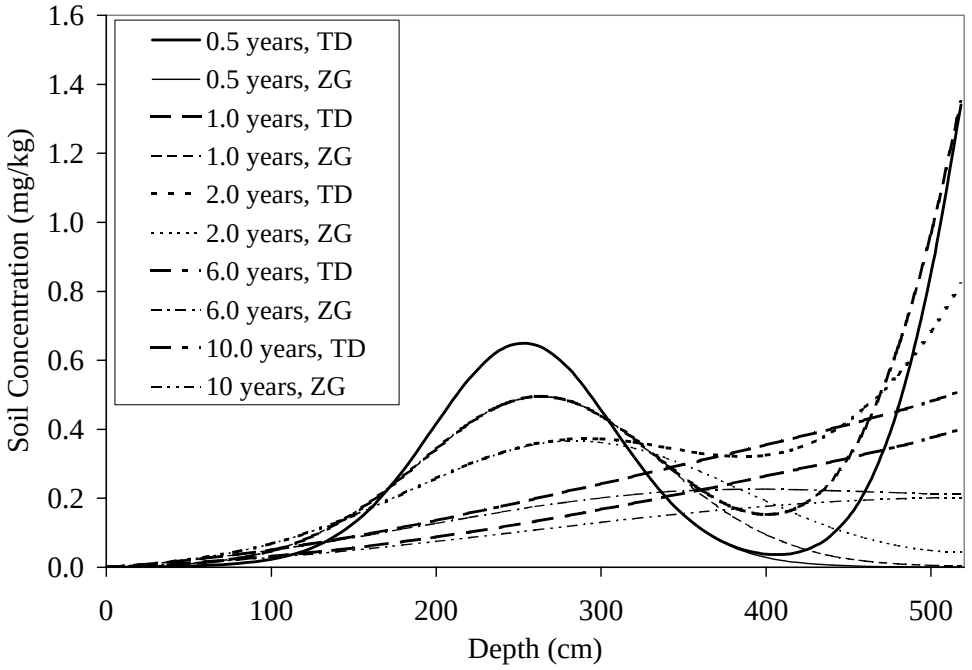

Figure 15.16 Total soil concentration as a function of time (0.5 - 10 years) and depth for low initial soil concentration profile and first-type, time-dependent (TD) and zero-gradient (ZG) lower boundary conditions. Water saturation = 0.9, NAPL absent, no degradation, q_w = 0.035 cm/d.

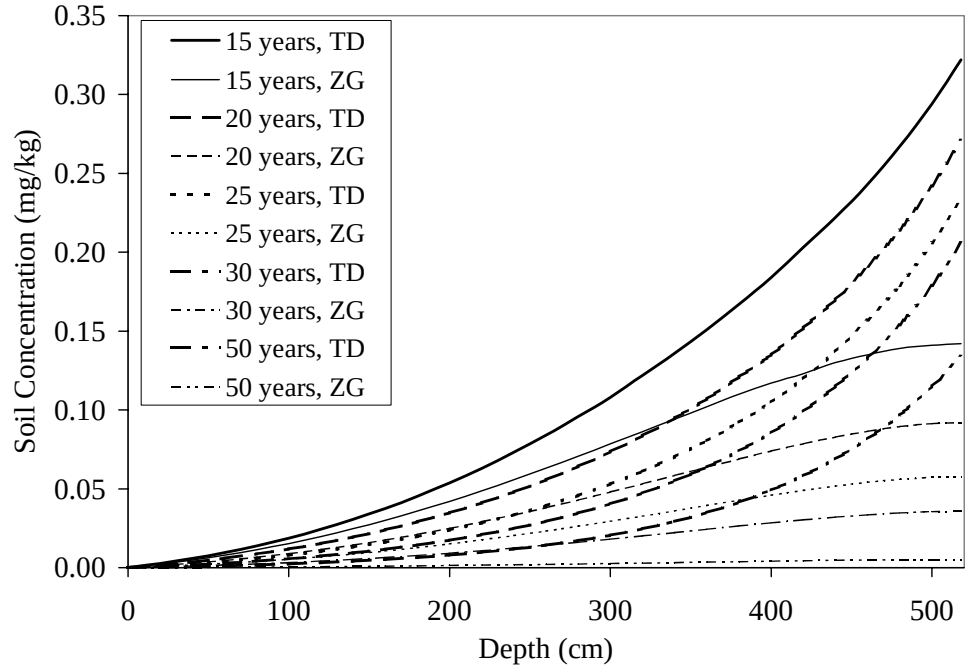

Figure 15.17 Total soil concentration as a function of time (15 - 50 years) and depth for low initial soil concentration profile and first-type, time-dependent (TD) and zero-gradient (ZG) lower boundary conditions.Water saturation = 0.9, NAPL absent, no degradation, q_w=0.035 cm/d.

time as the contaminant mass moves vertically downward peaking at a concentration of about 0.2 mg/kg at about 10 years time. From 10 to 50 years, the concentration at the interface slowly recedes to levels which would be difficult to detect in the field. For the first-type, time-dependent lower boundary condition however, the soil concentration at the interface immediately peaks to 1.4 mg/kg at early time due to mass flux from ground water and then slowly recedes over time. After 50 years simulation time though, concentration levels near the interface remain elevated due to vapor diffusion from ground-water. Similar to the high concentration profile, the affect of selection of the lower boundary condition propagates up the soil column with time only this time at a much faster rate. At time 0.5 years, there is large disparity in concentration profiles at about 400 cm. Concentration versus depth profiles at late time reflect what is frequently observed in the field during soil gas surveys to track ground-water plumes in initially uncontaminated soils. At late time, soil contamination is caused by vapor diffusion from contaminated ground water.

Finally, Figure 15.18 illustrates differences in soil-water concentrations with depth as a function of time (15 to 50 years) and depth. Since equilibrium conditions are presumed to prevail, Figure 15.18 is the same as Figure 15.17 adjusted by the retardation factor. Often, soil-water concentrations at MCLs or MCLs adjusted for a dilution attenuation factor (often 10) are required at the vadose zone - ground-water interface for vadose zone remediation closure, especially in the State of California. Since the MCL for TCE is 5 ug/l, a soil-water concentration

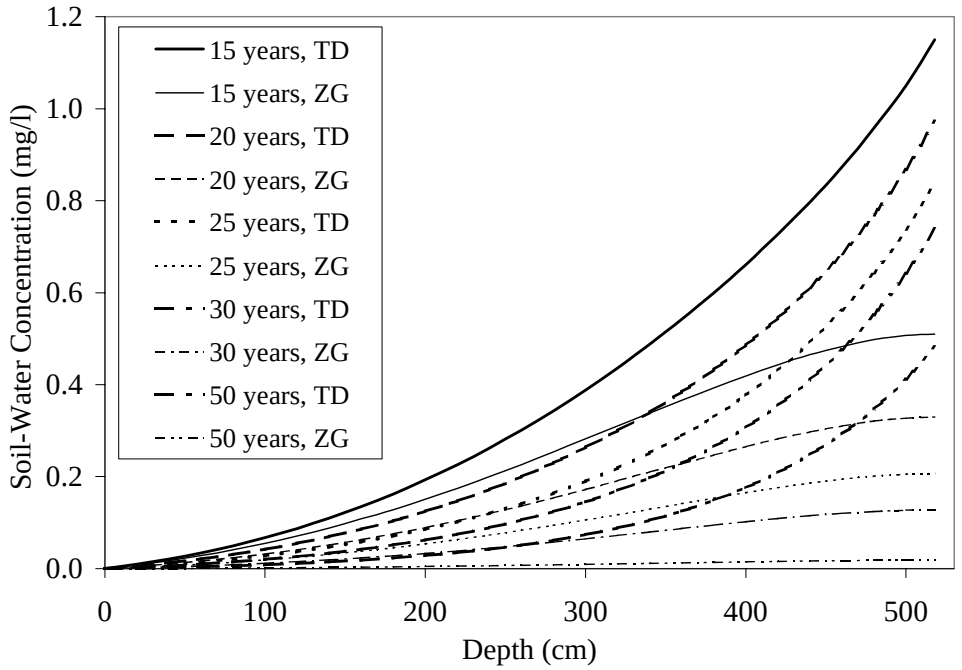

Figure 15.18 Soil-water concentration as a function of time (15 - 50 years) and depth for low initial soil concentration profile for first-type, time-dependent (TD) and zero-gradient (ZG) lower boundary conditions. Water saturation = 0.9, NAPL absent, no degradation, q_w = 0.035 cm/d.

between 5 and 50 ug/l or 0.005 to 0.05 mg/l would be required for closure. With the finite, zero-gradient boundary condition, it would take in excess of 50 years to achieve this level assuming a water saturation level of 0.9 and no degradation. Using a first-type, time-dependent lower boundary condition however, these soil-water concentration levels would not be achievable because of vapor diffusion from ground water. If this type of modeling reflects reality, then venting closure would be unattainable.

Given model output summarized in Figures 15.14 through 15.18 for soils contaminated at low levels, regulatory decision making on whether to initiate, continue, or cease venting or any other vadose zone remediation technology is directly contingent upon selection of the lower boundary condition. It would appear that use of a finite, zero-gradient lower boundary condition would require continued venting application, whereas, use of the first-type, time-dependent lower boundary condition would most likely lead to a decision to cease venting application. This disagreement in decision making was not present for more highly contaminated soils since mass flux to ground water overwhelmed mass flux from the ground water.

15.9 Conclusions

1. Selection of lower boundary conditions and highly sensitive input parameters such as water saturation, NAPL saturation, and degradation half-life significantly affect model output and decision making whether to initiate or cease venting application, especially when soil concentrations are low. A first-type, time-dependent lower boundary condition allows mass transfer across the vadose zone - ground-water interface by infiltration and diffusion. A finite, zero-gradient lower boundary condition only allows mass transfer across the interface by infiltration with soil and soil-water concentrations independent of boundary conditions. For more highly contaminated soils, the first-type, time-dependent lower boundary condition results in a higher magnitude but shorter duration pulse of mass to ground water and a higher cumulative mass fraction to ground water compared to the finite, zero-gradient lower boundary condition. For more highly contaminated soils, regardless of which lower boundary condition is chosen, model simulations clearly indicate a need to initiate or continue venting application. For soils at lower contaminant levels however, use of a first-type, time-dependent lower boundary condition may result in the primary direction of mass flux being from ground water to the vadose zone perhaps questioning the need to initiate or continue venting. The finite, zero-gradient lower boundary condition on the other hand results in sustained but low magnitude mass flux to ground water perhaps prompting a decision to initiate or continue venting. Thus, the two boundary conditions result in contradictory decisions.

2. As previously discussed, a coherent soil venting strategy should link progress in ground-water remediation to vadose zone remediation. A first-type, time-dependent lower boundary conditions accomplishes this with relative ease. Regulators though typically use the model VLEACH and a finite, zero-gradient lower boundary condition when assessing venting closure. This approach is more conservative than use of a first-type,

time-dependent lower boundary condition. Differences in model output inherent in use of these two boundary conditions have been explained and illustrated. Thus, if a finite, zero-gradient lower boundary condition is utilized in vadose zone modeling to assess closure of a venting system, limitations associated with this approach can be understood and taken into account during decision making.

REFERENCES

Abriola, L.M., J. Lang, and K. Rathfelder, Michigan Soil vapor extraction remediation (MISER) model: A computer program to model soil vapor extraction and bioventing of organic chemicals in unsaturated geologic material, U.S. EPA, Office of Research and Development, National Risk Management Research Laboratory, Ada, OK, 1996.

Acomb, L.J., D. McKay, P. Currier, S.T. Berglund, T.V. Sherhart, and C.V. Benediktsson, Neutron probe measurements of air saturation near an air sparging well, In *In Situ Aeration: Air Sparging, Bioventing, and Related Remediation Processes*, Eds. R.E. Hinchee, R.N. Miller and P.C. Johnson, 47-61, Columbus, Ohio. Battelle Press, 1995.

Ahlfeld, D. P., A. Dahmani, and W. Ji, A conceptual model of field behavior of air sparging and its implications for application, *Ground Water Monitoring and Remediation*, Fall, 132-139, 1994.

Ahlers, C.F., S. Finsterle, Y.S. Wu, and G.S. Bodvarsson, Characterization and prediction of subsurface pneumatic response at Yucca Mountain, Nevada, *J. Contam. Hydrol*., 38, 47-68, 1999.

Ahlers, C.F., S. Finsterle, Y.S. Wu, and G.S. Bodvarsson, Determination of pneumatic permeability of a multi-layered system by inversion of pneumatic pressure data, in *Proc. of the 1995 AGU Fall Meeting*, San Francisco, CA, 1995.

Alexander, M., Introduction to Soil Microbiology, John Wiley & Sons, New York, NY, 1977.

Allison, S.B., G.A. Pope, and K. Sepehrnoori, Analysis of field tracers for reservoir description, *J. Pet. Sci. Eng*., 5, 173, 1991.

American Petroleum Institute (API), Recommended practice for core analysis, Procedure RP-40, First Edition, API Production Dept., Dallas, TX, 1960.

American Society for Testing and Materials (ASTM), Standard test method for permeability of rocks by flowing air, Method D 4545, Section 4 Construction, Vol. 04.08 Soil and Rock, Philadelphia, PA, 1990.

Annable, M.D., P.S.C. Rao, K. Hatfield, W.D. Graham, and C.G. Enfield, Partitioning tracers for measuring residual NAPLs for field-scale test results, *J. Environ. Eng*., 124(4), 498-503, 1998.

Armstrong, J.E., E.O. Frind, and R.D. McClellan, Nonequilibrium mass transfer between the vapor, aqueous, and solid phases in unsaturated soils during soil vapor extraction, *Water Resour. Res.*, 30(2), 355-368, 1994.

Atlas, R.M., and R. Bartha, Microbial Ecology - Fundamentals and Applications (3rd ed), The Benjamin/Cummings Publishing Company, Inc., 1993.

Baehr, A.L., and C.J. Bruell, Application of Stefan-Maxwell equations to determine limitations of Fick's law when modeling organic vapor transport in sand columns, *Water Resour. Res.*, 26(6), 1990.

Baehr, A.L. G.E. Hoag, and M.C. Marley, Removing volatile contaminants from the unsaturated zone by inducing advective air phase transport, *J. Contam. Hydrol.*, 4(1),1-26, 1989.

Baehr, A.L., and M.F. Hult, Evaluation of Unsaturated Zone Permeability Through Pneumatic Tests, *Water Resour. Res.*, 27(10), 1991.

Baehr, A.L., and M.F. Hult, Determination of the air-phase permeability tensor of an unsaturated zone at the Bemidji, Minnesota Research Site, U.S. Geological Survey Program on Toxic Waste, Proceedings of the Fourth Technical Meeting, Phoenix, Arizona, September 25-29, Water Resour. Invest. Rep., 88-4220, 55-62, 1988.

Baehr, A.L. and C.J. Joss, An updated model of induced airflow in the unsaturated zone, *Water Resour. Res.*, 31(2), 417-421, 1995.

Bahr, J.M. and J. Rubin, Direct comparison of kinetic and local equilibrium formulations for solute transport affected by surface reaction, *Water Resour. Res.*, 23(3), 438-452, 1987.

Baker, R.S., M.E. Hayes, and S.H. Frisbie, Evidence of preferential vapor flow during insitu air sparging, In *In Situ Aeration:Air Sparging, Bioventing, and Related Remediation Processes*, Eds. R.E. Hinchee, R.N. Miller and P.C. Johnson, 63-74, Columbus, Ohio. Battelle Press, 1995.

Ball, W.P., and P.V. Roberts, Rate-limited sorption of halogenated aliphatics onto sandy aquifer material-experimental results and implications for solute transport, *ES*, 66, 894, 1985.

Barry, D.A., and G. Sposito, Application of the convection-dispersion model to solute transport in finite soil columns, *Soil Sci. Soc. Am. J.*, 52, 3-9, 1988.

Bear, J. Dynamics of fluids in porous media, Dover Publications, Inc., Mineola, NY, 1972.

Beckett, G.D., and D. Huntley, Characterization of flow parameters controlling soil vapor extraction, *Ground Water*, 32(2), 239-247, 1994.

Benson, W.B., and G.J. Farquhar, Experiments on movement of vapour in unsaturated soil, in *Subsurface Contamination by Immiscible Fluids*, 115-121, A.A. Balkema, Rotterdam, 1992.

Berndtson, M.J. and A.L. Bunge, A mechanistic study of forced aeration for in-place remediation

of vadose zone soils, In Proceedings Petroleum Hydrocarbons and Organic Chemicals in Ground Water, Houston, TX, 249-263, 1991.

Bird, B.B, W.E. Stewart, and E. N. Lightfoot, *Transport Phenomena*, John Wiley and Sons, Inc., NY, 1960.

Bloes, M.B., K.M. Rathfelder, and D.M. Mackay, Laboratory studies of vapor extraction for remediation of contaminated soil, in *Subsurface Contamination by Immiscible Fluids*, 255-262, A.A. Balkema, Rotterdam, 1992.

Blunt, M.J., D. Zhou, and D.H. Fenwick, Three-phase flow and gravity drainage in porous media, *Transport in Porous Media*, 20, 77-103, 1995.

Boersma, P.M., K.R. Piontek, and P.A.B Newman, Sparging effectiveness for groundwater restoration, In *In Situ Aeration:Air Sparging, Bioventing, and Related Remediation Processes*, Eds. R.E. Hinchee, R.N. Miller and P.C. Johnson, 39-46, Columbus, Ohio. Battelle Press, 1995.

Bouchard, D.C., A.L. Wood, M.L. Campbell, P. Nkedi-Kizza, and P.S.C. Rao, Sorption nonequilibrium during solute transport, *J. Contam. Hydrol*., 2, 209, 1988.

Brooks, R.H., and A.T. Corey, Hydraulic properties of porous media, *Hydrol. Pap. 3*, Dept. of Civ. Eng., Colo. State Univ., Fort Collins, 1964.

Brown, B.D., and D.E. Rolston, Transport and transformation of methyl bromide in soils, *Soil Sci.*, 130(2), 68-75, 1980.

Brusseau, M.L., The influence of solute size, pore water velocity, and intraparticle porosity on solute dispersion and transport in soil, *Water Resour. Res*., 29(4), 1071-1080, 1993.

Brusseau, M.L., Transport of reactive contaminants in heterogeneous porous media, *Rev. Geophys*., 32(3), 285-13, 1994.

Brusseau, M.L., Transport of organic chemicals by gas advection in structured or heterogeneous porous media: Development of a model and application to column experiments, *Water Resour. Res.*, 27(12), 3189-3199, 1991.

Brusseau, M.L. and P.S.C. Rao, Influence of sorbate structure on nonequilibrium sorption of organic compounds. *Environ. Sci. Technol.*, 25, 1501-1506, 1991.

Brusseau, M.L. and P.S.C. Rao, Sorption nonideality during organic contaminant transport in porous media. *CRC Crit. Rev. Environ. Control*, 19(1), 33-99, 1989a.

Brusseau, M.L. and P.S.C. Rao, The influence of sorbate-organic matter interactions or sorption

nonequilibrium, *Chemosphere*, 18(9/10) 1691-1706, 1989b.

Brusseau, M.L., J. Popovicova, and J.A.K. Silva, Characterizing gas-water interfacial and bulk-water partitioning for gas-phase transport of organic contaminants in unsaturated porous media, *Environ. Sci. Technol*., 31, 1645-1649, 1997.

Brusseau, M.L., R.E. Jessup, and P.S.C. Rao, Nonequilibrium sorption of organic chemicals: Elucidation of rate-limiting processes, *Environ. Sci. Technol.*, 25, 134-142, 1991.

Brusseau, M.L., R.E. Jessup, and P.S.C. Rao, Sorption kinetics of organic chemicals: Evaluation of gas-purge and miscible-displacement techniques, *Environ. Sci. Technol.*, 24(5), 727-735, 1990.

Brusseau, M.L., R.E. Jessup, and P.S.C. Rao, Modeling the transport of solutes influenced by multiprocess nonequilibrium, *Water Resour. Res.*, 25(9), 1971-1988, 1989.

Buckingham, E., Contributions to our knowledge of the aeration of soils, U.S. Dept. Of Agriculture Soils Bur. Bull. 25, 52p, 1904.

Burdine, N.T., Relative permeability calculations from pore size distribution data, *Trans. AIME*, 198, 71-78, 1953.

Butler, J.J., and W.Z. Liu, Pumping tests in nonuniform aquifers: The radially asymmetric case, Water Resour. Res., 29(2), 259-269, 1993.

Cain, B.R., G.R. Johnson, J.E. McCray, W.J. Blanford, and M.L. Brusseau, Partitioning tracer tests for evaluating remediation performance, *Ground Water*, 38(5), 752-761, 2000.

Cameron, D.R., and A. Klute, Convective-dispersive solute transport with a combined equilibrium and kinetic adsorption model, *Water Resour. Res*., 13, 183, 1977.

Carslaw, H.S. and J.C. Jaeger, *Conduction of Heat in Solids*. Oxford University Press Inc., New York, 1959.

Chandler, M.A., G. Kocurek, D.J. Goggin, and L.W. Lake, Effects of stratigraphic heterogeneity on permeability in eolian sandstone sequence, Page Sandstone, Northern Arizona, *AAPG Bull*., 73(5), 658-668, 1989.

Chatzis, I., N.R. Morrow, and H.T. Lin, Magnitude and detailed structure of residual oil saturation, *Soc. Pet. Eng. J.*, 23(2), 311-326, 1983.

Chen, X., An inverse method for soil permeability estimation from gas pump tests, *Computers & Geosciences*, 25, 751-763, 1999

Chen, X., and D.C. Gosselin, Numerical simulation of radial flow: Effects of soil anisotropy, well placement, and surface seal, *J. Hydrol. Eng*., 3(1), 52-61, 1998.

Chiou, C.T., and T.D. Shoup, Soil sorption of organic vapors and effects of humidity on sorptive mechanism and capacity. *Environ. Sci. Technol.*, 19, 1196-1200, 1985.

Chiou, C.T., P.E. Porter, and D.W. Schmedding, Partition equilibria of nonionic organic compounds between soil organic matter and water, *Environ. Sci. Technol.*, 17, 227-231, 1983.

Chiou, C.T., L.J. Peters, and V.H. Freed, A physical concept of soil-water equilibria for nonionic organic compounds. *Science*, 206, p. 831-832, 1979.

Cho, J.S., and D.C. DiGiulio, Pneumatic Pumping Test for Soil Vacuum Extraction. *Environ. Progress*, 11(3), 228-233, 1992.

Cline, P.V., J.J. Delfino, and P.S.C. Rao, Partitioning of aromatic constituents into water from gasoline and other complex mixtures, *Environ. Sci. Technol.*, 25, 914-920, 1991.

Coats, K.H., and B.D. Smith, Dead-end pore volume and dispersion in porous media, *J. Soc. Pet. Eng*., 4, 73, 1964.

Conant, B.H., and P.S.C. Rao, Struggling with the meaning(s) and measures of "success", *Ground Water*, 38(5), 641-642, 2000.

Conklin, M.H., T.L. Corley, P.A. Roberts, J. Hal Davis, and James G. van de Water, Nonequilibrium processes affecting forced ventilation of benzene and xylene in a desert soil, *Water Resour. Res*., 31(5), 1355-1365, 1995.

Cooke, D.E., Jr., Method of determining residual oil saturation, U.S. Patent 3,590,923, U.S. Pat. Off., Washington, D.C., 1971.

Costanza, M, and M.L. Brusseau, Contaminant vapor adsorption at the gas-water interface in soils, *Environ. Sci. Technol*., 34(1), 1-11, 2000.

Corey, A.T., Air permeability, in *Methods of Soil Analysis*, edited by A. Klute et al., pp. 1121-1136, Am. Soc. of Agron./Soil Sci. Soc. of Am., Madison, WI, 1986.

Croisé, J., J.E. Armstrong, and V. Kaleris, Numerical simulation of rate-limited vapour extraction of volatile organic compounds in wet sands, in *Transport and Reactive Processes in Aquifers*, edited by T. Dracos and f. Stauffer, IAHR/AIRH Proc. Ser., Vol. 5, pp. 569-575, A.A. Balkema, Rotterdam, Netherlands, 1994.

Croisé, J., W. Kinzelbach, and J. Schmolke, Computation of air flows induced in the zone of

aeration during in situ remediation of volatile hydrocarbon spills, in *Contaminant Transport in Groundwater*, edited by H.E. Kobus and W. Kinzelbach, pp. 437-444, Balkema, Rotterdam, Netherlands, 1989.

Curtis, G.P., P.V. Roberts, and M. Reinhard, A natural gradient experiment on solute transport in a sand aquifer. IV. Sorption of organic solutes and its influence on mobility, *Water Resour. Res*., 22, 2059, 1986.

Davies, B., and B. Martin, Numerical inversion of the Laplace transform: A survey and comparison of methods, *J. Computational Phy*., 33, 1-32, 1979

Davis, J.M., R.C. Lohmann, F.M. Phillips, J.L. Wilson, and D.W. Love, Architecture of the Sierra Ladrones Formation, Central New Mexico: Depositional controls on the permeability correlation structure, *Geol. Soc. Am. Bull*., 105(8), 998-1007, 1993.

Davis, J.M, J.L. Wilson, and F.M. Phillips, A portable air-minipermeamter for rapid in situ field measurements, *Ground Water*, 32(2), 258-266, 1994.

Deans, H.A., Method of determining fluid saturations in reservoirs, U.S. Patent no. 3,623,842, 1971.

Deans, H.A., Using chemical tracers to measure fractional flow and saturation in-situ, paper SPE 7076 presented at the SPPE Symposium on Improved Oil Recovery, Soc. Pet. Eng., Tulsa, OK, 1978.

Deeds, N.E., G.A. Pope, and D.C. McKinney, Vadose zone characterization at a contaminated field site using partitioning interwell tracer technology, *Environ. Sci. Technol*., 33(16), 2745-2751, 1999.

Detty, T.E., Determination of air and water relative permeability relationships for selected unconsolidated porous media, M.S. Thesis, Dept. of Hydrol. And Wat. Resour., University of Arizona, 1992.

DiGiulio, D.C., SVE systems: When to shut them off. In: U.S. EPA Technical Support Meeting - Technical Session Minutes, http://clu-in.org, tech_slc.pdf, Salt Lake City, Utah, Feb. 11-13, 1998a.

DiGiulio, D.C., Response to comments on SVE closure paper in supoort of the Picillo Farms Site (92-RO1-009), U.S. EPA memorandum to Anna Krasko, 16p, U.S. EPA Region I, Feb. 23, 1998b.

DiGiulio, D.C., Limitations of radius of influence testing for soil vapor extraction design. In: U.S. EPA Technical Support Meeting - Technical Session Minutes, http://clu-in.org,

tech1198.pdf, San Antonio, TX, Nov. 17-20, 1998c.

DiGiulio, D.C., Water displacement during sparging under perched water-table conditions. In: In Situ Aeration: Air Sparging, Bioventing, and Related Remediation Processes, Ed. R.E. Hinchee, R.N. Miller, and P.C. Johnson, Battelle Press, 1995a.

DiGiulio, D. C., Use of a combined air injection/extraction (CIE) well to minimize vacuum enhanced water recovery." In: Proceedings of the 9th National Outdoor Action Conference and Exposition, National Ground Water Association, Dublin, OH, 1995b.

DiGiulio, D.C. and V. Ravi. 1999. An approach for assessment of soil venting performance and closure. In: Subsurface Remediation: Improving long term monitoring and remedial systems performance, Federal Remediation Technologies Roundtable, St Louis, MI, June 8-11, 1999.

DiGiulio, D.C., and R. Varadhan, Steady-state, field-scale gas permeability estimation, pore-gas velocity, and stream function calculation, *Accepted for Publication in: The Journal of Environmental Cleanup Costs, Technologies & Techniques, 2000a*

DiGiulio, D.C. and R. Varadhan, Limitations of ROI testing for venting design: Description of an alternative approach based on attainment of critical pore-gas velocities in contaminated media, *Accepted for publication in Ground Water Monitoring and Remediation*, 2000b.

DiGiulio, D.C., and R. Varadhan, Analysis of water and NAPL saturation, degradation half-life, and boundary conditions on VOC transport modeling: Implications for venting closure, *Submitted to Ground Water Monitoring and Remediation, 2000*c.

DiGiulio, D.C., V. Ravi, and M.L. Brusseau, Evaluation of mass flux to and from ground water using a vertical flux model (VFLUX): Application to the Soil Vacuum Extraction Closure Problem, *Ground Water Monitoring and Remediation*, Spring, 1999.

DiGiulio, D.C., M.L, Brusseau, and V. Ravi, Use of diffusion modeling to aid assessment of rate-limited vapor transport for SVE closure, in *Proceedings of The First International Conference on Remediation of Chlorinated and Recalcitrant Compounds*, Monterey, CA, May 18-21, 1998, Battelle Press, 1998.

Dougherty, D.E., and D.K. Babu, Flow to a partially penetrating well in a double-porosity reservoir, *Water Resour. Res.*, 20(8), 1116-1122, 1984

Dragun, J., The Soil Chemistry of Hazardous Materials, Hazardous Materials Control Research Institute, Solver Spring, MD, 1988.

Domenico, P.A. and F.W. Schwartz, Physical and chemical hydrogeology, John Wiley & Sons, 1990.

Dreyer, T., A. Scheie, and O. Walderhaug, Minipermeameter-based study of permeability trends in channel sand bodies, *AAPG Bull*., 74(4), 359-374, 1990.

Dupont, R.R., Fundamentals of bioventing applied to fuel contaminated sites, *Environmental Progress*, 12(1), 45-53, 1993.

Dupont,R.R., W. Douchette, and R.E. Hinchee, Assessment of in situ bioremediation potential and the application of bioventing at a fuel-contaminated site. In: Hinchee, R.E. and R.F. Olfenbuttel, eds., In Situ and On-Site Bioreclamation. Butterworth-Heinemann, Pub., Stoneham, MA, 262-282, 1991.

Dury, O., U. Fisher, and R. Schulin, A comparison of relative nonwetting-phase permeability models, *Water Resour. Res*., 35(5), 1481-1493, 1999.

Earth Tech. 1997. Installation Restoration Program (IRP), Soil Vapor Extraction Closure Report, Buildings 673 and 763, TCE Source Area Remedial Action, Central Base Area Operable Unit, Norton AFB, San Bernardino, CA, Prepared for AFBCA/DD Norton, Norton AFB, San Bernardino, CA, USAF

Eijpe, R. and K.J. Weber, Mini-permeameters for rock and unconsolidated sand, *Am. Assoc. Petr. Geol. Bull*., 55, 307-309, 1971.

Ellgehausen, H., C.D'Hondt, and R. Fuerer, Reversed-phase chromatography as a general method for determining octan-1-ol/water partition coefficients, *Pesticide Science*, 12, 219-227, 1981.

Estes, R.K. and P.F. Fulton, Gas slippage and permeability measurements, *Trans. Am. Inst. Min, Metall. Pet. Eng*., 207, 338-342., 1956.

Falta, R.W., A program for analyzing transient and steady-state soil gas pump tests, *Ground Water*, 34(4), 750-755, 1996.

Falta, R.W. 1993. Analysis of soil gas pump tests. in: Proc. of the ER'93 Environmental Remediation Conf., Augusta, GA, October 24-28, v. 1, 441-447.

Falta, R.W., I. Javendel, K. Pruess, and P.A. Witherspoon, Density-driven flow of gas in the unsaturated zone due to the evaporation of volatile organic compounds, *Water Resour. Res.*, 25(10), 2159-2169, 1989.

Falta, R.W., K. Pruess, and D.A. Chestnut, Modeling advective contaminant transport during soil vapor extraction, *Ground Water*, 31, 1011-1020, 1993

Fancher, G.H., J.A. Lewis, and K.B. Barnes, Some physical characteristics of oil sands, Penn.

State College Mineral Industries Experimental Station Bulletin 12, 65, 1933.

Ferreira, L.E.A., F.J. Descant, M. Delshad, G.A. Pope, and K. Sepehrnoori, A single-well tracer test to estimate wettability, paper SPE 24136 presented at the SPE/DOE 8th Symposium on Enhanced Oil Recovery, Soc. Pet. Eng., Tulsa, OK, April 22-24, 1992.

Fetter, C.W. 1992. Contaminant hydrogeology, Macmillan Publishing Co., NY, NY

Fisher U., and M.A. Celia, Prediction of relative and absolute permeabilities of gas and water from soil water retention curves using a pore-scale network model, *Water Resour. Res*., 3, 1089-1100, 1999

Fisher, U., O. Dury, H. Flühler, and M.T. van Genuchten, Modeling nonwetting phase relative permeability accounting for a discontinuous nonwetting phase, *Soil Sci. Soc. Am. J*., 61, 1348-1354, 1997.

Fisher, U., C. Hinz. R. Schulin, and F. Stauffer, Assessment of nonequilibrium in gas-water mass transfer during advective gas-phase transport in soils, *J. Contam. Hydrol*., 33, 133-148, 1998.

Fisher, U., R. Schulin, M. Keller, and F. Stauffer, Experimental and numerical investigation of soil vapor extraction, *Water Resour. Res.*, 32(12), 3413-3427, 1996.

Fishtine, S.H., Reliable latent heats of vaporization, *Ind. Eng. Chem*., 55, 47, 1963

Fuller, C.M., and J.M. Sharp Jr., Permeability and fracture patterns in extrusive volcanic rocks: Implication from the Welded Santana Tuff, Trans-Pecos Texas, *Geol. Soc. Am. Bull*., 104, 1485-1496, 1992.

Garbesi, K., R.G. Sextro, A.L. Robinson, J.D. Wooley, J.A. Owens, and W.W. Nazaroff, Scale dependence of soil permeability to air; Measurement method and field investigation, *Water Resour. Res*., 32, 547-560, 1996.

Gelhar, L.W., A.L. Gutjahr, and R.L. Naff, Stochastic analysis of macrodispersion in aquifers. *Water Resour. Res.*, 19(1), 161-180, 1979.

Gierke, J.S., N.J. Hutzler, and J.C. Crittenden, Modeling the movement of volatile organic chemicals in columns of unsaturated soil, *Water Resour. Res.*, 26(7), 1529-1547, 1990.

Gierke, J.S., N.J. Hutzler, and D.B. McKenzie, Vapor transport in unsaturated soil columns: Implications for vapor extraction, *Water Resour. Res.*, 28(2), 323-335, 1992.

Gimmi, T. and H. Flühler, Flux and resident injection in gaseous advection experiments. *Water Resour. Res.*, 32(1), 11-7, 1996.

Gimmi, T, H. Flühler, B. Studer, and A. Rasmuson, Transport of volatile chlorinated hydrocarbons in unsaturated aggregated media, *Water Air Soil Pollut*., 68, 291–395, 1993.

Goggin, D.J., R. Thrasher, and L.W. Lake, A theoretical and experimental analysis of minipermeameter response including gas slippage and high velocity effects, *In Situ*, 12, 79-116, 1988a.

Goggin, D.J., M.A. Chandler, G. Korcurek, and L.W. Lake, Patterns of permeability in eolian deposits: Page Sandstone (Jurassic), northeastern Arizona, *SPE Formation Eval*., 3, 297-306, 1988b.

Goltz, M.N., and M.E. Okley, An analytical solution to equations describing rate-limited soil vapor extraction of contaminants in the vadose zone, *Water Resour. Res*., 30(10), 2691-2698, 1994.

Goss, K., and S.J. Eisenreich, Adsorption of VOCs from the gas phase to different minerals and a mineral mixture, *Environ. Sci. Technol*., 30, 2135-2142, 1996.

Grain, C.F., Vapor pressure, In: Handbook of chemical property estimation methods, Ed. W.J. Lyman, W.F. Reehl, and D.H. Rosenblatt, American Chemical Society, Washington, D.C., 1990.

Grathwohl. P, and M. Reinhard, Desorption of trichloroethylene in aquifer material: Rate limitation at the grain scale, *Environ. Sci. Technol.*, 27(2), 2360-2366, 1993.

Grathwohl, P. J. Farrell, and M. Reinhard, Desorption kinetics of volatile organic chemicals from aquifer materials, in Contaminated Soil '90, edited by F. Arendt, M. Hinsenveld, and W.J. van den Brink, pp. 343-350, Kluwer Academic, Norwell, Mass., 1990.

Gschwend, P.M. and S. Wu, On the constancy of sediment-water partition coefficients of hydrophobic organic pollutants. *Environ. Sci. Technol.*, 19, 90-96, 1985.

Gvirtzman, H. and P.V. Roberts, Pore scale analysis of two immiscible fluids in porous media, *Water Resour. Res*., 27, 1165-1176, 1991.

Hahne, T.W. and K.O. Thomsen, VOC distribution in vadose zone soil gas resulting from a fumigant release, In: Proceedings of the Fifth National Outdoor Action Conference on Aquifer Restoration, Ground Water Monitoring, and Geophysical Methods, NGWA, Dublin, OH, 1991.

Hantush, M.S., Hydraulics of wells, In Advances in Hydroscience, v. 1, Academic, San Diego, CA, p. 281-442, 1964

Hantush, M.S., and C.E. Jacob, Nonsteady radial flow in an infinite leaky aquifer, *Trans. Amer. Geophys. Union*, 36, 95-100, 1955.

Harper, B.M., W.H. Stiver, and R.G. Zytner, Influence of water content on SVE in a silt loam, *J. Environ. Eng*., 124(11), 1047-1053, 1998.

Hassler, G.L., U.S. Patent 2,345,935, 1944.

Hayden, N.J., and T.C. Voice, Microscopic observation of a NAPL in a three-fluid system, *J. Contam. Hydrol.,* 12, 217-226, 1993.

Hayden, N.J., and T.C. Voice, M.D. Annable, and R.B. Wallace, Change in gasoline constituent mass transfer during soil venting, *J. Environ. Eng.*, 120(6), 1598-1614, 1994.

Heid, J.G., J.J. McMahon, R.F. Nielson, and S.T. Yuster, Study of the permeability of rocks to homogeneous fluids, *In: Drilling and Production Practice*, 230-240, API, NY, 1950.

Hinchee, R.E., Bioventing of petroleum hydrocarbons. In: Handbook of Bioremdiation, CRC Press, Inc., pp. 39-59, 1994.

Hinchee, R.E., and M. Arthur, Bench-scale studies of the soil aeration process for bioremediation of petroleum hydrocarbons, *J. Appl. Biochem. Biotech*, 28/29, 901-906, 1991.

Hinchee, R.E., D.C. Downey, R.R. Dupont, P. Aggarwal, and R.N. Miller, Enhancing biodegradation of petroleum hydrocarbons through soil venting. *J. Hazardous Materials*, 27, 315-325, 1991.

Hinchee, R.E., and S.K. Ong, A rapid in situ respiration test for measuring aerobic biodegradation rates of hydrocarbons in soil, *J. Air & Waste Management Assoc*., 1992.

Ho, C.K., and K.S. Udell, An experimental investigation of air venting of volatile liquid hydrocarbon mixtures from homogeneous and heterogeneous porous media, *J. Contam. Hydrol.,* 11, 291-316, 1992.

Ho, C.K., S.-W Liu, and K.S. Udell, Propagation of evaporation and condensation fronts during multicomponent soil vapor extraction, *J. Contam. Hydrol.*, 16, 381-401, 1994.

Hoag, G.E., C.J. Bruell, and M.C. Marley, A study of the mechanisms controlling gasoline hydrocarbon partitioning and transport in groundwater systems, NTIS publication No. PB85-242907, 1984.

Hoff, J.T., D. Mackay, R. Gillham, and W.Y. Shiu, Partitioning of organic chemicals at the air-water interface in environmental systems, *Environ. Sci. Technol*., 27, 2174-2180, 1993.

Hoffman, G.D., D.R. Gan, L.M. Abriola, and K.D. Pennell, Rate limited processes that affect the performance of soil vapor extraction, in Proceedings of the 14th Annual Superfund Conference,

Washington, D.C., 960-967, 1993.

Hogg, D.S., R.J. Burden, and P.J. Riddell, In situ vadose zone bioremediation of soil contaminated with non-volatile hydrocarbon. Presented at HMCRI Conference, Feb. 4. San Francisco, 1992.

Hu, Q. and M.L. Brusseau, The effect of solute size on diffusive-dispersive transport in porous media. Journal of Hydrology, 158, p. 305-317, 1994.

Hu, Q, X. Wang, and M.L. Brusseau, Quantitative structure-activity relationships for evaluating the influence of sorbate structure on sorption of organic compounds by soil. *Environmental Toxicology and Chemistry*, v. 14, no. 7, p.1133-1140, 1995.

Huang, J. and M.N. Goltz, Solutions to equations incorporating the effect of rate-limited contaminant mass transfer on vadose zone remediation by soil vapor extraction, *Water Resour. Res*., 35(3), 879-883, 1999.

Huang, K., Y.W. Tsang, and G.S. Bodvarsson, Simultaneous inversion of air-injection tests in fractured unsaturated tuff at Yucca Mountain, *Water Resour. Res*., 35(8), 2375-2386, 1999.

Hubbert, M.K, The theory of groundwater motion, *J. Geol*., 38(8), 785-944, 1940.

Imhoff, P.T., and P.R. Jaffe, Effect of liquid distribution on gas-water phase mass transfer in an unsaturated sand during infiltration, *J. Contam. Hydrol*., 16, 359-380, 1994.

Jaffe, P.R., and R.A. Ferrara, Desorption kinetics in modeling toxic chemicals, *J. Environ. Eng. Div*., ASCE, 109, 859, 1983.

Jennings, A.A., and D.J. Kirkner, Instantaneous equilibrium approximation analysis, *Hydraul. Eng*., 110 (12), 1700-1717, 1984.

Ji, W., A. Dahmani, D. P. Ahlfeld, J. D. Lin, and E. Hill, Laboratory study of air sparging: Air flow visualization, *GWMR*, 13(4), 115-126, 1993.

Jin, M., G.W. Butler, R.E. Jackson, P.E. Mariner, J.F. Pickens, G.A. Pope, C.L. Brown, and D.C. McKinney, Sensitivity models and design protocol for partitioning tracer tests in alluvial aquifers, *Ground Water*, 35(6), 964-972, 1997.

Jin, M., M. Delshad, V. Dwarakanath, D.C. MkKinney, G.A. Pope, K. Sepehrnoori, C. Tilburg, and R.E. Jackson, Partitioning tracer test for detection, estimation and remediation performance assessment of subsurface nonaqueous phase liquids, *Water Resour. Res*. 31(5), 1201-1211, 1995.

Johnson, J.J., In situ air stripping: Analysis of data from a project near Benson, Arizona, M.S.

Thesis, Colorado School of Mines, CO, 1988.

Johnson, P.C. and R.A. Ettinger, Considerations for the design of in situ vapor extraction systems: radius of influence vs. zone of remedation. *GWMR,* Spring 1994, 123-128, 1994.

Johnson, P.C. and R.A. Ettinger, Heuristic model for predicting the intrusion rate of contaminant vapors into buildings, *Environ. Sci. Technol*., 25(8), 1445-1452, 1991.

Johnson, P.C., R.L. Johnson, C. Neaville, E.E. Hansen, S.M. Stearns, and I.J. Dortch, Do conventional monitoring practices indicate in situ air sparging performance?, In *In Situ Aeration:Air Sparging, Bioventing, and Related Remediation Processes*, Eds. R.E. Hinchee, R.N. Miller and P.C. Johnson, 1-20. Columbus, Ohio. Battelle Press, 1995.

Johnson, P.C., C.C. Stanley, M.W. Kemblowski, D.L. Byers, and J.D. Colthart, A practical approach to the design, operation, and monitoring of in-situ soil venting systems, *Ground Water Monit. Rev.*, 10(2), 159-178, 1990a.

Johnson, P.C., M.W. Kemblowski, and J.D. Colthart, Quantitative analysis for the cleanup of hydrocarbon contaminated soils by in-situ soil venting, *Ground Water*, 28(3), 413-429, 1990b.

Johnson, P.C., M.W. Kemblowski, and J.D. Colthart, Practical Screening Models for Soil Venting Applications, in NWWA/API Conference on Petroleum Hydrocarbons and Organic Chemicals in Groundwater, Houston, TX, 521-546, 1988.

Johnson, T.E. and D.K. Kreamer, Physical and mathematical modeling of diesel fuel liquid and vapor movement in porous media. *Ground Water*, 32(4), 551-560, 1994.

Jones, S.C., The profile permeameter-A new, fast, accurate minipermeameter, paper SPE 24757 presented at the 67th Annual Technical Conference, Soc. of Pet. Eng., Washington, D.C., Oct. 4-7, 1992.

Joss, C.J., and A.L. Baehr, AIR2D - Documentation of AIR2D, A computer program to simulate two-dimensional axisymmetric air flow in the unsaturated zone, U.S. Geological Survey Open File Report 97-588, 1997.

Joss, C.J., and A.L. Baehr. 1995. Documentation of AIR3D, An adaptation of the ground-water-flow code MODFLOW to simulate three-dimensional air flow in the unsaturated zone, U.S. Geological Survey Open-File Report 94-533

Joss, C. J., Baehr, A. L., and J. M. Fisher, A field technique for determining unsaturated zone air-permeability." In: Proceedings of the Symposium on Soil Venting, U.S. Environmental Protection Agency, EPA/600/R-92/174, Robert S. Kerr Environmental Research Laboratory, Ada, OK, 1991.

Jury, W.A., W.R. Gardner, and W.H. Gardner, *Soil Physics*, 5th Ed., John Wiley and Sons, Inc., New York, 1991.

Jury, W.A., W.J. Farmer, and W.F. Spencer, Behavior assessment model for trace organics in soil. II. Chemical classification and parameter sensitivity. *Journal of Environmental Quality*, 13:567-572, 1984a.

Jury, W.A., W.F. Spencer, and W.J. Farmer, Behavior assessment model for trace organics in soil. III. Application of screening model. *Journal of Environmental Quality*, 13:573-579, 1984b.

Jury, W.A., W.F. Spencer, and W.J. Farmer, Behavior assessment model for trace organics in soil, IV. Review of experimental evidence. *Journal of Environmental Quality*, 13:580-585, 1984c.

Kaleris, V. and J. Croisé, Estimation of cleanup time in layered soils by vapor extraction, *J. Contam. Hydrol*., 26, 105-129, 1999.

Kaleris, V. and J. Croisé, Estimation of cleanup time for continuous and pulsed soil vapor extraction, *J. Hydrol*., 194, 330-356, 1997.

Kaluarachchi, J.J., Analytical solution to two-dimensional axisymmetric gas flow with Klinkenberg effect, *J. Environ. Eng*., 121(5), 417-420, 1995.

Kampbell, D.H., J.T. Wilson, and C.J. Griffin, Bioventing of a gasoline spill at Traverse City, Michigan. In: Bioremediation of Hazardous Wastes. EPA/600/R-92/126. Office of Research and Development, 1992a.

Kampbell, D.H., J.T. Wilson, C.J. Griffin, and D.W. Ostendorf, Bioventing reclamation pilot project--aviation gasoline spill. In: Abstracts, Subsurface Restoration Conference. National Center for Ground Water Research. June 21-24, Dallas, Texas, 1992b.

Karger, B.L., R.C. Castells, P.A. Sewell, and A. Hartkopf, Study of the adsorption of insoluble and sparingly soluble vapors at the gas-liquid interface of water by gas chromatography, *J. Phys. Chem.*, 75, 3870-3879, 1971.

Karickhoff, S.W., Organic pollutant sorption in aquatic systems, *J. Hyd. Eng.*, 110(6), 707-735, 1984.

Karickhoff, S.W., Sorption kinetics of hydrophobic pollutants in natural sediments, in *Contaminants and Sediments*, Vol. 2, Chap. 11, Ed. R.A. Baker, Ann Arbor Science, Ann Arbor, MI, 1980

Karickhoff, S.W., D.S. Brown, and T.A. Scott, Sorption of hydrophobic pollutants on natural

sediments, *Water Resour. Res.*, 13, 241-248, 1979.

Karickhoff, S.W., and K.R. Morris, Sorption dynamics of hydrophobic pollutants in sediment suspensions, *Environ. Tox. Chem.*, 4, 469-479, 1985.

Katz, D.L., *Handbook of Natural Gas Engineering*, McGraw-Hill, New York, 1959.

Keelan, D.K., Automated core measurement system for enhanced core data at overburden conditions, *Soc. Petr. Eng.*, 15185: 155-167, 1986.

Kearl, P.M., N.E. Korte, T.A. Gleason, and J.S. Beale, Vapor extraction experiments with laboratory soil columns: Implications for field programs, *Waste Management*, 11, 231-239, 1991.

Kerfoot, H.B., Soil gas surveys in support of design of vapor extraction systems, In: *Soil Vapor Extraction Technology*, Pollution Technology Review, No. 204, Pedersen, T.A. and Curtis, J.T., Eds. Noyes Data Corporation, Park Ridge, NJ, 1991.

Khan, S.U., Interactions of organic matter with pesticides, in *Soil Organic Matter*, edited by M. Schnitzer and S.U. Khan, Elsevier, NY, 1978

Kidder, R.E., Unsteady flow of gas through a semi-infinite porous medium, *J. Applied Mechanics*, 229 - 332, September, 1957.

Kittridge, M.G., L.W. Lake, F.J. Lucia, and G.E. Fogg, Outcrop/subsurface comparisons of heterogeneity in the San Andres Formation, *SPE Form Eval.*, 5(3), 233-240, 1990.

Klinkenberg, L.J., The permeability of porous media to liquids and gases, *Drilling and Production Practice*, American Petroleum Institute, NY, 200-213, 1941.

Koch, R., Molecular connectivity index for assessing ecotoxicological behavior of organic compounds, *Toxicological and Environmental Chemistry*, 6, 87-96, 1983.

Kovalick. W. Jr., Oral presentation at: U.S. EPA Conference on: Abiotic In Situ Technologies for Groundwater Remediation, Dallas, TX, August 31 - September 2, 1999.

Kreft, A. and A. Zuber, On the physical meaning of the dispersion equation and its solutions for different initial and boundary conditions. *Chem. Eng. Sci.*, 33, 1471-1480, 1978.

Kreft, A., and A. Zuber, On the physical meaning of the dispersion equation and its solutions for different initial and boundary conditions, *Chem. Eng. Sci.*, 33, 1471-1480, 1978.

Kreft, A., and A. Zuber, Comments on "Flux-averaged and volume-averaged concentrations in continuum approaches to solute transport" by J.C. Parker and M. Th. van Genuchten, *Water*

Resour. Res., 22(7), 1157-1158, 1986.

Krishnayya, A.V., M.J. O'Conner, J.G. Agar, and R.D. King, Vapour extraction system factors affecting their design and performance, in *Proceedings of the NWWA/API Conference on Petroleum Hydrocarbons and Organic Chemicals in Groundwater-Prevention, Detection, and Restoration*, pp. 547-568, National Water Well Association, Dublin, OH, 1988.

Lee, L.S., M. Hagwall, J.J. Delfino, and P.S.C. Rao, Partitioning of polycyclic aromatic hydrocarbons from diesel fuel into water, *Environ. Sci. Technol*., 26(11), 2104-2110, 1992.

Lee, L.S., P.S.C. Rao, M.L. Brusseau, and R.A. Ogwada, Nonequilibrium sorption of organic contaminants during flow through columns of aquifer material, *Environ. Tox. Chem*., 110, 779, 1988.

Leinonen, P.J., D. Mackay, *Can. J. Chem. Eng*., 51, 230-233, 1973.

Lenhard, R.J. and J.C. Parker, A model for hysteretic constitutive relations governing mulitphase flow, 2, Permeability-saturations relations, *Water Resour. Res*, 23, 2197-2206, 1987.

Liang, H.C. and K.S. Udell, Experimental and theoretical investigation of vaporization of liquid hydrocarbon mixtures in water-wetted porous media, *Water Resour. Res*., 35(3), 635-649, 1999.

Lichtenberger, G.J., Field applications of interwell tracers for reservoir characterization of enhanced oil recovery pilot areas, paper SPE 21652 presented at the SPPE Symposium on Production Operations, Soc. Pet. Eng., Oklahoma City, OK, 1991.

Liikala, T.L., K.B. Olsen, S.S. Teel, and D.C. Lanigan, Volatile organic compounds: Comparison of two sample collection and preservation methods, *Environ. Sci. Technol*., 30(12), 3441-3447, 1996.

Lingineni, S. and V.K. Dhir, Modeling of soil venting processes to remediate unsaturated soils, *J. Environ. Eng.*, 118(1), 135-151, 1992.

Lorden, S.W., W. Chen, and L.W. Lion, Experiments and modeling of the transport of trichloroethene vapor in unsaturated aquifer material, *Environ. Sci. Technol*., 32(13), 2009-2017, 1998.

Luckner, L., M.T. van Genuchten, and D.R. Nielson, A consistent set of parametric models for the two-phase flow of immiscible fluids in the subsurface, *Water Resour. Res.*, 25, 2187-2193, 1989.

Lundegard, P.D., Air sparging: much ado about mounding. In *In Situ Aeration:Air Sparging, Bioventing, and Related Remediation Processes*, Eds. R.E. Hinchee, R.N. Miller and P.C.

Johnson, 21-30. Columbus, Ohio. Battelle Press, 1995.

Lundegard, P.D.and G. Andersen, Numerical simulation of air sparging performance. In *Proc. Petroleum Hydrocarbon and Organic Chemicals in Ground Water: Prevention, Detection, and Restoration*, 461-476. Dublin, Ohio. National Ground Water Association, 1993.

Mariner, P.E., M. Jin, J.E. Studer, and G.A. Pope, The first vadose zone partitioning interwell tracer test for nonaqueous phase liquid and water residual, *Environ. Sci. Technol*., 33(16), 2825-2828, 1999.

Marley, M.C., C.J. Bruell, and H.H. Hopkins, Air sparging technology: A practice update, In *In Situ Aeration:Air Sparging, Bioventing, and Related Remediation Processes*, Eds. R.E. Hinchee, R.N. Miller and P.C. Johnson, 31-37, Columbus, Ohio. Battelle Press, 1995.

Massmann, J.W., Applying groundwater flow models in vapor extraction system design, *J. Environ. Eng.*, 115(1), 129-149, 1989.

Massmann, J. and D.F. Farrier, Effects of atmospheric pressures on gas transport in the vadose zone, *Water Resour. Res.*, 28(), 777-791, 1992.

McCall, P.J., and G.L. Agin, Desorption kinetics of picloram as affected by residence time in the soil, *Environ. Tox. Chem*., 4, 37, 1985

McCarty, P.L., M. Reinhard, and B.E. Rittmann, Trace organics in groundwater. *Environmental Science and Technology*, 15, p. 40-51, 1981.

McClellan, R.D., and R.W. Gilham, Vapor extraction of trichloroethylene under controlled field conditions, paper presented at Conference on Subsurface Contamination by Immiscible Liquids, International Association of Hydrogeologists, Calgary, Alberta, Canada, April, 1992.

Means, J.C., S.G. Wood, J.J. Hasset, and W.L. Banwart, Sorption of polynuclear aromatic hydrocarbons by sediments and soils. *Environ. Sci. Technol.*, 14(12), 40-51, 1981.

Mendoza, C.A., and E.O. Frind, Advective-dispersive transport of dense organic vapors in the unsaturated zone, 1, Model development, *Water Resour. Res*., 26(3), 379-387, 1990a.

Mendoza, C.A., and E.O. Frind, Advective-dispersive transport of dense organic vapors in the unsaturated zone, 2, Sensitivity analysis, *Water Resour. Res*., 26(3), 388-398, 1990b.

Miller, R.N., A field scale investigation of enhanced petroleum hydrocarbon biodegradation in the vadose zone combining soil venting as an oxygen source with moisture and nutrient additions. Ph.D. Dissertation. Utah State University, Logan, Utah, 1990.

Miller, R.N., and C.C. Vogel, A field investigation of petroleum biodegradation in the vadose zone enhanced by soil venting at Tyndall AFB, Florida. In: Hinchee, R.E. and R.F. Olfenbuttel, eds., In Situ and On-Site Bioreclamation. Butterworth-Heinemann, Pub., Stoneham, MA. pp. 283-302, 1991.

Miller, R.N., R.E. Hinchee, C.M. Vogel, A field scale investigation of soil venting enhanced petroleum hydrocarbon biodegradation in the vadose-zone at Tyndall, AFB, Florida. In: Proceedings of the Symposium on Soil Venting. EPA/600/R-92/174, April 29-May 1, 1991, Houston, Texas, pp. 293-308, 1992.

Millington, R.J. and J.P. Quirk, Permeability of porous solids, *Trans. Faraday Soc*., 57, 1200-1207, 1961.

Mingelgrin, U., and Z. Gerstl, Reevaluation of partitioning as a mechanism of nonionic chemicals adsorption in soils, *J. Environ. Qual*., 12, 1-11, 1983.

Moench, A.F., and A. Ogata, A numerical inversion of the Laplace transform solution to radial dispersion in a porous medium, *Water Resour. Res*., 17(1), 250-252, 1981.

Mualem, Y., A new model for predicting the hydraulic conductivity of unsaturated porous media, *Water Resour. Res*., 12, 513-522, 1976.

Muskat, M. And H.G. Botset, Flow of gases through porous materials, *Physics*, 1, 27-47, 1931.

Muskat, M., Principles of Oil Production, McGraw Hill Book Co., New York, 1949.

Nadim, F., A. Nadim, G.E. Hoag, A.M. Dahmani, Desorption rate limitation in the extraction of organic molecules from unsaturated soils during soil venting operations, *J. Contam. Hydrol*., 25, 21-37, 1997.

National Research Council, Alternatives for ground water cleanup, National Academy Press, Washington, D.C., pp. 267-272, 1994.

Nelson, N.T., and M.L. Brusseau, Field study of the partitioning tracer method for detection of dense nonaqueous phase liquid in a trichloroethene-contaminated aquifer, *Environ. Sci. Technol*., 30(9), 2859-2863, 1996.

Nkedi-Kizza, P., P.S.C. Rao, R.E. Jessup, and J.M. Davidson, Ion exchange and diffusive mass transfer during miscible displacement through an aggregated oxisol, *Soil Sci. Soc. Am. J*., 46, 471, 1982.

Nkedi-Kizza, P., M.L. Brusseau, P.S.C. Rao, and A.G. Hornsby, Nonequilibrium sorption during displacement of hydrophobic organic chemicals and ^{45}Ca through soil columns with aqueous and

mixed solvents, *Environ. Sci. Technol.*, 23(7), 814-820, 1989.

Ng, Chiu-On, and C.C. Mei, Aggregate diffusion model applied to soil vapor extraction in unidirectional and radial flows. *Water Resources Research*, vol. 32, no 5, pp. 1289-1297, 1996.

Ng, C.O., C.C. Mei, and D.W. Ostendorf. A model for stripping multicomponent vapor from unsaturated soil with free and trapped residual nonaqueous phase liquid, *Water Resour. Res.*, 35(2), 385-406, 1999.

Novakowski, K.S., An evaluation of boundary conditions for one-dimensional solute transport 1. Mathematical development, *Water Resour. Res*., 28(9), 2399-2410, 1992.

Novakowski, K.S., An evaluation of boundary conditions for one-dimensional solute transport 2. Column experiments, *Water Resour. Res*., 28(9), 2411-2423, 1992.

Nyer, E.K, R.W. Macneal, and D.C. Schafer, VES design: Using simple or sophisticated design methods. *Ground Water Monitoring and Remediation*, Summer, 1994, p.101-104, 1994.

Oliver, B.G., Desorption of chlorinated hydrocarbons from spiked and anthropogenically contaminated sediments, *Chemosphere*, 14, 1087, 1985.

Olsen, R.L., and A. Davis, Predicting the fate and transport of organic compounds in groundwater: Part 1, *Hazardous Materials Control*, 3 (3), 38-64, 1990.

Or, D., and M. Tuller, Liquid retention and interfacial area in variably saturated porous media: Upscaling from single-pore to sample-scale model, *Water Resour. Res*., 35(12), 3591-3605, 1999.

Ostendorf, D.W., D.J. DeGroot, M.M. Meyer, and S.J. Pollock, Evaporation rates and reaction kinetics of petroleum biosparging from intact cores sleeves, in *Global Environmental Biotechnology*, edited by D.L. Wise, 639-659, Elvesier, NY, 1997.

Pankow, J.F., R.L. Johnson, and J.A. Cherry, Air sparging in gate well in cutoff walls and trenches for control of plumes of volatile organic compounds (VOCs), *Ground Water*, 31(4), 654-663, 1993.

Parker, J.C., and R.J. Lenhard. A model for hysteretic constitutive relations governing multiphase flow, 1. Saturation-pressure relations, *Water Resour. Res.*, 23(12), 2187-2196, 1987.

Parker, J.C., and A.J. Valocchi, Constraints on the validity of equilibrium and first-order kinetic transport models in structured soils, *Water Resour. Res*., 22, 399, 1986.

Parker, J.C., and van Genuchten, Flux-averaged and volume averaged concentrations in

continuum approaches to solute transport, *Water Resour. Res*., 20, 866-872, 1984.

Pennell, K.D., R.D. Rhue, P.S.C. Rao, and C.T. Johnston, Vapor-phase sorption of p-xylene and water on soils and clay minerals, *Environ. Sci. Technol*., 26, 756-763, 1992.

Persoff, P. and J.B. Hulen, Hydrologic characterization of four cores from the Geysers coring project, in: *Proc. Twenty-First Workshop on Geothermal Engineering*, Stanford University, CA, Jan. 22-24, 1996.

Pfannkuch, H.O., Contribution à l'étude des deplacement de fluides miscible dans un milieu poreux, *Rev. Inst. Fr. Petrol*., 18(2), 215-270, 1962

Piwoni, M.D., and P. Bannerjee, Sorption of volatile organic solvents from aqueous solution onto subsurface solids, J. Contam. Hydrol., 4, 163-179, 1989.

Pope, G.A., K. Sepehrnoori, M. Delshad, B. Rouse, V. Dwarakanath, and M. Jin, NAPL partitioning interwell tracer test in OU1 test cell at Hill Air Force Base, Utah, Final report for ManTech Environmental Research Services Corp, October, 1994.

Popovičová, J. and M.L. Brusseau, Dispersion and transport of gas-phase contaminants in dry porous media: effect of heterogeneity and gas velocity, *J. Contam. Hydrol*., 28,, 157-169, 1997.

Popovičová, J. and M.L. Brusseau, Contaminant mass transfer during gas-phase transport in unsaturated porous media, *Water Resour. Res*., 34(1), 83-92, 1998.

Rainwater, K., M.R. Zaman, B.J. Claborn, and H.W. Parker, Experimental and modeling studies of in situ volatilization: Vapor-liquid equilibrium or diffusion- controlled process?, in *Proceedings of Conference on Petroleum Hydrocarbons and Organic Chemicals in Ground Water: Prevention, Detection, and Restoration*, Natl. Well Water Assoc./Am. Pet. Inst., Houston, TX, 1989.

Rao, P.S.C., and R.E. Jessup, Sorption and movement of pesticides and other toxic organic substances in soils, in *Chemical Mobility and Reactivity in Soil Systems*, Soil Science Society of America, Madison, WI, 1983.

Rao, P.S.C., R.E. Jessup, and T.M. Addiscott, Experimental and theoretical aspects of solute diffusion in spherical and nonspherical aggregates, *Soil Sci.*, 133(6), 342-349, 1982.

Rao, P.S.C., R.E. Jessup, D.E. Rolston, J.M. Davidson, and D.P. Kilcrease, Experimental and mathematical description of nonadsorbed solute transfer in spherical aggregates, *Soil Sci. Soc. Am. J.*, 44, 684-688, 1980a.

Rao, P.S.C., D.E. Rolston, R.E. Jessup, and J.M. Davidson, Solute transport in aggregated

porous media: Theoretical and experimental evaluation, *Soil Sci. Soc. Am. J.*, 44, 1139, 1980b.

Rasmuson, A., The influence of particle shape on the dynamics of fixed beds, *Chem. Eng. Sci*., 40, 1115, 1985.

Rathfelder, K.W., W.G. Yeh, and D. Mackay, Mathematical simulation of soil vapor extraction systems: Model development and numerical examples, *J. Contam. Hydrol.*, 8, 263-297, 1991.

Rathfelder, K.W., J. Lang, and LM. Abriola, Soil vapor extraction and bioventing: Applications, limitations and future research directions, *U.S. Natl. Rep. Int. Union Geol. Geophys*., 1991-1994, *Rev. Geophys*., 1995.

Ravi, V. and J.A. Johnson, VLEACH - A one-dimensional finite difference vadose zone leaching model, Version 2.2, Robert S. Kerr Environmental Research Center, U.S. EPA, Ada, OK, 1997.

Rawlins, E.L., and M.A. Schellhardt, Back-pressure data on natural gas wells and their application to production practices, U.S. Bureau of Mines Monograph, 1936.

Reda, D.C., Slip flow experiments in welded tuff: The Knudson diffusion problem. In: Chin-Fu Tsang (ed.), Coupled Processes Associated with Nuclear Waste Repositories, 485-493, 1987.

Robbins, G.A., Deyo, B.G., Temple, M.R., Stuart, J.D., and Lacy, M.J., Soil Gas Surveying for Subsurface Gasoline Contamination Using Total Organic Vapor Detection Instruments: Part I, Theory and Laboratory Experimentation, *Ground Water Monitoring Review*, 10(3), 122-131, 1990a.

Robbins, G.A., Deyo, B.G., Temple, M.R., Stuart, J.D., and Lacy, M.J., Soil Gas Surveying for Subsurface Gasoline Contamination Using Total Organic Vapor Detection Instruments: Part II. Field Experimentation, *Ground Water Monitoring Review*, 10(4), 110-117, 1990b.

Roberts, P.A., The effects of system variables on soil-vapor extraction of benzene and p-xylene in an unsaturated desert soil, M.S. thesis, Univ. of Ariz., Tucson, 1990.

Rojstaczer, S. and J.P. Tunks, Field-based determination of air diffusivity using air and atmospheric pressure time series, *Water Resour. Res*., 31(12), 3337-3343, 1995.

Rosza, R.B., D.F. Snoeberger, and J.Baker, Permeability of a nuclear chimney and surface alluvium, Lawrence Livermore Laboratory Report UCID-16722, 11p, 1975.

Sabljic, A., On the prediction of soil sorption coefficients of organic pollutants from molecular structure: Application of molecular topology model. *Environmental Science and Technology*, 21, p. 358-366, 1987.

Sabljic, A., Modeling association of highly chlorinated biphenyls with marine humic substances. *Chemosphere*, 19, p. 1665-1676, 1989.

Sabljic, A. and M. Protic, Relationship between molecular connectivity indices and soil sorption coefficients of polycyclic aromatic hydrocarbons, *Bulletin of Environmental Contamination and Toxicology*, 28, 162-165, 1982.

Sallam, A., W.A. Jury, and J. Letey, Measurement of gas diffusion coefficient under relatively low air-filled porosity. Soil Sci. Soc. Am. J. 42:863-869, 1984.

Sanemasa, I., Y. Miyazaki, S. Arakawa, M. Kumamaru, and T. Degughi, *Bull. Chem. Soc. Jpn*., 60, 517-523, 1987.

Sawyer, C.S., and M. Kamakoti, Optimal flow rates and well locations for soil vapor extraction design, *J. Contam. Hydrol*., 32, 63-76, 1998.

Schnitzer, M., Humic substances, chemistry and reactions, in *Soil Organic Matter*, edited by M. Schnitzer and S.U. Khan, Elsevier, NY, 1978

Schwarzenbach, R.P. and J. Westall, Transport of nonpolar organic compounds from surface water to groundwater, Laboratory sorption studies, *Environ. Sci. Technol.*, 15(11), 1360-1367, 1981.

Schwarenbach, R.P., P.M. Gshwend, and D.M. Imboden, Environmental Organic Chemistry, Wiley-Interscience, New York, 1993.

Schwartz, R.C., K.J. McInnes, A.S.R. Juo, L.P. Wilding, and D.L. Reddell, Boundary effects on solute transport in finite soil columns, *Water Resour. Res*., 35(3), 671-681, 1999.

Selim, H.M., J.M. Davidson, and R.S. Mansell, Evaluation of a two-site adsorption-desorption model for describing solute transport in soils, in *Proc. Summer Computer Simulation Conf*., Washington, D.C., 1976.

Shan, C., Analytical solutions for determining vertical air permeability in unsaturated soils, *Water Resour. Res*., 31(9), 2193-2200, 1995.

Shan, C., I. Javandel, and P.A Witherspoon, Characterization of leaky faults: Study of air flow in faulted vadose zones, *Water Resour. Res*., 35(7), 2007-2013, 1999.

Shan, C., R.W. Falta, I. Javandel, Analytical solutions for steady state gas flow to a soil vapor extraction well, *Water Resour. Res*., 28(4), 1105-1120, 1992.

Sharp, J.M., Jr., L. Fu, P. Cortez, and E. Wheeler, An electronic minipermeameter for use in the

field and laboratory, *Ground Water*, 32(1), 41-46, 1993.

Sheely, C.Q., Description of field tests to determine residual oil saturation by single-well tracer method, *JPT J. Pet. Technol*., 194, 1978.

Sheely, C.Q., Jr., and D.E. Baldwin Jr., Single-well tracer tests for evaluating chemically enhanced oil recovery processes, *JPT J. Pet. Technol*., 34, 1887, 1982.

Siegrist, R.L., and P.D. Jenssen, Evaluation of sampling method effects on volatile organic compound measurements in contaminated soils, *Environ. Sci. Technol*., 24(9), 1387-1392, 1990.

Skopp, J., Estimation of true moments from truncated data, *AIChE Journal*, 30(1), 151-155, 1984.

Sleep, B.E., and J.F. Sykes. Modeling the transport of volatile organics in variably saturated media, *Water Resour. Res*., 25(1), 81-92, 1989.

Sorensen, D.L., and R.C. Sims, Habitat conditions affecting bioventing processes, In: Proceedings of the Symposium on Soil Venting, U.S. Environmental Protection Agency, Office of Research and Development, EPA/600/R-92/174, April 29- May 1, Houston, TX, 1991.

Springer, D.S., S.J. Cullen, and L.G. Everett, Laboratory studies on air permeability, in *Handbook of Vadose Zone Characterization and Monitoring*, edited by L.G. Wilson, and S.J. Cullen, pp. 217-247, Lewis Publishers, Boca Raton, FL, 1995.

Springer, D.S., H.A. Loaiciga, S. J. Cullen, and L.G. Everett, Air permeability of porous materials under controlled laboratory conditions, *Ground Water*, 36(4), 558-565, 1998.

Stallman, R.W., Flow in the zone of aeration, in V. T. Chow, ed., Advances in Hydroscience, v. 4, Academic Press, p. 151-195, 1967.

Stallman, R.W., and E.P. Weeks, The use of atmospherically induced gas-pressure fluctuations for computing hydraulic conductivity of the unsaturated zone (abs.), Geological Society of America abstracts with programs, rpt. 7, p.213, 1969.

Stehfest, H., Numerical inversion of Laplace transforms, Algorithm 368, *Communications of the ACM*, 13(1), 47-49, 1970.

Stephens, D.B., Vadose Zone Hydrology. CRC Press Inc, 1995.

Stonestrom, D.A., Co-determination and comparisons of hysteresis-affected parametric functions of unsaturated flow: Water content dependence on matric pressure, air trapping, and fluid permeabilities in a non-swelling soil, Ph.D. dissertation, Applied Earth Petroleum Engineering,

Stanford University, Stanford, CA, 1987.

Stonestrom, D.A. and J. Rubin, Water content dependence of trapped air in two soils, *Water Resour. Res.*, 25(9), 1959-1969, 1989a.

Stonestrom, D.A. and J. Rubin, Air permeability and trapped-air content in two soils, *Water Resour. Res*., 25(9), 1959-1969, 1989b.

Sun, Y.H., M.W. Davert, and W.W.-G. Yeh, Soil vapor extraction system design by combinatorial optimization, *Water Resour. Res*., 32(6), 1863-1873, 1996.

Tang, J.S., Interwell tracer test to determine residual oil saturation to waterflood at Judy Creek BHL "A" Pool, *J. Can. Pet. Technol*., 31(8), 61-71, 1992.

Tang, J.S., Partitioning tracers and in-situ fluid saturation measurements, *Soc. Pet. Eng. Form. Eval*., 10(1), 33-39, 1995.

Tang, J.S., and B. Harker, Interwell tracer test to determine residual oil saturation in a gas reservoir, I, Theory and design, *J. Can. Pet. Technol*., 30(3), 76, 1991a.

Tang, J.S., and B. Harker, Interwell tracer test to determine residual oil saturation in a gas reservoir, II, Field applications, *J. Can. Pet. Technol*., 30(4), 34, 1991b.

Texas Research Institute, Laboratory scale gasoline spill and venting experiment. American Petroleum Institute. Interim Report No. 7743-5:JST, 1980.

Texas Research Institute, Forced venting to remove gasoline vapor from a large scale model aquifer. American Petroleum Institute. Final Report No. 82101-F:TAV, 1984.

Thorstenson, D.C., and D.W. Pollock, Gas transport in unsaturated porous media: The adequacy of Fick's law, *Rev. Geophys*., 27(1), 61-78, 1989.

Theis, C.V., The relation between lowering of the piezometric surface and the rate and duration of discharge of a well using groundwater storage, *Trans. Amer. Geophys. Union*, 519-525, 1935.

Tidwell, V.C. and J.L. Wilson. Laboratory method for investigating permeability upscaling, *Water Resour. Res*., 33(7), 1607-1616, 1997.

Tomich, J.F., R.L. Dalton Jr., H.A. Deans, and L.K. Shallenberger, Single-well tracer method to measure residual oil saturation, *J. Pet. Technol*. 255, 211, 1973.

Tuller, M., D. Or, and L.M. Dudley, Adsorption and capillary condensation in porous media: Liquid retention and interfacial configurations in angular pores, *Water Resour. Res*., 35(7), 1949-

1964, 1999.

U.S. Army Corps of Engineers (USACE), Soil Vapor Extraction and Bioventing, EM 1110-1-4001, 1995.

U.S. Environmental Protection Agency (EPA), Letter from Nikki L. Tinsley to Congressman Dick Armey dated 12/7/98, 1998a.

U.S. Environmental Protection Agency (EPA), Technical protocol for evaluating natural attenuation of chlorinated solvents in ground water, EPA/600/R-98/128, 1998b.

U.S. Environmental Protection Agency (EPA), Guide for conducting treatability studies under CERCLA: Soil Vacuum Extraction, EPA/540/2-91/019A. Risk Reduction Engineering Laboratory, USEPA, Cincinnati, OH, 1991.

U.S. Environmental Protection Agency (EPA), Soil venting optimization guide, Office of Technology Innovation, Washington, D.C. (Undergoing review), 2000.

van Eyk, J., Bioventing-an in situ remedial technology: scope and limitations, In: Proceedings of the Symposium on Soil Venting. EPA/600/R-92/174, April 29-May 1, 1991, Houston, Texas, 317-334, 1992.

van Eyk, J., and C. Vreeken, Model of petroleum mineralization response to soil aeration to aid in site-specific, in situ biological remediation. In: Groundwater contamination: Use of models in decision-making, Proceedings of an international conference on groundwater contamination. Ed. G. Jousma. Kluwer Boston/London. pp. 365-371, 1989a.

van Eyk, J. and C. Vreeken, Venting-mediated removal of diesel oil from subsurface soil strata as a result of stimulated evaporation and enhanced biodegradation. In: Hazardous Waste and Contaminated Sites, Envirotech Vienna. v. 2, session 3, ISNB 389432-009-5. Westarp Wiss., Essen. pp. 475-485, 1989b.

van Genuchten, M. Th., A general approach for modeling solute transport in structured soils, in *Proc. Hydrogeology Rocks Low Hydraulic Conductivity*, Memoirs of the IAH, Vol. 17, (Part 1), 513, 1985.

Van Genuchten, M. Th., A closed-form equation for predicting the hydraulic conductivity of unsaturated soils, *Soil Sci. Soc. Am. J.*, 44, 892-898, 1980.

van Genuchten, M.Th., and J.C. Parker, Boundary conditions for displacement experiments through short laboratory columns, *Soil Sci. Soc. Am. J.*, 48, 703-708, 1984.

van Genuchten, M.Th., and P.J. Wierenga, Mass transfer studies in sorbing porous media:

analytical solutions, *Soil Sci. Sci. Am. J.*, 40, 473, 1976.

van Genuchten, M. Th. and J.C. Parker, Boundary conditions for displacement experiments through short laboratory soil columns. *Soil Sci. Soc. Am. J.*, 48, 703-708, 1984.

Varadhan, R., and D.C. DiGiulio, Models for transient pneumatic pressure response in the unsaturated zone considering wellbore storage. EPA Report (undergoing review), 2001.

Warrick, A.W., and A. Rojano, Effects of source cavity shape on steady, three-dimensional flow of soil gases, *Water Resour. Res*, 35(5), 1425-1433, 1999.

Weeks, E.P., Field determination of vertical permeability to air in the unsaturated zone, U.S. Geological Survey Professional Paper 1051, 41p, 1977.

Wehrle, K. and J. Brauns, Column experiments concerning rate limited vapour extraction of volatile organic compound from wet sands, In: *Transport and Reactive Processes in Aquifers*, IAHR/AIRH Proc. Ser., Vol. 5, Edited by T. Dracos and f. Stauffer, pp. 549-554, A.A. Balkema, Rotterdam, Netherlands, 1994.

White, N.F., D.K. Sunada, H.R. Duke, and A.T. Corey, Boundary effects in desaturation of porous media, *Soil Sci*., 113, 7-12, 1972.

Whitley, G.A., D.C. McKinney, B.A. rouse, and N.E. Deeds, Contaminated vadose zone characterization using partitioning gas tracers, *J. Environ. Eng*., 125(6), 574-582, 1999.

Wilkins, M.D., L.M. Abriola, and K.D. Pennel, An experimental investigation of rate-limited nonaqueous phase liquid volatilization in unsaturated porous media: Steady state mass transfer, *Water Resour. Res.*, 31(9), 2159-2172, 1995.

Wilson, D.E., R.E. Montgomery, and M.R. Sheller, A mathematical model for removing volatile subsurface hydrocarbons by miscible displacement, *Water Air and Soil Pollution*, 33, 231-255, 1987.

Wilson, D.J., A.N. Clarke, and J.H. Clarke. 1988. Soil Clean up by in-situ aeration, 1. Mathematical modeling, *Separation Science Technology*, 23(10-11), 991-1037, 1988.

Wilson, J.L., and S.H. Conrad, Is physical displacement of residual hydrocarbons a realistic possibility in aquifer restoration? Paper presented at NWWA/API Conference on Petroleum Hydrocarbons and Organic Chemicals in Ground Water-Prevention, Detection and Restoration, Houston, TX, 1984.

Wilson, R.D., and D.M. Mackay, Direct detection of residual nonaqueous phase liquid in the saturated zone using SF_6 as a partitioning tracer, *Environ. Sci. Technol*., 29(5), 1255-1258, 1995.

Woodward-Clyde and Envirogen, Draft 100% Design Report Picillo Farm Site, Coventry, Rhode Island, 1998.

Wu, S., and P.M. Gschwend, Sorption kinetics of hydrophobic organic compounds to natural sediments and soils, *Environ. Sci. Technol*., 20, 725, 1986.

Wu, U.S., K. Pruess, and P. Persoff, Gas flow in porous media with Klinkenberg effects, *Trans. Porous Media*, 32, 117-137, 1998.

Yates, S.R., S.K. Papiernik, F. Gao, and J. Gan, Analytical solutions for the transport of volatile organic chemicals in unsaturated layered systems, *Water Resour. Res*., 36(8), 1993-2000, 2000.

Young, C.M., R.E. Jackson, M. Jin, J.T. Londergan, P.E. Mariner, G.A. Pope, F.J. Anderson, and T. Houk, Characterization of a TCE DNAPL zone in alluvium by partitioning tracers, *Ground Water Monitoring and Remediation*, 19(1), 84-94, 1999.

Yu, L.L., Study of air flow through porous media, M.S. thesis, 114 p. Dept. of Civ. Eng., Univ. of Conn., Storrs, 1985.

Zaidel, J. and A. Zazovsky, Theoretical study of multicomponent soil vapor extraction: Propagation of evaporation-condensation fronts, *J. Contam. Hydrol*., 37, 225-268, 1999.

APPENDIX A (MFROAINV)

Sample Input File for MFROAINV

```
                /*  input file for test 3
298.0           /* temperature (K)
-56.90           /* mass pumping rate (g/sec)
518.16           /* thickness of formation  (cm)
396.24           /* distance to top of sandpack from surface  (cm)
426.72          /* distance to bottom of sandpack from surface  (cm)
7.5              /* radius of sandpack (cm)
1.e-10           /* convergence criterion
5.1e-07,5.4e-07  /* minimum and maximum radial permeability (cm^2)
1.09,1.20        /* minimum and maximum anisotropy ratio (K_r/K_z)
5000            /* number of random parameter guesses
25               /* number of "best" parameter sets for forward problem
15              /*number of observations
152.4   91.44   0.9985247        /* observations    r(cm)    z(cm)    P/P(atm)
152.4   274.32  0.9950823
152.4   426.72  0.9881975
304.8   91.44   0.9990165
304.8   274.32  0.9972953
304.8   426.72  0.9950823
457.2   91.44   0.9993853
457.2   274.32  0.9984017
457.2   426.72  0.9979100
609.6   91.44   0.9996312
609.6   274.32  0.9992623
609.6   426.72  0.9992623
914.4   91.44   0.9997049
914.4   274.32  0.9995082
914.4   426.72  0.9993361
```

Sample Output File for MFROAINV

```
 ------------------------------------------------------
     Steady-State Multi-Well Parameter Estimation
           Finite-Radius Model
         Top BC: Open to Atmosphere
 ------------------------------------------------------
```

Parameter Estimates Ordered from Best to Worst

K_r	K_z	RMS-Error	IFLAG
0.5272E-06	0.4614E-06	0.5243E-03	0
0.5269E-06	0.4615E-06	0.5243E-03	0
0.5280E-06	0.4606E-06	0.5243E-03	0
0.5271E-06	0.4616E-06	0.5243E-03	0
0.5281E-06	0.4609E-06	0.5243E-03	0
0.5282E-06	0.4602E-06	0.5243E-03	0
0.5275E-06	0.4604E-06	0.5243E-03	0
0.5262E-06	0.4616E-06	0.5243E-03	0
0.5287E-06	0.4606E-06	0.5243E-03	0
0.5263E-06	0.4624E-06	0.5243E-03	0

(only first ten shown)

Observed Versus Modeled Fit (only first ranked fit shown)

Parameter set - 1

K_r = 0.5272E-06
K_z = 0.4614E-06

R (cm)	Z (cm)	P_observed	P_model
0.1524E+03	0.9144E+02	0.9985E+00	0.9984E+00
0.1524E+03	0.2743E+03	0.9951E+00	0.9939E+00
0.1524E+03	0.4267E+03	0.9882E+00	0.9893E+00
0.3048E+03	0.9144E+02	0.9990E+00	0.9989E+00
0.3048E+03	0.2743E+03	0.9973E+00	0.9967E+00
0.3048E+03	0.4267E+03	0.9951E+00	0.9952E+00
0.4572E+03	0.9144E+02	0.9994E+00	0.9993E+00
0.4572E+03	0.2743E+03	0.9984E+00	0.9981E+00
0.4572E+03	0.4267E+03	0.9979E+00	0.9975E+00
0.6096E+03	0.9144E+02	0.9996E+00	0.9996E+00
0.6096E+03	0.2743E+03	0.9993E+00	0.9989E+00
0.6096E+03	0.4267E+03	0.9993E+00	0.9986E+00
0.9144E+03	0.9144E+02	0.9997E+00	0.9999E+00
0.9144E+03	0.2743E+03	0.9995E+00	0.9996E+00
0.9144E+03	0.4267E+03	0.9993E+00	0.9995E+00

Source Code for MFROAINV (author: Ravi Varadhan)

(A FORTRAN program for estimation of radial and vertical gas permeability in a domain open to the atmosphere)

```
c  Parameter estimation for the steady-state solution for finite well radius
c  BC: Open to the atmosphere on top
c  Multiple monitoring locations
c  version 1.0   07/19/99
      implicit real*8 (a-h,o-z)
      dimension rr(100),zz(100),pobs(100),p_r(5000),p_z(5000),
     >errmet(5000),wksp(5000),iwksp(5000),iflag(5000)
      integer*4 istart,ifinish
      character*15 prefix,fname1,fname2
      character*4 suffix1,suffix2
      write(*,*)' Parameter Estimation for Steady-State Multi-Well Test'
      write(*,*)' Finite-Radius Solution -  BC: Open to Atmosphere'
      write(*,*)
      write(*,*)'Enter the Prefix of the input file:  '
      write(*,*)'An output file is created w/ same prefix'
      write(*,*)' Input-file Prefix ?  '
      read(*,'(a)')prefix
      call getlen(prefix,' ',n0,n1)
      suffix1='.inp'
      suffix2='.dat'
      fname1=prefix(n0:n1)//suffix1
      fname2=prefix(n0:n1)//suffix2
      open(10,fname1,status='unknown')
      open(20,fname2,status='unknown')
      open(30,'seed.inp',status='unknown')
      read(10,*)
      read(10,101)temp,xmpr,xb,xd,xl,rw,tol
      read(10,*)prmin,prmax
      read(10,*)rmin,rmax
      read(10,101)nguess
      read(10,101)nbest
      read(10,101)nsim
      do 2 i=1,nsim
      read(10,*)rr(i),zz(i),pobs(i)
2     continue
      patm=1013200.
      visc=1.76e-04
      rgas=8.314e07
      xmw=28.8
      pi=4.0*datan(1.0)
c   patm = atmospheric pressure (g/cm/sec^2)
c   visc = viscosity of gas (g/cm/sec)
c   rgas = universal gas constant
c   temp = temperature of gas (K)
c   xmw = molecular weight of gas (g/mole)
c   xmpr = mass withdrawal rate (g/sec)
c   prad = radial permeability of the formation (cm^2)
c   pz = vertical permeability
```

```
c   pleak = permeability of the leaky confining unit
c   xb = thickness of the formation (cm)
c   xbp = thickness of the leaky unit
c   xl = distance from the bottom of leaky unit to the bottom of well screen
c   xd = distance from the bottom of leaky unit to the top of well screen
c   rw = nominal well radius (cm)
c   aa = radial cordinate (cm)
c   bb = vertical cordinate
c   cc = elapsed time (sec)
c   nsim = number of times solution will be generated
c   pobs = measured pneumatic pressure responses
c
      write(20,*)' ------------------------------------------------------'
      write(20,*)'      Steady-State Multi-Well Parameter Estimation'
      write(20,*)'              Finite-Radius Model   '
      write(20,*)'           Top BC: Open to Atmosphere '
      write(20,*)' ------------------------------------------------------'
      write(20,*)
      xll=xl/xb
      xdd=xd/xb
      r_w=rw/xb
      call timer(istart)
      read(30,*)iseed
      if(iseed.gt.0)iseed=-iseed
      do 1 j=1,nguess
      iflag(j)=0
      errmet(j)=0.
      sqerr=0.
      guess1=ran1(iseed)
      guess2=ran1(iseed)
      p_r(j)=prmin*(prmax/prmin)**guess1
      ratio=rmin+(rmax-rmin)*guess2
      p_z(j)=p_r(j)/ratio
      prad=p_r(j)
      pz=p_z(j)
      a=dsqrt(prad/pz)
      xm=xmpr*visc*rgas*temp/(pi*xmw*prad*patm*patm*xb)
c
      do 5 i=1,nsim
      r=rr(i)/xb
      z=zz(i)/xb
      n=0
      sum=0.0
10    continue
      n=n+1
      rm=n-0.5
      if(n.gt.1000)then
      iflag(j)=1
      goto 15
      endif
      vn=rm*pi
      wn=vn/a
```

```
      fn=bessk0(wn*r)/(wn*r_w*bessk1(wn*r_w))
      tsin=dsin(vn*z)
      tcos=dcos(vn*xdd)-dcos(vn*xll)
      trig=tcos*tsin
      fact=1./(vn*(xll-xdd))
      add=trig*fact*fn
      sum=sum+add
      if(dabs(sum).le.1.e-14)goto 15
      if(dabs(add/sum).gt.tol)goto 10
15    continue
      psqrd=1.0+2.0*xm*sum
      if(psqrd.lt.0.)then
      iflag(j)=2
      errmet(j)=1.e10
      goto 1
      endif
      popatm=dsqrt(psqrd)
      sqerr=sqerr+(popatm-pobs(i))**2
5     continue
      errmet(j)=dsqrt(sqerr/nsim)
      write(*,*)j,prad,pz,errmet(j),iflag(j)
1     continue
      call sort3(nguess,errmet,p_r,p_z,iflag,wksp,iwksp)
      write(20,107)
      write(20,102)
      do 20 j=1,nguess
      write(20,103)p_r(j),p_z(j),errmet(j),iflag(j)
20    continue

      do 30 j=1,nbest
      prad=p_r(j)
      pz=p_z(j)
      write(20,104)j,prad,pz
      write(20,105)
      a=dsqrt(prad/pz)
      xm=xmpr*visc*rgas*temp/(pi*xmw*prad*patm*patm*xb)
c
      do 35 i=1,nsim
      r=rr(i)/xb
      z=zz(i)/xb
      n=0
      sum=0.0
40    continue
      n=n+1
      rm=n-0.5
      if(n.gt.1000)goto 45
      vn=rm*pi
      wn=vn/a
      fn=bessk0(wn*r)/(wn*r_w*bessk1(wn*r_w))
      tsin=dsin(vn*z)
      tcos=dcos(vn*xdd)-dcos(vn*xll)
      trig=tcos*tsin
```

```
      fact=1./(vn*(xll-xdd))
      add=trig*fact*fn
      sum=sum+add
      if(dabs(sum).le.1.e-14)goto 45
      if(dabs(add/sum).gt.tol)goto 40
45    continue
      psqrd=1.0+2.0*xm*sum
      if(psqrd.ge.0.)then
      popatm=dsqrt(psqrd)
      else
      popatm=0.
      endif
      write(20,106)rr(i),zz(i),pobs(i),popatm
35    continue
30    continue
      call timer(ifinish)
      write(*,*)'Time of execution (sec)  =',(ifinish-istart)/100.
101   format(g15.0)
102   format(/5x,'K_r',11x,'K_z',9x,'RMS-Error',5x,'IFLAG'/)
103   format(2x,e10.4,4x,e10.4,5x,e10.4,5x,i2)
104   format(//20x,'Parameter set - ',i4//,3x,'K_r = ',e10.4/
     >3x,'K_z = ',e10.4//)
105   format(10x,'R (cm)',8x,'Z (cm)',9x,'P_observed',8x,'P_model'/)
106   format(7x,e10.4,5x,e10.4,8x,e10.4,6x,e10.4)
107   format(//10x,'Parameter Estimates Ordered from Best to Worst'//)
      rewind(30)
      write(30,*)-iseed
      stop
      end

      Double Precision Function Bessk0(x)
      implicit real*8 (a-h,o-z)
      data p1,p2,p3,p4,p5,p6,p7/-0.57721566,0.4227842,0.23069756,
     >0.348859d-1,0.262698d-2,0.10750d-3,0.74d-5/
      data q1,q2,q3,q4,q5,q6,q7/1.25331414,-0.7832358d-1,0.2189568d-1,
     >-0.1062446d-1,0.587872d-2,-0.25154d-2,0.53208d-3/
      if(x.le.2.0)then
      y=x*x/4.0
      bessk0=(-dlog(x/2.0)*bessi0(x))+(p1+y*(p2+y*(p3+y*(p4+y*(p5+y*(p6+
     >y*p7))))))
      else
      y=2.0/x
      bessk0=(dexp(-x)/dsqrt(x))*(q1+y*(q2+y*(q3+y*(q4+y*(q5+y*(q6+y*q7)
     >)))))
      endif
      return
      end

      DOUBLE PRECISION FUNCTION BESSI0(W)
      IMPLICIT real*8 (A-H,O-Z)
      T=W/3.75
      IF(DABS(T).LE.1.0) THEN
```

```
      Y=T*T
      BESSI0=1.0+Y*(3.5156229+Y*(3.0899424+Y*(1.2067492+Y*(0.2659732+
     >Y*(0.0360768+0.0045813*Y)))))
      ELSE
      AW=DABS(W)
      Y=3.75/AW
      TEMP=0.39894228+Y*(0.01328592+Y*(0.00225319+Y*(-0.00157565+Y*(
     >0.00916281+Y*(-0.02057706+Y*(0.02635537+Y*(-0.01647633+
     >0.00392377*Y)))))))
      BESSI0=DEXP(AW)*TEMP/DSQRT(AW)
      END IF
      RETURN
      END

      double precision FUNCTION bessk1(x)
CU    USES bessi1
      implicit real*8 (a-h,o-z)
      DOUBLE PRECISION p1,p2,p3,p4,p5,p6,p7,q1,q2,q3,q4,q5,q6,q7,y
      SAVE p1,p2,p3,p4,p5,p6,p7,q1,q2,q3,q4,q5,q6,q7
      DATA p1,p2,p3,p4,p5,p6,p7/1.0d0,0.15443144d0,-0.67278579d0,
     *-0.18156897d0,-0.1919402d-1,-0.110404d-2,-0.4686d-4/
      DATA q1,q2,q3,q4,q5,q6,q7/1.25331414d0,0.23498619d0,-0.3655620d-1,
     *0.1504268d-1,-0.780353d-2,0.325614d-2,-0.68245d-3/
      if (x.le.2.0) then
        y=x*x/4.0
        bessk1=(dlog(x/2.0)*bessi1(x))+(1.0/x)*(p1+y*(p2+y*(p3+y*(p4+y*
     *(p5+y*(p6+y*p7))))))
      else
        y=2.0/x
        bessk1=(dexp(-x)/dsqrt(x))*(q1+y*(q2+y*(q3+y*(q4+y*(q5+y*(q6+y*
     *q7))))))
      endif
      return
      END

      double precision FUNCTION bessi1(x)
      implicit real*8 (a-h,o-z)
      DOUBLE PRECISION p1,p2,p3,p4,p5,p6,p7,q1,q2,q3,q4,q5,q6,q7,q8,q9,y
      SAVE p1,p2,p3,p4,p5,p6,p7,q1,q2,q3,q4,q5,q6,q7,q8,q9
      DATA p1,p2,p3,p4,p5,p6,p7/0.5d0,0.87890594d0,0.51498869d0,
     *0.15084934d0,0.2658733d-1,0.301532d-2,0.32411d-3/
      DATA q1,q2,q3,q4,q5,q6,q7,q8,q9/0.39894228d0,-0.3988024d-1,
     *-0.362018d-2,0.163801d-2,-0.1031555d-1,0.2282967d-1,-0.2895312d-1,
     *0.1787654d-1,-0.420059d-2/
      if (abs(x).lt.3.75) then
        y=(x/3.75)**2
        bessi1=x*(p1+y*(p2+y*(p3+y*(p4+y*(p5+y*(p6+y*p7))))))
      else
        ax=abs(x)
        y=3.75/ax
        bessi1=(dexp(ax)/dsqrt(ax))*(q1+y*(q2+y*(q3+y*(q4+y*(q5+y*(q6+y*
     *(q7+y*(q8+y*q9))))))))
```

```
      if(x.lt.0.)bessi1=-bessi1
    endif
    return
    END

    double precision FUNCTION ran1(idum)
    implicit real*8 (a-h,o-z)
    INTEGER idum,IA,IM,IQ,IR,NTAB,NDIV
    PARAMETER (IA=16807,IM=2147483647,AM=1./IM,IQ=127773,IR=2836,
   *NTAB=32,NDIV=1+(IM-1)/NTAB,EPS=1.2e-7,RNMX=1.-EPS)
    INTEGER j,k,iv(NTAB),iy
    SAVE iv,iy
    DATA iv /NTAB*0/, iy /0/
    if (idum.le.0.or.iy.eq.0) then
      idum=max(-idum,1)
      do 11 j=NTAB+8,1,-1
        k=idum/IQ
        idum=IA*(idum-k*IQ)-IR*k
        if (idum.lt.0) idum=idum+IM
        if (j.le.NTAB) iv(j)=idum
11      continue
      iy=iv(1)
    endif
    k=idum/IQ
    idum=IA*(idum-k*IQ)-IR*k
    if (idum.lt.0) idum=idum+IM
    j=1+iy/NDIV
    iy=iv(j)
    iv(j)=idum
    ran1=dmin1(AM*iy,RNMX)
    return
    END

    SUBROUTINE sort3(n,ra,rb,rc,id,wksp,iwksp)
    implicit real*8 (a-h,o-z)
    INTEGER n,iwksp(n),id(n)
    dimension ra(n),rb(n),rc(n),wksp(n)
CU    USES indexx
    INTEGER j
    call indexx(n,ra,iwksp)
    do 11 j=1,n
      wksp(j)=ra(j)
11    continue
    do 12 j=1,n
      ra(j)=wksp(iwksp(j))
12    continue
    do 13 j=1,n
      wksp(j)=rb(j)
13    continue
    do 14 j=1,n
      rb(j)=wksp(iwksp(j))
14    continue
```

```
      do 15 j=1,n
        wksp(j)=rc(j)
15    continue
      do 16 j=1,n
        rc(j)=wksp(iwksp(j))
16    continue
      do 17 j=1,n
        wksp(j)=id(j)
17    continue
      do 18 j=1,n
        id(j)=wksp(iwksp(j))
18    continue
      return
      END

      SUBROUTINE indexx(n,arr,indx)
      implicit real*8 (a-h,o-z)
      INTEGER n,indx(n),M,NSTACK
      dimension arr(n)
      PARAMETER (M=7,NSTACK=50)
      INTEGER i,indxt,ir,itemp,j,jstack,k,l,istack(NSTACK)
      do 11 j=1,n
        indx(j)=j
11    continue
      jstack=0
      l=1
      ir=n
1     if(ir-l.lt.M)then
        do 13 j=l+1,ir
          indxt=indx(j)
          a=arr(indxt)
          do 12 i=j-1,1,-1
            if(arr(indx(i)).le.a)goto 2
            indx(i+1)=indx(i)
12        continue
          i=0
2         indx(i+1)=indxt
13      continue
        if(jstack.eq.0)return
        ir=istack(jstack)
        l=istack(jstack-1)
        jstack=jstack-2
      else
        k=(l+ir)/2
        itemp=indx(k)
        indx(k)=indx(l+1)
        indx(l+1)=itemp
        if(arr(indx(l+1)).gt.arr(indx(ir)))then
          itemp=indx(l+1)
          indx(l+1)=indx(ir)
          indx(ir)=itemp
        endif
```

```
      if(arr(indx(l)).gt.arr(indx(ir)))then
        itemp=indx(l)
        indx(l)=indx(ir)
        indx(ir)=itemp
      endif
      if(arr(indx(l+1)).gt.arr(indx(l)))then
        itemp=indx(l+1)
        indx(l+1)=indx(l)
        indx(l)=itemp
      endif
      i=l+1
      j=ir
      indxt=indx(l)
      a=arr(indxt)
3     continue
        i=i+1
      if(arr(indx(i)).lt.a)goto 3
4     continue
        j=j-1
      if(arr(indx(j)).gt.a)goto 4
      if(j.lt.i)goto 5
      itemp=indx(i)
      indx(i)=indx(j)
      indx(j)=itemp
      goto 3
5     indx(l)=indx(j)
      indx(j)=indxt
      jstack=jstack+2
      if(jstack.gt.NSTACK)pause 'NSTACK too small in indexx'
      if(ir-i+1.ge.j-l)then
        istack(jstack)=ir
        istack(jstack-1)=i
        ir=j-1
      else
        istack(jstack)=j-1
        istack(jstack-1)=l
        l=i
      endif
    endif
    goto 1
    END
c
    subroutine getlen(string,chr,n0,n1)
c
c     to determine the length of a string excluding any blank padding & heading
c     and return string(n0:n1) n0... position of first non-blank letter
c                              n1... position of last non-blank letter
c     else return the original string
c     ***Use | to keep blank space at the begining or the end of the
c      *** string
c
    character*(*) string
```

```
      character*160 string1
      character*1 chr
      string1=' '
      in0=0
      in1=0
      do 10 i=len(string),1,-1
      if(string(i:i).ne.chr) then
        if(in1.eq.0) then
        if(string(i:i).eq.'|') then
        n1=i-1
        else
        n1=i
        endif
        in1=1
        endif
        goto 11
      endif
10    continue
11    do 20 i=1,len(string)
      if(string(i:i).ne.chr) then
       if(in0.eq.0) then
       if(string(i:i).eq.'|') then
       n0=i+1
       else
       n0=i
       endif
       in0=1
       nk=n0-1
c      write(6,*) '|'//string(n0:n1)//'|', n0,n1
       do 30 k=n0,n1
       if(string(k:k).ne.'|') then
         nk=nk+1
         if(k.eq.n0) then
           string1=string(k:k)
         else
           string1=string1(1:nk-n0)//string(k:k)
         endif
       endif
c      write(6,*) '|'//string1(1:nk-n0)//'|'
30     continue
       string=string1
       n1=n1-n0+1
       n0=1
       endif
       return
      endif
20    continue
      n0=-1
      n1=-1
      return
      end
```

APPENDIX B (SAIRFLOW)

Sample Input File for SAIRFLOW

```
283.                /* temperature (K)
-75.11              /* mass pumping rate (g/sec)
6.10e-07            /* radial permeability (cm^2)
4.89e-07            /* vertical permeability  (cm^2)
0.2                 /* air-filled porosity
518.16              /* thickness of formation  (cm)
396.24              /* distance to top of sandpack (cm)
426.72              /* distance to bottom of sandpack (cm)
7.5                 /* well radius of sandpack (cm)
1.0e-06             /* convergence criterion
74,50               /*number of r and z points
10.0,20.0,30.0,40.0,50.0,60.0,70.0,80.0,90.0,100.0,
110.0,120.0,130.0,140.0,150.0,160.0,170.0,180.0,190.0,200.0,
210.0,220.0,230.0,240.0,250.0,260.0,270.0,280.0,290.0,300.0,
310.0,320.0,330.0,340.0,350.0,360.0,370.0,380.0,390.0,400.0,
410.0,420.0,430.0,440.0,450.0,460.0,470.0,480.0,490.0,500.0,
520.0,540.0,560.0,580.0,600.0,620.0,640.0,680.0,700.0,720.0,
740.0,760.0,780.0,800.0,820.0,840.0,860.0,880.0,900.0,920.0,
940.0,960.0,980.0,1000.0 /* radial distances (cm)
20.0,40.0,50.0,60.0,70.0,80.0,90.0,100.0,
110.0,120.0,130.0,140.0,150.0,160.0,170.0,180.0,190.0,200.0,
210.0,220.0,230.0,240.0,250.0,260.0,270.0,280.0,290.0,300.0,
310.0,320.0,330.0,340.0,350.0,360.0,370.0,380.0,390.0,400.0,
410.0,420.0,430.0,440.0,450.0,460.0,470.0,480.0,490.0,500.0,
510.0,518.0         /* vertical distance (cm)
n                   /* yes/no flag for particle tracking
1.0                 /* maximum step size (cm)
```

Sample Output File for SAIRFLOW

****

Results of Single-Well Airflow Simulation

Steady-state Finite-Radius Solution
Open to the Atmosphere

****

R_start	Z_start	Potential	Streamline	v_r	v_z	v (cm/s)
0.100E+02	0.200E+02	.999142E+00	.613049E+01	-0.4157E-03	0.3034E+00	0.3034E+00
0.200E+02	0.200E+02	.999143E+00	.612470E+01	-0.1630E-02	0.3030E+00	0.3030E+00
0.300E+02	0.200E+02	.999145E+00	.611509E+01	-0.2655E-02	0.3021E+00	0.3021E+00
0.400E+02	0.200E+02	.999149E+00	.610167E+01	-0.3618E-02	0.3008E+00	0.3008E+00
0.500E+02	0.200E+02	.999154E+00	.608450E+01	-0.4540E-02	0.2992E+00	0.2992E+00
0.600E+02	0.200E+02	.999159E+00	.606365E+01	-0.5424E-02	0.2971E+00	0.2972E+00
0.700E+02	0.200E+02	.999166E+00	.603918E+01	-0.6269E-02	0.2948E+00	0.2948E+00
0.800E+02	0.200E+02	.999174E+00	.601120E+01	-0.7073E-02	0.2920E+00	0.2921E+00
0.900E+02	0.200E+02	.999182E+00	.597980E+01	-0.7833E-02	0.2890E+00	0.2891E+00
0.100E+03	0.200E+02	.999191E+00	.594508E+01	-0.8546E-02	0.2857E+00	0.2858E+00

(Only first 10 simulations shown)

R_start	Z_start	Potential	Norm_Streamline
0.100E+02	0.200E+02	.999142E+00	.100000E+01
0.200E+02	0.200E+02	.999143E+00	.999057E+00
0.300E+02	0.200E+02	.999145E+00	.997488E+00
0.400E+02	0.200E+02	.999149E+00	.995299E+00
0.500E+02	0.200E+02	.999154E+00	.992499E+00
0.600E+02	0.200E+02	.999159E+00	.989097E+00
0.700E+02	0.200E+02	.999166E+00	.985107E+00
0.800E+02	0.200E+02	.999174E+00	.980542E+00
0.900E+02	0.200E+02	.999182E+00	.975419E+00
0.100E+03	0.200E+02	.999191E+00	.969757E+00

(Only first 10 simulations shown)

Source Code for SAIRFLOW (author Ravi Varadhan)

(A FORTRAN program for computation of pore-gas velocity, streamlines, and particle tracking for one well in a domain open to the atmosphere)

```
C  Particle tracking algorithm for Travel time calculation
C  Airflow due to one pumping well
C  Finite well radius -  Steady state flow field
C
C  Runge-Kutta Second Order scheme is used in Particle-Tracking
c
      implicit real*8 (a-h,o-z)
      dimension r(50),z(50),strm(50,50),pot(50,50)
      common/cseries/xk,zb,zd,zl,prad,pz,a,visc,theta,rw,tol,patm
      character*15 prefix,fname1,fname2
      character*4 suffix1,suffix2
      character*1 ptrack
      write(*,*)' Steady-State Airflow Simulation for a Single Well'
      write(*,*)' Finite-Radius Solution with Borehole Storage '
      write(*,*)' Top BC: Open to Atmosphere'
      write(*,*)
      write(*,*)'Enter the Prefix of the input file:  '
      write(*,*)'An output file is created w/ same prefix'
      write(*,*)' Input-file Prefix ?  '
      read(*,'(a)')prefix
      call getlen(prefix,' ',n0,n1)
      suffix1='.inp'
      suffix2='.dat'
      fname1=prefix(n0:n1)//suffix1
      fname2=prefix(n0:n1)//suffix2
      open(20,fname1,status='unknown')
      open(30,fname2,status='unknown')
      read(20,101)temp,xmpr,prad,pz,theta,zb,zd,zl,rw,tol
      read(20,*)nr,nz
      read(20,*)(r(i),i=1,nr)
      read(20,*)(z(i),i=1,nz)
      read(20,'(a)')ptrack
      read(20,*)delx
c
      write(*,*)'      Steady-state, Finite Radius-Open to Atmosphere'
      write(*,*)
      call timer(istart)
      patm=1013200.
      visc=1.76e-04
      rgas=8.314e07
      xmw=28.8
      pi=4.0*datan(1.0)
      a=dsqrt(prad/pz)
      qp=visc*rgas*temp/xmw*xmpr
      xk=2.0*qp/(pi*pi*prad*(zl-zd))
      write(30,106)
```

```
      if(ptrack.ne.'y' .and. ptrack.ne.'Y')then
      write(30,102)
      else
      write(30,104)
      endif
      strmax=-1.e10
      do 5 j=1,nz
      z0=z(j)
      if(z0.eq.zb)z0=0.999*zb
      do 5 i=1,nr
      r0=r(i)
      ttime=0.0
      rnew=r0
      znew=z0
      call series(rnew,znew,vr,vz,phi0,psi0)
      vres0=dsqrt(vr*vr+vz*vz)
      pot(i,j)=phi0
      strm(i,j)=psi0
      if(psi0.gt.strmax)strmax=psi0
      if(ptrack.ne.'y' .and. ptrack.ne.'Y')then
      write(30,103)r0,z0,phi0,psi0,vr,vz,vres0
      goto 5
      endif
      write(*,*)'r(0),z(0),psi  =  ',rnew,znew,psi0
C  loop for particle tracking
1     continue
      rold=rnew
      zold=znew
      call series(rold,zold,vr,vz,phi,psi)
      vres=dsqrt(vr*vr+vz*vz)
      delt=delx/vres
      delr1=vr*delt
      delz1=vz*delt
      call series(rold+delr1,zold+delz1,vr,vz,phi,psi)
      delr2=vr*delt
      delz2=vz*delt
      rnew=rold+(delr1+delr2)/2.
      znew=zold+(delz1+delz2)/2.
      ttime=ttime+delt
      dist1=dsqrt((rnew-rw)**2+(znew-zd)**2)
      dist2=rnew-rw
      dist3=dsqrt((rnew-rw)**2+(znew-zl)**2)
      if(znew.lt.zd)dist=dist1
      if(znew.ge.zd .and. znew.lt.zl)dist=dist2
      if(znew.ge.zl)dist=dist3
      if(dist.ge.delx)goto 1
C  Particle tracking loop is complete
      if(rnew.le.rw)rnew=rw
2     continue
      call series(rnew,znew,vr,vz,phi,psi)
      vres=dsqrt(vr*vr+vz*vz)
      write(*,*)'r(t),z(t),t,psi  =  ',rnew,znew,ttime,psi
```

```
      write(30,105)r0,z0,phi0,psi0,vr,vz,vres,ttime
5     continue
      write(30,107)
      do 6 j=1,nz
      do 6 i=1,nr
      write(30,108)r(i),z(j),pot(i,j),strm(i,j)/strmax
6     continue
      call timer(ifinish)
      write(*,*)'Execution time (sec): ',(ifinish-istart)/100.
101   format(g15.0)
102   format(4x,'R_start',7x,'Z_start',7x,'Potential',7x,'Streamline',
     >8x,'v_r',13x,'v_z',10x,'v (cm/s)'/)
103   format(2x,e10.3,4x,e10.3,5x,e11.4,5x,e11.4,4x,e11.4,5x,e11.4,4x,
     >e11.4)
104   format(3x,'R_start',6x,'Z_start',6x,'Potential',6x,'Streamline',
     >9x,'v_r',12x,'v_z',11x,'v (cm/s)',7x,'Travel-Time (s)'/)
105   format(1x,e10.3,3x,e10.3,3x,e11.4,5x,e11.4,5x,e11.4,5x,e11.4,5x,
     >e11.4,5x,e11.4)
106   format(//4x,65('*')//16x,'Results of Single-Well Airflow ',
     >'Simulation'//10x,'Steady-state Finite-Radius Solution'/,
     >10x,'Open to the Atmosphere'//4x,65('*')/)
107   format(///4x,'R_start',7x,'Z_start',7x,'Potential',7x,
     >'Norm_Streamline'/)
108   format(3x,e10.3,4x,e10.3,5x,e11.4,5x,e11.4)
      stop
      end

      subroutine series(r,z,vr,vz,phi,psi)
      implicit real*8 (a-h,o-z)
      common/cseries/xk,zb,zd,zl,prad,pz,a,visc,theta,rw,tol,patm
      pi=4.0*datan(1.0)
      n=0
      sumphi=0.0
      sumpsi=0.0
      sumvr=0.0
      sumvz=0.0
10    continue
      n=n+1
      if(n.gt.1000) goto 15
      rm=n-0.5
      xmn=rm*pi/zb
      sterm=dsin(xmn*z)
      cterm=dcos(xmn*z)
      am=(dcos(xmn*zd)-dcos(xmn*zl))/(xmn*rw/a*bessk1(xmn*rw/a))
      if(r.le.0.0)then
      write(*,*)'Step size for particle tracking is too large'
      return
      endif
      addphi=sterm*am/rm*bessk0(xmn*r/a)
      addpsi=cterm*am/rm*bessk1(xmn*r/a)
      addvr=sterm*am*xmn/rm*bessk1(xmn*r/a)
      addvz=cterm*am*xmn/rm*bessk0(xmn*r/a)
```

```
      sumphi=sumphi+addphi
      sumpsi=sumpsi+addpsi
      sumvr=sumvr+addvr
      sumvz=sumvz+addvz
      if (dabs(sumvr).le.1.e-14 .or. dabs(sumvz).le.1.e-14)goto 15
      if(dabs(addvr/sumvr).gt.tol .or. dabs(addvz/sumvz).gt.tol)goto 10
15    phi=xk*sumphi+patm*patm
      psi=-xk*r*sumpsi/(patm*patm)
      vr=-xk/a*sumvr*(-prad/(2.*visc*dsqrt(phi)))/theta
      vz=xk*sumvz*(-pz/(2.*visc*dsqrt(phi)))/theta
      phi=phi/(patm*patm)
      return
      end

      DOUBLE PRECISION FUNCTION BESSI0(W)
      IMPLICIT REAL*8 (A-H,O-Z)
      T=W/3.75
      IF(DABS(T).LE.1.0) THEN
      Y=T*T
      BESSI0=1.0+Y*(3.5156229+Y*(3.0899424+Y*(1.2067492+Y*(0.2659732+
     >Y*(0.0360768+0.0045813*Y)))))
      ELSE
      AW=DABS(W)
      Y=3.75/AW
      TEMP=0.39894228+Y*(0.01328592+Y*(0.00225319+Y*(-0.00157565+Y*(
     >0.00916281+Y*(-0.02057706+Y*(0.02635537+Y*(-0.01647633+
     >0.00392377*Y)))))))
      BESSI0=DEXP(AW)*TEMP/DSQRT(AW)
      END IF
      RETURN
      END

      Double Precision Function Bessk0(x)
      implicit real*8 (a-h,o-z)
      data p1,p2,p3,p4,p5,p6,p7/-0.57721566,0.4227842,0.23069756,
     >0.348859d-1,0.262698d-2,0.10750d-3,0.74d-5/
      data q1,q2,q3,q4,q5,q6,q7/1.25331414,-0.7832358d-1,0.2189568d-1,
     >-0.1062446d-1,0.587872d-2,-0.25154d-2,0.53208d-3/
      if(x.le.2.0)then
      y=x*x/4.0
      bessk0=(-dlog(x/2.0)*bessi0(x))+(p1+y*(p2+y*(p3+y*(p4+y*(p5+y*(p6+
     >y*p7))))))
      else
      y=2.0/x
      bessk0=(dexp(-x)/dsqrt(x))*(q1+y*(q2+y*(q3+y*(q4+y*(q5+y*(q6+y*q7)
     >)))))
      endif
      return
      end

      DOUBLE PRECISION FUNCTION BESSI1(W)
      IMPLICIT REAL*8 (A-H,O-Z)
```

```
      T=W/3.75
      IF(DABS(T).LE.1.0) THEN
      Y=T*T
      BESSI1=W*(0.5+Y*(0.87890594+Y*(0.51498869+Y*(0.15084934+Y*
     >(0.02658733+Y*(0.00301532+0.00032411*Y))))))
      ELSE
      AW=DABS(W)
      Y=3.75/AW
      TEMP=0.39894228+Y*(-0.03988024+Y*(-0.00362018+Y*(0.00163801+Y*
     >(-0.01031555+Y*(0.02282967+Y*(-0.02895312+Y*(0.01787654-
     >0.00420059*Y)))))))
      BESSI1=DEXP(AW)*TEMP/DSQRT(AW)
      IF(W.LT.0.)BESSI1=-BESSI1
      END IF
      RETURN
      END

      Double Precision Function Bessk1(x)
      implicit real*8 (a-h,o-z)
      data p1,p2,p3,p4,p5,p6,p7/1.d0,0.15443144d0,-0.67278579d0,
     >-0.18156897d0,-0.1919402d-1,-0.110404d-2,-0.4686d-4/
      data q1,q2,q3,q4,q5,q6,q7/1.25331414,0.23498619d0,-0.3655620d-1,
     >0.1504268d-1,-0.780353d-2,0.325614d-2,-0.68245d-3/
      if(x.le.2.0)then
      y=x*x/4.0
      bessk1=(dlog(x/2.0)*bessi1(x))+(1./x)*(p1+y*(p2+y*(p3+y*(p4+y*(p5+
     >y*(p6+y*p7))))))
      else
      y=2.0/x
      bessk1=(dexp(-x)/dsqrt(x))*(q1+y*(q2+y*(q3+y*(q4+y*(q5+y*(q6+y*q7)
     >)))))
      endif
      return
      end
c
      subroutine getlen(string,chr,n0,n1)
c
c     to determine the length of a string excluding any blank padding & heading
c     and return string(n0:n1) n0... position of first non-blank letter
c                              n1... position of last non-blank letter
c     else return the original string
c     ***Use | to keep blank space at the begining or the end of the
c      *** string
c
      character*(*) string
      character*160 string1
      character*1 chr
      string1=' '
      in0=0
      in1=0
      do 10 i=len(string),1,-1
      if(string(i:i).ne.chr) then
```

```
      if(in1.eq.0) then
      if(string(i:i).eq.'|') then
      n1=i-1
      else
      n1=i
      endif
      in1=1
      endif
      goto 11
     endif
10    continue
11    do 20 i=1,len(string)
     if(string(i:i).ne.chr) then
      if(in0.eq.0) then
      if(string(i:i).eq.'|') then
      n0=i+1
      else
      n0=i
      endif
      in0=1
      nk=n0-1
c     write(6,*) '|'//string(n0:n1)//'|', n0,n1
      do 30 k=n0,n1
      if(string(k:k).ne.'|') then
        nk=nk+1
        if(k.eq.n0) then
          string1=string(k:k)
        else
          string1=string1(1:nk-n0)//string(k:k)
        endif
      endif
c     write(6,*) '|'//string1(1:nk-n0)//'|'
30     continue
      string=string1
      n1=n1-n0+1
      n0=1
      endif
      return
     endif
20    continue
     n0=-1
     n1=-1
     return
     end
```

APPENDIX C (MFRLKINV)

Sample Input File for MFRLKINV

```
/*  Title - This is a sample input file for the MFRLKINV code
293.0                   /* temperature (K)  (TEMP)
-11.38                  /* mass pumping rate (g/sec)  (XMPR)
451.5                   /* thickness of formation  (XB)
190.5                   /* distance to top of well screen  (XD)
451.                    /* distance to bottom of well screen  (XL)
12.7                    /* radius of the borehole
1.e-10                  /* convergence criterion
1.74e-07,1.85e-07       /* minimum and maximum radial permeability (cm^2)
2.9,9.3                 /* minimum and maximum anisotropy ratio (K_r/K_z)
2.1e-10,1.0e-9          /* minimum and maximum leakance (cm)
5000                    /* number of random parameter guesses
1                       /* number of "best" parameter sets for forward problem
6
457.0,229.0,0.997049
1097.0,229.0,0.999238
1237.0,229.0,0.999189
1478.0,229.0,0.999336
1582.0,269.0,0.999607
1584.0,229.0,0.999754
1932.0,286.0,0.999705
```

Sample Output File for MFRLKINV

```
 ------------------------------------------------------
      Steady-State Multi-Well Parameter Estimation
            Finite-Radius Model
          Top BC: Semi-Confining Layer
 ------------------------------------------------------
```

Parameter Estimates Ordered from Best to Worst

K_r	K_z	Leakance	RMS-Error	IFLAG
0.1752E-06	0.5618E-07	0.2257E-09	0.1216E-03	0
0.1777E-06	0.5791E-07	0.2181E-09	0.1216E-03	0
0.1780E-06	0.5497E-07	0.2264E-09	0.1216E-03	0
0.1751E-06	0.5626E-07	0.2282E-09	0.1216E-03	0
0.1768E-06	0.5480E-07	0.2254E-09	0.1218E-03	0
0.1764E-06	0.5135E-07	0.2519E-09	0.1218E-03	0
0.1782E-06	0.4436E-07	0.3000E-09	0.1219E-03	0
0.1800E-06	0.4191E-07	0.3259E-09	0.1219E-03	0
0.1759E-06	0.4902E-07	0.2680E-09	0.1220E-03	0
0.1821E-06	0.4174E-07	0.3319E-09	0.1220E-03	0

(Only top ten listed)

Observed Versus Modeled Results

Parameter set - 1

K_r = 0.1752E-06
K_z = 0.5618E-07
K/b(leaky) = 0.2257E-09

R (cm)	Z (cm)	P_observed	P_model
0.4570E+03	0.2290E+03	0.9970E+00	0.9970E+00
0.1097E+04	0.2290E+03	0.9992E+00	0.9991E+00
0.1237E+04	0.2290E+03	0.9992E+00	0.9993E+00
0.1478E+04	0.2290E+03	0.9993E+00	0.9995E+00
0.1582E+04	0.2690E+03	0.9996E+00	0.9996E+00
0.1584E+04	0.2290E+03	0.9998E+00	0.9996E+00

Source Code for MFRLKINV (author: Ravi Varadhan)

(A FORTRAN program for estimation of radial gas permeability, vertical gas permeability, and leakance in a semi-confined domain)

```
c  Parameter estimation for the steady-state solution for finite well radius
c
c  BC: Semi-confining unit on top
c  Multiple monitoring locations
c
c  version 1.0   07/21/99
c
      implicit real*8 (a-h,o-z)
      common/ceigen/xlk
      dimension pobs(100),p_r(5000),p_z(5000),beta(5000),errmet(5000),
     >rr(100),zz(100),wksp(5000),iwksp(5000),iflag(5000),bn(1000)
      integer*4 istart,ifinish
      character*15 prefix,fname1,fname2
      character*4 suffix1,suffix2
      write(*,*)' Parameter Estimation for Steady-State Multi-Well Test'
      write(*,*)' Finite-Radius Solution -  BC: Leaky-Layer on Top'
      write(*,*)
      write(*,*)'Enter the Prefix of the input file:  '
      write(*,*)'An output file is created w/ same prefix'
      write(*,*)' Input-file Prefix ?  '
      read(*,'(a)')prefix
      call getlen(prefix,' ',n0,n1)
      suffix1='.inp'
      suffix2='.dat'
      fname1=prefix(n0:n1)//suffix1
      fname2=prefix(n0:n1)//suffix2
      open(10,fname1,status='unknown')
      open(20,fname2,status='unknown')
      open(30,'seed.inp',status='unknown')
      read(10,*)
      read(10,101)temp,xmpr,xb,xd,xl,rw,tol
      read(10,*)prmin,prmax
      read(10,*)rmin,rmax
      read(10,*)xlkmin,xlkmax
      read(10,101)nguess
      read(10,101)nbest
      read(10,101)nsim
      do 2 i=1,nsim
      read(10,*)rr(i),zz(i),pobs(i)
2     continue
      patm=1013200.
      visc=1.76e-04
      rgas=8.314e07
      xmw=28.8
      pi=4.0*datan(1.0)
c   patm = atmospheric pressure (g/cm/sec^2)
c   visc = viscosity of gas (g/cm/sec)
```

```
c   rgas = universal gas constant
c   temp = temperature of gas (K)
c   xmw = molecular weight of gas (g/mole)
c   xmpr = mass withdrawal rate (g/sec)
c   prad = radial permeability of the formation (cm^2)
c   pz = vertical permeability
c   xlk = leakance of the confining unit (cm):  xlk = k'/b'
c   por = gas filled porosity
c   xb = thickness of the formation (cm)
c   xbp = thickness of the leaky unit
c   xl = distance from the bottom of leaky unit to the bottom of well screen
c   xd = distance from the bottom of leaky unit to the top of well screen
c   rw = nominal well radius (cm)
c   aa = radial cordinate (cm)
c   bb = vertical cordinate
c   cc = elapsed time (sec)
c   nsim = number of times solution will be generated
c   pobs = measured pneumatic pressure responses
c
      write(20,*)' ------------------------------------------------------'
      write(20,*)'      Steady-State Multi-Well Parameter Estimation'
      write(20,*)'               Finite-Radius Model  '
      write(20,*)'           Top BC: Semi-Confining Layer '
      write(20,*)' ------------------------------------------------------'
      write(20,*)
      xll=xl/xb
      xdd=xd/xb
      r_w=rw/xb
      call timer(istart)
      read(30,*)iseed
      do 1 j=1,nguess
      iflag(j)=0
      errmet(j)=0.
      sqerr=0.
      guess1=ran1(iseed)
      guess2=ran1(iseed)
      guess3=ran1(iseed)
      p_r(j)=prmin*(prmax/prmin)**guess1
      ratio=rmin+(rmax-rmin)*guess2
      p_z(j)=p_r(j)/ratio
      beta(j)=xlkmin*(xlkmax/xlkmin)**guess3
      prad=p_r(j)
      pz=p_z(j)
      xlk=beta(j)/(pz/xb)
      a=dsqrt(prad/pz)
      xm=xmpr*visc*rgas*temp/(pi*xmw*prad*patm*patm*xb)
c
      call vnfunc(bn)
      do 5 i=1,nsim
      r=rr(i)/xb
      z=zz(i)/xb
      n=0
```

```
      sum=0.0
10    continue
      n=n+1
      if(n.gt.1000)then
      iflag(j)=1
      goto 15
      endif
      vn=bn(n)
      tcos=dcos(vn*(1.-z))
      tsin=dsin(vn*(1.-xdd))-dsin(vn*(1.-xll))
      trig=tcos*tsin
      fact=xlk/(vn*(xll-xdd)*(xlk+dsin(vn)**2))
      wn=vn/a
      fn=bessk0(wn*r)/(wn*r_w*bessk1(wn*r_w))
      add=trig*fact*fn
      sum=sum+add
      if(dabs(sum).le.1.e-14)goto 15
      if(dabs(add/sum).gt.tol)goto 10
15    continue
      psqrd=1.0+2.0*xm*sum
      if(psqrd.lt.0.)then
      iflag(j)=2
      errmet(j)=1.e10
      goto 1
      endif
      popatm=dsqrt(psqrd)
      sqerr=sqerr+(popatm-pobs(i))**2
5     continue
      errmet(j)=dsqrt(sqerr/nsim)
      write(*,*)j,prad,pz,beta(j),errmet(j),iflag(j)
1     continue
      call sort3(nguess,errmet,p_r,p_z,beta,iflag,wksp,iwksp)
      write(20,107)
      write(20,102)
      do 20 j=1,nguess
      write(20,103)p_r(j),p_z(j),beta(j),errmet(j),iflag(j)
20    continue
c
      do 30 j=1,nbest
      prad=p_r(j)
      pz=p_z(j)
      xlk=beta(j)/(pz/xb)
      write(20,104)j,prad,pz,beta(j)
      write(20,105)
      a=dsqrt(prad/pz)
      xm=xmpr*visc*rgas*temp/(pi*xmw*prad*patm*patm*xb)
      call vnfunc(bn)
c
      do 35 i=1,nsim
      r=rr(i)/xb
      z=zz(i)/xb
      n=0
```

```
      sum=0.0
40    continue
      n=n+1
      if(n.gt.1000)goto 45
      vn=bn(n)
      tcos=dcos(vn*(1.-z))
      tsin=dsin(vn*(1.-xdd))-dsin(vn*(1.-xll))
      trig=tcos*tsin
      fact=xlk/(vn*(xll-xdd)*(xlk+dsin(vn)**2))
      wn=vn/a
      fn=bessk0(wn*r)/(wn*r_w*bessk1(wn*r_w))
      add=trig*fact*fn
      sum=sum+add
      if(dabs(sum).le.1.e-14)goto 45
      if(dabs(add/sum).gt.tol)goto 40
45    continue
      psqrd=1.0+2.0*xm*sum
      if(psqrd.ge.0.)then
      popatm=dsqrt(psqrd)
      else
      popatm=0.
      endif
      write(20,106)rr(i),zz(i),pobs(i),dsqrt(psqrd)
35    continue
30    continue
      call timer(ifinish)
      write(*,*)'Time of execution (sec)  =',(ifinish-istart)/100.
101   format(g15.0)
102   format(/5x,'K_r',11x,'K_z',10x,'Leakance',9x,'RMS-Error',4x,
     >'IFLAG'/)
103   format(2x,e10.4,4x,e10.4,5x,e10.4,8x,e10.4,4x,i2)
104   format(//20x,'Parameter set - ',i4//,3x,'K_r = ',e10.4/
     >3x,'K_z = ',e10.4/3x,'K/b(leaky) = ',e10.4//)
105   format(7x,'R (cm)',10x,'Z (cm)',11x,'P_observed',7x,'P_model'/)
106   format(5x,e10.4,7x,e10.4,8x,e10.4,6x,e10.4)
107   format(//10x,'Parameter Estimates Ordered from Best to Worst'//)
      rewind(30)
      write(30,*)-iseed
      stop
      end
c
      subroutine vnfunc(x)
      implicit real*8 (a-h,o-z)
      dimension x(1000)
      external eigen
      common/ceigen/b
      pi=4.*datan(1.0)
      x1=1.e-06
      x2=pi
      kount=1
1     continue
      zero=rtsafe(eigen,x1,x2,1.e-06)
```

```
 x(kount)=zero
 x1=zero+0.5*pi
 x2=zero+1.5*pi
 kount=kount+1
 if(kount.le.1000)goto 1
 return
 end

 Double Precision FUNCTION rtsafe(funcd,x1,x2,xacc)
 implicit real*8 (a-h,o-z)
 EXTERNAL funcd
 PARAMETER (MAXIT=100)
 call funcd(x1,fl,df)
 call funcd(x2,fh,df)
 if((fl.gt.0..and.fh.gt.0.).or.(fl.lt.0..and.fh.lt.0.))write(*,*)
*'root must be bracketed in rtsafe'
 if(fl.eq.0.)then
   rtsafe=x1
   return
 else if(fh.eq.0.)then
   rtsafe=x2
   return
 else if(fl.lt.0.)then
   xl=x1
   xh=x2
 else
   xh=x1
   xl=x2
 endif
 rtsafe=.5*(x1+x2)
 dxold=dabs(x2-x1)
 dx=dxold
 call funcd(rtsafe,f,df)
 do 11 j=1,MAXIT
   if(((rtsafe-xh)*df-f)*((rtsafe-xl)*df-f).ge.0..or. dabs(2.*
*f).gt.dabs(dxold*df) ) then
     dxold=dx
     dx=0.5*(xh-xl)
     rtsafe=xl+dx
     if(xl.eq.rtsafe)return
   else
     dxold=dx
     dx=f/df
     temp=rtsafe
     rtsafe=rtsafe-dx
     if(temp.eq.rtsafe)return
   endif
   if(dabs(dx).lt.xacc) return
   call funcd(rtsafe,f,df)
   if(f.lt.0.) then
     xl=rtsafe
   else
```

```
        xh=rtsafe
      endif
11    continue
      write(*,*)'rtsafe exceeded maximum iterations'
      return
      END

      subroutine eigen(x,f,df)
      implicit real*8 (a-h,o-z)
      common/ceigen/b
      f=b*dcos(x)-x*dsin(x)
      df=-b*dsin(x)-dsin(x)-x*dcos(x)
      return
      end

      Double Precision Function Bessk0(x)
      implicit real*8 (a-h,o-z)
      data p1,p2,p3,p4,p5,p6,p7/-0.57721566,0.4227842,0.23069756,
     >0.348859d-1,0.262698d-2,0.10750d-3,0.74d-5/
      data q1,q2,q3,q4,q5,q6,q7/1.25331414,-0.7832358d-1,0.2189568d-1,
     >-0.1062446d-1,0.587872d-2,-0.25154d-2,0.53208d-3/
      if(x.le.2.0)then
      y=x*x/4.0
      bessk0=(-dlog(x/2.0)*bessi0(x))+(p1+y*(p2+y*(p3+y*(p4+y*(p5+y*(p6+
     >y*p7))))))
      else
      y=2.0/x
      bessk0=(dexp(-x)/dsqrt(x))*(q1+y*(q2+y*(q3+y*(q4+y*(q5+y*(q6+y*q7)
     >)))))
      endif
      return
      end

      DOUBLE PRECISION FUNCTION BESSI0(W)
      IMPLICIT real*8 (A-H,O-Z)
      T=W/3.75
      IF(DABS(T).LE.1.0) THEN
      Y=T*T
      BESSI0=1.0+Y*(3.5156229+Y*(3.0899424+Y*(1.2067492+Y*(0.2659732+
     >Y*(0.0360768+0.0045813*Y)))))
      ELSE
      AW=DABS(W)
      Y=3.75/AW
      TEMP=0.39894228+Y*(0.01328592+Y*(0.00225319+Y*(-0.00157565+Y*(
     >0.00916281+Y*(-0.02057706+Y*(0.02635537+Y*(-0.01647633+
     >0.00392377*Y)))))))
      BESSI0=DEXP(AW)*TEMP/DSQRT(AW)
      END IF
      RETURN
      END

      double precision FUNCTION bessk1(x)
```

```
CU    USES bessi1
      implicit real*8 (a-h,o-z)
      DOUBLE PRECISION p1,p2,p3,p4,p5,p6,p7,q1,q2,q3,q4,q5,q6,q7,y
      SAVE p1,p2,p3,p4,p5,p6,p7,q1,q2,q3,q4,q5,q6,q7
      DATA p1,p2,p3,p4,p5,p6,p7/1.0d0,0.15443144d0,-0.67278579d0,
     *-0.18156897d0,-0.1919402d-1,-0.110404d-2,-0.4686d-4/
      DATA q1,q2,q3,q4,q5,q6,q7/1.25331414d0,0.23498619d0,-0.3655620d-1,
     *0.1504268d-1,-0.780353d-2,0.325614d-2,-0.68245d-3/
      if (x.le.2.0) then
        y=x*x/4.0
        bessk1=(dlog(x/2.0)*bessi1(x))+(1.0/x)*(p1+y*(p2+y*(p3+y*(p4+y*
     *(p5+y*(p6+y*p7))))))
      else
        y=2.0/x
        bessk1=(dexp(-x)/dsqrt(x))*(q1+y*(q2+y*(q3+y*(q4+y*(q5+y*(q6+y*
     *q7))))))
      endif
      return
      END

      double precision FUNCTION bessi1(x)
      implicit real*8 (a-h,o-z)
      DOUBLE PRECISION p1,p2,p3,p4,p5,p6,p7,q1,q2,q3,q4,q5,q6,q7,q8,q9,y
      SAVE p1,p2,p3,p4,p5,p6,p7,q1,q2,q3,q4,q5,q6,q7,q8,q9
      DATA p1,p2,p3,p4,p5,p6,p7/0.5d0,0.87890594d0,0.51498869d0,
     *0.15084934d0,0.2658733d-1,0.301532d-2,0.32411d-3/
      DATA q1,q2,q3,q4,q5,q6,q7,q8,q9/0.39894228d0,-0.3988024d-1,
     *-0.362018d-2,0.163801d-2,-0.1031555d-1,0.2282967d-1,-0.2895312d-1,
     *0.1787654d-1,-0.420059d-2/
      if (abs(x).lt.3.75) then
        y=(x/3.75)**2
        bessi1=x*(p1+y*(p2+y*(p3+y*(p4+y*(p5+y*(p6+y*p7))))))
      else
        ax=abs(x)
        y=3.75/ax
        bessi1=(dexp(ax)/dsqrt(ax))*(q1+y*(q2+y*(q3+y*(q4+y*(q5+y*(q6+y*
     *(q7+y*(q8+y*q9))))))))
        if(x.lt.0.)bessi1=-bessi1
      endif
      return
      END

      double precision FUNCTION ran1(idum)
      implicit real*8 (a-h,o-z)
      INTEGER idum,IA,IM,IQ,IR,NTAB,NDIV
      PARAMETER (IA=16807,IM=2147483647,AM=1./IM,IQ=127773,IR=2836,
     *NTAB=32,NDIV=1+(IM-1)/NTAB,EPS=1.2e-7,RNMX=1.-EPS)
      INTEGER j,k,iv(NTAB),iy
      SAVE iv,iy
      DATA iv /NTAB*0/, iy /0/
      if (idum.le.0.or.iy.eq.0) then
        idum=max(-idum,1)
```

```
      do 11 j=NTAB+8,1,-1
        k=idum/IQ
        idum=IA*(idum-k*IQ)-IR*k
        if (idum.lt.0) idum=idum+IM
        if (j.le.NTAB) iv(j)=idum
11      continue
      iy=iv(1)
    endif
    k=idum/IQ
    idum=IA*(idum-k*IQ)-IR*k
    if (idum.lt.0) idum=idum+IM
    j=1+iy/NDIV
    iy=iv(j)
    iv(j)=idum
    ran1=dmin1(AM*iy,RNMX)
    return
    END

    SUBROUTINE sort3(n,ra,rb,rc,rd,ie,wksp,iwksp)
    implicit real*8 (a-h,o-z)
    INTEGER n,iwksp(n),ie(n)
    dimension ra(n),rb(n),rc(n),rd(n),wksp(n)
CU    USES indexx
    INTEGER j
    call indexx(n,ra,iwksp)
    do 11 j=1,n
      wksp(j)=ra(j)
11    continue
    do 12 j=1,n
      ra(j)=wksp(iwksp(j))
12    continue
    do 13 j=1,n
      wksp(j)=rb(j)
13    continue
    do 14 j=1,n
      rb(j)=wksp(iwksp(j))
14    continue
    do 15 j=1,n
      wksp(j)=rc(j)
15    continue
    do 16 j=1,n
      rc(j)=wksp(iwksp(j))
16    continue
    do 17 j=1,n
      wksp(j)=rd(j)
17    continue
    do 18 j=1,n
      rd(j)=wksp(iwksp(j))
18    continue
    do 19 j=1,n
      wksp(j)=ie(j)
19    continue
```

```
      do 20 j=1,n
        ie(j)=wksp(iwksp(j))
20    continue
      return
      END

      SUBROUTINE indexx(n,arr,indx)
      implicit real*8 (a-h,o-z)
      INTEGER n,indx(n),M,NSTACK
      dimension arr(n)
      PARAMETER (M=7,NSTACK=50)
      INTEGER i,indxt,ir,itemp,j,jstack,k,l,istack(NSTACK)
      do 11 j=1,n
        indx(j)=j
11    continue
      jstack=0
      l=1
      ir=n
1     if(ir-l.lt.M)then
        do 13 j=l+1,ir
          indxt=indx(j)
          a=arr(indxt)
          do 12 i=j-1,1,-1
            if(arr(indx(i)).le.a)goto 2
            indx(i+1)=indx(i)
12        continue
          i=0
2         indx(i+1)=indxt
13      continue
        if(jstack.eq.0)return
        ir=istack(jstack)
        l=istack(jstack-1)
        jstack=jstack-2
      else
        k=(l+ir)/2
        itemp=indx(k)
        indx(k)=indx(l+1)
        indx(l+1)=itemp
        if(arr(indx(l+1)).gt.arr(indx(ir)))then
          itemp=indx(l+1)
          indx(l+1)=indx(ir)
          indx(ir)=itemp
        endif
        if(arr(indx(l)).gt.arr(indx(ir)))then
          itemp=indx(l)
          indx(l)=indx(ir)
          indx(ir)=itemp
        endif
        if(arr(indx(l+1)).gt.arr(indx(l)))then
          itemp=indx(l+1)
          indx(l+1)=indx(l)
          indx(l)=itemp
```

```
      endif
      i=l+1
      j=ir
      indxt=indx(l)
      a=arr(indxt)
3      continue
        i=i+1
      if(arr(indx(i)).lt.a)goto 3
4      continue
        j=j-1
      if(arr(indx(j)).gt.a)goto 4
      if(j.lt.i)goto 5
      itemp=indx(i)
      indx(i)=indx(j)
      indx(j)=itemp
      goto 3
5      indx(l)=indx(j)
      indx(j)=indxt
      jstack=jstack+2
      if(jstack.gt.NSTACK)write(*,*) 'NSTACK too small in indexx'
      if(ir-i+1.ge.j-l)then
        istack(jstack)=ir
        istack(jstack-1)=i
        ir=j-1
      else
        istack(jstack)=j-1
        istack(jstack-1)=l
        l=i
      endif
    endif
    goto 1
    END

c
    subroutine getlen(string,chr,n0,n1)
c
c    to determine the length of a string excluding any blank padding & heading
c    and return string(n0:n1) n0... position of first non-blank letter
c                             n1... position of last non-blank letter
c    else return the original string
c    ***Use | to keep blank space at the begining or the end of the
c     *** string
c
    character*(*) string
    character*160 string1
    character*1 chr
    string1=' '
    in0=0
    in1=0
    do 10 i=len(string),1,-1
    if(string(i:i).ne.chr) then
      if(in1.eq.0) then
```

```
       if(string(i:i).eq.'|') then
       n1=i-1
       else
       n1=i
       endif
       in1=1
       endif
       goto 11
      endif
10     continue
11     do 20 i=1,len(string)
      if(string(i:i).ne.chr) then
       if(in0.eq.0) then
       if(string(i:i).eq.'|') then
       n0=i+1
       else
       n0=i
       endif
       in0=1
       nk=n0-1
c      write(6,*) '|'//string(n0:n1)//'|', n0,n1
       do 30 k=n0,n1
       if(string(k:k).ne.'|') then
         nk=nk+1
         if(k.eq.n0) then
           string1=string(k:k)
         else
           string1=string1(1:nk-n0)//string(k:k)
         endif
       endif
c      write(6,*) '|'//string1(1:nk-n0)//'|'
30     continue
       string=string1
       n1=n1-n0+1
       n0=1
       endif
       return
      endif
20     continue
      n0=-1
      n1=-1
      return
      end
```

Appendix D (TFRLK)

Sample Input File for TFRLK code

```
/*  Title - This is a sample input file for the TFRLK code
298.0              /* temperature (K)  (TEMP)
1.0                /* mass pumping rate (g/sec)  (XMPR)
2000.0             /* time of pumping (sec)
600.0              /* thickness of formation  (XB)
410.               /* distance to top of well screen  (XD)
470.               /* distance to bottom of well screen  (XL)
10.0               /* radius of the well (Rw)
1.e-09             /* convergence criterion
1
0.10               /* air-porosity
1
15000.0            /* well-bore storage volume
1
1.0e-09            /* radial permeability (cm^2/s)
6
2.e-09,1.0E-09,3.33E-10,2.0E-10,1.40E-10,1.0E-10          /* vertical permeability (cm^2/s)
1
1.e-11             /* leakance (cm)
1
10.0               /* radial distances (cm)
1
440.0              /* vertical distance (cm)
100                /*times(s)
1.0,2.0,3.0,4.0,5.0,6.0,7.0,8.0,9.0,10.0,
15.0,20.0,25.0,30.0,35.0,40.0,45.0,50.0,55.0,60.0,
70.0,80.0,90.0,100.0,110.0,120.0,130.0,140.0,150.0,175.0,
200.0,225.0,250.0,275.0,300.0,325.0,350.0,375.0,400.0,450.0,
500.0,550.0,600.0,650.0,700.0,750.0,800.0,850.0,900.0,950.0,
1000.0,1100.0,1200.0,1300.0,1400.0,1500.0,1600.0,1700.0,1800.0,1900.0,
2000.0,2001.0,2002.0,2003.0,2004.0,2005.0,2006.0,2007.0,2008.0,2009.0,
2010.0,2015.0,2020.0,2025.0,2030.0,2035.0,2040.0,2045.0,2050.0,2100.0,
2200.0,2300.0,2400.0,2500.0,2600.0,2700.0,2800.0,2900.0,3000.0,3100.0,
3200.0,3300.0,3400.0,3400.0,3500.0,3600.0,3700.0,3800.0,3900.0,4000.0
```

Sample Output File for TFRLK code

```
   ********************************************************************

                  Results of Sensitivity Analysis

        Transient Finite-Radius Solution with Well-Bore Storage &
        Semi-confining Layer on Top

   ********************************************************************


              Parameter Set:  1

        Porosity =     0.1000
        Storage  = 0.1500E+05
        K_radial  = 0.1000E-08
        K_vertical = 0.2000E-08
        Leakance =0.1000E-10

         r            z            t            P/P_atm       Flag

    0.100E+02      0.440E+03     0.100E+01      0.10468E+01      0
    0.100E+02      0.440E+03     0.200E+01      0.10849E+01      0
    0.100E+02      0.440E+03     0.300E+01      0.11179E+01      0
    0.100E+02      0.440E+03     0.400E+01      0.11464E+01      0
    0.100E+02      0.440E+03     0.500E+01      0.11711E+01      0
    0.100E+02      0.440E+03     0.600E+01      0.11933E+01      0
    0.100E+02      0.440E+03     0.700E+01      0.12131E+01      0
    0.100E+02      0.440E+03     0.800E+01      0.12307E+01      0
    0.100E+02      0.440E+03     0.900E+01      0.12470E+01      0
    0.100E+02      0.440E+03     0.100E+02      0.12608E+01      0
(first 10 simulations for parameter set)
```

Source Code for TFRLK (author: Ravi Varadhan)

```
c  Forward problem for the transient solution for finite well radius
c  including well-bore storage
c  Top BC: Semi-Confining Layer
c
c  version 1.0   07/14/99
c
      implicit real*8 (a-h,o-z)
      dimension rr(100),zz(100),tt(100),poros(20),stor(20),p_r(20),p_z
     >(20),p_lk(20),bn(1000)
      common/cfunc/r,r_w,vn,a,gama
      common/ceigen/xlk
      character*15 prefix,fname1,fname2
      character*4 suffix1,suffix2
      write(*,*)' Forward Problem - Transient State'
      write(*,*)' Finite-Radius Solution with Borehole Storage '
      write(*,*)' Top BC: Semi-Confining Layer'
      write(*,*)
      write(*,*)'Enter the Prefix of the input file:  '
      write(*,*)'An output file is created w/ same prefix'
      write(*,*)' Input-file Prefix ?  '
      read(*,'(a)')prefix
      call getlen(prefix,' ',n0,n1)
      suffix1='.inp'
      suffix2='.dat'
      fname1=prefix(n0:n1)//suffix1
      fname2=prefix(n0:n1)//suffix2
      open(10,fname1,status='unknown')
      open(20,fname2,status='unknown')
      read(10,*)
      read(10,110)temp,xmpr,ttpump,xb,xd,xl,rw,tol
      patm=1013200.
      visc=1.76e-04
      rgas=8.314e07
      xmw=28.8
      pi=4.0*datan(1.0)
c   patm = atmospheric pressure (g/cm/sec^2)
c   visc = viscosity of gas (g/cm/sec)
c   rgas = universal gas constant
c   temp = temperature of gas (K)
c   xmw = molecular weight of gas (g/mole)
c   xmpr = mass withdrawal rate (g/sec)
c   por = air-filled porosity
c   prad = radial permeability of the formation (cm^2)
c   pz = vertical permeability
c   plk = permeability of the leaky confining unit
c   xb = thickness of the formation (cm)
c   xbp = thickness of the leaky unit
c   xl = distance from the bottom of leaky unit to the bottom of well screen
c   xd = distance from the bottom of leaky unit to the top of well screen
c   rw = nominal well radius (cm)
```

```
c
      xll=xl/xb
      xdd=xd/xb
      r_w=rw/xb
c
c  parameters to be varied are: porosity,wellbore-storage,k_r,k_z,leakance
c
      read(10,*)npor
      read(10,*)(poros(i),i=1,npor)
      read(10,*)nstor
      read(10,*)(stor(i),i=1,nstor)
      read(10,*)nprad
      read(10,*)(p_r(i),i=1,nprad)
      read(10,*)npz
      read(10,*)(p_z(i),i=1,npz)
      read(10,*)nlk
      read(10,*)(p_lk(i),i=1,nlk)
      nparm=npor+nstor+nprad+npz+nlk
      read(10,*)nr
      read(10,*)(rr(i),i=1,nr)
      read(10,*)nz
      read(10,*)(zz(i),i=1,nz)
      read(10,*)nt
      read(10,*)(tt(i),i=1,nt)
      write(20,101)
      mlinv=-1
      kount=0
      do 1 i=1,nparm
      por=poros(1)
      vstor=stor(1)
      prad=p_r(1)
      pz=p_z(1)
      plk=p_lk(1)
      if(i.eq.1)goto 2
      if((i-npor).eq.1)goto 1
      if((i-npor-nstor).eq.1)goto 1
      if((i-npor-nstor-nprad).eq.1)goto 1
      if((i-npor-nstor-nprad-npz).eq.1)goto 1
      if(i.le.npor)por=poros(i)
      if(i.gt.npor .and. i.le.(npor+nstor))vstor=stor(i-npor)
      if(i.gt.(npor+nstor) .and. i.le.(npor+nstor+nprad))prad=p_r
     >(i-npor-nstor)
      if(i.gt.(npor+nstor+nprad) .and. i.le.(npor+nstor+nprad+npz))
     >pz=p_z(i-npor-nstor-nprad)
      if(i.gt.(npor+nstor+nprad+npz))plk=p_lk(i-npor-nstor-nprad-npz)
c
2     continue
      kount=kount+1
      write(20,102)kount
      write(*,*)'porosity  =',por
      write(*,*)'storage  =',vstor
      write(*,*)'K_r  =',prad
```

```
      write(*,*)'K_z  =',pz
      write(*,*)'leakance  =',plk
      write(*,*)
      write(20,103)por,vstor,prad,pz,plk
      gama=vstor/(2.*pi*(xl-xd)*xb*xb*por)
      a=dsqrt(prad/pz)
      xm=xmpr*visc*rgas*temp/(pi*xmw*prad*patm*patm*xb)
      tpump=ttpump*prad*patm/(visc*por*xb*xb)
      xlk=plk/(pz/xb)
      if(i.eq.1 .or. i.gt.(npor+nstor+nprad+npz))call vnfunc(bn)
c
      write(20,104)
      do 5 j1=1,nz
      z=zz(j1)/xb
      do 6 j2=1,nr
      r=rr(j2)/xb
      do 7 j3=1,nt
      t=tt(j3)*prad*patm/(visc*por*xb*xb)
      iflag=0
      n=0
      sum=0.0
10    continue
      n=n+1
      if(n.gt.1000)goto 15
      vn=bn(n)
      call linv(mlinv,t,fnrt)
      call linv(mlinv,t-tpump,fnrtp)
      tcos=dcos(vn*(1.-z))
      tsin=dsin(vn*(1.-xdd))-dsin(vn*(1.-xll))
      trig=tcos*tsin
      fact=xlk/(vn*(xll-xdd)*(xlk+dsin(vn)**2))
      ans=fnrt-fnrtp
      add=trig*fact*ans
      sum=sum+add
      if(dabs(sum).le.1.e-14)goto 15
      if(dabs(add/sum).gt.tol)goto 10
15    continue
      psqrd=1.0+2.0*xm*sum
      if(psqrd.lt.0.)then
      popatm=0.
      iflag=999
      else
      popatm=dsqrt(psqrd)
      endif
      write(20,105)rr(j2),zz(j1),tt(j3),popatm,iflag
7     continue
      write(20,106)
6     continue
      write(20,106)
5     continue
c
1     continue
```

```
101   format(//4x,65('*')//25x,'Results of Sensitivity Analysis'//10x,
     >'Transient Finite-Radius Solution with Well-Bore Storage & '/,
     >10x,'Semi-confining Layer on Top'//4x,65('*')/)
102   format(///20x,'Parameter Set: ',i2/)
103   format(10x,'Porosity  = ',f10.4/10x,'Storage  = ',e10.4/10x,
     >'K_radial  = ',e10.4/10x,'K_vertical = ',e10.4/10x,'Leakance =',
     >e10.4/)
104   format(8x,'r',15x,'z',14x,'t',15x,'P/P_atm',8x,'Flag'/)
105   format(3x,e10.3,7x,e10.3,5x,e10.3,7x,e12.5,6x,i3)
106   format(/)
110   format(g10.0)
      stop
      end

      subroutine linv(m,t,f)
      implicit real*8 (a-h,o-z)
      common/cfunc/r,r_w,vn,a,gama
      dimension g(50),v(50),h(25)
      f=0.
      if(t.le.0.)return
      n=14
      if(m.ne.n)then
      call auxvec(n,g,v,h)
      m=n
      endif
      ss=dlog(2.d0)/t
      xp=0.d0
      visum=0.d0
      do 50 l=1,n
      s=l*ss
      wn=dsqrt(s+(vn/a)**2)
      pnum=bessk0(wn*r)
      pden=s*(wn*r_w*bessk1(wn*r_w)+s*gama*bessk0(wn*r_w))
      fbar=pnum/pden
      xp=xp+v(l)*fbar
      visum=v(l)/l+visum
50    continue
      f=ss*xp
      return
      end
c
      subroutine auxvec(n,g,v,h)
      implicit real*8 (a-h,o-z)
      dimension g(0:50),v(50),h(25)
      g(0)=1
      nh=n/2
      do 90 i=1,n
      g(i)=i*g(i-1)
90    continue
      h(1)=2.d0/g(nh-1)
      do 100 i=2,nh
      h(i)=i**nh*g(2*i)/(g(nh-i)*g(i)*g(i-1))
```

```
100   continue
      sn=2*mod(nh,2)-1
      vsum=0.d0
      do 140 i=1,n
      v(i)=0
      k1=(i+1)/2
      k2=min0(i,nh)
      do 130 k=k1,k2
      v(i)=v(i)+h(k)/(g(i-k)*g(2*k-i))
130   continue
      v(i)=sn*v(i)
      vsum=vsum+v(i)
      sn=-sn
140   continue
      return
      end
c
      Double Precision Function Bessk0(x)
      implicit real*8 (a-h,o-z)
      data p1,p2,p3,p4,p5,p6,p7/-0.57721566,0.4227842,0.23069756,
     >0.348859d-1,0.262698d-2,0.10750d-3,0.74d-5/
      data q1,q2,q3,q4,q5,q6,q7/1.25331414,-0.7832358d-1,0.2189568d-1,
     >-0.1062446d-1,0.587872d-2,-0.25154d-2,0.53208d-3/
      if(x.le.2.0)then
      y=x*x/4.0
      bessk0=(-dlog(x/2.0)*bessi0(x))+(p1+y*(p2+y*(p3+y*(p4+y*(p5+y*(p6+
     >y*p7))))))
      else
      y=2.0/x
      bessk0=(dexp(-x)/dsqrt(x))*(q1+y*(q2+y*(q3+y*(q4+y*(q5+y*(q6+y*q7)
     >)))))
      endif
      return
      end
c
      DOUBLE PRECISION FUNCTION BESSI0(W)
      IMPLICIT real*8 (A-H,O-Z)
      T=W/3.75
      IF(DABS(T).LE.1.0) THEN
      Y=T*T
      BESSI0=1.0+Y*(3.5156229+Y*(3.0899424+Y*(1.2067492+Y*(0.2659732+
     >Y*(0.0360768+0.0045813*Y)))))
      ELSE
      AW=DABS(W)
      Y=3.75/AW
      TEMP=0.39894228+Y*(0.01328592+Y*(0.00225319+Y*(-0.00157565+Y*(
     >0.00916281+Y*(-0.02057706+Y*(0.02635537+Y*(-0.01647633+
     >0.00392377*Y)))))))
      BESSI0=DEXP(AW)*TEMP/DSQRT(AW)
      END IF
      RETURN
      END
```

```
c
      double precision FUNCTION bessk1(x)
CU    USES bessi1
      implicit real*8 (a-h,o-z)
      DOUBLE PRECISION p1,p2,p3,p4,p5,p6,p7,q1,q2,q3,q4,q5,q6,q7,y
      SAVE p1,p2,p3,p4,p5,p6,p7,q1,q2,q3,q4,q5,q6,q7
      DATA p1,p2,p3,p4,p5,p6,p7/1.0d0,0.15443144d0,-0.67278579d0,
     *-0.18156897d0,-0.1919402d-1,-0.110404d-2,-0.4686d-4/
      DATA q1,q2,q3,q4,q5,q6,q7/1.25331414d0,0.23498619d0,-0.3655620d-1,
     *0.1504268d-1,-0.780353d-2,0.325614d-2,-0.68245d-3/
      if (x.le.2.0) then
        y=x*x/4.0
        bessk1=(dlog(x/2.0)*bessi1(x))+(1.0/x)*(p1+y*(p2+y*(p3+y*(p4+y*
     *(p5+y*(p6+y*p7))))))
      else
        y=2.0/x
        bessk1=(dexp(-x)/dsqrt(x))*(q1+y*(q2+y*(q3+y*(q4+y*(q5+y*(q6+y*
     *q7))))))
      endif
      return
      END
c
      double precision FUNCTION bessi1(x)
      implicit real*8 (a-h,o-z)
      DOUBLE PRECISION p1,p2,p3,p4,p5,p6,p7,q1,q2,q3,q4,q5,q6,q7,q8,q9,y
      SAVE p1,p2,p3,p4,p5,p6,p7,q1,q2,q3,q4,q5,q6,q7,q8,q9
      DATA p1,p2,p3,p4,p5,p6,p7/0.5d0,0.87890594d0,0.51498869d0,
     *0.15084934d0,0.2658733d-1,0.301532d-2,0.32411d-3/
      DATA q1,q2,q3,q4,q5,q6,q7,q8,q9/0.39894228d0,-0.3988024d-1,
     *-0.362018d-2,0.163801d-2,-0.1031555d-1,0.2282967d-1,-0.2895312d-1,
     *0.1787654d-1,-0.420059d-2/
      if (abs(x).lt.3.75) then
        y=(x/3.75)**2
        bessi1=x*(p1+y*(p2+y*(p3+y*(p4+y*(p5+y*(p6+y*p7))))))
      else
        ax=abs(x)
        y=3.75/ax
        bessi1=(dexp(ax)/dsqrt(ax))*(q1+y*(q2+y*(q3+y*(q4+y*(q5+y*(q6+y*
     *(q7+y*(q8+y*q9))))))))
        if(x.lt.0.)bessi1=-bessi1
      endif
      return
      END
c
      subroutine vnfunc(x)
      implicit real*8 (a-h,o-z)
      dimension x(1000)
      external eigen
      common/ceigen/b
      pi=4.*datan(1.0)
      x1=1.e-06
      x2=pi
```

```
      kount=1
1     continue
      zero=rtsafe(eigen,x1,x2,1.e-06)
      x(kount)=zero
      x1=zero+0.5*pi
      x2=zero+1.5*pi
      kount=kount+1
      if(kount.le.1000)goto 1
      return
      end
c
      Double Precision FUNCTION rtsafe(funcd,x1,x2,xacc)
      implicit real*8 (a-h,o-z)
      EXTERNAL funcd
      PARAMETER (MAXIT=100)
      call funcd(x1,fl,df)
      call funcd(x2,fh,df)
      if((fl.gt.0..and.fh.gt.0.).or.(fl.lt.0..and.fh.lt.0.))write(*,*)
     *'root must be bracketed in rtsafe'
      if(fl.eq.0.)then
        rtsafe=x1
        return
      else if(fh.eq.0.)then
        rtsafe=x2
        return
      else if(fl.lt.0.)then
        xl=x1
        xh=x2
      else
        xh=x1
        xl=x2
      endif
      rtsafe=.5*(x1+x2)
      dxold=dabs(x2-x1)
      dx=dxold
      call funcd(rtsafe,f,df)
      do 11 j=1,MAXIT
        if(((rtsafe-xh)*df-f)*((rtsafe-xl)*df-f).ge.0..or. dabs(2.*
     *f).gt.dabs(dxold*df) ) then
          dxold=dx
          dx=0.5*(xh-xl)
          rtsafe=xl+dx
          if(xl.eq.rtsafe)return
        else
          dxold=dx
          dx=f/df
          temp=rtsafe
          rtsafe=rtsafe-dx
          if(temp.eq.rtsafe)return
        endif
        if(dabs(dx).lt.xacc) return
        call funcd(rtsafe,f,df)
```

```
      if(f.lt.0.) then
        xl=rtsafe
      else
        xh=rtsafe
      endif
11    continue
      write(*,*)'rtsafe exceeded maximum iterations'
      return
      END
c
      subroutine eigen(x,f,df)
      implicit real*8 (a-h,o-z)
      common/ceigen/b
      f=b*dcos(x)-x*dsin(x)
      df=-b*dsin(x)-dsin(x)-x*dcos(x)
      return
      end
c
      subroutine getlen(string,chr,n0,n1)
c
c     to determine the length of a string excluding any blank padding & heading
c     and return string(n0:n1) n0... position of first non-blank letter
c                              n1... position of last non-blank letter
c     else return the original string
c     ***Use | to keep blank space at the begining or the end of the
c      *** string
c
      character*(*) string
      character*160 string1
      character*1 chr
      string1=' '
      in0=0
      in1=0
      do 10 i=len(string),1,-1
      if(string(i:i).ne.chr) then
        if(in1.eq.0) then
        if(string(i:i).eq.'|') then
        n1=i-1
        else
        n1=i
        endif
        in1=1
        endif
        goto 11
      endif
10    continue
11    do 20 i=1,len(string)
      if(string(i:i).ne.chr) then
       if(in0.eq.0) then
       if(string(i:i).eq.'|') then
       n0=i+1
       else
```

```
      n0=i
      endif
      in0=1
      nk=n0-1
c     write(6,*) '|'//string(n0:n1)//'|', n0,n1
      do 30 k=n0,n1
      if(string(k:k).ne.'|') then
        nk=nk+1
        if(k.eq.n0) then
          string1=string(k:k)
        else
          string1=string1(1:nk-n0)//string(k:k)
        endif
      endif
c     write(6,*) '|'//string1(1:nk-n0)//'|'
30    continue
      string=string1
      n1=n1-n0+1
      n0=1
      endif
      return
     endif
20   continue
     n0=-1
     n1=-1
     return
     end
```

Appendix E (FRLKINV)

Sample Input File for FRLKINV

```
/*  Title -  This is a sample input file for the FRLKINV code
298.0            /* temperature (K)  (TEMP)
0.215            /* mass pumping rate (g/sec)  (XMPR)
76.0            /* time of pumping (sec)
521.2            /* thickness of formation  (XB)
198.1             /* distance to top of well screen  (XD)
259.1             /* distance to bottom of well screen  (XL)
10.48            /* radius of the well (Rw)
1.e-06           /* convergence criterion
0.01,0.1          /* minimum and maximum air-porosity
4.e-10,3.e-09     /* minimum and maximum radial permeability (cm^2)
1.,10.           /* minimum and maximum anisotropy ratio (K_r/K_z)
1.e-14,1.e-10       /* minimum and maximum leakance (K'/b') (cm)
7500.,12500.      /* Minimum and Maximum Storage volume (cm^3)
3000              /* number of random parameter guesses
10               /* number of "best" parameter sets for forward problem
500              /* number of observations  (NSIM)
0          1.000885189
0.5        1.010032139
1          1.034817425
1.5        1.051636012
2          1.066684221
2.5        1.078191675
3          1.08881394
3.5        1.098551016
4          1.106222652
4.5        1.114484414
(only first 10 observations shown)
```

Sample Output File for FRLKINV

```
 ----------------------------------------------------
     Transient Single-Well Parameter Estimation
     Finite-Radius Model with Well-Bore Storage
         Top BC: Semi-Confining Layer
 ----------------------------------------------------

         Parameter Estimates Ordered from Best to Worst

   K_r          K_z          Leakance     Porosity     Storage      RMS-Error   IFLAG

 0.1812E-08   0.2009E-09   0.7196E-11   0.8013E-02   0.1179E+05   0.3228E-02   0
 0.1763E-08   0.2311E-09   0.6141E-11   0.8087E-02   0.1186E+05   0.3229E-02   0
 0.1763E-08   0.2228E-09   0.6459E-10   0.8181E-02   0.1186E+05   0.3273E-02   0
 0.1764E-08   0.2347E-09   0.7404E-11   0.8228E-02   0.1164E+05   0.3287E-02   0
 0.1796E-08   0.2122E-09   0.6801E-11   0.8015E-02   0.1151E+05   0.3300E-02   0
 0.1805E-08   0.1999E-09   0.3735E-10   0.8924E-02   0.1148E+05   0.3365E-02   0
 0.1744E-08   0.2300E-09   0.5049E-10   0.8388E-02   0.1167E+05   0.3369E-02   0
 0.1829E-08   0.1864E-09   0.4269E-11   0.8148E-02   0.1156E+05   0.3374E-02   0
 0.1714E-08   0.2559E-09   0.5804E-10   0.9741E-02   0.1171E+05   0.3388E-02   0
 0.1722E-08   0.2467E-09   0.8233E-11   0.9450E-02   0.1188E+05   0.3420E-02   0

(Only first 10 estimates shown)

Observed Versus Simulated Pressure

Parameter set -    1

  K_r = 0.1812E-08
  K_z = 0.2009E-09
  K/b(leaky) = 0.7196E-11
  Air-porosity = 0.8013E-02
  Storage = 0.1179E+05

     Time (sec)       P_observed       P_model

     0.0000E+00       0.1001E+01       0.1000E+01
     0.5000E+00       0.1014E+01       0.1021E+01
     0.1000E+01       0.1032E+01       0.1039E+01
     0.1500E+01       0.1048E+01       0.1055E+01
     0.2000E+01       0.1062E+01       0.1070E+01
     0.2500E+01       0.1074E+01       0.1084E+01
     0.3000E+01       0.1086E+01       0.1096E+01
     0.3500E+01       0.1096E+01       0.1107E+01
     0.4000E+01       0.1106E+01       0.1117E+01
     0.4500E+01       0.1115E+01       0.1127E+01

(Only first 10 observations shown)
```

Source Code for FRLKINV

```
c  Parameter estimation for the transient solution for finite well radius
c  including well-bore storage
c
c  Single-well Test
c  BC:Leaky layer on top
c
c  Author:  Varadhan Ravi
c  version 1.0   07/21/99
c
      implicit real*8 (a-h,o-z)
      common/cfunc/r,r_w,vn,a,gama
      common/ceigen/xlk
      dimension tt(3600),pobs(3600),poros(5000),p_r(5000),p_z(5000),
     >beta(5000),errmet(5000),wksp(5000),iwksp(5000),iflag(5000),
     >stor(5000),bn(500)
      integer*4 istart,ifinish
      character*15 prefix,fname1,fname2
      character*4 suffix1,suffix2
      write(*,*)' Parameter Estimation for Transient Single-Well Test'
      write(*,*)' Finite-Radius Solution -  BC: Leaky Layer on Top'
      write(*,*)
      write(*,*)'Enter the Prefix of the input file:  '
      write(*,*)'An output file is created w/ same prefix'
      write(*,*)' Input-file Prefix ?  '
      read(*,'(a)')prefix
      call getlen(prefix,' ',n0,n1)
      suffix1='.inp'
      suffix2='.dat'
      fname1=prefix(n0:n1)//suffix1
      fname2=prefix(n0:n1)//suffix2
      open(10,fname1,status='unknown')
      open(20,fname2,status='unknown')
      open(30,'seed.inp',status='unknown')
      read(10,*)
      read(10,101)temp,xmpr,ttpump,xb,xd,xl,rw,tol
      read(10,*)pormin,pormax
      read(10,*)prmin,prmax
      read(10,*)rmin,rmax
      read(10,*)xlkmin,xlkmax
      read(10,*)vstmin,vstmax
      read(10,101)nguess
      read(10,101)nbest
      read(10,101)nsim
      read(10,*)(tt(i),pobs(i),i=1,nsim)
      patm=1013200.
      visc=1.76e-04
      rgas=8.314e07
      xmw=28.8
      pi=4.0*datan(1.0)
c   patm = atmospheric pressure (g/cm/sec^2)
```

```
c   visc = viscosity of gas (g/cm/sec)
c   rgas = universal gas constant
c   temp = temperature of gas (K)
c   xmw = molecular weight of gas (g/mole)
c   xmpr = mass withdrawal rate (g/sec)
c   prad = radial permeability of the formation (cm^2)
c   pz = vertical permeability
c   xlk = leakance of the confining unit (cm):  xlk = k'/b'
c   por = gas filled porosity
c   xb = thickness of the formation (cm)
c   xbp = thickness of the leaky unit
c   xl = distance from the bottom of leaky unit to the bottom of well screen
c   xd = distance from the bottom of leaky unit to the top of well screen
c   rw = nominal well radius (cm)
c   nsim = number of times solution will be generated
c   pobs = measured pneumatic pressure responses
c
      write(20,*)' ----------------------------------------------------'
      write(20,*)'      Transient Single-Well Parameter Estimation'
      write(20,*)'      Finite-Radius Model with Well-Bore Storage  '
      write(20,*)'           Top BC: Semi-Confining Layer '
      write(20,*)' ----------------------------------------------------'
      write(20,*)
      xll=xl/xb
      xdd=xd/xb
      r_w=rw/xb
      call timer(istart)
      read(30,*)iseed
      do 1 j=1,nguess
      iflag(j)=0
      errmet(j)=0.
      sqerr=0.
      guess1=ran1(iseed)
      guess2=ran1(iseed)
      guess3=ran1(iseed)
      guess4=ran1(iseed)
      guess5=ran1(iseed)
      poros(j)=pormin+(pormax-pormin)*guess1
      p_r(j)=prmin*(prmax/prmin)**guess2
      ratio=rmin+(rmax-rmin)*guess3
      p_z(j)=p_r(j)/ratio
      beta(j)=xlkmin*(xlkmax/xlkmin)**guess4
      stor(j)=vstmin+(vstmax-vstmin)*guess5
      prad=p_r(j)
      pz=p_z(j)
      por=poros(j)
      xlk=beta(j)/(pz/xb)
      vstor=stor(j)
      gama=vstor/(2.*pi*(xl-xd)*xb*xb*por)
      a=dsqrt(prad/pz)
      xm=xmpr*visc*rgas*temp/(pi*xmw*prad*patm*patm*xb)
      tpump=ttpump*prad*patm/(visc*por*xb*xb)
```

```
c
      call vnfunc(bn)
      mlinv=-10
      do 5 i=1,nsim
      r=r_w
      z=(xdd+xll)/2.
      t=tt(i)*prad*patm/(visc*por*xb*xb)
      n=0
      sum=0.0
10    continue
      n=n+1
      if(n.gt.500)then
      iflag(j)=1
      goto 15
      endif
      vn=bn(n)
      call linv(mlinv,t,fnrt)
      call linv(mlinv,t-tpump,fnrtp)
      tcos=dcos(vn*(1.-z))
      tsin=dsin(vn*(1.-xdd))-dsin(vn*(1.-xll))
      trig=tcos*tsin
      fact=xlk/(vn*(xll-xdd)*(xlk+dsin(vn)**2))
      ans=fnrt-fnrtp
      add=trig*fact*ans
      sum=sum+add
      if(dabs(sum).le.1.e-14)goto 15
      if(dabs(add/sum).gt.tol)goto 10
15    continue
      psqrd=1.0+2.0*xm*sum
      if(psqrd.lt.0.)then
      iflag(j)=2
      errmet(j)=1.e10
      goto 1
      endif
      popatm=dsqrt(psqrd)
      sqerr=sqerr+(popatm-pobs(i))**2
5     continue
      errmet(j)=dsqrt(sqerr/nsim)
      write(*,*)j,prad,pz,beta(j),por,stor(j),errmet(j),iflag(j)
1     continue
      call sort3(nguess,errmet,poros,p_r,p_z,beta,stor,iflag,wksp,iwksp)
      write(20,107)
      write(20,102)
      do 20 j=1,nguess
      write(20,103)p_r(j),p_z(j),beta(j),poros(j),stor(j),errmet(j),
     >iflag(j)
20    continue
c
      do 30 j=1,nbest
      prad=p_r(j)
      pz=p_z(j)
      por=poros(j)
```

```
      xlk=beta(j)/(pz/xb)
      write(20,104)j,prad,pz,beta(j),por,stor(j)
      write(20,105)
      gama=vstor/(2.*pi*(xl-xd)*xb*xb*por)
      a=dsqrt(prad/pz)
      xm=xmpr*visc*rgas*temp/(pi*xmw*prad*patm*patm*xb)
      tpump=ttpump*prad*patm/(visc*por*xb*xb)
      call vnfunc(bn)
c
      mlinv=-10
      do 35 i=1,nsim
      r=r_w
      z=(xdd+xll)/2.
      t=tt(i)*prad*patm/(visc*por*xb*xb)
      n=0
      sum=0.0
40    continue
      n=n+1
      if(n.gt.500)goto 45
      vn=bn(n)
      call linv(mlinv,t,fnrt)
      call linv(mlinv,t-tpump,fnrtp)
      tcos=dcos(vn*(1.-z))
      tsin=dsin(vn*(1.-xdd))-dsin(vn*(1.-xll))
      trig=tcos*tsin
      fact=xlk/(vn*(xll-xdd)*(xlk+dsin(vn)**2))
      ans=fnrt-fnrtp
      add=trig*fact*ans
      sum=sum+add
      if(dabs(sum).le.1.e-14)goto 45
      if(dabs(add/sum).gt.tol)goto 40
45    continue
      psqrd=1.0+2.0*xm*sum
      if(psqrd.ge.0.)then
      popatm=dsqrt(psqrd)
      else
      popatm=0.
      endif
      write(20,106)tt(i),pobs(i),popatm
35    continue
30    continue
      call timer(ifinish)
      write(*,*)'Time of execution (sec)  =',(ifinish-istart)/100.
101   format(g15.0)
102   format(/4x,'K_r',11x,'K_z',10x,'Leakance',6x,'Porosity',7x,
     >'Storage',7x,'RMS-Error',4x,'IFLAG'/)
103   format(1x,e10.4,4x,e10.4,5x,e10.4,4x,e10.4,5x,e10.4,5x,e10.4,4x,
     >i2)
104   format(//20x,'Parameter set - ',i4//,3x,'K_r = ',e10.4/
     >3x,'K_z = ',e10.4/3x,'K/b(leaky) = ',e10.4/3x,'Air-porosity = ',
     >e10.4/3x,'Storage = ',e10.4//)
105   format(7x,'Time (sec)',8x,'P_observed',8x,'P_model'/)
```

```
106   format(7x,e10.4,8x,e10.4,7x,e10.4)
107   format(//10x,'Parameter Estimates Ordered from Best to Worst'//)
108   format(/3x,'K_r = ',e10.4/3x,'K_r/K_z = ',e10.4/3x,'K/b(leaky) = '
     >,e10.4/3x,'Air-porosity = ',e10.4/3x,'Storage = ',e10.4/)
      rewind(30)
      write(30,*)-iseed
      stop
      end

      subroutine linv(m,t,f)
      implicit real*8 (a-h,o-z)
      common/cfunc/r,r_w,vn,a,gama
      dimension g(50),v(50),h(25)
      f=0.
      if(t.le.0.)return
      n=14
      if(m.ne.n)then
      call auxvec(n,g,v,h)
      m=n
      endif
      ss=dlog(2.d0)/t
      xp=0.d0
      visum=0.d0
      do 50 l=1,n
      s=l*ss
      wn=dsqrt(s+(vn/a)**2)
      pnum=bessk0(wn*r)
      pden=s*(wn*r_w*bessk1(wn*r_w)+s*gama*bessk0(wn*r_w))
      fbar=pnum/pden
      xp=xp+v(l)*fbar
      visum=v(l)/l+visum
50    continue
      f=ss*xp
      return
      end

      subroutine auxvec(n,g,v,h)
      implicit real*8 (a-h,o-z)
      dimension g(0:50),v(50),h(25)
      g(0)=1
      nh=n/2
      do 90 i=1,n
      g(i)=i*g(i-1)
90    continue
      h(1)=2.d0/g(nh-1)
      do 100 i=2,nh
      h(i)=i**nh*g(2*i)/(g(nh-i)*g(i)*g(i-1))
100   continue
      sn=2*mod(nh,2)-1
      vsum=0.d0
      do 140 i=1,n
      v(i)=0
```

```
      k1=(i+1)/2
      k2=min0(i,nh)
      do 130 k=k1,k2
      v(i)=v(i)+h(k)/(g(i-k)*g(2*k-i))
  130   continue
      v(i)=sn*v(i)
      vsum=vsum+v(i)
      sn=-sn
  140   continue
      return
      end

      subroutine vnfunc(x)
      implicit real*8 (a-h,o-z)
      dimension x(500)
      external eigen
      common/ceigen/b
      pi=4.*datan(1.0)
      x1=1.e-06
      x2=pi
      kount=1
  1    continue
      zero=rtsafe(eigen,x1,x2,1.e-06)
      x(kount)=zero
      x1=zero+0.5*pi
      x2=zero+1.5*pi
      kount=kount+1
      if(kount.le.500)goto 1
      return
      end

      Double Precision FUNCTION rtsafe(funcd,x1,x2,xacc)
      implicit real*8 (a-h,o-z)
      EXTERNAL funcd
      PARAMETER (MAXIT=100)
      call funcd(x1,fl,df)
      call funcd(x2,fh,df)
      if((fl.gt.0..and.fh.gt.0.).or.(fl.lt.0..and.fh.lt.0.))write(*,*)
     *'root must be bracketed in rtsafe'
      if(fl.eq.0.)then
        rtsafe=x1
        return
      else if(fh.eq.0.)then
        rtsafe=x2
        return
      else if(fl.lt.0.)then
        xl=x1
        xh=x2
      else
        xh=x1
        xl=x2
      endif
```

```
      rtsafe=.5*(x1+x2)
      dxold=dabs(x2-x1)
      dx=dxold
      call funcd(rtsafe,f,df)
      do 11 j=1,MAXIT
        if(((rtsafe-xh)*df-f)*((rtsafe-xl)*df-f).ge.0..or. dabs(2.*
     *f).gt.dabs(dxold*df) ) then
          dxold=dx
          dx=0.5*(xh-xl)
          rtsafe=xl+dx
          if(xl.eq.rtsafe)return
        else
          dxold=dx
          dx=f/df
          temp=rtsafe
          rtsafe=rtsafe-dx
          if(temp.eq.rtsafe)return
        endif
        if(dabs(dx).lt.xacc) return
        call funcd(rtsafe,f,df)
        if(f.lt.0.) then
          xl=rtsafe
        else
          xh=rtsafe
        endif
11      continue
      write(*,*)'rtsafe exceeded maximum iterations'
      return
      END

      subroutine eigen(x,f,df)
      implicit real*8 (a-h,o-z)
      common/ceigen/b
      f=b*dcos(x)-x*dsin(x)
      df=-b*dsin(x)-dsin(x)-x*dcos(x)
      return
      end

      Double Precision Function Bessk0(x)
      implicit real*8 (a-h,o-z)
      data p1,p2,p3,p4,p5,p6,p7/-0.57721566,0.4227842,0.23069756,
     >0.348859d-1,0.262698d-2,0.10750d-3,0.74d-5/
      data q1,q2,q3,q4,q5,q6,q7/1.25331414,-0.7832358d-1,0.2189568d-1,
     >-0.1062446d-1,0.587872d-2,-0.25154d-2,0.53208d-3/
      if(x.le.2.0)then
      y=x*x/4.0
      bessk0=(-dlog(x/2.0)*bessi0(x))+(p1+y*(p2+y*(p3+y*(p4+y*(p5+y*(p6+
     >y*p7))))))
      else
      y=2.0/x
      bessk0=(dexp(-x)/dsqrt(x))*(q1+y*(q2+y*(q3+y*(q4+y*(q5+y*(q6+y*q7)
     >)))))
```

```
      endif
      return
      end

      DOUBLE PRECISION FUNCTION BESSI0(W)
      IMPLICIT real*8 (A-H,O-Z)
      T=W/3.75
      IF(DABS(T).LE.1.0) THEN
      Y=T*T
      BESSI0=1.0+Y*(3.5156229+Y*(3.0899424+Y*(1.2067492+Y*(0.2659732+
     >Y*(0.0360768+0.0045813*Y)))))
      ELSE
      AW=DABS(W)
      Y=3.75/AW
      TEMP=0.39894228+Y*(0.01328592+Y*(0.00225319+Y*(-0.00157565+Y*(
     >0.00916281+Y*(-0.02057706+Y*(0.02635537+Y*(-0.01647633+
     >0.00392377*Y)))))))
      BESSI0=DEXP(AW)*TEMP/DSQRT(AW)
      END IF
      RETURN
      END

      double precision FUNCTION bessk1(x)
CU    USES bessi1
      implicit real*8 (a-h,o-z)
      DOUBLE PRECISION p1,p2,p3,p4,p5,p6,p7,q1,q2,q3,q4,q5,q6,q7,y
      SAVE p1,p2,p3,p4,p5,p6,p7,q1,q2,q3,q4,q5,q6,q7
      DATA p1,p2,p3,p4,p5,p6,p7/1.0d0,0.15443144d0,-0.67278579d0,
     *-0.18156897d0,-0.1919402d-1,-0.110404d-2,-0.4686d-4/
      DATA q1,q2,q3,q4,q5,q6,q7/1.25331414d0,0.23498619d0,-0.3655620d-1,
     *0.1504268d-1,-0.780353d-2,0.325614d-2,-0.68245d-3/
      if (x.le.2.0) then
        y=x*x/4.0
        bessk1=(dlog(x/2.0)*bessi1(x))+(1.0/x)*(p1+y*(p2+y*(p3+y*(p4+y*
     *(p5+y*(p6+y*p7))))))
      else
        y=2.0/x
        bessk1=(dexp(-x)/dsqrt(x))*(q1+y*(q2+y*(q3+y*(q4+y*(q5+y*(q6+y*
     *q7))))))
      endif
      return
      END

      double precision FUNCTION bessi1(x)
      implicit real*8 (a-h,o-z)
      DOUBLE PRECISION p1,p2,p3,p4,p5,p6,p7,q1,q2,q3,q4,q5,q6,q7,q8,q9,y
      SAVE p1,p2,p3,p4,p5,p6,p7,q1,q2,q3,q4,q5,q6,q7,q8,q9
      DATA p1,p2,p3,p4,p5,p6,p7/0.5d0,0.87890594d0,0.51498869d0,
     *0.15084934d0,0.2658733d-1,0.301532d-2,0.32411d-3/
      DATA q1,q2,q3,q4,q5,q6,q7,q8,q9/0.39894228d0,-0.3988024d-1,
     *-0.362018d-2,0.163801d-2,-0.1031555d-1,0.2282967d-1,-0.2895312d-1,
     *0.1787654d-1,-0.420059d-2/
```

```
      if (abs(x).lt.3.75) then
        y=(x/3.75)**2
        bessi1=x*(p1+y*(p2+y*(p3+y*(p4+y*(p5+y*(p6+y*p7))))))
      else
        ax=abs(x)
        y=3.75/ax
        bessi1=(dexp(ax)/dsqrt(ax))*(q1+y*(q2+y*(q3+y*(q4+y*(q5+y*(q6+y*
     *(q7+y*(q8+y*q9)))))))
        if(x.lt.0.)bessi1=-bessi1
      endif
      return
      END

      double precision FUNCTION ran1(idum)
      implicit real*8 (a-h,o-z)
      INTEGER idum,IA,IM,IQ,IR,NTAB,NDIV
      PARAMETER (IA=16807,IM=2147483647,AM=1./IM,IQ=127773,IR=2836,
     *NTAB=32,NDIV=1+(IM-1)/NTAB,EPS=1.2e-7,RNMX=1.-EPS)
      INTEGER j,k,iv(NTAB),iy
      SAVE iv,iy
      DATA iv /NTAB*0/, iy /0/
      if (idum.le.0.or.iy.eq.0) then
        idum=max(-idum,1)
        do 11 j=NTAB+8,1,-1
          k=idum/IQ
          idum=IA*(idum-k*IQ)-IR*k
          if (idum.lt.0) idum=idum+IM
          if (j.le.NTAB) iv(j)=idum
11      continue
        iy=iv(1)
      endif
      k=idum/IQ
      idum=IA*(idum-k*IQ)-IR*k
      if (idum.lt.0) idum=idum+IM
      j=1+iy/NDIV
      iy=iv(j)
      iv(j)=idum
      ran1=dmin1(AM*iy,RNMX)
      return
      END

      SUBROUTINE sort3(n,ra,rb,rc,rd,re,rf,ig,wksp,iwksp)
      implicit real*8 (a-h,o-z)
      INTEGER n,iwksp(n),ig(n)
      dimension ra(n),rb(n),rc(n),rd(n),re(n),rf(n),wksp(n)
CU    USES indexx
      INTEGER j
      call indexx(n,ra,iwksp)
      do 11 j=1,n
        wksp(j)=ra(j)
11    continue
      do 12 j=1,n
```

```
      ra(j)=wksp(iwksp(j))
12    continue
      do 13 j=1,n
        wksp(j)=rb(j)
13    continue
      do 14 j=1,n
        rb(j)=wksp(iwksp(j))
14    continue
      do 15 j=1,n
        wksp(j)=rc(j)
15    continue
      do 16 j=1,n
        rc(j)=wksp(iwksp(j))
16    continue
      do 17 j=1,n
        wksp(j)=rd(j)
17    continue
      do 18 j=1,n
        rd(j)=wksp(iwksp(j))
18    continue
      do 19 j=1,n
        wksp(j)=re(j)
19    continue
      do 20 j=1,n
        re(j)=wksp(iwksp(j))
20    continue
      do 21 j=1,n
        wksp(j)=rf(j)
21    continue
      do 22 j=1,n
        rf(j)=wksp(iwksp(j))
22    continue
      do 23 j=1,n
        wksp(j)=ig(j)
23    continue
      do 24 j=1,n
        ig(j)=wksp(iwksp(j))
24    continue
      return
      END

      SUBROUTINE indexx(n,arr,indx)
      implicit real*8 (a-h,o-z)
      INTEGER n,indx(n),M,NSTACK
      dimension arr(n)
      PARAMETER (M=7,NSTACK=50)
      INTEGER i,indxt,ir,itemp,j,jstack,k,l,istack(NSTACK)
      do 11 j=1,n
        indx(j)=j
11    continue
      jstack=0
      l=1
```

```
      ir=n
1     if(ir-l.lt.M)then
        do 13 j=l+1,ir
          indxt=indx(j)
          a=arr(indxt)
          do 12 i=j-1,1,-1
            if(arr(indx(i)).le.a)goto 2
            indx(i+1)=indx(i)
12        continue
          i=0
2         indx(i+1)=indxt
13      continue
        if(jstack.eq.0)return
        ir=istack(jstack)
        l=istack(jstack-1)
        jstack=jstack-2
      else
        k=(l+ir)/2
        itemp=indx(k)
        indx(k)=indx(l+1)
        indx(l+1)=itemp
        if(arr(indx(l+1)).gt.arr(indx(ir)))then
          itemp=indx(l+1)
          indx(l+1)=indx(ir)
          indx(ir)=itemp
        endif
        if(arr(indx(l)).gt.arr(indx(ir)))then
          itemp=indx(l)
          indx(l)=indx(ir)
          indx(ir)=itemp
        endif
        if(arr(indx(l+1)).gt.arr(indx(l)))then
          itemp=indx(l+1)
          indx(l+1)=indx(l)
          indx(l)=itemp
        endif
        i=l+1
        j=ir
        indxt=indx(l)
        a=arr(indxt)
3       continue
          i=i+1
        if(arr(indx(i)).lt.a)goto 3
4       continue
          j=j-1
        if(arr(indx(j)).gt.a)goto 4
        if(j.lt.i)goto 5
        itemp=indx(i)
        indx(i)=indx(j)
        indx(j)=itemp
        goto 3
5       indx(l)=indx(j)
```

```
      indx(j)=indxt
      jstack=jstack+2
      if(jstack.gt.NSTACK)write(*,*) 'NSTACK too small in indexx'
      if(ir-i+1.ge.j-l)then
        istack(jstack)=ir
        istack(jstack-1)=i
        ir=j-1
      else
        istack(jstack)=j-1
        istack(jstack-1)=l
        l=i
      endif
    endif
    goto 1
    END

c
    subroutine getlen(string,chr,n0,n1)
c
c    to determine the length of a string excluding any blank padding & heading
c    and return string(n0:n1) n0... position of first non-blank letter
c                             n1... position of last non-blank letter
c    else return the original string
c    ***Use | to keep blank space at the begining or the end of the
c     *** string
c
    character*(*) string
    character*160 string1
    character*1 chr
    string1=' '
    in0=0
    in1=0
    do 10 i=len(string),1,-1
    if(string(i:i).ne.chr) then
      if(in1.eq.0) then
      if(string(i:i).eq.'|') then
      n1=i-1
      else
      n1=i
      endif
      in1=1
      endif
      goto 11
    endif
10    continue
11    do 20 i=1,len(string)
    if(string(i:i).ne.chr) then
      if(in0.eq.0) then
      if(string(i:i).eq.'|') then
      n0=i+1
      else
      n0=i
```

```
      endif
      in0=1
      nk=n0-1
c      write(6,*) '|'//string(n0:n1)//'|', n0,n1
      do 30 k=n0,n1
      if(string(k:k).ne.'|') then
        nk=nk+1
        if(k.eq.n0) then
          string1=string(k:k)
        else
          string1=string1(1:nk-n0)//string(k:k)
        endif
      endif
c      write(6,*) '|'//string1(1:nk-n0)//'|'
30     continue
      string=string1
      n1=n1-n0+1
      n0=1
      endif
      return
     endif
20    continue
     n0=-1
     n1=-1
     return
     end
```

APPENDIX F (MAIRFLOW)

Sample Input File for MAIRFLOW

```
293.            /* temperature (K)  (TEMP)
1.42e-07        /* radial permeability (cm^2)  (PRAD)
1.44e-07        /* vertical permeability (cm^2)  (PZ)
3.62e-11        /* leaky-layer permeability (cm^2) (PLEAK)
465.5           /* thickness of formation (cm) (XB)
1.0             /* thickness of leaky-layer (cm) (XBLK)
0.24            /* air-filled porosity (THETA)
6               /* number of wells
1707.,1250.     /* X,Y coordinates of TW-1 (cm)
208.,465.       /* screened interval of TW-1 (cm)
12.7            /* effective well radius of TW-1 (cm)
-11.0           /* pumping rate of TW-1 (std. cu.ft per min)(+/- injection/extraction)
0               /* integer flag for particle tracking of TW-1 (0/1  no/yes)
3109.,2743      /* X,Y coordinates of TW-3 (cm)
190.,465.       /* screened interval of TW-3 (cm)
12.7            /* effective well radius of TW-3 (cm)
-20.0           /* pumping rate of TW-3 (std. cu.ft per min)(+/- injection/extraction)
0               /* integer flag for particle tracking of TW-3 (0/1  no/yes)
4816.,3353.     /* X,Y coordinates of TW-4 (cm)
193.,465.       /* screened interval of TW-4 (cm)
12.7            /* effective well radius of TW-4 (cm)
-9.0            /* pumping rate of TW-4 (std. cu.ft per min)(+/- injection/extraction)
0               /* integer flag for particle tracking of TW-4 (0/1  no/yes)
3688.,1219.     /* X,Y coordinates of TW-5 (cm)
213.,465.       /* screened interval of TW-5 (cm)
12.7            /* effective well radius of TW-5 (cm)
-29.0           /* pumping rate of TW-5 (std. cu.ft per min)(+/- injection/extraction)
0               /* integer flag for particle tracking of TW-5 (0/1  no/yes)
1219.,3200.     /* X,Y coordinates of TW-6 (cm)
198.,465.       /* screened interval of TW-6 (cm)
12.7            /* effective well radius of TW-6 (cm)
-11.0           /* pumping rate of TW-6 (std. cu.ft per min)(+/- injection/extraction)
0               /* integer flag for particle tracking of TW-6 (0/1  no/yes)
2195.,4084.     /* X,Y coordinates of TW-7 (cm)
178.,465.       /* screened interval of TW-7 (cm)
12.7            /* effective well radius of TW-7 (cm)
-24.0           /* pumping rate of TW-7 (std. cu.ft per min)(+/- injection/extraction)
0               /* integer flag for particle tracking of TW-7 (0/1  no/yes)
0.,6000.        /* X-min and X-max for simulations
0.,6000.        /* Y-min and Y-max for simulations
460.0,460.      /* Z-min and Z-max for simulations
50.,50.,10.     /* X,Y,Z grid spacing for simulation (cm)
2.4e-03         /* minimum darcy velocity for adequate airflow (cm/s)
0.0             /* step size for particle tracking (cm)
```

Sample Output File for MAIRFLOW

Total pumping (g/s) = 58.7993904877061

X (cm)	Y (cm)	Z (cm)	P/P_atm	qx	qy	qz	q (cm/s)
0.000E+00	0.000E+00	0.460E+03	0.99888E+00	0.6013E-03	0.4918E-03	0.2656E-05	0.7768E-03
0.500E+02	0.000E+00	0.460E+03	0.99884E+00	0.6186E-03	0.5144E-03	0.2744E-05	0.8045E-03
0.100E+03	0.000E+00	0.460E+03	0.99880E+00	0.6360E-03	0.5382E-03	0.2835E-05	0.8332E-03
0.150E+03	0.000E+00	0.460E+03	0.99876E+00	0.6537E-03	0.5631E-03	0.2929E-05	0.8628E-03
0.200E+03	0.000E+00	0.460E+03	0.99872E+00	0.6714E-03	0.5893E-03	0.3025E-05	0.8933E-03
0.250E+03	0.000E+00	0.460E+03	0.99868E+00	0.6893E-03	0.6166E-03	0.3124E-05	0.9248E-03
0.300E+03	0.000E+00	0.460E+03	0.99864E+00	0.7071E-03	0.6452E-03	0.3225E-05	0.9573E-03
0.350E+03	0.000E+00	0.460E+03	0.99860E+00	0.7249E-03	0.6752E-03	0.3329E-05	0.9906E-03
0.400E+03	0.000E+00	0.460E+03	0.99855E+00	0.7425E-03	0.7066E-03	0.3436E-05	0.1025E-02
0.450E+03	0.000E+00	0.460E+03	0.99851E+00	0.7599E-03	0.7394E-03	0.3545E-05	0.1060E-02

(Only first 10 simulations shown)

Source Code for MAIRFLOW (author Ravi Varadhan)

(A FORTRAN program written to compute a three-dimensional pressure and pore-gas velocity field from injection or extraction of multiple wells)

```
c ************************************************************************
c  MAIRFLO W -  Airflow induced by Multiple Wells
c ************************************************************************
C  Analytical solution for steady air flow in a well field.
C  Top BC: Semi-Confining Layer
c  Refer to Baehr and Hult (1995) - WRR - for the solution
c  Analytical solution obtained using the superposition principle.
c  Particle tracking using the Simple Runge-Kutta (second-order) method.
c
c  This code could be used to space venting wells such that there is adequate
c  airflow between wells.  It could also be used in bioventing applications
c  to identify whether there is any flow of contaminated air to the surface.
      implicit real*8 (a-h,o-z)
      common/ceigen/h
      common/cparam/bn,xb,a,prad,pz,visc,patm
      common/cwell/nwell,xw(200),yw(200),xl(200),xd(200),rw(200),xm(200)
      dimension bn(100),x(1000),y(1000),z(1000),xmpr(200),itrack(200)
      character*1 reply
      character*15 prefix,fname1,fname2,fname3
      character*4 suffix1,suffix2,suffix3
      write(*,*)' Steady-State Airflow Simulation for Multiple-Wells'
      write(*,*)' Finite-Radius Solution with Borehole Storage '
      write(*,*)' Top BC: Semi-Confining Layer'
      write(*,*)
      write(*,*)'Enter the Prefix of the input file:  '
      write(*,*)'An output file is created w/ same prefix'
      write(*,*)' Input-file Prefix ?  '
      read(*,'(a)')prefix
      call getlen(prefix,' ',n0,n1)
      suffix1='.inp'
      suffix2='.dat'
      suffix3='.ptk'
      fname1=prefix(n0:n1)//suffix1
      fname2=prefix(n0:n1)//suffix2
      fname3=prefix(n0:n1)//suffix3
      open(10,fname1,status='unknown')
      open(20,fname2,status='unknown')
      open(30,fname3,status='unknown')
      read(10,101)temp,prad,pz,pleak,xb,xblk,theta
      patm=1013200.
      visc=1.76e-04
      rgas=8.3143e07
      xmw=28.8
      a=dsqrt(prad/pz)
      h=pleak*xb/(pz*xblk)
      pi=4.0*datan(1.0)
      call vnfunc(bn)
```

```
      read(10,*)nwell
      totpmp=0.
c
      do 1 i=1,nwell
      read(10,*)xw(i),yw(i)
      read(10,*)xd(i),xl(i)
      read(10,*)rw(i)
      read(10,*)xmpr(i)
      read(10,*)itrack(i)
      xmpr(i)=xmpr(i)*471.947*28.8/(82.05*293.0)
      totpmp=totpmp+dabs(xmpr(i))
      qp=xmpr(i)*visc*rgas*temp/xmw
      xm(i)=2.*h*qp*a*xb/(pi*prad*(xl(i)-xd(i))*rw(i))
1     continue
c
      read(10,*)xmin,xmax
      read(10,*)ymin,ymax
      read(10,*)zmin,zmax
      read(10,*)dx,dy,dz
      read(10,*)qmin
      read(10,*)delx
      nx=nint((xmax-xmin)/dx)+1
      ny=nint((ymax-ymin)/dy)+1
      nz=nint((zmax-zmin)/dz)+1
c
      write(*,108)
      write(20,*)
      write(*,*)'Total pumping(g/s)  =',totpmp
      write(20,*)'Total pumping(g/s)  =',totpmp
      write(20,102)
c
      kount=0
      pmin=1.e10
      do 5 k=1,nz
      z(k)=zmin+(k-1)*dz
      do 5 j=1,ny
      y(j)=ymin+(j-1)*dy
      do 5 i=1,nx
      x(i)=xmin+(i-1)*dx
      call solution(x(i),y(j),z(k),popatm,qx,qy,qz)
      spdisch=dsqrt(qx*qx+qy*qy+qz*qz)
      write(20,103)x(i),y(j),z(k),popatm,qx,qy,qz,spdisch
      if(spdisch.le.qmin)kount=kount+1
      pmin=dmin1(pmin,popatm)
5     continue
      pinadq=100.*kount/(nx*ny*nz)
      pmin=(1.-pmin)*407.
      write(*,*)'Maximum vaccum in the domain (in water)  ',pmin
      write(20,*)'Maximum vaccum in the domain (in water)  ',pmin
      write(20,*)'% Volume receiving inadequate airflow   =',pinadq
      write(*,*)'% Volume receiving inadequate airflow   =',pinadq
c
```

```
c  Particle tracking segment
c
      write(*,108)
      write(*,*)'  Particle Tracking is going to commence '
      write(*,*)' Do you want to continue (y/n)?  '
      read(*,109)reply
      if (.not.(reply.eq.'y' .or. reply.eq.'Y')) stop
      dist1=dsqrt((xmax-xmin)**2+(ymax-ymin)**2)/(nwell*100.0)
      dist2=(zmin+zmax)/(2.*100.)
      if(delx.le.0.)delx=dmin1(dist1,dist2)
      write(*,*)'Max. particle tracking step (cm):',delx
      do 20 i=1,nwell
      if(itrack(i).eq.0)goto 20
      sign=1
      if(xmpr(i).lt.0.)sign=-1
      write(30,108)
      write(30,106)xw(i),yw(i)
      if(sign.gt.0)then
      write(30,*)'  Forward Tracking from Injection Well '
      kount=0
      else
      write(30,*)'  Backward Tracking from Extraction Well'
      endif
      write(30,105)
      do 30 iz=1,5
      zz=xd(i)+dfloat(iz-1.)*(xl(i)-xd(i))/4.
      do 30 iang=1,12
      alpha=dfloat(iang-1.)*pi/6.
      xx=xw(i)+rw(i)*dcos(alpha)
      yy=yw(i)+rw(i)*dsin(alpha)
      xnew=xx
      ynew=yy
      znew=zz
      ttime=0.
      nsteps=0
25    continue
      nsteps=nsteps+1
      angold=datan(ynew/xnew)
      xold=xnew
      yold=ynew
      zold=znew
      call solution(xold,yold,zold,popatm,qx,qy,qz)
      qres=dsqrt(qx*qx+qy*qy+qz*qz)
      if(qres.lt.1.e-07)then
      write(30,110)alpha*180./pi,zz
      goto 30
      endif
      delt=delx*theta/qres
      xk1=delt*qx/theta
      yk1=delt*qy/theta
      zk1=delt*qz/theta
      call solution(xold+xk1,yold+yk1,zold+zk1,popatm,qx,qy,qz)
```

```
      xk2=delt*qx/theta
      yk2=delt*qy/theta
      zk2=delt*qz/theta
      xnew=xold+sign*(xk1+xk2)/2.
      ynew=yold+sign*(yk1+yk2)/2.
      znew=zold+sign*(zk1+zk2)/2.
      ttime=ttime+delt
      if(znew.le. 1.e-07)then
      znew=0.
      if(sign.gt.0)kount=kount+1
      write(30,107)alpha*180./pi,zz,xnew,ynew,znew,ttime/86400.
      write(*,107)alpha*180./pi,zz,xnew,ynew,znew,ttime/86400.
      goto 30
      endif
      do 40 j=1,nwell
      if(j.eq.i)goto 40
      dist=dsqrt((xw(j)-xnew)**2+(yw(j)-ynew)**2)
      if(dist.le.rw(j))then
      write(30,107)alpha*180./pi,zz,xw(j),yw(j),znew,ttime/86400.
      write(*,107)alpha*180./pi,zz,xw(j),yw(j),znew,ttime/86400.
      goto 30
      endif
40    continue
      angnew=datan(ynew/xnew)
      if(nsteps.gt.1000 .and. dabs(angold-angnew).lt.1.e-15)then
      write(30,111)alpha*180./pi,zz
      goto 30
      endif
      goto 25
30    continue
      if(sign.gt.0)then
      escape=100.*dfloat(kount)/60.
      write(30,108)
      write(30,*)'Percent airflow escaping to the surface from injection
     >well:  ',escape
      endif
20    continue
C
101   format(g15.0)
102   format(/4x,'X (cm)',6x,'Y (cm)',6x,'Z (cm)',9x,'P/P_atm',11x,
     >'qx',15x,'qy',14x,'qz',11x,'q (cm/s)'/)
103   format(2x,e9.3,3x,e9.3,4x,e9.3,5x,e11.5,5x,e11.4,6x,e11.4,5x,e11.4
     >,4x,e10.4)
104   format(3x,'Particle-tracking from the Well @ ',2x,e10.4,2x,
     >e10.4/)
105   format(/10x,'Origin',20x,'Destination',16x,'Travel time(d)'//,
     >2x,'Angle(deg)',6x,'Z ',12x,'X',9x,'Y',9x,'Z'/)
106   format(4x,'Particles released from the Well at:',2(2x,e9.2)/)
107   format(4x,f5.1,4x,e9.3,6x,e9.3,2x,e9.3,2x,e9.3,8x,e9.3)
108   format(//)
109   format(a1)
110   format(4x,f5.1,4x,e9.3,8x,'Stagnation Point')
```

```
111   format(4x,f5.1,4x,e9.3,8x,'Indeterminate')
      stop
      end

      subroutine solution(xx,yy,zz,popatm,qx,qy,qz)
      implicit real*8 (a-h,o-z)
      common/ceigen/h
      common/cparam/bn,xb,a,prad,pz,visc,patm
      common/cwell/nwell,xw(200),yw(200),xl(200),xd(200),rw(200),xm(200)
      dimension bn(100)
      sump=0.
      sumqx=0.
      sumqy=0.
      sumqz=0.
      do 20 nw=1,nwell
      rr=dsqrt((xx-xw(nw))**2+(yy-yw(nw))**2)
      if(rr.lt.rw(nw))rr=rw(nw)
      xdd=xd(nw)
      xll=xl(nw)
      rrw=rw(nw)
      n=0
      sum1=0.0
      sum2=0.0
      sum3=0.0
10    continue
      n=n+1
      if(n.gt.100)goto 15
      vn=bn(n)
      tcos=dcos(vn*(1.-zz/xb))
      if((xll-xdd)/xb .le. 0.99) then
      tsin=(dsin(vn*(1.-xdd/xb))-dsin(vn*(1.-xll/xb)))/(vn*vn*(h+dsin
     >(vn)**2))
      else
      tsin=(xll-xdd)/(xb*(h+dsin(vn)**2))
      endif
      trig=tcos*tsin
      bess0=bessk0(vn*rr/a/xb)
      bess1=bessk1(vn*rrw/a/xb)
      add1=bess0/bess1*trig
      add2=trig*(-vn/a/xb)*bessk1(vn*rr/a/xb)/bess1
      add3=tsin*bess0/bess1*(vn/xb)*dsin(vn*(1.-zz/xb))
      sum1=sum1+add1
      sum2=sum2+add2
      sum3=sum3+add3
      if(sum1.eq.0. .or. sum2.eq.0. .or.sum3.eq.0.)goto 15
      convg=dmax1(dabs(add1/sum1),dabs(add2/sum2),dabs(add3/sum3))
      if(convg.gt.1.e-07)goto 10
15    continue
      sump=sump+xm(nw)*sum1
      sumqx=sumqx+xm(nw)*sum2*(xx-xw(nw))/rr
      sumqy=sumqy+xm(nw)*sum2*(yy-yw(nw))/rr
      sumqz=sumqz+xm(nw)*sum3
```

```
20    continue
      phi=sump+patm*patm
      popatm=dsqrt(phi/patm/patm)
      qx=-prad/(2.*visc*dsqrt(phi))*sumqx
      qy=-prad/(2.*visc*dsqrt(phi))*sumqy
      qz=-pz/(2.*visc*dsqrt(phi))*sumqz
      return
      end

      subroutine vnfunc(x)
      implicit real*8 (a-h,o-z)
      dimension x(*)
      external eigen
      common/ceigen/h
      pi=4.*datan(1.0)
      x1=1.e-07
      x2=pi
      kount=1
1     continue
      zero=rtsafe(eigen,x1,x2,1.e-06)
      x(kount)=zero
      x1=zero+0.5*pi
      x2=zero+1.5*pi
      kount=kount+1
      if(kount.le.100)goto 1
      return
      end

      Double Precision FUNCTION rtsafe(funcd,x1,x2,xacc)
      implicit real*8 (a-h,o-z)
      EXTERNAL funcd
      PARAMETER (MAXIT=100)
      call funcd(x1,fl,df)
      call funcd(x2,fh,df)
      if((fl.gt.0..and.fh.gt.0.).or.(fl.lt.0..and.fh.lt.0.))pause
     *'root must be bracketed in rtsafe'
      if(fl.eq.0.)then
        rtsafe=x1
        return
      else if(fh.eq.0.)then
        rtsafe=x2
        return
      else if(fl.lt.0.)then
        xl=x1
        xh=x2
      else
        xh=x1
        xl=x2
      endif
      rtsafe=.5*(x1+x2)
      dxold=dabs(x2-x1)
      dx=dxold
```

```
      call funcd(rtsafe,f,df)
      do 11 j=1,MAXIT
        if(((rtsafe-xh)*df-f)*((rtsafe-xl)*df-f).ge.0..or. dabs(2.*
     *f).gt.dabs(dxold*df) ) then
          dxold=dx
          dx=0.5*(xh-xl)
          rtsafe=xl+dx
          if(xl.eq.rtsafe)return
        else
          dxold=dx
          dx=f/df
          temp=rtsafe
          rtsafe=rtsafe-dx
          if(temp.eq.rtsafe)return
        endif
        if(dabs(dx).lt.xacc) return
        call funcd(rtsafe,f,df)
        if(f.lt.0.) then
          xl=rtsafe
        else
          xh=rtsafe
        endif
11    continue
      pause 'rtsafe exceeding maximum iterations'
      return
      END

      subroutine eigen(x,f,df)
      implicit real*8 (a-h,o-z)
      common/ceigen/h
      f=h*dcos(x)-x*dsin(x)
      df=-h*dsin(x)-dsin(x)-x*dcos(x)
      return
      end

      Double Precision Function Bessk0(x)
      implicit real*8 (a-h,o-z)
      data p1,p2,p3,p4,p5,p6,p7/-0.57721566,0.4227842,0.23069756,
     >0.348859d-1,0.262698d-2,0.10750d-3,0.74d-5/
      data q1,q2,q3,q4,q5,q6,q7/1.25331414,-0.7832358d-1,0.2189568d-1,
     >-0.1062446d-1,0.587872d-2,-0.25154d-2,0.53208d-3/
      if(x.le.2.0)then
      y=x*x/4.0
      bessk0=(-dlog(x/2.0)*bessi0(x))+(p1+y*(p2+y*(p3+y*(p4+y*(p5+y*(p6+
     >y*p7))))))
      else
      y=2.0/x
      bessk0=(dexp(-x)/dsqrt(x))*(q1+y*(q2+y*(q3+y*(q4+y*(q5+y*(q6+y*q7)
     >)))))
      endif
      return
      end
```

```
      DOUBLE PRECISION FUNCTION BESSI0(W)
      IMPLICIT REAL*8 (A-H,O-Z)
      T=W/3.75
      IF(DABS(T).LE.1.0) THEN
      Y=T*T
      BESSI0=1.0+Y*(3.5156229+Y*(3.0899424+Y*(1.2067492+Y*(0.2659732+
     >Y*(0.0360768+0.0045813*Y)))))
      ELSE
      AW=DABS(W)
      Y=3.75/AW
      TEMP=0.39894228+Y*(0.01328592+Y*(0.00225319+Y*(-0.00157565+Y*(
     >0.00916281+Y*(-0.02057706+Y*(0.02635537+Y*(-0.01647633+
     >0.00392377*Y)))))))
      BESSI0=DEXP(AW)*TEMP/DSQRT(AW)
      END IF
      RETURN
      END

      double precision FUNCTION bessk1(x)
CU    USES bessi1
      implicit real*8 (a-h,o-z)
      DOUBLE PRECISION p1,p2,p3,p4,p5,p6,p7,q1,q2,q3,q4,q5,q6,q7,y
      SAVE p1,p2,p3,p4,p5,p6,p7,q1,q2,q3,q4,q5,q6,q7
      DATA p1,p2,p3,p4,p5,p6,p7/1.0d0,0.15443144d0,-0.67278579d0,
     *-0.18156897d0,-0.1919402d-1,-0.110404d-2,-0.4686d-4/
      DATA q1,q2,q3,q4,q5,q6,q7/1.25331414d0,0.23498619d0,-0.3655620d-1,
     *0.1504268d-1,-0.780353d-2,0.325614d-2,-0.68245d-3/
      if (x.le.2.0) then
        y=x*x/4.0
        bessk1=(dlog(x/2.0)*bessi1(x))+(1.0/x)*(p1+y*(p2+y*(p3+y*(p4+y*
     *(p5+y*(p6+y*p7))))))
      else
        y=2.0/x
        bessk1=(dexp(-x)/dsqrt(x))*(q1+y*(q2+y*(q3+y*(q4+y*(q5+y*(q6+y*
     *q7))))))
      endif
      return
      END

      double precision FUNCTION bessi1(x)
      implicit real*8 (a-h,o-z)
      DOUBLE PRECISION p1,p2,p3,p4,p5,p6,p7,q1,q2,q3,q4,q5,q6,q7,q8,q9,y
      SAVE p1,p2,p3,p4,p5,p6,p7,q1,q2,q3,q4,q5,q6,q7,q8,q9
      DATA p1,p2,p3,p4,p5,p6,p7/0.5d0,0.87890594d0,0.51498869d0,
     *0.15084934d0,0.2658733d-1,0.301532d-2,0.32411d-3/
      DATA q1,q2,q3,q4,q5,q6,q7,q8,q9/0.39894228d0,-0.3988024d-1,
     *-0.362018d-2,0.163801d-2,-0.1031555d-1,0.2282967d-1,-0.2895312d-1,
     *0.1787654d-1,-0.420059d-2/
      if (abs(x).lt.3.75) then
        y=(x/3.75)**2
        bessi1=x*(p1+y*(p2+y*(p3+y*(p4+y*(p5+y*(p6+y*p7))))))
      else
```

```
      ax=abs(x)
      y=3.75/ax
      bessi1=(dexp(ax)/dsqrt(ax))*(q1+y*(q2+y*(q3+y*(q4+y*(q5+y*(q6+y*
     *(q7+y*(q8+y*q9))))))))
      if(x.lt.0.)bessi1=-bessi1
     endif
     return
     END

c
     subroutine getlen(string,chr,n0,n1)
c
c    to determine the length of a string excluding any blank padding & heading
c    and return string(n0:n1) n0... position of first non-blank letter
c                             n1... position of last non-blank letter
c    else return the original string
c    ***Use | to keep blank space at the begining or the end of the
c     *** string
c
     character*(*) string
     character*160 string1
     character*1 chr
     string1=' '
     in0=0
     in1=0
     do 10 i=len(string),1,-1
     if(string(i:i).ne.chr) then
      if(in1.eq.0) then
      if(string(i:i).eq.'|') then
      n1=i-1
      else
      n1=i
      endif
      in1=1
      endif
      goto 11
     endif
10    continue
11    do 20 i=1,len(string)
     if(string(i:i).ne.chr) then
      if(in0.eq.0) then
      if(string(i:i).eq.'|') then
      n0=i+1
      else
      n0=i
      endif
      in0=1
      nk=n0-1
c     write(6,*) '|'//string(n0:n1)//'|', n0,n1
      do 30 k=n0,n1
      if(string(k:k).ne.'|') then
       nk=nk+1
```

```
        if(k.eq.n0) then
          string1=string(k:k)
        else
          string1=string1(1:nk-n0)//string(k:k)
        endif
      endif
c     write(6,*) '|'//string1(1:nk-n0)//'|'
30    continue
      string=string1
      n1=n1-n0+1
      n0=1
      endif
      return
     endif
20   continue
     n0=-1
     n1=-1
     return
     end
```

APPENDIX G (Vapor Diffusion)

Source Code for Vapor Diffusion Problem (author: Dominic DiGiulio)

```
PROGRAM Vapor_Diff
IMPLICIT NONE
EXTERNAL Func
REAL*8,PARAMETER::Pi=3.141592654
REAL*8,DIMENSION(:),ALLOCATABLE::arr_v !variables
REAL*8,DIMENSION(:),ALLOCATABLE::arr_z !depth array
REAL*8,DIMENSION(:),ALLOCATABLE::arr_c !concentration array
REAL*8,DIMENSION(:),ALLOCATABLE::arr_t !time array
REAL*8,DIMENSION(:),ALLOCATABLE::arr_w !water saturation array
REAL*8::func,a,b,s,t,tt
INTEGER::M,J,Q,P
INTEGER::N_conc  !number of discrete soil concentrations in simulation
INTEGER::N_times !number of times to simulate
INTEGER::N_sat   !number of moisture saturations to simulate
!variables
REAL*8::theta_a !volumetric air content
REAL*8::theta_w !volumetric water content
REAL*8::theta_o !volumetric NAPL content
REAL*8::rho_b   !bulk density  [g/cm**3]
REAL*8::rho_o   !density of NAPL [g/cm**3]
REAL*8::H       !Henry's constant [dimensionless]
REAL*8::K_d     !solids/water partition coefficient
REAL*8::S_w     !water solubility [g/cm**3]
REAL*8::M_o     !average molecular weight of NAPL [g/mole]
REAL*8::M_i     !molecular weight of compound [g/mole]
REAL*8::D_a     !free air gas diffusion coefficient [cm**2/d]
REAL*8::D_w     !free water diffusion coefficient [cm**2/d]
REAL*8::L       !length of domain [cm]
REAL*8::R               !retardation factor [dimensionless]
REAL*8::por     !porosity
REAL*8::Si_a    !tortuosity factor for air phase [dimensionless]
REAL*8::Si_w !tortuosity factor for water phase [dimensionless]
REAL*8::k               !diffusion coefficient [cm**2/d]
REAL*8::K_a      !soil-air partition coefficient [dimensionles]
REAL*8::NAPL_sat,water_sat
REAL*8::term1,term2,term3,sum,sum_1,B_n,C_n,C_T_avg

COMMON/cfunc/tt

OPEN (1,FILE='diff_var.in')
OPEN (2,FILE='conc.in')
OPEN (3,FILE='depth.in')
```

```
OPEN (4,FILE='time.in')
OPEN (5,FILE='avg_conc.out')
OPEN (6,FILE='water_sat.in')

ALLOCATE (arr_v(15)) !allocate 15 spaces for variables
READ (1,*) arr_v  !read diff_var.in
N_conc=arr_v(13)  !read number of discrete soil conc.from diff_var.in (13th line)
N_times=arr_v(14) !read number of sim.times from diff_var.in (14th line)
N_sat=arr_v(15)   !read number of water saturations from diff_var.in (15th line)
ALLOCATE (arr_c(N_conc))  !allocate space in arr_c for N_conc
ALLOCATE (arr_z(N_conc-1))!allocate space in arr_z for N_conc - 1 depths
                  !do not include first and last depth z=0 and L
ALLOCATE (arr_t(N_times)) !allocate space for N_times
ALLOCATE (arr_w(N_sat))   !allocate space for N_sat
READ (2,*) arr_c !read conc.in file
READ (3,*) arr_z !read depth.in file
READ (4,*) arr_t !read time.in file
READ (6,*) arr_w !read water_sat.in

por=arr_v(1)
NAPL_sat=arr_v(2)
rho_b=arr_v(3)
rho_o=arr_v(4)
S_w=arr_v(5)
H=arr_v(6)
K_d=arr_v(7)
M_i=arr_v(8)
M_o=arr_v(9)
D_a=arr_v(10)
D_w=arr_v(11)
L=arr_v(12)

WRITE(5,*)     "time (yrs)     avg. conc. (ug/Kg)"
WRITE(5,*)

DO P=1,N_sat
water_sat=arr_w(P)
WRITE(5,*)
WRITE(5,20) water_sat
20 FORMAT(1X,F10.2)
theta_w=por*water_sat
theta_a=por*(1.0-water_sat-NAPL_sat)
theta_o=por*NAPL_sat
R=theta_a*H+theta_w+K_d*rho_b+(M_i*rho_o*theta_o)/(S_w*M_o)
K_a=R/H
Si_a=(theta_a**3.333)/por**2
Si_w=(theta_w**3.333)/por**2
```

```
k=(Si_a*D_a*H+Si_w*D_w)/R
a=0.0

DO Q=1,N_times
t=arr_t(Q)*365

  !summation loop
  sum=0.0
  DO M=1,10000,2

    tt=k*M**2*Pi**2*t/L**2
          b=tt
    !calc B_n
    CALL qtrap(func,a,b,s)
    B_n=K_a*s !ug/cm**3 soil

    !calc A_n
    sum_1=0.0
    DO J=1,N_conc-1
    term1=(arr_c(J+1)-arr_c(J))*dcos(arr_z(J)*M*Pi/L)
    sum_1=sum_1+term1
    END DO
    C_n=1./2.*(sum_1+arr_c(1)+(-1)**(M+1)*arr_c(5)) !ug/kg
          C_n=0.001*rho_b*C_n !ug/cm**3

  term1=C_n*dexp(-tt)
  term2=B_n
  term3=1./(M**2*Pi**2)*(term1+term2)
  sum=sum+term3
  IF ((dABS(term3/SUM) <= 1.0E-04) .or. (M > 1000)) EXIT
  PRINT 30, term3/SUM,M,t/365
  30 FORMAT(E10.5,I10,F10.2)
  END DO
  C_T_avg=8.*sum*(1000/rho_b) !ug/kg
WRITE(5,10) t/365.0,C_T_avg
10 FORMAT(1X,2F10.2)
END DO

END DO
CONTAINS

SUBROUTINE qtrap(func,a,b,s)
     INTEGER JMAX
     REAL*8 a,b,func,s,EPS
     EXTERNAL func
     PARAMETER (EPS=1.e-5, JMAX=20)
!    USES trapzd
```

```
      INTEGER j
      REAL*8 olds
      olds=-1.e30
      do 11 j=1,JMAX
        call trapzd(func,a,b,s,j)
        if (dabs(s-olds).lt.EPS*dabs(olds)) return
        if (s.eq.0..and.olds.eq.0..and.j.gt.6) return
        olds=s
11    continue
      !pause 'too many steps in qtrap'
      END SUBROUTINE qtrap

SUBROUTINE trapzd(func,a,b,s,n)
      INTEGER n
      REAL*8 a,b,s,func
      EXTERNAL func
      INTEGER it,j
      REAL*8 del,sum,tnm,x
      if (n.eq.1) then
        s=0.5*(b-a)*(func(a)+func(b))
      else
        it=2**(n-2)
        tnm=it
        del=(b-a)/tnm
        x=a+0.5*del
        sum=0.
        do 11 j=1,it
          sum=sum+func(x)
          x=x+del
11      continue
        s=0.5*(s+(b-a)*sum/tnm)
      endif
      return
      END SUBROUTINE trapzd

END PROGRAM Vapor_Diff

FUNCTION func(x)
REAL*8:: func,x,tt
COMMON/cfunc/tt
a=0.71761
b=0.0023179721
c=0.0054
fx=a*c/(1.0+a*b*x)
func=dexp(x-tt)*fx
END FUNCTION func
```

APPENDIX H (VFLUX)

Example Input File for VFLUX

```
0.35          /*  porosity
0.0           /* NAPL saturation (napl volume / pore volume)
0.70          /* water saturation (water volume / pore volume)
0.38          /* dimensionless Henry's law constant
131.5         /* average molecular weight of NAPL (g/mole)
131.5         /* molecular weight of compound (g/mole)
1100.0        /* aqueous solubility of pure-phase compound (mg/L)
126.          /* organic carbon partition coefficient (mL/g)
0.001         /* fraction organic carbon (unitless)
2.15          /* bulk density of soil (g/cm^3)
1.462         /* density of NAPL (g/cm^3)
0.035         /* average annual infiltration flux (cm/d)
6367.0        /* free-air diffusion coefficient of compound (cm^2/d)
0.804         /* free-water diffusion coefficient of compound (cm^2/d)
30.0          /* longitudinal dispersivity (cm)
3.65e6        /* degradation half life of compound (d)
11            /* number of depths for initial soil concentration
50      1006.635905   /* depth (cm) and the measured soil concentration (ug/kg)
100     4809.263006
150     35200.72357
200     266876.3314
250     1528360.581
300     210637.9515
350     28260.94547
400     3882.013805
450     913.4462901
500     656.0163567
11          /* number of times for groundwater concentration (mg/l)
1       4.999994228
5       1.998388846
10      1.445123207
15      1.165824718
20      0.984167078
30      0.74981552
40      0.598388867
50      0.489243244
60      0.405386745
80      0.282682286
74                  /* number of times (years) for outputting results
0.5,1.0,1.5,2.0,2.5,3.0,3.5,4.0,4.5,5.0,5.5,6.0,6.5,7.0,7.5,
8.0,8.5,9.0,9.5,10.0,10.5,11.0,11.5,12.0,12.5,13.0,13.5,14.0,14.5,15.0,
15.5,16.0,16.5,17.0,17.5,18.0,18.5,19.0,19.5,20.0,20.5,21.0,21.5,22.0,22.5,
23.0,23.5,24.0,24.5,25.0,25.5,26.0,26.5,27.0,27.5,28.0,28.5,29.0,29.5,30.0,
35.0,40.0,45.0,50.0,55.0,60.0,65.0,70.0,75.0,80.0,85.0,90.0,95.0,100.0 /* time unit is  (year)
27                  /* number of depths (cm) for outputting results
0.0,20.0,40.0,60.0,80.0,100.0,120.0,140.0,160.0,180.0,200.,220.0,240.0,260.0,280.0,
300.0,320.0,340.0,360.0,380.0,400.0,420.0,440.0,460.0,480.0,500.0,518.16   /*  depth unit is  (cm)
y           /* flag for mass balance if y or Y
```

Example Parameter File for VFLUX

***** Input Parameters prescribed by the user *****

Porosity = 0.350000000000000
NAPL saturation = 0.000000000000000
Water saturation = 0.700000000000000
Dimensionless Henrys constant = 0.380000000000000
Average molecular weight of NAPL = 131.500
Molecular weight of compound of interest = 131.500
Aqueous solubility of compound (mg/L) = 1100.00000000000
Organic carbon partition coefficient (cc/g) = 126.000
Fraction organic carbon content = 0.100000000000000D-002
Bulk density of soil (g/cc) = 2.15000000000000
density of NAPL (g/cc) = 1.46200000000000
Average annual recharge rate (cm/d) = 0.350000E-01
Free-air diffusion coefficient of compound (cm^2/d) = 6367.00000000000
Free-water diffusion coefficient of compound (cm^2/d) = 0.804000000000000
Hydrodynamic dispersivity (cm) = 30.0000000000000
Degradation half-life of compound (d) = 3650000.00000000
Number of initial soil concentrations = 11
Initial soil concentration versus depth (cm)

0.500E+02	0.101E+04
0.100E+03	0.481E+04
0.150E+03	0.352E+05
0.200E+03	0.267E+06
0.250E+03	0.153E+07
0.300E+03	0.211E+06
0.350E+03	0.283E+05
0.400E+03	0.388E+04
0.450E+03	0.913E+03
0.500E+03	0.656E+03
0.520E+03	0.645E+03

Number of groundwater concentrations = 11
Groundwater concentrations versus time (yrs)

0.100E+01	0.500E+01
0.500E+01	0.200E+01
0.100E+02	0.145E+01
0.200E+02	0.984E+00
0.300E+02	0.750E+00
0.400E+02	0.598E+00
0.500E+02	0.489E+00
0.600E+02	0.405E+00
0.800E+02	0.283E+00
0.100E+03	0.195E+00

Number of time values for simulation results = 75
Times (yr) at which results are produced

0.000000000000000	0.500000000000000	1.00000000000000
1.50000000000000	2.00000000000000	2.50000000000000
3.00000000000000	3.50000000000000	4.00000000000000
4.50000000000000	5.00000000000000	5.50000000000000
6.00000000000000	6.50000000000000	7.00000000000000

7.50000000000000 8.00000000000000 8.50000000000000
9.00000000000000 9.50000000000000 10.0000000000000
10.5000000000000 11.0000000000000 11.5000000000000
12.0000000000000 12.5000000000000 13.0000000000000
13.5000000000000 14.0000000000000 14.5000000000000
15.0000000000000 15.5000000000000 16.0000000000000
16.5000000000000 17.0000000000000 17.5000000000000
18.0000000000000 18.5000000000000 19.0000000000000
19.5000000000000 20.0000000000000 20.5000000000000
21.0000000000000 21.5000000000000 22.0000000000000
22.5000000000000 23.0000000000000 23.5000000000000
24.0000000000000 24.5000000000000 25.0000000000000
25.5000000000000 26.0000000000000 26.5000000000000
27.0000000000000 27.5000000000000 28.0000000000000
28.5000000000000 29.0000000000000 29.5000000000000
30.0000000000000 35.0000000000000 40.0000000000000
45.0000000000000 50.0000000000000 55.0000000000000
60.0000000000000 65.0000000000000 70.0000000000000
75.0000000000000 80.0000000000000 85.0000000000000
90.0000000000000 95.0000000000000 100.000000000000
Number of depth values for simulation results = 27
Depths (cm) at which results are produced
0.000000000000000 20.0000000000000 40.0000000000000
60.0000000000000 80.0000000000000 100.000000000000
120.000000000000 140.000000000000 160.000000000000
180.000000000000 200.000000000000 220.000000000000
240.000000000000 260.000000000000 280.000000000000
300.000000000000 320.000000000000 340.000000000000
360.000000000000 380.000000000000 400.000000000000
420.000000000000 440.000000000000 460.000000000000
480.000000000000 500.000000000000 518.160000000000
Length of domain (cm) = 520.000
****** Calculated Model Parameters *******
Volumetric NAPL saturation = 0.000000000000000
Volumetric water saturation = 0.245000000000000
Volumetric air saturation = 0.105000000000000
Lumped diffusion coefficient - D (cm^2/d) = 15.1325989906785
Half-Peclet number - a = 0.601350768916067
First-order decay constant (/d) = 0.189903E-06
Dimensionless decay constant = 0.188601131871932D-002
Parameter Delta = 0.602916875360662
Aqueous solubility (g/cc) = 0.109999999722277D-002
Soil-water partition coefficient - Kd = 0.126000
Total Retardation coefficient - R = 0.555800004357100

Example Flux File for VFLUX

Average Soil Concentration as a Function of Time

Time (yr)	Average Soil Concentration (ug/kg)
0.0000E+00	0.1790E+06
0.5000E+00	0.1739E+06
0.1000E+01	0.1528E+06
0.1500E+01	0.1287E+06
0.2000E+01	0.1073E+06
0.2500E+01	0.8909E+05
0.3000E+01	0.7393E+05
0.3500E+01	0.6131E+05
0.4000E+01	0.5085E+05
0.4500E+01	0.4217E+05

(First 10 times shown)

Mass flux To/From Groundwater

Time (yr)	Total Mass-flux (ug/cm^2/d)	Advective flux	Dispersive flux
0.0000E+00	0.000E+00	0.000E+00	0.000E+00
0.5000E+00	0.419E+02	0.175E+00	0.417E+02
0.1000E+01	0.845E+02	0.175E+00	0.843E+02
0.1500E+01	0.854E+02	0.105E+00	0.853E+02
0.2000E+01	0.754E+02	0.105E+00	0.753E+02
0.2500E+01	0.642E+02	0.874E-01	0.641E+02
0.3000E+01	0.539E+02	0.874E-01	0.538E+02
0.3500E+01	0.450E+02	0.771E-01	0.449E+02
0.4000E+01	0.374E+02	0.771E-01	0.374E+02
0.4500E+01	0.311E+02	0.699E-01	0.310E+02

(first 10 times shown)

Mass Flux to and from Atmosphere

Time (yr)	Flux to Atmosphere (ug/cm^2/d)
0.0000E+00	0.000E+00
0.5000E+00	-0.488E+02
0.1000E+01	-0.643E+02
0.1500E+01	-0.557E+02
0.2000E+01	-0.457E+02
0.2500E+01	-0.373E+02
0.3000E+01	-0.306E+02
0.3500E+01	-0.252E+02
0.4000E+01	-0.208E+02
0.4500E+01	-0.172E+02

(first 10 times shown)

Example of Mass Balance File for VFLUX

********** Summary of Mass Balance **********
(Note: The mass units are - ug/cm^2)

Time(yr)	M_remaining	M_Atm	M_Gw	M_decay
0.000E+00	0.2002E+06	0.0000E+00	0.0000E+00	0.0000E+00
0.500E+00	0.1945E+06	0.3513E+04	0.2182E+04	0.7146E+01
0.100E+01	0.1708E+06	0.1462E+05	0.1471E+05	0.1396E+02
0.150E+01	0.1439E+06	0.2567E+05	0.3059E+05	0.2010E+02
0.200E+01	0.1199E+06	0.3491E+05	0.4532E+05	0.2498E+02
0.250E+01	0.9960E+05	0.4245E+05	0.5808E+05	0.2880E+02
0.300E+01	0.8265E+05	0.4863E+05	0.6885E+05	0.3196E+02
0.350E+01	0.6855E+05	0.5370E+05	0.7787E+05	0.3459E+02
0.400E+01	0.5685E+05	0.5789E+05	0.8538E+05	0.3675E+02
0.450E+01	0.4715E+05	0.6135E+05	0.9163E+05	0.3856E+02
0.500E+01	0.3910E+05	0.6421E+05	0.9681E+05	0.4006E+02
0.550E+01	0.3243E+05	0.6658E+05	0.1011E+06	0.4130E+02
0.600E+01	0.2691E+05	0.6854E+05	0.1047E+06	0.4233E+02
0.650E+01	0.2232E+05	0.7016E+05	0.1076E+06	0.4319E+02
0.700E+01	0.1853E+05	0.7151E+05	0.1101E+06	0.4389E+02
0.750E+01	0.1538E+05	0.7263E+05	0.1121E+06	0.4448E+02
0.800E+01	0.1278E+05	0.7356E+05	0.1138E+06	0.4497E+02
0.850E+01	0.1061E+05	0.7432E+05	0.1152E+06	0.4538E+02
0.900E+01	0.8822E+04	0.7496E+05	0.1163E+06	0.4572E+02
0.950E+01	0.7336E+04	0.7549E+05	0.1173E+06	0.4600E+02
0.100E+02	0.6107E+04	0.7593E+05	0.1181E+06	0.4623E+02
0.105E+02	0.5085E+04	0.7629E+05	0.1187E+06	0.4643E+02
0.110E+02	0.4240E+04	0.7660E+05	0.1193E+06	0.4659E+02
0.115E+02	0.3538E+04	0.7685E+05	0.1197E+06	0.4673E+02
0.120E+02	0.2957E+04	0.7706E+05	0.1201E+06	0.4684E+02
0.125E+02	0.2474E+04	0.7723E+05	0.1204E+06	0.4694E+02
0.130E+02	0.2075E+04	0.7738E+05	0.1207E+06	0.4702E+02
0.135E+02	0.1742E+04	0.7750E+05	0.1209E+06	0.4709E+02
0.140E+02	0.1467E+04	0.7760E+05	0.1210E+06	0.4714E+02
0.145E+02	0.1238E+04	0.7768E+05	0.1212E+06	0.4719E+02
0.150E+02	0.1049E+04	0.7775E+05	0.1213E+06	0.4723E+02
0.155E+02	0.8902E+03	0.7781E+05	0.1214E+06	0.4727E+02
0.160E+02	0.7598E+03	0.7786E+05	0.1215E+06	0.4730E+02
0.165E+02	0.6503E+03	0.7790E+05	0.1216E+06	0.4732E+02
0.170E+02	0.5602E+03	0.7793E+05	0.1216E+06	0.4734E+02
0.175E+02	0.4843E+03	0.7796E+05	0.1217E+06	0.4736E+02
0.180E+02	0.4220E+03	0.7799E+05	0.1217E+06	0.4738E+02
0.185E+02	0.3691E+03	0.7801E+05	0.1217E+06	0.4739E+02
0.190E+02	0.3260E+03	0.7803E+05	0.1218E+06	0.4741E+02
0.195E+02	0.2890E+03	0.7804E+05	0.1218E+06	0.4742E+02
0.200E+02	0.2589E+03	0.7806E+05	0.1218E+06	0.4743E+02
0.205E+02	0.2329E+03	0.7807E+05	0.1218E+06	0.4744E+02
0.210E+02	0.2119E+03	0.7808E+05	0.1218E+06	0.4745E+02
0.215E+02	0.1934E+03	0.7809E+05	0.1218E+06	0.4745E+02

Source Code for VFLUX (authors: Ravi Varadhan and Dominic DiGiulio)

```
c  This code, VFLUX, calculates an exact solution to the one-simensional
c  solute transport equation under time dependent boundary conditions.
c  The code calculates soil concentration profile, average soil concentrations
c  and mass flux to/from  groundwater.
c  Refer to DiGiulio et al. (1999) for details regarding the analytical model
c
c  Date: March 1999
c
c  Code modified 04/21/99 to account for zero-gradient BC at the bottom
c  of the soil column and also for g(T)=0; with these features the code
c  almost completely supersedes VLEACH - the only feature lacking is
c  the ability to simulate multiple polygons
c
c  Modified on 06/29/99 to generate a summary of mass balance at user-
c  specified times.  This option slows the execution of the code due to
c  slower convergence of the resulting fourier series for cumulative mass
c  flux.
c
c  modified on October 12, 1999 - moved the line, calculating
c  the conversion of aqsol from (mg/L) to (g/cc), up before the determination
c  of retardation factor
c
      implicit real*8 (a-h,o-z)
      dimension ctinit(500),zct(500),t(100),z(100),ctavg(100),
     >gwcon(500),tgw(500),eign(1000),an(1000),cmgw(100),cmatm(100)
      real mavg,mcomp,l,lambda,koc,kd,infil
      character*10 prefix,fname1,fname2,fname3,fname4,fname5
      character*4 suffix1,suffix2,suffix3,suffix4,suffix5
      character*1 mbl
      common/cmain/a
      common/cflux/an,eign,biglamb,tgw,gwcon,r,d,infil,l,ngw
      external funcd
      write(*,*)'Enter the Prefix of the input file:  '
      write(*,*)'3 different output files are created w/ same prefix'
      write(*,*)' Input-file Prefix ?  '
      read(*,'(a)')prefix
      call getlen(prefix,' ',n0,n1)
      suffix1='.inp'
      suffix2='.par'
      suffix3='.prf'
      suffix4='.flx'
      suffix5='.mbl'
      fname1=prefix(n0:n1)//suffix1
      fname2=prefix(n0:n1)//suffix2
      fname3=prefix(n0:n1)//suffix3
      fname4=prefix(n0:n1)//suffix4
      fname5=prefix(n0:n1)//suffix5
      open(10,fname1,status='unknown')
      open(20,fname2,status='unknown')
      open(30,fname3,status='unknown')
```

```
      open(40,fname4,status='unknown')
      open(50,fname5,status='unknown')
c
c  The following parameter definitions and units are used:
c
c  por = void volume / total volume
c  vnapl = NAPL volume / total volume
c  vwater = water volume / total volume
c  henry = dimensionless henry's law coefficient
c  mavg = average molecular weight (g/mole)
c  mcomp = molecular weight of component of interest
c  aqsol = aqueous solubility (mg/L)
c  koc = organic carbon partition coefficient (mL/g)
c  foc = fraction organic carbon (unitless)
c  rhob = bulk density of soil (g/cm^3)
c  rhonapl = density of NAPL (g/cm^3)
c  infil = average annual infiltration rate (cm/d)
c  dair = free-air diffusion coefficient of compound (cm^2/d)
c  dwater = free-water diffusion coefficient of compound (cm^2/d)
c  disp = longitudinal dispersivity (cm)
c  hlife = half-life of degradation (d)
c  zct = depths at which initial soil concentrations are measured (cm)
c  ctinit = initial soil concentrations (ug/kg)
c  tgw = times at which groundwater concentrations are measured (yr)
c  gwcon = groundwater concentrations (mg/L)
c  t = times at which outputs are calculated (yr)
c  z = depths at which soil concentration profile is evlauated (cm)
c
      read(10,101)por,vnapl,vwater,henry,mavg,mcomp,aqsol,koc,foc,rhob,
     >rhonapl
      read(10,101)infil,dair,dwater,disp,hlife
      read(10,101)nzct
      do 41 i=1,nzct
      read(10,*)zct(i),ctinit(i)
41    continue
      read(10,101)ngw
      if(ngw.le.0)goto 43
      do 42 i=1,ngw
      read(10,*)tgw(i),gwcon(i)
42    continue
43    continue
      read(10,101)nt
      read(10,*)(t(i),i=1,nt)
      if(t(1).ne.0.)then
      do 44 i=nt+1,2,-1
      t(i)=t(i-1)
44    continue
      t(1)=0.
      nt=nt+1
      endif
      read(10,101)nz
      read(10,*)(z(i),i=1,nz)
```

```
      l=zct(nzct)
      read(10,'(a1)')mbl
c
      write(20,*)'***** Input Parameters prescribed by the user *****'
      write(20,*)
      write(20,*)'Porosity  =',por
      write(20,*)'NAPL saturation  =', vnapl
      write(20,*)'Water saturation  =',vwater
      write(20,*)'Dimensionless Henrys constant  =',henry
      write(20,*)'Average molecular weight of NAPL  =',mavg
      write(20,*)'Molecular weight of compound of interest  =',mcomp
      write(20,*)'Aqueous solubility of compound (mg/L)  =',aqsol
      write(20,*)'Organic carbon partition coefficient (cc/g)  =',koc
      write(20,*)'Fraction organic carbon content  =',foc
      write(20,*)'Bulk density of soil (g/cc)  =',rhob
      write(20,*)'density of NAPL (g/cc)  =',rhonapl
      write(20,*)'Average annual recharge rate (cm/d)  =',infil
      write(20,*)'Free-air diffusion coefficient of compound (cm^2/d)  =
     >',dair
      write(20,*)'Free-water diffusion coefficient of compound (cm^2/d)
     >=',dwater
      write(20,*)'Hydrodynamic dispersivity (cm)  =',disp
      write(20,*)'Degradation half-life of compound (d)  =',hlife
      write(20,*)
      write(20,*)'Number of initial soil concentrations  =',nzct
      write(20,*)
      write(20,*)'Initial soil concentration versus depth (cm)'
      do 120 i=1,nzct
      write(20,109)zct(i),ctinit(i)
120   continue
      write(20,*)
      write(20,*)'Number of groundwater concentrations  =',ngw
      write(20,*)
      write(20,*)'Groundwater concentrations versus time (yrs)'
      if(ngw.gt.0)then
      do 130 i=1,ngw
      write(20,109)tgw(i),gwcon(i)
130   continue
      endif
      write(20,*)
      write(20,*)'Number of time values for simulation results  =',nt
      write(20,*)
      write(20,*)'Times (yr) at which results are produced  '
      write(20,*)(t(i),i=1,nt)
      write(20,*)
      write(20,*)'Number of depth values for simulation results  =',nz
      write(20,*)'Depths (cm) at which results are produced '
      write(20,*)(z(i),i=1,nz)
      write(20,*)
      write(20,*)'Length of domain (cm)  =',l
c
c  output times are converted from years to days
```

```
c
      do 45 i=1,nt
      t(i)=t(i)*365.2
45    continue
c
c  NAPL and water saturations are converted to bulk volumetric contents
c
      vnapl=vnapl*por
      vwater=vwater*por
c
c  soil concentrations which are input as (ug/kg) are converted to (ug/cm^3)
c
      sum=0.
      do 46 k=1,nzct
      ctinit(k)=ctinit(k)*rhob/1000.
      sum=sum+ctinit(k)*(zct(k)-zct(k-1))
46    continue
      ctavg(1)=sum/l
c
c  The conversion of aquqous solubility from mg/L to g/cc was moved to just
c  below this line so that the Retardation factor could be properly
c  calculated
c
      aqsol=aqsol*1.e-06
      vair=por-vnapl-vwater
      kd=koc*foc
      r=vair*henry+vwater+kd*rhob+mcomp*rhonapl*vnapl/(aqsol*mavg)
      psia=vair**(10./3.)/(por*por)
      psiw=vwater**(10./3.)/(por*por)
      d=dair*psia*henry+dwater*psiw+disp*infil/vwater
      a=infil*l/(2.*d)
      lambda=0.
      if(hlife.gt.0.)lambda=dlog(2.0)/hlife
      biglamb=lambda*r*l*l/d
      delta=dsqrt(a*a+biglamb)
      pi=4.*datan(1.0)
c
      write(20,*)
      write(20,*)'****** Calculated Model Parameters ******* '
      write(20,*)
      write(20,*)'Volumetric NAPL saturation  =',vnapl
      write(20,*)'Volumetric water saturation  =',vwater
      write(20,*)'Volumetric air saturation  =',vair
      write(20,*)'Lumped diffusion coefficient - D (cm^2/d)  =',d
      write(20,*)'Half-Peclet number - a   =',a
      write(20,*)'First-order decay constant (/d)  =',lambda
      write(20,*)'Dimensionless decay constant   =',biglamb
      write(20,*)'Parameter Delta  =',delta
      write(20,*)'Aqueous solubility (g/cc)  =',aqsol
      write(20,*)'Soil-water partition coefficient - Kd  =',kd
      write(20,*)'Total Retardation coefficient - R  =',r
c
```

```
c  groundwater concentrations (mg/L) are converted to interface soil
c  concentrations (ug/cm^3)
c  times are converted from (yrs) to (days)
c
      if(ngw.gt.0)then
      do 60 k=1,ngw
      tgw(k)=tgw(k)*365.2
      gwcon(k)=gwcon(k)*r
60    continue
      endif
c
c
c  calculation of eigen values
c
      if(ngw.ge.0)then
      do 1 n1=1,1000
      eign(n1)=n1*pi
1     continue
      else
      x1=0.01
      x2=pi
      do 1001 kount=1,1000
      zero=rtsafe(funcd,x1,x2,1.e-06)
      eign(kount)=zero
      x1=zero+0.5*pi
      x2=zero+1.5*pi
1001  continue
      endif
c
c  calculation of fourier coeffiecients
c
      do 1003 i=1,1000
      sum1=0.
      do 1002 k=1,nzct
      zzctk=zct(k-1)/l
      zzctk1=zct(k)/l
      hzk=dexp(-a*zzctk)*(a*dsin(eign(i)*zzctk)+eign(i)*dcos(eign(i)*
     >zzctk))
      hzk1=dexp(-a*zzctk1)*(a*dsin(eign(i)*zzctk1)+eign(i)*dcos(eign(i)*
     >zzctk1))
      sum1=sum1+ctinit(k)*(hzk-hzk1)
1002  continue
      if(ngw.ge.0)xnorm=1./2.
      if(ngw.lt.0)xnorm=(a+a*a+eign(i)**2)/(2.*(a*a+eign(i)**2))
      an(i)=sum1/(xnorm*(a*a+eign(i)**2))
1003  continue
c
c  calculation of soil concentration profile
c
      do 3 i=1,nt
      tt=d*t(i)/(r*l*l)
      if(tt.eq.0.)goto 3
```

```
c
c The profile is not calculated for t=0, since it is the
c initial distribution, which is known.
c
      write(30,103)t(i)/365.2
      write(30,108)
      do 4 j=1,nz
      zz=z(j)/l
      sum2=0.
      n2=0
5     continue
      n2=n2+1
      if(n2.gt.1000)goto 6
      wn2sq=biglamb+a*a+eign(n2)**2
      term=an(n2)*dexp(-wn2sq*tt)
      sterm=dsin(eign(n2)*zz)
      add=term*sterm
      sum2=sum2+add
      if(abs(sum2).le.1.e-14)goto 6
      if(abs(term/sum2).gt.1.e-07)goto 5
6     continue
      ct1=dexp(a*zz)*sum2
      ct2=0.
      ct3=0.
      if(ngw.le.0)goto 71
      n3=0
      sum3=0.
      fact=1
7     continue
      n3=n3+1
      if(n3.gt.1000)goto 8
      fact=-fact
      wn3sq=biglamb+a*a+(eign(n3))**2
      term=n3*fact/(wn3sq)*dexp(-wn3sq*tt)
      sum3=sum3+term*dsin(eign(n3)*zz)
      if(abs(sum3).le.1.e-14) goto 8
      if(abs(term/sum3).gt.1.e-07)goto 7
8     continue
      ct2=gwcon(1)*dexp(a*(zz-1.))*(2.*pi*sum3+dsinh(delta*zz)/dsinh
     >(delta))
      ct3=0.
      do 9 k=1,ngw
      ttgw=d*tgw(k)/(r*l*l)
      if(ttgw.ge.tt)goto 9
      n4=0
      sum4=0.
      fact=1
10    continue
      n4=n4+1
      if(n4.gt.1000)goto 11
      fact=-fact
      wn4sq=biglamb+a*a+(eign(n4))**2
```

```
      term=n4*fact/(wn4sq)*dexp(-wn4sq*(tt-ttgw))
      sum4=sum4+term*dsin(eign(n4)*zz)
      if(abs(sum4).le.1.e-14) goto 11
      if(abs(term/sum4).gt.1.e-07)goto 10
11    continue
      ct3=ct3+(gwcon(k+1)-gwcon(k))*dexp(a*(zz-1.))*(2.*pi*sum4+
     >dsinh(delta*zz)/dsinh(delta))
9     continue
71    continue
      ct=ct1+ct2+ct3
      ctmass=ct*1000./rhob
      cair=ct*henry/r
      csolid=ct*kd/r
      cwater=ct/r
      write(30,109)z(j),ctmass,csolid,cair,cwater
4     continue
3     continue
c
c  Calculation of average soil concentration
c
      write(40,104)
      write(40,105)t(1)/365.2,ctavg(1)*1000./rhob
      do 30 i=1,nt
      tt=d*t(i)/(r*l*l)
      if(tt.eq.0.)goto 30
      sum5=0.
      n5=0
12    continue
      n5=n5+1
      if(n5.gt.1000)goto 13
      wn5sq=biglamb+a*a+(eign(n5))**2
      t1=a*dsin(eign(n5))-eign(n5)*dcos(eign(n5))+dexp(-a)*eign(n5)
      term=an(n5)*dexp(-wn5sq*tt)*t1/(a*a+(eign(n5))**2)
      sum5=sum5+term
      if(abs(sum5).le.1.e-14)goto 13
      if(abs(term/sum5).gt.1.e-07)goto 12
13    continue
      ctavg1=dexp(a)*sum5
      ctavg2=0.
      ctavg3=0.
      if(tt.eq.0. .or. ngw.le.0)goto 72
      n6=0
      sum6=0.
      fact=1.
14    continue
      n6=n6+1
      if(n6.gt.1000)goto 15
      fact=-fact
      wn6sq=biglamb+a*a+(eign(n6))**2
      term=(eign(n6))**2/wn6sq/(a*a+(eign(n6))**2)*dexp(-wn6sq*tt)*
     >(fact*dexp(-a)-1.)
      sum6=sum6+term
```

```
      if(abs(sum6).le.1.e-14)goto 15
      if(abs(term/sum6).gt.1.e-07)goto 14
15    continue
      if(abs(a-delta).ge.1.e-14)then
      ctavg2=gwcon(1)*((a*dsinh(delta)-delta*dcosh(delta)+delta*dexp(-a)
     >)/(dsinh(delta)*(a*a-delta*delta))+2.*sum6)
      else
      ctavg2=gwcon(1)*((1./delta-dexp(-delta)/dsinh(delta))/2.+2.*sum6)
      endif
      do 16 k=1,ngw
      ttgw=d*tgw(k)/(r*l*l)
      if(ttgw.ge.tt)goto 16
      n7=0
      sum7=0.
      fact=1.
17    continue
      n7=n7+1
      if(n7.gt.1000)goto 18
      fact=-fact
      wn7sq=biglamb+a*a+(eign(n7))**2
      term=(eign(n7))**2/wn7sq/(a*a+(eign(n7))**2)*dexp(-wn7sq*(tt-ttgw)
     >)*(fact*dexp(-a)-1.)
      sum7=sum7+term
      if(abs(sum7).le.1.e-14)goto 18
      if(abs(term/sum7).gt.1.e-07)goto 17
18    continue
      if(abs(a-delta).ge.1.e-14)then
      ctavg3=ctavg3+(gwcon(k+1)-gwcon(k))*((a*dsinh(delta)-delta*dcosh
     >(delta)+delta*dexp(-a))/(dsinh(delta)*(a*a-delta*delta))+2.*sum7)
      else
      ctavg3=ctavg3+(gwcon(k+1)-gwcon(k))*((1./delta-dexp(-delta)/dsinh
     >(delta))/2.+2.*sum7)
      endif
16    continue
72    continue
      ctavg(i)=ctavg1+ctavg2+ctavg3
      write(40,105)t(i)/365.2,ctavg(i)*1000./rhob
30    continue
c
c  Calculation of groundwater flux
c
      write(40,106)
      do 40 i=1,nt
      tt=d*t(i)/(r*l*l)
      call gwflux(tt,gwflx,advflx,dspflx)
      write(40,107)t(i)/365.2,gwflx,advflx,dspflx
40    continue
c
c  Calculation of flux to the atmosphere
c
      write(40,110)
      do 50 i=1,nt
```

```
      tt=d*t(i)/(r*l*l)
      call atmflux(tt,atmflx)
      write(40,111)t(i)/365.2,atmflx
50    continue
c
c  Summary of mass balance
c
c
      if(mbl.eq.'y' .or. mbl.eq.'Y')then
c
      if(lambda.eq.0.)write(50,112)
      if(lambda.gt.0.)write(50,114)
      do 80 i=1,nt
      tt=d*t(i)/(r*l*l)
      call gwmass(tt,cgwm)
      call atmass(tt,catm)
      cmatm(i)=-catm*r*l*l/d
      cmgw(i)=cgwm*r*l*l/d
      cmdis=ctavg(1)*l-(ctavg(i)*l+cmatm(i)+cmgw(i))
      write(50,113)t(i)/365.2,ctavg(i)*l,cmatm(i),cmgw(i),cmdis
80    continue
c
      endif
c
101   format(g10.0)
102   format(g10.0,g10.0)
103   format(75('*')/'Soil Concentration Profile @ time (yr)=',e10.3/)
104   format(75('*')/5x,'Time',12x,'Average Soil Concentration '/5x,
     >'(yr)',21x,'(ug/kg)'/)
105   format(2x,e10.4,16x,e10.4)
106   format(75('*'),//10x,'Mass flux To/From Groundwater'//5x,'Time',
     >9x,'Total Mass-flux',4x,'Advective flux',4x,'Dispersive flux'/5x,
     >'(yr)',12x,'(ug/cm^2/d)'/)
107   format(3x,e10.4,8x,e10.3,8x,e10.3,10x,e10.3)
108   format(/6x,'Depth',9x,'C_soil',9x,'C_solids',9x,'C_air',8x,
     >'C_water'/,7x,'(cm)',9x,'(ug/kg)',7x,'(ug/kg)',9x,'(ug/cm^3)',
     >5x,'(ug/cm^3)'/)
109   format(4x,e9.3,5x,e10.3,5x,e10.3,5x,e10.3,5x,e10.3)
110   format(75('*'),/7x,'Time',10x,'Flux to Atmosphere'/,7x,'(yr)',
     >13x,'(ug/cm^2/d)'/)
111   format(3x,e10.4,12x,e10.3)
112   format(///5x,20('*'),3x,'Summary of Mass Balance',3x,20('*')/3x,
     >'(Note:  The mass units are - ug/cm^2)'///5x,'Time(yr)',5x,
     >'M_remaining',7x,'M_Atm',11x,'M_Gw',13x,'M_error'/)
113   format(3x,e9.3,7x,e10.4,6x,e10.4,4x,e10.4,8x,e10.4)
114   format(///5x,20('*'),3x,'Summary of Mass Balance',3x,20('*')/3x,
     >'(Note:  The mass units are - ug/cm^2)'///5x,'Time(yr)',5x,
     >'M_remaining',7x,'M_Atm',11x,'M_Gw',13x,'M_decay'/)
      stop
      end
c
      double precision FUNCTION rtsafe(funcd,x1,x2,xacc)
```

```
      implicit real*8 (a-h,o-z)
      EXTERNAL funcd
      PARAMETER (MAXIT=100)
      call funcd(x1,fl,df)
      call funcd(x2,fh,df)
      if((fl.gt.0..and.fh.gt.0.).or.(fl.lt.0..and.fh.lt.0.))pause
     *'root must be bracketed in rtsafe'
      if(fl.eq.0.)then
        rtsafe=x1
        return
      else if(fh.eq.0.)then
        rtsafe=x2
        return
      else if(fl.lt.0.)then
        xl=x1
        xh=x2
      else
        xh=x1
        xl=x2
      endif
      rtsafe=.5*(x1+x2)
      dxold=dabs(x2-x1)
      dx=dxold
      call funcd(rtsafe,f,df)
      do 11 j=1,MAXIT
        if(((rtsafe-xh)*df-f)*((rtsafe-xl)*df-f).ge.0..or. dabs(2.*
     *f).gt.dabs(dxold*df) ) then
          dxold=dx
          dx=0.5*(xh-xl)
          rtsafe=xl+dx
          if(xl.eq.rtsafe)return
        else
          dxold=dx
          dx=f/df
          temp=rtsafe
          rtsafe=rtsafe-dx
          if(temp.eq.rtsafe)return
        endif
        if(dabs(dx).lt.xacc) return
        call funcd(rtsafe,f,df)
        if(f.lt.0.) then
          xl=rtsafe
        else
          xh=rtsafe
        endif
11    continue
      pause 'rtsafe exceeding maximum iterations'
      return
      END
c
      subroutine funcd(x,f,df)
      implicit real*8 (a-h,o-z)
```

```
      common/cmain/a
      f=x*dcos(x)+a*dsin(x)
      df=dcos(x)-x*dsin(x)+a*dcos(x)
      return
      end
c
      subroutine gwflux(tt,gwflx,advflx,dspflx)
      implicit real*8 (a-h,o-z)
      dimension an(1000),eign(1000),tgw(500),gwcon(500)
      real l,infil
      common/cflux/an,eign,biglamb,tgw,gwcon,r,d,infil,l,ngw
      common/cmain/a
      advflx2=0.
      advflx3=0.
      dspflx1=0.
      dspflx2=0.
      dspflx3=0.
      advflx=0.
      dspflx=0.
      gwflx=0.
      delta=dsqrt(a*a+biglamb)
      if(tt.eq.0.)goto73
      sum8=0.
      n8=0
      fact=1.
19    continue
      n8=n8+1
      if(n8.gt.1000)goto 20
      fact=-fact
      wn8sq=biglamb+a*a+(eign(n8))**2
      if(ngw.ge.0)term=an(n8)*dexp(-wn8sq*tt)*eign(n8)*fact
      if(ngw.lt.0)term=an(n8)*dexp(-wn8sq*tt)*dsin(eign(n8))
      sum8=sum8+term
      if(abs(sum8).le.1.e-14)goto 20
      if(abs(term/sum8).gt.1.e-07)goto 19
20    continue
      dspflx1=-sum8*dexp(a)*d/(r*l)
      if(ngw.lt.0)then
      advflx=infil*dexp(a)*sum8/r
      gwflx=advflx+dspflx
      elseif(ngw.eq.0)then
      dspflx=dspflx1
      gwflx=advflx+dspflx
      endif
      if(ngw.le.0) goto 73
      n9=0
      sum9=0.
21    continue
      n9=n9+1
      if(n9.gt.1000)goto 22
      wn9sq=biglamb+a*a+(eign(n9))**2
      term=(eign(n9))**2/wn9sq*dexp(-wn9sq*tt)
```

```
      sum9=sum9+term
      if(abs(sum9).le.1.e-14)goto 22
      if(abs(term/sum9).gt.1.e-07)goto 21
   22   continue
      advflx2=gwcon(1)*infil/r
      dspflx2=-gwcon(1)*d/(r*l)*(a+delta*dcosh(delta)/dsinh(delta)+2.*
     >sum9)
      do 23 k=1,ngw
      ttgw=d*tgw(k)/(r*l*l)
      if(ttgw.ge.tt)goto 23
      n10=0
      sum10=0.
   24   continue
      n10=n10+1
      if(n10.gt.1000)goto 25
      wn10sq=biglamb+a*a+(eign(n10))**2
      term=(eign(n10))**2/wn10sq*dexp(-wn10sq*(tt-ttgw))
      sum10=sum10+term
      if(abs(sum10).le.1.e-14)goto 25
      if(abs(term/sum10).gt.1.e-07)goto 24
   25   continue
      advflx3=advflx3+(gwcon(k+1)-gwcon(k))*infil/r
      dspflx3=dspflx3-d/(r*l)*(gwcon(k+1)-gwcon(k))*(a+delta*dcosh(delta
     >)/dsinh(delta)+2.*sum10)
   23   continue
      advflx=advflx2+advflx3
      dspflx=dspflx1+dspflx2+dspflx3
      gwflx=advflx+dspflx
   73   continue
      return
      end
c
      subroutine atmflux(tt,atmflx)
      implicit real*8 (a-h,o-z)
      dimension an(1000),eign(1000),tgw(500),gwcon(500)
      real l,infil
      common/cflux/an,eign,biglamb,tgw,gwcon,r,d,infil,l,ngw
      common/cmain/a
      atmflx1=0.
      atmflx2=0.
      atmflx3=0.
      if(tt.eq.0.)goto 74
      delta=dsqrt(a*a+biglamb)
      sum12=0.
      n12=0
   51   continue
      n12=n12+1
      if(n12.gt.1000)goto 52
      wn12sq=biglamb+a*a+(eign(n12))**2
      term=an(n12)*dexp(-wn12sq*tt)*eign(n12)
      sum12=sum12+term
      if(abs(sum12).le.1.e-14)goto 52
```

```
      if(abs(term/sum12).gt.1.e-07)goto 51
   52   continue
      atmflx1=-sum12*d/(r*l)
      if(ngw.le.0.)goto 74
      n13=0
      sum13=0.
      fact=1.
   53   continue
      n13=n13+1
      fact=-fact
      if(n13.gt.1000)goto 54
      wn13sq=biglamb+a*a+(eign(n13))**2
      term=fact*(eign(n13))**2/wn13sq*dexp(-wn13sq*tt)
      sum13=sum13+term
      if(abs(sum13).le.1.e-14)goto 54
      if(abs(term/sum13).gt.1.e-07)goto 53
   54   continue
      atmflx2=-d/(r*l)*gwcon(1)*dexp(-a)*(delta/dsinh(delta)+2.*sum13)
      do 55 k=1,ngw
      ttgw=d*tgw(k)/(r*l*l)
      if(ttgw.ge.tt)goto 55
      n14=0
      sum14=0.
      fact=1
   56   continue
      n14=n14+1
      fact=-fact
      if(n14.gt.1000)goto 57
      wn14sq=biglamb+a*a+(eign(n14))**2
      term=fact*(eign(n14))**2/wn14sq*dexp(-wn14sq*(tt-ttgw))
      sum14=sum14+term
      if(abs(sum14).le.1.e-14)goto 57
      if(abs(term/sum14).gt.1.e-07)goto 56
   57   continue
      atmflx3=atmflx3-d/(r*l)*(gwcon(k+1)-gwcon(k))*dexp(-a)*(delta/
     >dsinh(delta)+2.*sum14)
   55   continue
   74   continue
      atmflx=atmflx1+atmflx2+atmflx3
      return
      end
c
      subroutine gwmass(tt,cgwm)
      implicit real*8 (a-h,o-z)
      dimension an(1000),eign(1000),tgw(500),gwcon(500)
      real l,infil
      common/cflux/an,eign,biglamb,tgw,gwcon,r,d,infil,l,ngw
      common/cmain/a
      delta=dsqrt(a*a+biglamb)
      if(tt.eq.0.)goto73
      sum21=0.
      n8=0
```

```
      fact=1.
19    continue
      n8=n8+1
      if(n8.gt.1000)goto 20
      fact=-fact
      wn8sq=biglamb+a*a+(eign(n8))**2
      if(ngw.ge.0)cmtrm=an(n8)*eign(n8)*fact*(1.-dexp(-wn8sq*tt))/wn8sq
      if(ngw.lt.0)cmtrm=an(n8)*dsin(eign(n8))*(1.-dexp(-wn8sq*tt))/wn8sq
      sum21=sum21+cmtrm
      if(abs(sum21).le.1.e-14)goto 20
      if(abs(cmtrm/sum21).gt.1.e-07)goto 19
20    continue
      if(ngw.lt.0)cgwm=infil*dexp(a)*sum21/r
      if(ngw.eq.0)cgwm=-sum21*dexp(a)*d/(r*l)
      if(ngw.le.0) goto 73
      cmgw1=-dexp(a)*sum21*d/(r*l)
      n9=0
      sum22=0.
21    continue
      n9=n9+1
      if(n9.gt.1000)goto 22
      wn9sq=biglamb+a*a+(eign(n9))**2
      cmtrm=(eign(n9))**2*(1.-dexp(-wn9sq*tt))/wn9sq**2
      sum22=sum22+cmtrm
      if(abs(sum22).le.1.e-14)goto 22
      if(abs(cmtrm/sum22).gt.1.e-07)goto 21
22    continue
      cmgw2=gwcon(1)/r*(infil*tt-d/l*((a+delta*dcosh(delta)/dsinh(delta)
     >)*tt+2.*sum22))
      cmgw3=0.
      do 23 k=1,ngw
      ttgw=d*tgw(k)/(r*l*l)
      if(ttgw.ge.tt)goto 23
      n10=0
      sum23=0.
24    continue
      n10=n10+1
      if(n10.gt.1000)goto 25
      wn10sq=biglamb+a*a+(eign(n10))**2
      cmtrm=(eign(n10))**2*(1.-dexp(-wn10sq*(tt-ttgw)))/wn10sq**2
      sum23=sum23+cmtrm
      if(abs(sum23).le.1.e-14)goto 25
      if(abs(cmtrm/sum23).gt.1.e-07)goto 24
25    continue
      cmgw3=cmgw3+(gwcon(k+1)-gwcon(k))/r*(infil*(tt-ttgw)-d/l*((a+delta
     >*dcosh(delta)/dsinh(delta))*(tt-ttgw)+2.*sum23))
23    continue
      cgwm=cmgw1+cmgw2+cmgw3
73    continue
      return
      end
```

```
      subroutine atmass(tt,catm)
      implicit real*8 (a-h,o-z)
      dimension an(1000),eign(1000),tgw(500),gwcon(500)
      real l,infil
      common/cflux/an,eign,biglamb,tgw,gwcon,r,d,infil,l,ngw
      common/cmain/a
      if(tt.eq.0.)goto 74
      delta=dsqrt(a*a+biglamb)
      sum24=0.
      n12=0
   51   continue
      n12=n12+1
      if(n12.gt.1000)goto 52
      wn12sq=biglamb+a*a+(eign(n12))**2
      cmtrm=an(n12)*eign(n12)*(1.-dexp(-wn12sq*tt))/wn12sq
      sum24=sum24+cmtrm
      if(abs(sum24).le.1.e-14)goto 52
      if(abs(cmtrm/sum24).gt.1.e-07)goto 51
   52   continue
      catm=-sum24*d/(r*l)
      if(ngw.le.0.)goto 74
      n13=0
      sum25=0.
      fact=1.
   53   continue
      n13=n13+1
      fact=-fact
      if(n13.gt.1000)goto 54
      wn13sq=biglamb+a*a+(eign(n13))**2
      cmtrm=fact*(eign(n13))**2*(1.-dexp(-wn13sq*tt))/wn13sq**2
      sum25=sum25+cmtrm
      if(abs(sum25).le.1.e-14)goto 54
      if(abs(cmtrm/sum25).gt.1.e-07)goto 53
   54   continue
      cmatm1=-d/(r*l)*gwcon(1)*dexp(-a)*(delta/dsinh(delta)*tt+2.*sum25)
      cmatm2=0.
      do 55 k=1,ngw
      ttgw=d*tgw(k)/(r*l*l)
      if(ttgw.ge.tt)goto 55
      n14=0
      sum26=0.
      fact=1
   56   continue
      n14=n14+1
      fact=-fact
      if(n14.gt.1000)goto 57
      wn14sq=biglamb+a*a+(eign(n14))**2
      cmtrm=fact*(eign(n14))**2*(1.-dexp(-wn14sq*(tt-ttgw)))/wn14sq**2
      sum26=sum26+cmtrm
      if(abs(sum26).le.1.e-14)goto 57
      if(abs(cmtrm/sum26).gt.1.e-07)goto 56
   57   continue
```

```
      cmatm2=cmatm2-d/(r*l)*(gwcon(k+1)-gwcon(k))*dexp(-a)*(delta/dsinh
     >(delta)*(tt-ttgw)+2.*sum26)
55    continue
      catm=catm+cmatm1+cmatm2
74    continue
      return
      end


      subroutine getlen(string,chr,n0,n1)
c
c     to determine the length of a string excluding any blank padding & heading
c     and return string(n0:n1) n0... position of first non-blank letter
c                              n1... position of last non-blank letter
c     else return the original string
c     ***Use | to keep blank space at the begining or the end of the
c      *** string
c
      character*(*) string
      character*160 string1
      character*1 chr
      string1=' '
      in0=0
      in1=0
      do 10 i=len(string),1,-1
      if(string(i:i).ne.chr) then
        if(in1.eq.0) then
        if(string(i:i).eq.'|') then
        n1=i-1
        else
        n1=i
        endif
        in1=1
        endif
        goto 11
      endif
10    continue
11    do 20 i=1,len(string)
      if(string(i:i).ne.chr) then
       if(in0.eq.0) then
       if(string(i:i).eq.'|') then
       n0=i+1
       else
       n0=i
       endif
       in0=1
       nk=n0-1
c      write(6,*) '|'//string(n0:n1)//'|', n0,n1
       do 30 k=n0,n1
       if(string(k:k).ne.'|') then
         nk=nk+1
         if(k.eq.n0) then
```

```
          string1=string(k:k)
        else
          string1=string1(1:nk-n0)//string(k:k)
        endif
      endif
c     write(6,*) '|'//string1(1:nk-n0)//'|'
30    continue
      string=string1
      n1=n1-n0+1
      n0=1
      endif
      return
     endif
20   continue
     n0=-1
     n1=-1
     return
     end
```